UNIVERSITY *of* TASMANIA

Department of Physical Sciences

A long-term single-pulse study of the Vela pulsar

Jim Palfreyman M.Sc.

Version 1.05
2018-10-31
MJD 58422.1

Supervisors:
Prof. John Dickey
Prof. Simon Ellingsen
Dr Aidan Hotan

Submitted in fulfilment of the requirements for the Degree of
Doctor of Philosophy

Declaration of Originality

This thesis contains no material which has been accepted for a degree or diploma by the University or any other institution, except by way of background information and duly acknowledged in the thesis, and to the best of my knowledge and belief no material previously published or written by another person, except where due acknowledgement is made in the text of the thesis, nor does the thesis contain any material that infringes copyright.

Signed:

Date: 31-Oct-2018

Dedication

This work is dedicated to Stephen Atkinson (MJD 37693.2 to 58313.4). Technically the oldest of my oldest friends.

In my teenage years, and being two years his junior, I followed in his footsteps through high school, college, and then completed a Computer Science degree. This opened my eyes to the world of science and commenced my academic career. I ended up adding a mathematics degree to my B.Sc., then I completed Honours. Thirty years passed and I lost contact with Stephen until we re-connected online. After completing my Masters in Astrophysics and during this Ph.D. he was very supportive and the first to comment upon me lecturing in mathematics and also being published in Nature.

My hatred of European wasps was only equalled by Stephen.

His untimely death occurred as this work was been finalised and it was particularly devastating for me.

I would have loved to have been able to personally hand him a copy of this thesis. Instead I will hand it to his younger brother (and my oldest friend) Richard.

Authority of Access

Signed:

Date: 31-Oct-2018

Statement of Co-Authorship

The following people contributed to the publication of work undertaken as part of this thesis:

Candidate	Palfreyman, J. L.	University of Tasmania
Co-Author 1	Dickey, J. M.	University of Tasmania
Co-Author 2	Ellingsen, S. P.	University of Tasmania
Co-Author 3	Hotan, A. W.	CSIRO Astronomy & Space Science
Co-Author 4	Jones, I. R.	University of Tasmania
Co-Author 5	van Straten, W	Auckland University of Technology

Sections 6.1-6.4: *Temporal evolution of the Vela pulsar's pulse profile*
Candidate (85%), Co-Author 1, 2, 3, and 4 (15%)
Candidate was the primary author and Co-Authors 1, 2, 3, and 4 contributed to the idea, its formalisation, development and refinement. Writing was done primarily by the Candidate. Feedback and editing for the purposes of publication was provided by the Co-Authors 1, 2, 3 and 4.

Appendix C: *Alteration of the magnetosphere of the Vela pulsar during a glitch*
Candidate (85%), Co-Author 1, 2, 3, and 5 (15%)
Candidate was the primary author and Co-Authors 1, 2, 3, and 5 contributed to the idea, its formalisation, development and refinement. Writing was done primarily by the Candidate. Polarisation calibration was done by Co-Author 5. Feedback and editing for the purposes of publication was provided by the Co-Authors 1, 2, 3 and 5.

We the undersigned agree with the above stated "proportion of work undertaken" for each of the above published peer-reviewed manuscripts contributing to this thesis:

Signed:

Date: 31-Oct-2018

Prof. John Dickey
Primary Supervisor
School of Natural Sciences
University of Tasmania

Signed:

Date: 31-Oct-2018

Prof. Mark Hunt
Head of School
School of Natural Sciences
University of Tasmania

"I'm looking at a stellar crematorium, staring down the throat of a spinning dead star with a 1 pixel movie camera trying to figure out what the hell happened."

— "Dumbed down" version of this thesis as it would appear as per the Facebook and reddit memes.

Abstract

The mechanisms of emission and changes in rotation frequency (*glitches*) of the Vela pulsar (J0835−4510) are a fascinating area of study. Further insight into these mechanisms can be achieved by long-term studies of integrated pulse width, timing residuals, and bright pulse rates. We have undertaken an intensive observing campaign of Vela and collected over 14000 hours of single-pulse data. The data shows that the pulse width changes with time, including marked jumps in width after micro-glitches. The abundance of bright pulses also changes after some micro-glitches, but not all. The secular changes in pulse width have cyclic periods, some of which match with X-Ray periodicities of a helical jet that are interpreted as free precession. Some radio pulsars make excellent natural clocks because of their fast rotation and immense angular inertia. However the Vela pulsar, which has rotation frequency $\nu = 11.2$ Hz, suddenly speeds up by $\frac{\Delta\nu}{\nu} \approx 10^{-6}$ during a glitch which happens roughly every three years. Glitches have never been observed with a telescope and receiver sensitive enough to detect individual pulses, from Vela or any other pulsar, until now. On 2016-12-12 at UT 11:36 a glitch with magnitude $\frac{\Delta\nu}{\nu} = 1.431 \times 10^{-6}$ was captured by the University of Tasmania's 26m and 30m telescopes at a frequency of 1376 MHz and a bandwidth of 64 MHz. Here we show that just near the glitch epoch, the pulse shape shows a sudden change. One pulse is a null, i.e. there is no emission detected, and the pulse before the null is very broad. Just after the null there is a 2.6 second interval when the pulsar shows *decreased* pulse frequency, i.e. an effect in the opposite direction to the glitch. Along with the slight spin-down during these 2.6 seconds, the variance of the pulse arrival time decreases, suggesting that either or both the magnetic field configuration and the crustal rotation period have been stabilised during this interval, perhaps by a brief but strong dynamical connection between the superfluid interior and the outer layers of the pulsar. The null pulse and the change in arrival time statistics are both extremely rare; that they are nearly simultaneous with the glitch strongly suggests that all three are aspects of a single event.

Acknowledgements

I have many people to thank over the duration of this work. The data-gathering was probably the most annoying aspect, especially as the glitch approached. For this I would like to mainly thank Brett Reid and Eric Baynes for keeping the 26 m telescope up and running. As well as providing day and night support, they also cut me some slack when the Y-drive was leaking oil, solved the burned-out hydraulics motor issue (multiple times), fixed the capacitors in the main drives (multiple times), and kept the L-band receiver cooled (multiple times).

Special mention goes to Bev Bedson at Ceduna who kept the 30 m telescope running through many issues. This involved driving out at odd hours and this was no doubt extremely tiresome at times.

I'd like to thank all the other observers for putting up with my persistence as the glitch approached - especially Jamie McCallum who also provided much patience and assistance.

The Dean's Summer Students for 2016/17, Nicholas Bochenek and Wesley Kean Tai, provided valuable assistance in the tedious "eyeballing" of many thousands of pulsar plots for the removal of RFI and tracking down *nulls*. Job Carr-Turbitt also found a lovely sequence of consecutive bright pulses.

I'd like to thank Ogilvie High School student Scarlett Marston for asking such a fantastic question at one of my school visits when I was explaining how glitches work.

There were also numerous inter-departmental and tea-room chats where problems were solved and new ideas seemed to just pop out of nowhere. Mentions go to Dr Kym Hill, David Hughes, Melissa Humphries, and also Emeritus Professor Peter McCulloch for providing me with historical data to analyse. A special mention goes to Karen Bradford who provided much support with regard to the machinations of the bureaucratic entity that is a University.

Internet resources, when carefully selected, can be excellent and the folks on the *time-nuts* and the Facebook *astrostatistics* forums have also been invaluable. A special mention goes to *time-nuts* administrator Tom Van Baak.

Supervision is an incredibly important part of a Ph.D and my main supervisors Professor John Dickey and Professor Simon Ellingsen gave me the support, and especially the freedom, to explore the aspects of this work that I needed.

Dr Aidan Hotan, who not only 10 years ago introduced me to the wonderful world of pulsars, but also gave me support throughout this work and never failed to answer any

question I had. I would also like to thank Dr Willem van Straten for his insights with regard to the pulsar magnetosphere and neutron star cores.

I would also like to officially acknowledge the Australian Government Research Training Program Scholarship which helped fund this research and the Tasmanian Partnership for Advanced Computing (TPAC) at the University of Tasmania, with funding from the Australian Government through its NCRIS and RDSI programs for the use of the 2.3 PB storage facility, without which this project would not have been possible.

A penultimate acknowledgement goes to my mum, Jennie Clarke, and my aunt, Wendy Weight, who proof-read this thesis from a non-scientific perspective.

Finally, and most importantly, I'd like to thank my partner Zonia Bell for suffering through the four years of a hard-slog that is a Ph.D.

But it's all worth it.

Contents

List of Figures

List of Tables

List of Equations

Chapter 1

Thesis overview

We begin this thesis with an introduction to pulsar theory that is relevant to this work. Then we discuss the Vela pulsar (J0835−4510) and the other pulsars that have also been observed during this study. This is followed by an introduction to the hardware and software used at the Mount Pleasant and Ceduna observatories. Observed radio frequency interference is then covered along with a discussion of major statistical tools used throughout.

Bright and giant pulses observed at both Mount Pleasant and Ceduna observatories are then discussed.

The paper that appeared in *The Astrophysical Journal* titled *Temporal Evolution of the Vela Pulsar's Pulse Profile* is presented along with a postscript discussing updated data that was gathered since the paper was accepted for publication.

The glitch that was caught live in single-pulse mode at both Mount Pleasant and Ceduna observatories on 12 December 2016 is then discussed. The observed *null*, changes in timing, and flux density are presented. This result appeared in *Nature*.

The conclusion summarises the content and then three appendices are included. Appendix A provides a list of scripts and commands so that future researchers can continue pulsar work, Appendix B is a summary table of each day's recording, including brief notes, and Appendix C is the paper that appeared in *Nature* on 2018-04-12 titled *Alteration of the magnetosphere of the Vela pulsar during a glitch.*

1.1 Notes on style

Scientific writing has a requirement to be precise, however this style also constantly evolves over the decades. We have used *Scientific Style and Format* (Huth 1994) as a general guide. Some exceptions and options arose, and so we had to adopt some specific choices. When deciding, the option making the script *easier to read* was used as a major guideline. The key selections made were:

- British English spelling is used throughout.
- The Oxford comma is always used. Here's why: "At school I learned from my teachers, Marie Curie and Albert Einstein." and *with* the Oxford comma: "At school I learned from my teachers, Marie Curie, and Albert Einstein."
- Double quote marks " " have been used not single quotes ' '. This is more of a United States style, but we've adopted it simply to avoid confusion with apostrophes.
- If an abbreviation has been used, we write as if the abbreviation has been said as letters and not its full expansion. For example, FRB as an abbreviation for Fast Radio Burst, we would say "in the case of an FRB" and not "in the case of a FRB".
- We have adopted the modern style of using the word *data* as singular or plural depending on context. The singular form *datum* is very rarely used nowadays (except when explaining why it is not used), and other Latin based words have followed this path. For example, the words *agenda* and *agendum*. This sentence would never now be written: "the agenda show that Albert was present".
- All pulsar designations are quoted using the J2000 form, but without the leading "PSR". For example the Vela pulsar was originally labelled B0833−45 but its J2000 version is PSR J0835−4510. We write J0835−4510. This looks neater in tables and provides consistency in layout. Note that care must be taken by researchers when using on-line searches, as the older names may have been the only ones used in earlier publications.
- A number such as 3×10^{-6} would not normally be written as 3000×10^{-9}. However since pulsar glitch sizes quote $\frac{\Delta\nu}{\nu}$, we always express this in terms of 10^{-9} as this appears neater in tables, and makes for easier comparisons when reading.
- We adopt the sign convention of the spectral index to be $S \propto f^{\xi}$.
- Equations on their own line do not have punctuation marks at the end, in particular, commas or full stops. We consider this confusing and unnecessary.

Chapter 2

Introduction

A full introduction of pulsars is not really possible in a single chapter. So for this work we have focused on key areas that are relevant to later chapters. For an excellent overall introduction to pulsars, *Handbook of Pulsar Astronomy* (Lorimer and Kramer 2004) is highly recommended.

In summary we briefly cover the formation of pulsars, emission mechanisms, drifting sub-pulses, nulling, mode changes, bright and giant pulses, characteristic age, braking index, interstellar medium, dispersion measure, arrival times, timing noise, polynomial fits and their associated timing artefacts, fast radio bursts, and finally basic glitch theory.

2.1 Formation of pulsars

In simple terms, at the end of a sufficiently large star's life, the hydrogen runs out, nuclear fusion ends, the star collapses, and a Type II supernova occurs. The remains of the star ($M \approx 1.4 M_{\odot}$) collapse further until the neutron degeneracy limit is reached and as long as the star is not sufficiently large to create a black hole, a neutron star with a radius of $R \approx 10$ km is formed.

The magnetic field at the surface of a typical neutron star is $B \approx 10^{12}$ Gauss, approximately a trillion times that on the surface of the earth. The axis of the magnetic field is thought to be close to perpendicular to the axis of rotation at the pulsar's birth, but then moves slowly to align with the axis of rotation over the lifetime of the pulsar (Tong and Kou 2017). Once the neutron star is an *aligned rotator* it is no longer visible as a pulsar.

Initial rotation frequencies of pulsars are not accurately known, but by comparing characteristic age ($\tau_{\rm c}$) with a real known age (e.g. with the Crab pulsar - see Equation 2.7

on page 16 and related text), a value of $\nu_0 \approx 60$ Hz can be estimated.

2.2 Emission

The pulsar emission mechanism is still, after nearly 50 years of study, not as well understood as would be expected. Within a few months of the publication of pulsar discovery, Gold (1968) stated that rotating neutron stars were the origin of pulsating radio sources. Despite only a short amount of time for research, this paper is surprisingly accurate to this day. Here are a number of selected quotes from the paper:

"Since the distances are known approximately from interstellar dispersion of the different radio frequencies, it is clear that the emission per unit emitting volume must be very high; the size of the region emitting any one pulse can, after all, not be much larger than the distance light travels in the few milliseconds that represents the lengths of the individual pulses. No such concentration of energy can be visualized except in the presence of an intense gravitational field."

"... the emission derives its energy from the rotation energy of the star (very likely the principal remaining energy source), and is a result of relativistic effects in a co-rotating magnetosphere."

"A magnetic field of a neutron star may well have a strength of 10^{12} *gauss at the surface of the 10 km object."*

"... the configuration discussed here may be particularly favourable for the generation of a coherent radiation mechanism."

"If this basic picture is the correct one it may be possible to find a slight, but steady, slowing down of the observed repetition frequencies."

"Also, one would then suspect that more sources exist with higher rather than lower repetition frequency, because the rotation rates of neutron stars are capable of going up

to more than 100/s, and the observed periods would seem to represent the slow end of the distribution."

This was a very short paper and the majority of the statements proved ultimately to be correct. Twelve months later Goldreich and Julian (1969) published an influential paper on the emission process. It has since been shown that the true model is more complex than originally proposed, however their explanation is still essential in understanding the pulsar emission mechanism.

Within a magnetised sphere that is rotating there will be an induced electric field. This electric force acts on the charged particles on the surface of the pulsar and since this force is many orders of magnitude greater than gravity, these particles are pulled from the surface. This leads to a plasma surrounding the neutron star and is called the magnetosphere (Lorimer and Kramer 2004).

This plasma co-rotates with the neutron star out to a point where it reaches the speed of light. This is called the *light cylinder* and the distance from the centre of the neutron star to the light cylinder ($R_{\rm LC}$) is given by:

$$R_{\rm LC} = \frac{cP}{2\pi} \approx 4.77 \times 10^4 \times P \text{ km} \tag{2.1}$$

where P is the period of the pulsar in seconds and c is the speed of light. For Vela (using 2016 data), $R_{\rm LC} = 4262.1$ km and grows on average by 190 m y^{-1} and shrinks 140 m on each major glitch (see Section 3.1.2 on page 33).

Magnetic field lines that meet within the light cylinder are called *closed field lines* and those that do not meet within the light cylinder are called *open field lines*. The area where these open field lines leave the surface of the neutron star defines the *polar cap*.

Radio emission along these open field lines due to curvature radiation is stronger when the radius of curvature is at its smallest (Komesaroff 1970). This means at the last open field line, radiation is at its strongest, and emission vanishes along the magnetic axis. This is known as the *hollow cone* model. Figure 2.1 on page 6 is a reproduction from Komesaroff (1970) showing how curvature radiation is emitted under this model.

As of this writing there are currently 2613 pulsars in the Australia Telescope National Facility's Pulsar Catalogue (Manchester et al. 2005), providing a cross-section of the wide variety of known pulsars at different states and ages.

One of the key "signatures" of an individual pulsar is its *pulse profile*. This describes the flux density vs time of the pulsar beam as it sweeps across the observer. The pulse

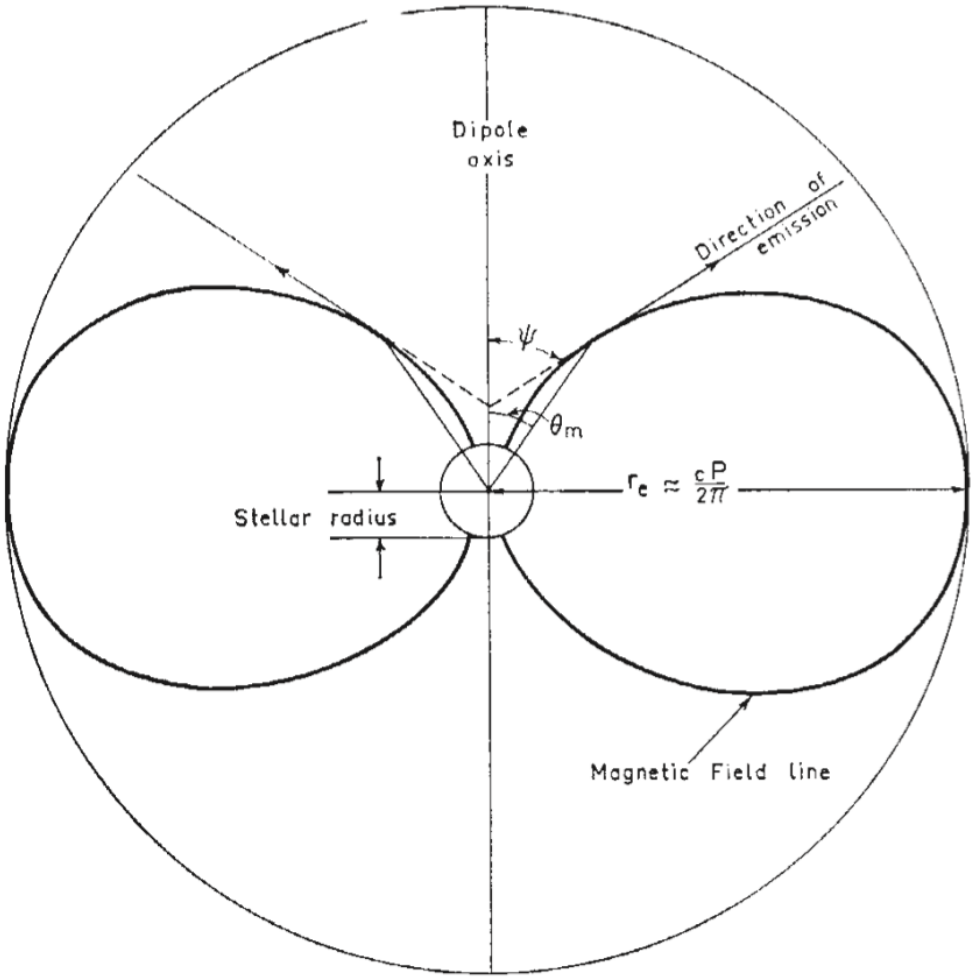

Figure 2.1: View of a pulsar down onto the rotational axis showing the light cylinder as a circle and the direction of emission of radiation. This is taken from Komesaroff (1970).

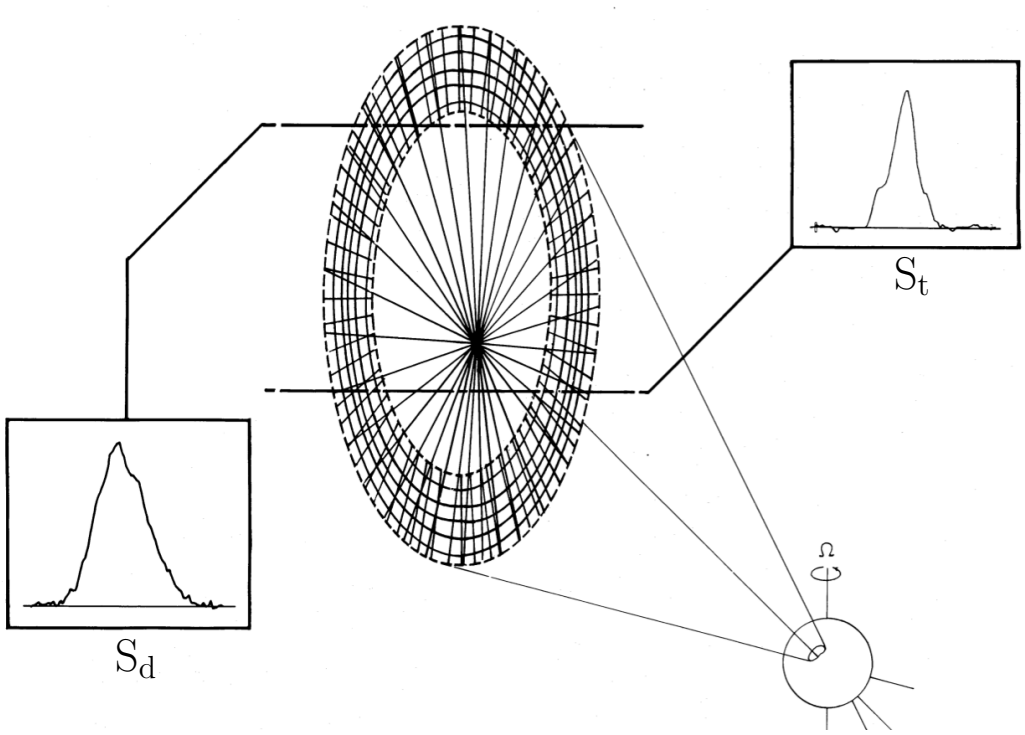

Figure 2.2: Profiles of type *core-single* (S_t) and *conal-single* (S_d). Reproduction of Figure 21b from Rankin (1983b).

profiles of the pulsar population are many and varied and can help provide information on the pulsar itself.

However, *individual* pulse profiles either vary greatly from pulse to pulse or are not even detectable, therefore the *integrated* pulse profile is most commonly used for analysis.

The *Toward an Empirical Theory of Pulsar Emission* series of publications by Rankin (1983a,b, 1986, 1990); Radhakrishnan and Rankin (1990); Rankin (1993); Rankin and Ramachandran (2003); Mitra and Rankin (2002); Rankin and Ramachandran (2003); Mitra and Rankin (2011); Basu et al. (2015); Rankin (2015) provides a foundation for pulsar emission theory, including morphological taxonomy of pulsars based on their integrated pulse profiles, which assists in the analysis of their emission. Table 2.1 on page 8 is a table of pulsar morphological taxonomy with the description duplicated verbatim from the summaries in Rankin (1983b).

The hollow cone model was modified by Michel (1987) (and covered more in depth in Michel (1991)) who suggested that *fan beams* from different emission zones could explain the bifurcated components in the profile that the hollow cone model could not explain. Recently Dyks (2017) proposed that observed profiles that change at different frequencies (ν) can be explained by a rotating spiral of emission. Figure 2.4 on page 10 is a reproduction of Figure 2 from their paper along with their description. This model explains bifurcated components and the idea of a spiral at the magnetic pole is not

Table 2.1: Morphological taxonomy of pulsar integrated profiles. The text in the column *Description* is a verbatim reproduction of the summaries in Rankin (1983b).

Code	Type	Description
S_t	Core-single	"Profiles are dominated by central beam emission. They exhibit widths (HWHM) of typically $\lesssim 10^\circ$ which tend to broaden more shallowly at low frequency than $f^{-0.25}$. At high frequency, they evolve toward formal triplicity by adding adjacent conal outriders. At even higher frequencies, these conal components can come to dominate the profile entirely, imposing a well-resolved double form of profile."
S_d	Conal-single	"Profiles represent a highly non-central trajectory across a hollow-conical emission beam. Core radiation does not manifest itself as a distinct distinguishable component, but it can be diffusely present. The profile width increases as about $f^{\sim -0.25}$ and evolves toward a well-resolved double profile at low frequency."
D	Double	"Profiles are characterised by prominent conal components and broad, low amplitude, core emission in the "bridge" region between them. Vestigial core emission tends to become weaker at high frequency; at low frequency, the conal components separate as $f^{\sim -0.25}$, and the core emission may resolve itself into a separate component, thus tending toward triplicity."
T	Triple	"Profiles entail a discernible core component flanked by conal outriders. In some cases the core component is asymmetrically placed and can merge with, or even be coincident with, one of the outriders. Triple profiles seem to occur in "wide", well resolved, and "narrow", poorly resolved classes, and evolve towards double and core-single profiles at high and low frequencies respectively. The conal components separate as $f^{\sim -0.25}$."
M	Multiple	"Profiles prototypically exhibit five components and thus clearly involve both a core component and distinct inner and outer conal emission zones. The core emission can be more or less prominent but is seemingly always present, possibly owing to highly central line-of-sight trajectories. The profiles tend to evolve to wide triples (separating as $f^{\sim -0.25}$) and probably ultimately to core-single profiles at very low frequency."

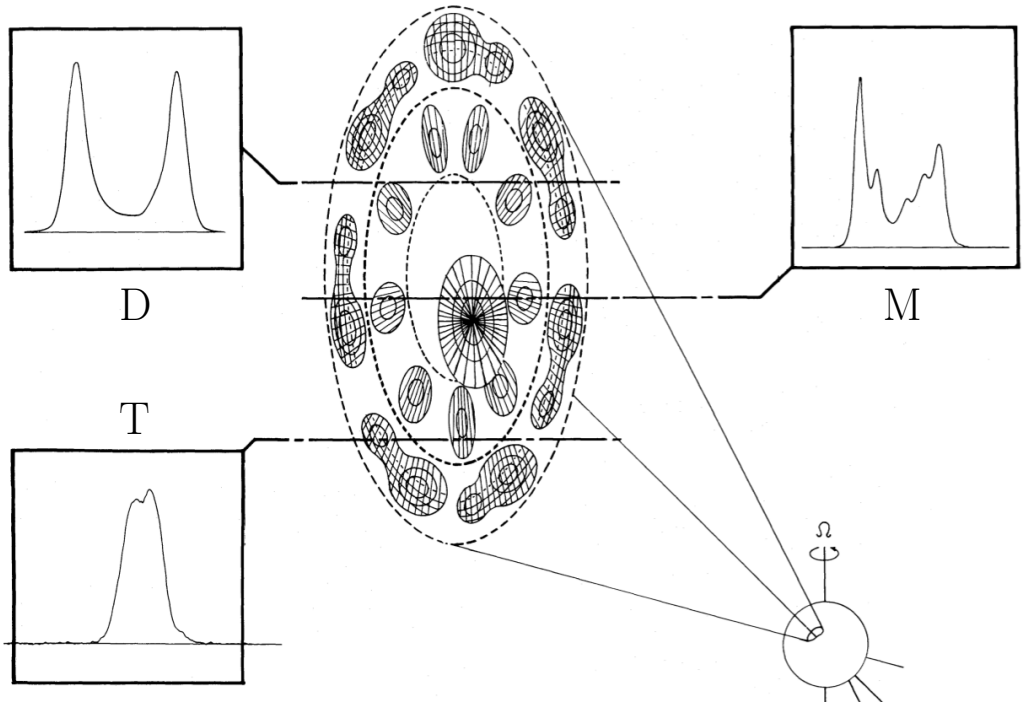

Figure 2.3: Profiles of type Double (D), Multiple (M), and Triple (T). Reproduction of Figure 21a from Rankin (1983b).

unreasonable.

The "patchy beam" model (Lyne and Manchester 1988) is an alternative model that states "the emission within the beam boundary is often patchy and that the distribution of component locations within the beam is essentially random".

2.2.1 Drifting, nulling, mode changing, and switching

Whether it be individual pulse profiles or integrated pulse profiles, four different key types of changes in profile have been reported:

1. *Drifting subpulses.* First discovered by Drake and Craft (1968), drifting subpulses are a phenomenon where successive single pulses "walk" in phase over time. Figure 2.5 on page 12 is a reproduction from Deshpande and Rankin (1999) and shows this occurring in J0946+0951. Drifting subpulses are thought to be a rotating carousel of sub-beams moving through the line-of-sight to the earth.

2. *Mode changing.* Noted by Backer (1970a), mode changing is where an integrated pulse profile changes between two (or even more) distinct shapes.

3. *Nulling.* Also first noted by Backer (1970b), nulling is a phenomenon where pulses vanish for a number of pulse periods.

4. *Intermittent or switching.* This class of pulsar is similar to nulling pulsars and

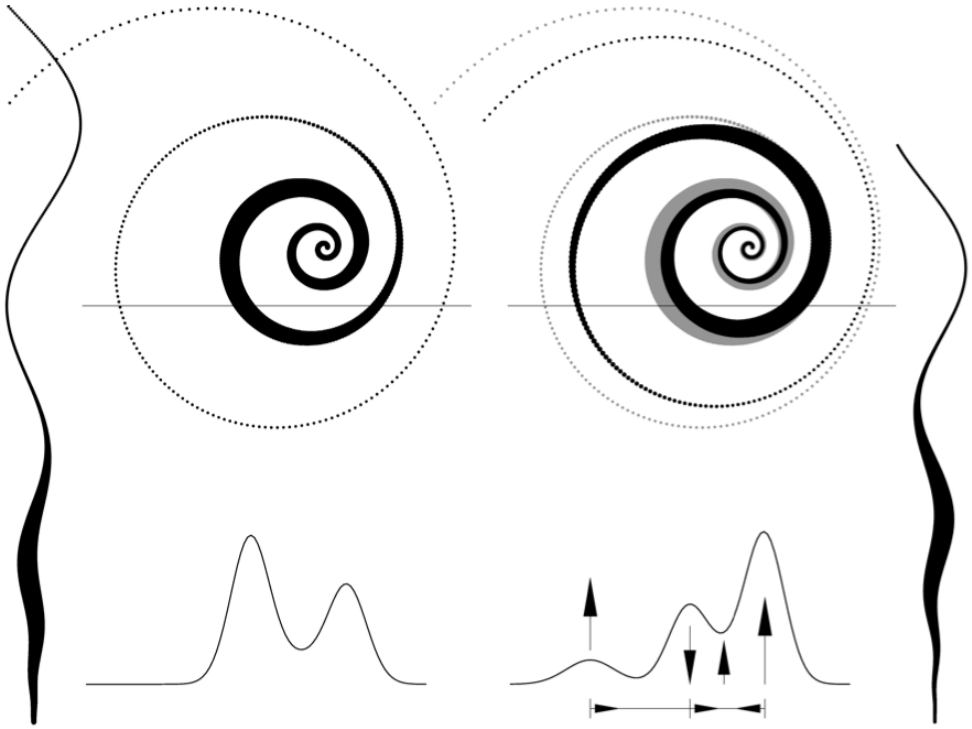

Figure 2.4: "A spiral radio pulsar beam viewed head on at two different frequencies (the left low-ν spiral is plotted on the right in grey for reference). Side views of the associated emission region are shown near the left and right edge of the figure. The local radio emissivity along each spiral is marked by line thickness, and reaches maximum at the altitude of 3% (left) and 4% (right) of the light cylinder radius. The thick parts of the spirals are therefore misaligned in azimuth. The horizontal straight sections mark the path of the sightline through the beams, and result in the profile differences shown below. Note the seemingly random change of the profile with ν. The origin of each spiral is dislocated rightwards, because of the aberration-retardation effects, which in the presented case are smaller at higher ν despite the higher locus of the average high-ν region." Figure and text from Dyks (2017).

is of special interest to this work. First noted by Kramer et al. (2006) when observing J1933+2421 which behaved like a typical pulsar and then suddenly (in < 10 s) switched off for 25-35 days (rather than just a short sequence which the nulling pulsars do). During the "on" phase, the slow-down in rotation was 50% faster than when in the "off" phase. Jones (2012) and Young et al. (2013) are further studies of this interesting group of pulsars. Naidu et al. (2018) is a recent paper discussing a pulsar that shows both nulling and intermittent characteristics.

It is thought that these types of phenomena are linked, as they mainly appear in older pulsars, and sometimes together.

Vela, the main topic of this work, is classified as *core-single* (S_t) and these types of pulsars are *not* known to null (or switch), mode-change, or have drifting sub-pulses.

2.2.2 Bright and giant pulses

Initially it was thought that Vela's flux density was very steady (Radhakrishnan et al. 1969), but a few months later (Cooke 1969) noted that Vela's flux density was "extremely variable". These two papers were not contradicting each other, they had first detected the temporal changes in Vela's pulse flux density characteristics which is a major focus of this work.

There are typically two ways of measuring a pulsar's flux density. *Peak flux density* is simply the highest level that a pulse reaches in a pulse period, and *mean flux density* is the "area under the curve" or *fluence* over the entire pulse window.

The unit of flux density used in pulsar astrophysics is the Jansky (Jy) where:

$$1 \text{ Jy} = 10^{-26} \frac{W}{\text{m}^2 \times \text{Hz}} \tag{2.2}$$

The mean flux density for Vela is 1.1 Jy (Manchester et al. 2005) and the peak flux density is ≈ 60 Jy. The large difference is because the mean flux density is taken over the *entire* pulse period, not just the on-pulse profile.

Giant pulses are ones which have a mean flux density which is greater than 10 times the average pulse's mean flux density. Since Vela is not considered to emit giant pulses but rather *micro-giants* (Johnston et al. 2001) we use the term *bright* pulses for pulses that have a mean flux density which is greater than 5 times the average pulse (Palfreyman et al. 2011).

Note that accurate flux density calibration for a radio telescope is a time consuming process, especially for large numbers of observations. In this work, many flux

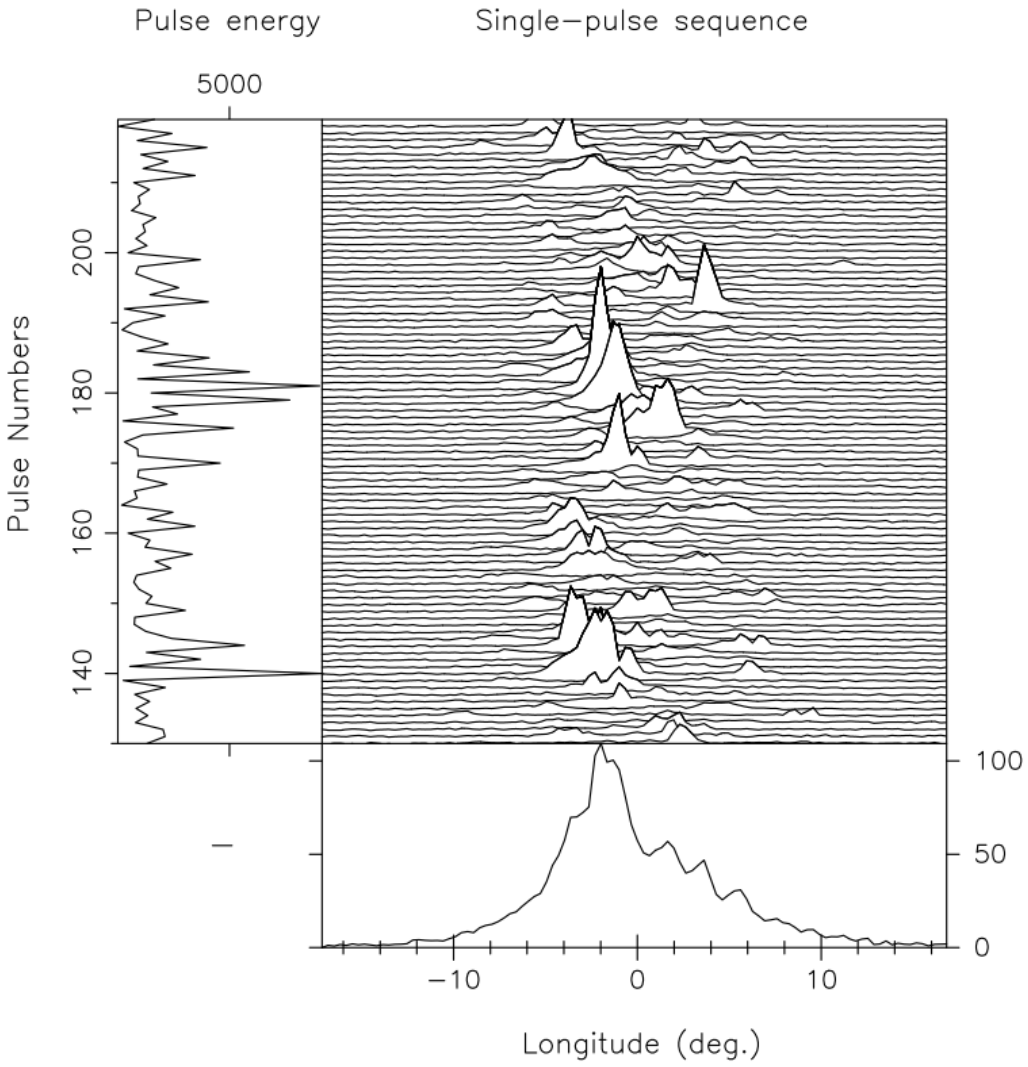

Figure 2.5: Drifting sub-pulses from J0946+0951. The X-axis is pulse longitude, the Y-axis is time (running upwards), and the Z-axis of the major panel is pulse flux density. The left panel shows the total pulse energy for the entire pulse, and the bottom panel shows the integrated pulse. Note how the individual pulse peaks drift in longitude. Figure reproduced from Deshpande and Rankin (1999).

density measurements are presented in *arbitrary* units. These arbitrary units have been calibrated at various points in time, and at 1376 MHz we typically have 1 arbitrary unit $\approx$ 45 Jy.

2.3 Rotation and age

2.3.1 Characteristic age

The P-$\dot{P}$ diagram is an important plot that shows where each pulsar is in its lifetime. It is shown in Figure 2.6 on page 14. It's a plot of the relationship of period (P) versus period derivative ($\dot{P}$), and pulsars tend to form in two major groups: "normal" pulsars and millisecond pulsars. Millisecond pulsars are formed by matter from a companion star accreting onto the pulsar which increases the rotational frequency ν. This high angular rotation rate ($\nu \gtrsim 100$ Hz) forms an extremely stable timing system with accuracies that can rival atomic clocks.

In the normal pulsar case we have that the pulsar spin frequency ν, and frequency derivative $\dot{\nu}$ satisfy the differential equation:

$$\begin{aligned} \dot{\nu} &\propto -\nu^n \\ \dot{\nu} &= -K\nu^n \end{aligned} \tag{2.3}$$

where K is a constant, and the *braking index* $n = 3$ would assume that all loss of rotation energy is due to magnetic dipole radiation. Using period P, so $\nu = \frac{1}{P}$, and taking the derivative we get:

$$\begin{aligned} \nu &= \frac{1}{P} \\ \dot{\nu} &= -\frac{\dot{P}}{P^2} \end{aligned}$$

and substituting into Equation 2.3 (with n not explicitly defined) results in:

$$\begin{aligned} -\frac{\dot{P}}{P^2} &= -K\left(\frac{1}{P}\right)^n \\ \dot{P} &= KP^{2-n} \\ P^{n-2}\dot{P} &= K \end{aligned} \tag{2.4}$$

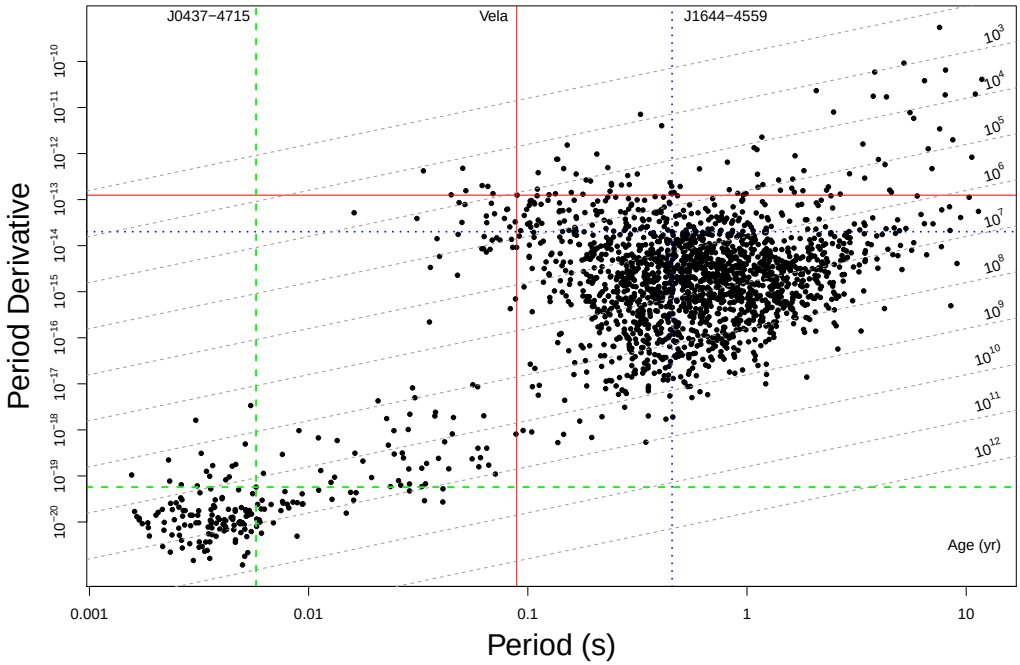

Figure 2.6: The P-$\dot{P}$ diagram of all known pulsars. Vela is shown with solid red lines, J1644−4559 with dotted blue lines, and J0437−4715 with the dashed green lines. The characteristic age τ_c is shown with dotted grey lines. Raw data for this plot was extracted from PSRCAT (Manchester et al. 2005).

Integrating with respect to time:

$$\int P^{n-2}\frac{dP}{dt}dt = \int K dt$$
$$\int P^{n-2}dP = \int K dt$$
$$\frac{P^{n-1}}{n-1} = Kt + C$$

Assuming we have period P_0 at time t=0, we get:

$$\frac{P^{n-1}}{n-1} = Kt + \frac{P_0^{n-1}}{n-1}$$
$$t = \frac{P^{n-1} - P_0^{n-1}}{(n-1)K}$$

Using K from Equation 2.4 on page 13:

$$
\begin{aligned}
K &= P^{n-2}\dot{P} \\
t &= \frac{P^{n-1} - P_0^{n-1}}{(n-1)P^{n-2}\dot{P}} \\
t &= \frac{P^{n-1}}{(n-1)P^{n-2}\dot{P}} - \frac{P_0^{n-1}}{(n-1)P^{n-2}\dot{P}} \\
t &= \frac{P}{(n-1)\dot{P}} - \frac{PP_0^{n-1}}{(n-1)\dot{P}P^{n-1}} \\
t &= \frac{P}{(n-1)\dot{P}}\left(1 - \left(\frac{P_0}{P}\right)^{n-1}\right)
\end{aligned} \tag{2.5}
$$

Assuming that $P_0 \ll P$ and n=3 we get the characteristic age :

$$\tau_c = \frac{P}{2\dot{P}} \tag{2.6}$$

which are shown as the grey dotted lines in the $P - \dot{P}$ diagram in Figure 2.6 on page 14.

The characteristic age may not line up with the actual age of a pulsar. The assumptions above that $P_0 \ll P$ and n=3 may not actually be correct in many cases. However τ_c is a useful figure for comparisons and is usually the only age estimate we actually have available.

For the Vela pulsar we have:

$$
\begin{aligned}
\tau_c &= \frac{0.089327}{2 \times 1.26933 \times 10^{-13}} \text{ s} \\
&= 3.518665 \times 10^{11} \text{ s} \\
&= 11150 \text{ y}
\end{aligned}
$$

Rather than assuming the effect of P_0 in Equation 2.5 is negligible, we can provide a better estimation by assuming P_0 is a value similar to other young (non-accreting) pulsars with a known age. Rearranging Equation 2.5 with $n = 3$, we get:

$$
\begin{aligned}
t &= \frac{P}{2\dot{P}}\left(1 - \left(\frac{P_0}{P}\right)^2\right) \\
t &= \frac{P}{2\dot{P}} - \frac{P_0^2}{2P\dot{P}} \\
t &= \frac{P^2 - P_0^2}{2P\dot{P}} \\
2P\dot{P}t &= P^2 - P_0^2 \\
P_0 &= \sqrt{P^2 - 2P\dot{P}t}
\end{aligned} \tag{2.7}
$$

Using the well documented supernova explosion of 1054 that formed the Crab pulsar (J0534+2200) as a benchmark, at MJD=40000, $P = 0.03308471603$, $\dot{P} = 4.22765 \times 10^{-13}$, and $t = 2.8844 \times 10^{10}$ s, we get $P_0 = 17$ ms or $\nu = 58.8$ Hz.

Using this derived figure of P_0 in Equation 2.5 on page 15 we get an age estimate of the Vela pulsar as $t = 10746$ y, which is ≈ 400 y younger than the characteristic age $\tau_c = 11150$ y.

Lyne et al. (1996) have assumed that $n = 3$ is not necessarily valid and have shown that Vela has a current braking index of $n = 1.4 \pm 0.2$. Figure 2.7 on page 17 shows a plot of of the Vela pulsar's characteristic age against braking index using Equation 2.5 on page 15, with $P_0 = 17$ ms, and Vela's current P and $\dot{P}$. As can be seen, the range of τ_c is many tens of thousands of years with regard to braking index n.

Johnston and Karastergiou (2017) as well as Tong and Kou (2017) challenge the view that n is invariant over time. We have expanded on this in Section 8.7.4 on page 242.

2.3.2 Energy loss

The theoretical energy loss rate of a pulsar can be estimated from the rate of change of rotational frequency. Starting with basic physics of a rotating object where I is the moment of inertia and Ω is the angular frequency we have rotational kinetic energy given by:

$$E_{\text{ROT}} = \frac{1}{2} I \Omega^2 \tag{2.8}$$

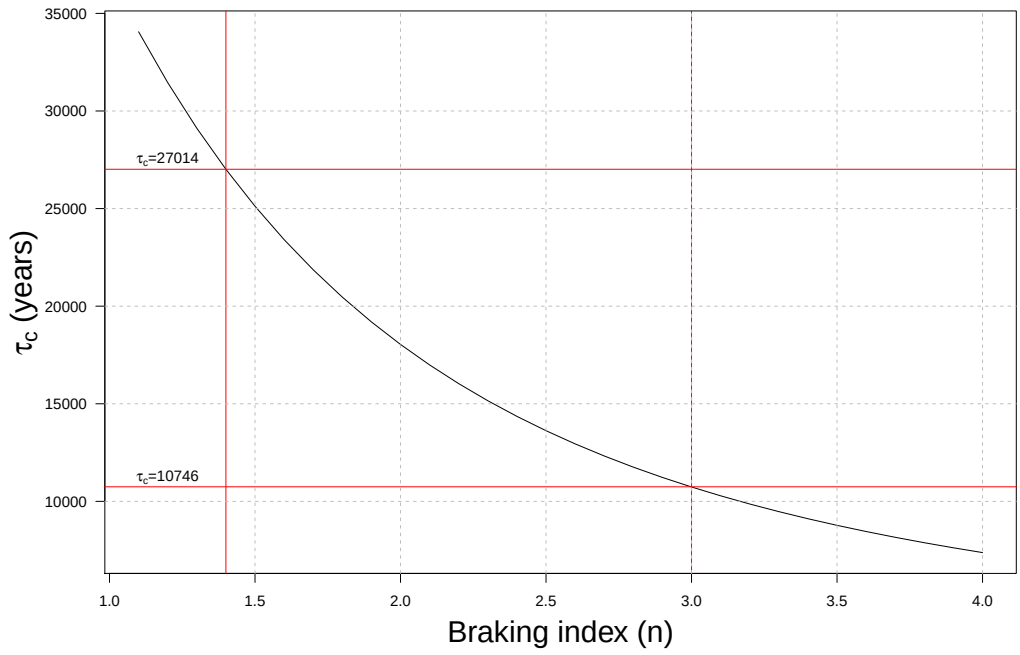

Figure 2.7: A plot of characteristic age (τ_c) vs braking index (n) of Vela using Equation 2.5 on page 15. The following have been set: $P_0 = 17$ ms, $P = 89.3$ ms, and $\dot{P} = 1.27 \times 10^{-13}$ s s^{-1}. The vertical red lines mark the potential range of n and how this affects the potential range of τ_c.

The energy loss rate is the first derivative of E_{ROT}:

$$\begin{aligned} \dot{E} &= \frac{d}{dt} E_{\mathrm{ROT}} \\ &= \frac{d}{dt}\left(\frac{1}{2} I\Omega^2\right) \\ &= -I\Omega\dot{\Omega} \\ &= -4\pi^2 I\nu\dot{\nu} \end{aligned} \tag{2.9}$$

when we substitute rotational frequency (ν) for angular frequency (Ω) using $\Omega = 2\pi\nu$.

Classical physics says that the moment of inertia I for a sphere of uniform density with mass M and radius R is:

$$I = \frac{2}{5} MR^2 \tag{2.10}$$

Using $M = 1.4M_\odot = 1.4 \times 1.989 \times 10^{30}$ kg and $R = 10^4$ m, we get $I = 1.11 \times 10^{38}$ kg m^2. However a canonical value of $I = 10^{38}$ kg m^2 $= 10^{45}$ g cm^2 is typically used (Lorimer and Kramer 2004, page 58).

Note that this assumes I is invariant with time - which is almost certainly not the case with a neutron star. Substituting the canonical I and Vela figures for ν and $\dot{\nu}$ into Equation 2.9 on page 17 we get an energy loss rate of:

$$\begin{aligned}\dot{E} &\approx -4\pi^2 \times 10^{38} \times 11.2 \times -1.56 \times 10^{-11} \\ &= 6.89 \times 10^{29} \text{ J s}^{-1}\end{aligned} \tag{2.11}$$

In comparison, this energy loss rate of 6.89×10^{29} J s^{-1}($= 6.89 \times 10^{36}$ erg s^{-1}) is ≈ 1800 L$_\odot$.

2.4 Interstellar medium

As electromagnetic radiation travels through the interstellar medium (ISM), arrival times of pulses are delayed by intervening free electrons. The lower the frequency, the longer the delay, given by:

$$\Delta t = \frac{e^2}{2\pi mcf^2} \int_0^d n_e \mathrm{d}l \tag{2.12}$$

where e and m are the charge and mass of an electron respectively, c is the velocity of light, f is the frequency of observation, and the density of particles along the line of sight:

$$\mathrm{DM} = \int_0^d n_e \mathrm{d}l \tag{2.13}$$

is called the *dispersion measure*, with n_e being the number of electrons between the observer and the pulsar (from $0 \rightarrow d$, the pulsar distance). Substituting appropriate values into Equation 2.12, the delay of a pulse (in ms) between two frequencies (in MHz) is:

$$\Delta t \approx 4.15 \times 10^6 \ \times \left(\frac{1}{f_1^2} - \frac{1}{f_2^2} \right) \times \mathrm{DM} \tag{2.14}$$

By observing pulsar arrival times at different frequencies (even within the bandwidth of a single receiver), Equation 2.14 can be rearranged to estimate the dispersion measure of a pulsar.

Cordes and Lazio (2002) in a pre-eminent study modelled the free electron density of

the galactic surroundings, but Yao et al. (2017) recently improved this model taking into account 189 pulsars and recent fits of galactic HII regions, the galactic disk, the Gum nebula, Galactic Loop I, and the Local Bubble.

These studies enable dispersion measure measurements to approximately relate to actual distances. These distances are not necessarily correct, but are a good estimation when no other method of distance measurement is available.

The interstellar medium also diffracts the point source of the pulsar and causes scintillation effects as the Earth moves through the solar system and the pulsar moves through the galaxy. This is a large topic on its own and will not be covered further in this work.

2.5 Arrival times

2.5.1 Solar system barycentre

At a frequency of 1376 MHz, the time of arrival of a bright single pulse from the Vela pulsar at the observatory at Mt Pleasant is typically measured to an accuracy of ≈ 10 μs. Integrated pulses over 10 s can be determined to an accuracy of ≈ 2 μs, and integrated over 19 hours, to an accuracy of ≈ 300 ns. Note that this is different from the RMS of the arrival times which is, for example, typically ≈ 50 μs for the 10 s integration.

Lorimer and Kramer (2004) state that $\sigma_{TOA} \propto 1/\sqrt{N_{\text{pulses}}}$, however this is only part of the TOA uncertainty. The main other factors are the interstellar medium, spin noise, polarisation calibration errors, and timing model errors. Frequency dependence on the pulse shape is also important, but not relevant to these results as the frequency was fixed throughout.

To make use of this accuracy at different times and at different observatories, all arrival times need to be shifted to the barycentre of the solar system for useful comparison. This transformation needs to take into account the precise location of the observatory, the centre of the Earth, and the current rotational position of the Earth.

Also, objects in the solar system (mainly the Sun and Jupiter) curve spacetime and affect the arrival time of the pulse - this is known as *Shapiro delay*. A lesser effect (but important for high-precision timing) is the *Einstein delay* which dilates time due to gravitational redshift and is caused by the motion of solar system bodies.

TEMPO2 (see Section 4.4.5 on page 57) accounts for all of these factors when calculating pulse arrival times.

2.5.2 Timing noise

A pulsar would be rotating at a frequency ν and slowing down with a frequency first derivative $\dot{\nu}$, with all further derivatives ($\ddot{\nu}, \dddot{\nu}, \ldots$) being possibly non zero. In reality, the timing model for Vela only includes ν and $\dot{\nu}$, with $\ddot{\nu}$ being fixed. For Vela, $\ddot{\nu}$ has been estimated by Lyne et al. (1996) and this is discussed in Section 8.7.3 on page 240.

If the timing model is ideal then it would be expected that the timing residuals would be Gaussian noise. This is not what typically occurs. Long-term timing, especially of young pulsars like Vela, show long period undulations when only basic timing models using ν and $\dot{\nu}$ (and a fixed $\ddot{\nu}$) are used. This is called red noise.

2.5.2.1 Polynomial fits and timing artefacts

When modelling the arrival times of pulses from a pulsar, it is typical to include rotation frequency (ν) and a rate of change in frequency ($\dot{\nu}$) in the model - this is due to neutron stars slowing down because they are emitting radiation. In the case where $\dot{\nu}$ is changing, $\ddot{\nu}$ can also be modelled. As many frequency derivatives as desired can be included and we get the well known Taylor series expanded about some point a:

$$f(x) = f(a) + f'(a)(x-a) + \frac{f''(a)}{2!}(x-a)^2 + \frac{f^{(3)}(a)}{3!}(x-a)^3 + \cdots + \frac{f^{(n)}(a)}{n!}(x-a)^n + \cdots \tag{2.15}$$

Substituting pulsar notation for some reference epoch t_0 we get:

$$\nu(t) = \nu_0 + \dot{\nu}_0(t-t_0) + \frac{\ddot{\nu}_0}{2!}(t-t_0)^2 + \frac{\dddot{\nu}_0}{3!}(t-t_0)^3 + \cdots \tag{2.16}$$

where $\nu_0 = \nu(t_0)$, $\dot{\nu}_0 = \dot{\nu}(t_0)$ and so on.

Whilst in principle this appears sound and in fact this is the de facto standard method of modelling arrival times, it does have some issues.

Consider the function $y = e^x$ and a least-squares fit to that function using a degree 4 polynomial:

$$y = 870.53 - 2284.30x + 1337.47x^2 - 269.82x^3 + 17.81x^4 \tag{2.17}$$

and a degree 10 polynomial:

$$\begin{aligned} y = 1.76067304 - 8.41345323x + 29.62596538x^2 - 38.58070636x^3 \\ +27.45113657x^4 - 11.43350072x^5 + 2.96681904x^6 - 0.48383465x^7 \\ +0.04866477x^8 - 0.00276827x^9 + 0.00006999x^{10} \end{aligned} \tag{2.18}$$

These along with residuals are shown in Figure 2.8 on page 23. Note that whilst there is a drastic improvement in fit, there are still characteristic x^5 and x^{11} shapes appearing in the residuals.

When observing timing residuals in real pulsar data, such observed shapes must not be confused with cycles that are not actually present. According to the Lomb-Scargle Periodogram (see Section 4.6.2 on page 69), the degree 10 residual shown in Figure 2.8 on page 23 has a period of 2.38 - which is of course non-existent in the original $y = e^x$ curve.

Consider now a function with a genuine cycle: $y = 100\sin(x)$. Fitting a degree 4 polynomial:

$$y = -24.800 + 227.569x - 127.580x^2 + 21.657x^3 - 1.128x^4 \tag{2.19}$$

and a degree 10 polynomial:

$$\begin{aligned} y = -0.01473268 + 100.07686197x - 0.18066417x^2 - 17.62324474x^3 \\ +1.33940212x^4 - 0.09493381x^5 + 0.37082564x^6 - 0.10969840x^7 \\ +0.01301768x^8 - 0.00071429x^9 + 0.00001513x^{10} \end{aligned} \tag{2.20}$$

These are shown in Figure 2.9 on page 24. Again the cycles appear in the degree 10 residual, with an apparent period of 2.32 - and totally unrelated to the genuine period of $2\pi \approx 6.28$.

In summary, it is important to note that any long-period cycles or *red noise* in timing residuals do not necessarily imply any undiscovered circular motion.

Fitting high degree polynomials does have one advantage - it visually highlights micro-

glitches (see Section 3.1.2 on page 33) in the data. Figure 2.10 on page 25 shows the curve $y = 100\sin(x)$, but at X=6 and onwards an identical function has been used which has been translated to the left by 0.002 and down by an appropriate amount so the curves are continuous. The plot on the left shows that this small change cannot be seen, but the residuals from the degree 10 polynomial fit highlight the discontinuity in gradient clearly. We use this technique in Section 7.1 on page 150.

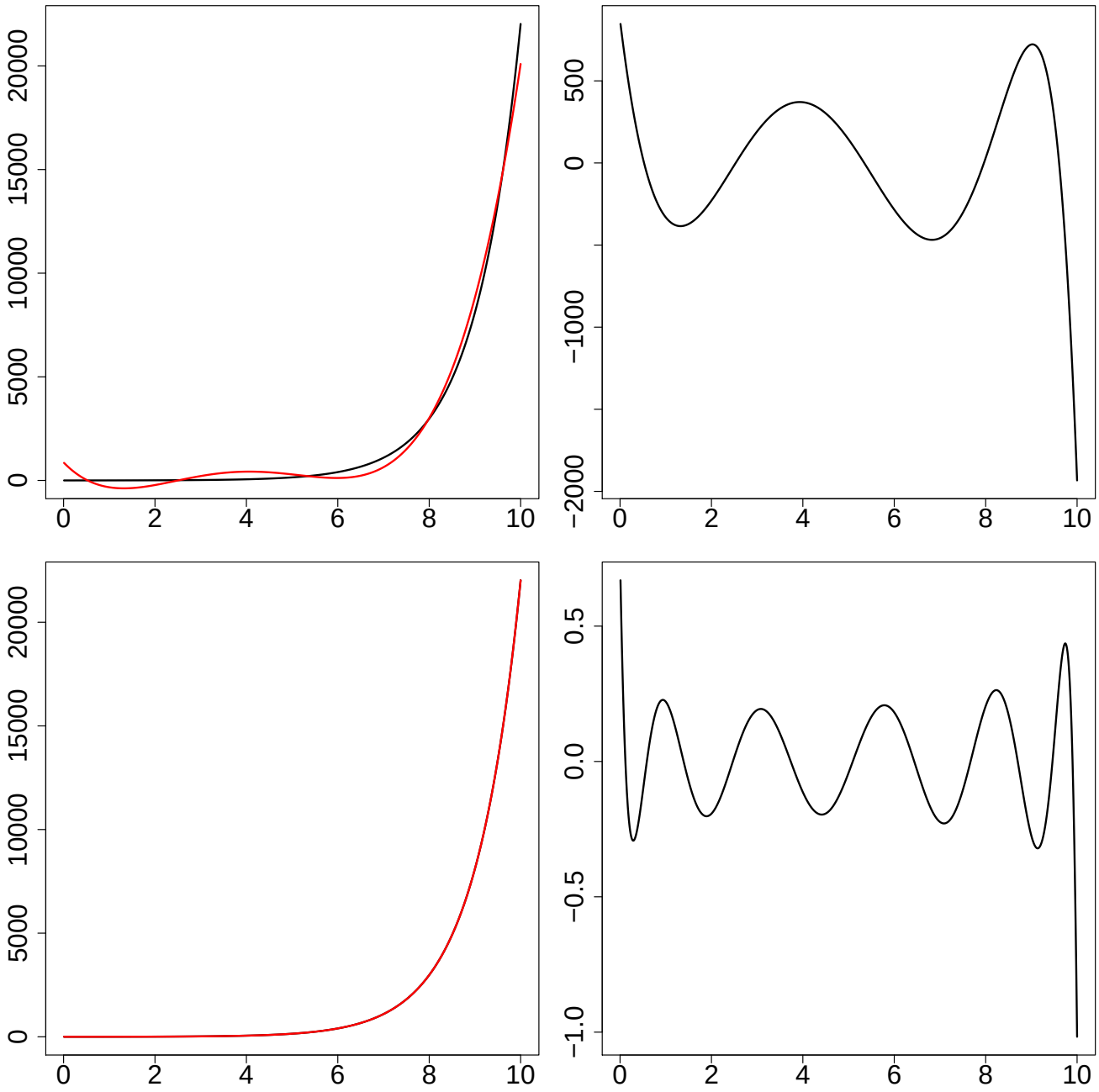

Figure 2.8: This highlights the potential issues of fitting polynomials by using a simple function as an example. The top left panel shows $y = e^x$ (black) and a least-squares fit polynomial of degree 4 (red). The top right panel shows the residuals and appears as a degree 5 polynomial. The bottom left panel again shows $y = e^x$ but fitted with a degree 10 polynomial. The bottom right panel again shows residuals and even though the errors are small, the characteristic shape of a degree 11 polynomial appears.

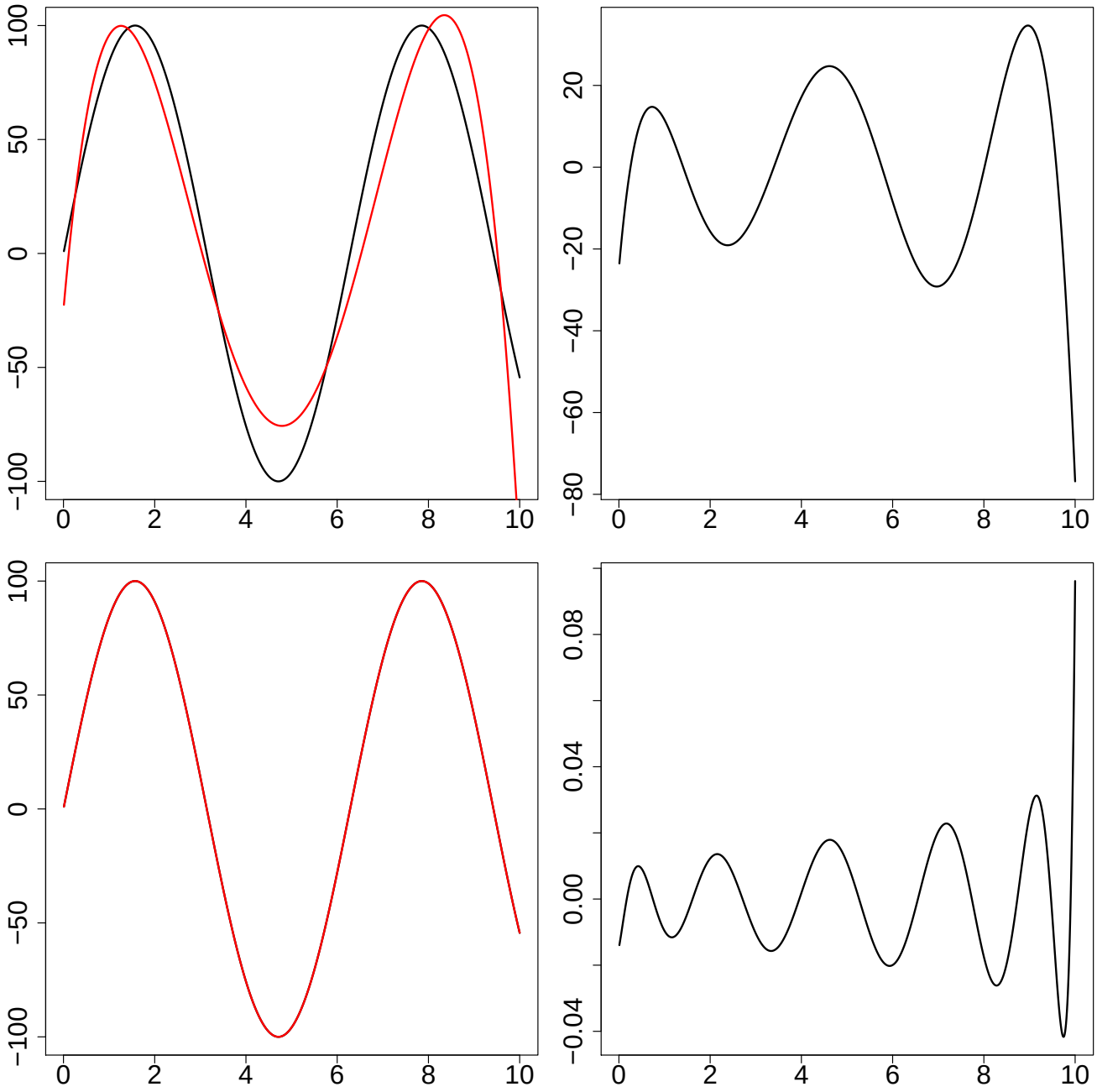

Figure 2.9: This highlights the potential issues of fitting polynomials by using a periodic function as an example. The top left panel shows $y = \sin(x)$ (black) and a least-squares fit polynomial of degree 4 (red). The top right panel shows the residuals and appears as a degree 5 polynomial. The bottom left panel again shows $y = \sin(x)$ but fitted with a degree 10 polynomial. The bottom right panel again shows residuals and even though the errors are small, the characteristic shape of a degree 11 polynomial appears.

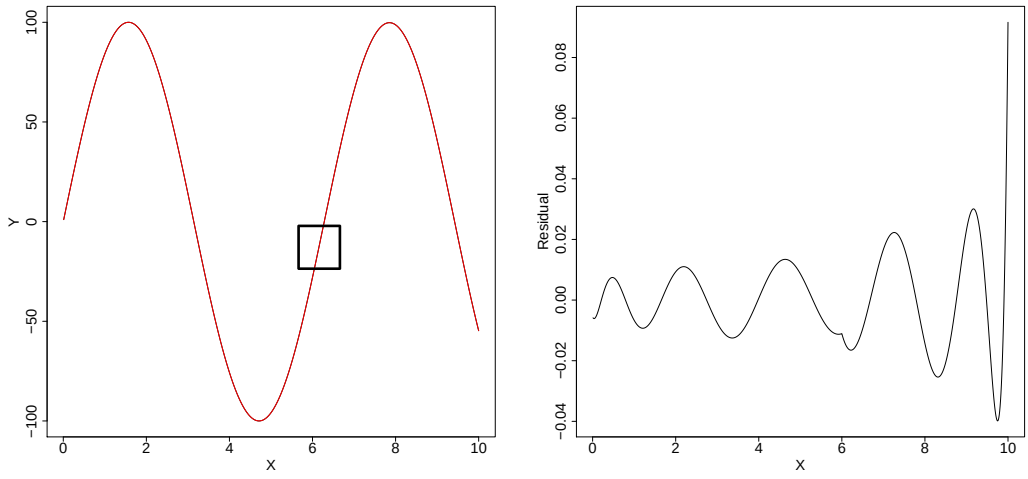

Figure 2.10: This highlights the advantage of polynomial fitting in detecting small changes. The left plot is $y = 100\sin(x)$ with a small piece of the function removed, but with a translation in X and Y to keep the function continuous. The effect is a tiny shift in gradient at X=6 which is not visible. The right plot is residuals from a degree 10 polynomial of best fit of the left plot showing how the discontinuity in gradient is highlighted.

2.6 Fast Radio Bursts

Fast Radio Bursts (FRBs) are a recently discovered phenomenon that possibly have a link with pulsars. FRBs appear in observations as a single pulse, although a single case (FRB 121102) has been known to occasionally repeat (Scholz et al. 2016). They have a high dispersion measure, implying that they are at large distances, and therefore inherently from a very bright source. One hypothesis is that "super-giant" pulses from pulsars are a possible cause (Katz 2016). Section 5.1.2 on page 83 examines this possibility using the data gathered from Vela.

2.7 Glitch theory

The sudden increase in pulsar rotation frequency (ν) is called a *glitch* and officially appears in that context in the *Oxford English Dictionary* (Stevenson 2015). The first use of the word in the scientific literature is in Rees and Trimble (1971) but Rees claims the first use of the word is not his. He does not recall where the use of the word (with regard to pulsars) came from.[§]

When glitches were first discovered (Radhakrishnan and Manchester 1969; Reichley and Downs 1969) the explanation was put down to "star quakes" caused by the hard

[§]Lord Rees, personal communication

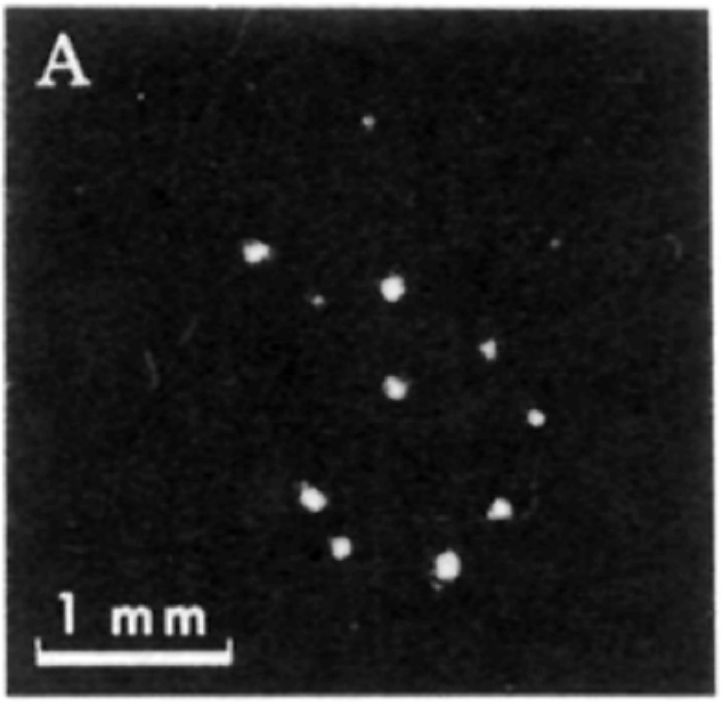

Figure 2.11: One of the first photographs of discrete quantised vortex lines in superfluid He II. They were rotating at $\omega = 0.25$ Hz, at a temperature of 75 mK, and the exposure time was 60 ms. The distinct bright spots mark the positions of the lines where they meet the free surface (Williams and Packard 1974).

outer crust trying to revert from being an oblate spheroid to a more spherical shape as the rotational frequency reduced (due to magnetic dipole radiation). These stresses would build up until the hard outer crust would "crack", reduce in radius, and due to conservation of angular momentum, would then speed up (Ruderman 1969).

This hypothesis was challenged due to the very low probability of observing glitches in both Vela and the Crab so soon after discovery (Smoluchowski 1970). This is because the "star quake" model would not have Vela glitching for orders of magnitude more years than it does.

Also, the post-glitch recovery showed an exponential decay component over a number of months, and this implied a superfluid core (Baym et al. 1969). Then Anderson and Itoh (1975) proposed catastrophic unpinning of superfluid vortices as an explanation for glitches.

The current hypotheses of the internal structure of a neutron star is highly complex. We will provide a basic overview. First, however, an understanding of rotating superfluids is required.

When superfluids are rotated, they do not behave like ordinary fluids. Instead they store their angular momentum in vortices (Zwierlein et al. 2005). Figure 2.11 shows one of the first photographs of these obtained by Williams and Packard (1974). These

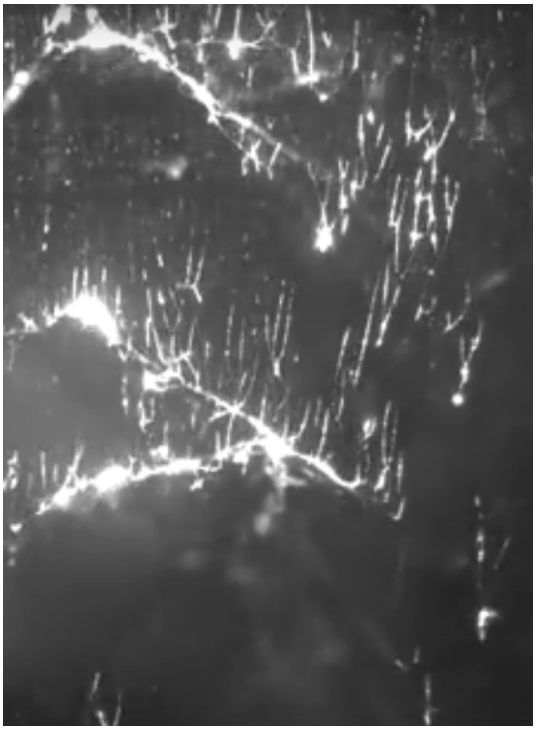

Figure 2.12: A frame from a video taken by Bewley et al. (2006) showing vortices in superfluid helium. The rotational axis is vertical and the vortices are highlighted using iced hydrogen. The temperature is only tens of mK below the phase transition at 2.712 K and the container was rotating at 2 Hz.

vortices are tiny, with a core $\approx 10^{-14}$ m across. This implies that the superfluid itself *does not rotate*, and it causes confusion to assume that superfluids behave like normal fluids in such situations. To quote Chamel and Haensel (2008):

"The confusion between velocity and momentum is very misleading and makes generalizations of the two-fluid model to multi-fluid systems (like the interior of neutron stars) unnecessarily difficult."

Bewley et al. (2006) shows a more recent view of quantised vortices as a video* and a single frame is shown in Figure 2.12.

As shown in Figure 2.13 on page 28, a neutron star has a solid crust and a core. Starting from the centre, the inner core is extremely dense and is of unknown structure. The outer core is a superfluid. The inner crust is solid but is *permeated* by the superfluid outer core. The outer crust is solid.

As the star rotates, the superfluid forms vortices which hold the superfluid's angular

*https://www.youtube.com/watch?v=I6dhnrXXXtc

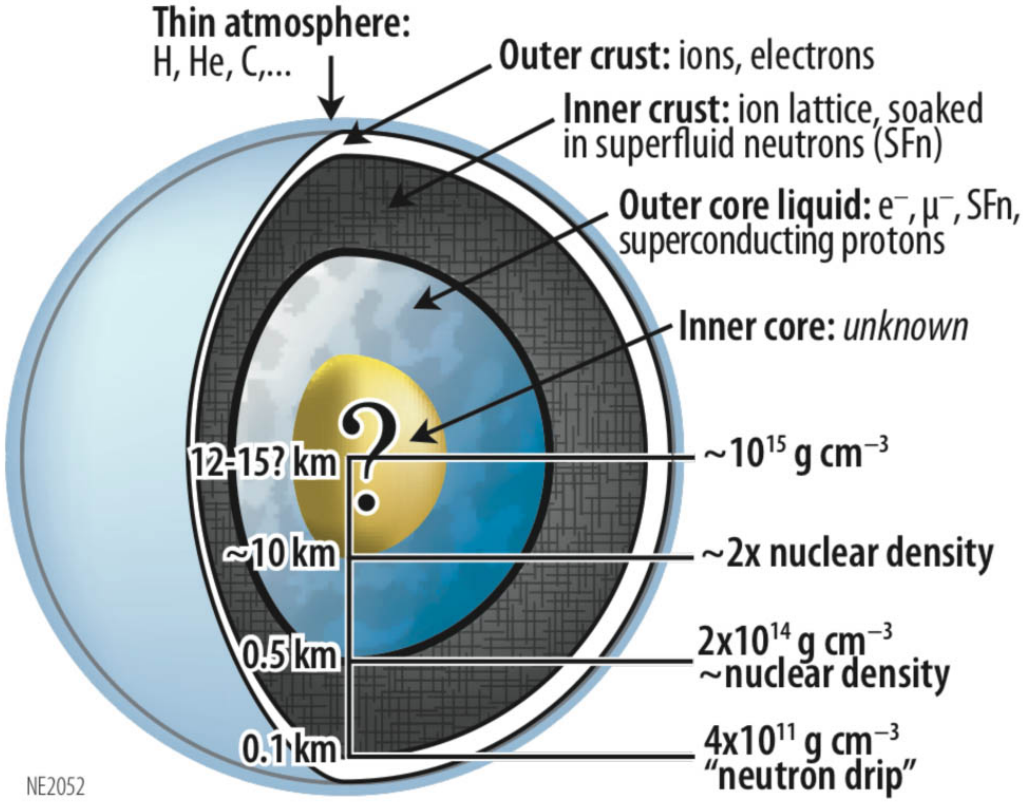

Figure 2.13: Simple diagram of neutron star interior. *Image courtesy NASA.*

momentum. In the inner crust these vortices attach or "pin" themselves to the nuclei in the lattice. In the outer core these vortices may also pin to the magnetic flux tubes that emanate from the outer crust.

The angular velocity of the outer crust is denoted by Ω^* and the angular velocity of the superfluid is denoted by Ω_n (the n is for neutrons). As the star slows down in rotation due to magnetic dipole radiation, a lag ($\Delta\Omega = \Omega_n - \Omega$) in the angular velocity between the outer crust and the *irrotational* superfluid core increases.[†]

Once the lag ($\Delta\Omega$) reaches a point where the Magnus[‡] force is greater than the pinning force, the vortices unpin from the nuclei, and angular momentum from the core to the crust is transferred. The crust increases in rotational velocity and a glitch occurs (Sourie et al. 2017).

Figure 2.14 on page 29 is a reproduction of Figure 1 from Sourie et al. (2017) which shows the change in $\Omega_{\rm n}$ and Ω over time, and as glitches occur.

As noted earlier the vortices in the outer core probably also pin to the magnetic flux

*or sometimes Ω_p - the p is for protons.

†recall that superfluids do not rotate like normal fluids because the angular momentum is stored in the vortices.

‡the force that causes a golf ball to curve through the air.

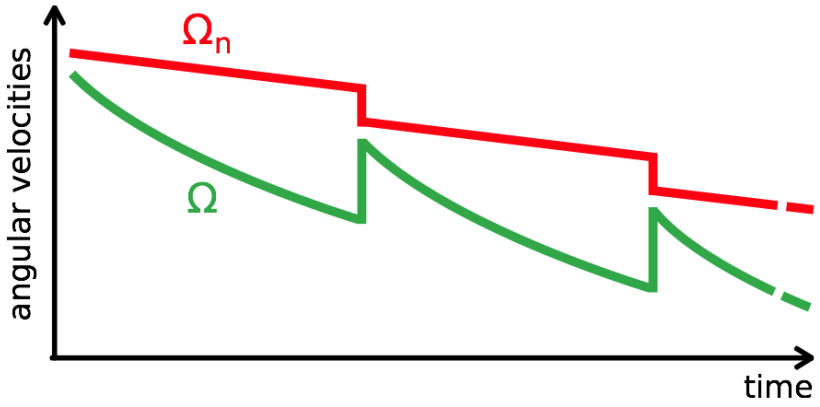

Figure 2.14: Angular velocity of the superfluid core (Ω_n) compared with the crust (Ω) as glitches occur. The X-axis is time, and the gap between glitches is approximately 3 years for Vela. Reproduced from Figure 1 of Sourie et al. (2017).

tubes from the intense (10^{12} G) magnetic field. During a glitch, whether these vortices unpin first and then catastrophically cause the vortices in the inner crust to unpin from the lattice, *or* the vortices in the inner crust alone unpin due to the Magnus force, is unknown.

Key to the understanding of this hypothesis is the glitch rise time τ_r. This is the time taken for Ω to move from the lower angular velocity to the higher when the glitch occurs. Dodson et al. (2002) from the University of Tasmania observing with the 14 m telescope have put a limit on $\tau_r < 40$ s. Accurately determining τ_r is an important step in the understanding of neutron star interiors and the equation of state.

It is worth noting here that the surface speed of the Vela pulsar (rotation frequency 11.2 s^{-1} and assume a radius of 10 km) is $2\pi \times 10000 \times 11.2 \approx 7 \times 10^5$ ms^{-1} which is $\approx 0.2\%$ of the speed of light. Some authors on neutron star glitch theory have ignored relativistic effects, whereas Sourie et al. (2017) have reached the conclusion that they are significant and need to be included.

What happens in the inner core with regards to the existence of vortices, magnetic flux tubes, and other strange matter is unknown, but still could be relevant to the results in this thesis.

Sedrakian and Cordes (1999) show that the interface between the crust and the core acts as a "*potential barrier to the peripheral neutron vortices approaching the interface*" and one of their conclusions suggests that changes in the angle of the dipole field may occur during a glitch. This may be important and is discussed in Section 8.4 on page 228.

Chapter 3

Pulsars of interest

The main topic of this thesis is, of course, the Vela pulsar, but since this is below the 26 m telescope's horizon for ≈ 5 hours each day, this time was used to observe other bright pulsars to act as controls for the Vela observations.

This chapter is a brief summary of Vela and the other pulsars regularly observed.

3.1 The Vela Pulsar - J0835−4510

The Vela pulsar is an extremely well-studied pulsar with to date over 4000 papers in the *SAO/NASA Astrophysics Data System* containing Vela's designation in the abstract or keywords. Vela is a close (0.28 kpc) and southerly placed ($\delta \approx -45°$) pulsar which is visible in the radio (Large et al. 1968), optical (Wallace et al. 1977), gamma ray (Pellizzoni et al. 2009), and X-Ray (Durant et al. 2013) bands of the electromagnetic spectrum. As a relatively young pulsar ($\tau_c = 11.3$ ky) that regularly speeds up in rotation ("glitches") it is a fascinating object for study. Table 3.1 on page 32 shows a summary of known parameters.

3.1.1 Discovery

The Vela pulsar was discovered by Large et al. (1968) using the Molongolo Radio Observatory at a frequency of 408 MHz.

The search for an optical image was initially inconclusive and there was debate about which star was actually the pulsar. Wallace et al. (1977) confirmed pulsed images at a blue magnitude of 25.1 and this was the faintest measured magnitude of a star at that time (Murdin et al. 1979). With the deployment of the Hubble Space Telescope, a massive improvement in optical imaging became available. Figure 3.1 on page 34 shows

Table 3.1: Summary of The Vela Pulsar from the ATNF Pulsar Catalogue (Manchester et al. 2005) with updated data from this work in bold. For brevity, errors are omitted.

Description	PSRCAT Parameter	Value	Units
Name (J2000)	PSRJ	J0835−4510	
Name (B1950)	PSRB	B0833−45	
Right Ascension J2000 (α)	RAJ	08:35:20.61149	h m s
Declination J2000 (δ)	DECJ	−45:10:34.8751	° ’ ”
Proper Motion ($\dot{\alpha}\cos\delta$)	PMRA	−49.68	mas y^{-1}
Proper Motion ($\dot{\delta}$)	PMDEC	29.9	mas y^{-1}
Total Proper Motion	PMTOT	57.98	mas y^{-1}
Ecliptic Longitude	ELONG	153.37	°
Ecliptic Latitude	ELAT	−60.36	°
Galactic Longitude	GL	263.55	°
Galactic Latitude	GB	−2.79	°
X in X-Y-Z Galactic Coordinates	XX	-0.28	kpc
Y in X-Y-Z Galactic Coordinates	YY	8.53	kpc
Z in X-Y-Z Galactic Coordinates	ZZ	−0.01	kpc
Epoch of Position	POSEPOCH	51544	MJD
Rotation Measure	RM	31.38	rad m^{-2}
Dispersion Measure	DM	67.99	cm^3 pc
Epoch of Dispersion Measure	DMEPOCH	51559.32	MJD
Barycentric Rotation Frequency (ν)	F0	**11.1862256**	Hz
Frequency Derivative ($\dot{\nu}$)	F1	$\mathbf{-1.56301 \times 10^{-11}}$	Hz s^{-1}
Frequency Second Derivative ($\ddot{\nu}$)	F2	3.1×10^{-23}	Hz s^{-2}
Period	P0	**89.39565814**	ms
Period Derivative	P1	$\mathbf{1.249093 \times 10^{-13}}$	s s^{-1}
Epoch of Frequency/Period	PEPOCH	**57900**	MJD
Pulse Width 50%	W50	**2.1**	ms
Pulse Width 10%	W10	**4.5**	ms
Mean Flux 400 MHz	S400	5000	mJy
Mean Flux 1400 MHz	S1400	1100	mJy
Characteristic Age (τ_c)	AGE	1.13×10^4	y
Temporal Broadening at 1 GHz	TAU_SC	4.7×10^{-5}	s
Annual Parallax	PX	3.5	mas
Number of Glitches	NGLT	**18**	
Date of Discovery	DATE	1968	y
Distance	DIST	0.28	kpc
Energy Flux at the Sun	EDOTD2	8.8×10^{37}	ergs kpc^{-2} s^{-1}
Radio Luminosity at 400 MHz	R_LUM	392.00	mJy kpc^2
Radio Luminosity at 1400 MHz	R_LUM14	86.24	mJy kpc^2
Transverse Velocity	VTRANS	76.97	km s^{-1}
Surface Magnetic Flux Density	BSURF	3.38×10^{12}	Gauss
Magnetic Field at Light Cylinder	B_LC	4.45×10^4	Gauss
Spin Down Energy Loss Rate	EDOT	6.9×10^{36}	ergs s^{-1}

four images from 1979 to 2011 with the proper motion ($\mu_{\alpha cos\delta} = -49.68 \pm 0.06, \mu_\delta = 29.9 \pm 0.1$ mas y^{-1}) being apparent. Figure 3.2 on page 35 shows Vela in X-Rays as viewed from Chandra. Note the jet with a "kink" in it that suggests the possibility of precession (Durant et al. 2013).

3.1.2 Glitches

Four months after the publication of the discovery of the Vela pulsar by Large et al. (1968), the very first glitch was observed (Radhakrishnan and Manchester 1969; Reichley and Downs 1969) with an increase in frequency of $\frac{\Delta\nu}{\nu} = 2338 \times 10^{-9}$.

Approximately two decades later, Cordes et al. (1988) analysed all the Vela glitch data that was available at that time, and stated that glitches could be classified as being of two types: "microjumps" ($\frac{\Delta\nu}{\nu} < 1000 \times 10^{-9}$) and "macrojumps" ($\frac{\Delta\nu}{\nu} > 1000 \times 10^{-9}$). We will hereafter refer to these as *micro-glitches* and *glitches* respectively.

Cordes et al. (1988) also noted that micro-glitches and glitches appeared to have different signatures: glitches always had $\frac{\Delta\nu}{\nu} > 0$ and $\frac{\Delta\dot{\nu}}{\dot{\nu}} < 0$, whereas micro-glitches had $\frac{\Delta\nu}{\nu} \lesseqgtr 0$ and $\frac{\Delta\dot{\nu}}{\dot{\nu}} \lesseqgtr 0$. They suggest that micro-glitches and glitches may have different underlying causes. Section 7.1 on page 150 and Section 8.5 on page 229 expand on this.

3.1.3 Pulse flux density

There are many published papers focusing specifically on the Vela pulsar - simply because it's the brightest pulsar in the sky (Manchester et al. 2005), and being a young pulsar, it has some extremely interesting characteristics.

Krishnamohan and Downs (1983) is arguably one of the most important papers ever published specifically on this pulsar.[§] Of special interest is their idea of breaking down the individual pulses into 15 different intensity bins (they called them "gates") and then analysing both the pulse profiles and arrival times for each of these different flux levels. It was in this paper that it was first noticed that the brighter the pulse, the earlier it arrived. They also showed how the pulse profile is composed of four separate components each with a Gaussian profile. This analysis was achieved from 87040 single pulses recorded by the 64 m dish at Goldstone, California at a latitude of +35°. This meant Vela would not have been higher than 10° above the horizon at maximum.

Their frequency was 2.3 GHz and they only had a time resolution of 750 μs due to the limitations of the recording hardware at the time. To improve on this Johnston

[§]Joanna Rankin, personal communication.

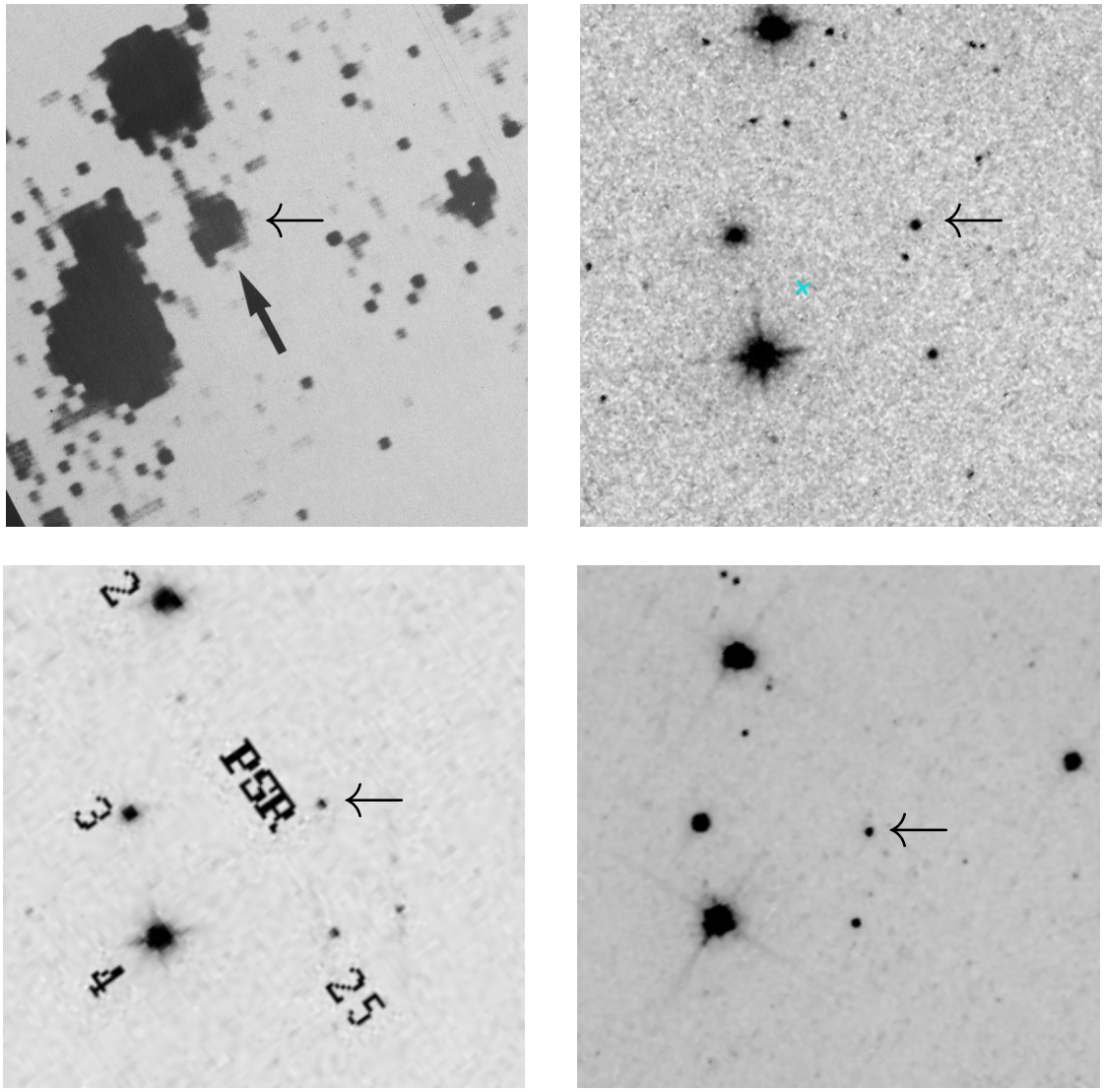

Figure 3.1: Optical images of the Vela pulsar from top left to bottom right: 1979[a], 1997[b], 2001[c], and 2011[b]. Note the proper motion and the massive improvement of resolution from the Hubble Space Telescope.

[a] Murdin et al. (1979)

[b] Based on observations made with the NASA/ESA Hubble Space Telescope, and obtained from the Hubble Legacy Archive, which is a collaboration between the Space Telescope Science Institute (STScI/NASA), the Space Telescope European Coordinating Facility (ST-ECF/ESA) and the Canadian Astronomy Data Centre (CADC/NRC/CSA)

[c] Caraveo et al. (2001)

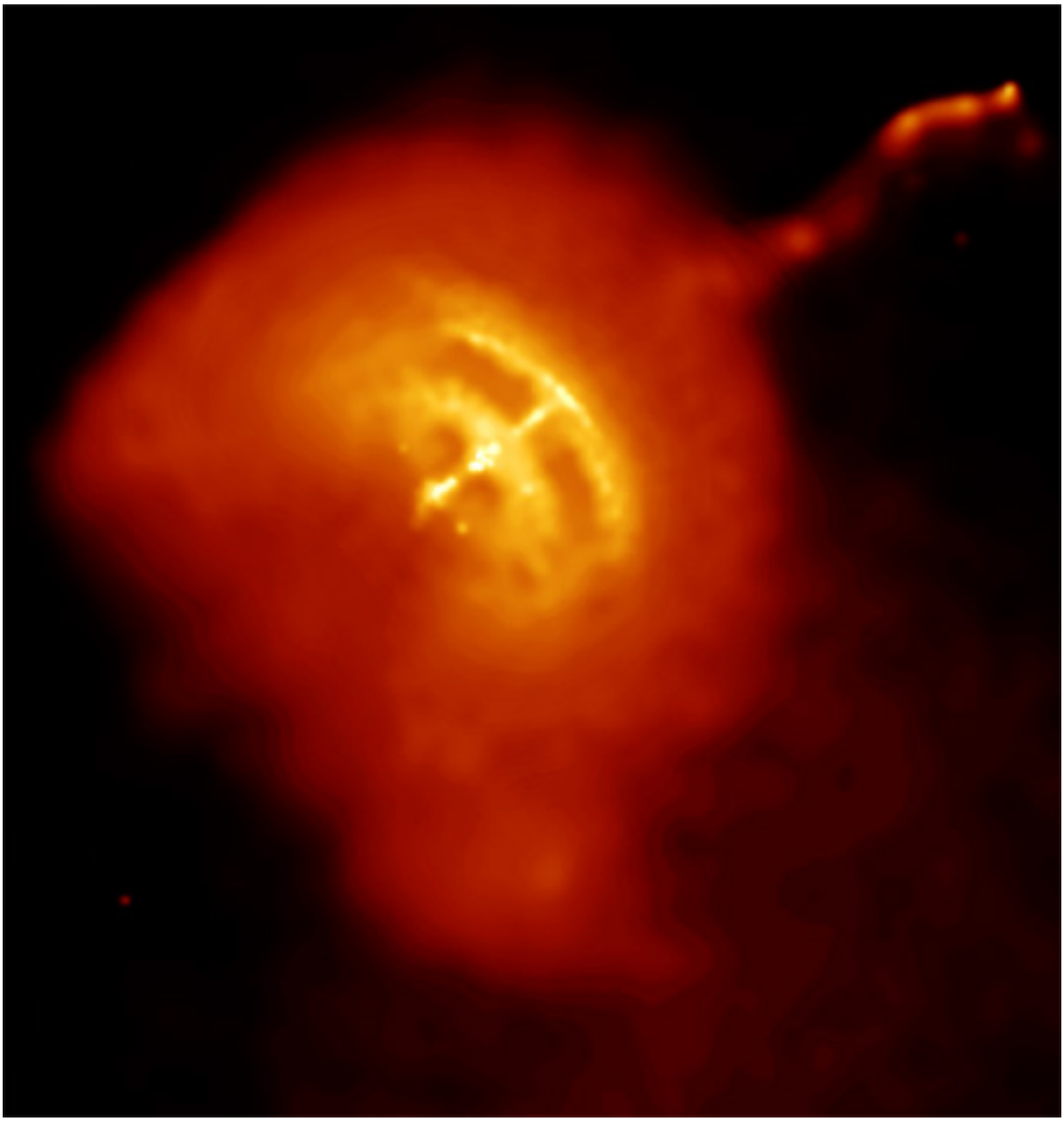

Figure 3.2: Chandra X-Ray image of the Vela Pulsar. Created by combining 8 separate images from the Advanced CCD Imaging Spectrometer (ACIS) for a total observing time of 44.7 hours. Scale: 4 x 3.5 arcmin. NASA/CXC/PSU and Pavlov et al. (2001).

et al. (2001) observed at a time resolution of 44 μs and at 1413 MHz, but they only observed 20000 pulses (30 min). Even with such a short recording time, they showed the existence of *giant micro-pulses* which were pulses with a high peak flux density, but not large enough to be classified as genuine giant pulses (mean flux density 10 times the average pulse). They were observed to arrive early and were also fairly narrow with a Full Width at Half Maximum (FWHM) of 50 μs.

3.1.4 Consecutive bright pulses

Palfreyman et al. (2011) showed that bright pulses (mean flux density 5 times the average pulse) tended to arrive consecutively. At the time of those observations, bright pulses arrived approximately once every 190 pulses (every $\approx$ 17 s). Assuming these were independent events, six consecutive pulses should only arrive once every $190^6 = 4.7 \times 10^{13}$ pulses, or once every 133 ky. However a pulse train of 6 consecutive pulses was detected twice in 300 h of observation. This, combined with other multiple consecutive sequences of 3 to 5 pulses arriving, led to the rejection of the assumption that consecutive bright pulses were independent events.

3.2 J1644−4559

J1644−4559 is a much older and slower pulsar that is bright and well-placed for southern observatories. See Table 3.2 on page 37 for its known parameters. Manchester et al. (1978) discovered that it glitches, and Johnston (2004) studied its pulse flux densities and showed that the distribution was log-normal with no bright pulses.

Table 3.2: Summary of J1644−4559 from the ATNF Pulsar Catalogue (Manchester et al. 2005) with updated data from this work in bold. For brevity, errors are omitted.

Description	PSRCAT Parameter	Value	Units
Name (J2000)	PSRJ	J1644−4559	J2000
Name (B1950)	PSRB	B1641−45	B1950
Right Ascension J2000 (α)	RAJ	16:44:49.281	h m s
Declination J2000 (δ)	DECJ	−45:59:09.5	° ’ ”
Ecliptic Longitude	ELONG	255.87	°
Ecliptic Latitude	ELAT	−23.46	°
Galactic Longitude	GL	339.19	°
Galactic Latitude	GB	−0.19	°
X in X-Y-Z Galactic Coordinates	XX	−1.6	kpc
Y in X-Y-Z Galactic Coordinates	YY	4.29	kpc
Z in X-Y-Z Galactic Coordinates	ZZ	−0.02	kpc
Epoch of Position	POSEPOCH	46800	MJD
Rotation Measure	RM	−617	rad m^{-2}
Dispersion Measure	DM	478.8	cm^3 pc
Epoch of Dispersion Measure	DMEPOCH	46800	MJD
Barycentric Rotation Frequency (ν)	F0	**2.19742204**	Hz
Frequency Derivative ($\dot{\nu}$)	F1	$\mathbf{-9.6781 \times 10^{-14}}$	Hz s^{-1}
Frequency Second Derivative ($\ddot{\nu}$)	F1	$\mathbf{8.27 \times 10^{-24}}$	Hz s^{-2}
Period	P0	**455.07871**	ms
Period Derivative	P1	$\mathbf{2.0043 \times 10^{-14}}$	s s^{-1}
Epoch of Frequency/Period	PEPOCH	**57900**	MJD
Pulse Width 50%	W50	**8.2**	ms
Mean Flux 400 MHz	S400	375	mJy
Mean Flux 1400 MHz	S1400	310	mJy
Characteristic Age (τ_c)	AGE	3.59×10^5	y
Temporal Broadening at 1 GHz	TAU_SC	1.12×10^{-2}	s
Date of Discovery	DATE	1973	y
Distance	DIST	4.5	kpc
Energy Flux at the Sun	EDOTD2	4.2×10^{32}	ergs kpc^{-2} s^{-1}
Radio Luminosity at 400 MHz	R_LUM	7593.75	mJy kpc^2
Radio Luminosity at 1400 MHz	R_LUM14	6277.5	mJy kpc^2
Surface Magnetic Flux Density	BSURF	3.06×10^{12}	Gauss
Magnetic Field at Light Cylinder	B_LC	3.04×10^2	Gauss
Spin Down Energy Loss Rate	EDOT	8.4×10^{33}	ergs s^{-1}

3.3 J0437−4715

Johnston et al. (1993) discovered the millisecond pulsar J0437−4715 and it is one of the closest and brightest pulsars in the sky. With a rotation frequency of $\nu \approx 173.7$ Hz this pulsar also rivals atomic clocks in its accuracy of rotation. It has not been known to glitch nor does it emit bright or giant pulses. J0437−4715 also has a binary companion with an estimated mass of 0.16 $M_{\odot}$with an orbital period of 5.74 days. Table 3.3 on page 39 shows a number of current parameters shown to their known precision. Of note is the extraordinarily low error in the period which is 1.7×10^{-17} s.

Table 3.3: Summary of J0437−4715 from the ATNF Pulsar Catalogue (Manchester et al. 2005). For brevity, errors are omitted.

Description	PSRCAT Parameter	Value	Units
Name (J2000)	PSRJ	J0437−4715	J2000
Right Ascension J2000 (α)	RAJ	04:37:15.8961737	h m s
Declination J2000 (δ)	DECJ	−47:15:09.110714	° ’ ”
Ecliptic Longitude	ELONG	50.47	°
Ecliptic Latitude	ELAT	−67.87	°
Galactic Longitude	GL	253.39	°
Galactic Latitude	GB	−41.96	°
X in X-Y-Z Galactic Coordinates	XX	−0.11	kpc
Y in X-Y-Z Galactic Coordinates	YY	8.53	kpc
Z in X-Y-Z Galactic Coordinates	ZZ	−0.10	kpc
Epoch of Position	POSEPOCH	54500.00	MJD
Rotation Measure	RM	0.0	rad m^{-2}
Dispersion Measure	DM	2.64476	cm^3 pc
Epoch of Dispersion Measure	DMEPOCH	54500.00	MJD
Barycentric Rotation Frequency (ν)	F0	173.6879458121843	Hz
Frequency Derivative ($\dot{\nu}$)	F1	$-1.728361 \times 10^{-15}$	s^{-2}
Period	P0	0.005757451936712637	s
Period Derivative	P1	5.729215×10^{-20}	s s^{-1}
Epoch of Frequency/Period	PEPOCH	54500	MJD
Pulse Width 50%	W50	0.410	ms
Mean Flux 400 MHz	S400	550	mJy
Mean Flux 1400 MHz	S1400	149	mJy
Characteristic Age (τ_c)	AGE	1.59×10^9	y
Annual Parallax	PX	6.37	mas
Date of Discovery	DATE	1993	y
Distance	DIST	0.16	kpc
Energy Flux at the Sun	EDOTD2	4.8×10^{35}	ergs kpc^{-2} s^{-1}
Radio Luminosity at 400 MHz	R_LUM	13.52	mJy kpc^2
Radio Luminosity at 1400 MHz	R_LUM14	3.66	mJy kpc^2
Surface Magnetic Flux Density	BSURF	5.81×10^8	Gauss
Magnetic Field at Light Cylinder	B_LC	2.85×10^4	Gauss
Spin Down Energy Loss Rate	EDOT	1.2×10^{34}	ergs s^{-1}
Binary period of pulsar	PB	5.7410459	days
Eccentricity	ECC	1.91811×10^{-5}	
Median companion mass	MEDMASS	0.163681	$M_\odot$

3.4 The Crab Pulsar - J0534+2200

The Crab pulsar was formed after the supernova which was observed in 1054. This pulsar has high flux density at low frequencies ($S_{400} = 550$ mJy) but is comparatively faint at the L-band frequencies we observe at ($S_{1400} = 14$ mJy). This is $\approx \frac{1}{78}$ that of Vela.

However the Crab pulsar emits very high flux density giant pulses that have been stated as *"The Brightest Pulses in the Universe"* (Cordes et al. 2004). The Crab pulsar was discovered because of these giants (Staelin and Reifenstein 1968), and they can be used as a comparison when examining the bright pulses that are emitted from Vela. Table 3.4 on page 41 shows a number of current parameters shown to their known precision.

Table 3.4: Summary of J0534+2200 from the ATNF Pulsar Catalogue (Manchester et al. 2005). For brevity, errors are omitted.

Description	PSRCAT Parameter	Value	Units
Name	PSRJ	J0534+2200	J2000
Right Ascension J2000 (α)	RAJ	05:34:31.973	h m s
Declination J2000 (δ)	DECJ	+22:00:52.06	° ’ ”
Ecliptic Longitude	ELONG	84.10	°
Ecliptic Latitude	ELAT	−1.29	°
Galactic Longitude	GL	184.56	°
Galactic Latitude	GB	−5.78	°
X in X-Y-Z Galactic Coordinates	XX	−0.16	kpc
Y in X-Y-Z Galactic Coordinates	YY	10.48	kpc
Z in X-Y-Z Galactic Coordinates	ZZ	−0.20	kpc
Epoch of Position	POSEPOCH	40000.00	MJD
Rotation Measure	RM	−42.3	rad m^{-2}
Dispersion Measure	DM	56.791	cm^3 pc
Epoch of Dispersion Measure	DMEPOCH	40000.00	MJD
Barycentric Rotation Frequency (ν)	F0	30.2254370	Hz
Frequency Derivative ($\dot{\nu}$)	F1	-3.86228×10^{-10}	s^{-2}
Period	P0	0.03308471603	s
Period Derivative	P1	4.22765×10^{-13}	s s^{-1}
Epoch of Frequency/Period	PEPOCH	40000.00	MJD
Pulse Width 50%	W50	3.0	ms
Pulse Width 10%	W10	4.7	ms
Mean Flux 400 MHz	S400	550	mJy
Mean Flux 1400 MHz	S1400	14	mJy
Age (actual)	AGE	1.24×10^3	y
Date of Discovery	DATE	1968	y
Distance	DIST	2.00	kpc
Energy Flux at the Sun	EDOTD2	1.2×10^{38}	ergs kpc^{-2} s^{-1}
Radio Luminosity at 400 MHz	R_LUM	2200	mJy kpc^2
Radio Luminosity at 1400 MHz	R_LUM14	56	mJy kpc^2
Surface Magnetic Flux Density	BSURF	3.78×10^{12}	Gauss
Magnetic Field at Light Cylinder	B_LC	9.80×10^5	Gauss
Spin Down Energy Loss Rate	EDOT	4.6×10^{38}	ergs s^{-1}

Chapter 4

Instrumentation and software

4.1 Mount Pleasant

The Mount Pleasant 26 m radio telescope was donated to the University of Tasmania by NASA in the mid 1980s and currently has 8 receivers at frequencies from 1200 MHz to 22 GHz. The telescope has an X-Y mount with the X-axis controlling the north/south and the Y-axis controlling the east/west direction.

Since pulsars generally emit higher flux densities at lower frequencies, but the lower frequencies are smeared by the interstellar medium, the selection of an optimum frequency for a given dish size is an important decision for a long-term study. For the Vela pulsar using a 26 m dish, we selected $\approx$ 1400 MHz. Since the Mount Pleasant telescope is only 12 km from the Hobart CBD with the ability to observe at a bandwidth of 64 MHz, a centre frequency selection for a three year project (and beyond) is very dependent on local radio frequency interference (RFI), the nature of the emission of the pulsar, and the intervening interstellar medium (ISM).

A central frequency of 1376 MHz (i.e. a range of 1344-1408 MHz) was finally chosen since it minimised RFI within the band, was high enough to have minimal scattering from the ISM, and low enough that single pulses were still clearly seen. This was all with the knowledge that RFI could become an issue later on.

For this work, most of the observations were conducted at 1376 MHz, but multi-frequency observations were also performed on Vela and other pulsars. Table 4.1 on page 44 shows the sky frequencies and oscillator settings we used.

An important consideration in such a long project was stability. To this end, there were no changes in the receiver and only minor changes in cables and local oscillator hardware. Most importantly, *no software upgrades* in the processing chain were made. In particular TEMPO2, DSPSR, and PSRCHIVE were left at the same versions

Table 4.1: Receivers, observation frequencies, oscillator settings, and feed types at Mount Pleasant for observations used throughout this study.

Receiver		Sky freq	Agilent		LO	SML		Attenuation		Feed
id	Band	MHz	MHz	dBm	MHz	MHz	dBm	L dBm	R dBm	type
2	L	1376	4100	16	5200	876	7	12	12.6	Linear
3	S	2230	7800	16	5200	782	7	9.5	16.7	Circular
4	C	4800	10500	16	5200	652	7	N/A‡	12.6	Circular
5	X	6658	12200	16	5200	810	7	12.8	9.2	Circular
6	X	8425	14000	16	5200	777	7	14.4	17.5	Circular
7	Ku	12200	17800	16	5200	752	7	15	N/A‡	Circular
8	K	22214	16600	16	5200	738	7	N/A‡	21.2	Circular

‡Feed was defective.

throughout. This was to minimise any risk of unexpected software changes affecting the results.

To maximise the probability of catching the upcoming glitch, we extended the negative limit of the X-axis to -85° which was the maximum that could be achieved without stretching cables and helium pipelines beyond their capability. This lowered the southern elevation limit to 4.3° and increased the maximum daily observing by $\approx$ 1 h to $18^{\mathrm{h}}57^{\mathrm{m}}06^{\mathrm{s}}$, or in other words a probability of catching the glitch at $p = 0.7897$ (assuming observing all day, every day was possible).

A typical observing session began by moving the telescope to the rise-point (for the telescope, not the horizon) 7 minutes prior to Vela being visible. As soon as Vela moved to the centre of the field, recording and tracking began. A 19 hour observing run typically cuts across two UTC days and so the observing was recorded under the day-of-year that had the majority of observing hours in it.

Table 4.2 on page 46 shows a summary of Mt Pleasant instrumentation, sampling, and total data collected. Figure 4.1 on page 45 shows the mixing and digitisation chain that occurs on the 26 m telescope up to and including writing data to disk by the machine `hovsi` which has a dedicated network link to a 24 TB datastore on `sirius`. This link used a Gigabit ethernet card and was mounted via NFS.

A small undesirable side effect of this was a 2 second buffering that occasionally occurred at the start of recording. This had no effect on pulsar timing as timestamps from the hydrogen maser were recorded in the sampled data. However it meant that the *filenames* of the datafiles were sometimes 2 s earlier than the first data recorded in them. This is important to remember when examining `pav -Y` plots like in Figure 8.9 on page 165.

Data was continuously copied off `sirius` to RDSI (see Section 4.4.3 on page 52). The 24 TB disk storage on `sirius` provided a buffer of up to 6 days in the event of network

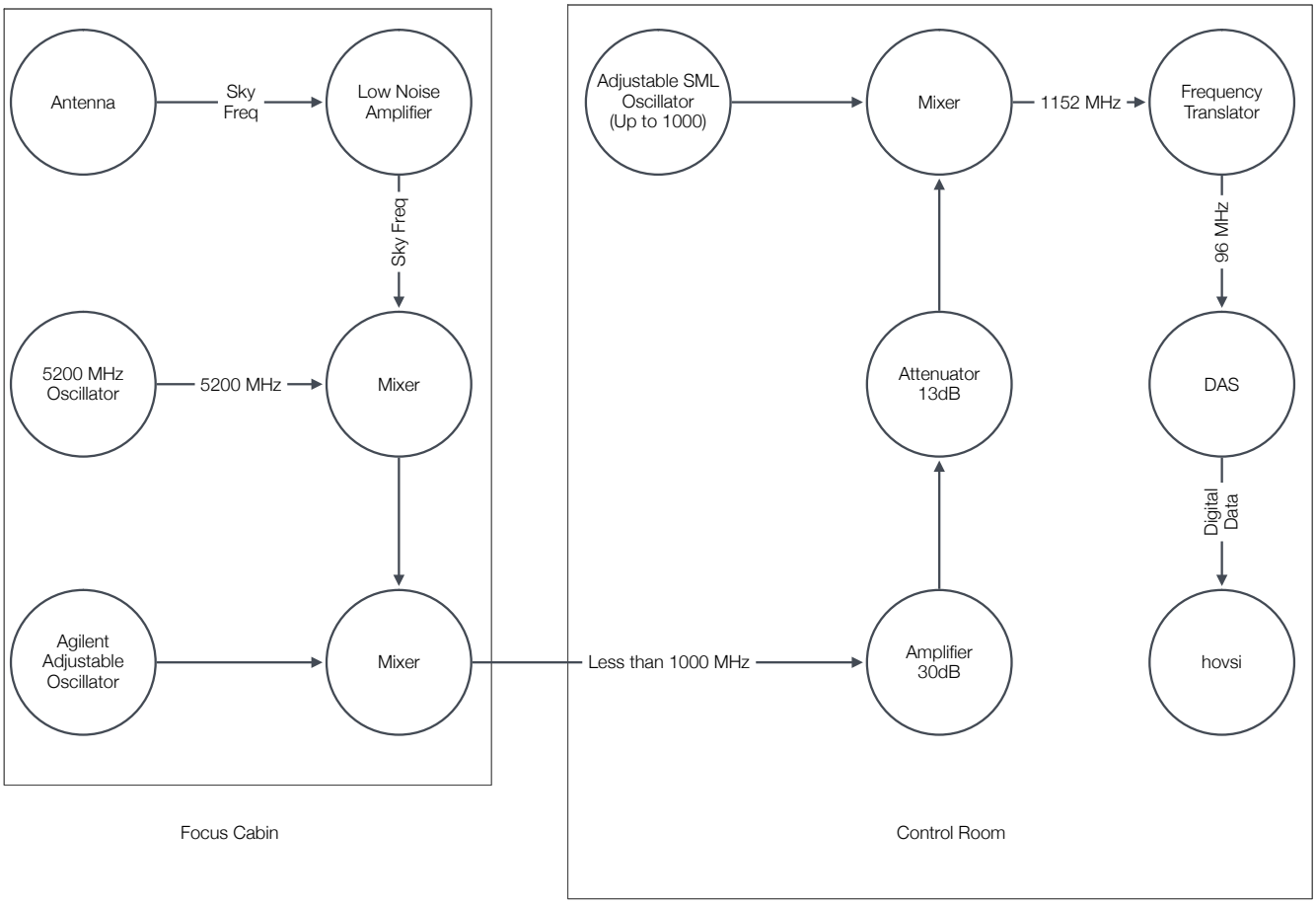

Figure 4.1: Mt Pleasant receiver, mixing, digitisation, and recording chain. The left panel shows the focus cabin and the right panel shows what happens down in the control room.

or RDSI issues.

4.1.1 Calibration

Polarisation calibration was conducted by firing orthogonal noise diodes (internally installed in the L-band receiver) for 2 min as a 5 Hz square wave with a 50 per-cent duty cycle during each daily observation. With larger telescopes this process should be performed just prior or after each observation as the Vela pulsar's signal is too strong for accurate calibration. However with a 26 m telescope, Vela's signal is weak enough when folded at 5 Hz that it doesn't interfere with the calibration (Willem Van Straten, private communication). Figure 4.2 on page 47 shows the firing of the noise diodes appearing as mild RFI. Vela's individual pulses can be seen as a vertical column around phase 0.5, with a bright pulse appearing at ≈ 1 s from the start.

Flux density calibration for L-band was performed on a less regular schedule as changes

Table 4.2: Mount Pleasant instrumentation, sampling, and total data collected. The number of phase bins and frequency channels shown is what all data was initially processed with. Higher resolutions were available if required (e.g. for giant pulses).

Category	Description	Value	Units
Telescope	Diameter	26	m
Location	Longitude	147°26′25″.87 E	WGS84
	Latitude	42°48′12″.90 S	WGS84
	Altitude (GPS)	65.09	m
Receiver	Frequency	1376	MHz
	Bandwidth	64	MHz
	Feeds	Dual Cooled	
	Polarisations	Linear	
	SEFD	470	Jy
Sampling	System	LBA DAS	
	Bits	2	
	Rate	128	MS s^{-1}
	File length	10	s
	File size	113	MB
Processing	Frequency channels	16	
	Phase bins	8192	
	Resolution	10.9	μs
	Data Collected		
Vela	Total	14074	hours
	Pulses recorded	5.55×10^8	
	"Good" pulses recorded	5.11×10^8	
	Data recorded	2.949	PB
J1644−4559	Total	657	hours
	Pulses recorded	4.99×10^6	
	"Good" pulses recorded	4.79×10^6	
	Data recorded	0.137	PB
J0437−4715	Total	160	hours
	Data recorded	0.033	PB
J0534+2200	Total	14.4	hours
	Data recorded	0.003	PB

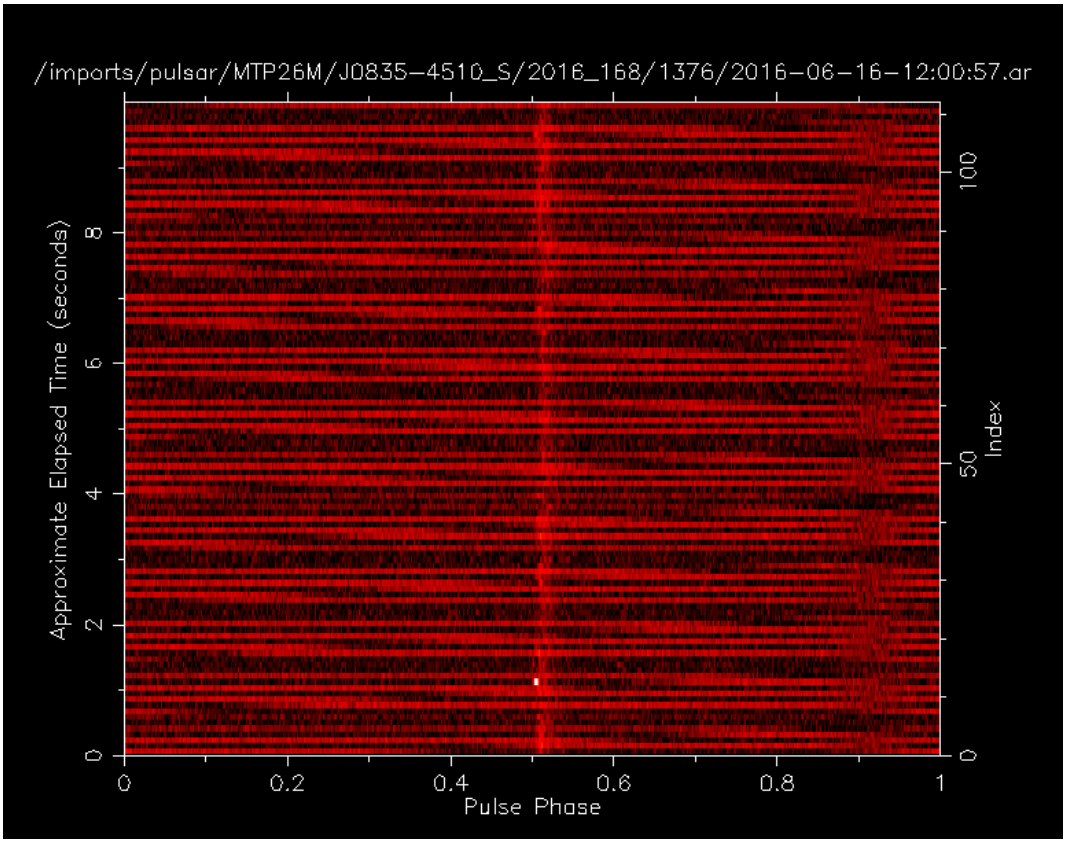

Figure 4.2: Firing of the noise diodes during an observation of the Vela pulsar at Mount Pleasant. This is a time vs time plot with the 89.3 ms period being shown as phase along the X-axis, and 10 s of time on the Y-axis. Flux density is shown by colour. The vertical strip at a phase of 0.5 is the Vela pulsar and the horizontal lines are the noise diode being fired.

in the receiving chain were relatively rare. It was typically performed when Vela was set, that is, LMST between 18:04:00 and 23:07:44.

Applying the flux calibration to the normal Vela data at 1376 MHz wasn't always necessary as the relative arbitrary units could be used.

For multi-frequency observations specific calibration *was* important. PSRCHIVE flux calibration software uses a configurable file of known calibrators. It has two formats:

1. A simple spectral index and a reference frequency.
2. A more accurate equation based on fitting a polynomial of the logarithm of the frequency (Perley and Butler 2013).

The first format (using spectral index) is useful when the observed frequency is close to the reference. However, with a wide range of frequencies the second format is preferable. Specifically it is:

$$\log S = A_0 + A_1 \log(f_g) + A_2 \log^2(f_g) + A_3 \log^3(f_g) \tag{4.1}$$

where S is flux density in Jy, f_g is the frequency in GHz, and A_0-A_3 are the supplied polynomial calibration parameters.

However, calibration references Baars et al. (1977) and Ott et al. (1994) use the frequency specified in MHz (f_m):

$$\log S = a_0 + a_1 \log(f_m) + a_2 \log^2(f_m) + a_3 \log^3(f_m) \tag{4.2}$$

Our major calibration references (3C218, 3C274, and 3C353) were not included in Perley and Butler (2013) because they are no longer considered quality calibrators. For our purposes however, they are sufficient.

So we converted the polynomial parameters for these calibrators from Ott et al. (1994), which used f_m, to equivalent parameters using f_g. Note that the a_3 term was not used by earlier authors and so we have simply set $a_3 = 0$.

For reference, the full conversion is:

$$A_0 = a_0 + 3a_1 + 9a_2 + 27a_3 \tag{4.3}$$

$$A_1 = a_1 + 6a_2 + 27a_3 \tag{4.4}$$

$$A_2 = a_2 + 9a_3 \tag{4.5}$$

$$A_3 = a_3 \tag{4.6}$$

Table 4.3: Flux density calibration sources where S is in Jy and f_g is frequency in GHz.

$$\log S = A_0 + A_1 \log(f_g) + A_2 \log^2(f_g)$$

Name	aka	α J2000	δ J2000	A_0	A_1	A_2
3C218	Hyd A	09:18:06	−12:05:44	1.771	-0.947	0.013
3C274	Vir A	12:30:49	+12:23:28	2.423	-0.771	-0.028
3C353		17:20:28	−00:58:47	1.857	-0.704	-0.091

Table 4.3 shows the list of our calibration sources and their polynomial parameters based on frequency referenced in GHz. 3C353 was selected most often due to its right ascension and availability when Vela was set. Its referenced maximum frequency was 10550 MHz, and so the pulsar flux densities observed at higher frequencies may be slightly in error.

4.2 Ceduna

The Ceduna 30 m radio telescope was donated to the University by what is now Telstra and has 7 receivers. Each has to be manually changed and all are uncooled. Apart from slight differences in local oscillators, the receiving and recording chain is very similar to Mt Pleasant. Compared with the 26 m, this dish has the advantage of an extra 33% surface area, but being uncooled its overall performance is less, with the SEFD of Ceduna being about three times that of the 26 m.

There is no connected fibre optic cable to the observatory and so any large data collection needs to be shipped using portable disks. Because of this data restriction, we used the Ceduna observatory to:

1. Confirm our bright pulses with dual observations using the same frequency as Mt Pleasant (1376 MHz). Once we found bright pulses in Hobart we could simply process the single data file at the Ceduna observatory, and confirm the bright pulse observation.

2. Observe our bright pulses with dual observations using a higher frequency than Mt Pleasant. Similarly, when a bright pulse was found locally, that single file was processed and checked at Ceduna.

3. A major goal of this project was to catch the glitch in single-pulse mode. Mt Pleasant could be used up to 19 hours a day, but when this was not possible due to other observers, Ceduna could be used instead. Data was collected and discarded if the glitch didn't happen. Being further north, it was not possible to

Table 4.4: Ceduna instrumentation, sampling, and data collected

Category	Description	Value	Units
Telescope	Diameter	30	m
Location	Longitude	133°48′36″ E	WGS84
	Latitude	31°52′05″ S	WGS84
	Altitude (GPS)	157.75	m
Receiver	Frequency	1376	MHz
	Bandwidth	64	MHz
	Feeds	Dual Uncooled	
	Polarisations	Linear	
	SEFD	≈ 1500	Jy
Sampling	System	LBA DAS	
	Bits	2	
	Rate	128	MS s^{-1}
	File length	10	s
	File size	113	MB
Processing	Frequency channels	16	
	Phase bins	8192	
	Resolution	10.9	μs

observe for as long as Mt Pleasant (just under 16 h as compared to 19 h), so the probability of catching the glitch at Ceduna was reduced.

4. Even when Mt Pleasant was observing Vela, Ceduna was also used at the same frequency so confirmation of pulse changes due to the glitch could be confirmed.

Table 4.5: Observation frequencies, oscillator settings, and feed types at Ceduna for observations used throughout this study.

Sky freq	Agilent	LO	SML	Type
	MHz	MHz	MHz	MHz
1376	6200	4100	428	Linear
4800	N/A	4100	452	Circular‡

‡One of the feeds became defective part-way through this study.

4.3 Sampling

For both Mount Pleasant and Ceduna, similar digital sampling systems were used. The LBA DAS is configured for 128 mega samples s^{-1} using 2 bit sampling. This rate is required for the 64 MHz bandwidth which is used for pulsar observations due to the Nyquist sampling theorem (Nyquist 1928). This theorem states that to avoid aliasing, sampling at least twice the highest frequency contained in the data is required.

The automatic gain control (AGC) on the DAS is disabled due to the compensation effect it has on pulsar signals. In tracking a pulsar across the sky for 19 hours some form of AGC is required. We produced a script that monitored the output of the `vsib_record` command on `hovsi` every 5 min and adjusted (and logged) the attenuator levels to keep the input to the DAS centred. Keeping these attenuation levels centred was important since poor timing results otherwise occurred.

4.4 Software processing

4.4.1 Data flow

Figure 4.3 on page 53 shows the dataflow after recording from the sampler. DSPSR coherently de-dispersed each `.lba` datafile to produce a `.ar` file containing 10 s worth of timing data broken up by frequency, polarisation, and time.

The `.ar` files were then "scrunched" in frequency, polarisation, and time to produce a single `.ft` file showing the integrated 10 s pulse. This was then aligned with a standard pulse profile for the observed frequency to produce an arrival time.

Arrival times for the day were then manually examined in TEMPO2 to remove RFI, wind stows, and other interruptions. Those clean timings were stored in `fixed.tim` in the `timing` directory. Then a fit of ν and $\dot{\nu}$ was performed whilst keeping $\ddot{\nu}$ fixed. The parameters for the day were then saved in `timing/today.par`. The script `create_pulsewidths` then measured the width of daily integrated pulse.

The collection of good timings were then used to generate images (using `pav -Y`) of bright pulses. These were then manually examined to make sure they were genuine.

4.4.2 Processing hardware

The Mount Pleasant observatory's `hex` cluster was used for all major processing. This consists of 12 machines (`hex0` to `hexb`), each with 8 cores, 4GB of RAM, and running the Debian Linux operating system. The top six (`hex7` to `hexb`) were newer, had faster processors, and ran the bulk of the processing. With access to 96 cores, we had the ability to process raw data in real time, but this was not implemented because efficiently parallelising incoming data files for processing over 96 cores is not a trivial task. It was also not necessary for this project. The one exception was that some real-time processing was needed for timely glitch detection and this is discussed in Section 4.4.7 on page 58.

4.4.3 RDSI petabyte disk storage

The main requirement of our data processing was storage. With 4 TB day^{-1} of raw data being recorded, and an extra 1 TB day^{-1} needed for the de-dispersed and folded data files, this project would not have been possible without a large datastore. Fortunately at the start, the Research Data Storage Infrastructure (RDSI) came online with its 2.3 PB facility. Our allocation was 250 TB but with a flexible buffer, the size of which depended on other users. This enabled us to retain raw data files for approximately 6 months before deleting them. Raw data files that contained "interesting" data on them were permanently retained.

4.4.4 DSPSR

After recording of the raw baseband file, phase coherent de-dispersion (see Section 2.4 on page 18) and folding to the pulsar's period is achieved using DSPSR (van Straten and Bailes 2011).

With our observations for Vela, a single-pulse 10 s file after processing by DSPSR contains 111 (or 112) pulses, 8192 phase bins, 16 frequency channels and 2 polarisations.

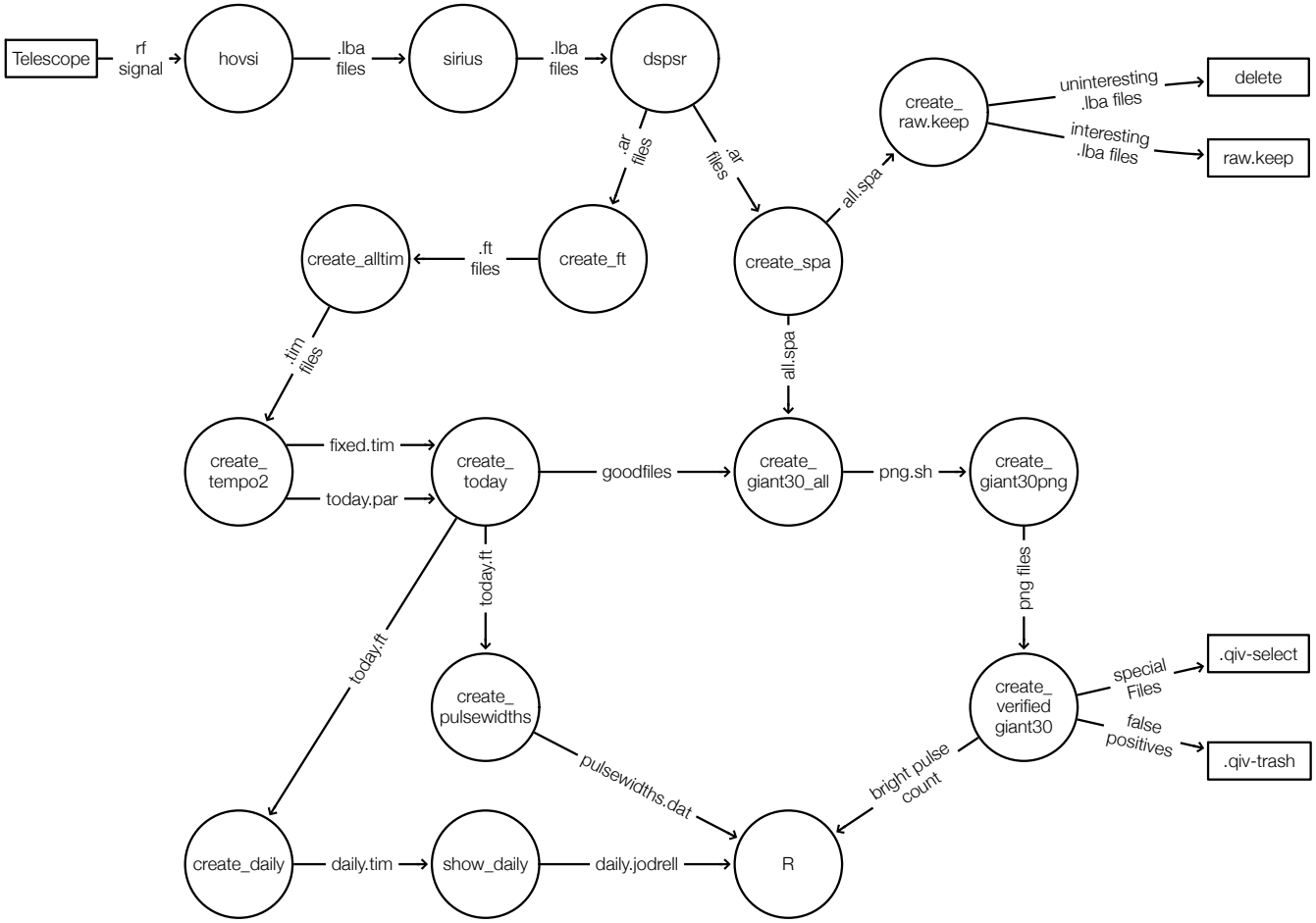

Figure 4.3: Data flow diagram of the software processing chain. Circles indicate processes and lines show the flow of data. Rectangles mark start or end points that are out of scope of the diagram.

Table 4.6: Number of simultaneous DSPSR processes running on each node for the throughput test.

Node	Processes
hex0	3
hex1	4
hex2	5
hex3	6
hex4	7
hex5	8
hex6	3
hex7	4
hex8	5
hex9	6
hexa	7
hexb	8

This DSPSR processing is the most computationally intensive of all the stages, so efficient loading of the `hex` cluster was paramount. We performed a test to discover the most efficient number of processes per node. Table 4.6 shows how many DSPSR processes were loaded onto each machine for the test. Figure 4.4 on page 55 shows a box plot of processing times for each node. The upper hex cluster with newer processors is clearly faster.

What is of importance though is total throughput. Figure 4.5 on page 56 shows the number of files processed in 200 min by each node.

It is quite clear from this chart that eight processes should be run on each processor for maximum throughput. However, this left no overhead for anything else and made system response for other ad-hoc commands very poor. We elected to run with seven DSPSR processes per node throughout. Note that hex4 appeared to perform poorly with seven processes, this was most likely that it also had the extra duty of being the cluster's "head node" at that time.

The average processing times at the end of 4 years are shown in Figure 4.6 on page 56 and total number of files processed is shown in Figure 4.7 on page 57. The upper hex cluster was mainly used for DSPSR, with the exception of hex9 which was dedicated to other pulsar processing. Also, hex0 and hex4 were rarely used. Pulsars other than Vela were processed mainly in the lower hex cluster, and so their processing times varied significantly.

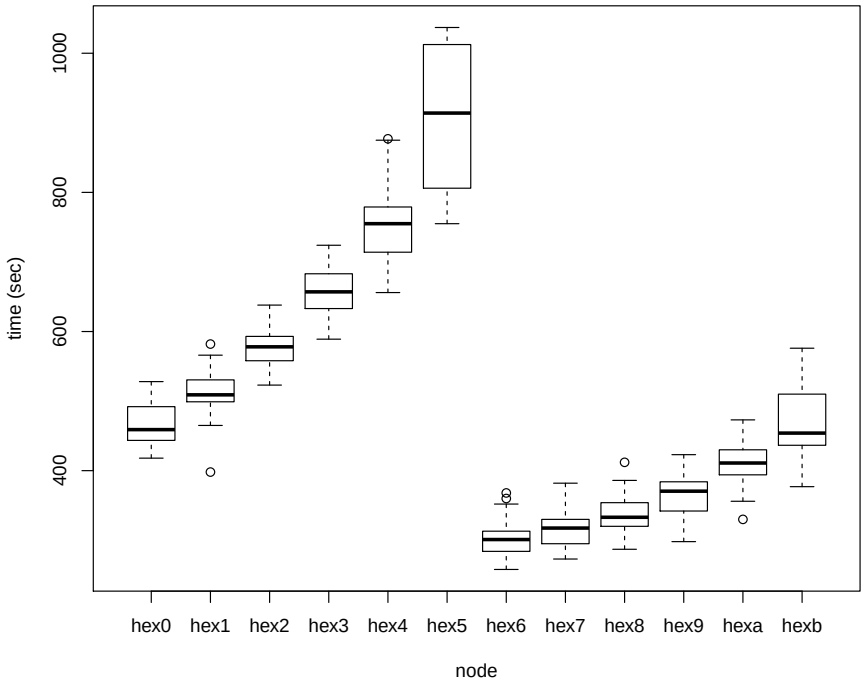

Figure 4.4: Processing times with each node running varying numbers of simultaneous DSPSR processes (from 3 to 8) as shown in Table 4.6 on page 54. Each box and whisker plot shows the median processing time (dark horizontal line), with the box showing the inter-quartile range. The extrema are marked by whiskers and extreme outliers by circles.

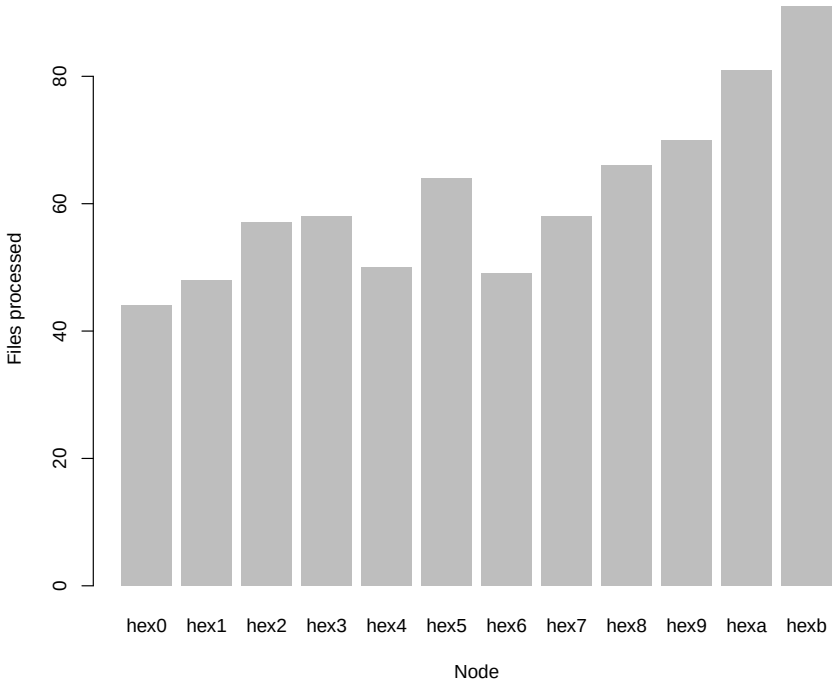

Figure 4.5: Processing throughput with each node running varying numbers of simultaneous DSPSR processes as shown in Table 4.6 on page 54.

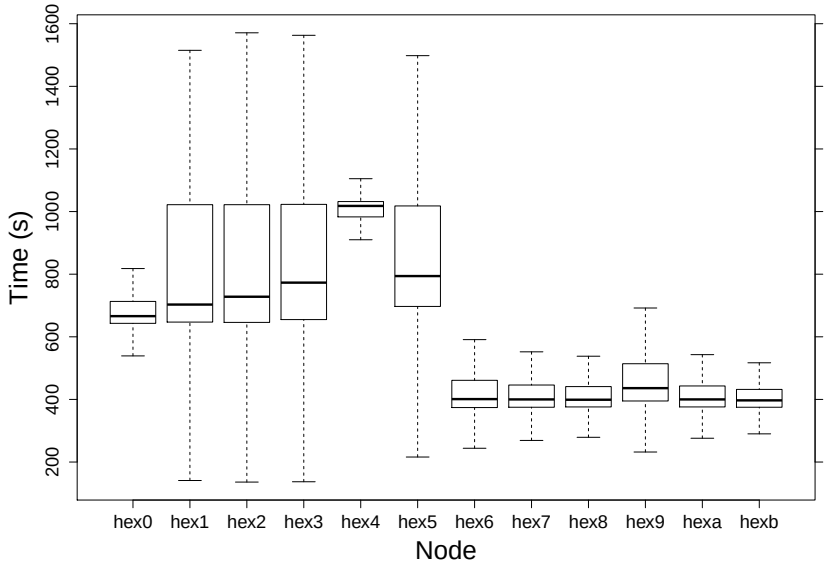

Figure 4.6: Processing times by node after processing 4 years worth of pulsar data. Machines hex6-hexb were mainly used for DSPSR processing, but hex9 was reserved for other processing.

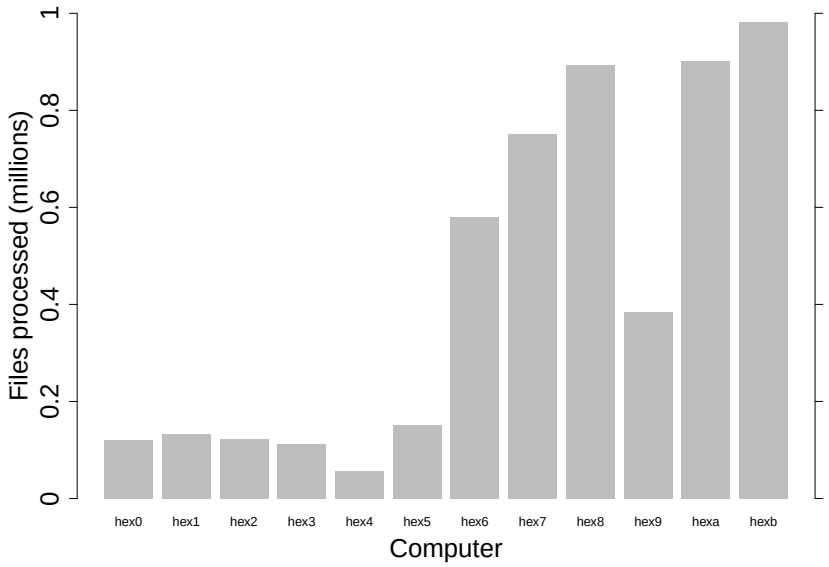

Figure 4.7: Number of files processed by node after 4 years worth of pulsar data had been collected and analysed. Machines hex6-hexb were mainly used for DSPSR processing, but hex9 was reserved for other processing.

4.4.5 TEMPO2

Once a 10 s file has been processed by DSPSR, a time-averaged pulse of that file is created and an arrival time is calculated. These arrival times are then loaded into TEMPO2 (Hobbs et al. 2006; Edwards et al. 2006) for long term analysis and glitch detection.

TEMPO2 is a graphics-based software package designed to fit polynomials (i.e. Taylor series) to the arrival times and then plot the residuals. TEMPO2 also accounts for barycentric arrival time correction, Shapiro delay, and Einstein delay. TEMPO2 has been the main pulse arrival-time analysis tool for over a decade, and it is based on the 1970s TEMPO that was written in FORTRAN.

4.4.6 PSRCHIVE

PSRCHIVE (Hotan et al. 2004) is a suite of freely available software packages for pulsar analysis. It is written in C++ and hence processing and manipulation of the large files produced is efficient. PSRCHIVE has the ability to produce publication quality graphs, although we mostly exported the results and used R for any statistical analysis and subsequent plots.

4.4.7 Real time glitch detection

Catching the glitch was one of the major goals of this project and with 19 hours daily observations there was a 79% chance of it being captured. With wind stows and other observers taken into account the probability was lower.

If the glitch was captured, timely reporting to *The Astronomer's Telegram* was paramount. With 7 cores typically dedicated to each day's observing, our standard processing chain typically takes 110 hours to process the full 19 hours worth of data. This was not timely.

So an additional process was installed. Every 15 min during data collection, a sample raw file was copied and processed using DSPSR and TEMPO2. The residual for that single 10 s observation was then emailed to the author. A glitch would cause a sizeable jump in that residual and so could be acted upon. The turn-around time for this glitch detection process was 4 minutes. Additionally, when a glitch occurred an automated text message was sent.

As Vela has a significant amount of red timing noise, these real-time residuals would drift over time periods of months - sometimes into the glitch trigger-zone. To overcome this, a regular re-fitting of ν and $\dot{\nu}$ to the most recent data was required. This was typically done after each micro-glitch.

4.5 Radio frequency interference

RFI is a major issue at Mt Pleasant, and less so at Ceduna. Part of this project was identifying different patterns of RFI and trying to localise their sources. Once identified, the RFI was mitigated if possible.

After processing, strong sporadic RFI was mostly identified in the timing residuals, and was indicated by a timing residual being outside the 50 μs RMS figure that was typical. Care was required since when giant pulses occur, they arrive earlier in the pulse period, so sometimes timings with an RMS < -50 μs would not be RFI.

When there was doubt, examining the file (using `pav -D` or `pav -Y`) could then indicate if the pulse was genuine. If the pulse was RFI, the file was removed from further analysis at this stage.

At the bright-pulse identification stage, less intense RFI can appear and it was removed if the RFI was being incorrectly counted as a bright pulse. Single sporadic pulses at a different phase than Vela's pulses could be checked by comparing frequency over time

to see if the pulse was smeared by dispersion. This was just in case a bright FRB occurred. Unfortunately no such pulses were discovered.

4.5.1 Out-of-band RFI

Radio frequency interference that has a frequency range *outside* of the observed receiver bandwidth can still interfere with observations. If strong enough it can "lift" the overall baseband signal. Figure 8.13 on page 167 shows a typical example.

4.5.2 4G mobile tower

Early in the project a strong out-of-band transmission appeared and prevented *any* observation using the L-band receiver. It was identified as a newly installed Telstra 4G tower 9.15 km away at an azimuth of 147.7°. For future reference, its Device Registration ID was 9391246, the frequency was 1815 MHz, bandwidth 10 MHz, and mean transmission power was 39.8 Watts. The transmitter was pointing at an azimuth of 310°, and it's power directed at the telescope was 35.7 dBm per 30 kHz. Figure 4.8 on page 60 shows the radiated pattern with Mt Pleasant being on azimuth of 327.7° with respect to the transmitter.[§]

As a trial, extremely simple "notch" filters were installed on each channel after the low-noise amplifiers. These consisted of simply a shorted stub of coaxial cable with the length being selected by experiment. Since these simple trial filters completely removed the out-of-band RFI, properly constructed filters were built and installed.

4.5.3 Lightning

Thunderstorms are relatively rare around Hobart with an average of 6 thunderdays* per year (Crowder 1997). However on 2015-02-22 (day 53) a number of lightning strikes occurred around the Hobart area. Utilising social media to get approximate times of strikes we identified a file containing a lightning strike.[†] Figure 4.9 on page 61 shows the overall result. Figures 4.10 to 4.14 on pages 62–64 show the sequence of events during the strike, and Figures 4.15 to 4.16 on pages 64–65 show the return stroke in greater detail.

Proctor et al. (1988) describe various features of lightning strikes at radio wavelengths. Of interest here is what they label Q-noise, and describe it as "*very short spikes su-*

[§]www.acma.gov.au

*A thunderday is defined as a day in which thunder is heard.

[†]Thanks to Andrew Strugnell for the original timing estimate of the lightning bolt.

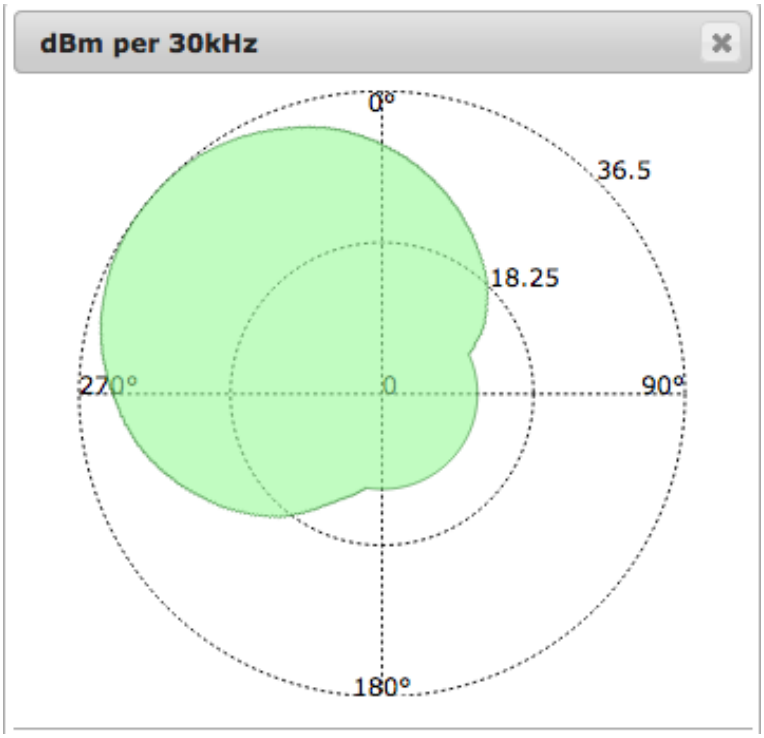

Figure 4.8: Telstra interfering transmitter beaming pattern. Mt Pleasant is at a bearing of 327.7° and is 9.15 km away. (ACMA website https://web.acma.gov.au/rrl/register_search.main_page Device Registration ID 9391246)

perimposed on the positive half cycle of a slowly varying low frequency component", which describes what is shown in Figure 4.12 on page 63, Figure 4.15 on page 64, and Figure 4.16 on page 65.

This lightning strike can be used as a baseline to show how the telescope and observing system handles pulses in flux density and in particular how reprocessing at higher resolution will appear. We examine bright pulses at nanosecond resolution in Section 5.1.3 on page 85 and this lightning shows that what we see with giant pulses are not system artefacts.

Lightning is also of interest with regards to Fast Radio Bursts (see Section 2.6 on page 25). Katz (2017) states that FRBs could be an analogy to lightning here on Earth. Just as lightning is a breakdown in insulation in a cumulonimbus cloud, the author proposes that an FRB is the results of a breakdown of the insulating vacuum gap that exists in pulsar magnetospheres. Another FRB cause that is proposed is that of giant pulses from neutron stars. We will be able to look for similarities in our lightning data and our giant pulse data.

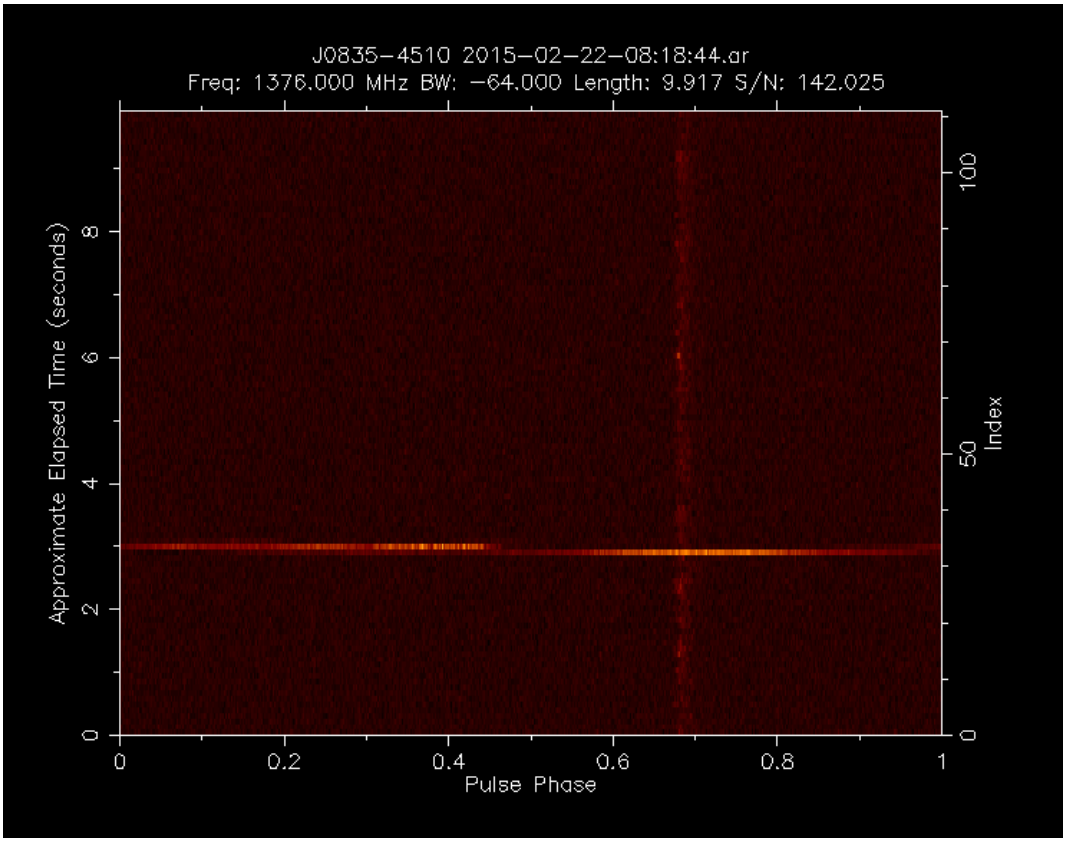

Figure 4.9: A lightning strike that occurred ≈ 10 km away. This is a time vs time plot with the 89.3 ms period being shown as phase along the X-axis, and 10 s of time on the Y-axis. Flux density is shown by colour. The vertical strip at a phase of 0.7 is the Vela pulsar and the horizontal lines are lightning.

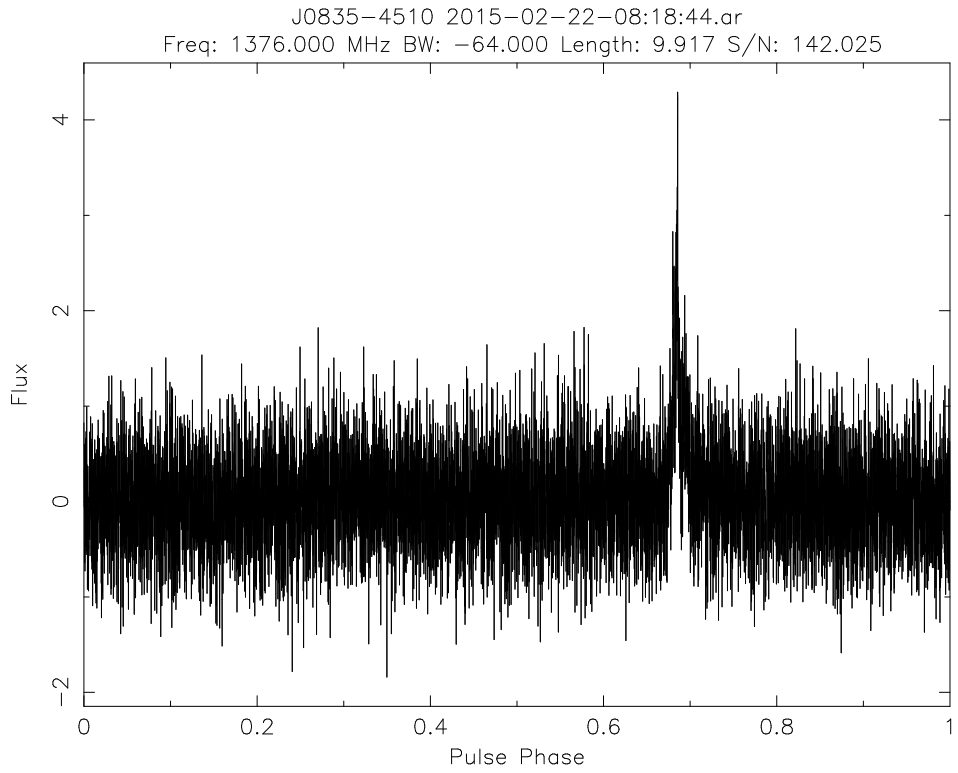

Figure 4.10: A lightning strike sequence (subint 31). This shows a typical single pulse prior to the event. This is a flux density vs time plot with the 89.3 ms period being shown as phase along the X-axis, and flux density (in arbitrary units) are on the Y-axis.

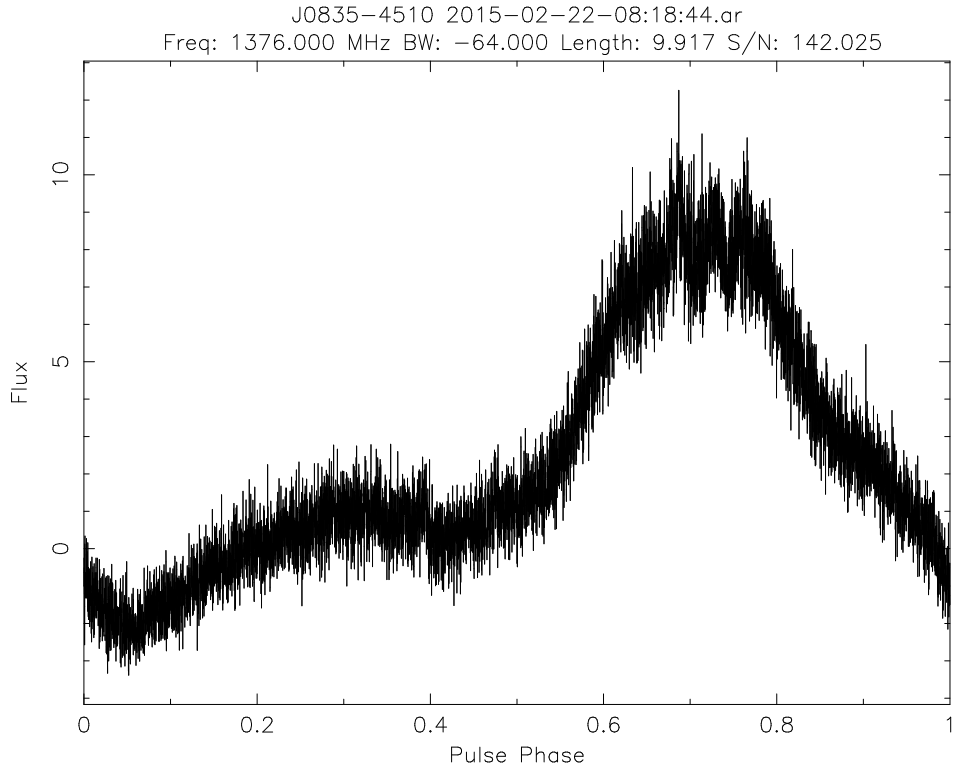

Figure 4.11: A lightning strike sequence (subint 32). This is showing the downstroke.

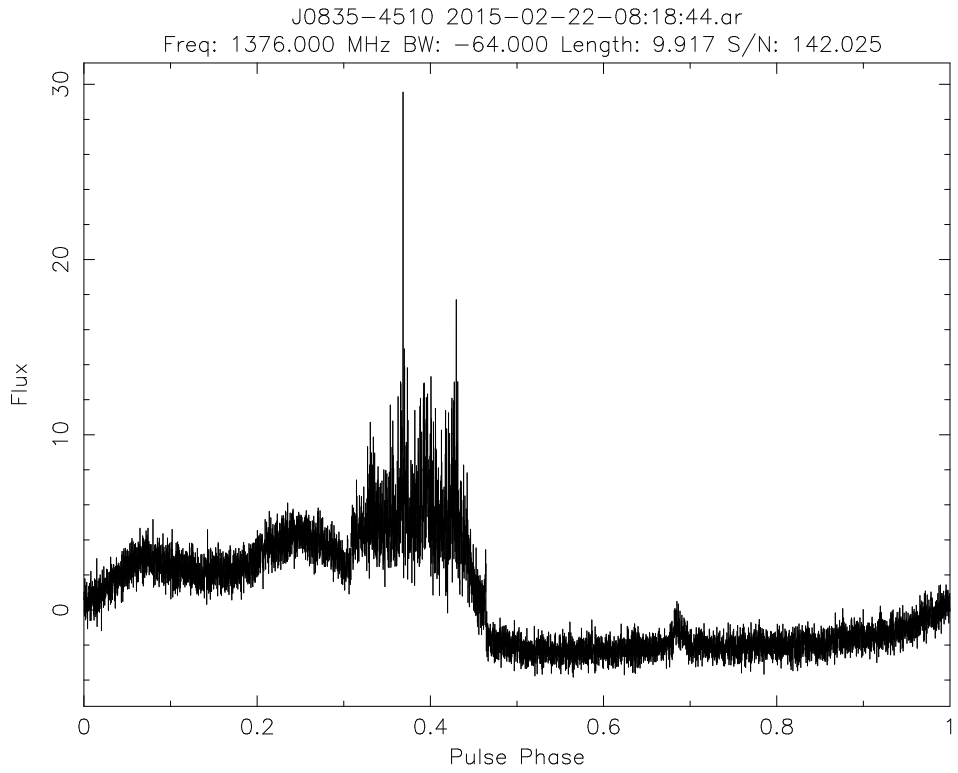

Figure 4.12: A lightning strike sequence (subint 33). This is showing the return stroke. Note the change in scale on the Y-axis and also the Vela pulsar is visible at phase 0.7.

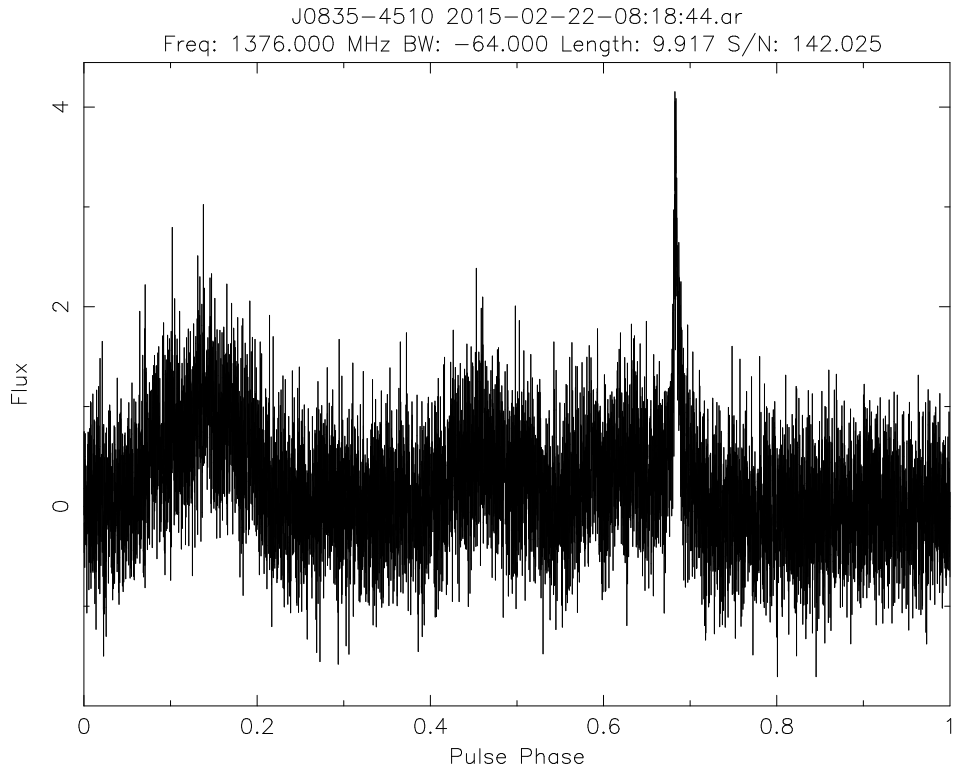

Figure 4.13: A lightning strike sequence (subint 34). This shows the final remnants of the strike, and the Vela pulsar is at phase 0.7.

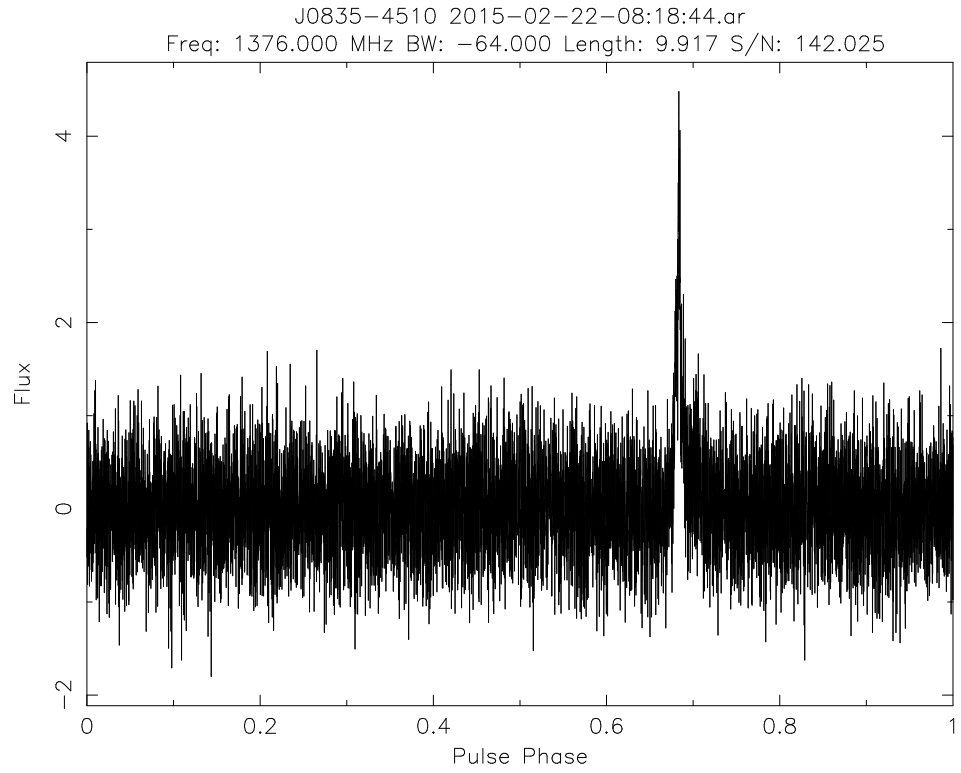

Figure 4.14: A lightning strike sequence (subint 35). This shows a normal single pulsar pulse after the strike.

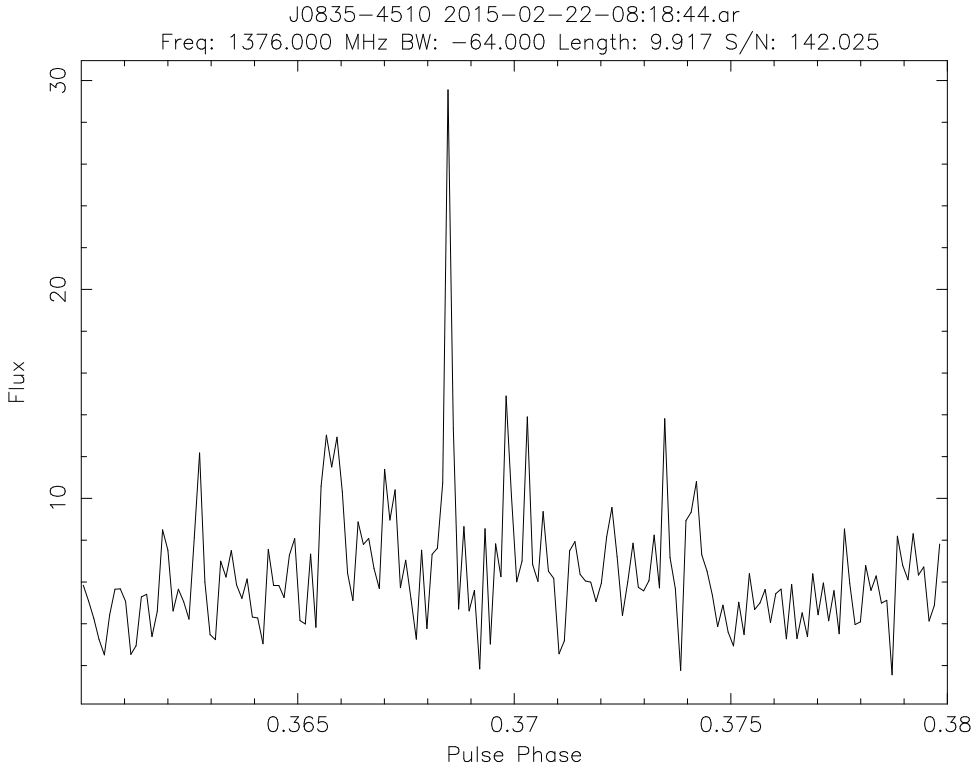

Figure 4.15: This shows a zoomed-in version of the return stroke of a lightning strike from Figure 4.12 on page 63. Resolution is 10.9 μs and the time on the X-axis shown is 0.02 of a pulse period which is 1.78 ms.

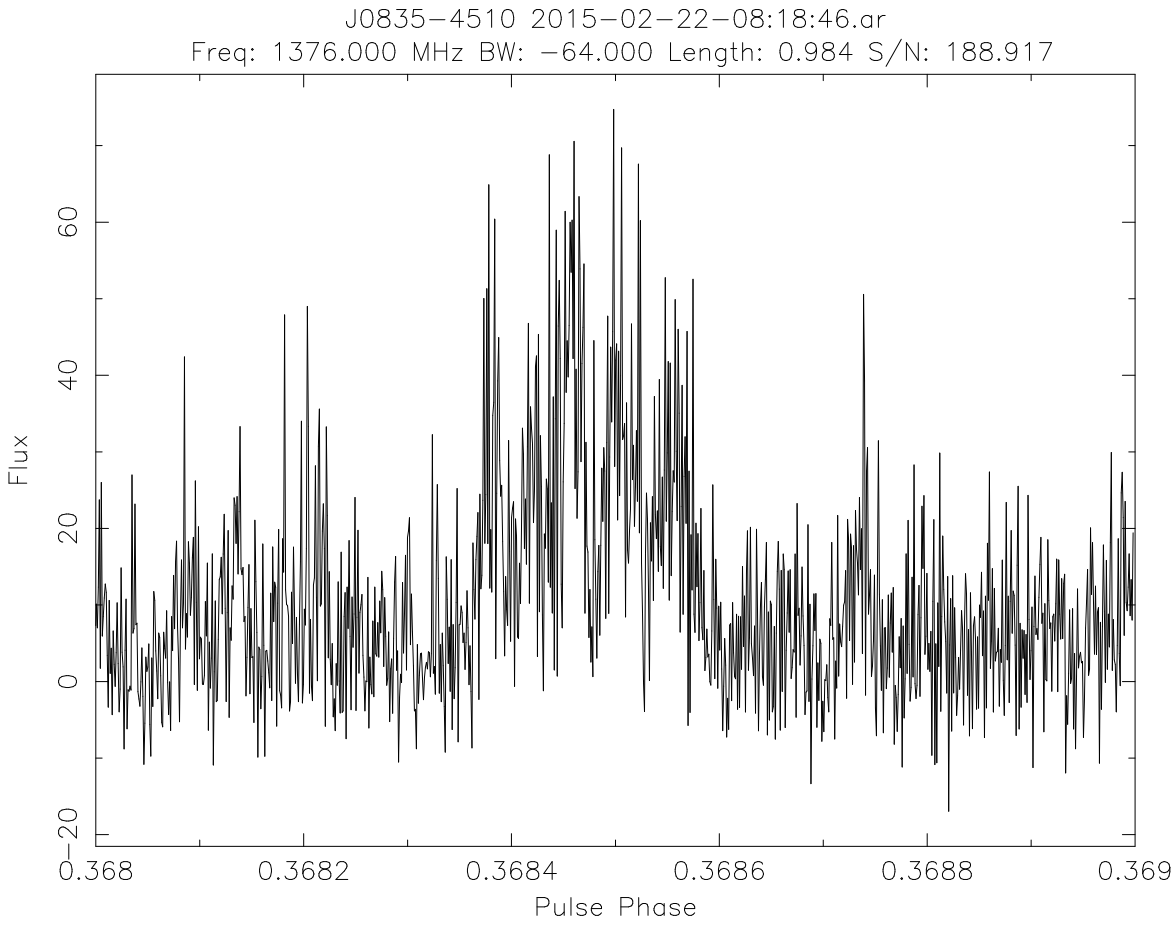

Figure 4.16: This shows an even more zoomed-in version of the return stroke of a lightning strike from Figure 4.12 on page 63. Resolution is 85.2 ns and the time on the X-axis shown is 0.001 of a pulse period which is 89.3 μs.

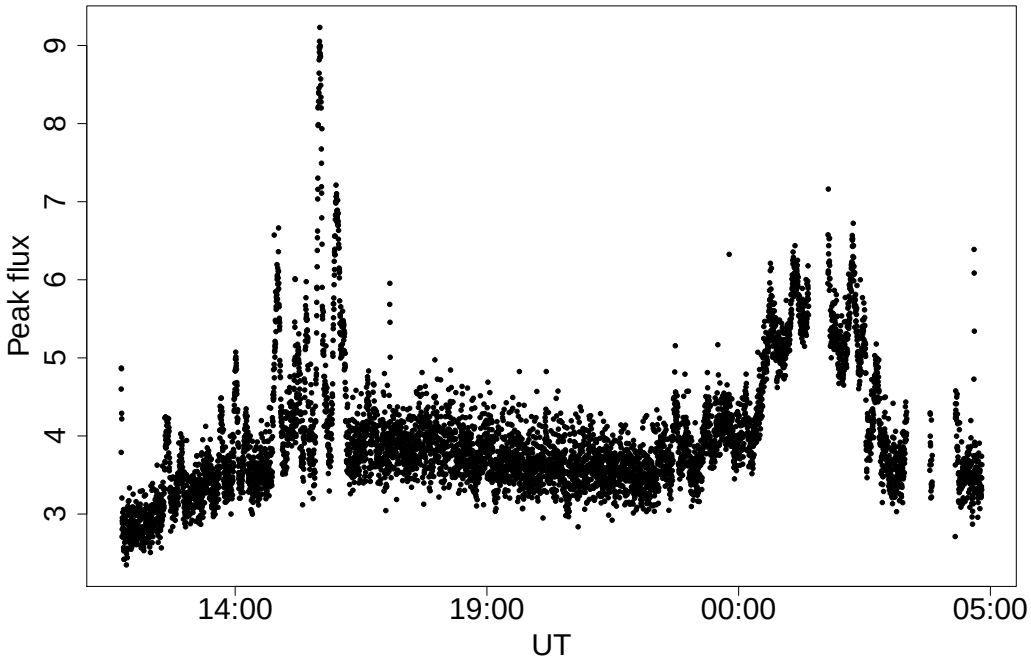

Figure 4.17: Moving average of relative flux density levels throughout a typical 19 h observation of Vela using the 26 m radio telescope at Mt Pleasant. The peak on the left is RFI from Hobart airport and the peak on the right is from Hobart city.

4.5.4 Local transmission towers

Nearby transmission towers and the general Hobart city area sometimes interfere at regular azimuths and elevations. As these are mostly out-of-band RFI these can affect the background flux density levels. Figure 4.17 shows a moving average of relative flux levels for a typical 19 h observation. The two "noisy" areas are when the telescope is pointing over Hobart Airport (left) and Hobart City (right). The one on the right could also be influenced by communications towers on nearby Mount Rumney. These peaks occur in every observation.

4.5.5 Local mobile phones

Certain mobile phone handsets do cause RFI, but which models and carriers is unknown. When large groups of people tour the nearby Grote Reber Museum, and the telescope itself, RFI is typically worse than normal. When University Open Day is held, where thousands of people tour the facilities, most of the day's observations need to be discarded.

4.5.6 Sparking terminal block

Figure 4.18 on page 68 shows a peculiar type of RFI that surfaced on occasions. It appeared to be evenly spread across the 64 MHz of frequencies and of note was that it was $\approx$ 20 ms wide. As the frequency of mains AC power was at 50 Hz this was most likely a spark. As it turned out, on day 287 in 2016, the power to the cryogenic systems failed. The cause was a faulty terminal block on the incoming mains power to the cryogenic power supply. It had been arcing and gradually melting the plastic of the terminal block. Finally it melted through to the metal case and shorted - triggering the circuit breaker. After repair that particular type of RFI disappeared.

4.5.7 Aircraft

A possible source of RFI was aircraft of various types flying through the telescope beam. Whilst this was impossible to verify with commercial flights using Hobart Airport, an opportunity to test whether a helicopter could have an effect was possible. Whilst the author was on a birthday helicopter ride, the pilot was instructed to hover in the beam getting as close as possible to the telescope. The estimate was that the craft was about 30-50 m from the focus cabin and hovered for about 20 s. There was no resultant effect on the Vela observations. Whilst this is not conclusive for all types of aircraft, it was definitive for helicopters.

4.5.8 Unknown

Many different types of unclassified RFI appeared. Some could have been caused by artificial satellites, especially GPS which transmits in L-band.

Radar was also considered as a possible cause, and nearby Hobart Airport was assumed to be the source. Discussions with the operators confirmed that Hobart Airport radars run continuously and since this type of RFI was sporadic it was concluded they were not responsible. Radio communication between boats in the nearby waterways could also cause interference.

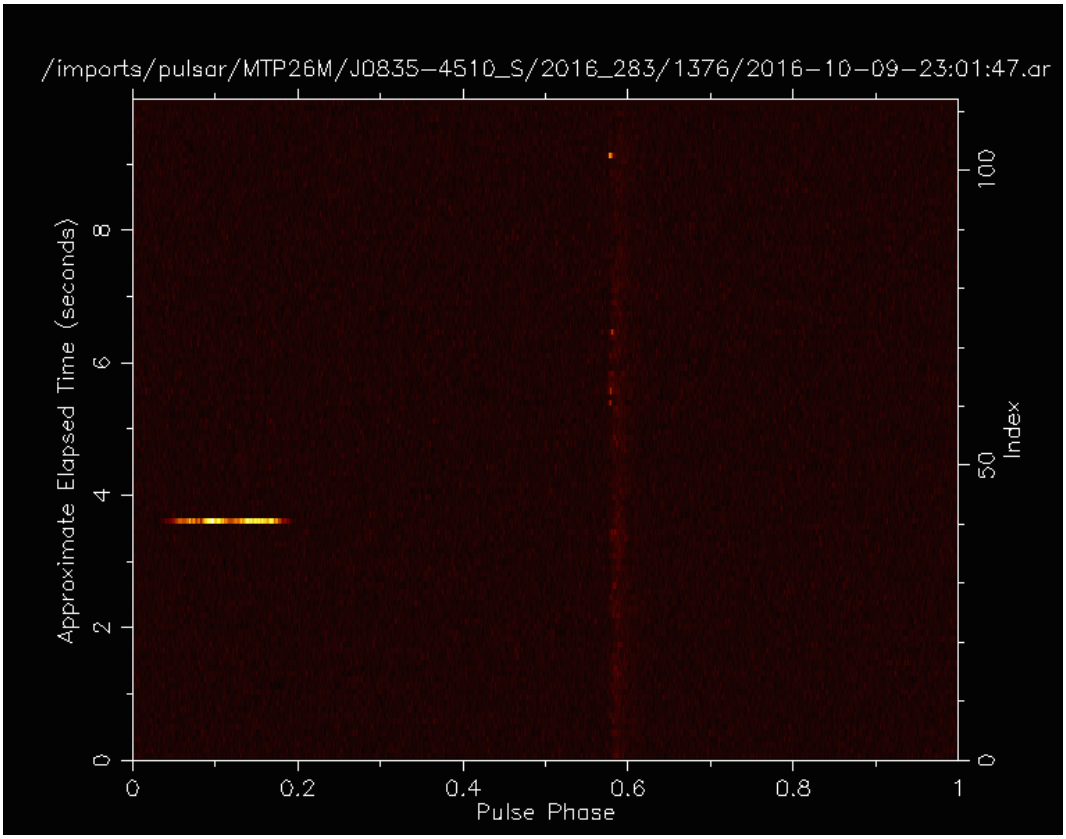

Figure 4.18: Spark RFI caused by a faulty terminal block. This is a time vs time plot with the 89.3 ms period being shown as phase along the X-axis, and 10 s of time on the Y-axis. Flux density is shown by colour. The vertical strip at a phase of 0.6 is the Vela pulsar and the horizontal line of 20 ms duration is the sparking terminal block on an incoming 240 V, 50 Hz line.

4.6 Statistical tools

4.6.1 R

With most of the "heavy" processing completed using DSPSR, PSRCHIVE, TEMPO2, Unix shell scripts, and to a lesser extent some custom C code, the decision was made to use R (R Core Team 2018) for statistical analysis and most of the publication data plotting (Feigelson 2017). Python is another serious contender for this, but the decision to use R was based on the vast amount of statistical packages that are instantly available for use. Secondly, many statisticians know and use R, which is an advantage when needing statistical advice.

R is a vector based language meaning its variables are vectors not numbers (although numbers are simply represented as vectors of length 1). This is a huge advantage when it comes to processing astrophysical data.

Another serious advantage is that R is typically used in interpretive mode (rather than compiled) and is available on all modern platforms, the downloaded libraries work almost universally, and most importantly, *easily*. In the past, interpreters rather than compilers were a huge disadvantage due to speed, but modern hardware has made this disadvantage almost moot.

The plots produced by R are simple to make publication quality. For example the plot in Figure 7.1 on page 144 had the following code to produce a pdf:

```
pdf("newwidth.pdf",width=298/25.4,height=210/25.4)
par(mar=c(5,5,4,2)+0.1)
plot(wg$w50*89.3~wg$mjd,pch=20,cex.lab=2,cex.axis=2,lwd=2,xlab="Modified Julian
   Date",ylab="Width (ms)")
abline(v=microglitches,col="red",lwd=2,lty=3)
dev.off()
```

where the vector `microglitches` contained the dates of observed micro-glitches and the data-frame `wg` contained the columns `w50` and `mjd` which contained pulse width (in units of pulse period) and the modified julian date respectively.

4.6.2 Lomb-Scargle periodogram

Finding repeating patterns in regularly spaced data can be typically achieved by transforming to the frequency domain using a Fourier transform and creating a periodogram. This has a major disadvantage in that the time series must be regular. That is, there can be no missing data points. Unfortunately this is a huge disadvantage for astrophysical data which often has this issue.

The Lomb-Scargle Periodogram was first introduced by Lomb (1976) and refined by Scargle (1982). It finds repeating patterns in time series even if data points are missing. It uses a least-squares approach to search for matching sine waves, and an α level (i.e. p-value) can be provided as a target in certain implementations.

If h_i are the data values at observation times t_i, then power at a particular angular frequency $\omega = 2\pi f$ is:

$$P_N(\omega) = \frac{1}{2\sigma^2}\left(\frac{\left(\sum_{i=1}^{N}(h_i - \bar{h})\cos\left(\omega\left(t_i - \tau\right)\right)\right)^2}{\sum_{i=1}^{N}\cos^2(\omega(t_i - \tau))} + \frac{\left(\sum_{i=1}^{N}(h_i - \bar{h})\sin(\omega(t_i - \tau))\right)^2}{\sum_{i=1}^{N}\sin^2(\omega(t_i - \tau))}\right) \tag{4.7}$$

where the mean

$$\bar{h} = \frac{1}{N}\sum_{i=1}^{N} h_i \tag{4.8}$$

and variance

$$\sigma^2 = \frac{1}{N-1}\sum_{i=1}^{N}(h_i - \bar{h})^2 \tag{4.9}$$

and τ is computed using:

$$\tan(2\omega\tau) = \frac{\sum_{i=1}^{N}\sin(2\omega t_i)}{\sum_{i=1}^{N}\cos(2\omega t_i)} \tag{4.10}$$

The Lomb-Scargle periodogram was initially developed as an astrophysical tool, but has also proved useful in the biomedical sciences (Ruf 1999). It is implemented in R and is publicly available in the standard R repositories. Usage is simple:

```
flux_lsp<-lsp(data$flux, type="period")
```

This plots a graph and stores results in `flux_lsp` for later use if required. Note that this is for a complete set of data points, if data is missing a time vector must be supplied:

```
flux_lsp<-lsp(data$flux, times=data$time, ofac=10, from=100, to=500, type="period")
```

This example also oversamples by a factor of 10 (for more accuracy in periods) and only scans from periods of 100 to 500 to save computing time.

To test the capabilites of the Lomb-Scargle periodogram, we added together three pure sine waves of amplitude 1 and periods of 120, 360, and 2520:

$$y = \sin\left(\frac{2\pi}{120}x\right) + \sin\left(\frac{2\pi}{360}x\right) + \sin\left(\frac{2\pi}{2520}x\right)$$

We set $\alpha = 0.01$ and a Lomb-Scargle periodogram (see Figure 4.19 on page 72) shows three clear signals with the dotted line showing the required p-value. Also note that as the period increases, less data is available for each cycle and so the uncertainty of the signal frequency increases. This can be improved with the `ofac=`n option which sets the oversampling factor, but at the cost of computing time. We plotted the default oversampling factor of 1 and also with an oversampling factor of 10.

Uniform noise was then added at amplitudes of 5, 10, 20, and 30 (see Figures 4.20 to 4.21 on pages 73–74). Once the noise gets to an amplitude of about 20 above the signal, only one of the frequencies remains above the $\alpha = 0.01$ level. Note that the signals are still appearing in the Lomb-Scargle periodogram.

Gaussian noise was added with $\mu = 0$ and σ =2.5, 5, 10, and 15 (see Figures 4.22 to 4.23 on pages 75–76). This made approximately 95% of the noise fall within the levels similar to the uniform noise. This time, the LSP successfully extracted the correct frequencies above the $\alpha = 0.01$ level for all but $\sigma = 15$.

The Lomb-Scargle periodogram has a major advantage in being able to extract the periods of repeating data even with data points missing. For this, an extra time vector must be supplied (which is not needed if no data points are missing). Figures 4.24 to 4.25 on pages 78–79 show a matrix of Lomb-Scargle periodograms with Gaussian noise of various levels (σ=0, 2.5, 5, 10, and 15) along with various numbers of random data points (0, 1000, 2000, 5000, and 9000) out of the initial 10000 being *removed*.

The results appear quite remarkable. Even with Gaussian noise with σ=10, it takes removal of 9000 (out of 10000) data points before the sinusoid signals disappear completely. With less amounts of noise, missing data points seem to have little effect.

The major *disadvantage* of the Lomb-Scargle Periodogram is computation time which is stated to be O(n^2) (with no oversampling). Ruf (1999) states that it is much slower than other popular methods and so Press and Rybicki (1989) introduced an improved algorithm that is O(nlog(n)). This was essential because in 1989 anything approaching 10^4 points required a supercomputer. Of course this has become less of an issue as computational power has improved many millions of times since Lomb published his original paper in 1975.

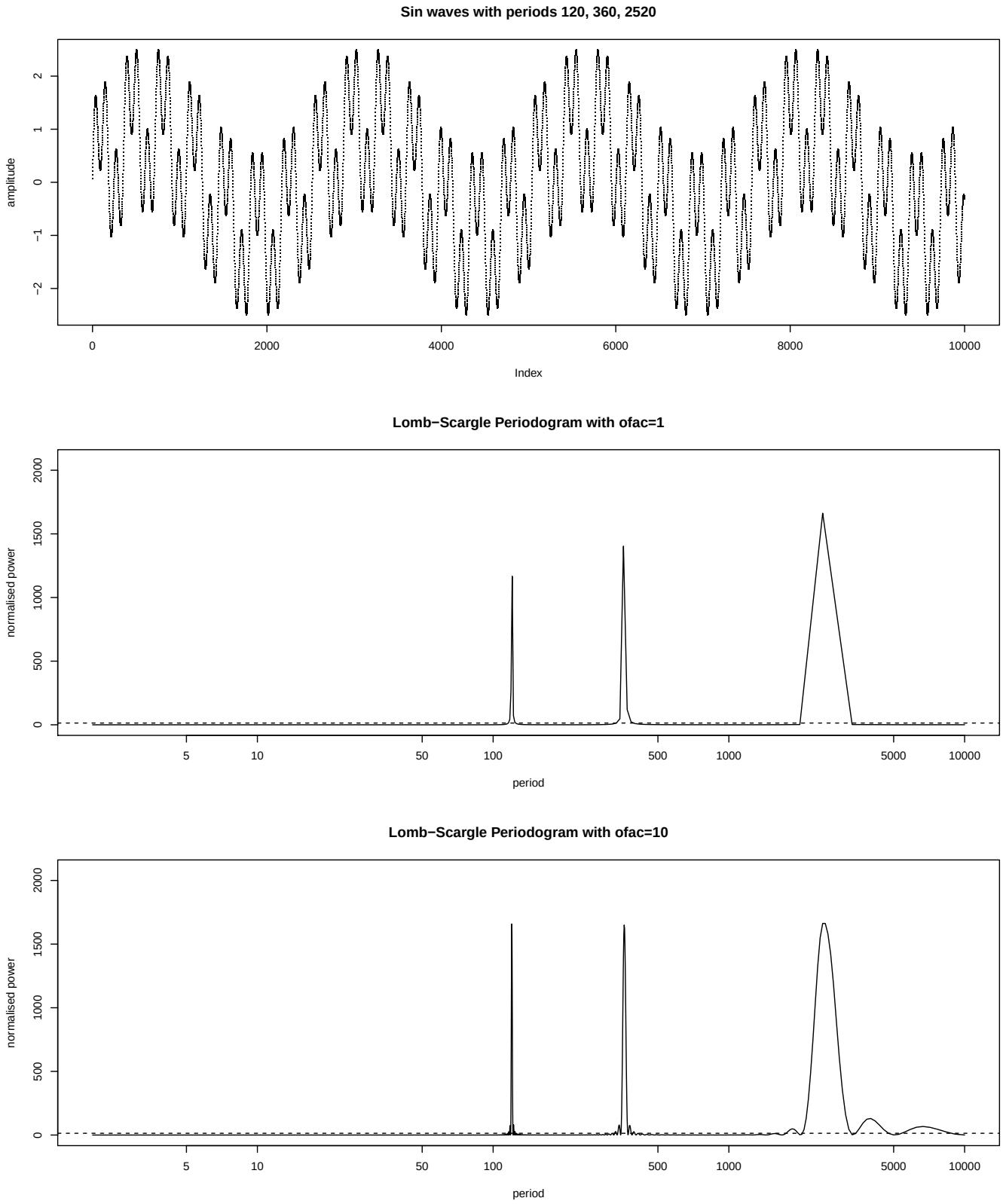

Figure 4.19: Lomb-Scargle periodograms (LSP) of sinusoidal waves with multiple periods. The top panel shows the source data of three sine waves combined. The middle panel shows the LSP of the source data, and the bottom panel also shows the LSP, but with 10× oversampling.

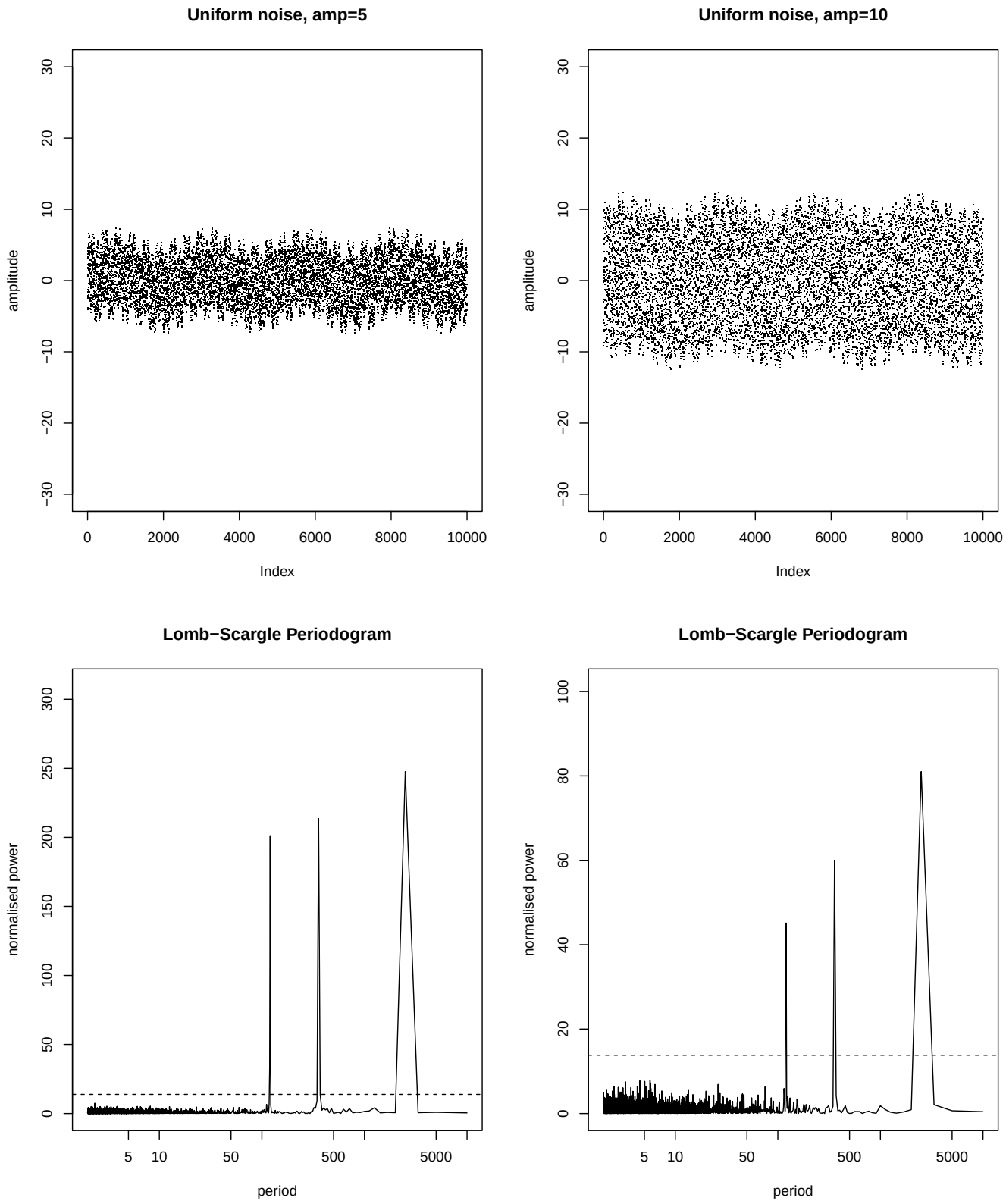

Figure 4.20: Top panels show source data of three sine waves combined, but with uniform noise of amplitude 5 (top left) and 10 (top right). The bottom panels show the Lomb-Scargle periodograms of the waveforms above them.

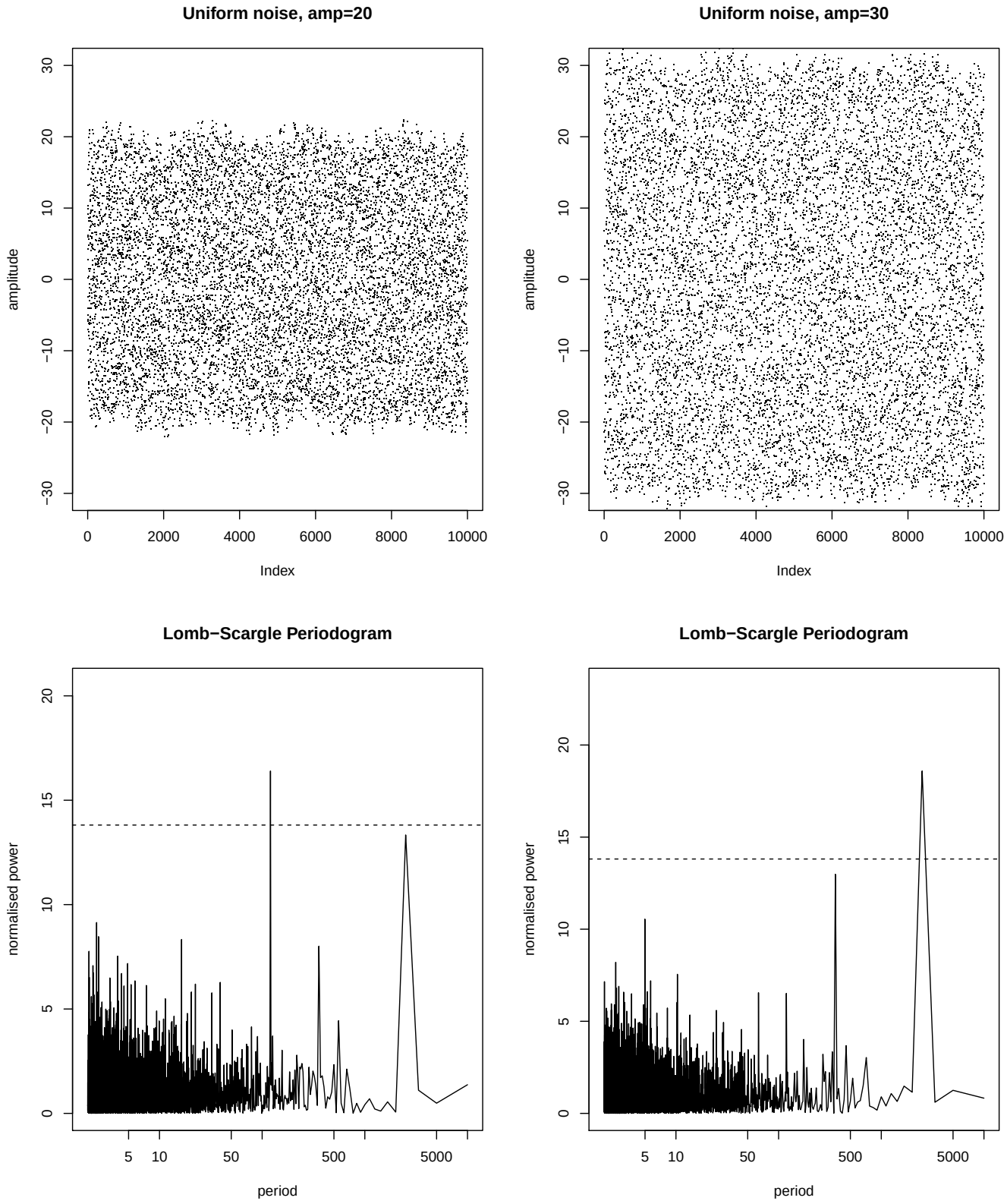

Figure 4.21: Top panels show source data of three sine waves combined, but with uniform noise of amplitude 20 (top left) and 30 (top right). The bottom panels show the Lomb-Scargle periodograms of the waveforms above them.

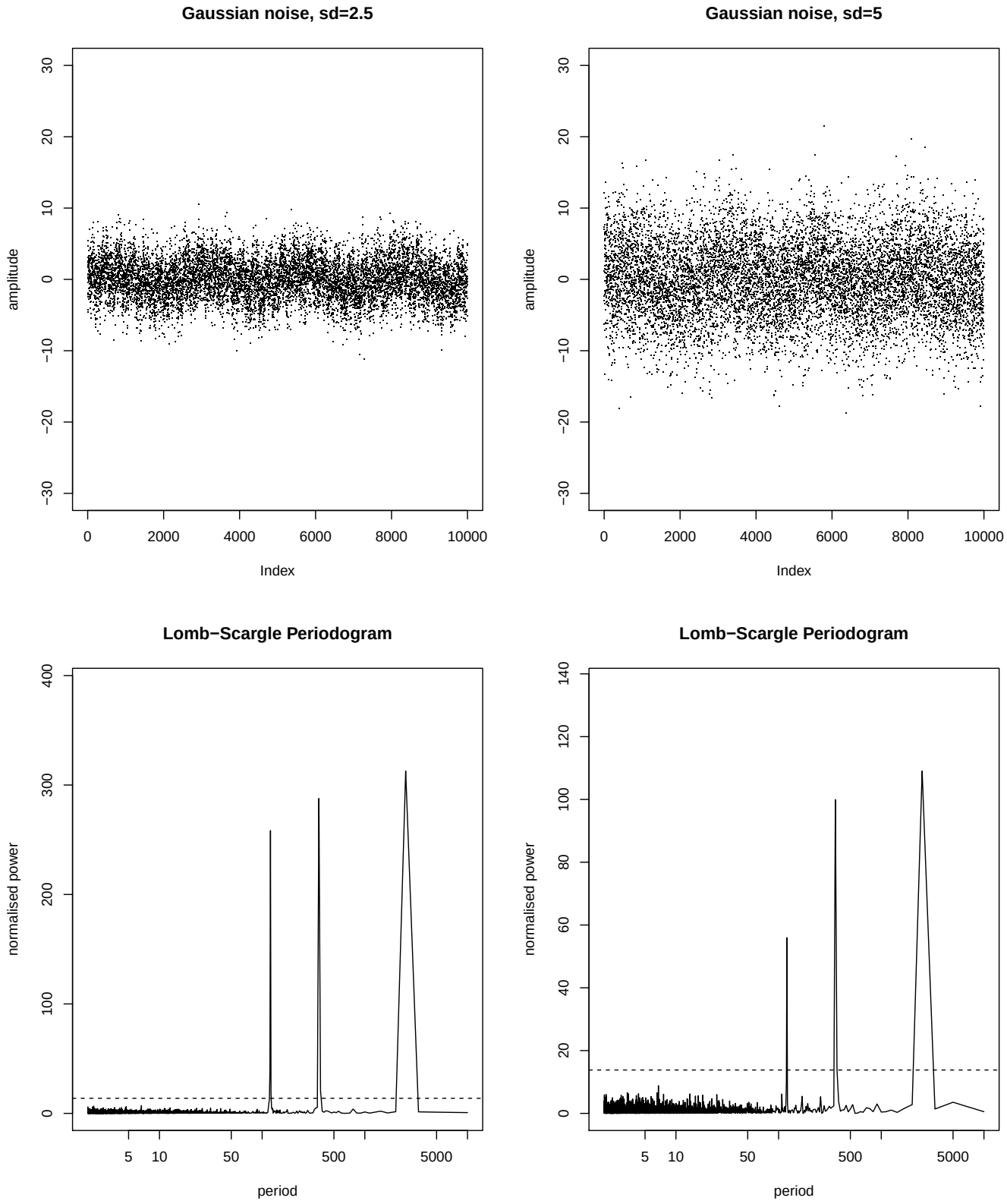

Figure 4.22: Top panels show source data of three sine waves combined, but with Guassian noise of standard deviation 2.5 (top left) and 5 (top right). The bottom panels show the Lomb-Scargle periodograms of the waveforms above them.

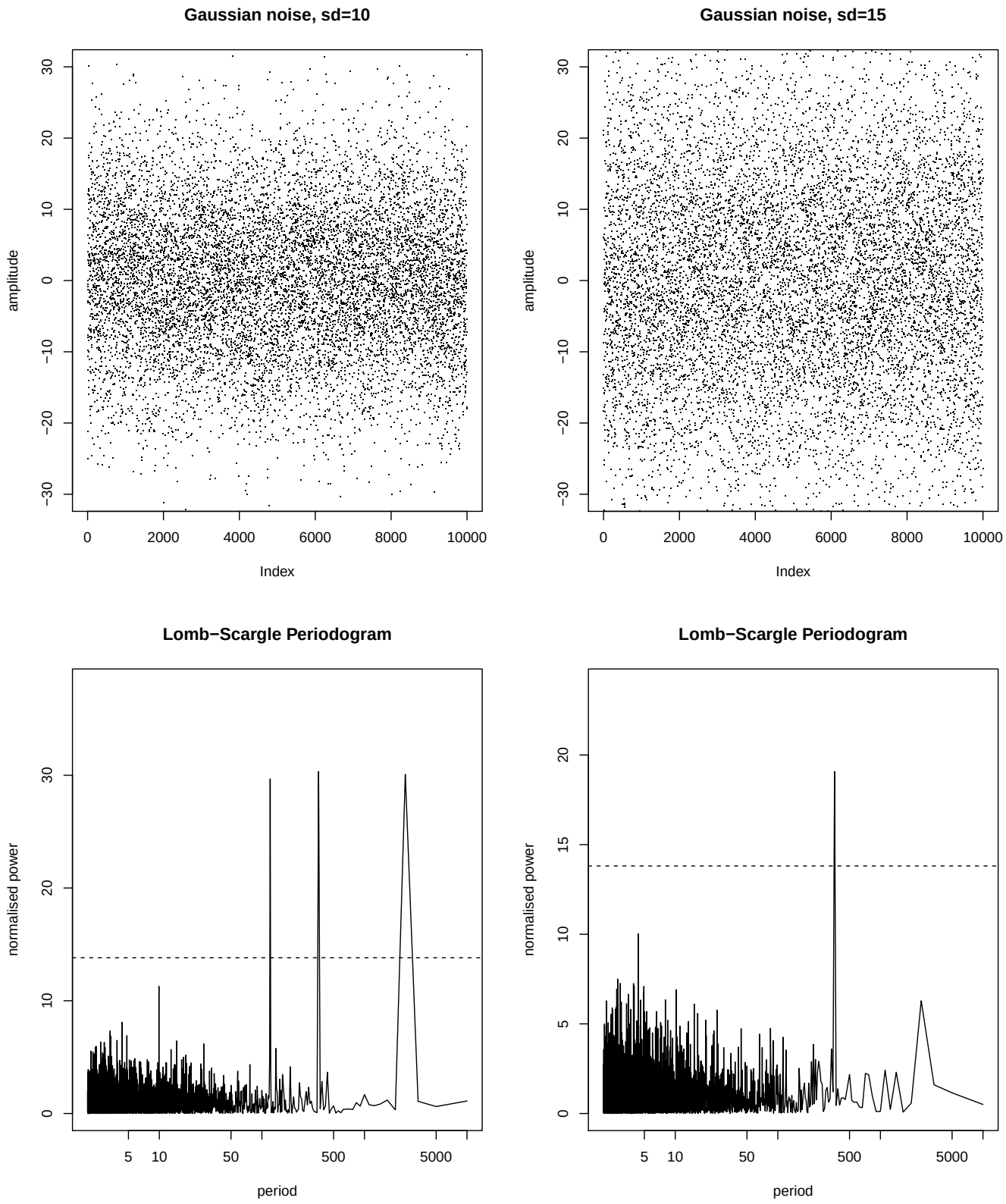

Figure 4.23: Top panels show source data of three sine waves combined, but with Guassian noise of standard deviation 10 (top left) and 15 (top right). The bottom panels show the Lomb-Scargle periodograms of the waveforms above them.

Table 4.7: Computation times for the Lomb-Scargle Periodogram on a 2014 MacBook Pro with a 2.6 GHz i5 CPU and 16 GB of RAM.

Data points	User s	System s	Elapsed s
100	0.032	0.004	0.074
1000	0.078	0.005	0.110
10000	5.598	1.994	7.564
15000	12.538	4.474	16.971
20000	22.696	15.701	38.296
25000	35.434	21.073	56.399
30000	58.578	36.391	325.815
50000	166	84	580
100000	598	261	1585

We measured times (user+system) on a 2014 MacBook Pro with a 2.6 GHz i5 CPU and 16 GB of RAM. These are in Table 4.7 and plotted in Figure 4.26 on page 80. These show that the algorithm implemented in R appears to be the original one with $O(n^2)$. Extrapolating using the fitted curve we predict 10^6 points should take ≈ 22.3 hours and a full day of observations ($> 7.6 \times 10^5$ points) should take ≈ 13 hours. Note that these are user+system times and not elapsed times - which could be up to double.

We conclude that the Lomb-Scargle periodogram is an excellent tool for extracting repeating time series data within noisy environments - even with many data points missing.* Computing time may only become an issue for data sets in excess of 10^5 points.

*It is worth mentioning that there is another major algorithm CLEAN (Roberts et al. 1987) that is widely used. It has not been evaluated in this work.

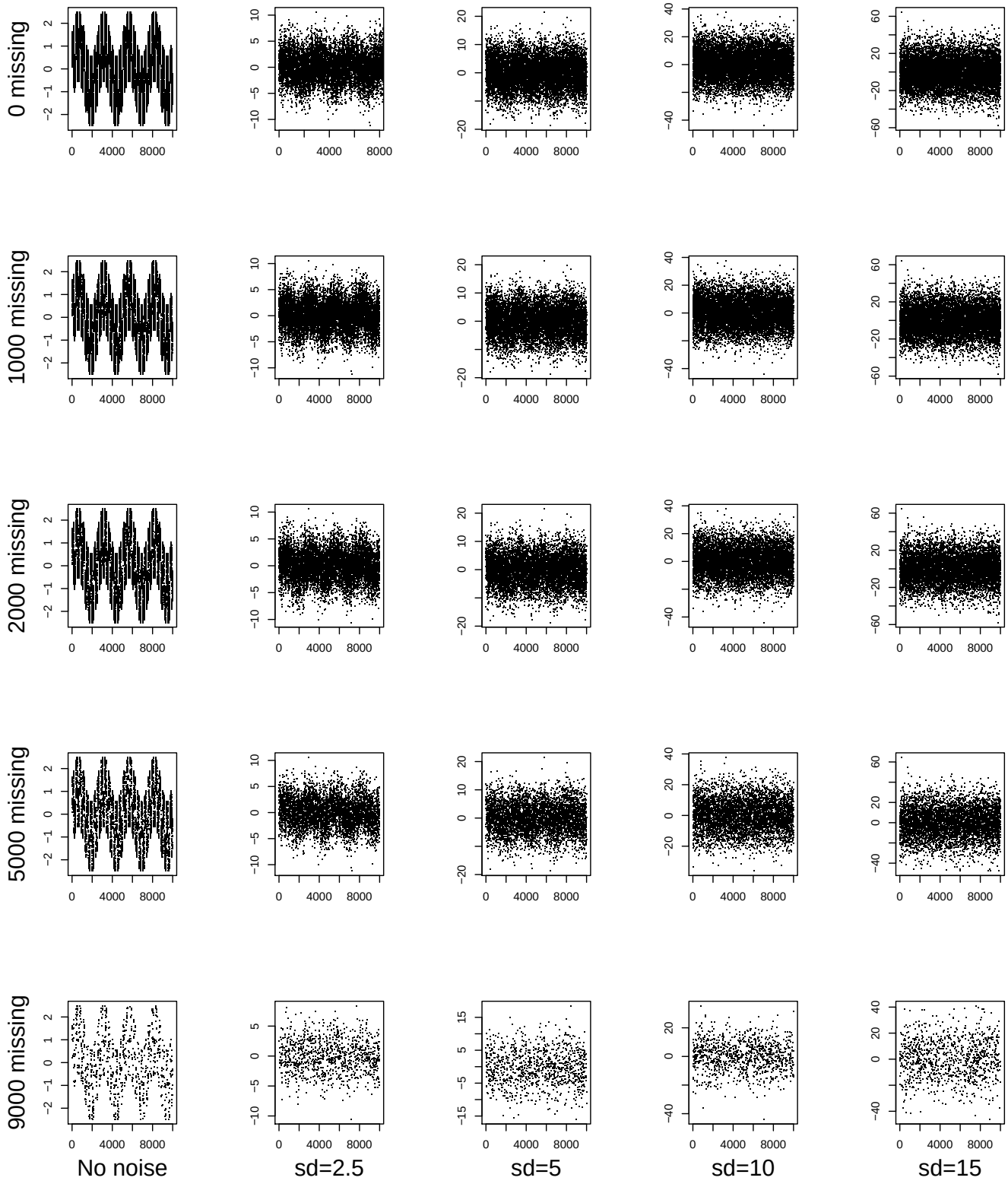

Figure 4.24: Sinusoidal signals with added Gaussian noise of various standard deviations with a number of random data points (out of 10000) being removed.

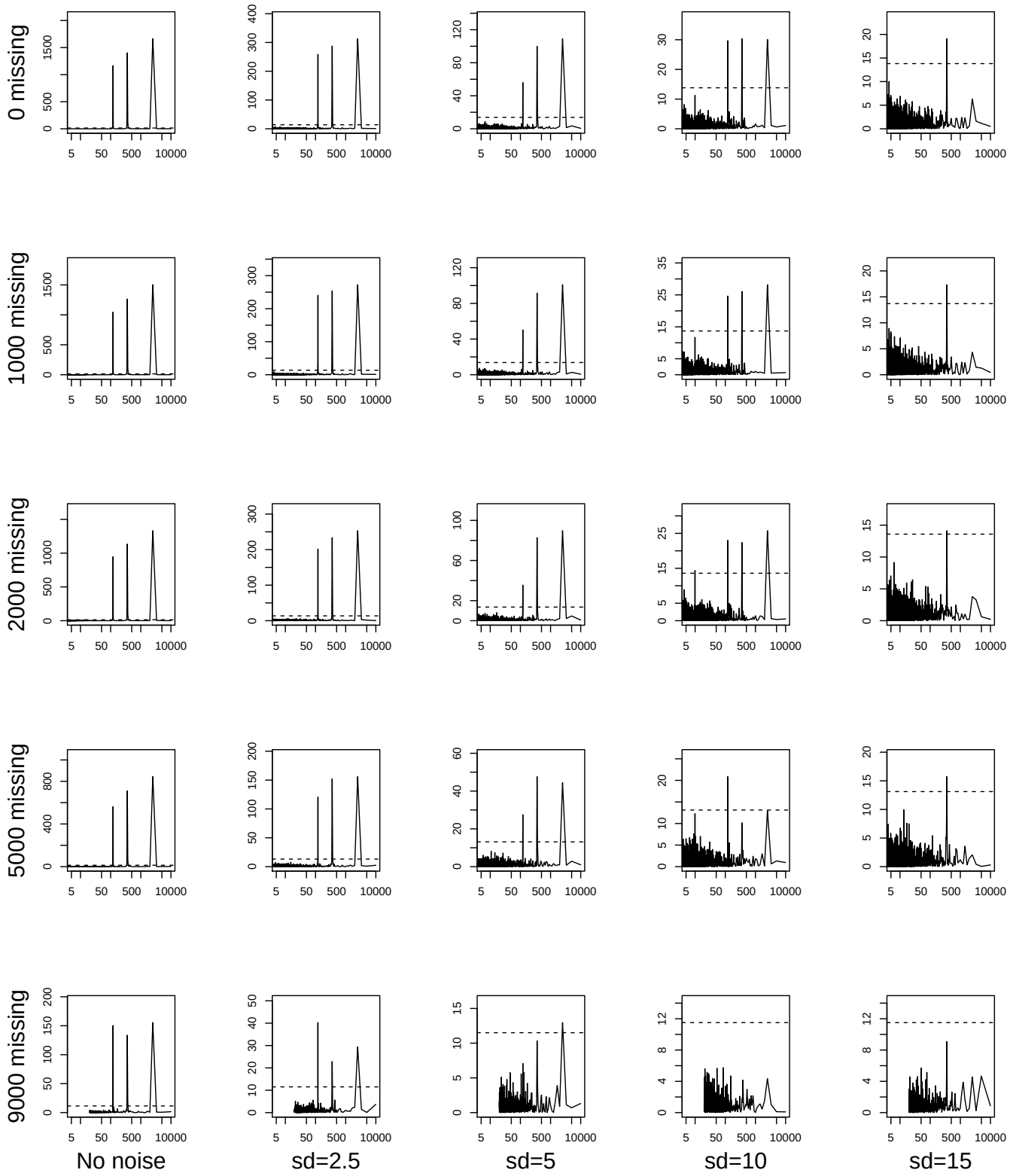

Figure 4.25: Lomb-Scargle periodograms of sinusoidal signals with added Gaussian noise of various standard deviations with a number of random data points (out of 10000) being removed.

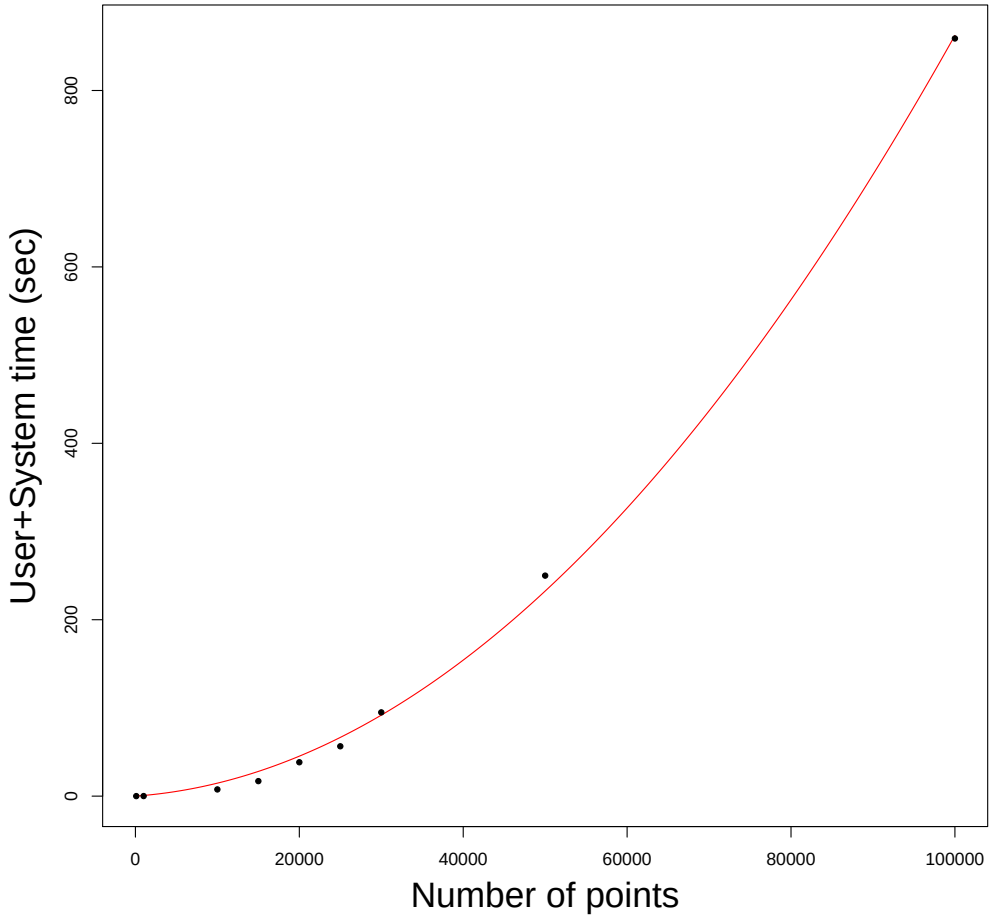

Figure 4.26: Lomb-Scargle periodogram computation times vs. number of data points with no oversampling. The quadratic of best fit is also shown. This shows that the LSP algorithm is O(n^2).

Chapter 5

Bright and giant pulses

5.1 Mount Pleasant observations

5.1.1 Integrated pulse profile flux density variations

The daily integrated pulse profiles of Vela showed a wide variation in peak flux density over a $\approx$ 3 year observing period, but in comparison J1644−4559 showed no such variability. Figure 5.1 on page 82 shows a comparison of average flux densities for both pulsars. This confirmed that the variation in Vela was not equipment dependent, but most likely real. Note that J1644−4559 was typically integrated over 5 hours and Vela over 19 hours. Superimposed with dotted red lines are the micro glitches that occurred in Vela, and the glitch is in blue. There appears to be no apparent pattern with regard to average flux density and micro-glitch occurrence.

However Figure 5.2 on page 82 shows a Lomb-Scargle periodogram of the Vela component (J1644−4559 had no significant periodicities). A number of significant peaks appear with 88 days being the highest. Comparing this with Figure 7.5 on page 146 shows a few potential overlaps, but 88 days is not present.

Interestingly though is the appearance of 78, 99, and 137 days which line up with the possible precessional values discussed in Section 6.3 on page 135.

The variation in average Vela flux densities could be caused by the interstellar medium (ISM), but the scintillation timescale in the direction of Vela is $\approx$ 30 s (Cordes and Lazio 2002) whereas these flux density variations are well above that. The cyclical nature of some of these variations imply that the cause is from the pulsar itself or its immediate surroundings.

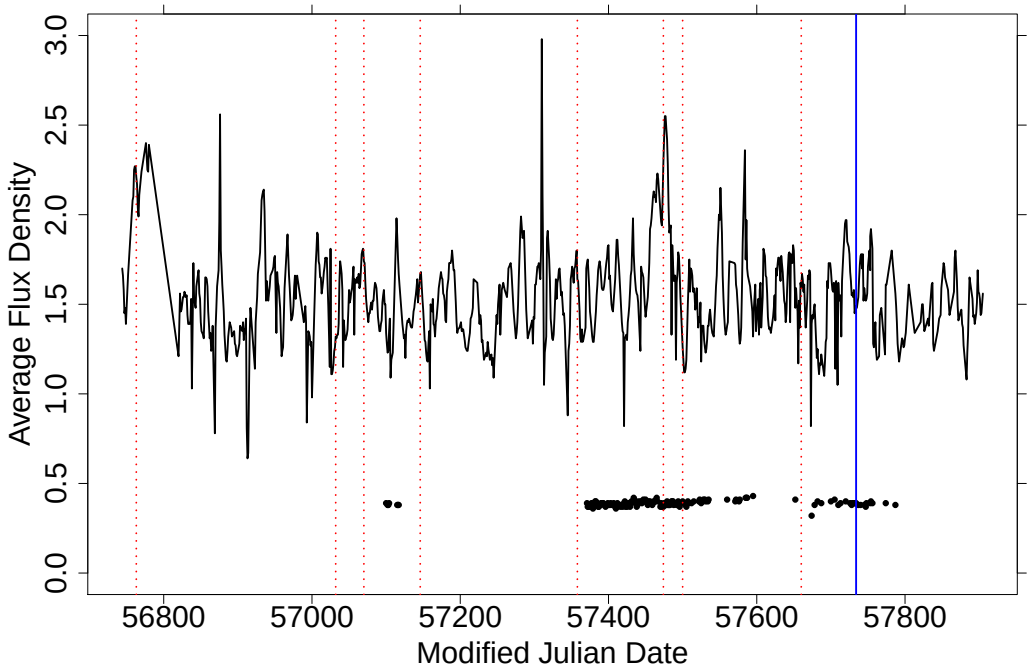

Figure 5.1: Variation in the daily average peak pulse flux density for Vela (top) and J1644−4559 (bottom). Flux density is in relative units. Dashed red lines mark micro glitches, and the solid blue line marks the glitch.

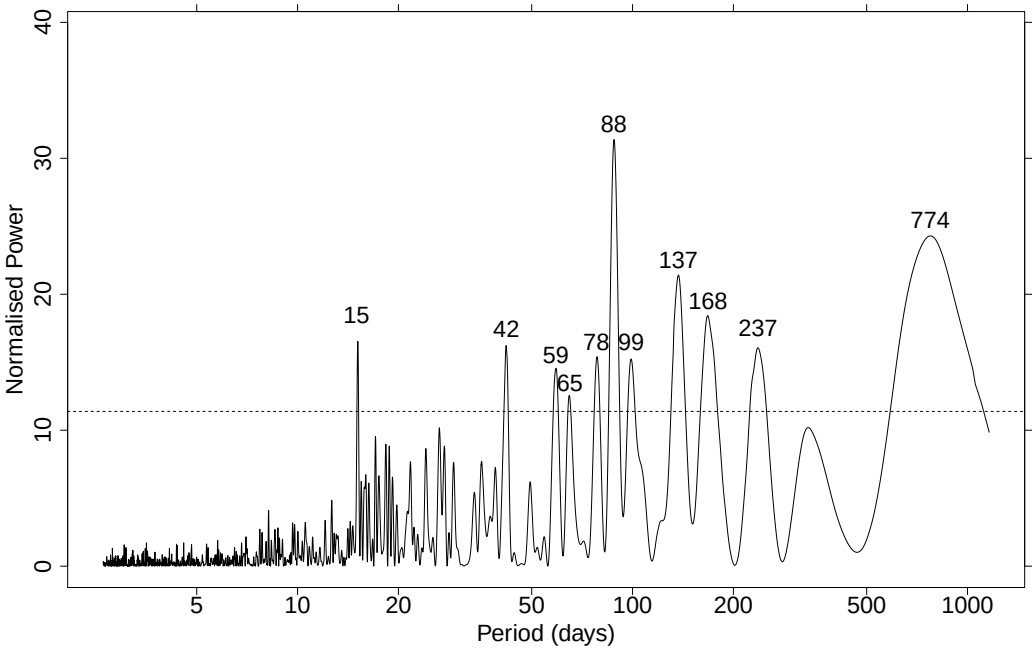

Figure 5.2: Lomb-Scargle periodogram of the Vela component of Figure 5.1.

5.1.2 Individual pulse flux density variations

By collecting such a large data set, we were able to gain statistics on high flux density pulses which have never been obtained before for the Vela pulsar. For measurement we typically used the relative flux scale explained earlier. Flux density calibration has been performed on particular pulses of interest, but calibrating the entire data set is a large computational task.

As a guide, the brightest pulse we observed had a peak of 130 on our relative scale which calibrated to 6000 Jy whereas the mean pulse had a flux density of ≈ 70 Jy.

Figure 5.3 on page 86 shows a histogram of flux density of 3.31×10^8 pulses with a bin width of 0.1 and plotted with and without log scales. As can be seen from the lower left plot, we have what is very close to a log-normal distribution. The top right scale brings out any subtleties that might appear at the higher flux density levels.

By assuming a log-normal distribution and fitting a model, we could potentially make a prediction as to how often a pulse of a given flux density would occur with a Vela-like pulsar.

Using a non-linear model fit in R the equation of best fit for the log-normal graph came to:

$$N = 13.903 \times 10^6 \times \exp\left(-\frac{(x - 0.4653)^2}{0.0335}\right) \tag{5.1}$$

where x is the log of the flux density level (relative units) and N is the number of events of that flux density level expected when observing 3.31×10^8 pulses (approximately a year of continuous observing). This distribution can be used to predict the likelihood of even higher flux density levels than we observed.

As of this writing, Fast Radio Bursts (FRBs) are a current topic and there is much discussion as to their origin (Katz 2016). FRBs are typically a single pulse in radio with a high dispersion measure (DM) indicating extra-galactic origin. Since one FRB has been observed to repeat, young pulsars emitting "super-giant" pulses have been indicated as a possible cause (Cordes and Wasserman 2016).

Caraveo et al. (2001) measured the parallax of the Vela pulsar using the Hubble Space Telescope at 3.4 ± 0.7 mas implying a distance of 294^{-50}_{+76} pc. Note that this is different from the dispersion measure figure of 280 pc shown in Table 3.1 on page 32, but is well within the error bars.

Now simplistically assuming the inverse-square law holds:

$$S = \frac{L_p}{4\pi d^2} \tag{5.2}$$

where S is the observed flux density of the Vela pulsar in Jy, L_p is the pseudo luminosity of the pulsar, and d is the distance in pc. Rearranging and substituting the figures of 6000 Jy (the brightest pulse we observed) and 294 pc we get:

$$\begin{aligned} L_p &= 4\pi S d^2 \\ &= 4\pi \times 6000 \times 294^2 \\ &= 6.52 \times 10^9 \end{aligned}$$

Thus Equation 5.2 becomes:

$$S = \frac{6.52 \times 10^9}{4\pi d^2} \tag{5.3}$$

or rearranging:

$$d = \sqrt{\frac{6.52 \times 10^9}{4\pi S}} \tag{5.4}$$

So using an observed flux density figure of 1 Jy for an FRB (Petroff et al. 2016), we get $d \approx 22.8$ kpc, which is the distance a Vela-like pulsar emitting its brightest giant pulse (observed to date), would have to be at, to have a similar observed flux density level of a median sized FRB. Using the Cordes and Lazio (2002) electron density model,* in the direction of one of the lowest Dispersion-Measure FRBs, the *Lorimer burst* (Lorimer et al. 2007), and the above 22.8 kpc, we get a DM=45 cm^3 pc which is only $\approx 12\%$ of the 375 cm^3 pc observed for the *Lorimer burst*.

Assuming it might be possible for Vela to produce brighter pulses following the log-normal distribution above, we need to find the flux level required at extra-galactic distances.

Now for a hypothetical FRB with an observed flux density of 1 Jy at 500 Mpc we get:

*https://www.nrl.navy.mil/rsd/RORF/ne2001

$$\begin{aligned} L_p &= 4\pi S d^2 \\ &= 4\pi \times 1 \times (500 \times 10^6)^2 \\ &= 3.14 \times 10^{18} \end{aligned}$$

So:

$$S = \frac{3.14 \times 10^{18}}{4\pi d^2} \tag{5.5}$$

and placing our FRB at the distance of the Vela pulsar (294 pc) we would observe a peak flux density of 2.9×10^{12} Jy. This massive figure means that a Vela-like pulsar is unlikely to be the cause of Fast Radio Bursts.

5.1.3 Genuine giant pulses

Bright pulse activity from the Vela pulsar is variable over time (see Figure 7.3 on page 145). At times of high activity, genuine giant pulses are emitted. Figure 5.4 on page 87 shows the brightest pulse we found. Using our relative scale, the peak flux density was just under 130, which equates to approximately 6000 Jy. To examine the microstructure in further detail, we re-processed the original source file using 16384, 32768, and 65536 timing bins (instead of the usual 8192). This gave us a timing resolution of 5.45, 2.73, and 1.36 μs respectively. See Figures 5.5 to 5.7 on pages 88–89.

As can be seen, further microstructure appears as the resolution improves. In Figure 5.8 on page 90 we focused on the peak and reprocessed with 1048576 timing bins each 85.2 ns wide. There appear to be some very short *nanoshots* of very high intensity. A similar pattern was also shown by Hankins et al. (2003) on giant pulses in the Crab pulsar. Their peaks had peak fluxes of $\approx$ 2000 Jy whereas Vela appears to be $\approx$ 18000 Jy. An important difference is that their pulses rise up from a low baseline, whereas Vela's rises up from 6000 Jy, which means these could be just radiometer noise. It should also be noted that Hankins et al. (2003) did have a much better resolution of 2 ns. The only model that they concluded explains the cause of their results was a "*collapse of plasma-turbulent wave packets in the pulsar magnetosphere*".

As a comparison, in Figure 5.31 on page 104 we examined a giant pulse from the Crab using 262144 timing bins (128.68 ns) which is nowhere near the resolution (2 ns) described by Hankins et al. (2003).

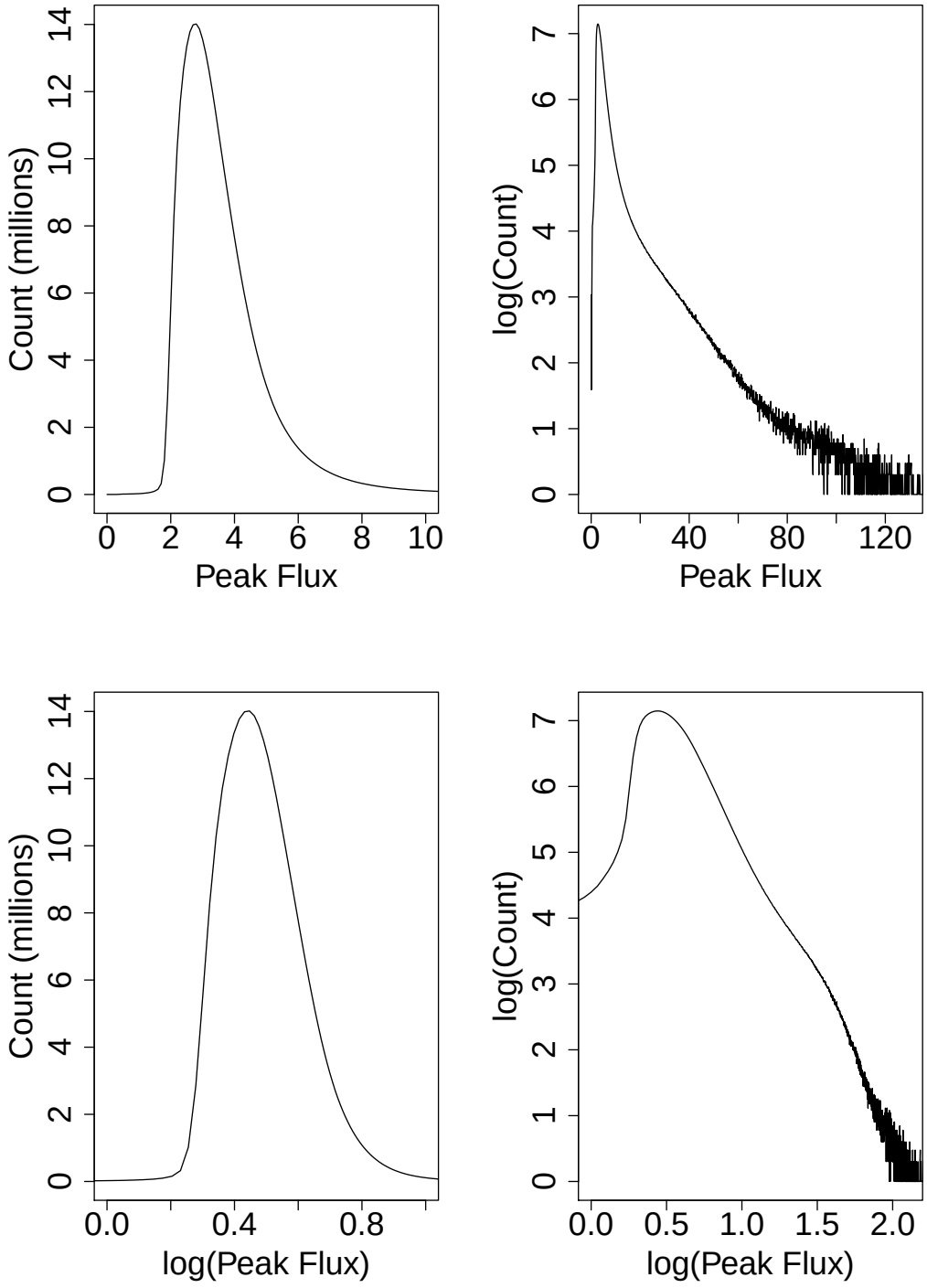

Figure 5.3: Histograms of pulse flux density (relative units) showing a nearly log-normal distribution. Data is from 3.31×10^8 pulses with a bin width of 0.1.

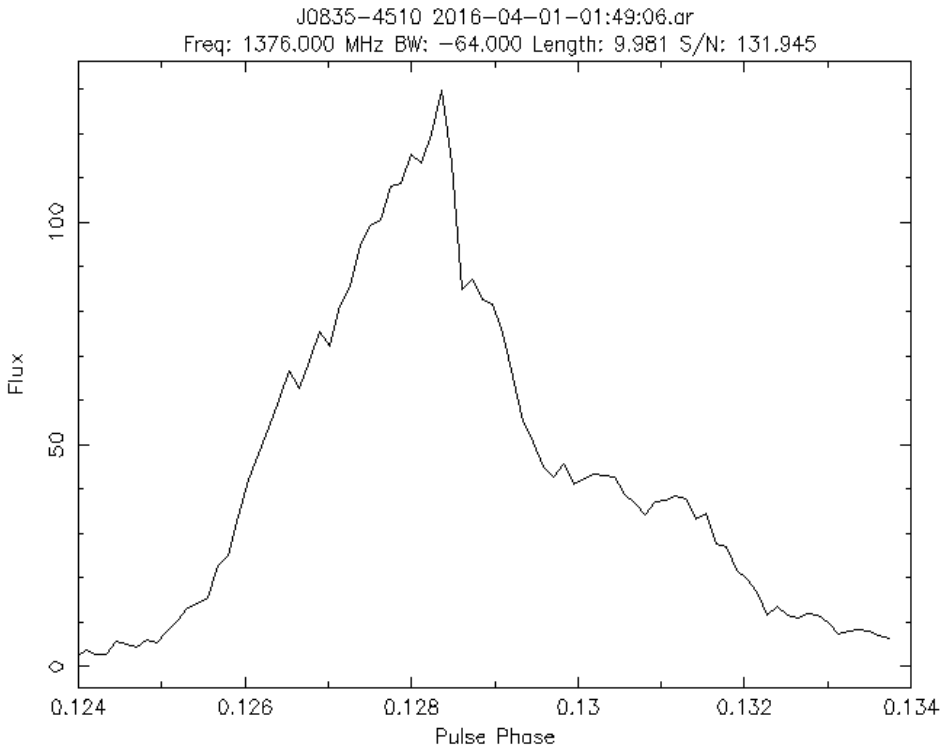

Figure 5.4: The brightest pulse we found, sampled using 8192 bins, each 10.9 μs wide. The X-axis spans 0.01 of a pulse period which is 893 μs.

Figure 5.9 on page 91 shows frequency versus arrival time (reprocessed using 1024 frequency bins) and clearly shows the range of frequencies due to dispersion measure. Figures 5.10 to 5.17 on pages 92–95 show frames of a movie of the arrival of this brightest giant pulse viewing the baseband recording in the frequency domain. The X-axis shows frequency (in bins, highest frequency to the left) and the Y-axis shows power using arbitrary units. Remember that Vela is highly linearly polarised and this is shown by the different powers in each channel. The command to produce this movie was:

```
fauto -n 1000 -N 20 -ymax 30 -s 233000000 PSR_J0835-4510_092_014906.lba
```

As stated earlier, Katz (2017) proposed that FRBs could be an analogy to lightning here on earth, and be a breakdown of the insulating vacuum gap that exists in the pulsar magnetosphere. We have no FRB data to analyse, but it is clear that our giant pulses have no resemblance to our lightning data discussed in Section 4.5.3 on page 59.

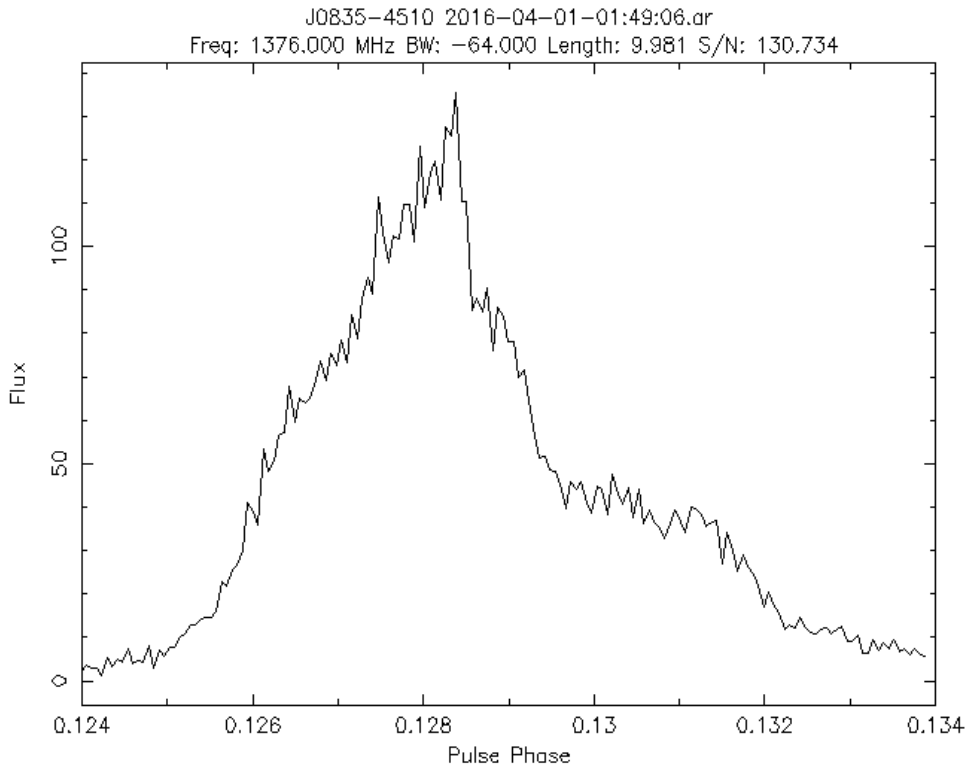

Figure 5.5: The brightest pulse we found, sampled using 16384 bins, each 5.45 μs wide. The X-axis spans 0.01 of a pulse period which is 893 μs.

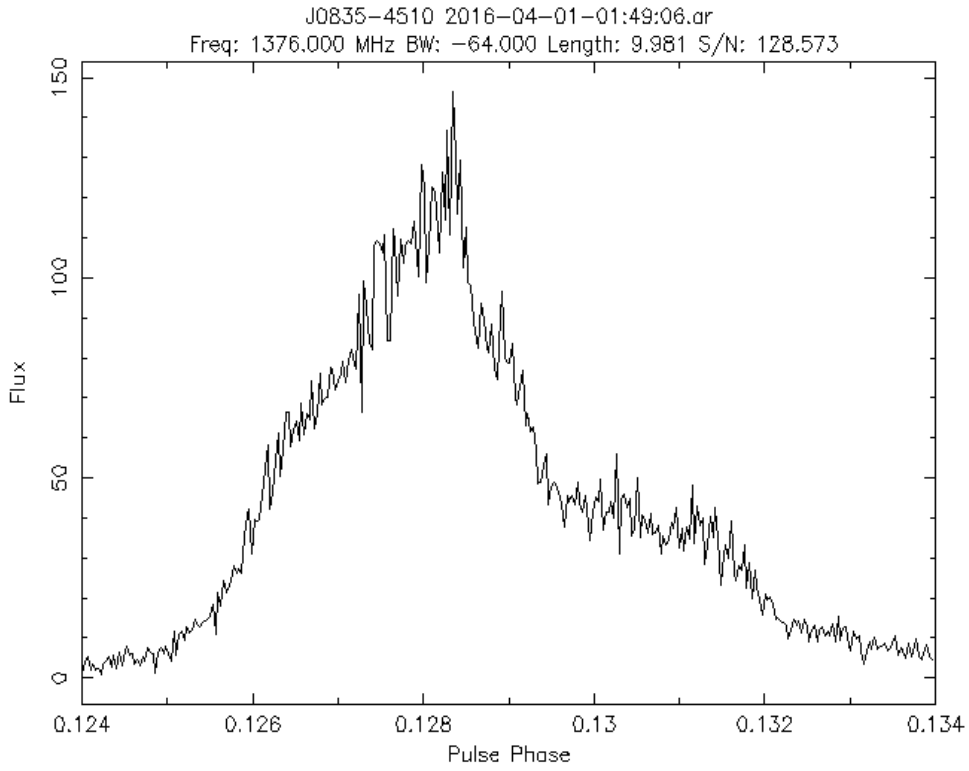

Figure 5.6: The brightest pulse we found, sampled using 32768 bins, each 2.73 μs wide. The X-axis spans 0.01 of a pulse period which is 893 μs.

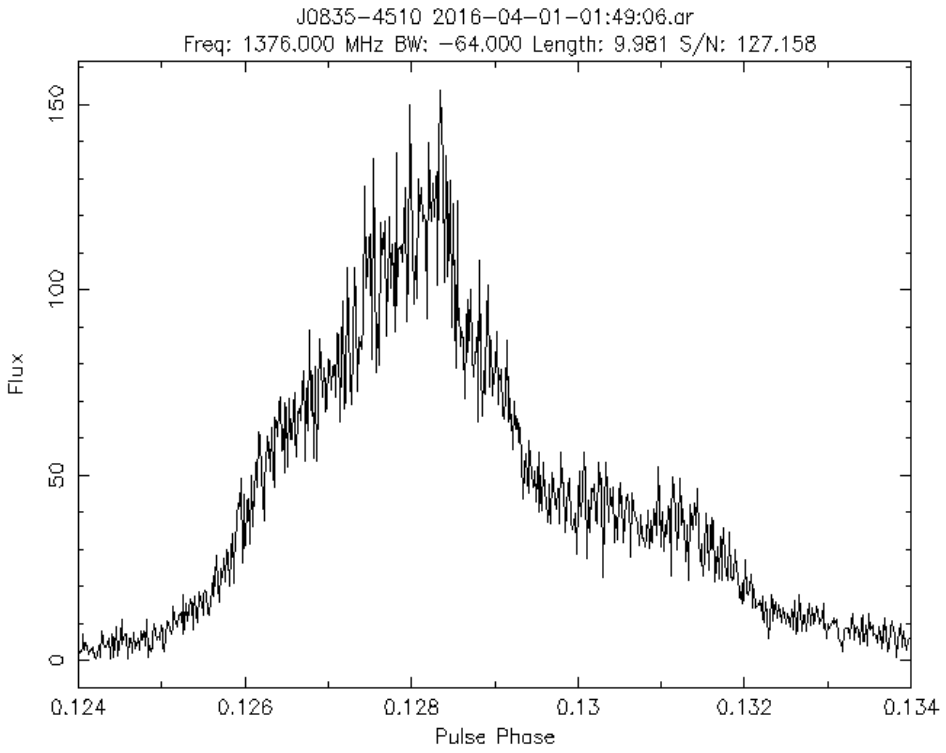

Figure 5.7: The brightest pulse we found, sampled using 65536 bins, each 1.36 μs wide. The X-axis spans 0.01 of a pulse period which is 893 μs.

5.1.4 Consecutive bright pulses

In Palfreyman et al. (2011) (and discussed in Section 3.1.4 on page 36) it was shown that sequences of 6 consecutive bright pulses appeared to occur with billions of times the expected probability, assuming bright pulses were independent events. We have discovered subsequent confirmation of long sequences of consecutive bright pulses as shown in Figure 5.18 on page 96.*

These consecutive pulses appear to drift in phase. Drifting sub-pulses have been analysed by Deshpande and Rankin (2001) in B0943+10 but have not been noted to appear in the Vela pulsar. Figure 5.19 on page 96 shows what certainly could be described as drifting sub-pulses. Figure 1 in Palfreyman et al. (2011) also shows this drift. However, since the drifts appear to occur in both directions a rotating carousel could not explain this. If such a carousel exists then it would have to be oscillating not rotating. With the pulsar precessing (see Sections 6.1 to 6.4 on pages 133–142) emission zones would move in and out of the sight-line as shown in Figure 5.22 on page 98.

Vela being a young pulsar would not be expected to have conal emission - only core emission (Rankin 1990) however it could be possible to have some core outriders

*Thanks to Job Carr-Turbitt for finding this sequence.

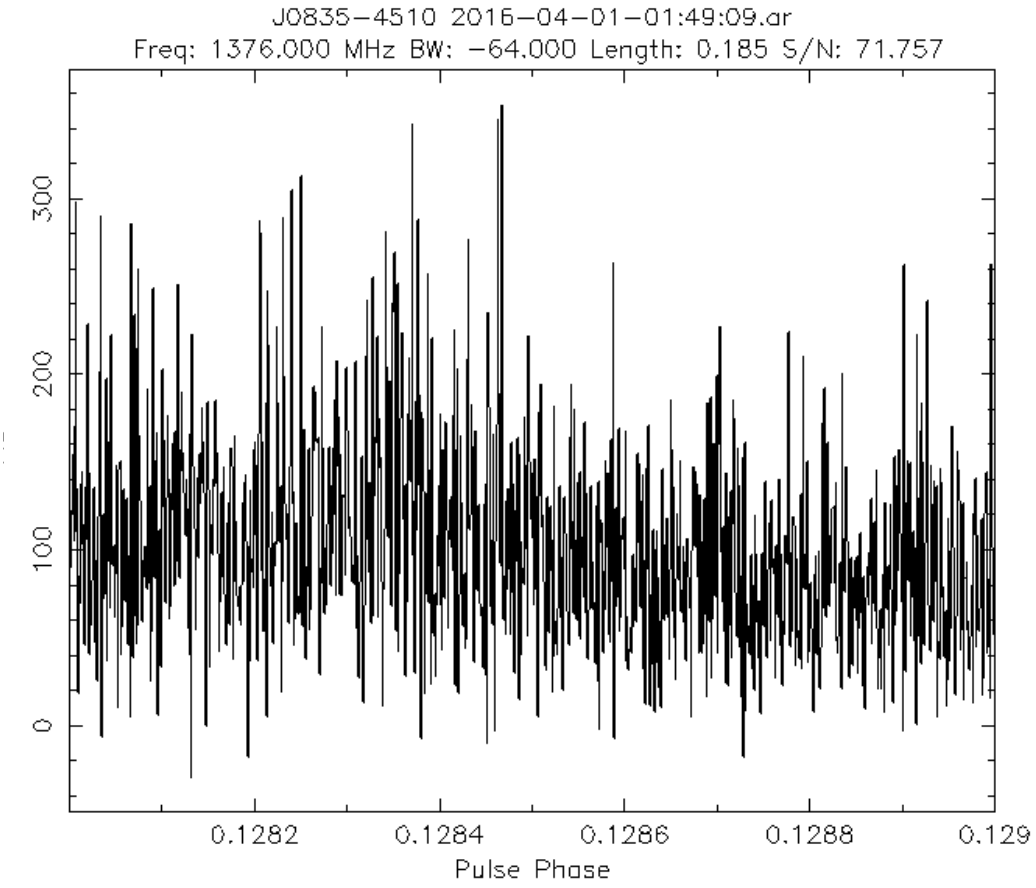

Figure 5.8: The brightest pulse we found, zoomed into the highest peak, sampled using 1048576 bins, each 85.2 ns wide. A filterbank of only 4 frequency channels could be utilised due to computer memory constraints.

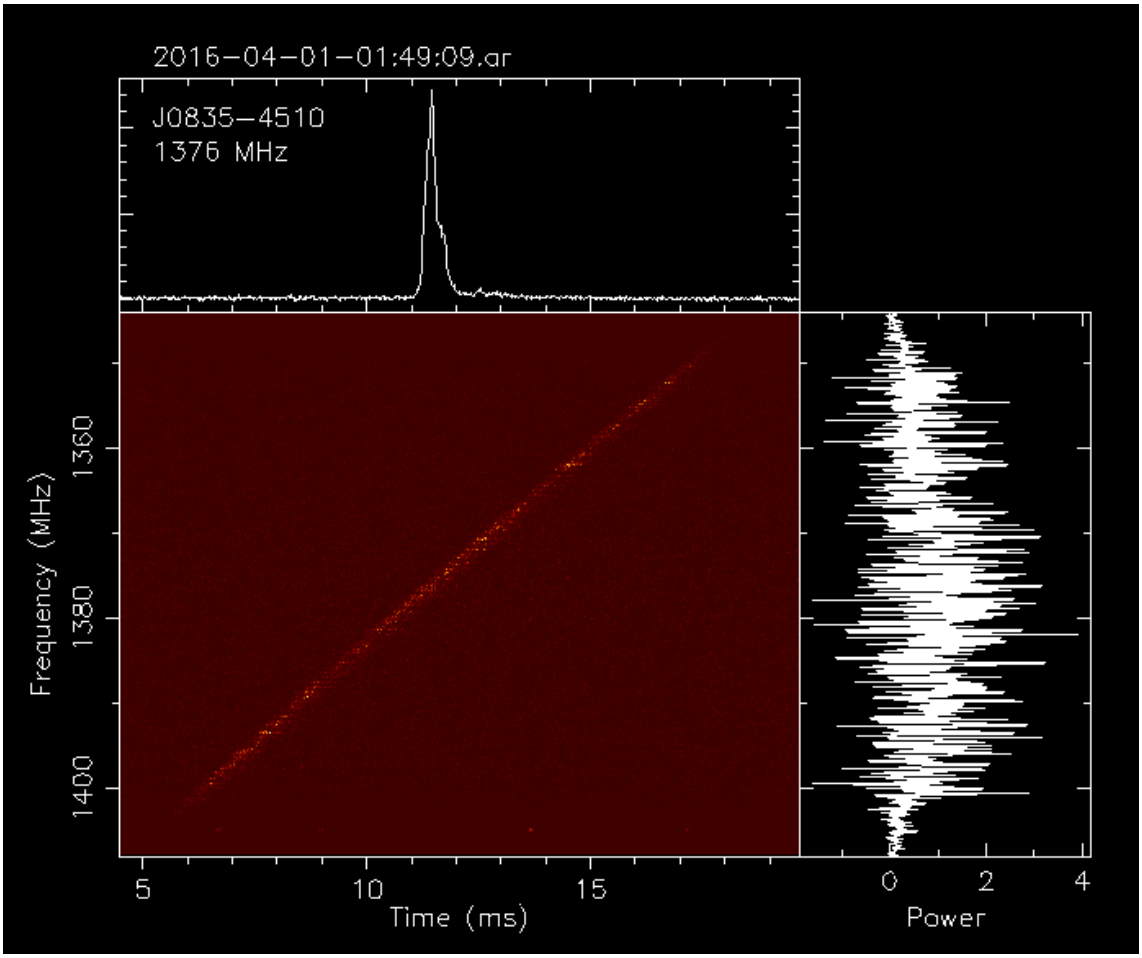

Figure 5.9: Frequency vs Phase of the brightest pulse we found, processed using 4096 timing bins, and 1024 frequency channels. Note that this pulse took about 15 ms to arrive over the 64 MHz bandwidth and the power is evenly spread across those frequencies. The filename is different from previous plots because due to the file's size, processing was commenced part way through the file.

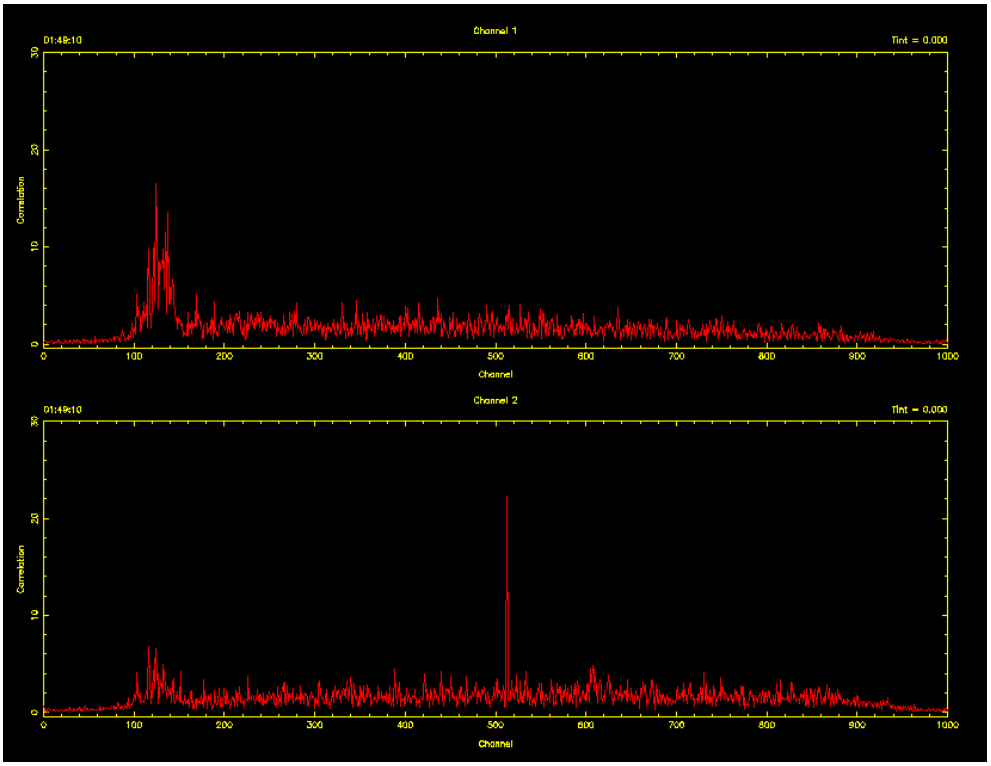

Figure 5.10: Brightest pulse arrival in real time. Frame 1 of 8. The signal at the centre is artificial.

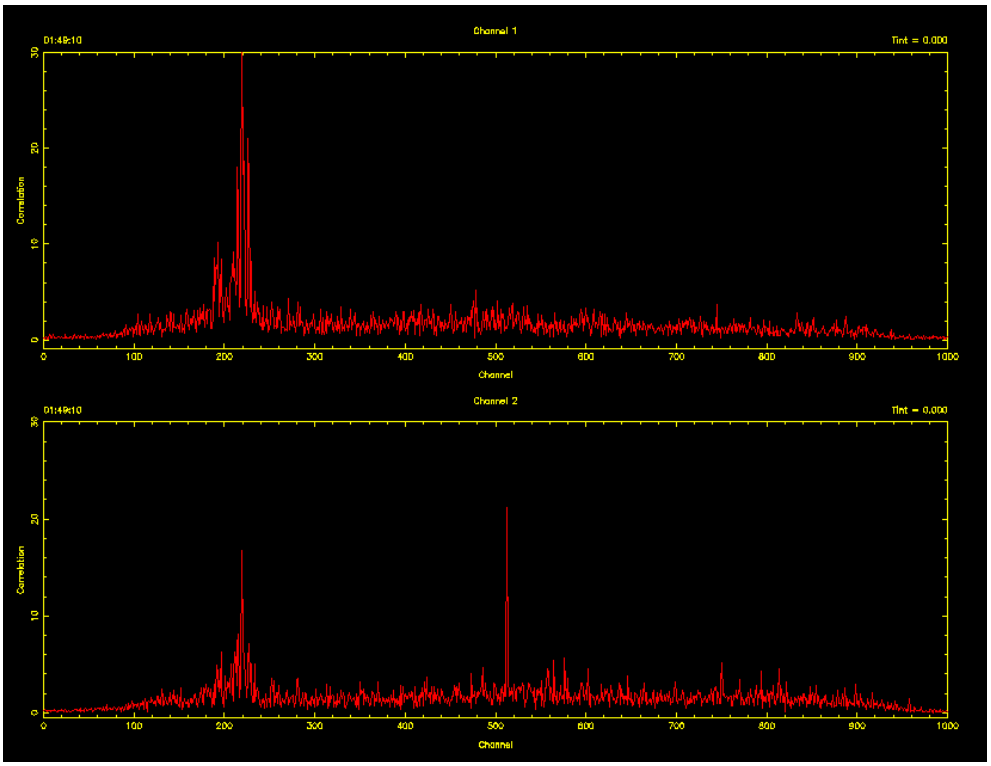

Figure 5.11: Brightest pulse arrival in real time. Frame 2 of 8.

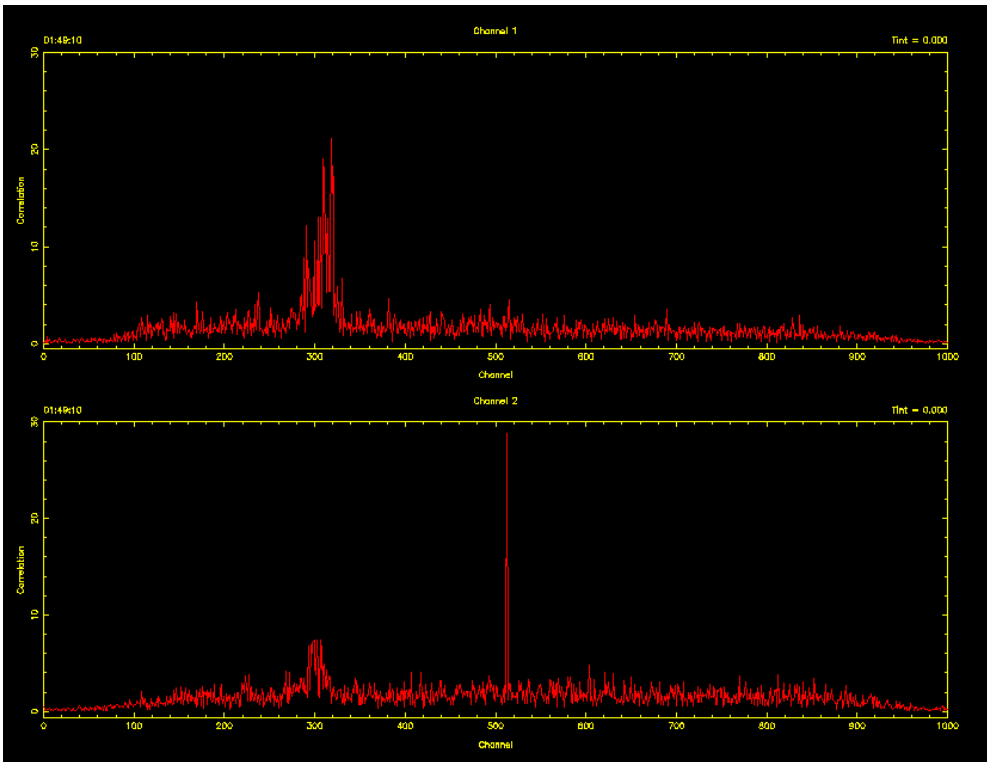

Figure 5.12: Brightest pulse arrival in real time. Frame 3 of 8.

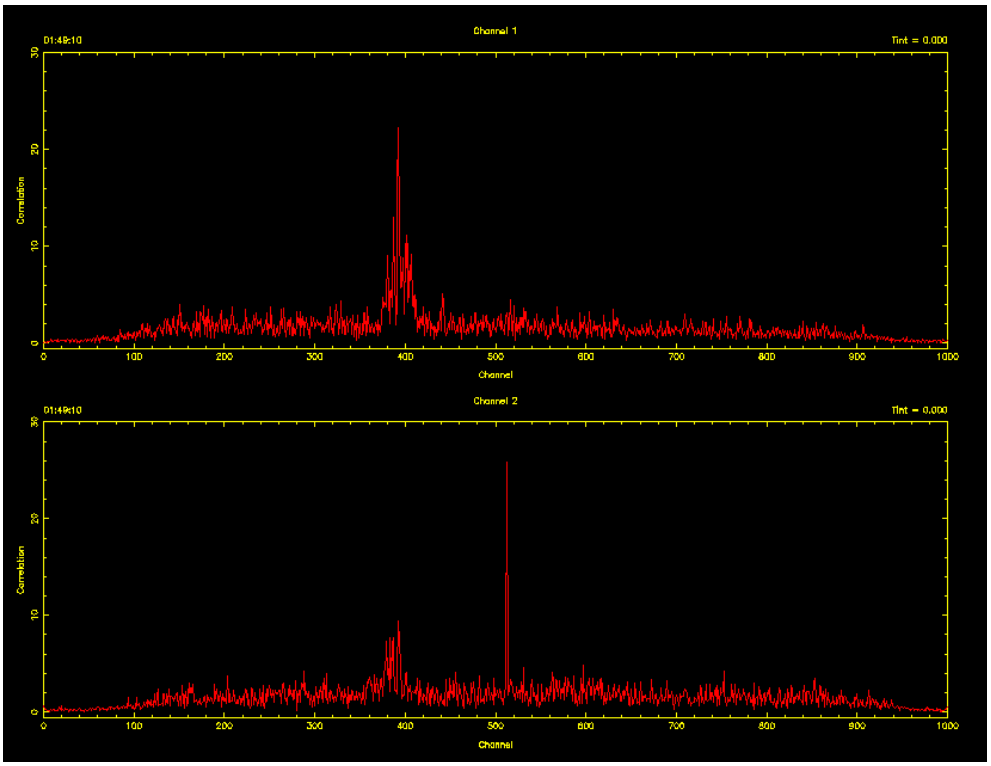

Figure 5.13: Brightest pulse arrival in real time. Frame 4 of 8.

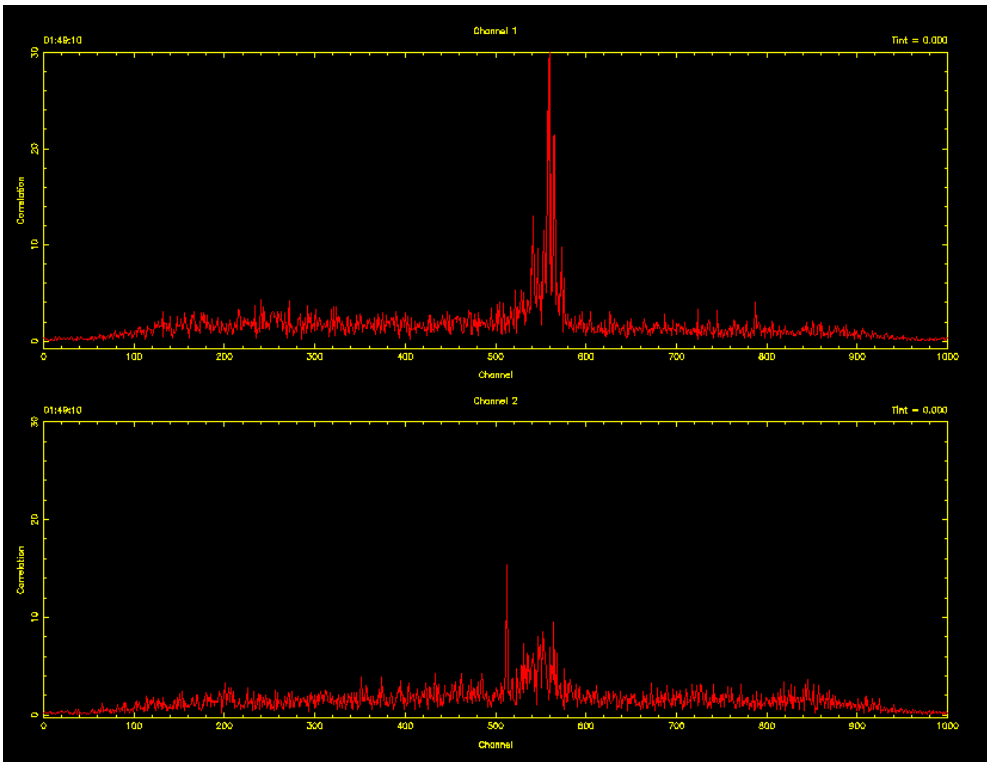

Figure 5.14: Brightest pulse arrival in real time. Frame 5 of 8.

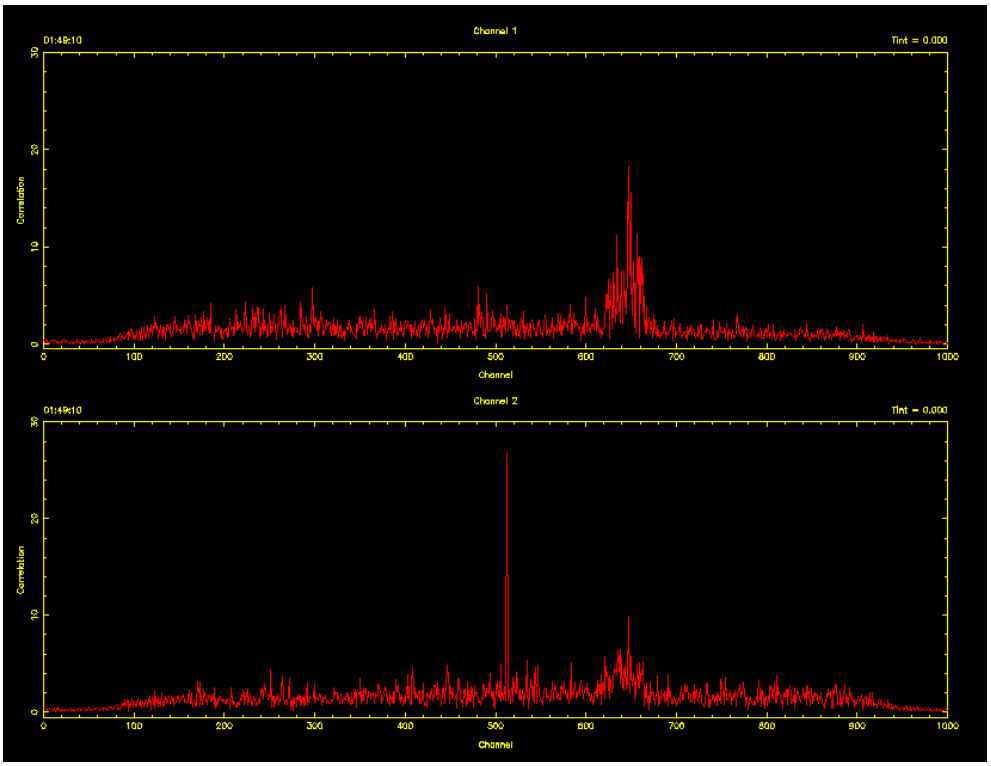

Figure 5.15: Brightest pulse arrival in real time. Frame 6 of 8.

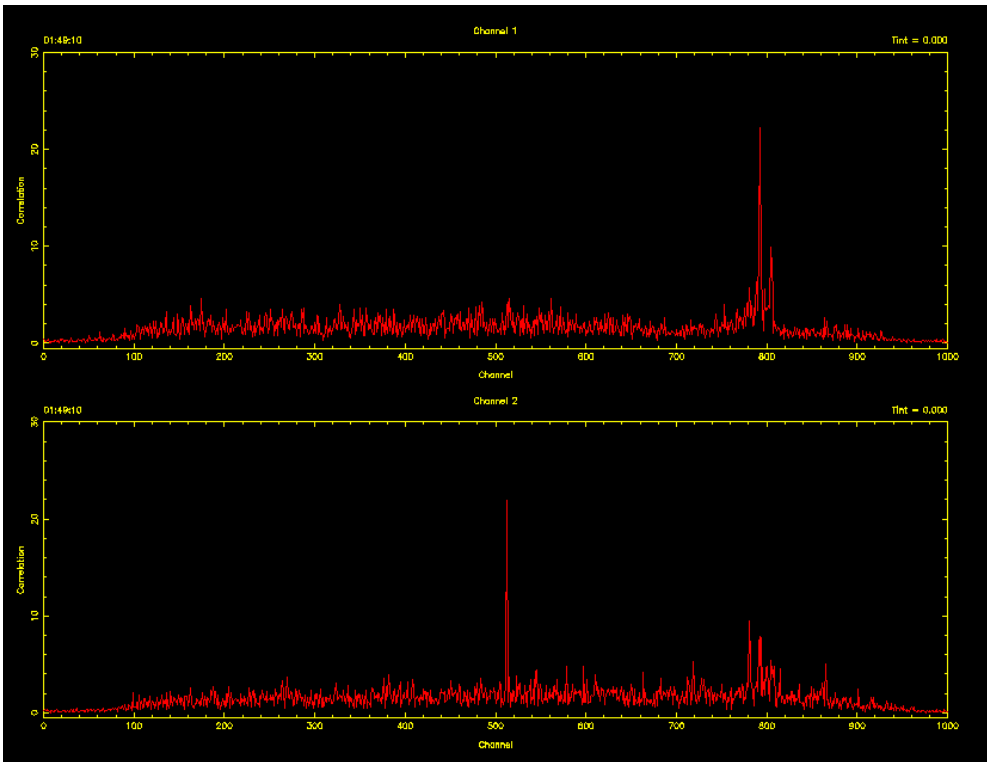

Figure 5.16: Brightest pulse arrival in real time. Frame 7 of 8.

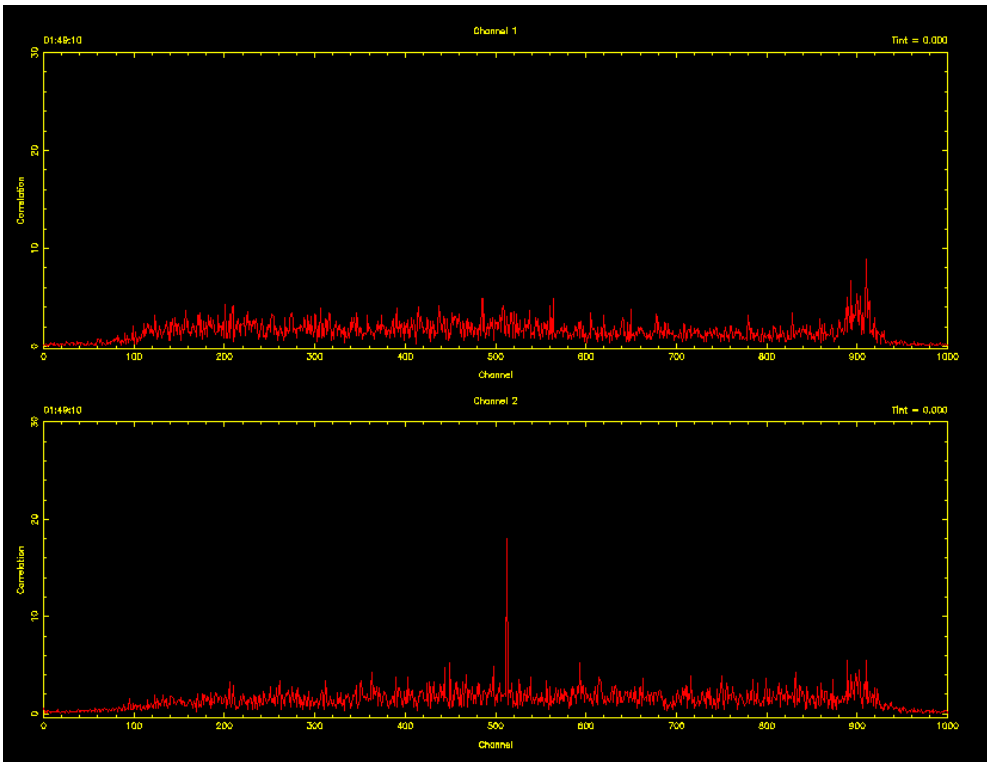

Figure 5.17: Brightest pulse arrival in real time. Frame 8 of 8.

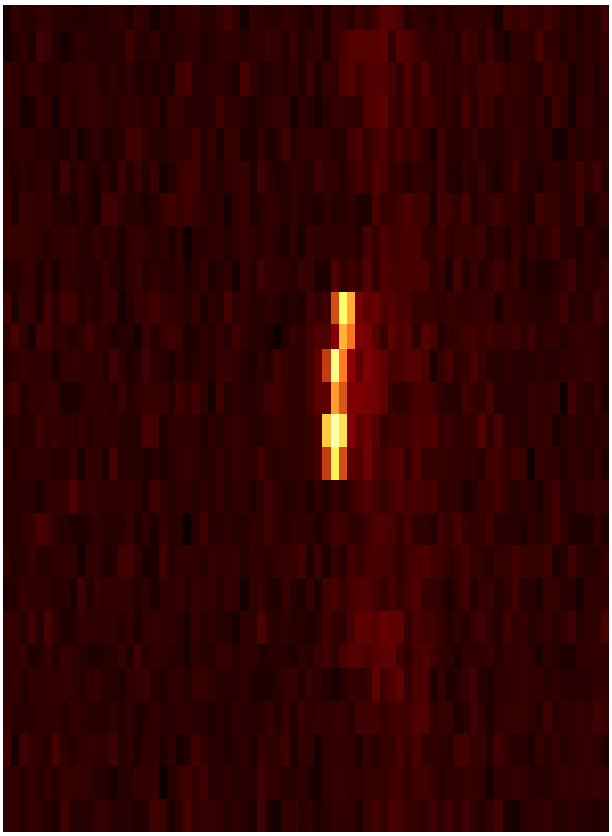

Figure 5.18: The brightest 6 consecutive bright pulses we've discovered so far.

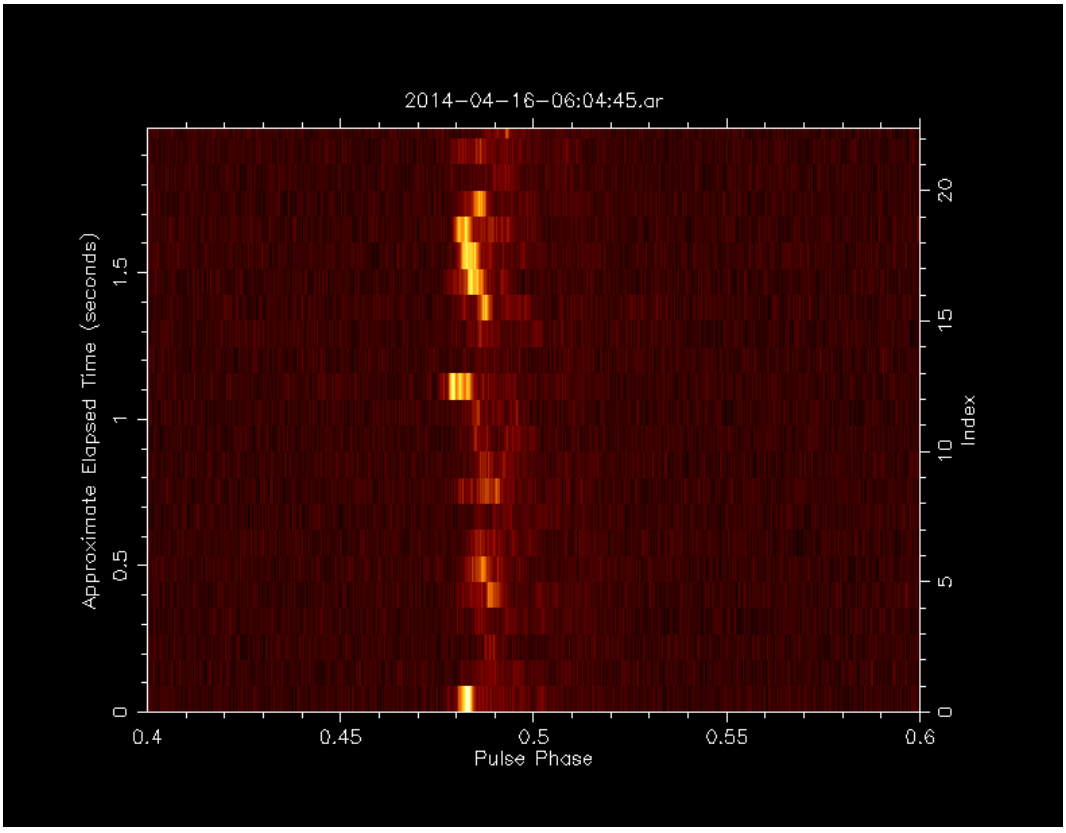

Figure 5.19: Drifting sub-pulses on the Vela pulsar.

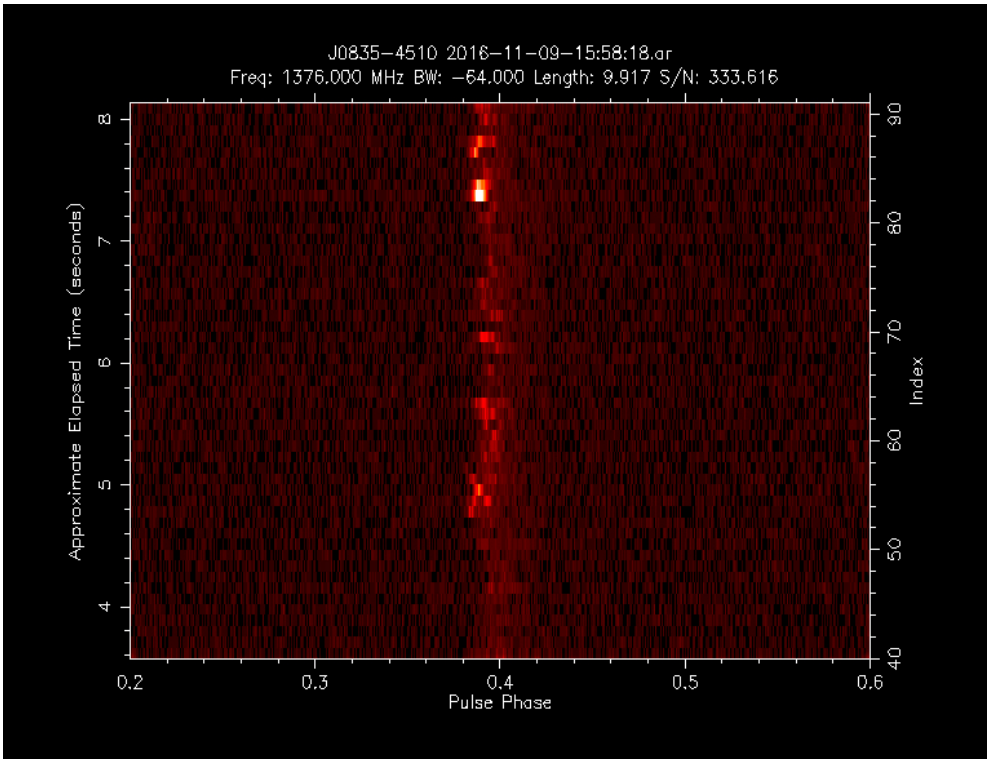

Figure 5.20: Drifting sub-pulses in opposite directions at the same time. Note the "λ" shape at $t \approx 5$ s.

(Rankin, private communication).

In Figure 5.20 we see a very interesting phenomenon. Note the "λ" shape in the lower third of the diagram. We've seen Vela pulses drift in both directions, but this shows pulses drift in opposite directions *at the same time*.

Cordes and Shannon (2008) discuss the possibility of supernova fallback material entering the light cylinder. Brook et al. (2014) examine pulse profile shape changes and postulate the cause is an asteroid or in-falling debris, and Kotera et al. (2016) also discuss this possibility.

An intriguing pattern has also revealed itself with regard to consecutive giant pulses. Often the consecutive pulses have the same "shape". Normally the shape is typically Gaussian in appearance but occasionally this is not the case. An excellent example is shown in Figures 5.23 to 5.24 on page 99: two consecutive wide triple-peaked giant pulses. Even though the amplitudes change, the locations of the peaks are similar. This supports the notion inferred in Palfreyman et al. (2011) that we are seeing multiple passes of a single emission zone (in this case multi-peaked) passing through the line-of-sight.

As stated earlier, Vela being a young pulsar should have only core emission and not conal emission (Rankin 1990) and certainly not a rotating carousel of emission zones like B0943+10, as shown in Deshpande and Rankin (2001). The above results appear

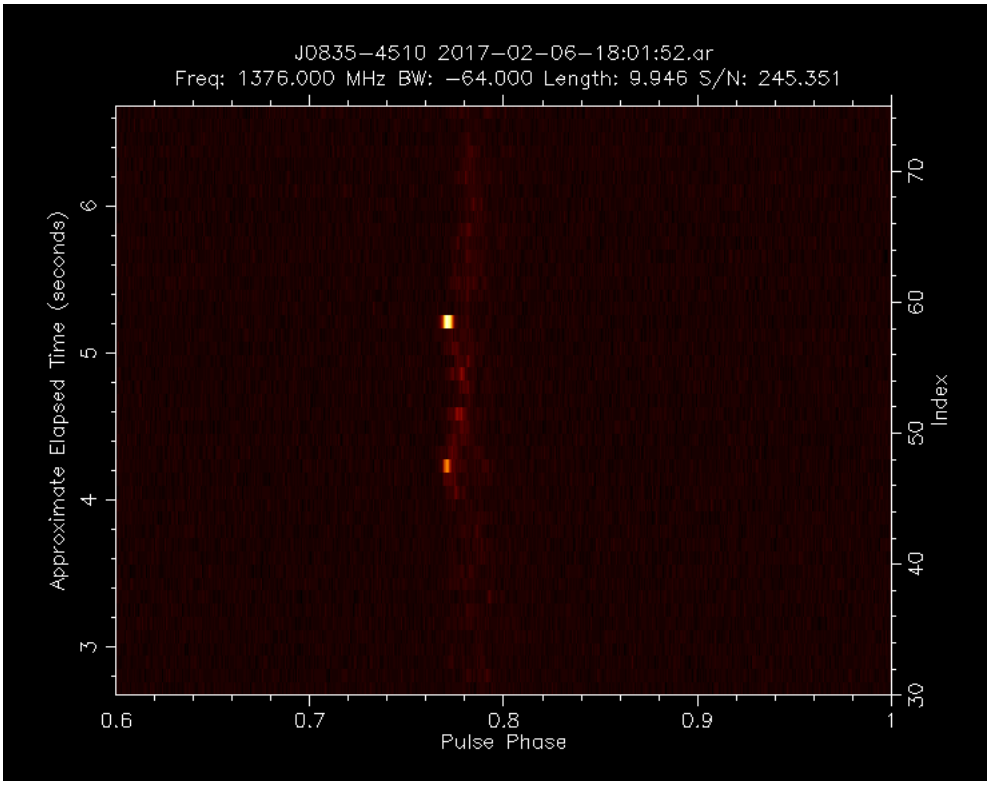

Figure 5.21: A large curving drifting sub-pulse which could not occur if there were emission zones rotating around the magnetic pole. Epicycles within the major rotation could cause this effect.

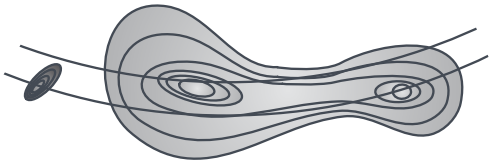

Figure 5.22: Simple graphic of potential core emission with some outriders. The two sight-lines in this diagram show how precession could change the pulse profile and why bright pulses only occur at the leading edge.

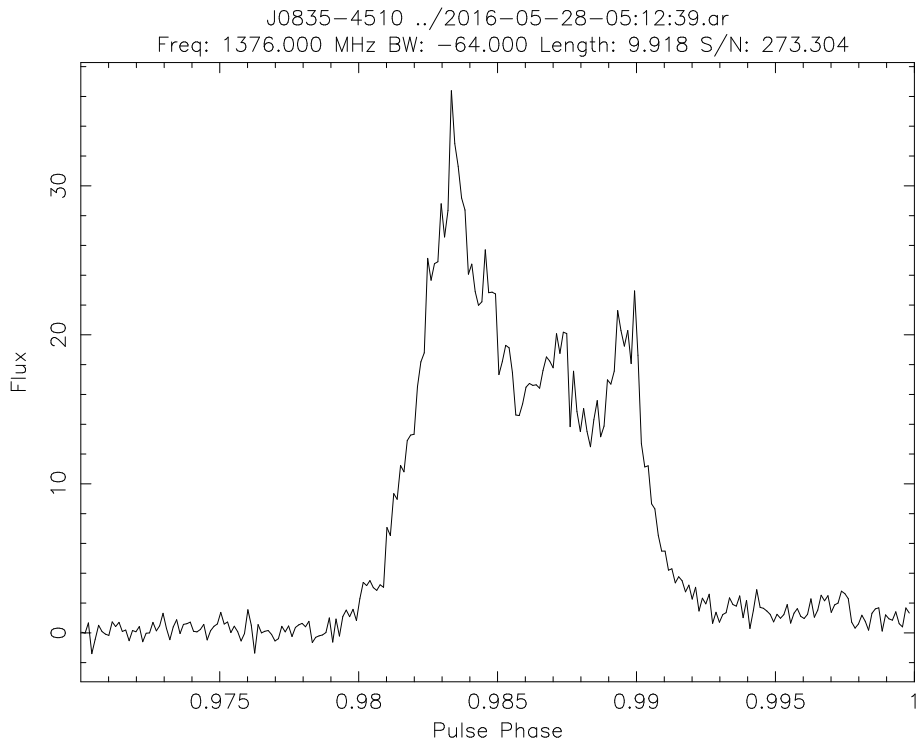

Figure 5.23: The first pulse of two consecutive bright pulses. Note the unusual shape in both pulses.

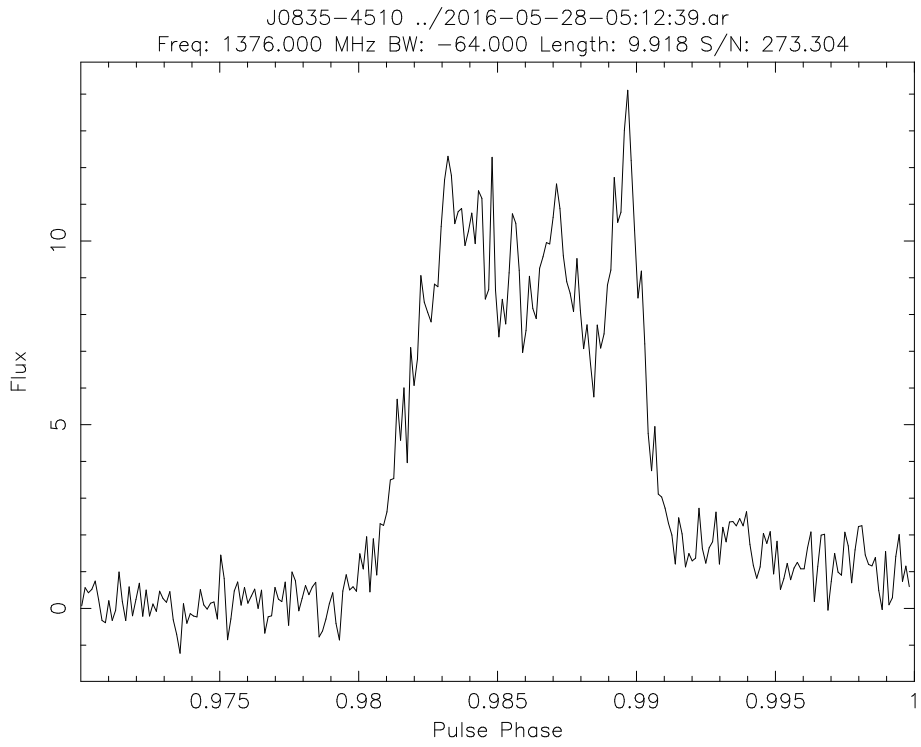

Figure 5.24: The second pulse of two consecutive bright pulses. Note the unusual shape in both pulses.

to contradict this, but Vela could just have emission zones that are "wobbling" into the line-of-sight due to precession or some other cause.

Another intriguing sequence is shown in Figure 5.21 on page 98. This large curving stream of pulses could not be explained by the rotating carousel of Deshpande and Rankin (1999). This pattern could be explained if such a carousel had emission zones of rotating epicycles.

5.1.5 Bright pulse from J1644−4559

Johnston (2004) stated that *"single pulses from this pulsar are rather featureless"*, but we found *one* example of a pulse with a peak flux density 5.1 times the peak flux of the integrated pulse. Figure 5.25 on page 101 shows this pulse and Figure 5.27 on page 102 confirms this is a genuine pulse emitted by the pulsar by showing the effect of dispersion measure. This bright pulse also occurred at the same phase as the integrated pulse which is notably different from the Vela pulsar where bright pulses arrive earlier.

Keith et al. (2011) shows a precursor pulse at 17 GHz. This was present 10° prior to the normal peak which equates to a phase difference of −0.028. In Figure 5.25 on page 101, the peak is at 0.77 and so any precursor would appear at 0.74. There is a *hint* of a small peak, but it could of course be random noise. The integrated pulse shown in Figure 5.26 on page 101 does also show a slight "bump" at that point, and this is most likely the precursor, which is labelled as "component 1" as discussed in Johnston (2004).

It is worth highlighting that the pulse shown in Figure 5.25 on page 101 was the *only* bright* pulse recorded in the 4.8 million single pulses we observed.

J1644−4559 is ≈ 350000 years older than Vela and this shows that bright pulse activity reduces as pulsars age. It also shows that the magnitude of the bright pulses also appears to drop (keep in mind though we have a sample of $n = 1$).

5.1.6 Giant pulses from J0534+2200

The Crab is an extremely well studied pulsar and typical single pulses at 1376 MHz are not possible to detect with the Mt Pleasant 26 m telescope since the average flux density over the entire pulse period is $S_{1400} = 14$ mJy as compared to Vela $S_{1400} = 1100$ mJy (Manchester et al. 2005).

*strictly speaking it is not a *bright* pulse as defined in Palfreyman et al. (2011), but it still was the only pulse recorded that was notably brighter than the standard pulse.

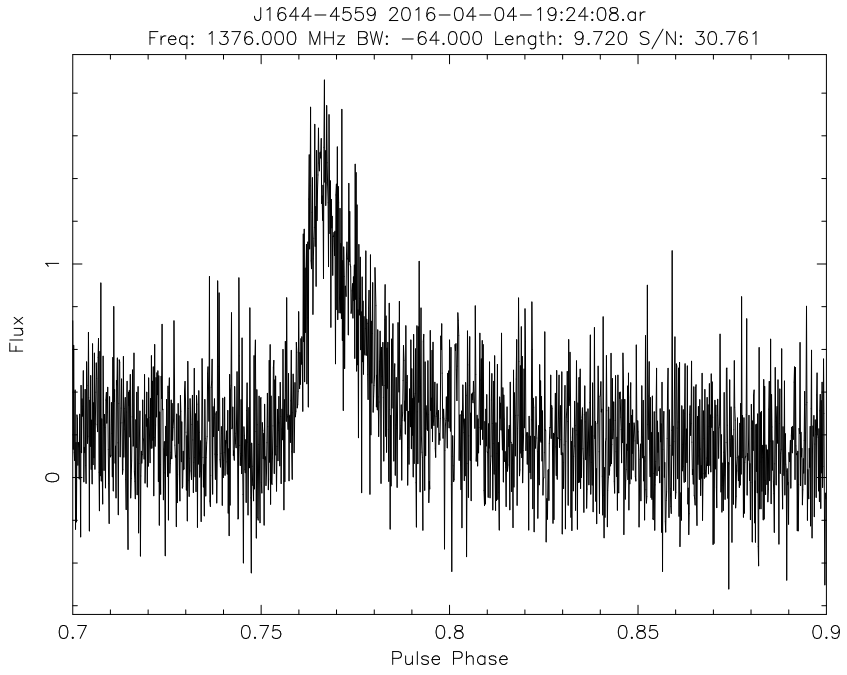

Figure 5.25: A bright pulse from J1644−4559. On the relative scale it has a peak flux of 1.94 as compared with 0.38 for the integrated pulse (5.1 times the peak flux of the integrated pulse).

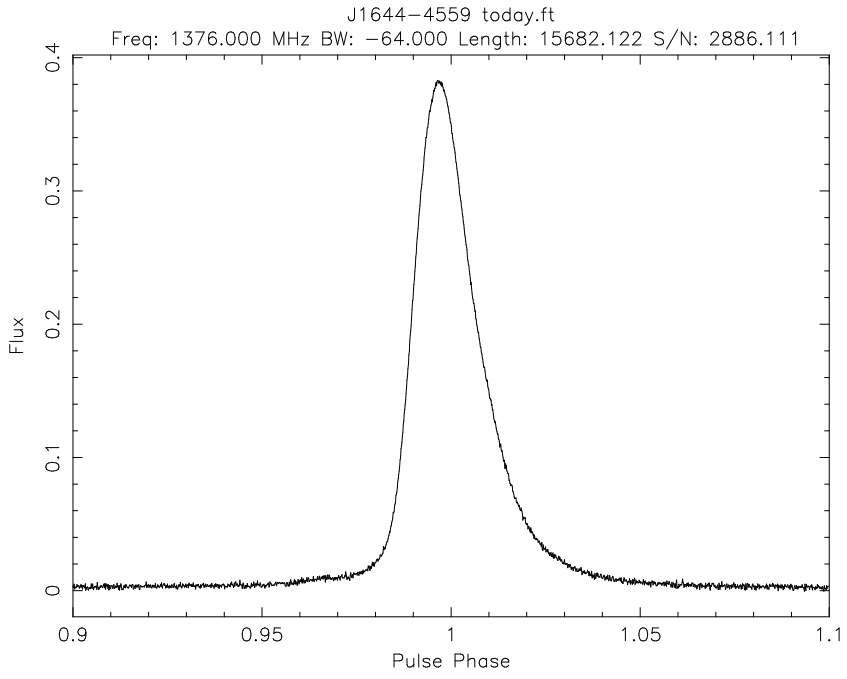

Figure 5.26: The integrated pulse from J1644−4559 over 4.4 h of observations. On the relative scale it has a peak flux of 0.38.

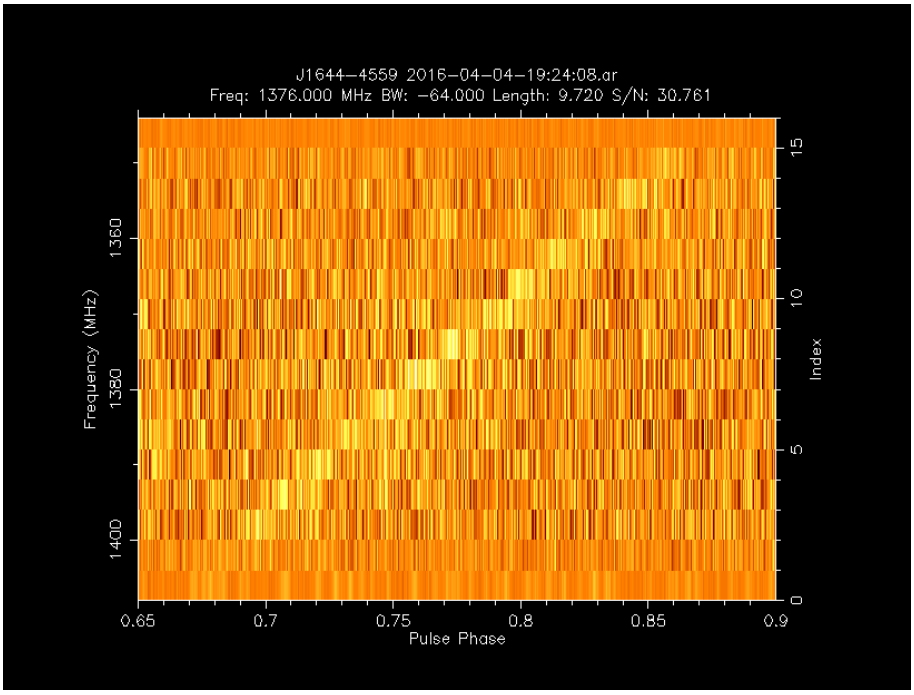

Figure 5.27: Frequency vs phase of a bright pulse from J1644−4559 showing dispersion and so confirming it's a genuine bright pulse.

However since the Crab is observable for a maximum of ≈ 8 h each day at Mt Pleasant, an integrated pulse profile is visible at 1376 MHz. This is shown in Figure 5.28 on page 103. The Crab has $\alpha \approx 90°$ and so an *interpulse*[*] is visible. Note the peak flux density of the main pulse is around 0.015 on the relative scale which is ≈ 700 mJy. The interpulse has a peak flux density of ≈ 225 mJy. Figure 5.29 on page 103 shows a zoomed-in version of the main pulse profile and Figure 5.30 on page 104 shows the interpulse.

Despite the low pulse flux density at this frequency, the Crab pulsar emits very high flux density giant pulses which are easily visible with the 26 m telescope. An example is shown in Figure 5.31 on page 104. Note the size of the peak, the extremely sharp, rise and slow decay (which is almost certainly scattering). This figure was reprocessed using $2^{18} = 262144$ timing bins (each point being 128.68 ns), and the X-axis spans only 33.7 μs.

The Crab's giant pulses have quite a different profile from those of Vela at this frequency (see Figure 5.4 on page 87), and their relative size (compared with the normal pulse) is also significantly larger. Even though both Vela and the Crab are both young pulsars, one could conclude that this could be caused by the angle of the magnetic axis to the rotational axis.

[*]with an inclination angle that is near orthogonal, both emission zones from the magnetic dipole are visible during the pulse period.

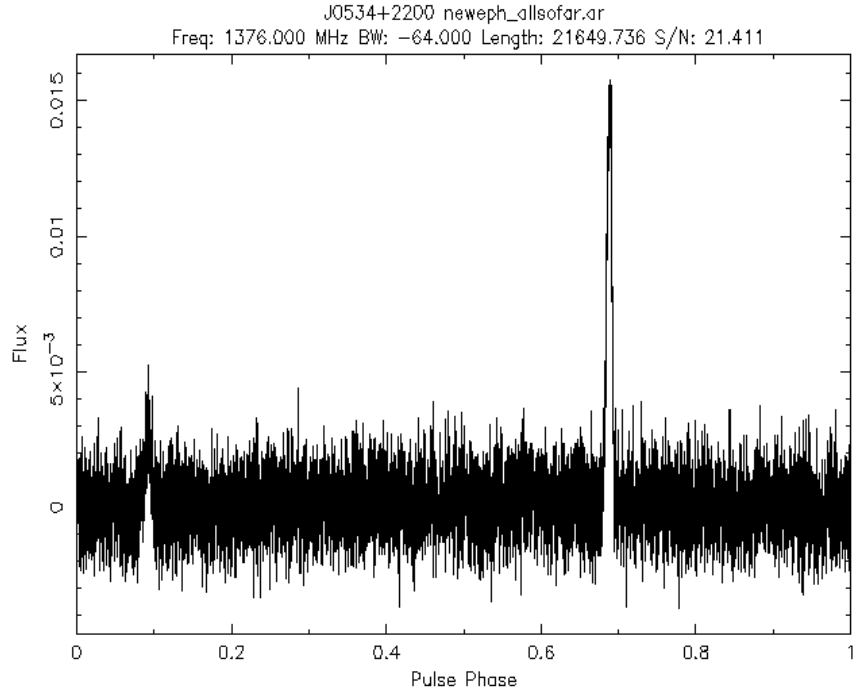

Figure 5.28: Integrated pulse over ≈ 8 h from J0534+2200 at 1376 MHz. The X-axis spans the full pulse period of 33.7 ms and the Y-axis is in relative flux units. Since J0534+2200 has $\alpha \approx 90°$, an interpulse is visible.

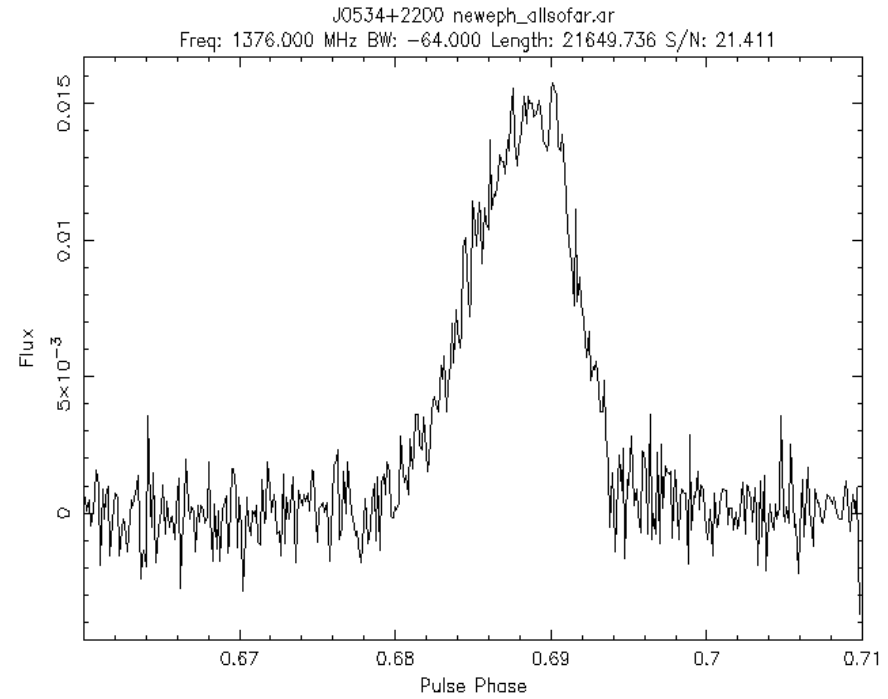

Figure 5.29: The main pulse from J0534+2200 at 1376 MHz. The X-axis spans 1.685 ms and the Y-axis is in relative flux units.

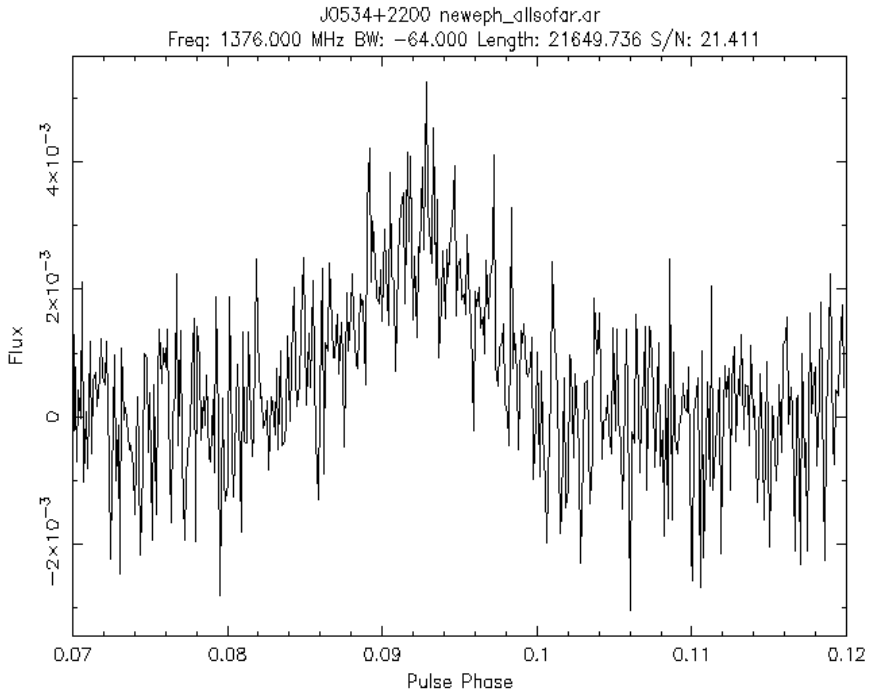

Figure 5.30: The interpulse from J0534+2200 at 1376 MHz. The X-axis spans 1.685 ms and the Y-axis is in relative flux units.

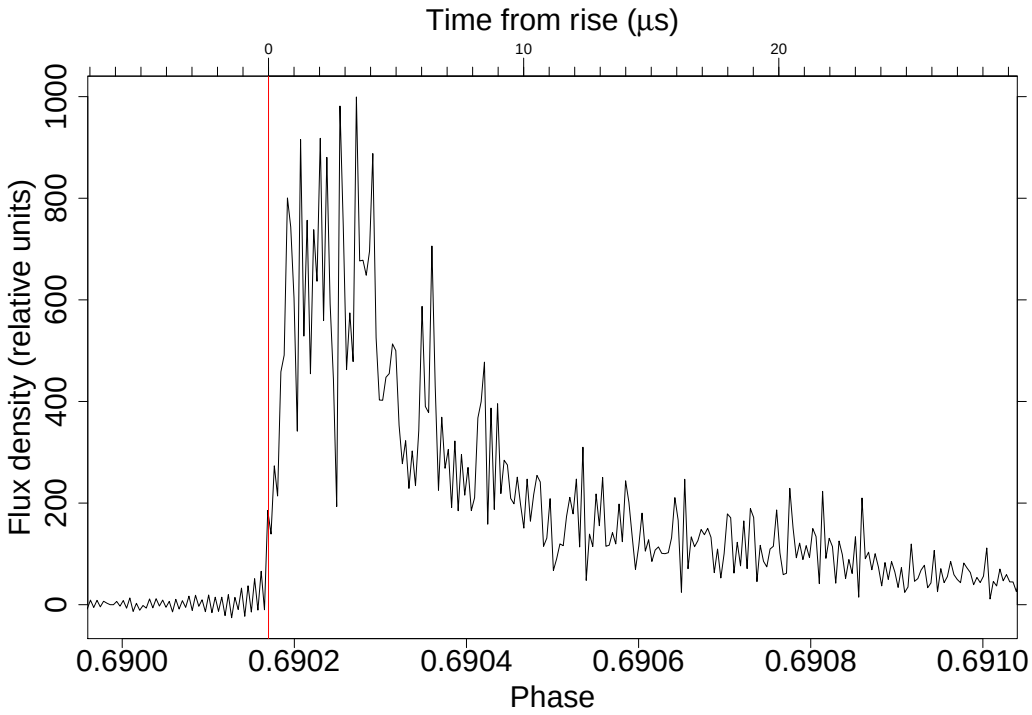

Figure 5.31: A giant pulse from J0534+2200 at 1376 MHz. The X-axis spans 33.7 μs and the Y-axis is in relative flux units. This was reprocessed using $2^{18} = 262144$ timing bins meaning each point represents 128.68 ns. The red line marks the peak of the normal pulse.

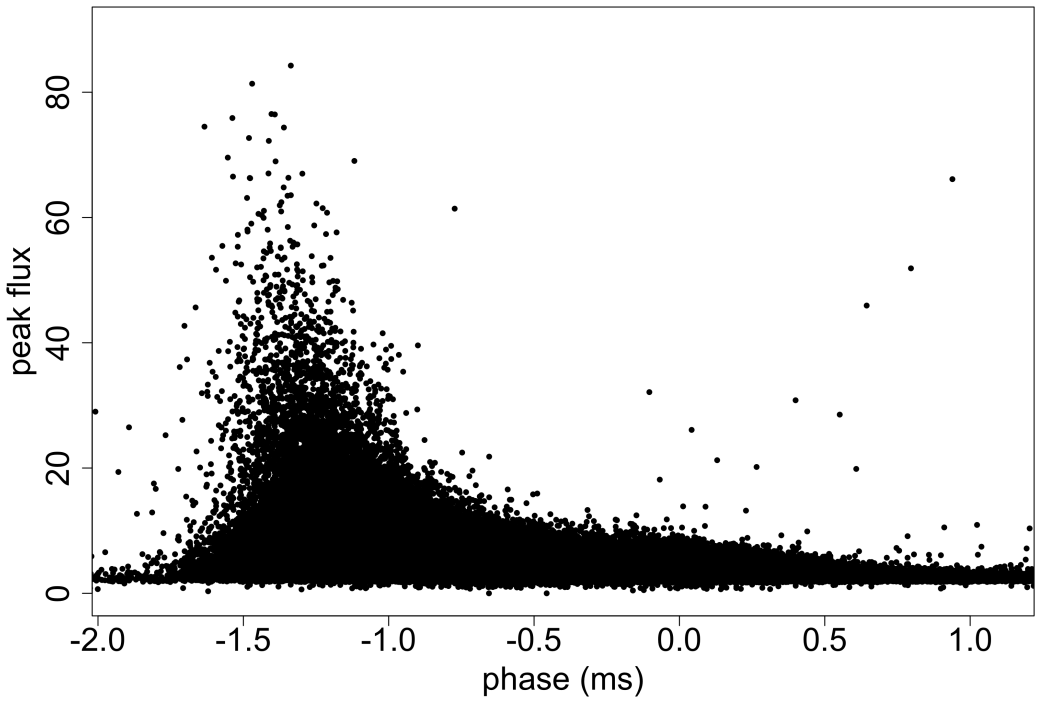

Figure 5.32: Peak flux density versus phase for Vela, with 0 marking the peak of the normal integrated pulse. Note the brighter the pulse is, the earlier it arrives. Also note that RFI is present.

5.1.7 Bright pulses leading the main pulse on Vela

It has been noted in the literature as early as Krishnamohan and Downs (1983) that the brighter pulses on Vela arrive earlier in phase. Figure 5.32 shows a typical 19 h observation. Here is shown $\approx 7.6 \times 10^5$ pulses as a plot of flux density against phase. Note that phase 0.0 is the centre of the integrated pulse and that occasional RFI is present.

Most important to note is that the brighter the pulse, the earlier it arrives. Our reviews of the literature* have not found an explanation for this effect.

The equivalent diagram for the Crab pulsar over a 7 h observation (see Figure 5.33 on page 106 and a zoomed-in version in Figure 5.34 on page 107) is quite different from Vela, and shows no sign of such correlation. Also see Figure 5.35 on page 107 and Figure 5.36 on page 108 for giants on the interpulse. These show a similar pattern.

Further research on this is needed. Examining whether the plot in Figure 5.32 changes over time (including before and after glitches) might give some insight into changes that might be occurring in the magnetosphere.

*as far as we have been able to discover.

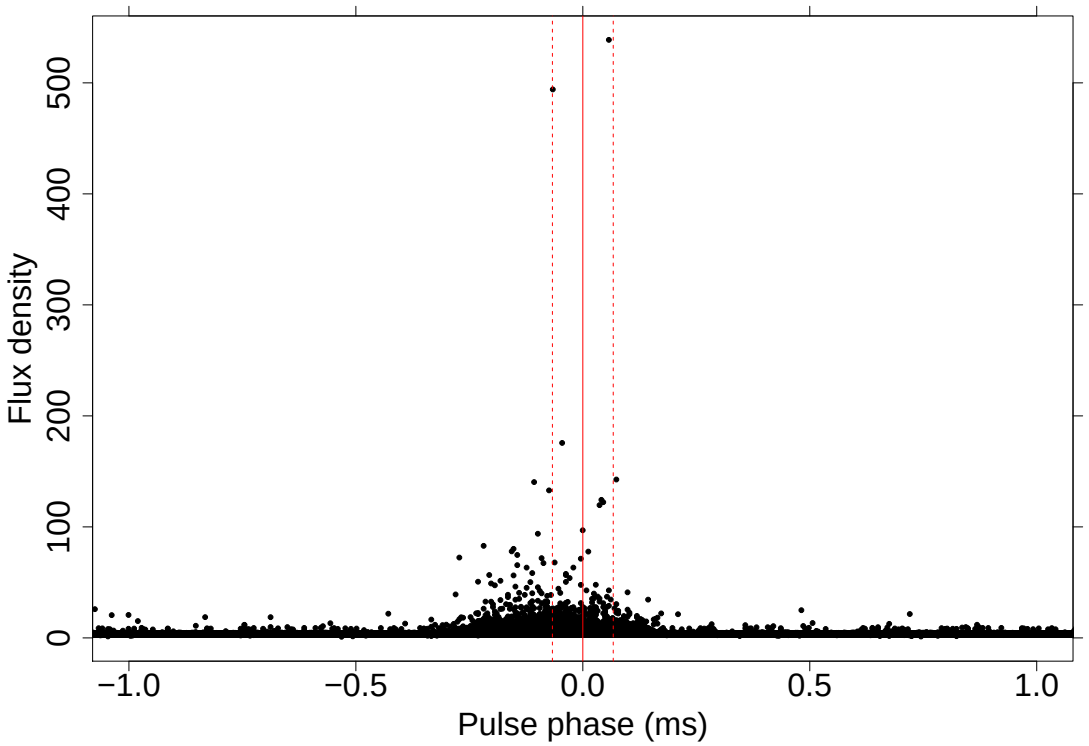

Figure 5.33: Peak flux density versus phase for J0534+2200 at the main pulse. The red line at 0 marks the peak of the normal integrated pulse and the dotted red lines mark the width of the peak. Note the contrast to Vela in that bright pulses do not arrive earlier.

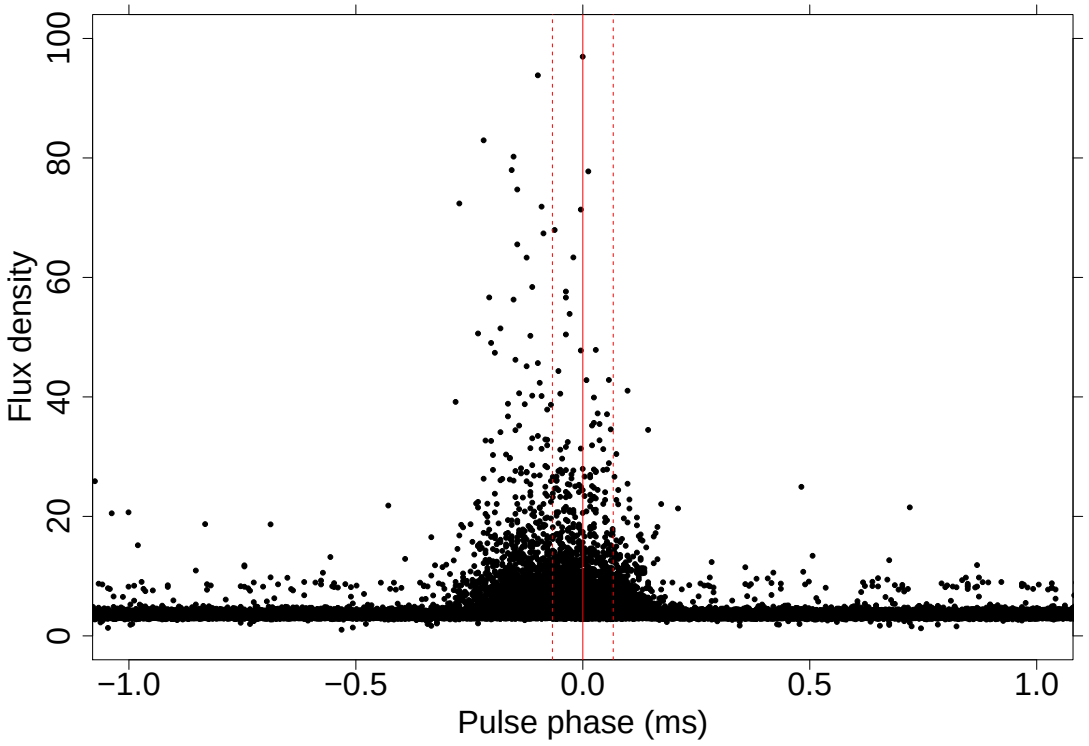

Figure 5.34: Zoomed-in plot of peak flux density versus phase for J0534+2200 at the main pulse. The red line at 0 marks the peak of the normal integrated pulse and the dotted red lines mark the width of the peak.

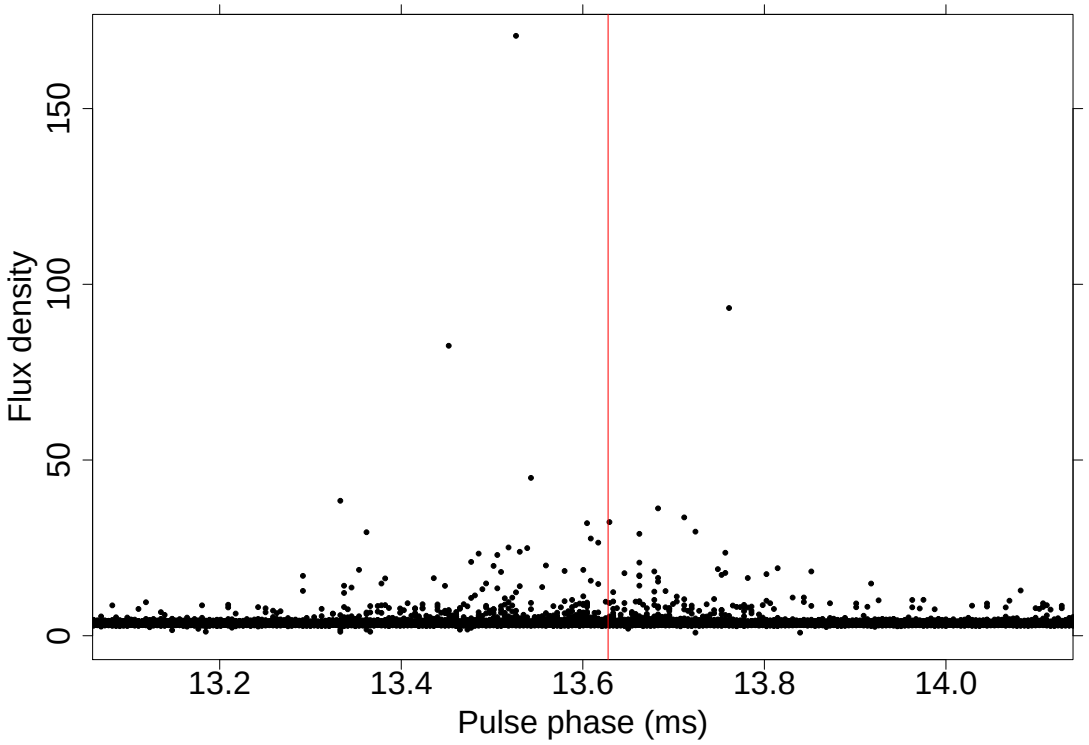

Figure 5.35: Peak flux density versus phase for J0534+2200 at the interpulse. The red line at 0 marks the peak of the normal integrated pulse.

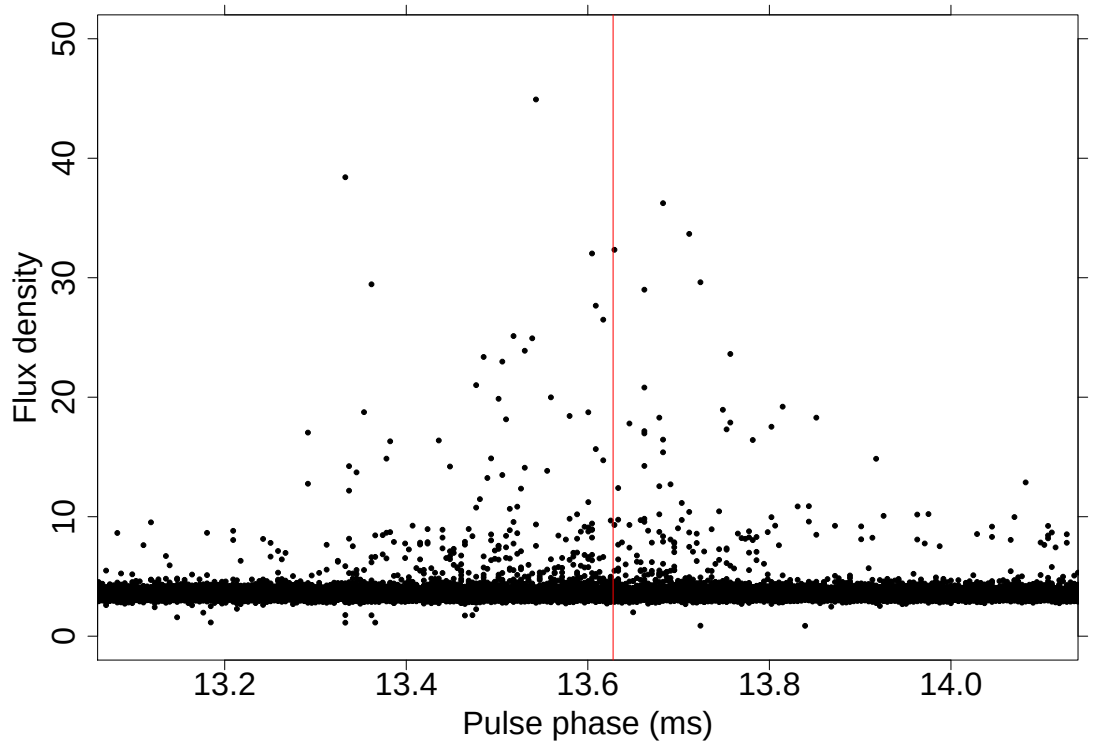

Figure 5.36: Zoomed-in plot of peak flux density versus phase for J0534+2200 at the interpulse. The red line at 0 marks the peak of the normal integrated pulse.

5.2 Vela pulse profile components by frequency

As far as we are aware, an examination of the flux density for different pulse profile components of Vela over a *wide* range of frequencies has not been properly evaluated. Kern et al. (2000) mentioned that the spectral indices were "different" between 1400-8400 GHz, but no figures were given.

We dedicated a full day of observing on each of the different receivers available at Mount Pleasant to compare the flux densities of each component.

Using the calibration method described in Section 4.1.1 on page 45 provided poor results, and it turned out the noise diode was saturating some of the receivers. For this result we instead calibrated using the radiometer equation:

$$\sigma_T \propto \frac{T_S}{\sqrt{B\tau}} \tag{5.6}$$

where T_S is the System Equivalent Flux Density for the receiver (in Jy), B is the bandwidth (always 64×10^6 Hz in our case), and τ is the integration time in seconds (which is doubled if both receivers are in operation).

The final column in Table 5.1 on page 109 shows the calculated multiplier to convert

Table 5.1: Receivers, SEFD, and calibration scale factors used at Mount Pleasant for multi-frequency observations.

Freq MHz	Working receivers	Average SEFD	Int. time (s)	Obs. σ_T $\times 10^{-6}$	Calc. σ_T $\times 10^{-6}$	Ratio Calc/Obs	L-Band relative
1376	2	450	67980	819.21	175.35	0.2140	1.000
2230	2	840	67980	‡4184.57	327.31	0.0782	0.365
4800	1	630	51550	506.83	398.67	0.7866	3.675
6658	2	850	63020	680.05	344.00	0.5058	2.363
8425	2	510	65580	699.21	202.33	0.2894	1.352
12200	1	1200	67980	518.98	661.27	1.2742	5.953
22214	1	1800	66480	819.15	1003.04	1.2245	5.721

‡This frequency was heavily affected by RFI.

other frequencies to "L-band equivalents" in flux density.

Note that the receiver at 2230 MHz was highly saturated with local RFI and so its calibration using this method was next to useless. Comparisons from this frequency to other frequencies have been ignored in future plots.

We fitted three Gaussian components (Krishnamohan and Downs 1983) labelled *a*, *b*, and *c* to pulse profiles at frequencies of 1376, 2230, 4800§, 6658, 8425, 12200§, and 22214§ MHz and these can be seen in Figures 5.37 to 5.43 on pages 113–119. Each of these observations were for close to 19 hours and were carefully aligned with an ephemeris based on observations at 1376 MHz on days surrounding the observation. This was required because of the need for precise alignment of the profile over such a long time frame. It is also important since an accurate comparison of location of profile components at different frequencies was required.

All these observations were completed within ten days and so the changes in flux density of Vela over time were not an issue.

Of note is the result at 22 GHz shown in Figure 5.43 on page 119. We were not expecting to see any pulse profile at such a high frequency with only a 26 m telescope, but the pulse profile is clear. This was obtained with a 19 h observation, and for $\approx$ 13 h the pulsar was $\geq 25^\circ$ above the horizon which is important as H_2O in the atmosphere affects observations at this frequency and compromises observations below this altitude.

The change in intensity of the three main components as frequency increases is quite striking. Component *a* is the strongest at the lower frequencies, but quickly drops in flux density to be below component *b* at 4800 MHz. At 6658 MHz, *a* is $\approx$ 20% of *b*, and *c* is no longer visible. Component *a* is still contributing at 12200 MHz, but has

§As stated earlier, these receivers had one polarisation faulty, but Vela has no circular polarisation and so pulse shape of Stokes I would not be affected.

completely vanished at 22214 MHz.

Figure 5.44 on page 120 shows a plot of intensity, pulse phase mean, and standard deviation for each of the profile components. The pulse phase mean varies slightly and the standard deviation is relatively steady. However the pulse intensity varies greatly. This is because of the *spectral index* (ξ):

$$S(f) \propto f^{\xi} \tag{5.7}$$

where S is flux density and f is frequency. Slee et al. (1986) states that the spectral index of Vela is $\xi_{160}^{400} = -1.13$ and $\xi_{400}^{1400} = -1.21$.

Now Lyne and Manchester (1988) has stated that the general pulsar population has different spectral indices, and so rather than assuming the spectral index for each component is the same, we have plotted the change in peak intensity of the emission zones versus frequency in Figure 5.45 on page 121 as a $\log_{10}$-$\log_{10}$ graph. We have confirmed that between frequencies of 1376-22210 MHz emission zone a has a different spectral index than the b, c, or d. This supports what was stated by Johnston et al. (2006).

Component a which is the predominant feature at lower frequencies (and this study) has a spectral index of $\xi_{1376}^{12200} = -3.162$, and hence drops in flux density quickly as frequency increases and is not visible after 12200 MHz. Component b has a flatter spectral index of $\xi_{1376}^{22210} = -1.958$ and so remains visible to the highest frequency we could observe of 22210 MHz. Component c has a spectral index of $\xi_{1376}^{6658} = -2.696$ and so also vanishes quickly and hence is not visible after 6658 MHz.

These numbers are lower than the $\xi_{400}^{1400} = -1.21$ as quoted by Slee et al. (1986), but ours is for a substantially different frequency range, and we are breaking the overall emission down by its components.

Keith et al. (2011) conducted a similar experiment using the Parkes radio telescope although they fitted von Mises functions, and they also used four components (not including the bright pulse component). Their spectral indices (using our component labelling and sign convention) came to $\xi_a = -2.7$, $\xi_b = -1.56$, and $\xi_c = -2.32$.

5.2.1 Giant pulses as a component

In Figure 5.46 on page 122 we have taken the 10 s file which includes the largest giant pulse we observed and fitted *four* Gaussian components. The giant pulse highlights component d and is 1.1 ms prior to the main component.

The only data we have on the spectral index of component d is with the giant pulse observed at both Ceduna at 4816 MHz and Mount Pleasant at 1376 MHz shown in Figures 5.55 to 5.56 on page 131. Unfortunately no proper flux density calibration was conducted on the 4.8 GHz receiver at Ceduna as the receiver subsequently failed. Ignoring the calibration issues and just using the relative levels reported from both telescopes* we get the spectral index of component d as

$$\begin{aligned} \xi_{1376}^{4816} &= \frac{\log_{10}(8.35) - \log_{10}(63.82)}{\log_{10}(4816) - \log_{10}(1376)} \\ &= -1.623 \end{aligned} \tag{5.8}$$

which is noticeably flatter than the spectral index for component a and c, but not b. This is in line with Lyne and Manchester (1988) which states that inner components have steeper spectral indices than outer components. However, as stated, we need to be careful as this could be due to calibration issues. Regardless, $\xi_d < 0$ which implies synchrotron or curvature emission as suggested by Johnston and Romani (2004).

The *Radius to frequency mapping* (RFM) hypothesis states that different frequencies are emitted at different heights in the magnetosphere, with the higher frequencies emitted closer to the surface of the neutron star. However this emission could be directly from that height or could be ducted to that height from a single emission zone (Lorimer and Kramer 2004).

5.2.2 Profile edges

With a 19 h integration, it was possible to examine the very edges of the pulse profile. Figure 5.47 on page 123 shows a zoomed-in version of Figure 5.37 on page 113 at either edge of the profile. At these extreme edges, the pulse profile has a 0 level width† of 26.8 ms which is over 3 times the typically quoted profile width of 8 ms (Krishnamohan and Downs 1983). It is debatable how relevant this width figure is, but it could be indicating the furthest edges of the magnetic field lines.

More relevant is that the half-way point between these edges is actually closest to the peak of profile c which is not the peak of the average pulse, which is used for the fiducial point for timings at 1376 MHz.

*This normally would be invalid as you cannot compare relative non-calibrated flux density levels between different telescopes, however the relative uncalibrated flux densities for the peak of the integrated pulse at 4816 MHz for both telescopes were very similar, so we progressed regardless. Use this result with caution.

†not a strictly correct term, but since the context is clear we will use it.

Of further interest is that the width doesn't appear to change over time. That is, the 0% level width seems identical at times when the 50% level is widest or narrowest.

At 6658 MHz and 8425 MHz the 0% level width is 5.5 and 5.7 ms respectively. These figures were both obtained with 19 h integrations. The 22 GHz 0% level width was not measurable.

5.2.3 J0437−4715

Figures 5.48 to 5.51 on pages 124–127 show the pulse profiles of the bright millisecond pulsar J0437−4715 at frequencies of 1376, 4800, 6658, and 8425 MHz. The plot of 1376 MHz shows a number of small outlying peaks that quickly vanish at higher frequencies. As stated previously, a steeper spectral index is expected from emission zones that are further from the core. Figure 5.52 on page 128 shows a $\log_{10}$-$\log_{10}$ plot of the central peak of J0437−4715 and shows the spectral index $\xi = -1.822$.

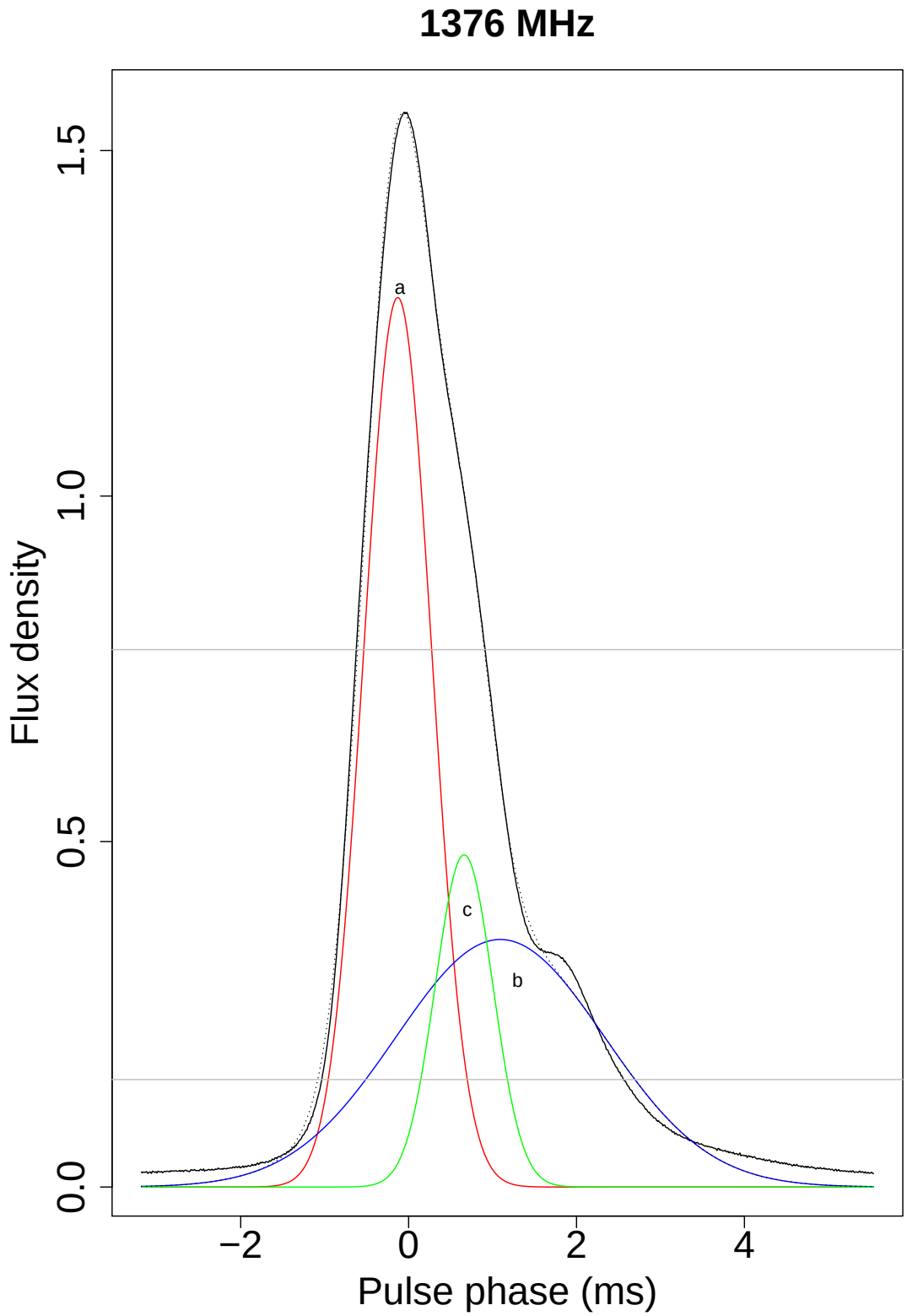

Figure 5.37: 1376 MHz daily pulse profile broken into Gaussian components a, b, c, and the normally unseen bright pulse component d is not visible. The dotted line shows the actual sum of the components. The horizontal grey lines show the 10 and 50 per cent levels.

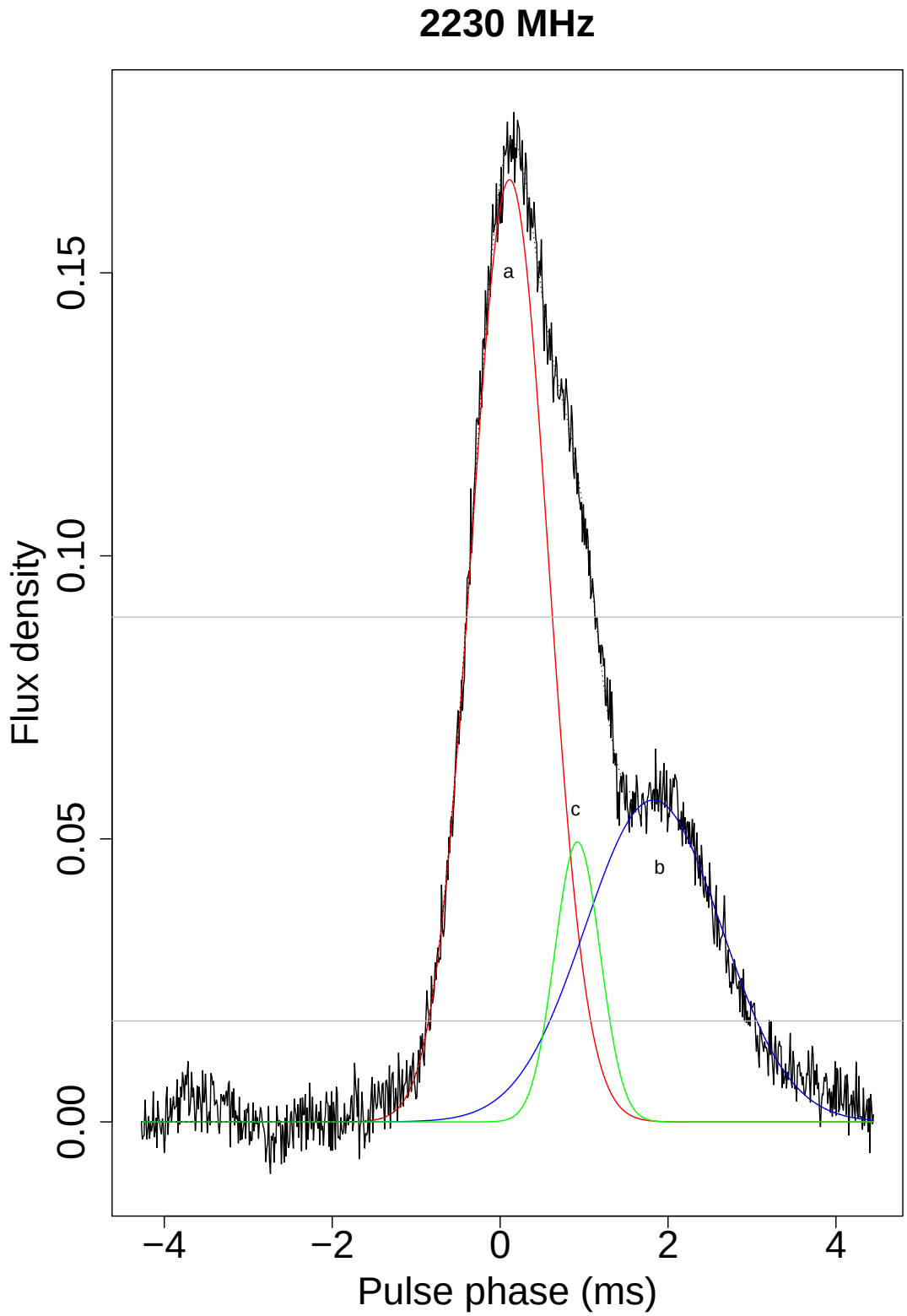

Figure 5.38: 2230 MHz pulse profile broken into three Gaussian components. The dotted line shows the actual sum of the components. This frequency range is *heavily* influenced by RFI and most 10 s integrations are un-useable. Integrating over 19 h however, produced useable results.

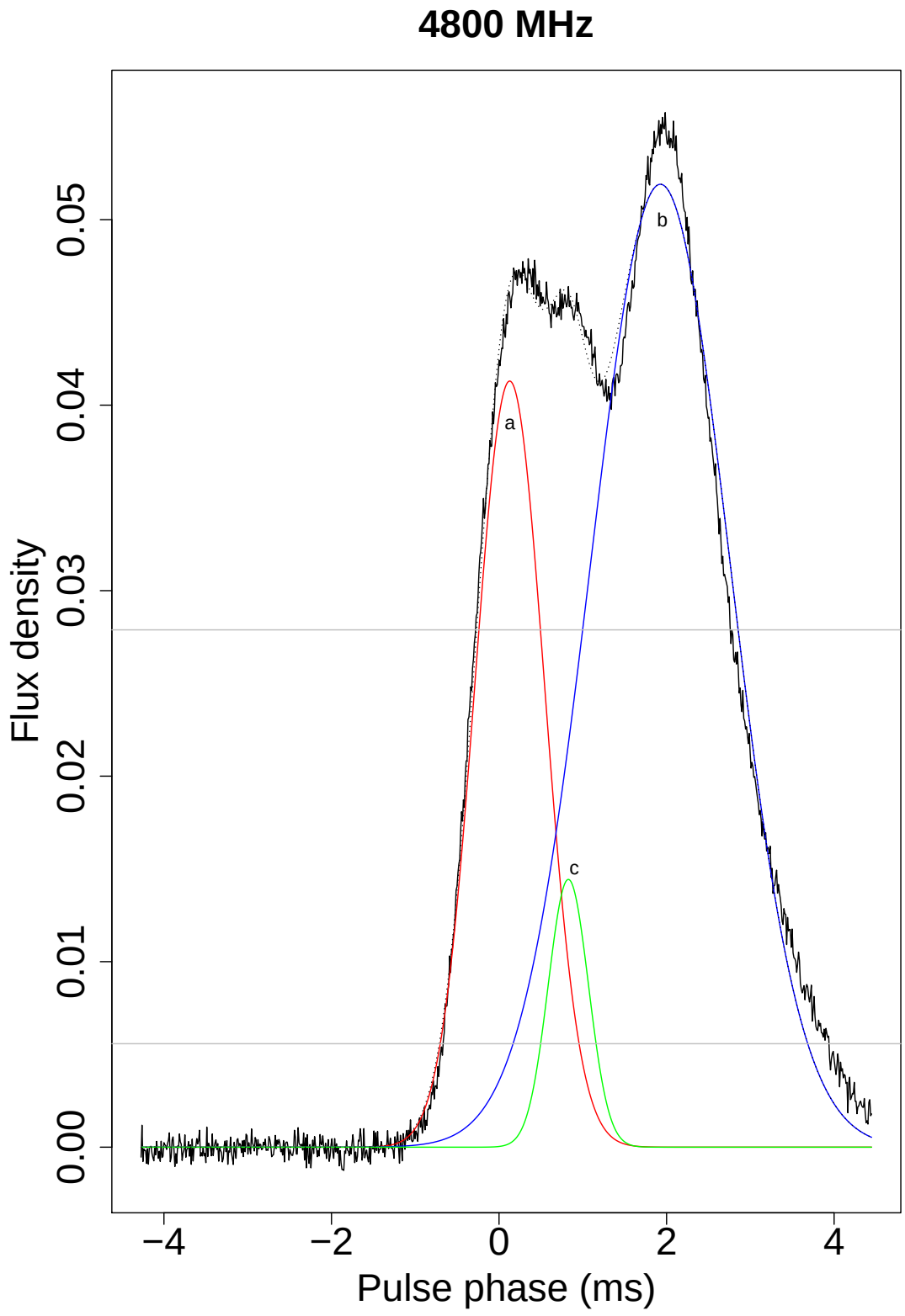

Figure 5.39: 4800 MHz pulse profile broken into Gaussian components. Note the change of size of components a, b, and c from previous figures. The dotted line shows the actual sum of the components. The receiver had a faulty channel and so this profile was generated from a single polarisation. This was circular and so total intensity would not be affected.

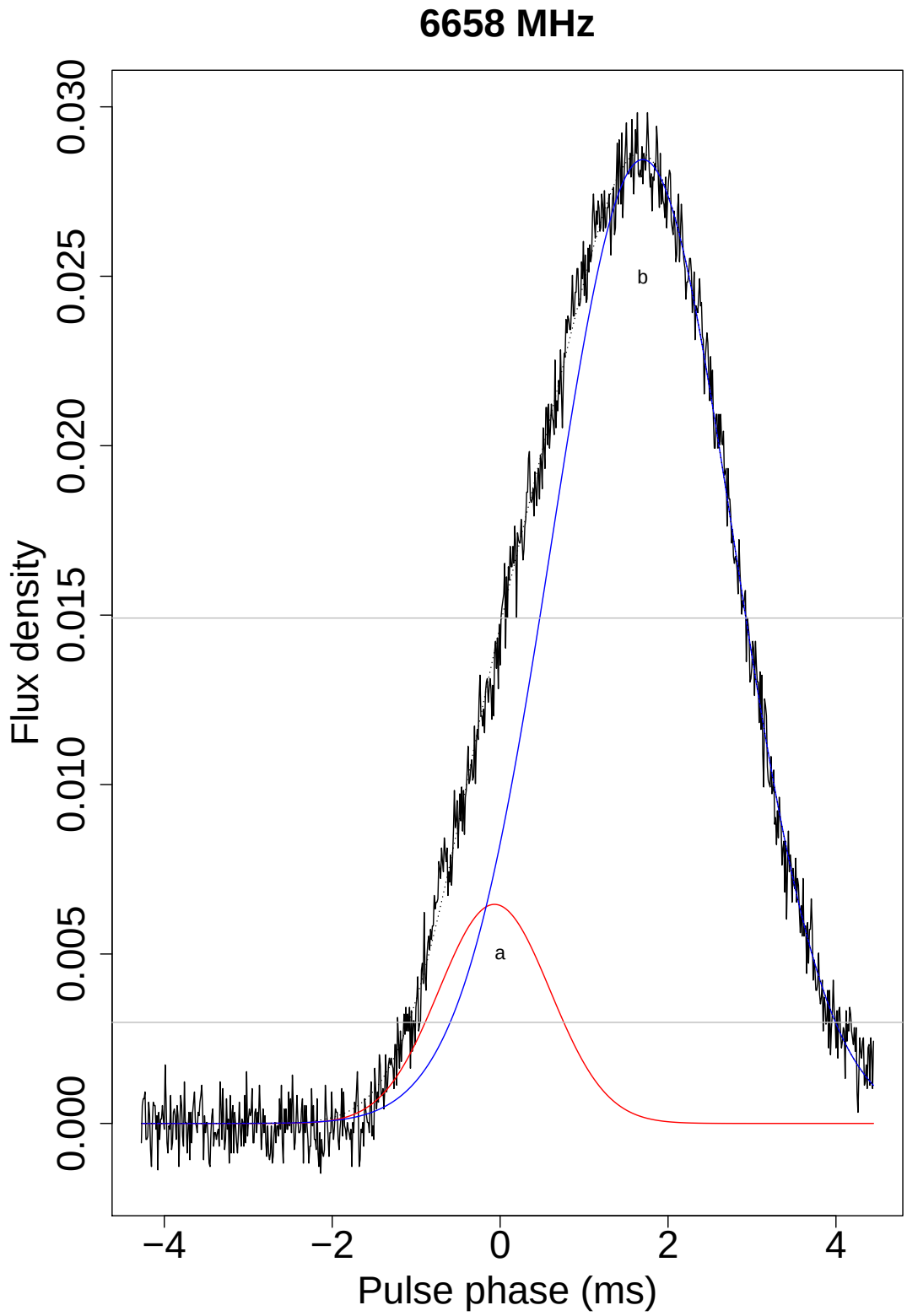

Figure 5.40: 6658 MHz pulse profile broken into two Gaussian components. Component *c* is no longer visible. The dotted line shows the actual sum of the components.

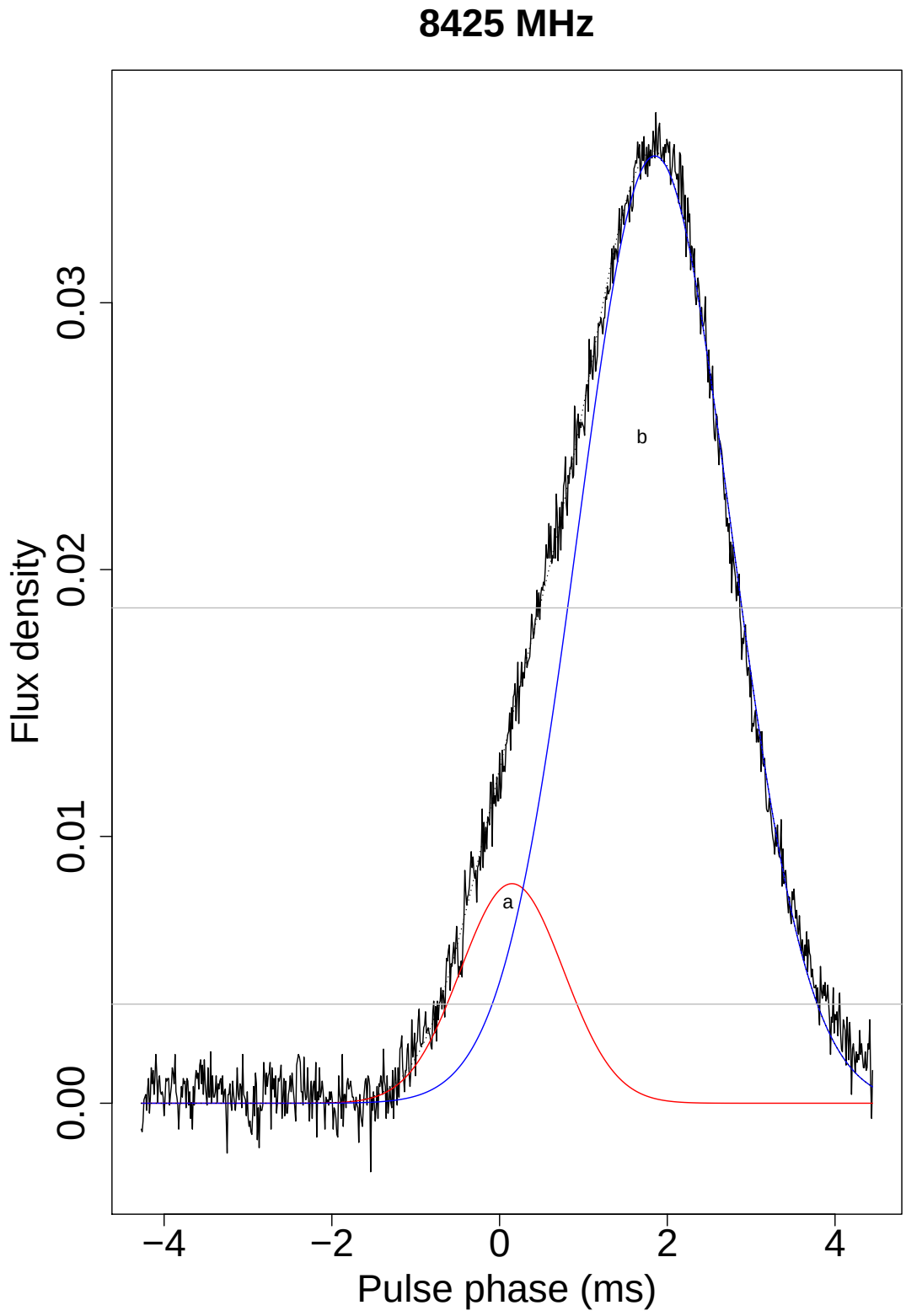

Figure 5.41: 8425 MHz pulse profile broken into two Gaussian components. The dotted line shows the actual sum of the components.

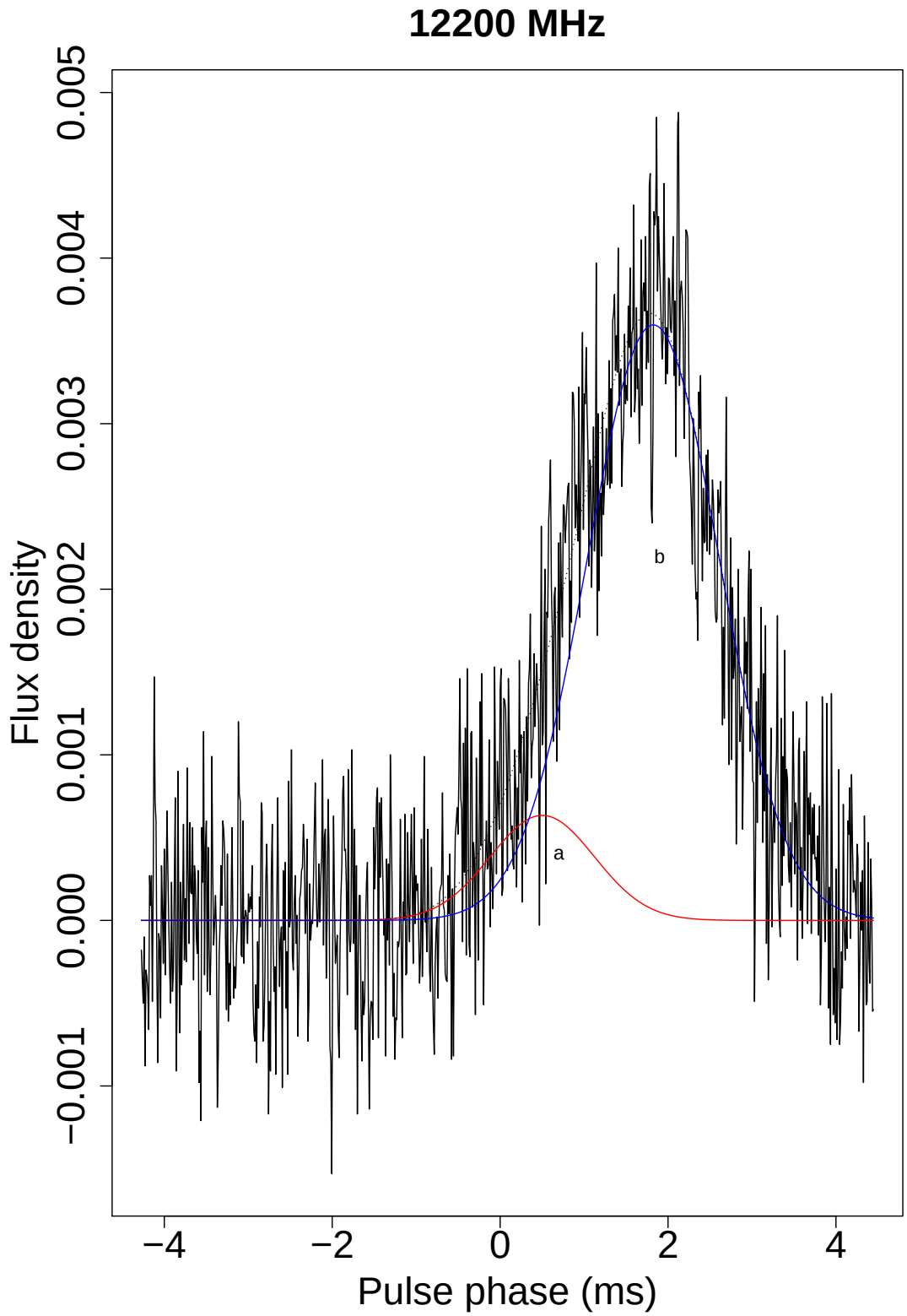

Figure 5.42: 12200 MHz pulse profile broken into two Gaussian components. The dotted line shows the actual sum of the components. The receiver had a faulty channel and so this profile was generated from a single polarisation. This was circular and so total intensity would not be affected.

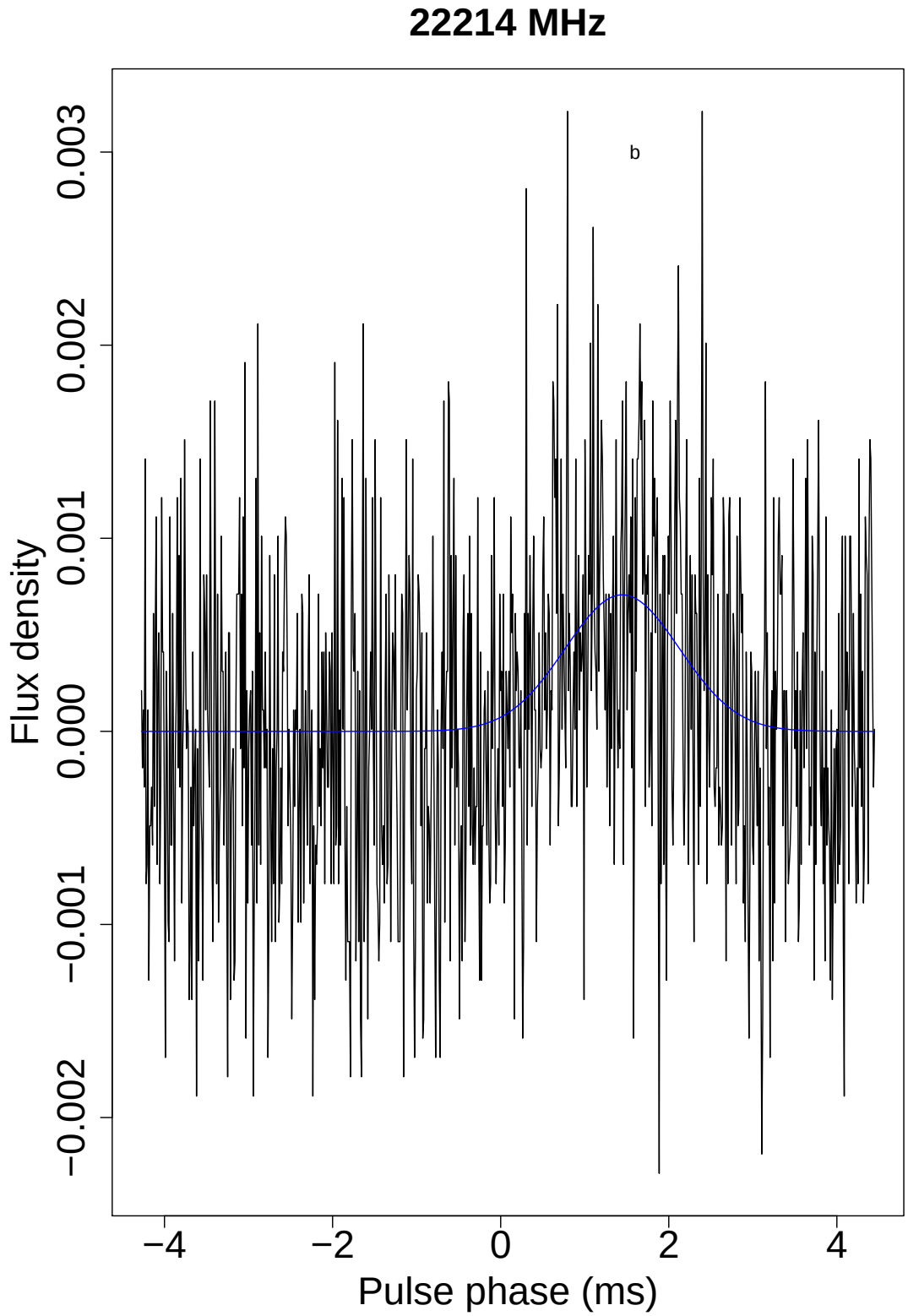

Figure 5.43: 22214 MHz pulse profile comprising a single Gaussian component (b).

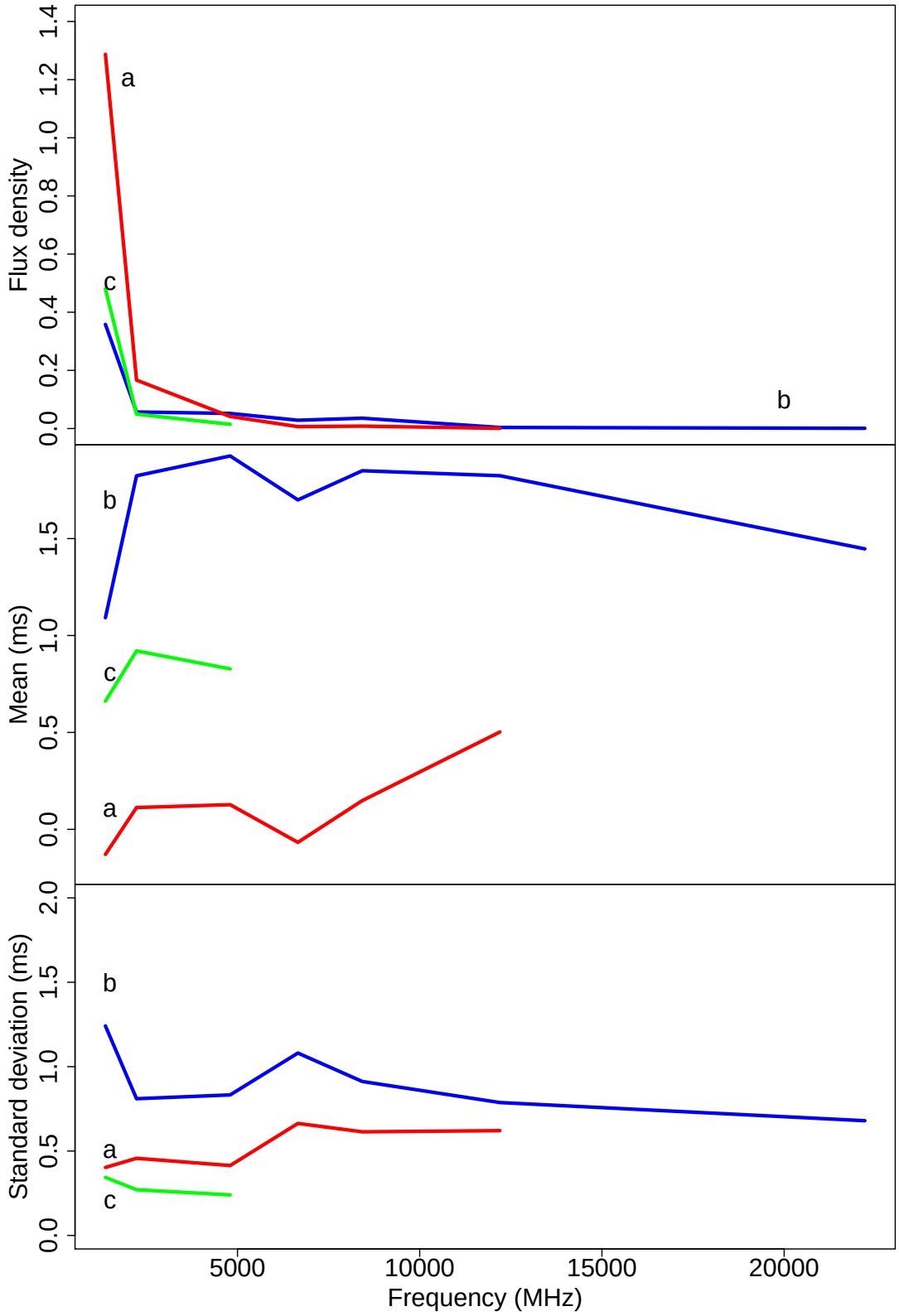

Figure 5.44: Changes of intensity, pulse phase mean, and standard deviation of each of the component profiles *a*, *b*, and *c* from Figures 5.37 to 5.43 on pages 113–119. Pulse phase mean and standard deviation are relatively steady, but intensity varies considerably - which is expanded on in Figure 5.45 on page 121.

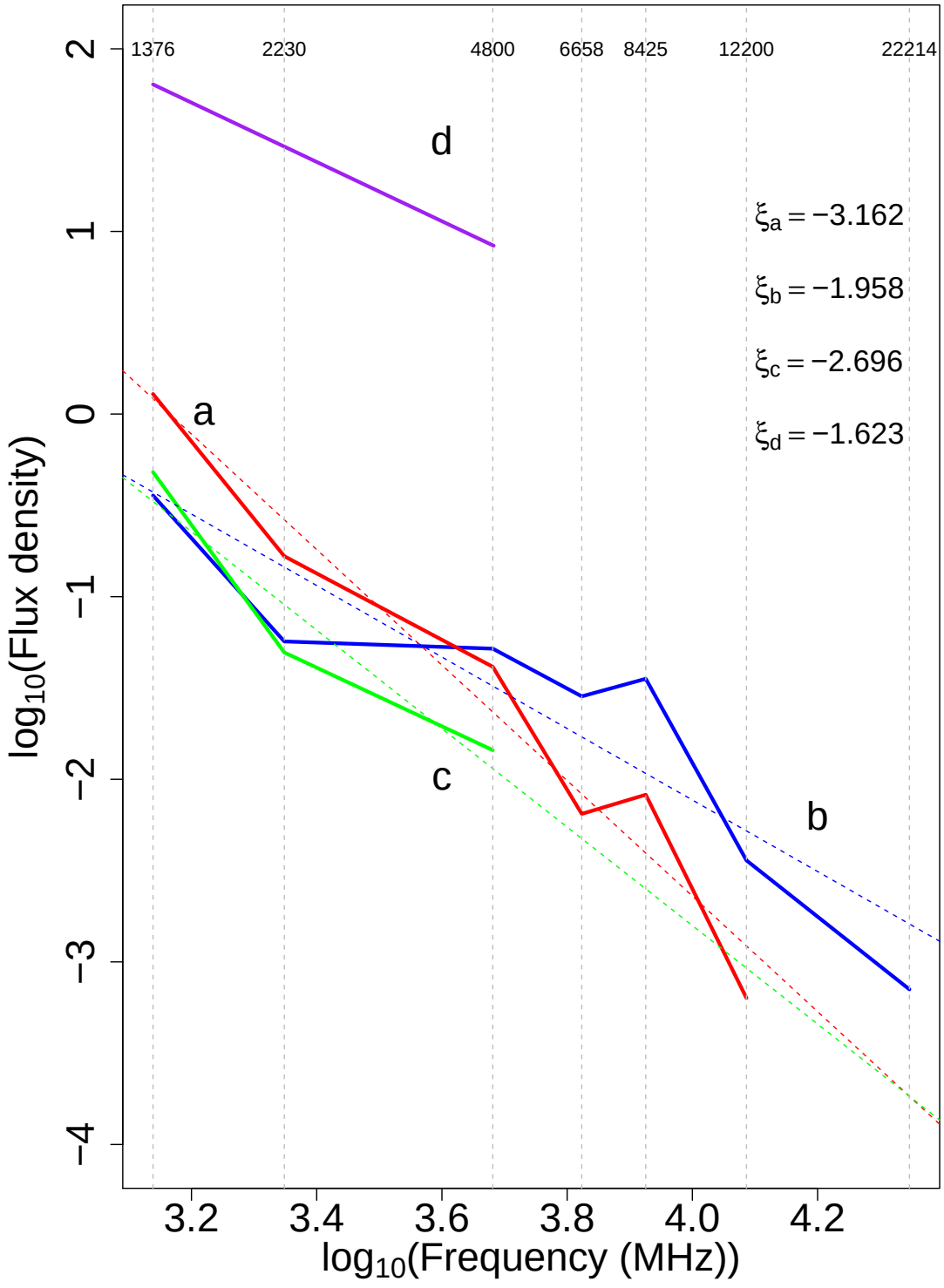

Figure 5.45: $\log_{10}$(amplitude) versus $\log_{10}$(frequency). The gradient of the line of best fit for each emission zone is shown as the dotted line of similar colour. The spectral index (ξ) of each emission zone is shown. The spectral index of component d is shown here (ξ_d) based on a single giant pulse of $\approx$ 3000 Jy at 1376 MHz. See text.

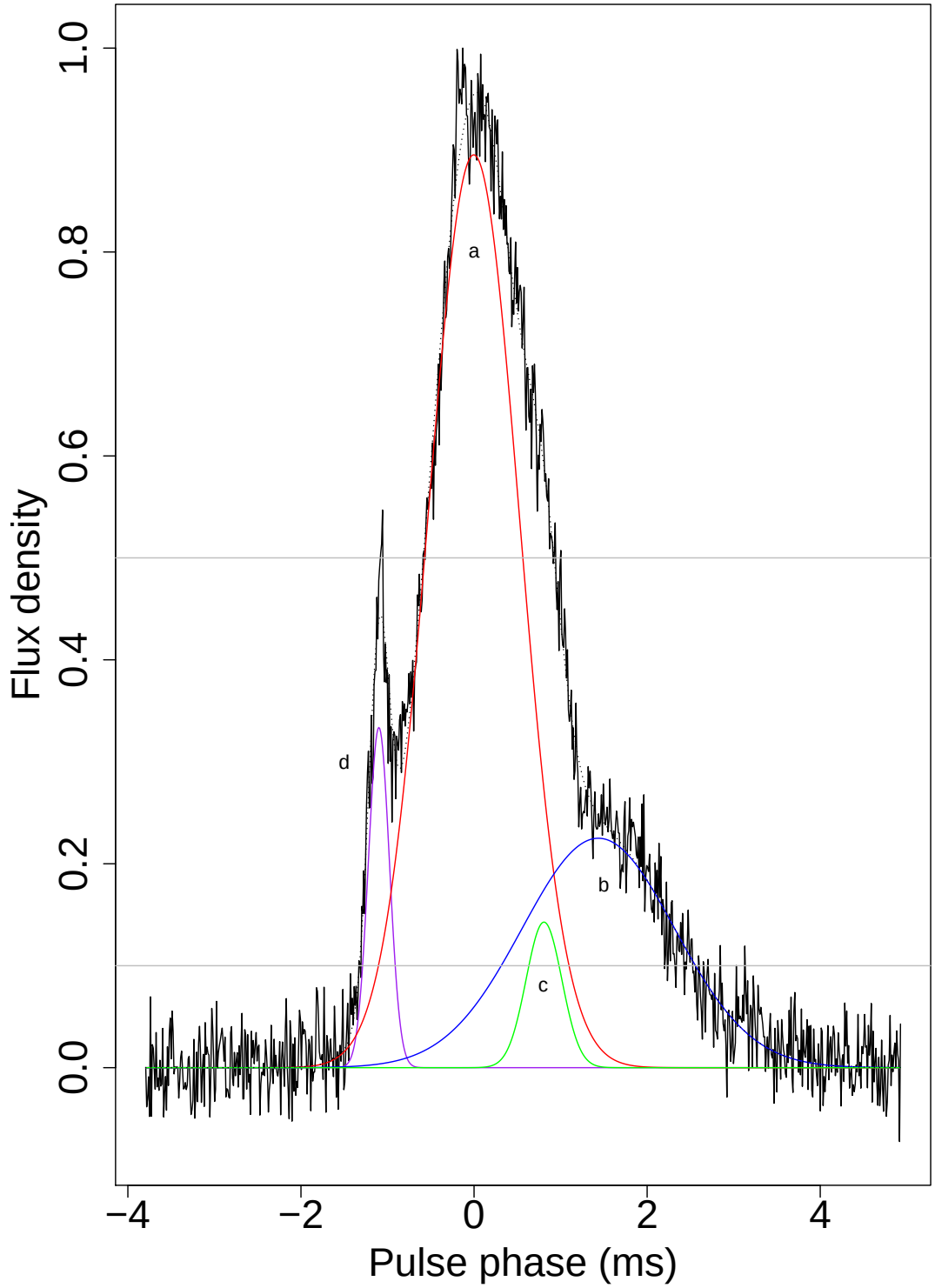

Figure 5.46: 1376 MHz pulse profile (10 s) which includes the largest giant pulse we observed broken into Gaussian components with a, b, c, and the normally unseen bright pulse component d. The dotted line shows the actual sum of the components.

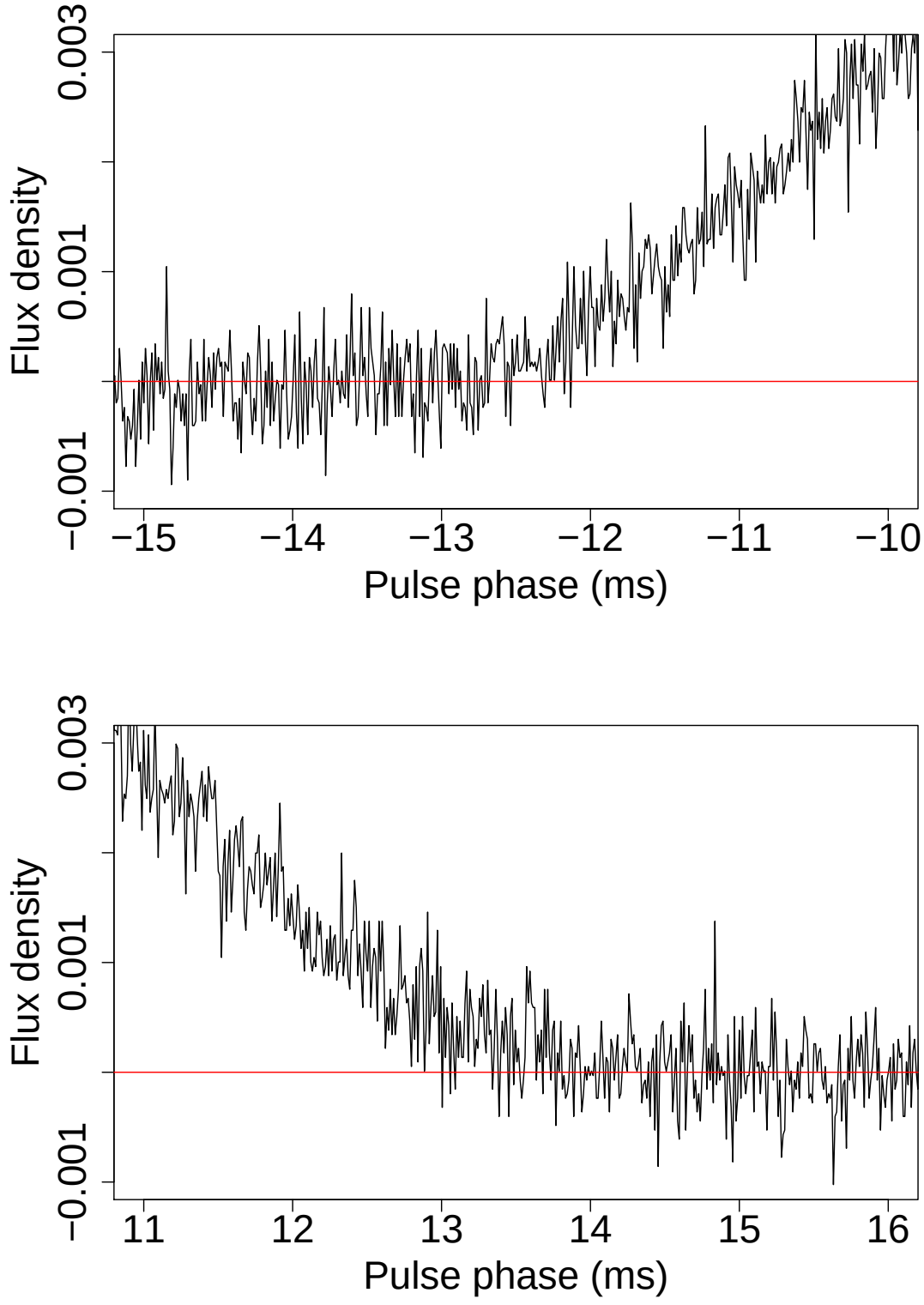

Figure 5.47: The start and end of the 1376 MHz integrated profile after 19 h of observation. Note that this makes the profile width around 26 ms.

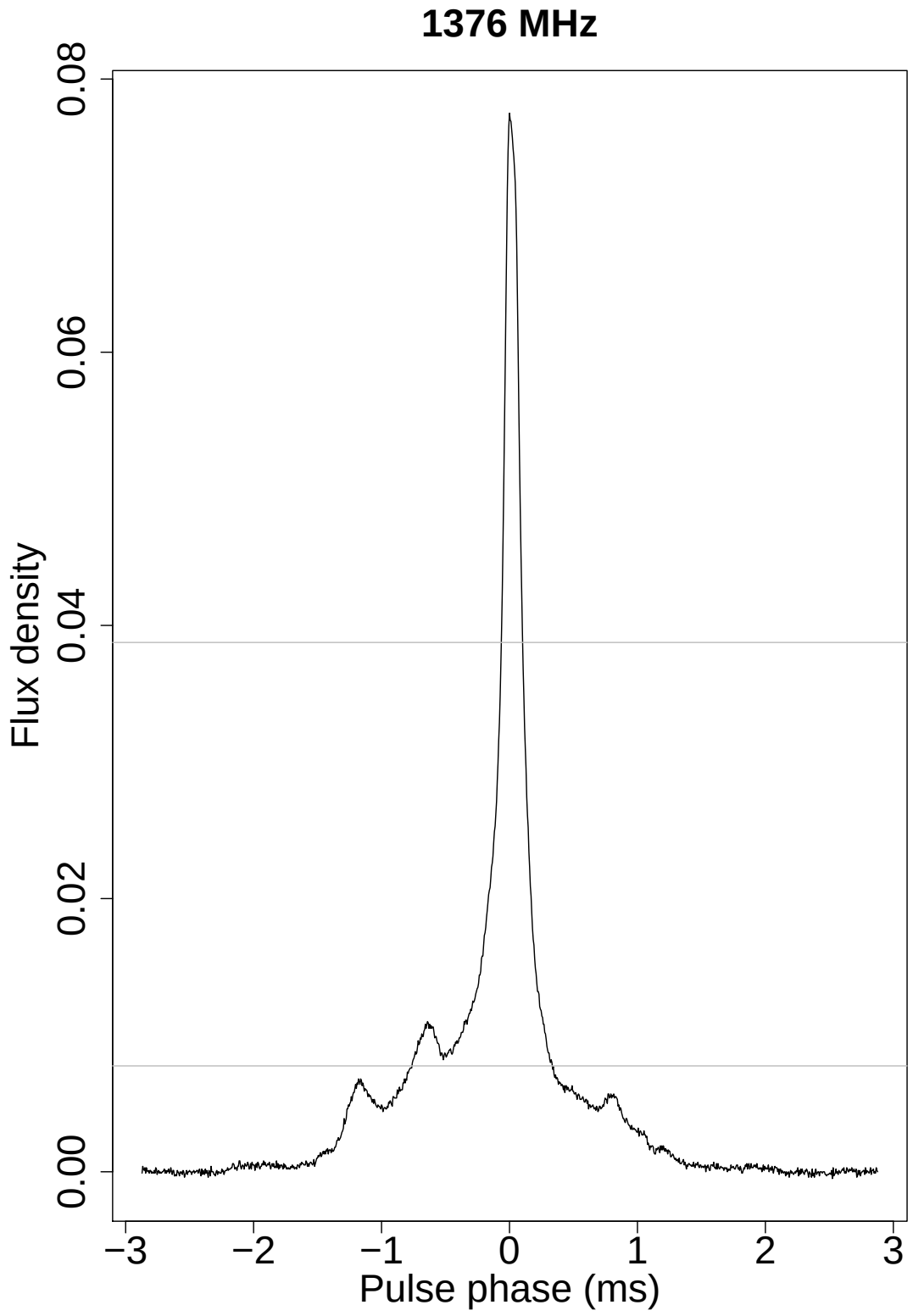

Figure 5.48: 1376 MHz pulse profile of the millisecond pulsar J0437−4715. This was integrated from 19 hours of observation. The grey lines mark the 50% and 10% levels.

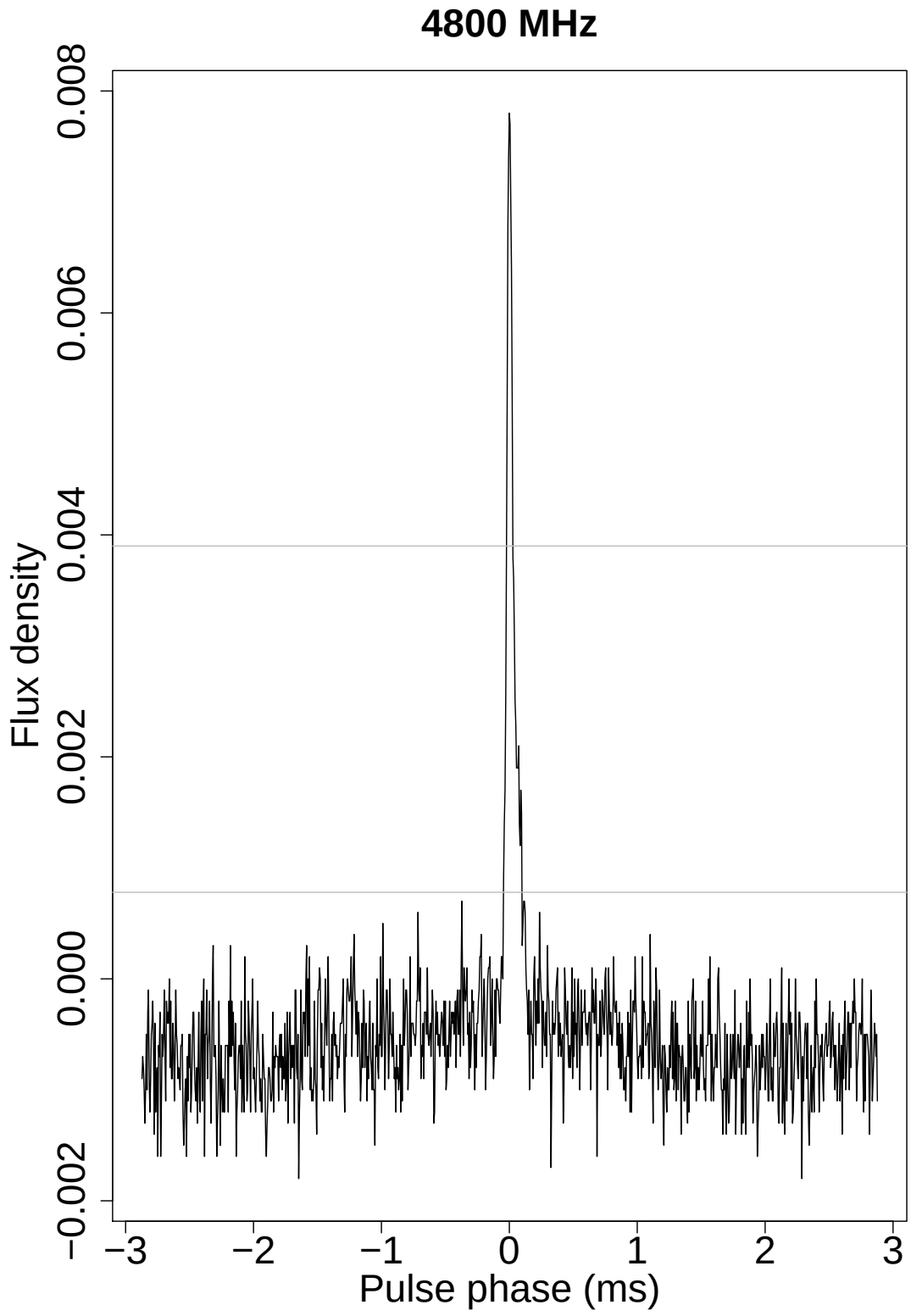

Figure 5.49: 4800 MHz pulse profile of the millisecond pulsar J0437−4715. This was integrated from 6.5 hours of observation. The grey lines mark the 50% and 10% levels.

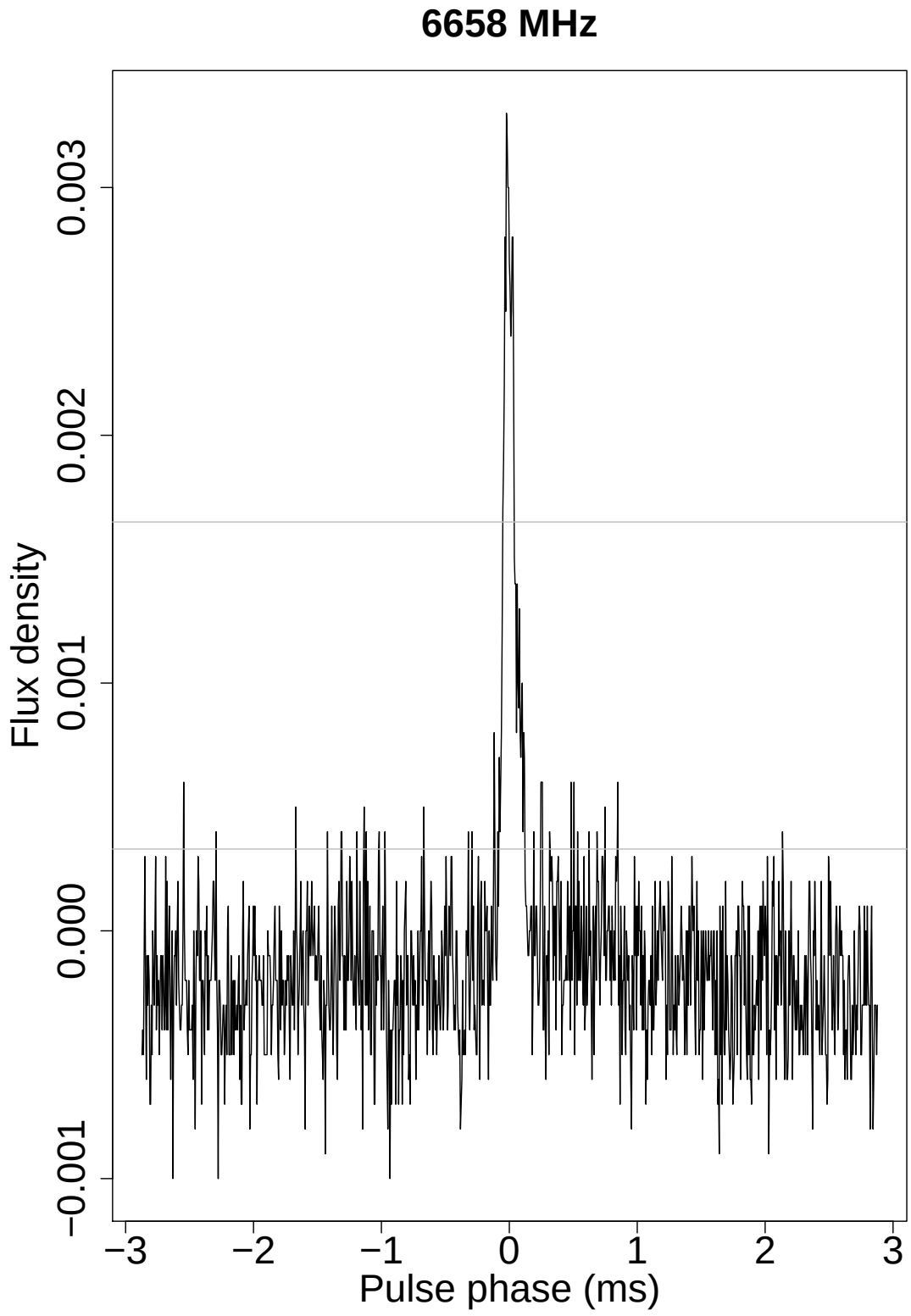

Figure 5.50: 6658 MHz pulse profile of the millisecond pulsar J0437−4715. This was integrated from 19 hours of observation. The grey lines mark the 50% and 10% levels.

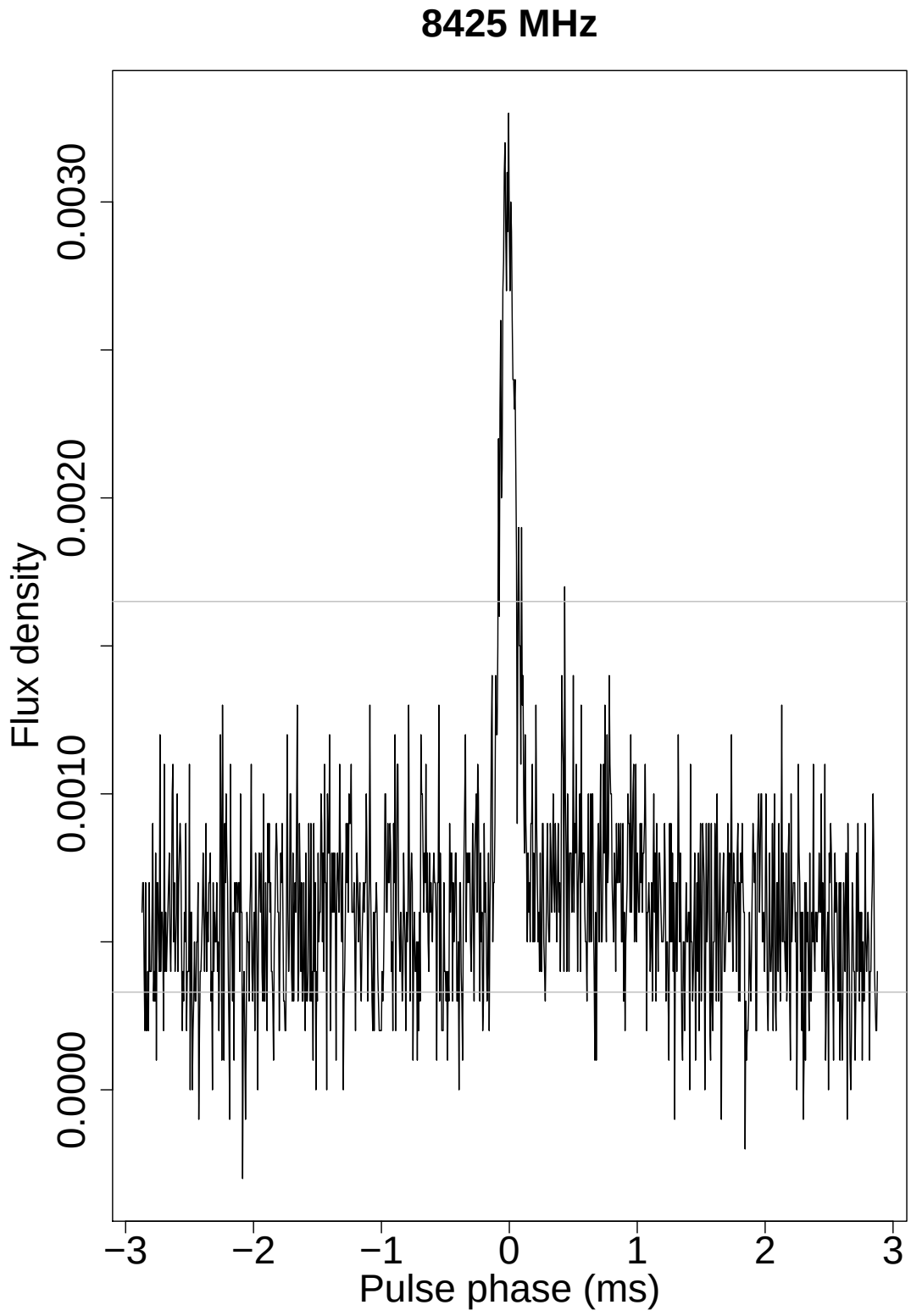

Figure 5.51: 8425 MHz pulse profile of the millisecond pulsar J0437−4715. This was integrated from 18.3 hours of observation. The grey lines mark the 50% and 10% levels.

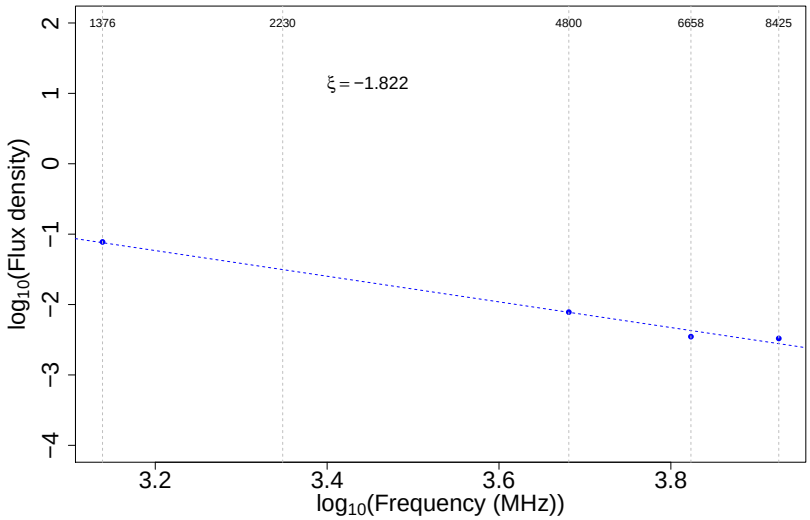

Figure 5.52: $\log_{10}$(Flux density) versus $\log_{10}$(Frequency) of J0437−4715 showing the spectral index. The line of best fit is shown as the dotted blue line.

5.3 Ceduna confirmation

With access to a second telescope in Ceduna, South Australia (1708 km away), simultaneous observations were occasionally used to verify the observations of bright pulses. For this confirmation we observed at both identical frequencies and different frequencies throughout the observing program.

5.3.1 Same frequency

Bright and consecutive bright pulses have been observed at Mt Pleasant previously (Palfreyman et al. 2011). We have confirmed bright pulses are not some local anomaly: Figure 5.53 on page 129 shows a direct comparison of the same set of pulses from Mt Pleasant and Ceduna.

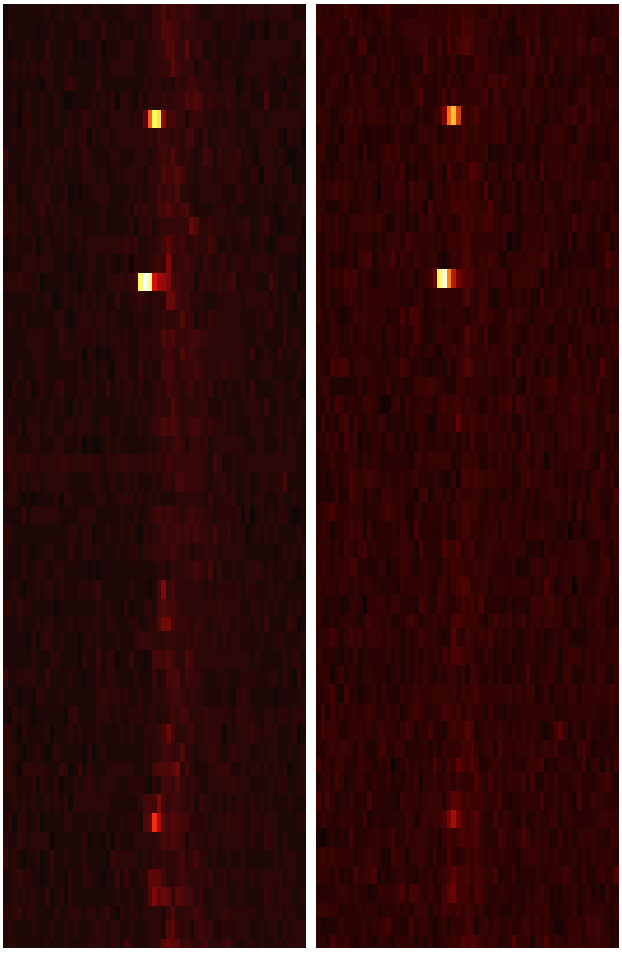

Figure 5.53: Comparison of bright pulses as viewed from Mount Pleasant (left) and Ceduna (right). This conclusively shows that bright pulses are not a local phenomenon.

5.3.2 Different frequency

Single pulses at 4800 MHz cannot normally be seen at the Ceduna observatory. With dual observations at 1376 MHz at Mt Pleasant and 4800 MHz at Ceduna we've shown that giant pulses can be seen (see Figure 5.54 on page 130). The individual pulses can be seen in Figures 5.55 to 5.56 on page 131. Note the similarity in shape.

The giant pulse arrives 0.9 ms prior to the main peak at *both* 1376 MHz and at 4815 MHz. This is an interesting result and future research could examine if this is true for different frequencies and/or times.

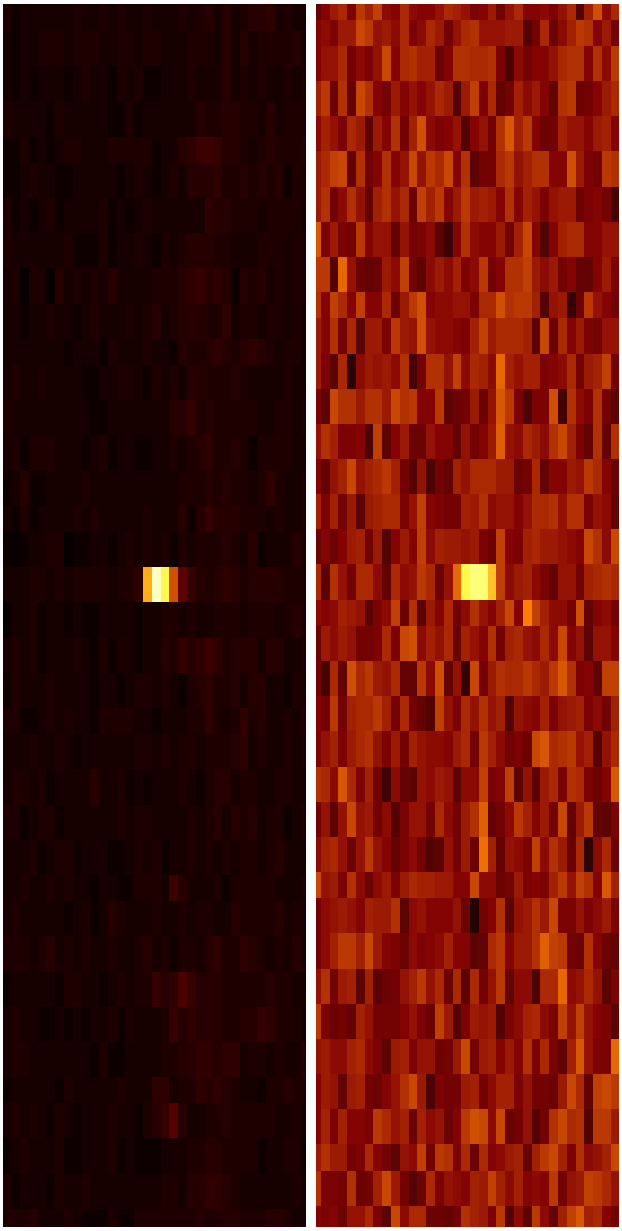

Figure 5.54: Comparison of a bright pulse as viewed from Mt Pleasant (left) at 1376 MHz and Ceduna (right) at 4800 MHz. Arrival was 2014, day 318 $\approx$ 14:47:53.5.

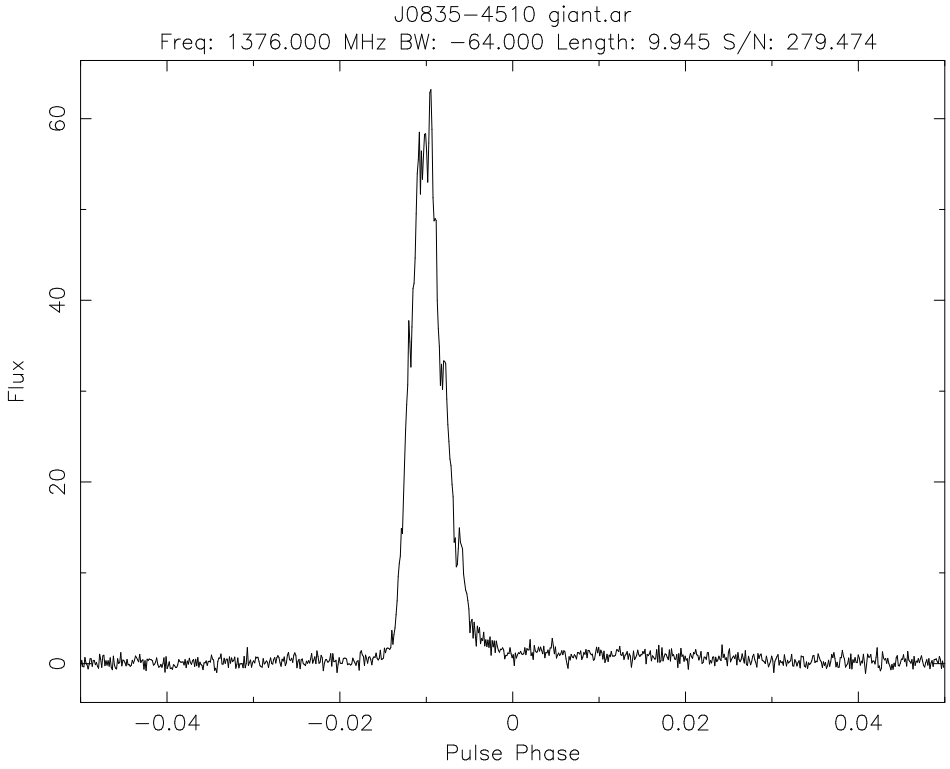

Figure 5.55: The giant pulse from J0835−4510 at Mt Pleasant at 1376 MHz. It appeared 0.9 ms prior to the main peak (at phase 0).

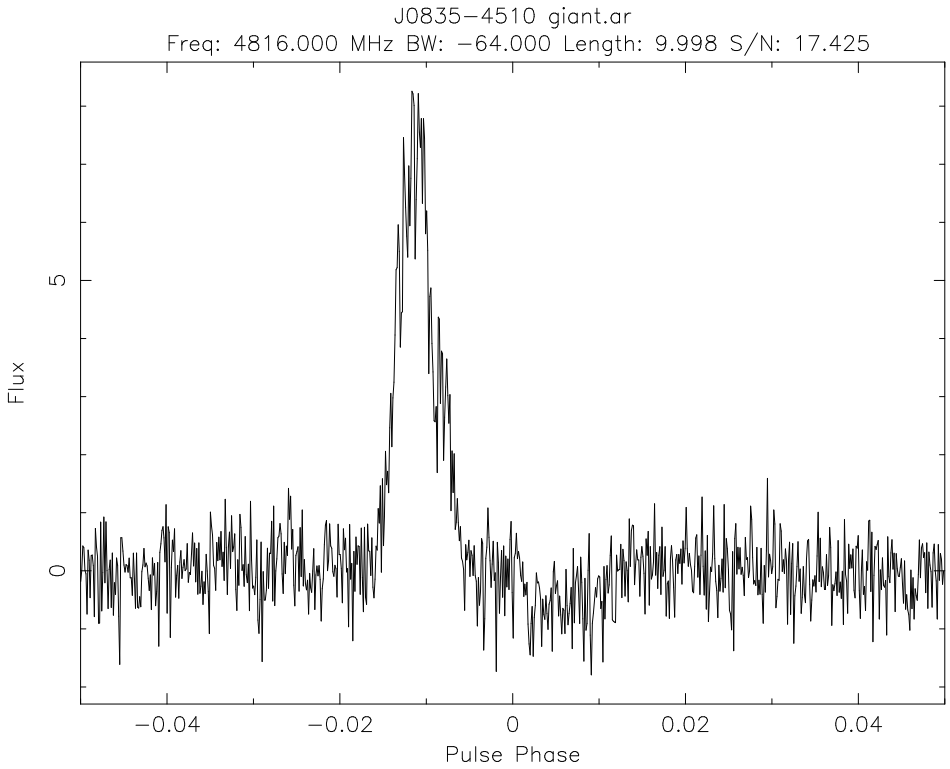

Figure 5.56: The giant pulse from J0835−4510 at Ceduna at 4815 MHz. It appeared 0.9 ms prior to the main peak (at phase 0).

Chapter 6

Temporal evolution of the pulse profile

This chapter appeared in the Astrophysical Journal (Palfreyman et al. 2016) and is reproduced here with minimal changes.[§] The chapter following is a postscript since over a year's worth of additional data was collected and analysed after publication.

6.1 Introduction

The Vela pulsar (J0835−4510) has been the focus of many studies. Much of this has focused on either long-term timing (e.g. Dodson et al. 2007) or short-term single pulse studies (e.g. Johnston et al. 2001). Here we report on both a long-term and single pulse study of the Vela pulsar.

Vela is a young, close, and bright pulsar with characteristic age τ_c=11.3 kyr, distance D≈280 pc, flux S_{1400}=1100 mJy, (Manchester et al. 2005) making it a good candidate for studies using medium-sized radio telescopes. Vela regularly *glitches* or speeds up in rotation frequency ν with $\Delta\nu/\nu \approx 2000 - 3000 \times 10^{-9}$ (Radhakrishnan and Manchester 1969; Reichley and Downs 1969).

Dodson et al. (2007) have previously demonstrated that Vela glitches approximately every three years. Micro-glitches, as defined by Cordes et al. (1988) as $\Delta\nu/\nu \lesssim 1000 \times 10^{-9}$ also typically occur a number of times per year (D'Alessandro 1995).

Giant pulses are considered as ones which have mean flux densities of at least 10 times the average pulse. Johnston et al. (2001) reported "giant micro-pulses" and Palfreyman et al. (2011) showed that Vela has bright pulses (5 times the average

[§]only to match the spelling and style of this thesis - incorrect grammar has been left as published.

pulse), and consecutive bright pulses. No genuine giant pulses have been mentioned in the literature.

Vela's integrated pulse profile is well known to change with frequency (Cordes 1978), but despite the variation in the brightness of individual pulses there has been minimal mention in the literature of pulse profile changes in Vela over time at a fixed frequency. The exception is Cordes (1993) where a single tantalising sentence mentions a pulse shape variability in the Vela profile with a period of 100 days.

In this paper we show that not only does Vela's pulse width change over time, it changes sharply after a micro-glitch, and that the rate of bright pulse activity also changes with micro-glitches. We also show that the profile changes have three quasi-periodic components (one of which has a period of ≈ 100 days) that match with periods found in X-Ray observations of a helical jet by Durant et al. (2013).

6.2 Observations and data reduction

In March 2014 we commenced a long-term single-pulse study of the Vela pulsar, collecting up to 19 h of data each day. After 18 months we have collected over 6000 h of single-pulse data.

We used the Mt Pleasant 26 m radio telescope (see Table 4.2 on page 46) with a centre frequency of 1376 MHz and a bandwidth of 64 MHz. The receiver consists of a 20 cm prime-focus feed-horn with cooled dual linear polarisation feeds that are sampled with 2 bit precision at 128 million samples per second.

Each 10 s "raw" baseband file is 640 MB in size producing 4 TB of data each day. The data is then folded and phase-coherently de-dispersed using DSPSR (van Straten and Bailes 2011) with 16 frequency channels and 8192 pulse phase bins giving a time resolution of 10.9 μs. Currently, raw files containing "interesting" events are retained, with the remainder being discarded after about 6 months. All the data is stored on the local RDSI 2.3 PB storage facility for later analysis using PSRCHIVE (Hotan et al. 2004).

Then each file was folded in frequency, polarisation, and time, then matched to a fixed standard profile template to produce a time of arrival. Residuals for the day were then calculated using TEMPO2 (Hobbs et al. 2006) and bad timing data was removed - typically caused by radio frequency interference (RFI) or wind stows. A best fit of ν and $\dot{\nu}$ was performed producing a residual plot appearing as white noise with a typical RMS of ≈ 50 μs. Finally all of the day's 10 s files were phase aligned and integrated using the ν and $\dot{\nu}$ just calculated. A successful full day's observing of 19 h

would produce an integrated profile from over 7.5×10^5 individual pulses and have a signal-to-noise ratio of around 2×10^4. Days that were shortened ($\lesssim 3$ h) due to other observers or wind stows were removed from the analysis.

The arrival time residuals of these daily integrated profiles were then used to search for micro-glitches. The PSRCHIVE utility `pdv` was used to produce the pulse widths at 10% and 50% of the pulse heights of the integrated profile.

We developed an algorithm to select a pulse as being "bright", but yet not include any RFI that passed through the timing residual stage, if two conditions were met:

1. the pulse has a peak flux of 10 or more times the average pulse.
2. the pulse at the 50% level has a width (FWHM) of between ≈ 160 and 550 μs (15-50 timing bins).

To confirm the algorithm's effectiveness we manually checked all 41442 bright pulses to verify how many were actually RFI. Only $\approx 5\%$ were falsely selected by the algorithm and these were removed from the analysis.

6.3 Pulse shape changes

Figure 6.1 on page 136 shows a plot of the 50% and 10% profile widths, timing residuals, and bright pulse rate for MJD 56746 to 57281. At MJD=57143 a micro-glitch of magnitude $\Delta\nu/\nu = 75.6 \times 10^{-9}$ occurred (see Figure 6.2 on page 137), and a noticeable and sustained reduction in the pulse width at both 50% and 10% of the pulse height can be seen.

Jankowski et al. (2015) reported a micro-glitch at MJD=56922 with a magnitude of $\Delta\nu/\nu = 0.4 \times 10^{-9}$ (see Figure 6.3 on page 138). This coincided with a large increase in bright pulse activity.

The plot of pulse width over a year shows distinct cyclical variations on the order of 20-30 μs. Figure 6.4 on page 139 shows a Lomb-Scargle periodogram (Lomb 1976; Scargle 1982) which has significant (p=0.001) period peaks at 78±5, 100±7, and 137±12 days.

We also found a strong correlation (r=0.914) between the pulse widths at 10% and 50% of the peak (see Figure 6.5 on page 139) through the entire dataset.

This implies that what is affecting pulse width is affecting the entire pulse shape.

Our observations show that after the second and larger micro-glitch the pulse has decreased in width by about 40 μs (2.6%) at the 50% level and about 60 μs (1.7%)

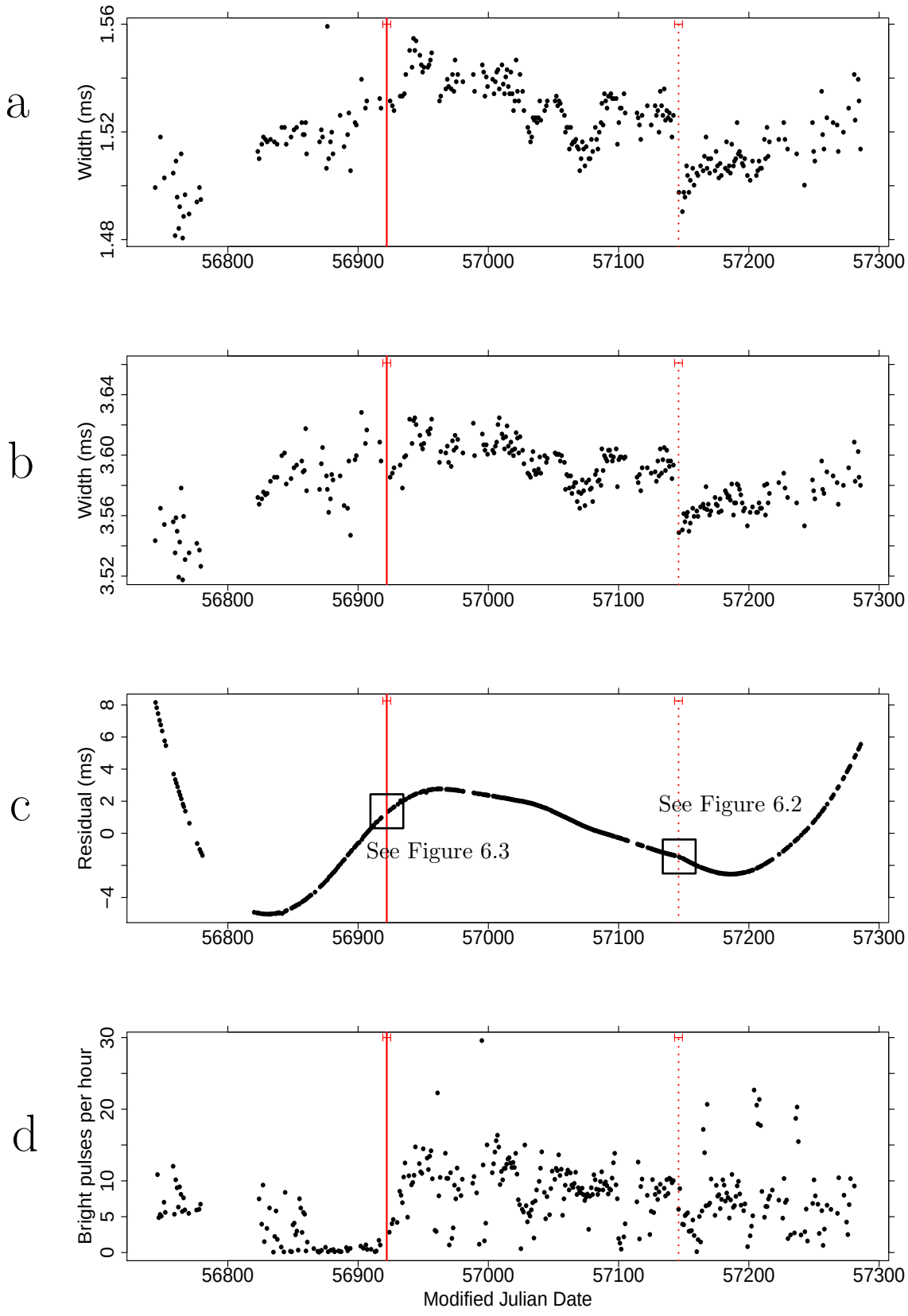

Figure 6.1: (a) Plot of pulse width (in ms) at 50% of the peak of the integrated pulse, (b) pulse width at 10% of the peak, (c) timing residuals, and (d) bright pulse rate. Note the sudden decrease in both pulse widths when the magnitude $\frac{\Delta\nu}{\nu} = 75.6 \times 10^{-9}$ micro-glitch at MJD=57143 occurred (dotted line). Note the 50 day quiet period and then sudden increase in bright pulse rate after the first glitch of magnitude $\frac{\Delta\nu}{\nu} = 0.4 \times 10^{-9}$ that occurred at MJD=56922 (solid line). Each dot is a day of observing and all errors bars are smaller than the dots.

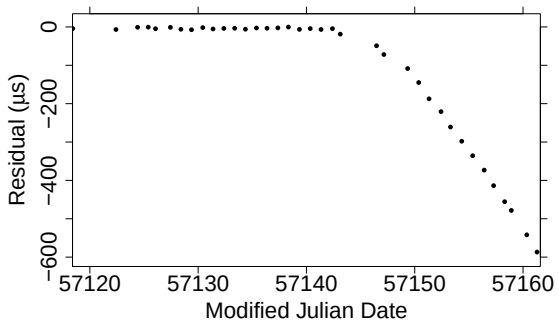

Figure 6.2: Daily timing residuals showing the $\Delta\nu/\nu = 75.6 \times 10^{-9}$ magnitude micro-glitch at MJD=57143±3.

at the 10% level.

Note that even though we observed with a bin width of 10.9 μs, we have from Lorimer and Kramer (2004):

$$\sigma_T \approx \frac{W}{S/N} = \frac{5\ ms}{20000} = 0.250\ \mu s, \tag{6.1}$$

where σ_T is the timing error, W is the pulse width, and S/N is the signal to noise ratio. This shows that the error bars in Figure 6.1a, Figure 6.1b, and Figure 6.1c on page 136 would be smaller than the plotted points after integrating over 19 hours.

Pulse profile width changes like this could be caused by a slight change in our sight-line to the pulsar's magnetic axis β (see Figure 6.6 on page 140) both generally throughout the year and also a step change associated with the micro-glitch. For this to occur either a change in the pulsar's rotational axis relative to the earth (geodetic precession), or a change in the magnetic axis angle (α) relative to the rotational axis (free precession) has occurred.

Precession of the Vela pulsar has been raised in the literature previously. Durant et al. (2013) reveal a helical X-Ray jet streaming from the rotational axis of the Vela pulsar potentially caused by precession. The jet has "acceptable" periods of 122 ± 5, 73 ± 2 or 91 ±5 days. We see three definite periods in our pulse width data and the ranges of these fall within the ranges of the "acceptable" periods mentioned in Durant et al. as shown by Figure 6.7 on page 140.

Stairs et al. (2000) also discuss precession in a different pulsar (J1830−1059) and the periodicity in their timing residuals is very clear. However J1830−1059 does not glitch like Vela and so the cycles are easy to measure over a long period of time. They conclude that precession is the simplest explanation for their observations.

The change in α for Vela has also been discussed by Link and Epstein (1997). They

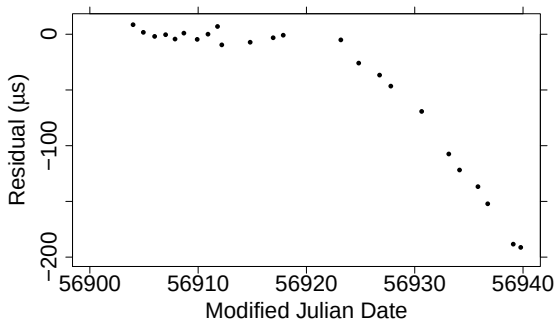

Figure 6.3: Daily timing residuals showing the $\Delta\nu/\nu = 0.4 \times 10^{-9}$ magnitude micro-glitch at MJD=56922±3.

contend that its very low braking index of 1.4 ± 0.2 is caused by an increase of α over time. For Vela, $\alpha = 55°$ and $\beta = -6°$ (Johnston et al. 2001) and so since β is negative we have an inside sight-line (see Figure 6.6 on page 140). An increase in α implies the pulse width should be shrinking overall. Our data shows a pattern of pulse width increase and then decrease following the small micro-glitch at MJD=56922. After the much larger micro-glitch at MJD=57143, we see a sharp decrease in pulse width followed by a steady increase.

Link and Epstein (1997) also state that the evolution of α is not monotonic and that it seems to be different with older pulsars as compared to younger ($t_{age} \lesssim 10^4$ y) ones.

Profile width changes could also be caused by a change in the width of the emission cone (ρ). This has been discussed in Rankin (1993) which shows a link between conal width and pulse period — the slower the pulsar, the narrower the emission cone. Now since a glitch is a fractional increase in rotation frequency, this would imply a widening of the emission cone. With the larger micro-glitch, we observed a sharp decrease followed by a slow increase in pulse width. Regardless, the rotational increase is so small that Rankin's relation ($W = 5.8^o P^{-1/2}$) predicts a pulse width change of only 0.178 ns. Of interest is that changes in emission cone width are linked to rotational frequency, and that a micro-glitch could be linked to a change in pulse width.

There are three distinct visible and one non-visible features in the integrated profile of the Vela pulsar (see Figure 6.8 on page 141):

a. large main peak

b. 'ledge' to the right

c. gentle point of inflection

d. bright pulse emission zone

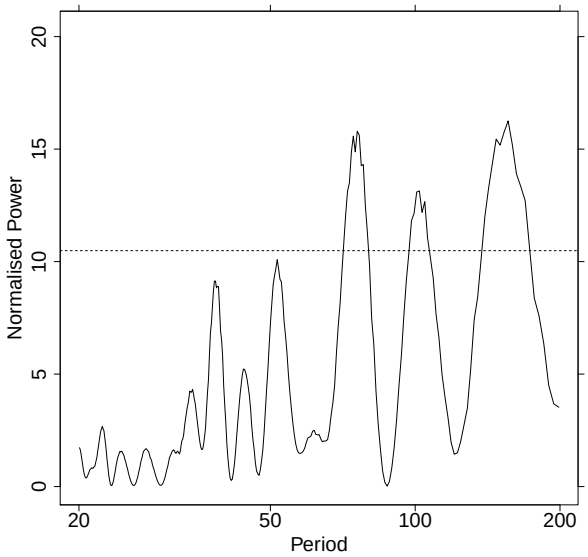

Figure 6.4: Lomb-Scargle periodogram of the pulse width at the 50% level with a cutoff level set at p=0.001. Significant peaks are at periods of 78±5, 100±7, and 137±12 days. Due to the discontinuity, data after the micro glitch at MJD=57143 was excluded from this analysis.

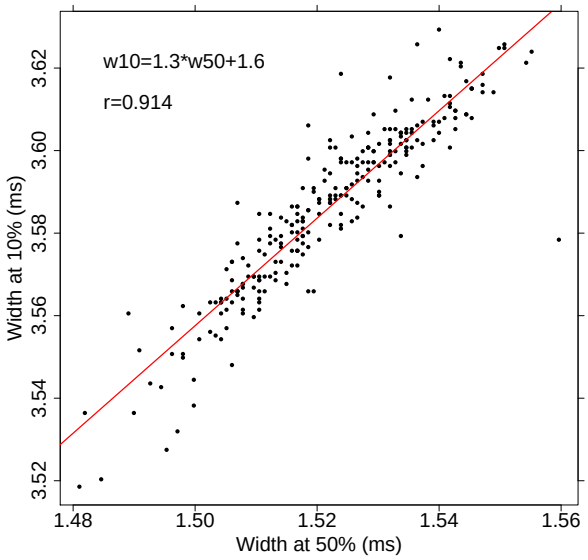

Figure 6.5: Correlation of pulse width at 10% of the peak to 50% of the peak. Low signal-to-noise days have been removed.

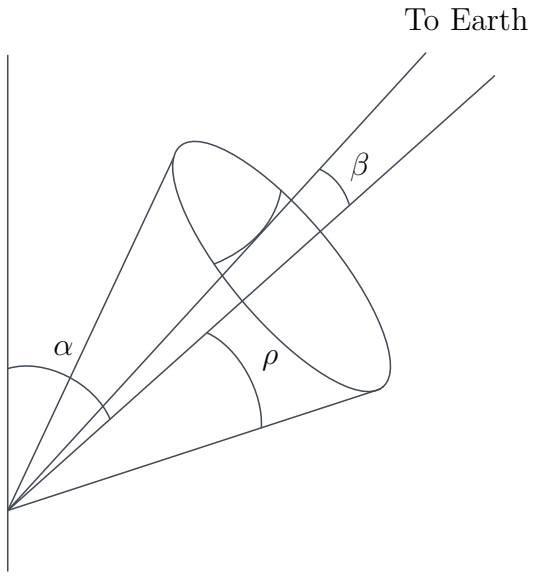

Figure 6.6: Simple graphic showing angles for the Vela pulsar where α is the angle between the rotational and magnetic axes (55°), β is the angle between the sight-line and the magnetic axis (−6°), ρ is the angular half-width of the emission cone (12°). See text for references.

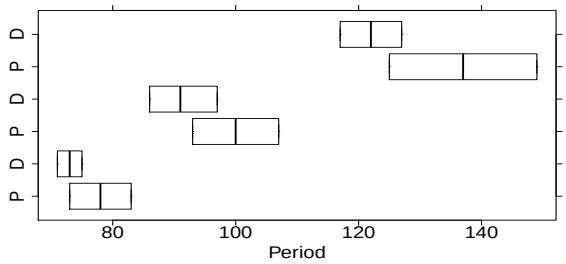

Figure 6.7: Periods (in days) from (P) our Lomb-Scargle plot (Figure 6.4 on page 139) compared to the periods from the (D) X-Ray observations from Durant et al. (2013).

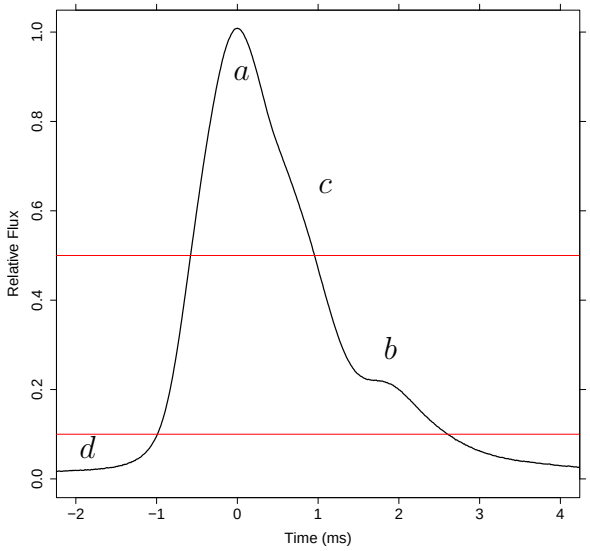

Figure 6.8: Typical daily integrated pulse profile (over 750000 pulses) of J0835−4510 at 1376 MHz showing the 10% and 50% levels. The letters *a,b,c,d* label emission zones discussed in Krishnamohan and Downs (1983). See text.

Krishnamohan and Downs (1983) discuss these four pulse components, their distributions, and their emission heights.

The leading edge bright-pulse component (*d*) is not visible in the integrated profile because it only appears rarely. However, when the pulsar does emit a bright pulse, it is always on the leading edge, and it affects the pulse width strongly at both the 10% and 50% levels. Therefore an increase in bright pulse rates should positively correlate with an increase in pulse width. It can be seen this is the case around the first small micro-glitch (MJD=56922), but it is clearly not the case with the large micro-glitch (MJD=57143) where the sudden decrease in pulse width did not appear alongside a sudden drop in bright pulse rate. A Lomb-Scargle periodogram of the bright pulse rates shows no significant periodicities.

This is a paradox. The first micro-glitch coincides with a sudden increase in bright pulse rates, with no apparent change in pulse width. The second micro-glitch coincides with a sudden decrease in pulse width with no apparent change in bright pulse rate.

This can be explained in the model of Wright (2003) who considers that emission zones might be mathematically chaotic in nature, however this hypothesis relies on the emission zones occurring in the cone, whereas Vela (being a young pulsar) should have main core emission rather than conal emission (Rankin 1990).

Finally, note in Figure 6.1d on page 136, the 50 day "quiet time" just before the first micro-glitch and the gradual overall "settling" of the bright pulse rate over time. This may settle to another "quiet time" which might indicate that another glitch is

imminent.

6.4 Conclusion

We are carrying out an intensive single-pulse observation campaign of the Vela pulsar and have collected over 6000 hours of data. We have shown that the daily integrated pulse profile width changes both slowly over time and has a discontinuity after a micro-glitch. Bright-pulse rates are also shown to be affected by micro-glitches, but in an inconsistent manner.

We have found periodicities in the pulse width changes that match (within error bars) the exciting X-Ray results from Durant et al. (2013) that imply free precession.

We hope that these results might shed some new light on the pulsar emission and glitching process, and to this end, we intend to produce further papers from this large data set.

Chapter 7

Postscript with updated data

The paper in the previous chapter was originally submitted in October 2015, and further data has since been added. Figures 7.1 to 7.3 on pages 144–145 show Figure 6.1 on page 136 with the additional data. As previously, this plot shows temporal changes in the 50% and 10% pulse widths over time along with dotted red lines marking further drops in the pulse width and *all* coincide with micro-glitches with $\frac{\Delta\nu}{\nu} > 0$ in the timing residuals. The tiny micro-glitch ($\frac{\Delta\nu}{\nu} = 0.4 \times 10^{-9}$) on MJD 56922 has been removed from the plot as the drop in pulse width is small at best. The intriguing result here is that the rapid shrinking of pulse width coinciding with $\frac{\Delta\nu}{\nu} > 0$ micro-glitches has continued. The strong correlation of changes in the pulse width at the 10% and 50% levels (as originally shown in Figure 6.5 on page 139) has also continued and is shown in Figure 7.4 on page 146.

The Lomb-Scargle periodogram of the time series in Figure 7.1 on page 144 is shown with the new data in Figure 7.5 on page 146. The published version (Figure 6.4 on page 139) only included data prior to the micro-glitch at MJD 57143. In Figure 7.5 on page 146 all data has been included and periods of 154, 372, 101, 76, 126, and 39 days (in descending order of normalised power) have appeared. The original periods that coincided with Durant et al. (2013) still appear, but more interestingly two very significant periods of 372 and 155 days have surfaced.

Deshpande and McCulloch (1996) suggested a precessional period of 330 days in Vela which would support this finding.

Weisberg et al. (2010) conducted an analysis of the change in ψ (the position angle of the linear polarisation or PPA) of 81 pulsars and produced sinusoidal fits to 19 of these with periods from 200-1300 days. They stated that these sinusoidal changes could be explained by precession. Unfortunately Vela was not included in their analysis, but their results show that precession is certainly a decent possibility in many pulsars.

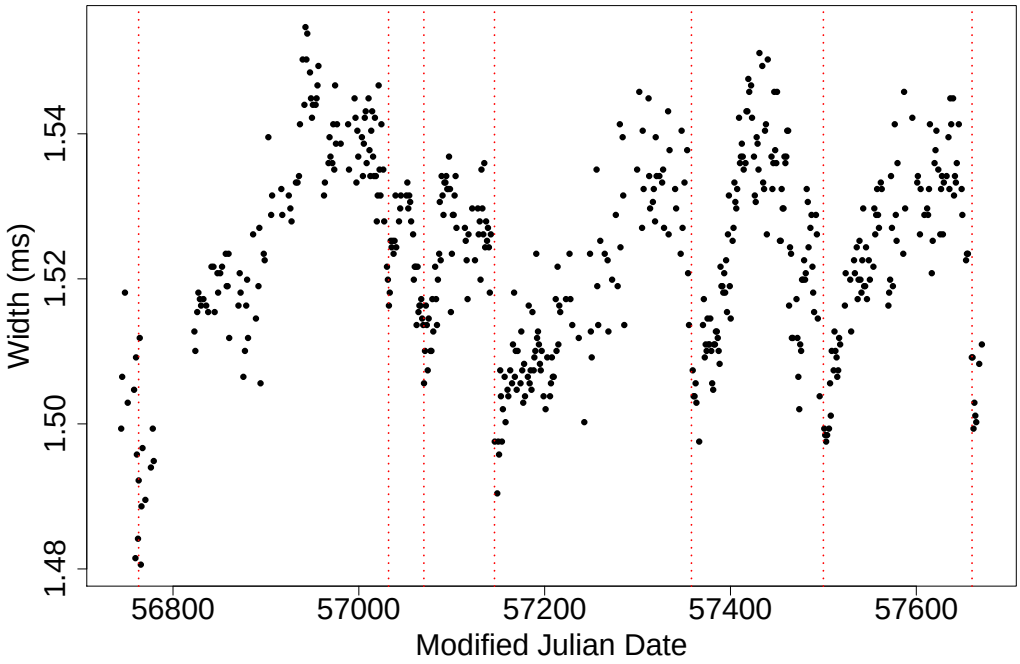

Figure 7.1: Pulse profile width at the 50% level of Vela over time. The dotted red lines mark sudden drops in the pulse width and all coincide with micro-glitches with $\frac{\Delta\nu}{\nu} > 0$ in the timing residuals.

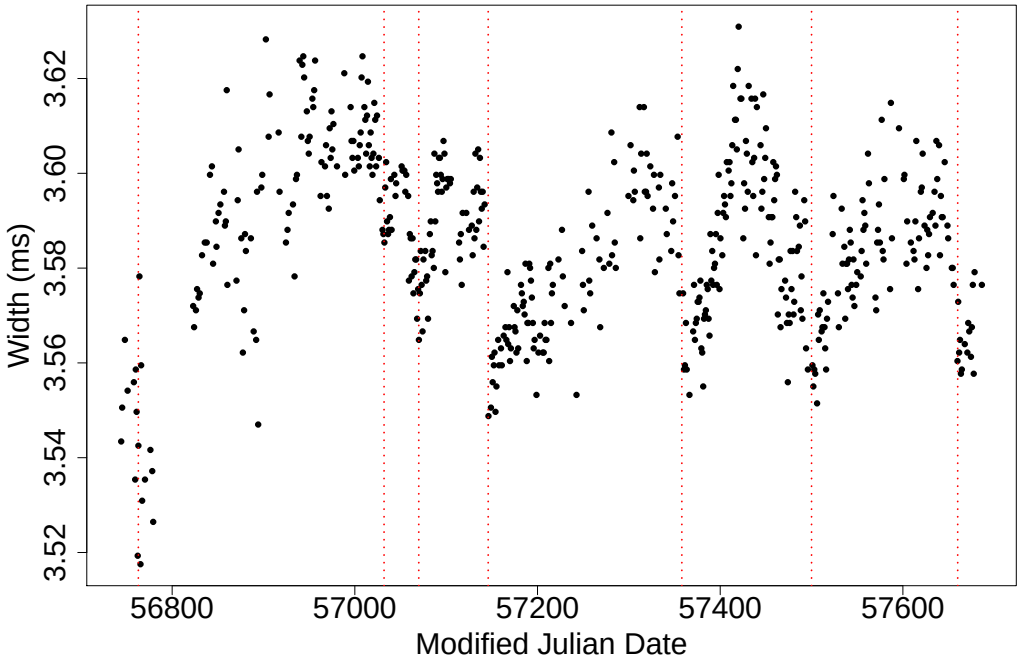

Figure 7.2: Pulse profile width at the 10% level of Vela over time. The dotted red lines mark sudden drops in the pulse width and all coincide with micro-glitches with $\frac{\Delta\nu}{\nu} > 0$ in the timing residuals.

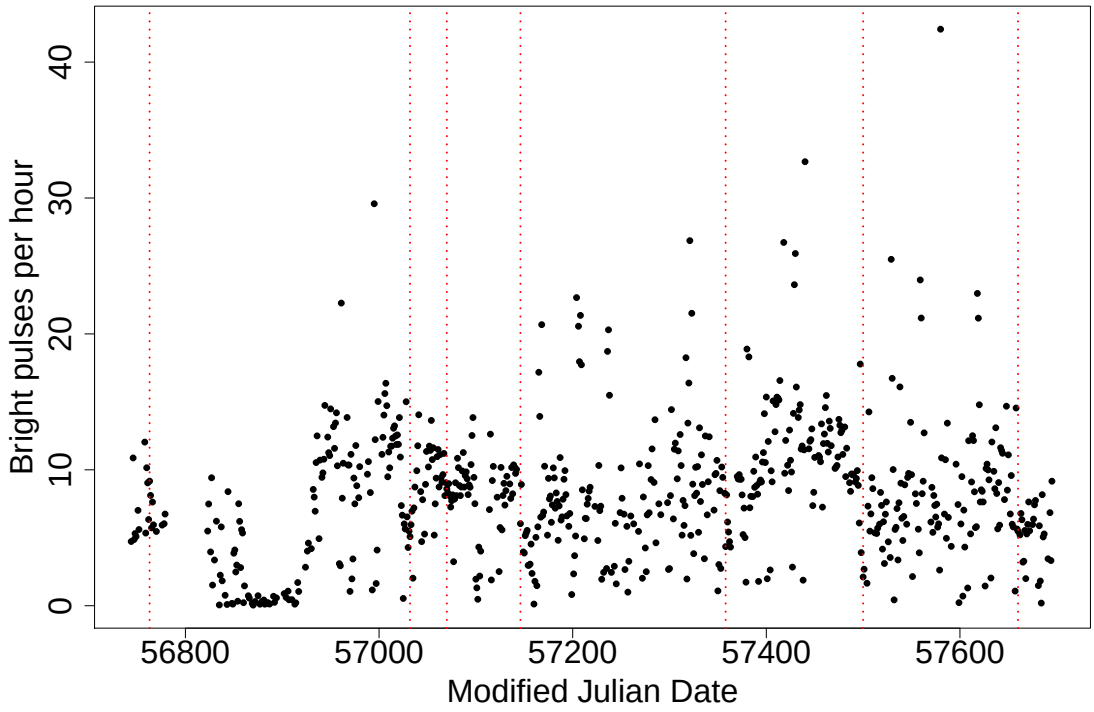

Figure 7.3: Bright pulses per hour versus time for Vela. The dotted red lines mark micro-glitches. Note that there is never any high bright pulse activity (bright pulse rate$>$ 20) near micro-glitches.

To confirm that the variations in pulse width of the Vela pulsar's pulse profile were not system or processing artefacts, the same analysis was performed on J1644−4559. This pulsar is second only to Vela in flux density (the average over the pulse period is 310 mJy compared to 1100 mJy at 1400 MHz) and was typically only observed for at most 5 hours when Vela was below the horizon limits of the 26 m telescope. Being both fainter and observed for less time made the signal-to-noise ratio an order of magnitude worse ($\approx$ 2000 at best compared to $\approx$ 20000 for Vela) and using Equation 6.1 on page 137 with figures for J1644−4559:

$$\sigma_T \approx \frac{W}{S/N} = \frac{8.2 \text{ ms}}{2000} = 4.1 \ \mu\text{s} \tag{7.1}$$

the pulse width errors are significantly larger (and probably even worse if pulse jitter is taken into account). Figure 7.6 on page 148 shows the plot of pulse width at the 50% level over time. The general trend can be clearly seen and this means the pulse width is increasing at the rate of 454 ns day^{-1}.

Tong and Kou (2017) hypothesise that the magnetic axis of a pulsar moves towards the rotational axis ($\alpha \to 0$) over time so the oblique rotator ultimately turns into an aligned

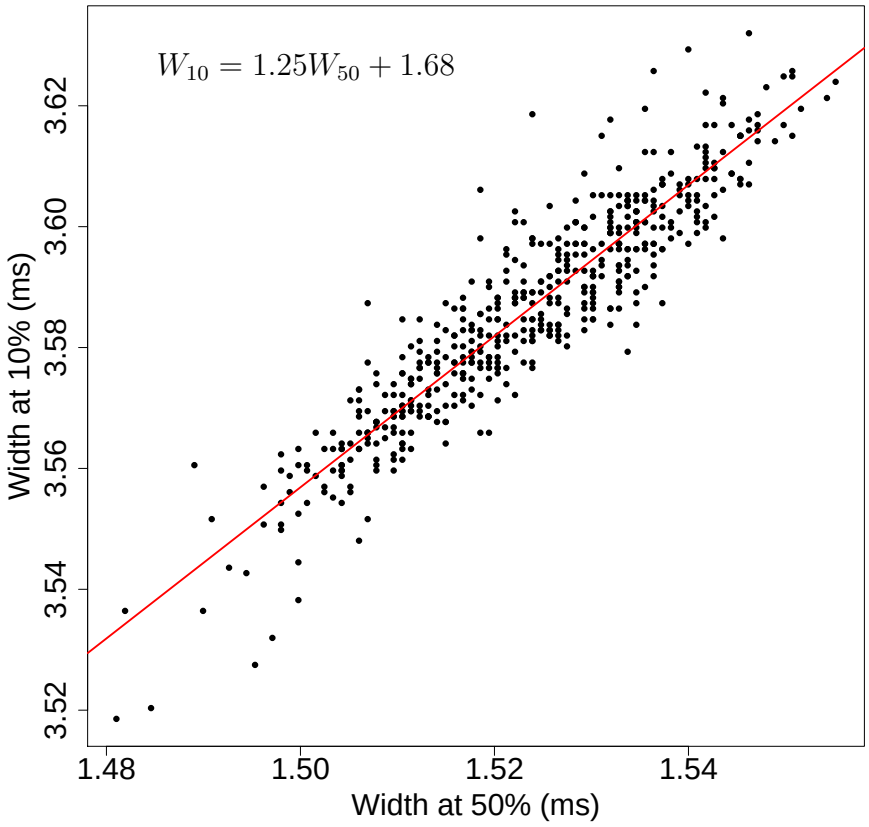

Figure 7.4: Correlation over time of Vela's pulse profile width at the 50% versus 10% level. Correlation coefficient $r = 0.925$.

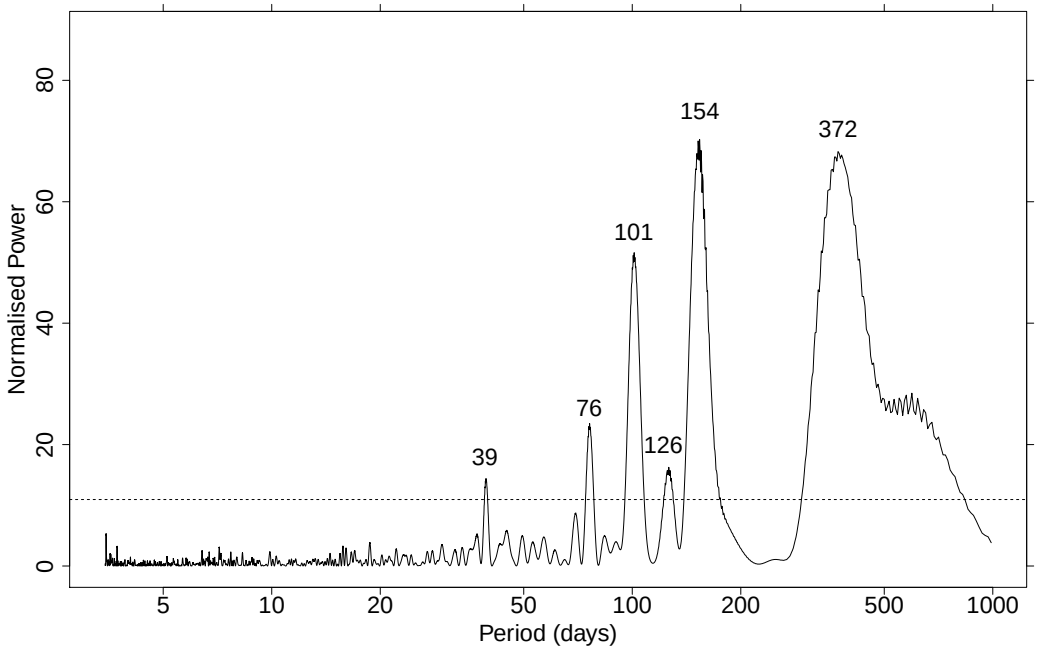

Figure 7.5: Lomb-Scargle periodogram of the Vela time series in Figure 7.1 on page 144. Significant peaks occurs at 154, 372, 101, 76, 126, and 39 days (in descending order of normalised power).

Table 7.1: Results of manually removing RFI from a number of selected days' observing of Vela.

Day	Old Width	New Width	Change (ms)	per cent	Old S/N	New S/N	Files Removed	Analyst
2016_053	1.55025	1.55025	+0.00000	+0.00	22471	21506	783	N
2016_114	1.49935	1.50024	+0.00089	+0.06	16004	15063	1156	W
2016_263	1.52882	1.53596	+0.00714	+0.46	22044	20552	1902	W
2016_274	1.49935	1.50024	+0.00089	+0.06	21118	20337	1137	N

rotator. Assuming this magnetic axis migration is true and given that the width of the pulse of J1644−4559 is increasing, this implies the pulsar has an inside sight-line and $\beta < 0$, but increasing. This is similar to Vela, (see Figure 6.6 on page 140), although as J1644−4559 is much older (characteristic age $\tau = 3.59 \times 10^5$ y compared with Vela's $\tau = 1.13 \times 10^4$ y) we can expect α to be much less than Vela's 55°.

A Lomb-Scargle periodogram of the pulse width data of J1644−4559 after MJD 57350 initially showed no indications of statistically significant periods. However when older archived data from around MJD 57100 was included (see Figure 7.7 on page 148), a peak at 273 days surfaced. It will be interesting to see if this cycle remains as further data is gathered.

Importantly there was no indication of a 374 day period in the data, confirming that this period in Vela was not due to instrument or software issues. J1644−4559 is at a distance of ≈ 4.5 kpc which is a parallax of 0.22 mas, (which is 6% of Vela) and so is too small to be reflected in changes in the pulse width, especially with only 5 hours of data (maximum) in each observation.

Another source of potential error in the pulse width statistic for Vela is the ever-present RFI. To check this, we chose 4 days and visually examined *every single* 10 s data file (using the `pav -Y` diagram) and removed files that showed the slightest hint of RFI.[‡] The four selected days had two with the pulse width near maximum and two near minimum. Each analyst was given a day of wide and a day of narrow pulses.

With the RFI removed, a comparison of integrated pulse widths before and after RFI mitigation is shown in Table 7.1. As can be seen the removal of RFI had a minimal effect on pulse width. Analyst "W" was much harsher on removing RFI than analyst "N", but all serious RFI was removed by both.

Figure 7.8 on page 149 shows a plot of pulse widths of each 10 s integrated pulse at the 50% level on a single day for Vela. Day 267 in 2016 was chosen as Vela was observed from rise to set, there were no breaks in observing, and no radio frequency interference occurred in either the timing residuals or bright pulses (of course RFI no

[‡]Thanks to Summer Scholarship students Nicholas Bochenek and Wesley Kean Tai for this task.

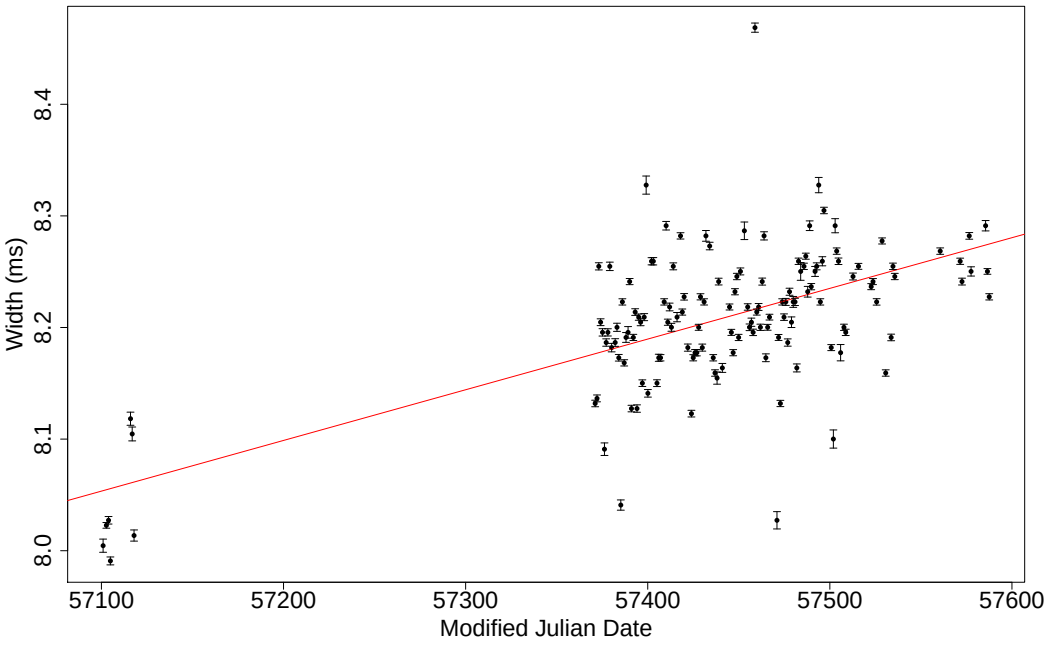

Figure 7.6: Pulse profile width at the 50% level of J1644-4559 over time. The red line shows the line of best fit and has a slope of 454 ns day^{-1}.

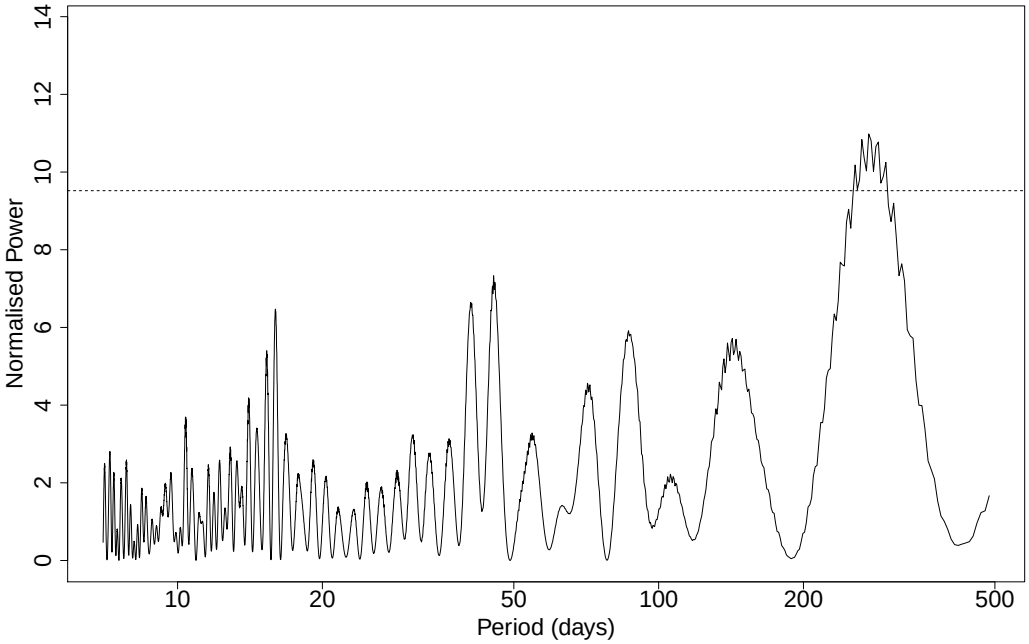

Figure 7.7: Lomb-Scargle periodogram of the time series of profile width of J1644−4559 shown in Figure 7.6. A significant peak occurs at 273 days.

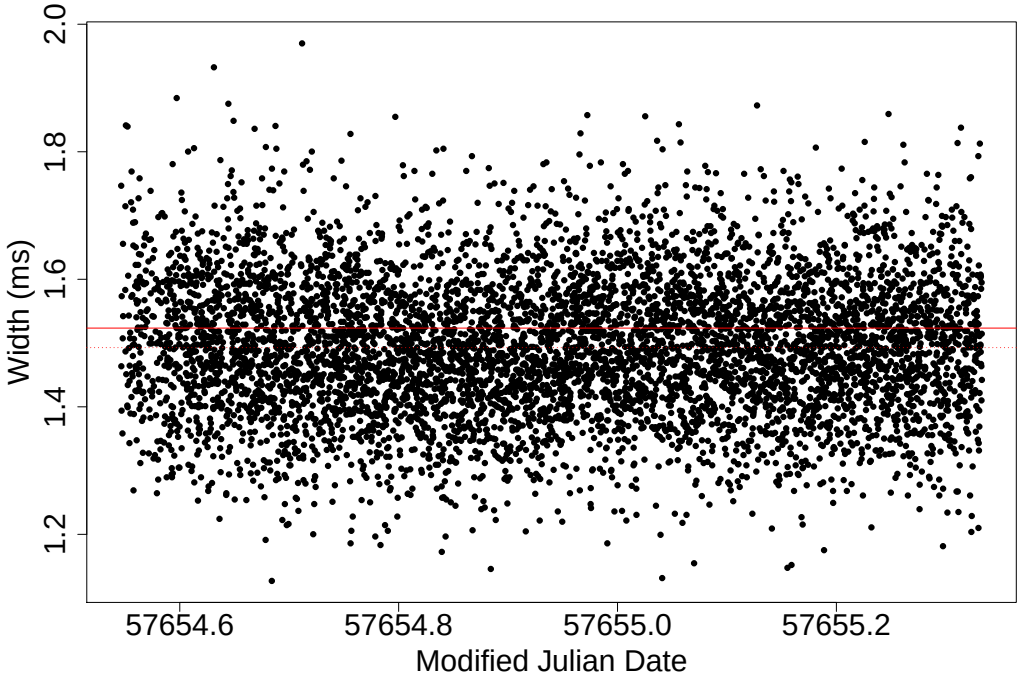

Figure 7.8: Vela pulse profile width at the 50% level on day 267 in 2016. These are widths of 10 second integrations. The solid red line marks the mean pulse width for the day as measured from the 19 hour profile, and the dotted red line marks the mean of the 10 s pulse widths.

doubt occurred - it was just particularly low that day). Each 10 s file was integrated and folded in frequency and polarisation (these were the identical files to those which were used to measure the daily timing residuals).

The solid red line marks the mean pulse width for the day as measured from the average profile, and the dotted red line marks the mean of the 10 s pulse widths. The error between the two means (1.523 and 1.493 ms) is 2% which is within the statistical expectation. The pulse widths of the 10 s profiles contain noise and some RFI which is effectively removed by the 19 hour integration and so the 1.523 ms (solid red line) is the more accurate figure. The Lomb-Scargle periodogram of Figure 7.8 showed no significant periodicities.

In summary this shows that there were no significant variations in pulse width that occurred *during* a 19 hour observation.

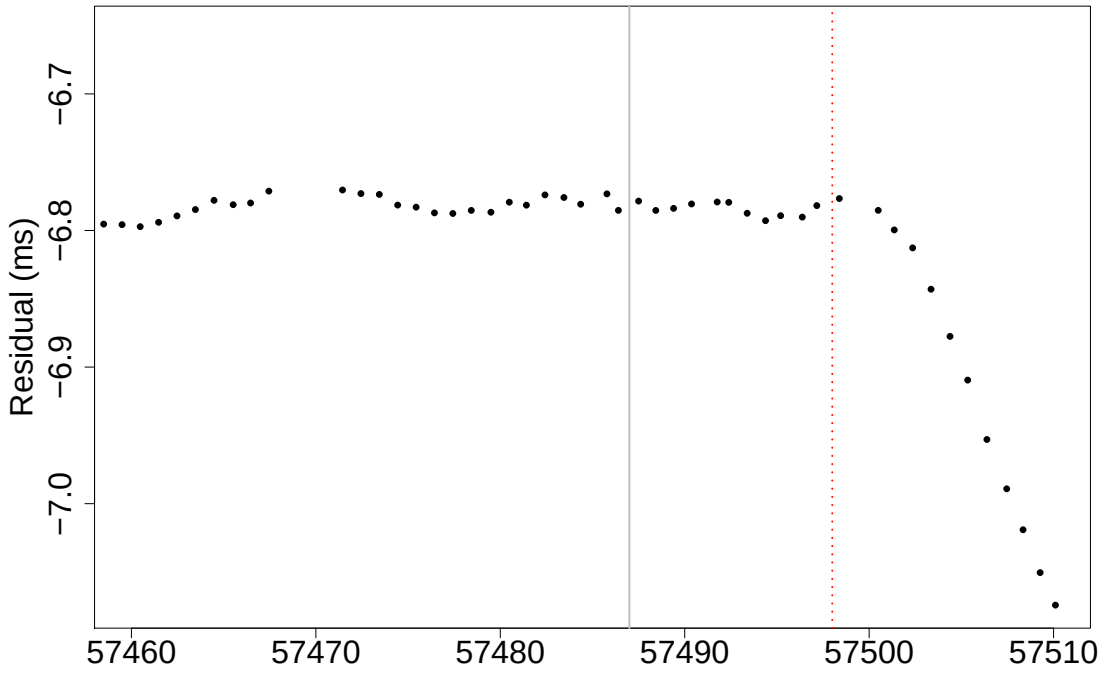

Figure 7.9: Timing residuals of Vela using pulse profiles based on the narrowest pulse profile (left of solid grey line) vs widest pulse profile (right of solid grey line). The dotted red line marks a genuine micro-glitch. This shows that changing timing profiles do not cause glitch-like signatures.

7.1 Micro-glitches

7.1.1 Real or artefact?

As shown in Figures 7.1 to 7.2 on page 144 there is a strong link between micro-glitches and pulse width. However, timing of pulses is based on a single fixed pulse profile template and it is possible that if the pulse profile is changing daily, then this could affect the timing residuals and create fake micro-glitches which were in reality an artefact of the changing pulse width.

To resolve this issue, two pulse profiles were selected. One integrated from a 19 h day when the width at the 50% profile was narrowest, and one from when it was widest. A quiescent time between micro-glitches was selected (MJD 57487) and the timing residuals were recalculated using the narrowest profile as a template prior to that date and the widest profile as a template afterwards. The timing residuals are shown in Figure 7.9. The grey solid line is the changeover from the narrowest to the widest pulse template. The red dotted line is a genuine micro-glitch using the fixed profile throughout this work.

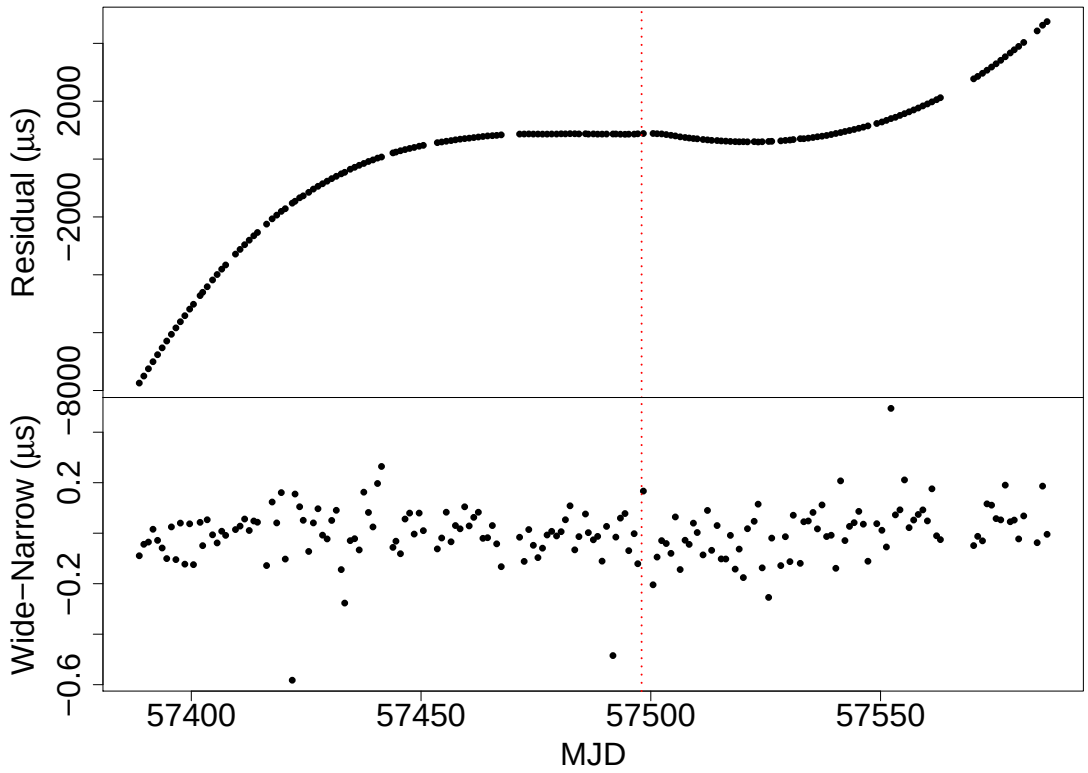

Figure 7.10: The top panel is timing residuals of Vela over 191 days (with the dotted red line marking a micro-glitch) and the bottom panel is the difference (in the sense widest−narrowest) in timing residuals based on pulse profile templates at their widest and narrowest. As can be seen, the difference is at the nanosecond level and irrelevant.

As can be seen, the switch from the narrowest to the widest pulse profile template made no difference to the timing residuals.

To examine this further we plotted the difference in timing residuals based on the two profile templates over 191 days (in the sense widest−narrowest) and this is shown in Figure 7.10. As can be seen, the residual differences are less than a microsecond, and hence irrelevant.

This rules out that the changing pulse profiles affected the timing residuals, and being the cause of micro-glitches and general red noise.

7.1.2 Linking micro-glitches to pulse width

Micro-glitches are an intriguing phenomenon. Their change in $\frac{\Delta\nu}{\nu}$ being both positive and negative set them apart from normal glitches where $\frac{\Delta\nu}{\nu} > 0$.

Assuming that they are from the same process, then by examining Figure 2.14 on page 29 we see that the angular velocity of the crust ($\Omega = 2\pi\nu$) compared with the angular velocity of the core ($\Omega_{\rm n}$) is different for most times except when a glitch oc-

curs.

The crust, being composed of iron nuclei, protons, electrons, and neutrons in a crustal superfluid, has a stronger magnetic field than the super-fluid core (Sourie et al. 2017). So a hypothesis is that when $\Delta\Omega = \Omega_{\rm n} - \Omega$ is non-zero, the magnetic field of the core and crust may be affecting the magnetosphere, and possibly making the emission cone wider. Then after a (micro) glitch in which $\Delta\Omega$ is reduced, the magnetic field of the crust and core line up and hence affect the magnetosphere less, and so would make the pulse width narrower.

However, as will be shown in Section 8.5 on page 229, glitches and micro-glitches appear to have different causes. There is little doubt that glitches are occurring in the neutron star itself, but micro-glitches could be occurring in the magnetosphere.

7.2 Morphology of pulse shape

The changes of pulse width at the 50% level shown in Figure 7.1 on page 144 are comparatively small and comparing the shapes of the widest vs the narrowest pulse by eye reveals no visible change. However Figure 7.11 on page 153 shows the difference in intensity between the two (in the sense widest−narrowest) superimposed on the pulse profile and its Gaussian components. Interestingly the two troughs line up with Gaussian components *a* and *c*, and the point of inflection lines up with component *b*.

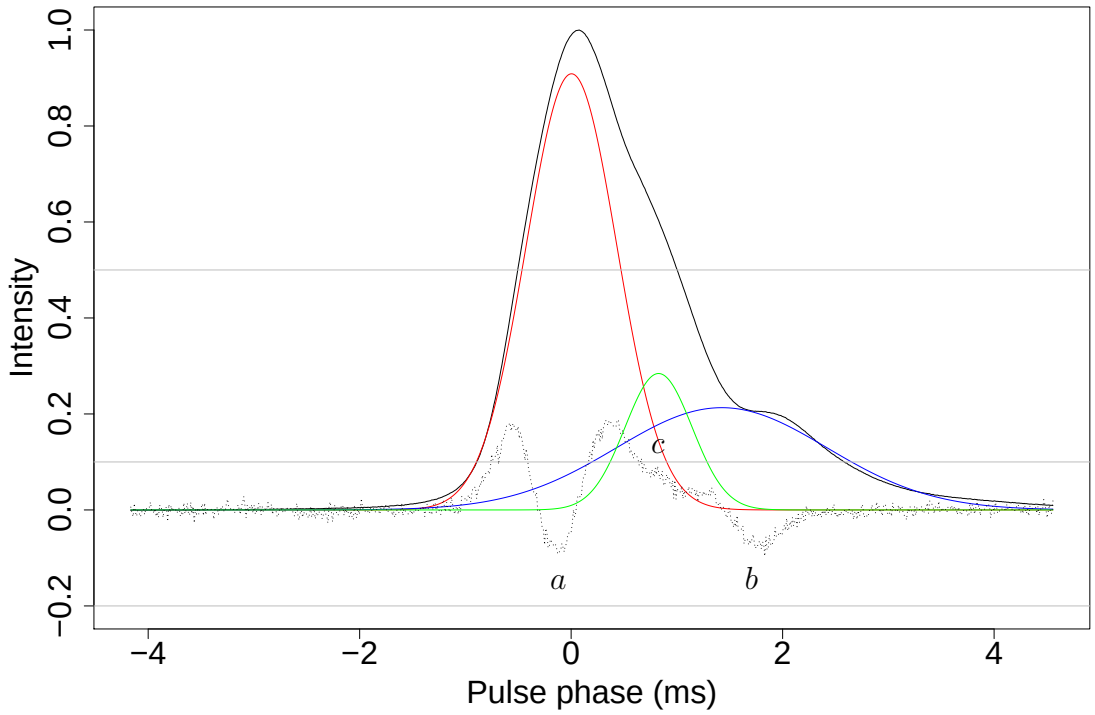

Figure 7.11: The difference in flux density of Vela between the widest and narrowest daily integrated pulses (dotted line) superimposed on a normalised plot of Figure 5.37 on page 113 which shows the pulse profile and underlying Gaussian components. Note that the dotted line showing flux density difference is not to scale. The horizontal grey lines mark the 50% and 10% levels of pulse flux density.

Chapter 8

The glitch of 2016

8.1 Summary

A summary of this chapter appeared in *Nature* (Palfreyman et al. 2018) and is reproduced in Appendix C on page 311.

On 2016-12-12 at 11:36 UT a glitch of magnitude 1431×10^{-9} was observed at both the Mount Pleasant and Ceduna observatories. The alert system via SMS described in Section 4.4.7 on page 58 was successful in its notification as shown in Figure 8.1 on page 156, and an *Astronomer's Telegram* (Palfreyman 2016) was sent out at 12:22 UT which was 44 min after the glitch occurred. The arrival of the glitch at the solar system barycentre was initially estimated to be at MJD 57734.485 (11:38 UT).

The glitch was recorded at both radio telescopes at a frequency of 1376 MHz. Whilst the Mount Pleasant data was successfully recorded, the Ceduna data was very poor due to a loose connection in a cable connector.[‡] This meant that overall timing data based on 10 s integrations was available, but very little single pulse timing information was obtained from Ceduna.

Table 8.1 on page 156 shows an overall summary of glitch arrival times at the solar system barycentre from both telescopes. The Mount Pleasant figures for $\frac{\Delta\nu}{\nu}$ and $\frac{\Delta\dot{\nu}}{\dot{\nu}}$ were obtained using 4 days of 10 s integrated data, whereas the fitting of the glitch epoch is based on 72 min of single pulse data. The Ceduna data is based on 15 h of 10 s integrated data, but with only ≈ 1 h of pre-glitch timings available, this meant $\frac{\Delta\nu}{\nu}$ was not ideal and $\frac{\Delta\dot{\nu}}{\dot{\nu}}$ was not able to be determined. The difference in $\frac{\Delta\nu}{\nu}$ between the two telescopes is because TEMPO2 underestimates the uncertainties due to the unmodelled effects of red noise (Shannon et al. 2016).

[‡]Ironically similar to the faster-than-light neutrino error (https://profmattstrassler.com/articles-and-posts/particle-physics-basics/neutrinos/neutrinos-faster-than-light/opera-what-went-wrong/).

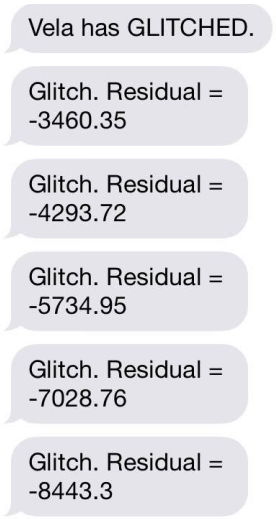

Figure 8.1: SMS messages that were received when the glitch occurred.

Table 8.1: The 2016 Glitch of the Vela pulsar. Shown are barycentre arrival time estimates based on data recorded at each observatory. Data for Ceduna was poor due to the cable fault, and because we only had 1 h of pre-glitch data, $\frac{\Delta\dot{\nu}}{\dot{\nu}}$ was not able to be determined.

Location	MJD	Time (UTC)	$\frac{\Delta\nu}{\nu}$	$\frac{\Delta\dot{\nu}}{\dot{\nu}}$
Mount Pleasant	57734.484991	11:38:23.2	1431.24×10^{-9}	9.2×10^{-3}
uncertainty	$\pm 2.9 \times 10^{-5}$	± 2.5 s	$\pm 0.069 \times 10^{-9}$	$\pm 0.83 \times 10^{-3}$
Ceduna	57734.484973	11:38:21.7	1433.5×10^{-9}	N/A
uncertainty	$\pm 3.2 \times 10^{-5}$	± 2.8 s	$\pm 0.21 \times 10^{-9}$	N/A

8.2 Mount Pleasant results

Figure 8.2 on page 158 shows a plot of arrival time residuals of individual pulses recorded at Mount Pleasant as the glitch occurred. The residuals were the difference from the usual model of ν, $\dot{\nu}$, and $\ddot{\nu}$ just prior to the glitch. Of note is the slight upturn just before the glitch occurred. This result will be discussed shortly, but the glitch fitting process needs to be first covered in-depth.

8.2.1 Fitting for the glitch

Accurate glitch fitting using single pulses has never been performed with real data in TEMPO2 previously. To this end, we will describe our method in detail.

There are 6 fitting parameters used by TEMPO2, they are shown in Table 8.2. The "_1" after each parameter implies the glitch number being referred to, as TEMPO2 can model an arbitrary number of glitches.

Table 8.2: Glitch fitting parameters.

TEMPO2 name	Symbol	Description
GLEP_1	t_g	Glitch epoch
GLPH_1	$\Delta\phi$	Phase increment
GLF0_1	$\Delta\nu$	Change in frequency
GLF1_1	$\Delta\dot{\nu}$	Change in frequency derivative
GLF0D_1	$\Delta\nu_d$	Change in decaying pulse frequency
GLTD_1	τ_d	Decay time constant

The last two parameters GLF0D_1 ($\Delta\nu_d$) and GLTD_1 (τ_d) are used to model the post-glitch decay, which is typically over a time span of weeks or months. At first we set these to 0, since our analysis time span was only 72 min. However Sarkissian et al. (2017) showed that for this glitch $\tau_d = 0.96$ d. This result meant that these parameters could not be ignored even at the 72 min range. So when fitting for the predicted time of the glitch (t_g), we set $\tau_d = 0.96$ and $\Delta\nu_d = 1.29 \times 10^{-7}$ as per their paper.

When fitting for a glitch, TEMPO2 requires an initial estimate of GLEP_1 (t_g), but TEMPO2 will *not* fit for this, even if selected. The results of the fit instead are reflected in the phase increment GLPH_1 ($\Delta\phi$) which ideally needs to be as close to 0 as possible. We plotted a number of different points (t_g,$\Delta\phi$) around the estimated glitch epoch, and then calculated the line of best fit, and used this to calculate the value of t_g when $\Delta\phi = 0$.

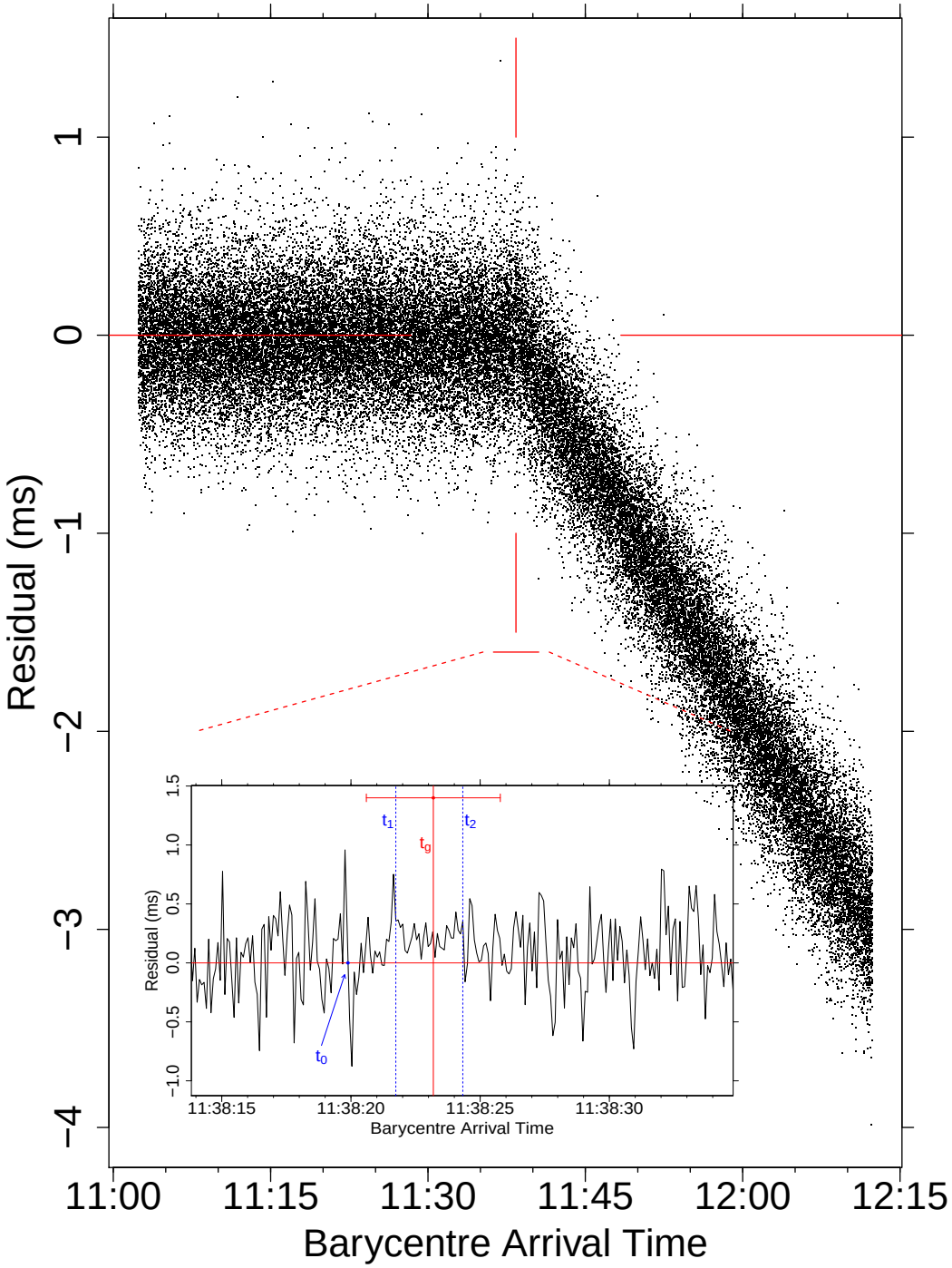

Figure 8.2: Timing residuals of *individual* pulses at the time of the glitch. The X-axis shows arrival time (hh:mm) at the solar system barycentre on MJD 57734, and the Y-axis shows the residual of the arrival time from the pre-glitch model. The vertical red line marks the fitted time of the glitch (t_g). The inset shows a zoomed-in version. Just 3.3 s prior to t_g a *null* occurred (t_0), and an unusual change in the timing residuals followed: in particular the mean arrival times were early, and the variance was reduced. Note the null cannot be timed and so it has been placed between the points on either side, but on the 0.0 line.

With 72 min worth of single-pulse data and the glitch approximately in the centre, we explicitly used these manual steps to calculate the glitch epoch and other parameters:

1. We estimated a value for GLEP_1 from the plot and set it explicitly (using right-click in TEMPO2).
2. We fitted only for F0, F1, GLPH_1, GLF0_1, and GLF1_1. We did multiple fits (≈ 3) to confirm the fit parameters and that the RMS converges, and also that the plot looks like random Gaussian noise.
3. We recorded GLEP_1 and the *post-fit* value of GLPH_1 and plotted them on a graph.
4. We picked another value for GLEP_1 paying attention to the sign and magnitude of GLPH_1. For the best fit we wanted both positive and negative values of GLPH_1 on the graph.
5. We repeated steps 2-4 until we had ≈ 10 data points. We found the line of best fit and calculated the value of GLEP_1 to make GLPH_1=0.
6. We repeated step 2 using the calculated value of GLEP_1. Then we repeated the entire process again (if necessary) with much closer values of GLEP_1 trying to get GLPH_1 as small as possible.

Following the process above we got $\Delta\phi = 6.98 \times 10^{-8}$ which equates to 6 ms. The reported *Uncertainty* (ϵ) in t_g from TEMPO2 was $\epsilon = 2.9 \times 10^{-5}$ which equates to ± 2.5 s.

After this approximation, we adjusted t_g manually to minimise the RMS residuals in the arrival time (data - model). Then we adjusted ν to minimise RMS, and then $\dot{\nu}$. This was repeated a number of times until convergence was achieved. In each step of this process, the RMS plot was a parabola that was smooth enough that we had confidence in our best fit determination. The final RMS in the 72 min of single pulse timing residuals was ≈ 252 μs and is shown in Figure 8.3 on page 160.

Figure 8.4 on page 160 shows the same timing residuals but zoomed-in to the time of the glitch as predicted from TEMPO2. The vertical red line marks the glitch epoch (t_g) and the horizontal red line marks the reported errors bars ($t_g - \epsilon$ and $t_g + \epsilon$).

8.2.2 A null

Figures 8.8 to 8.15 on pages 165–168 show 80 s of intensity data over the glitch epoch. They are in reverse time order so that they flow continuously from last to first. There

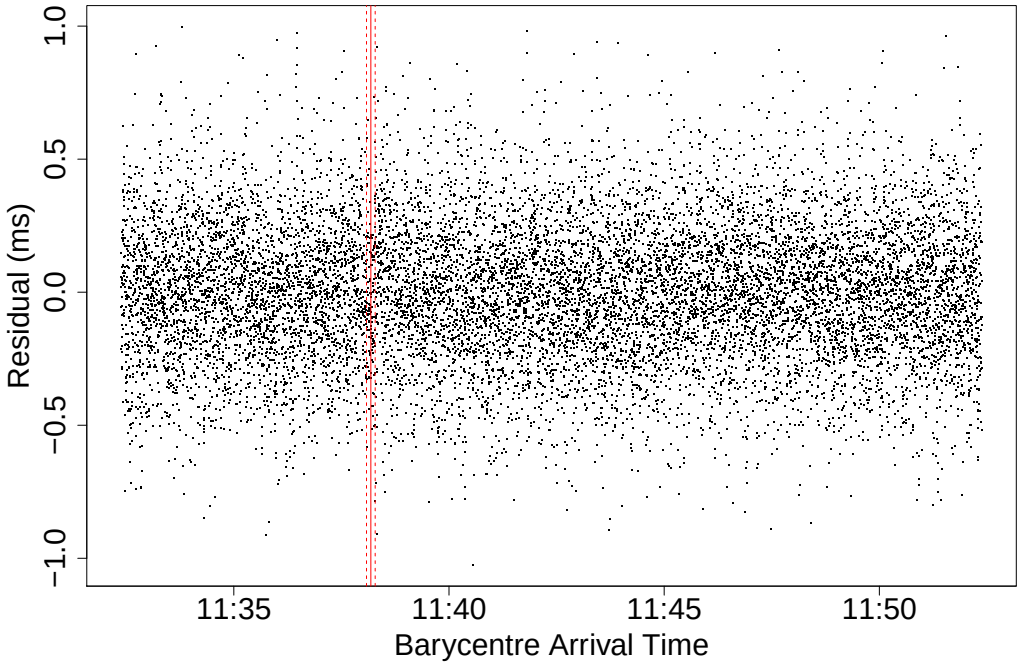

Figure 8.3: Residuals of arrival times of individual pulses for the glitch of 2016 after glitch modelling had been applied. The red lines show the glitch epoch with error bars.

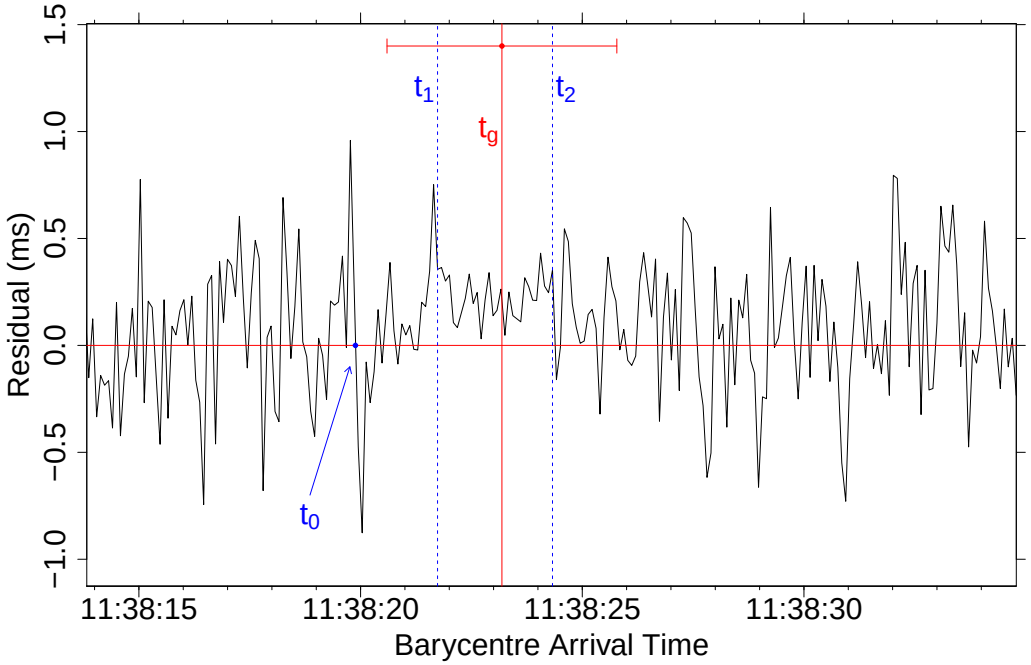

Figure 8.4: Residuals of arrival times of individual pulses for the glitch of 2016 zoomed-in to the time of the glitch. The solid red line marks the glitch epoch (t_g) with error bars. The dashed blue lines mark t_1 and t_2. Note the null (t_0) cannot be timed and so it has been placed between the points on either side, but on the 0.0 line.

are smatterings of RFI, but at first glance there seems to be no sharp changes in bright pulse activity near the glitch.

However in Figure 8.11 on page 166, a few seconds before the glitch epoch t_g, there is a notable fading of pulse flux density and a closer inspection shows that pulse 76 was a *null*.

That is, *no measurable signal from the pulsar was received*.

We will label the time of the null as t_0. Recall that the predicted time of the glitch is labelled as t_g with the error bars at $t_g - \epsilon$ and $t_g + \epsilon$. Figure 8.4 on page 160 shows the timing residuals on a line graph with the null marked. Note that there is obviously no timing residual recorded for a null, so the point has been marked at a residual of 0 and on a straight line between the recorded points either side. Curiously, both of those points have a large variance.

8.2.3 Change in mean and variance

Figure 8.2 on page 158 shows a hint of an upturn just prior to the glitch occurring. This effect also appeared in the 2000 glitch as shown in Dodson et al. (2002) and their plot is reproduced in Figure 8.5 on page 162. We have replicated this figure format using our 2016 glitch data and this is shown in Figure 8.6 on page 162.

At first glance this upturn appears quite notable, but consider Figure 8.7 on page 163 which shows Figure 8.6 on page 162 zoomed-in to ≈ 14 min. There is a considerable rise to a large peak just before the glitch, but if that peak were to be removed, the preceding points would be possibly unremarkable.

In Figure 8.4 on page 160 a notable change in mean (μ) and variance (σ^2) appears between $t_g - \epsilon$ and $t_g + \epsilon$. This is quite a significant change but it also appears in a section of mild RFI.

All the Figures 8.8 to 8.15 on pages 165–168 show sections of out-of-band RFI. This changes the level of the entire band and so appears as light streaks. An artificially generated version of something similar is shown with the firing of the noise diodes in Figure 4.2 on page 47.

8.2.4 Significance of RFI on timing and flux density

The appearance of a null and these striking changes in mean and variance may be affected by RFI and so a close analysis of each individual pulse over this time period

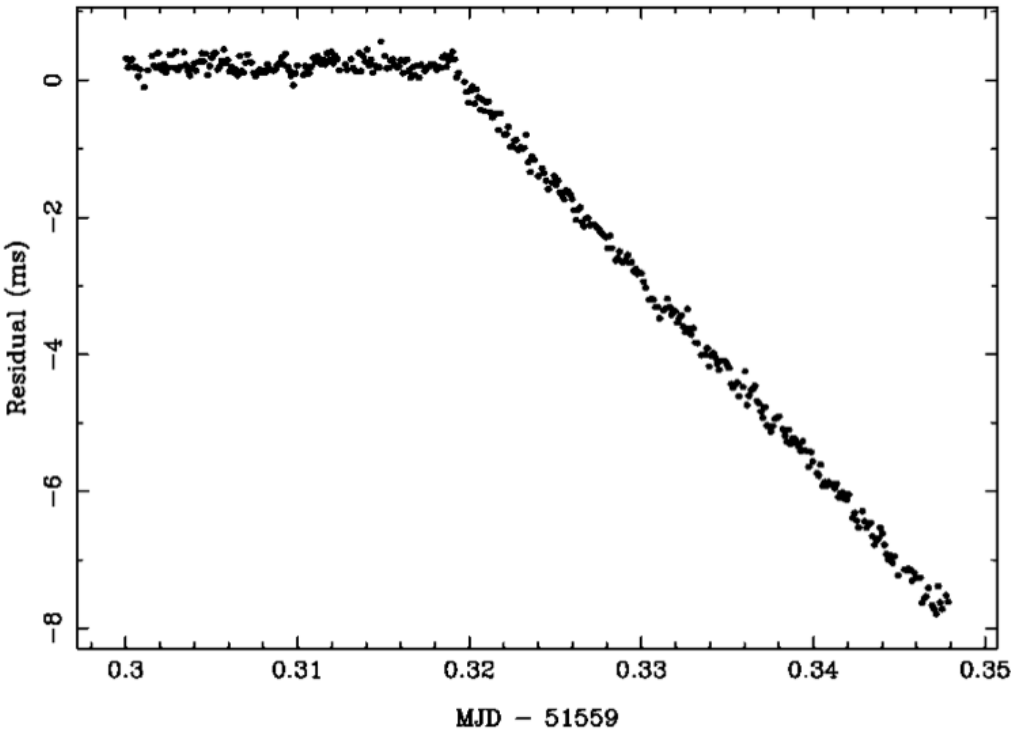

Figure 8.5: A copy of the figure from Dodson et al. (2002) showing residuals of arrival times using 10 s integrations for the glitch of 2000. Note the slight upturn of the residuals just before the glitch occurs.

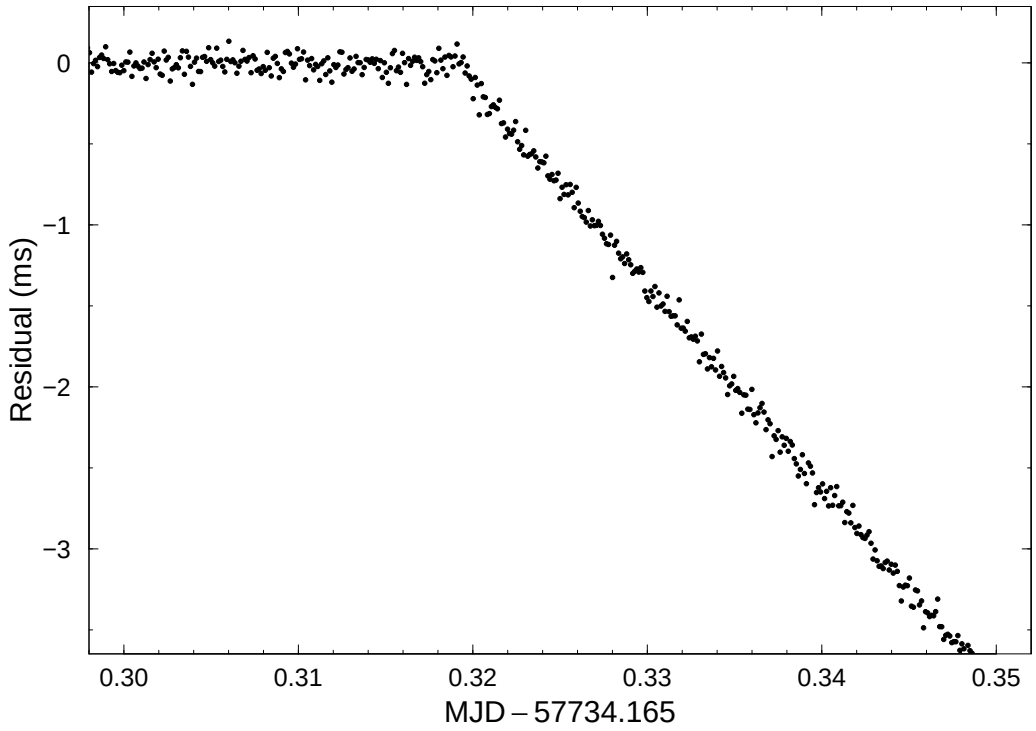

Figure 8.6: A plot of the 2016 glitch using 10 s integrations designed to replicate Figure 8.5. The X-axis has been adjusted to have the same values. The Y-axis is different as the 2000 glitch had a $\frac{\Delta\nu}{\nu} = 3085 \times 10^{-9}$. Note the very similar upturn of the residuals just before the glitch occurs.

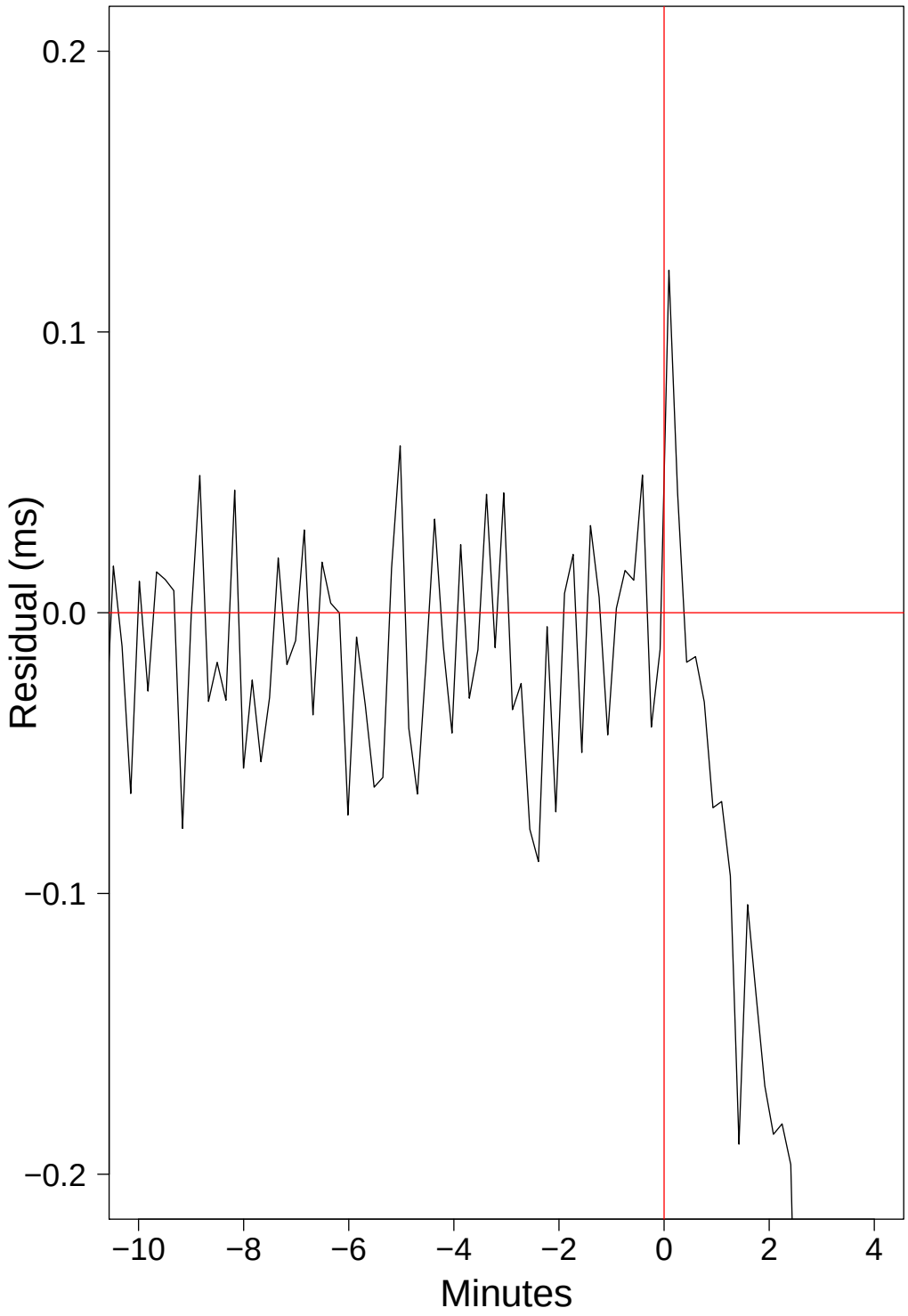

Figure 8.7: A plot of the 2016 glitch using 10 s integrations zoomed-in to the pre-glitch rise.

is warranted.

Figures 8.19 to 8.39 on pages 170–190 respectively, show 332 pulses over a period of 30 s extracted from files `2016-12-12-11:35:53.ar` to `2016-12-12-11:36:13.ar`.[‡] The flux density reference 0.0 on the graph (and marked with a horizontal red line) has been calculated as the mean of the off-pulse data for each pulse. The vertical dotted red line marks a timing residual of 0 and pulse 32 in Figure 8.30 on page 181 is the reference pulse for this as its timing residual was 12.76 μs.

The null (t_0) is "pulse" 76 in Figure 8.35 on page 186, and the sequence of 30 pulses with increased μ and decreased σ is marked on the plots as "$\mu^+\sigma^-$". There were two pulses within that sequence that could not be timed (due to RFI) and are marked with "Bad timing".

Pulse 75 just prior to the null *appears* to be affected by out-of-band RFI when looking at Figure 8.11 on page 166, however when examining Figure 8.35 on page 186 it is symmetrical about the timing residual of 0. This seems highly coincidental and since it is the pulse prior to the null, the assumption it is RFI is probably incorrect.

Normally to decide if a pulse is genuine, the frequency versus time plot is analysed to see if arrival times are affected by dispersion (see Figure 8.16 on page 169, which shows the *integrated* pulse of `2016-12-12-11:35:53.ar`, as a clear example). Figure 8.17 on page 169 shows the "broad" pulse 75, and Figure 8.18 on page 169 shows pulse 74 (a "normal" pulse) as a comparison. The dispersion is hard to see, but it appears present in both pulses.

[‡]as previously noted in Section 4.1 on page 44 there was a ≈ 2 s error in file naming.

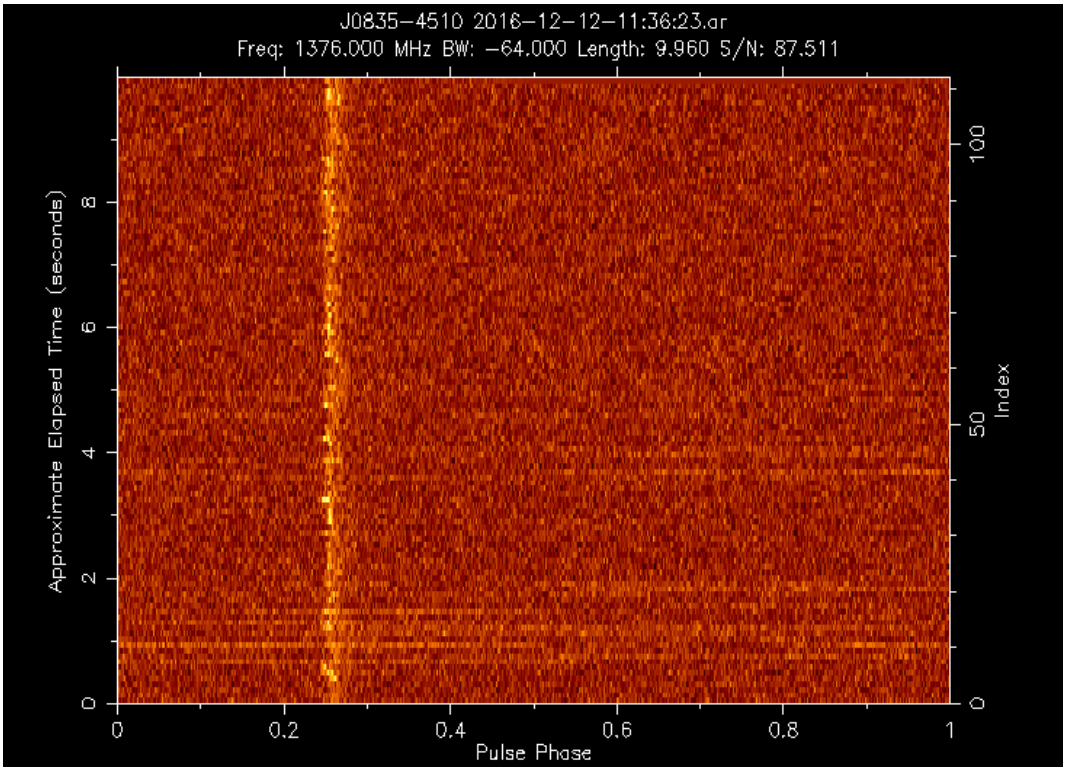

Figure 8.8: Plot of intensity near the time of the glitch. File 2016-12-12-11:36:23.ar and note the filenames of these 8 files are ≈ 2 s in error as explained in Section 4.1 on page 44.

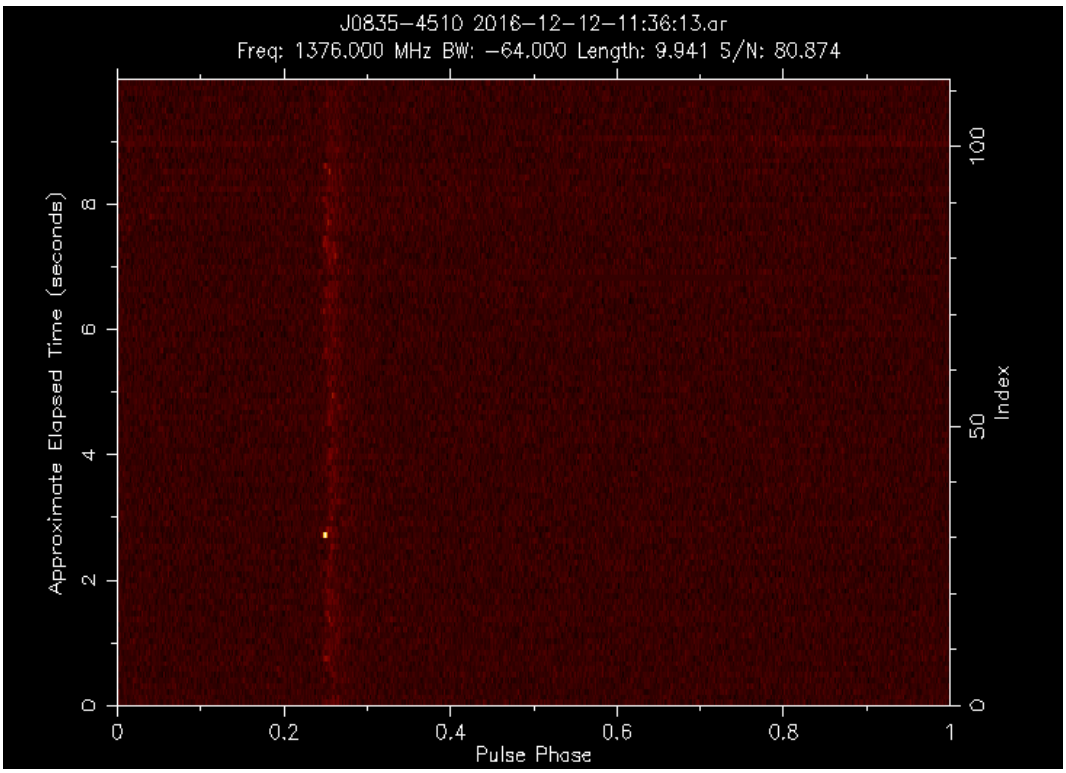

Figure 8.9: Plot of intensity near the time of the glitch. File 2016-12-12-11:36:13.ar

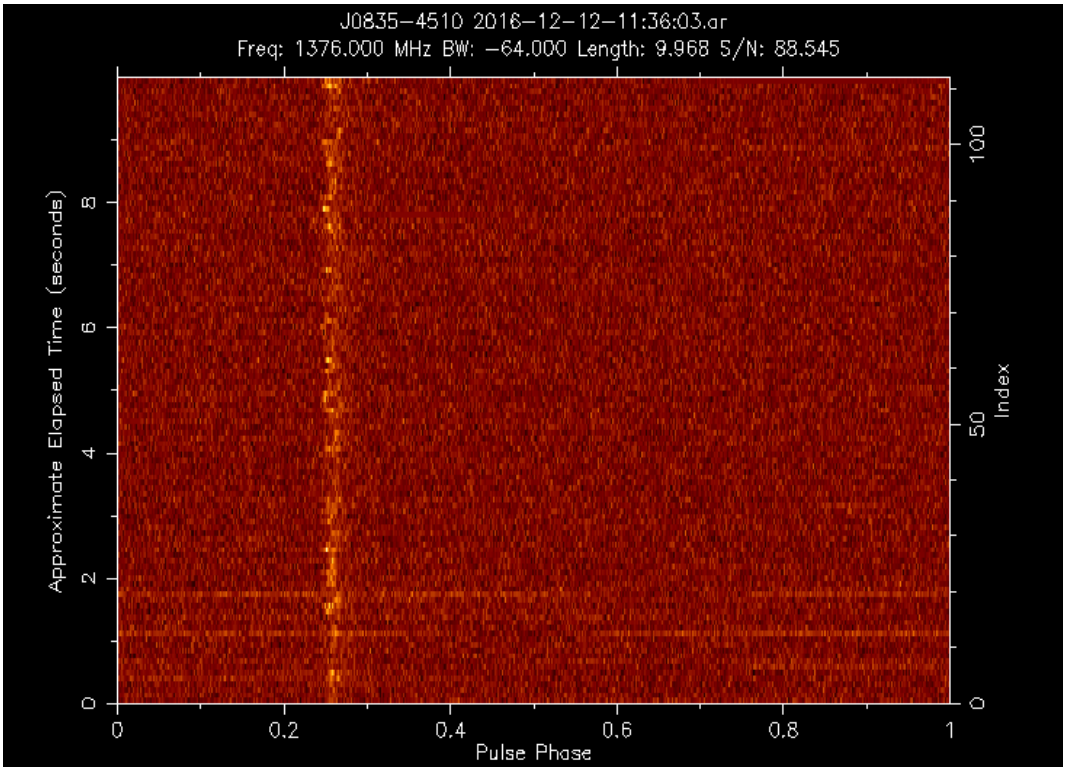

Figure 8.10: Plot of intensity near the time of the glitch. File 2016-12-12-11:36:03.ar

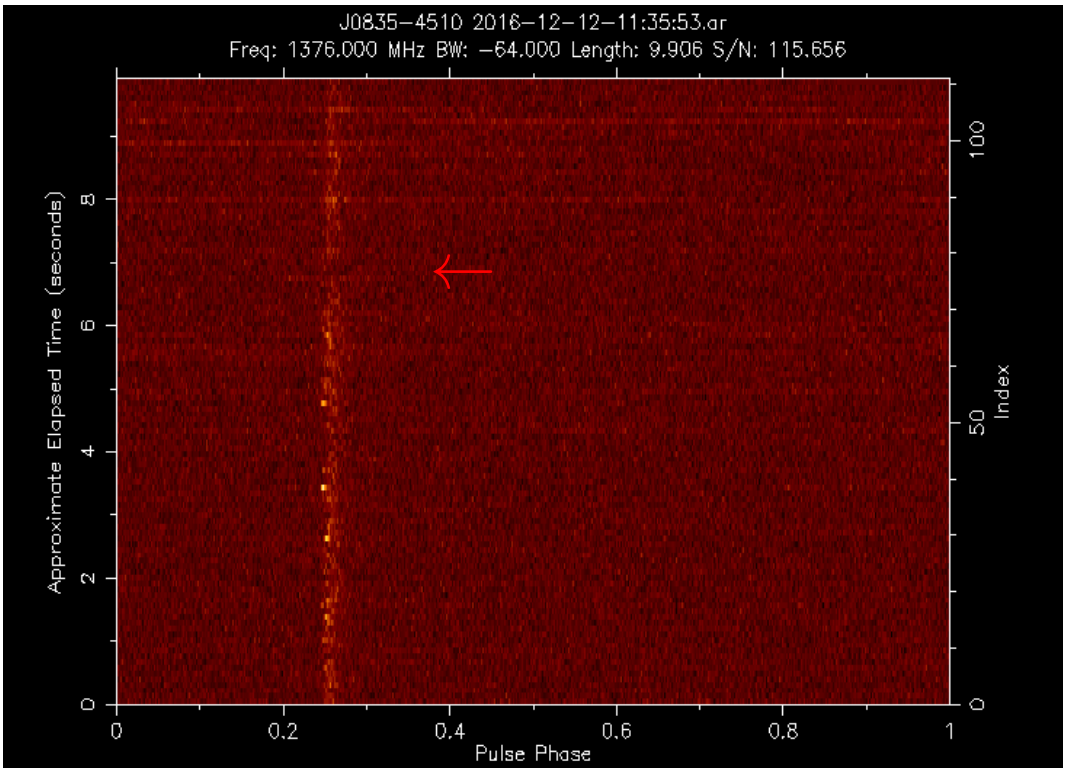

Figure 8.11: Plot of intensity near the time of the glitch and the null (t_0) shown with an arrow. File 2016-12-12-11:35:53.ar

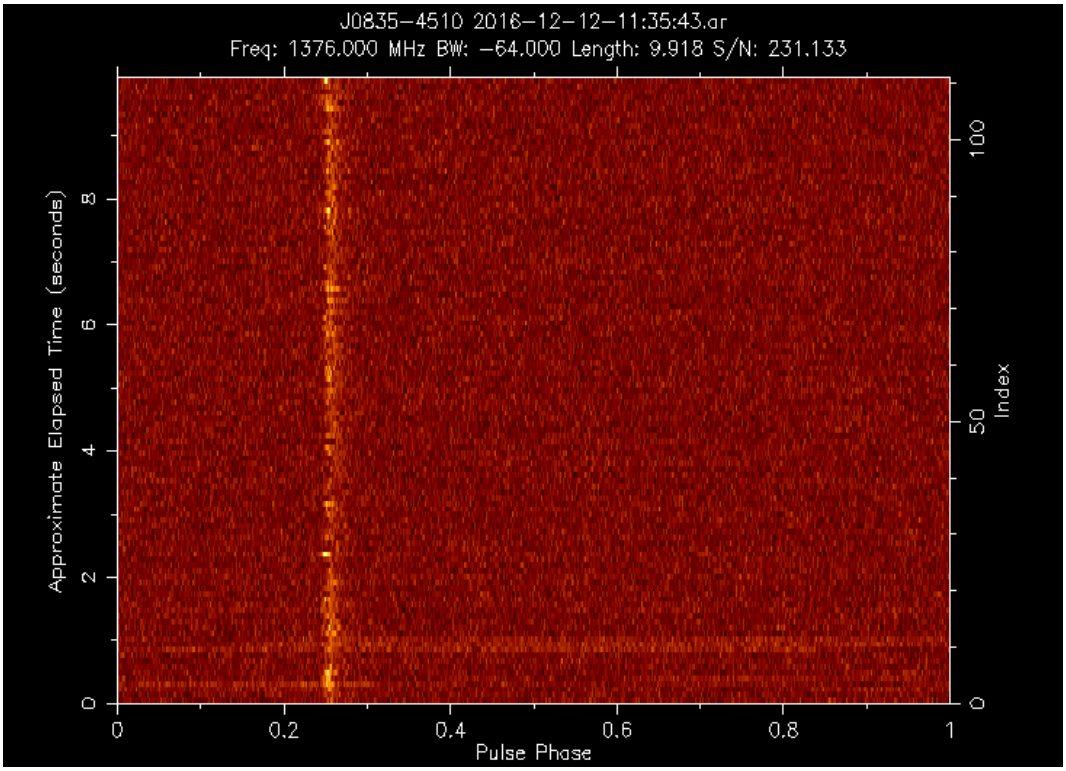

Figure 8.12: Plot of intensity near the time of the glitch. File 2016-12-12-11:35:43.ar

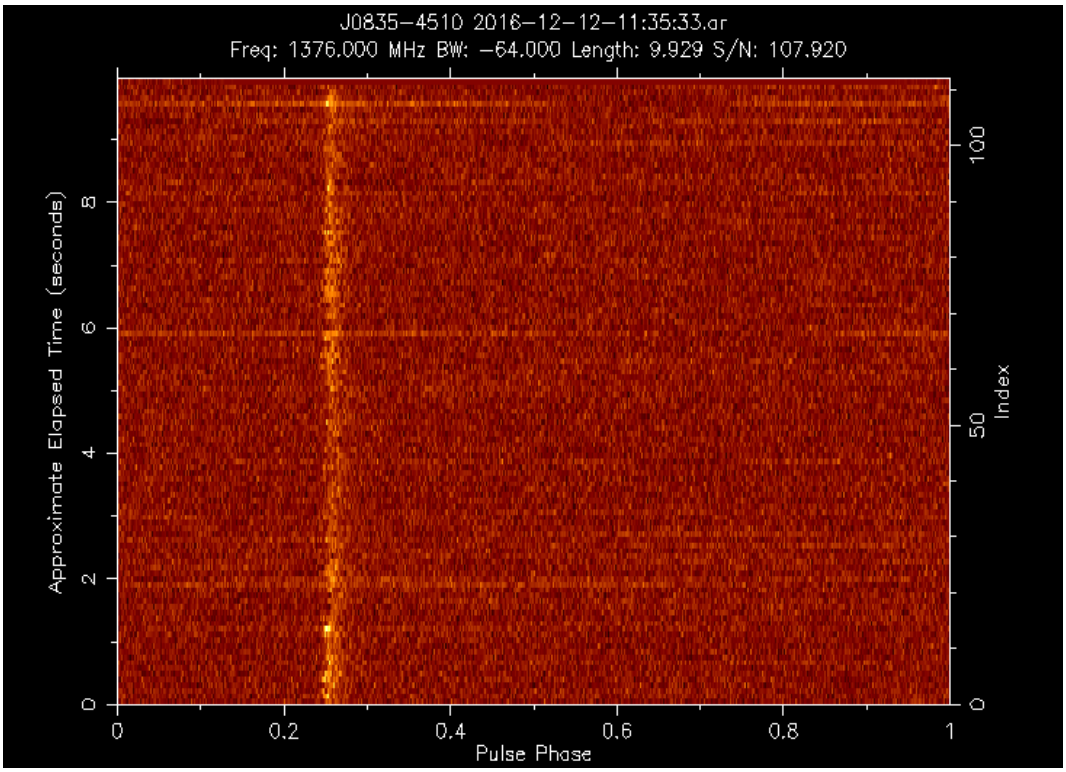

Figure 8.13: Plot of intensity near the time of the glitch. File 2016-12-12-11:35:33.ar

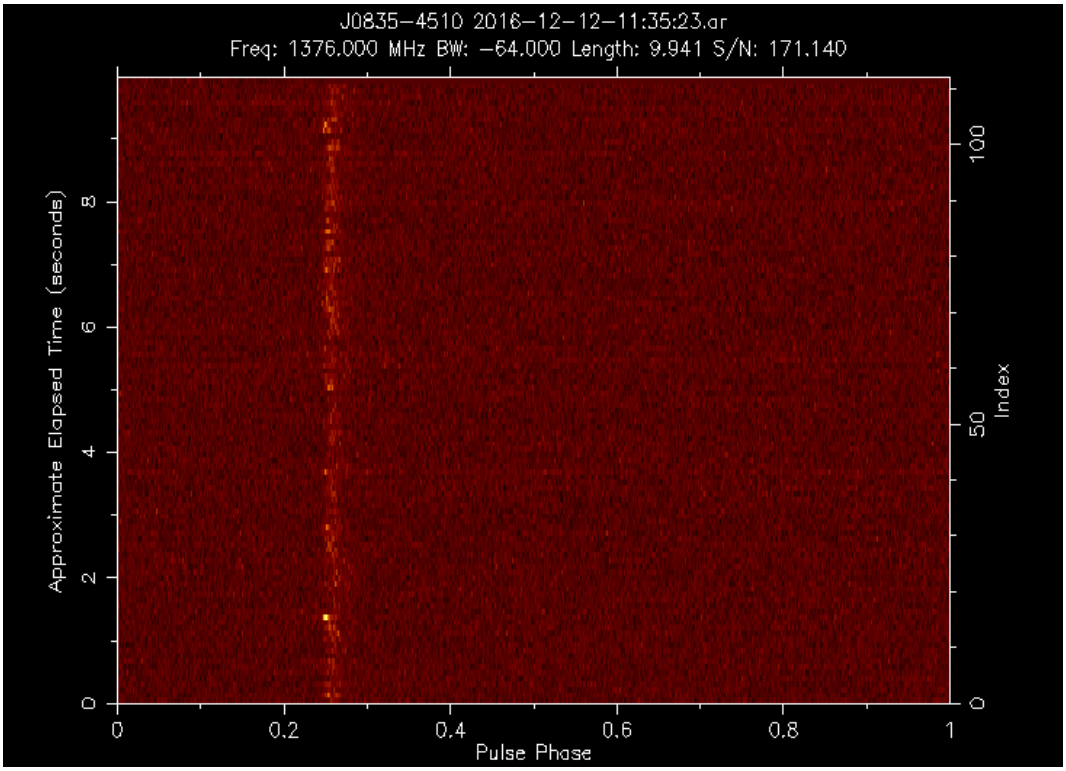

Figure 8.14: Plot of intensity near the time of the glitch. File 2016-12-12-11:35:23.ar

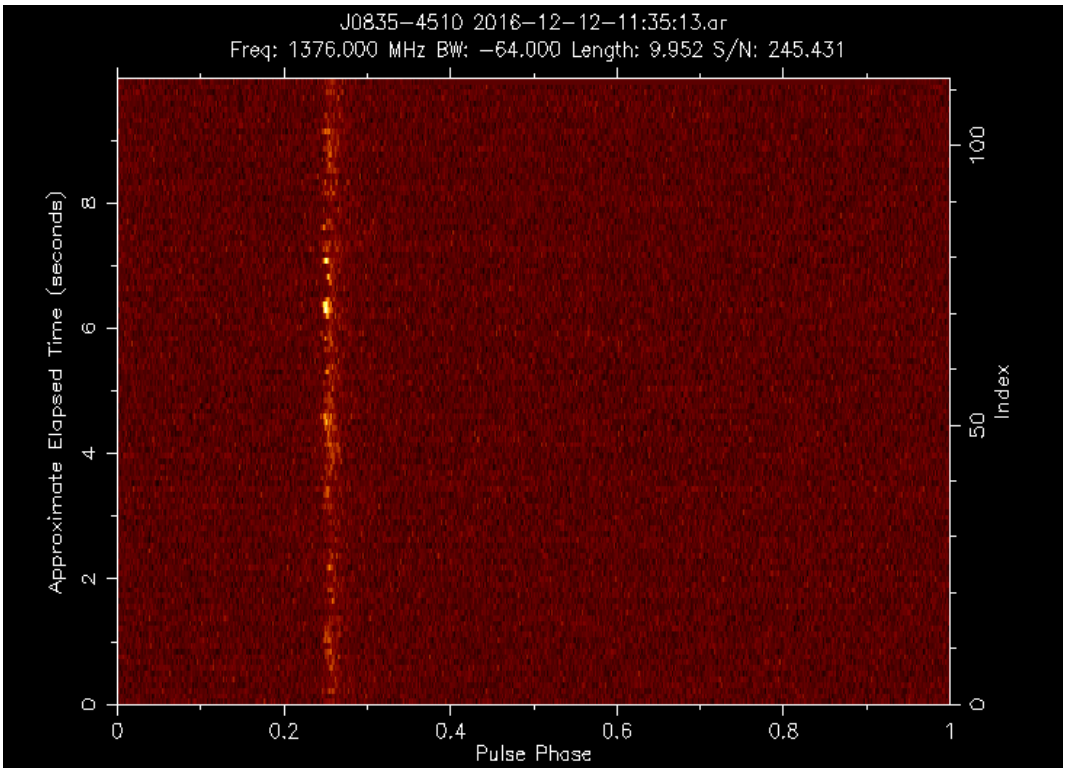

Figure 8.15: Plot of intensity near the time of the glitch. File 2016-12-12-11:35:13.ar

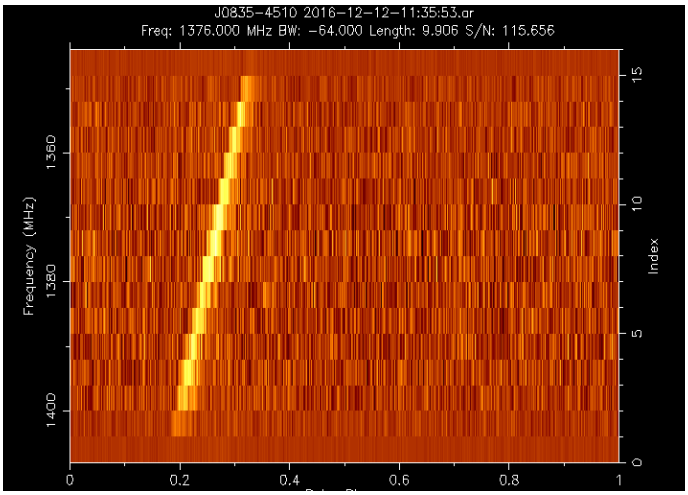

Figure 8.16: Frequency vs time plot of integrated pulse, file 2016-12-12-11:35:53.ar

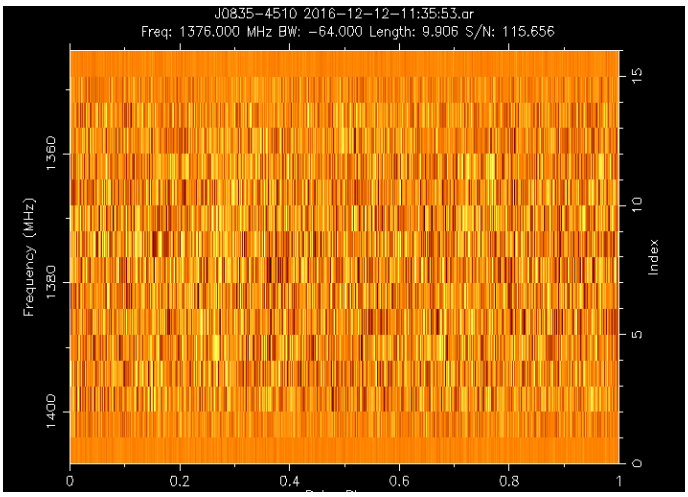

Figure 8.17: Frequency vs time plot of pulse 75 (the broad pulse), file 2016-12-12-11:35:53.ar

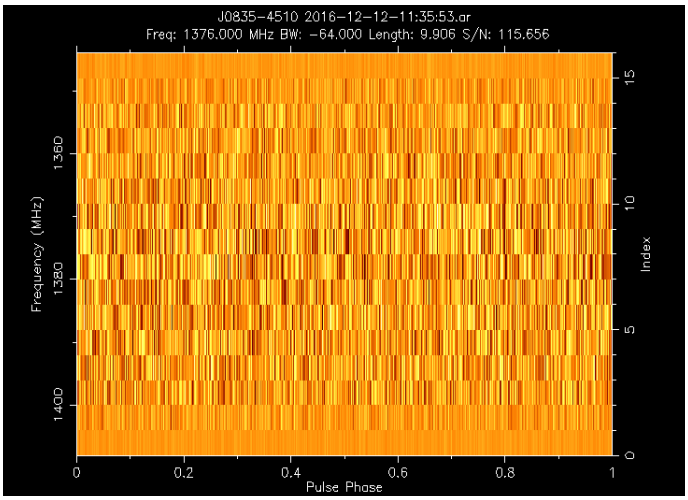

Figure 8.18: Frequency vs time plot of pulse 74, (a normal pulse) file 2016-12-12-11:35:53.ar

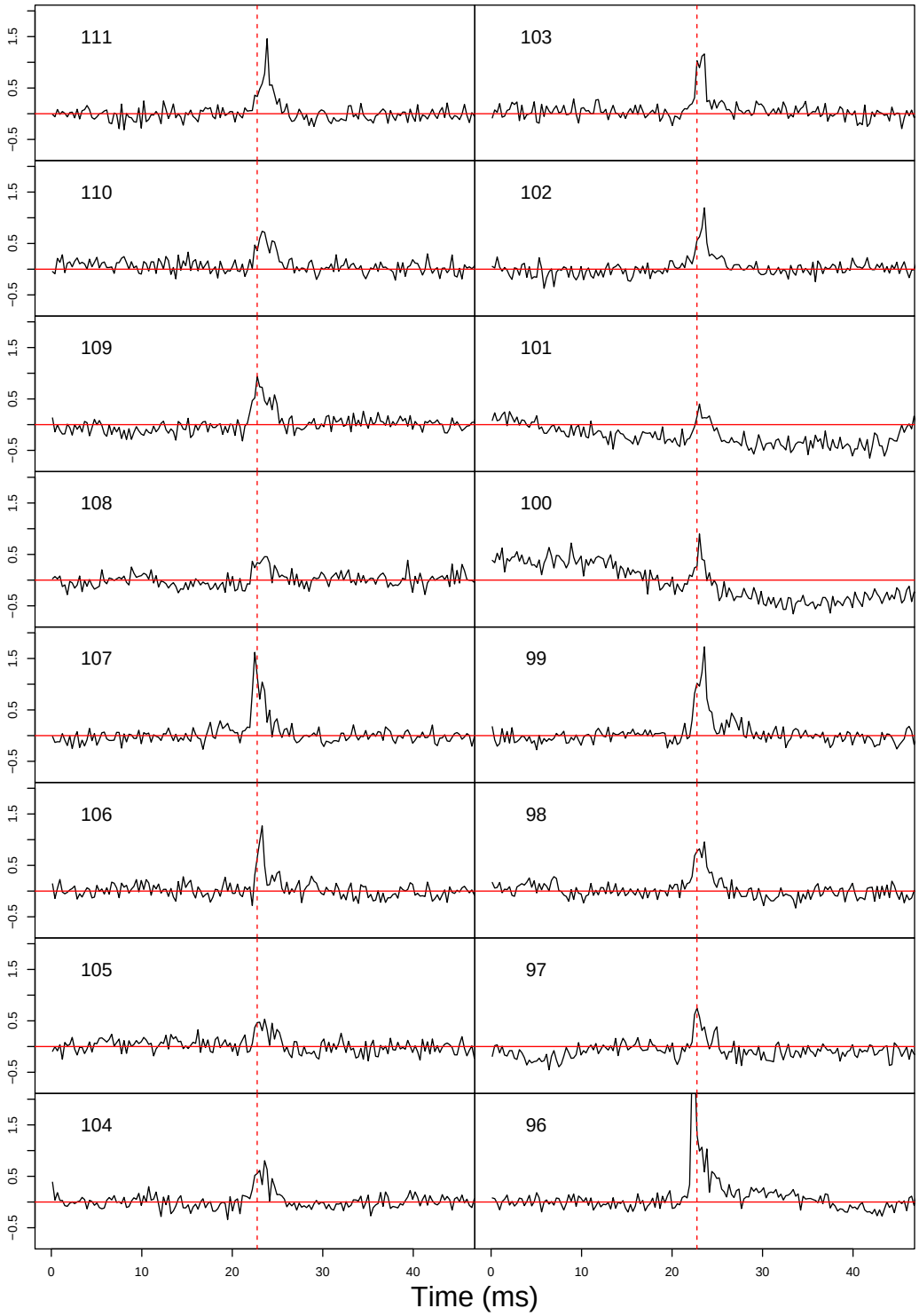

Figure 8.19: File 2016-12-12-11:36:13.ar, pulses 111-96, binned with $n = 25$. The X-axis is time in ms and the Y-axis is flux density in arbitrary units with all axes having the same scale. The solid red line marks a flux density of 0 and the dotted line marks the location of the peak of the full day's integrated pulse. Note that the full pulse period is not shown.

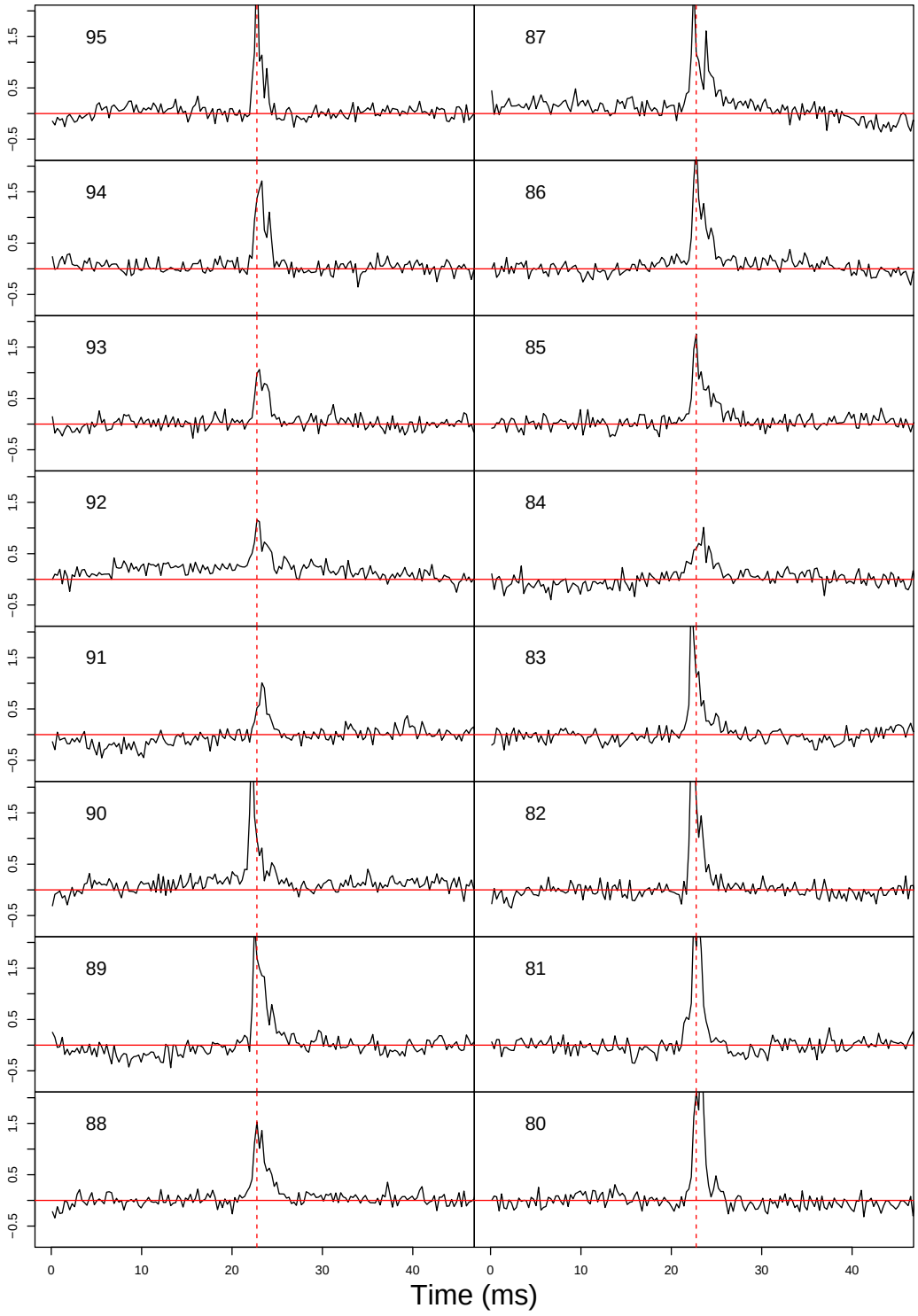

Figure 8.20: File 2016-12-12-11:36:13.ar, pulses 95-80, binned with $n = 25$. The X-axis is time in ms and the Y-axis is flux density in arbitrary units with all axes having the same scale. The solid red line marks a flux density of 0 and the dotted line marks the location of the peak of the full day's integrated pulse. Note that the full pulse period is not shown.

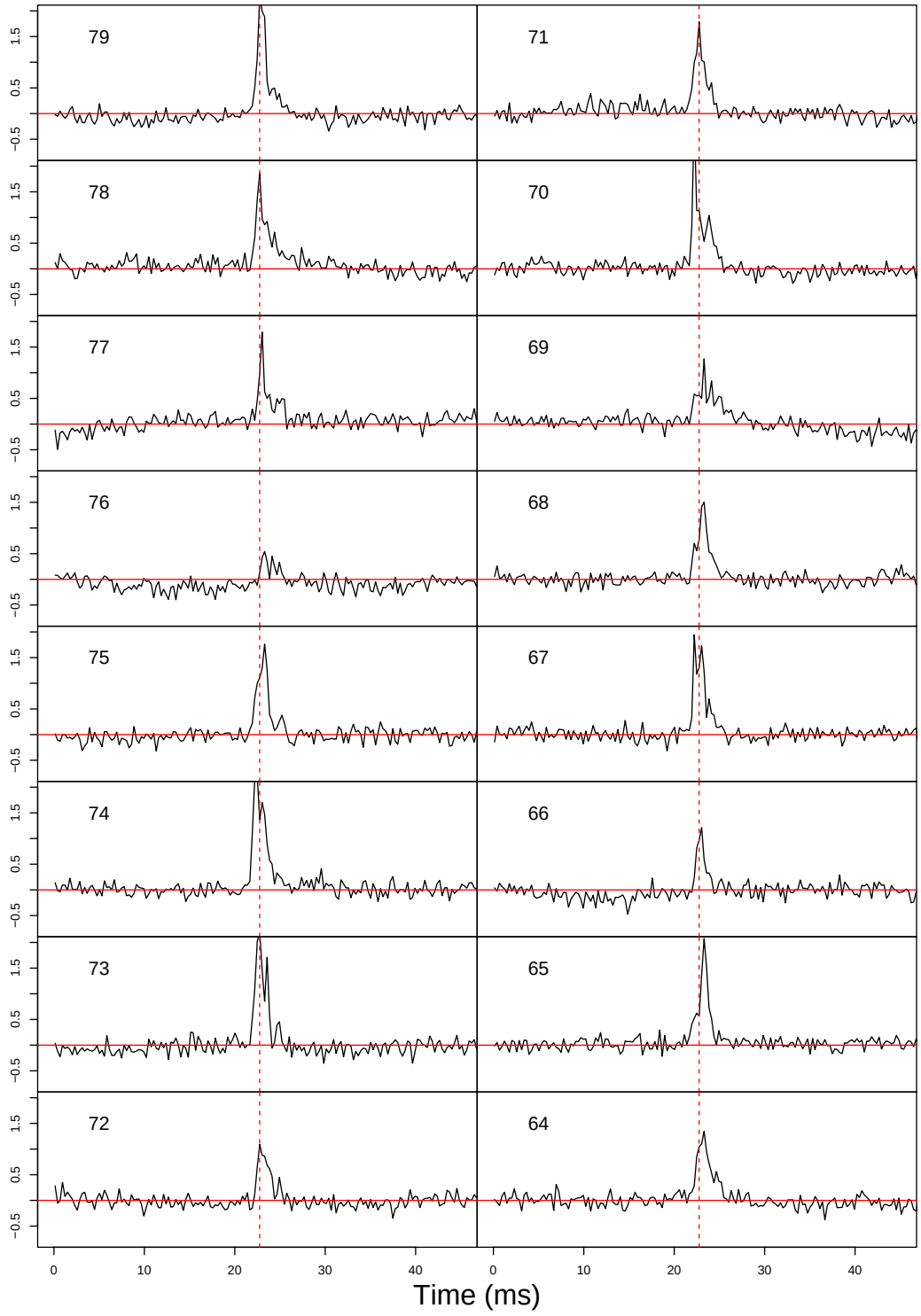

Figure 8.21: File 2016-12-12-11:36:13.ar, pulses 79-64, binned with $n = 25$. The X-axis is time in ms and the Y-axis is flux density in arbitrary units with all axes having the same scale. The solid red line marks a flux density of 0 and the dotted line marks the location of the peak of the full day's integrated pulse. Note that the full pulse period is not shown.

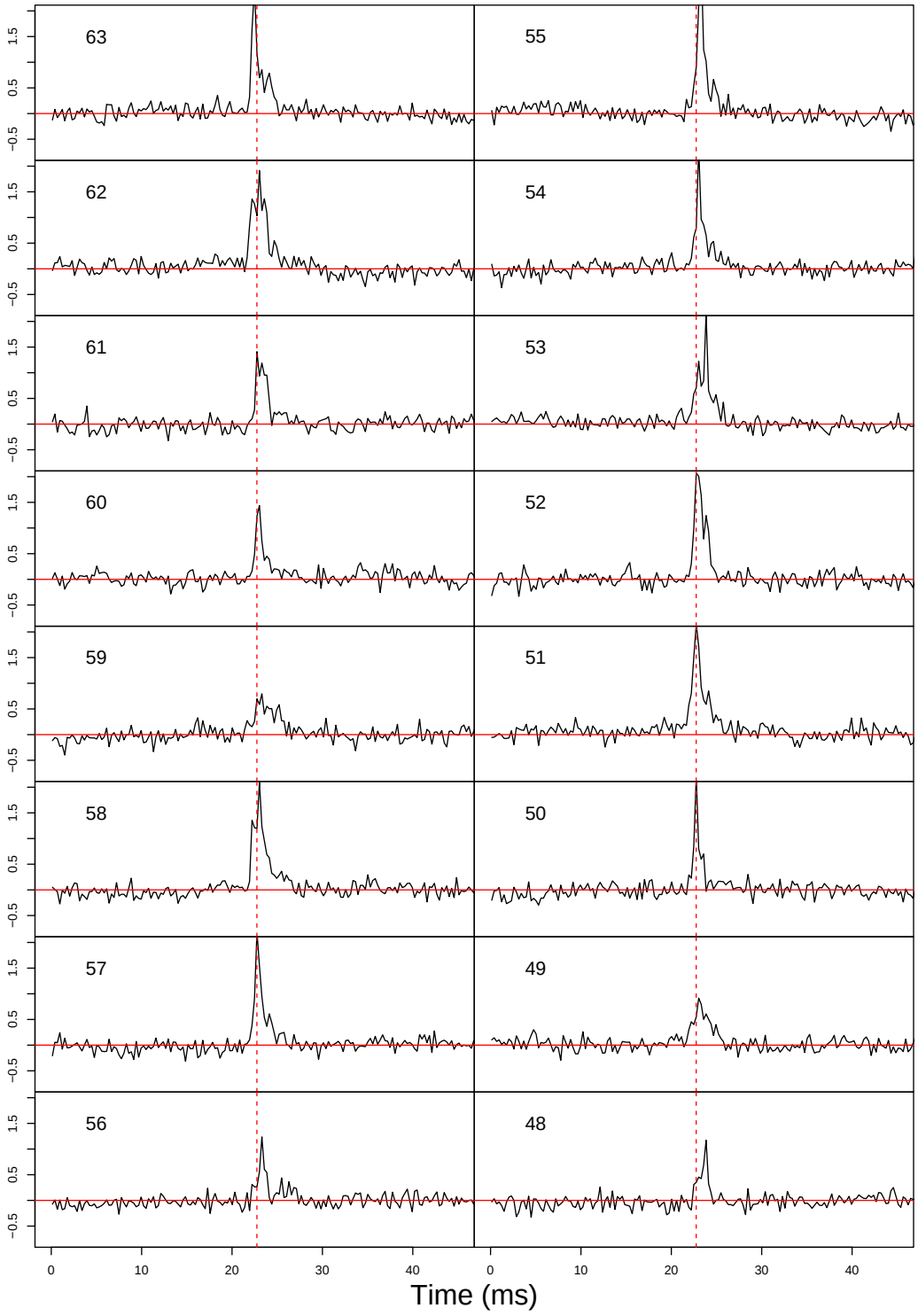

Figure 8.22: File 2016-12-12-11:36:13.ar, pulses 63-48, binned with $n = 25$. The X-axis is time in ms and the Y-axis is flux density in arbitrary units with all axes having the same scale. The solid red line marks a flux density of 0 and the dotted line marks the location of the peak of the full day's integrated pulse. Note that the full pulse period is not shown.

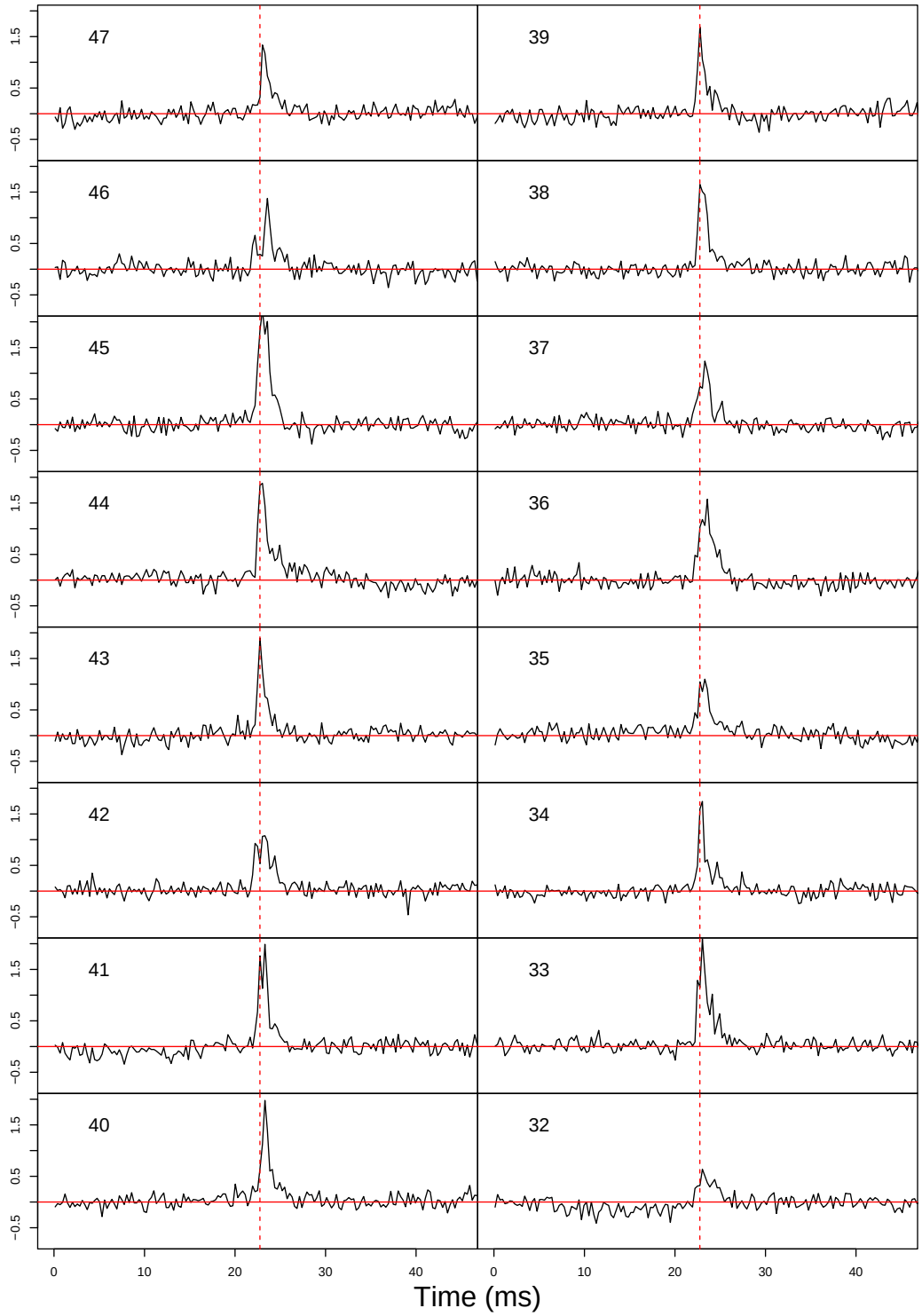

Figure 8.23: File 2016-12-12-11:36:13.ar, pulses 47-32, binned with $n = 25$. The X-axis is time in ms and the Y-axis is flux density in arbitrary units with all axes having the same scale. The solid red line marks a flux density of 0 and the dotted line marks the location of the peak of the full day's integrated pulse. Note that the full pulse period is not shown.

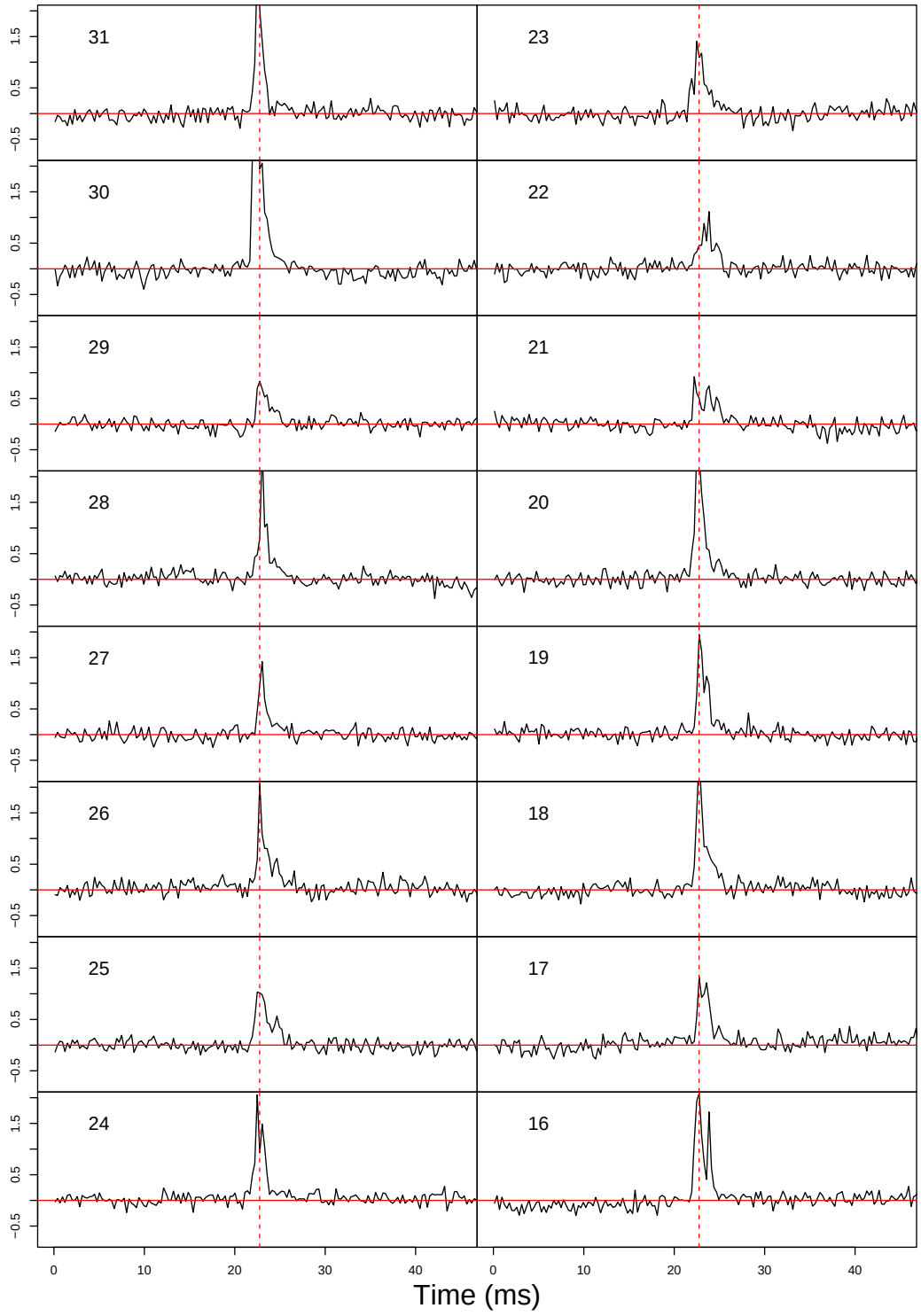

Figure 8.24: File 2016-12-12-11:36:13.ar, pulses 31-16, binned with $n = 25$. The X-axis is time in ms and the Y-axis is flux density in arbitrary units with all axes having the same scale. The solid red line marks a flux density of 0 and the dotted line marks the location of the peak of the full day's integrated pulse. Note that the full pulse period is not shown.

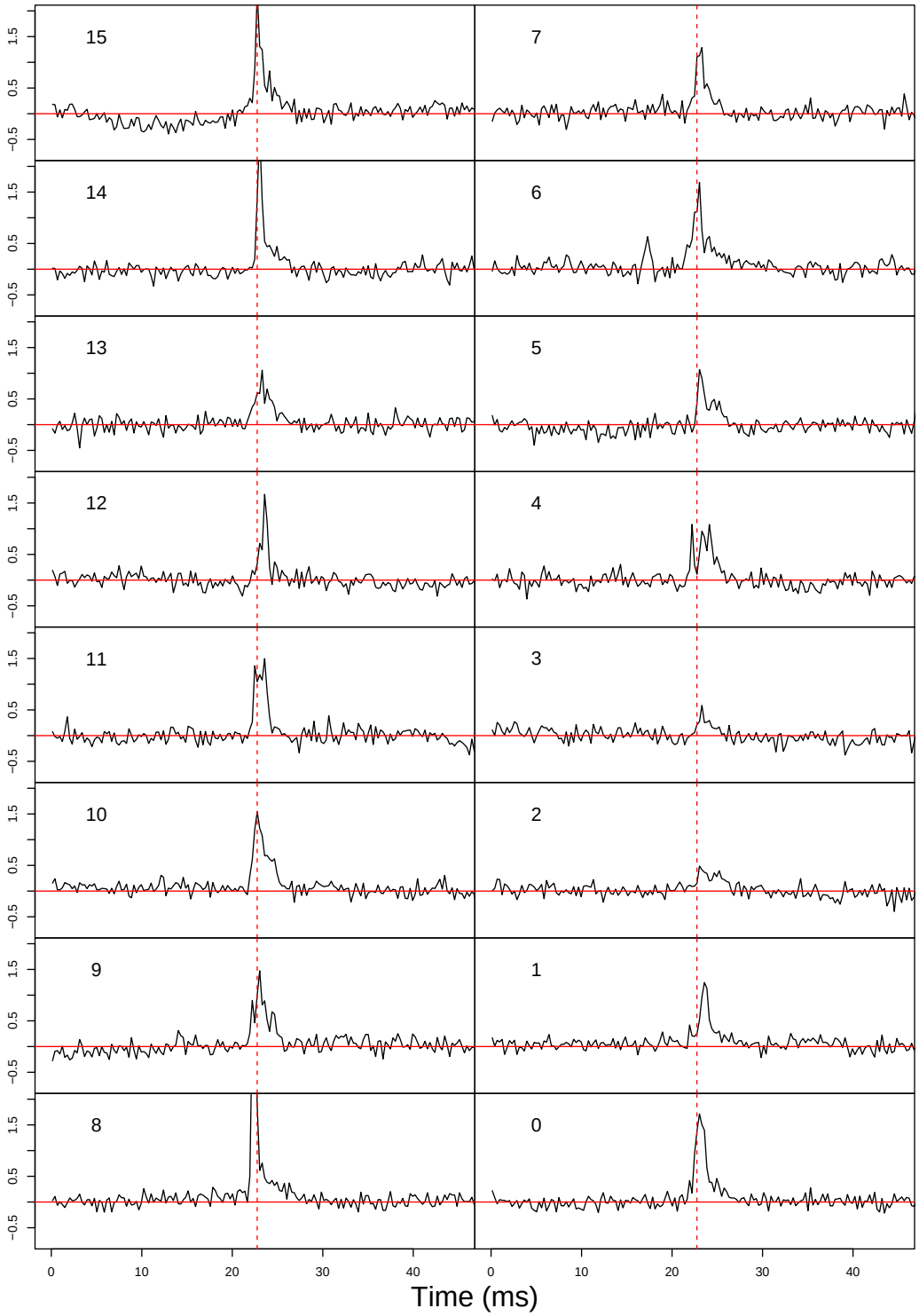

Figure 8.25: File 2016-12-12-11:36:13.ar, pulses 15-0, binned with $n = 25$. The X-axis is time in ms and the Y-axis is flux density in arbitrary units with all axes having the same scale. The solid red line marks a flux density of 0 and the dotted line marks the location of the peak of the full day's integrated pulse. Note that the full pulse period is not shown.

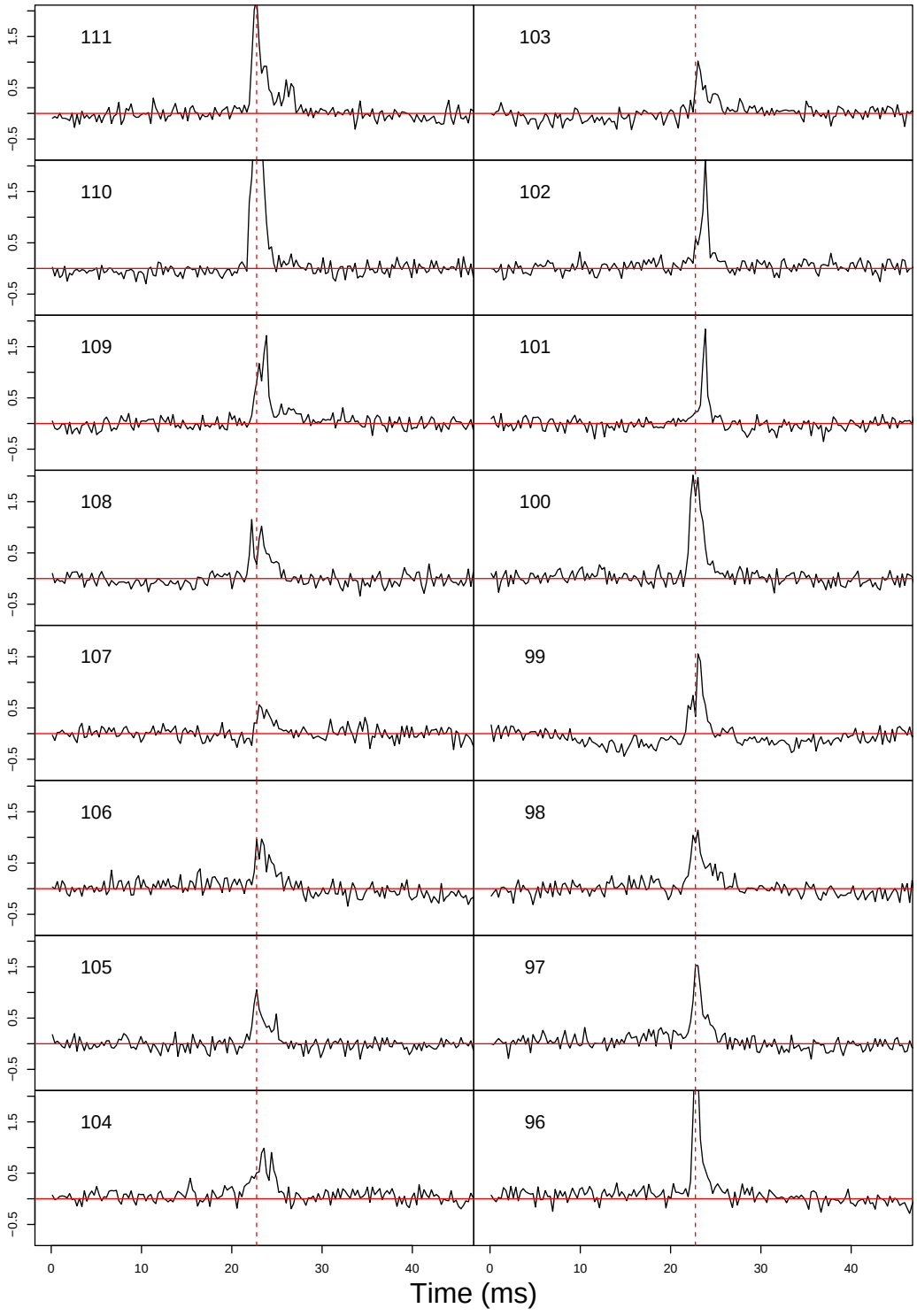

Figure 8.26: File 2016-12-12-11:36:03.ar, pulses 111-96, binned with $n = 25$. The X-axis is time in ms and the Y-axis is flux density in arbitrary units with all axes having the same scale. The solid red line marks a flux density of 0 and the dotted line marks the location of the peak of the full day's integrated pulse. Note that the full pulse period is not shown and that pulse 99 has RFI affecting the baseline.

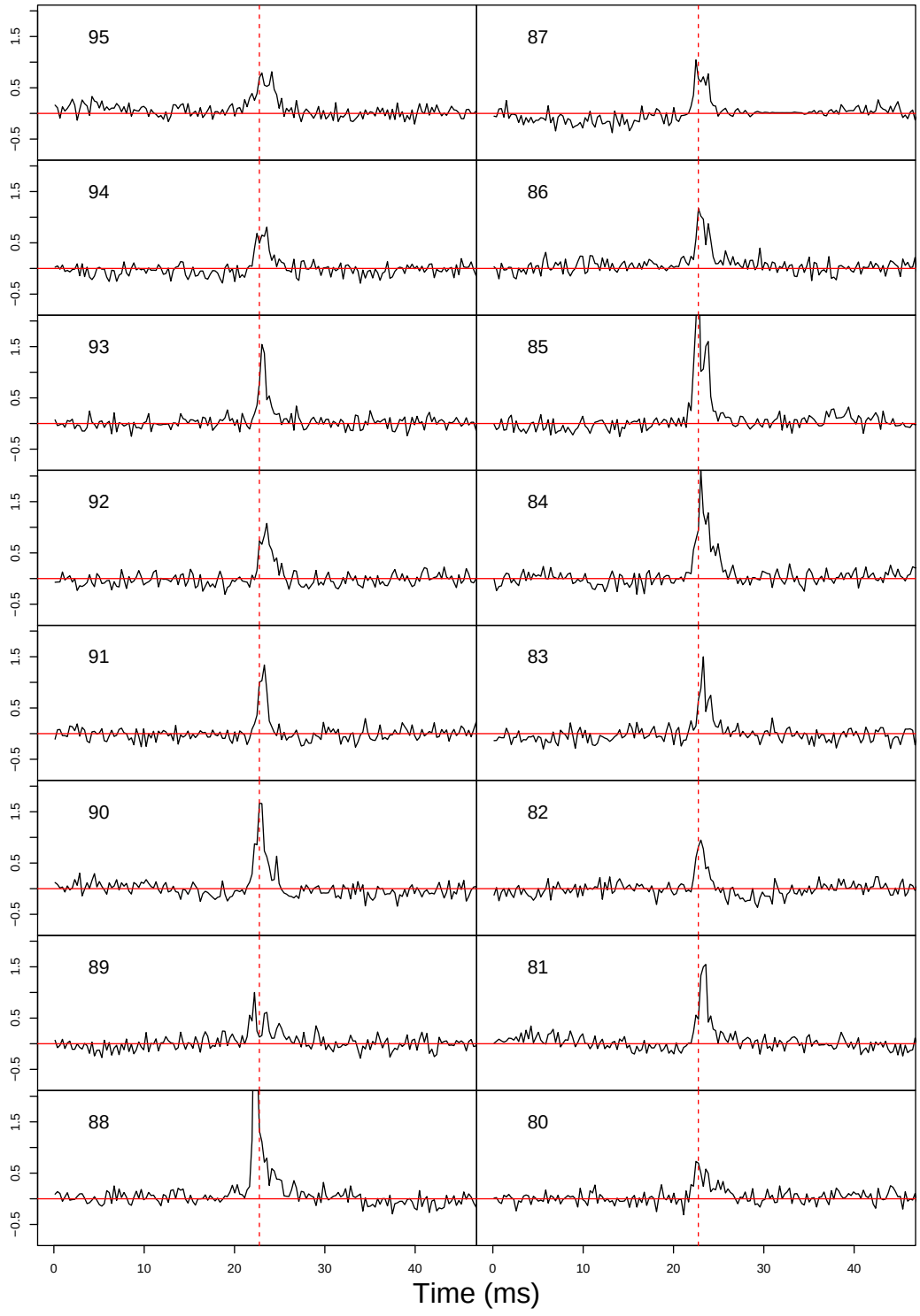

Figure 8.27: File 2016-12-12-11:36:03.ar, pulses 95-80, binned with $n = 25$. The X-axis is time in ms and the Y-axis is flux density in arbitrary units with all axes having the same scale. The solid red line marks a flux density of 0 and the dotted line marks the location of the peak of the full day's integrated pulse. Note that the full pulse period is not shown.

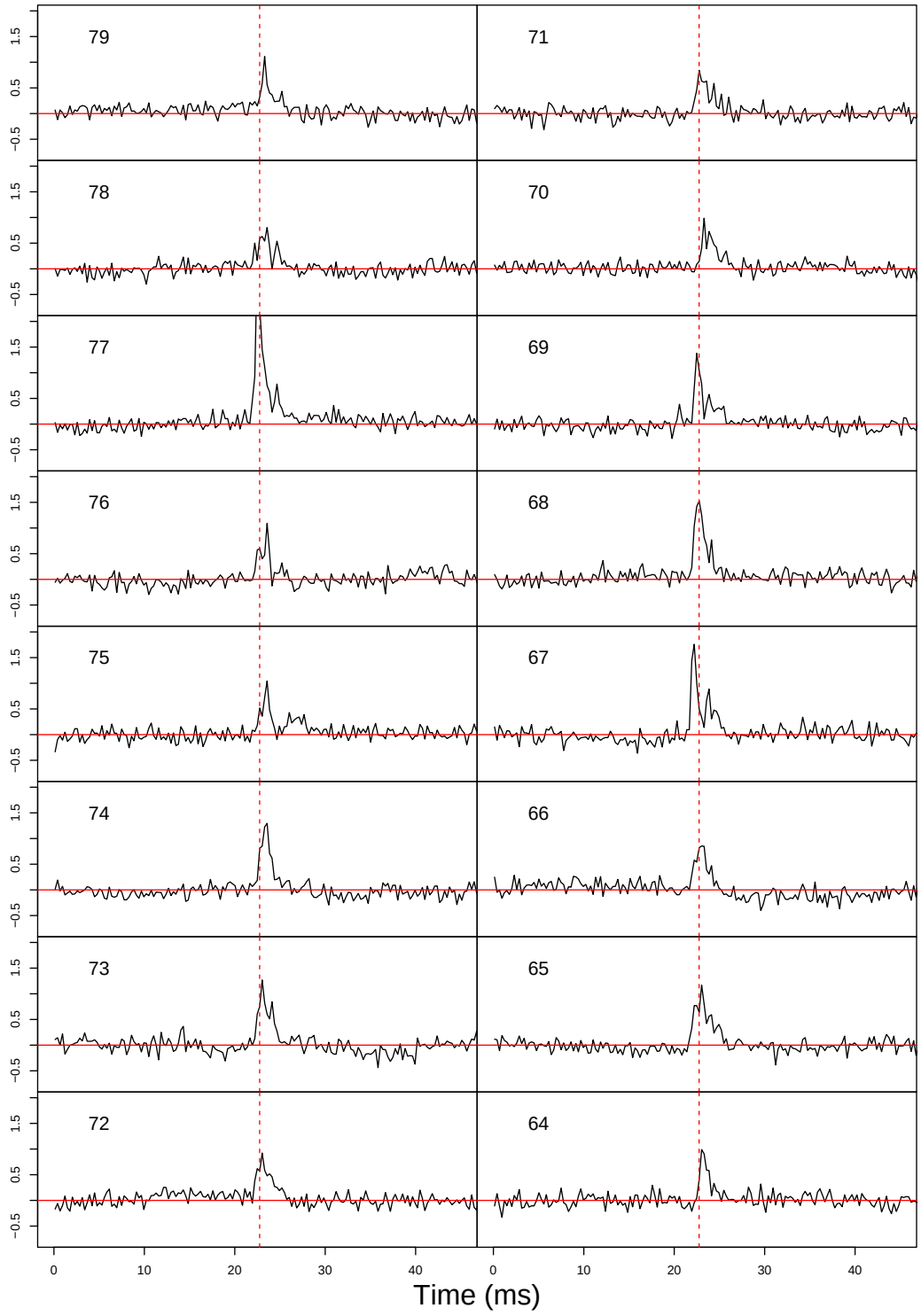

Figure 8.28: File 2016-12-12-11:36:03.ar, pulses 79-64, binned with $n = 25$. The X-axis is time in ms and the Y-axis is flux density in arbitrary units with all axes having the same scale. The solid red line marks a flux density of 0 and the dotted line marks the location of the peak of the full day's integrated pulse. Note that the full pulse period is not shown.

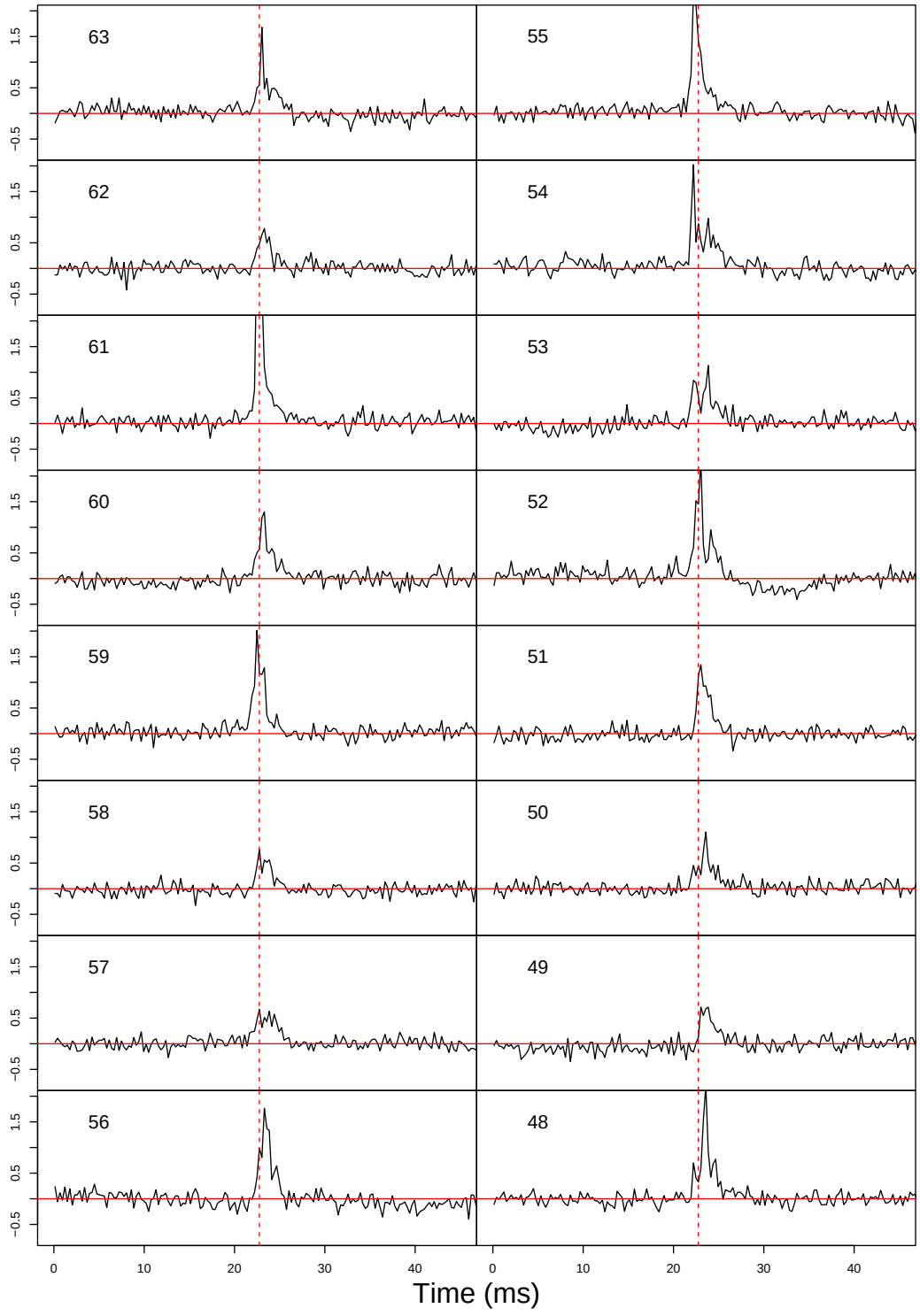

Figure 8.29: File 2016-12-12-11:36:03.ar, pulses 63-48, binned with $n = 25$. The X-axis is time in ms and the Y-axis is flux density in arbitrary units with all axes having the same scale. The solid red line marks a flux density of 0 and the dotted line marks the location of the peak of the full day's integrated pulse. Note that the full pulse period is not shown.

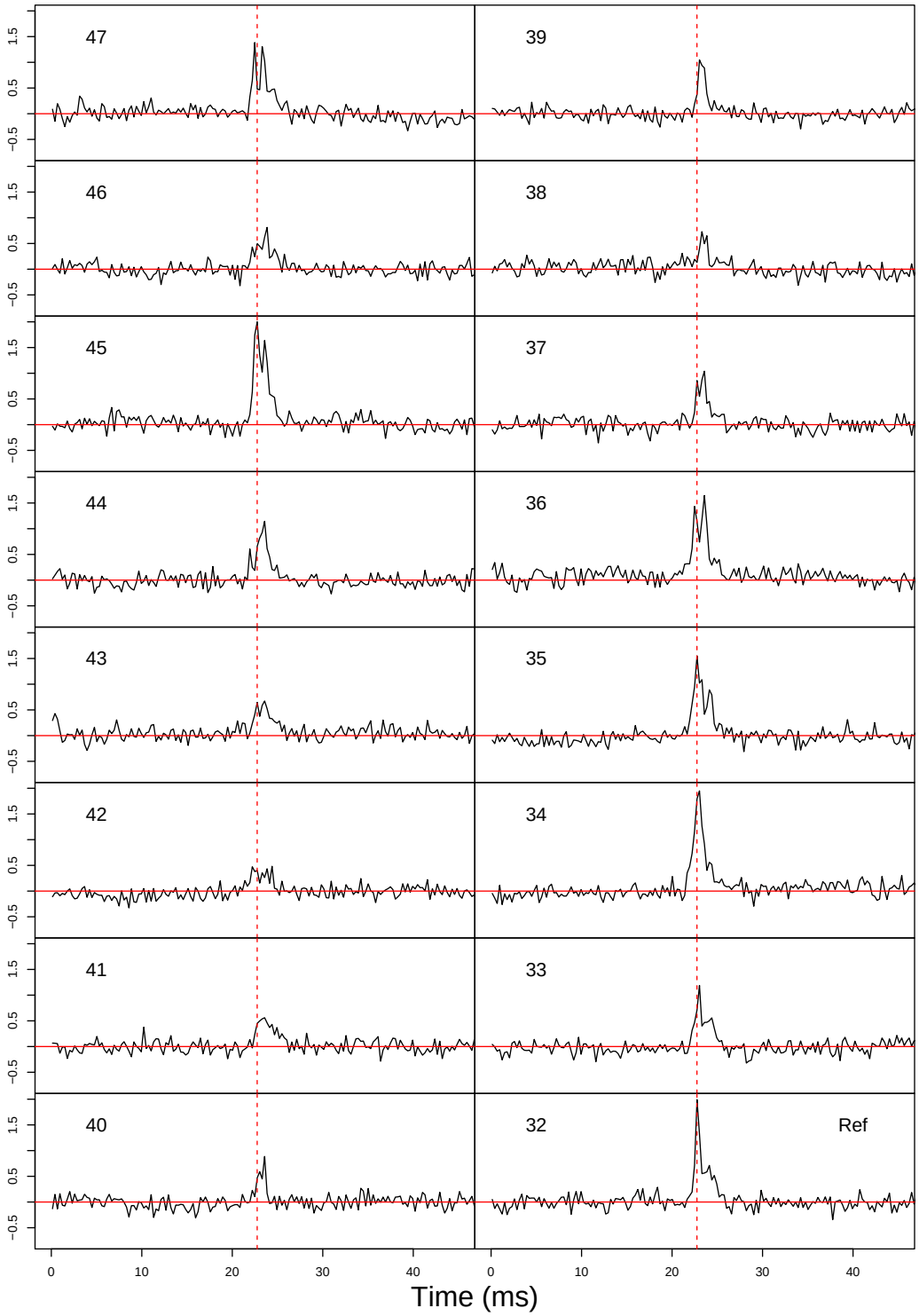

Figure 8.30: File 2016-12-12-11:36:03.ar, pulses 47-32, binned with $n = 25$. The X-axis is time in ms and the Y-axis is flux density in arbitrary units with all axes having the same scale. The solid red line marks a flux density of 0 and the dotted line marks the location of the peak of the full day's integrated pulse. Note that the full pulse period is not shown.

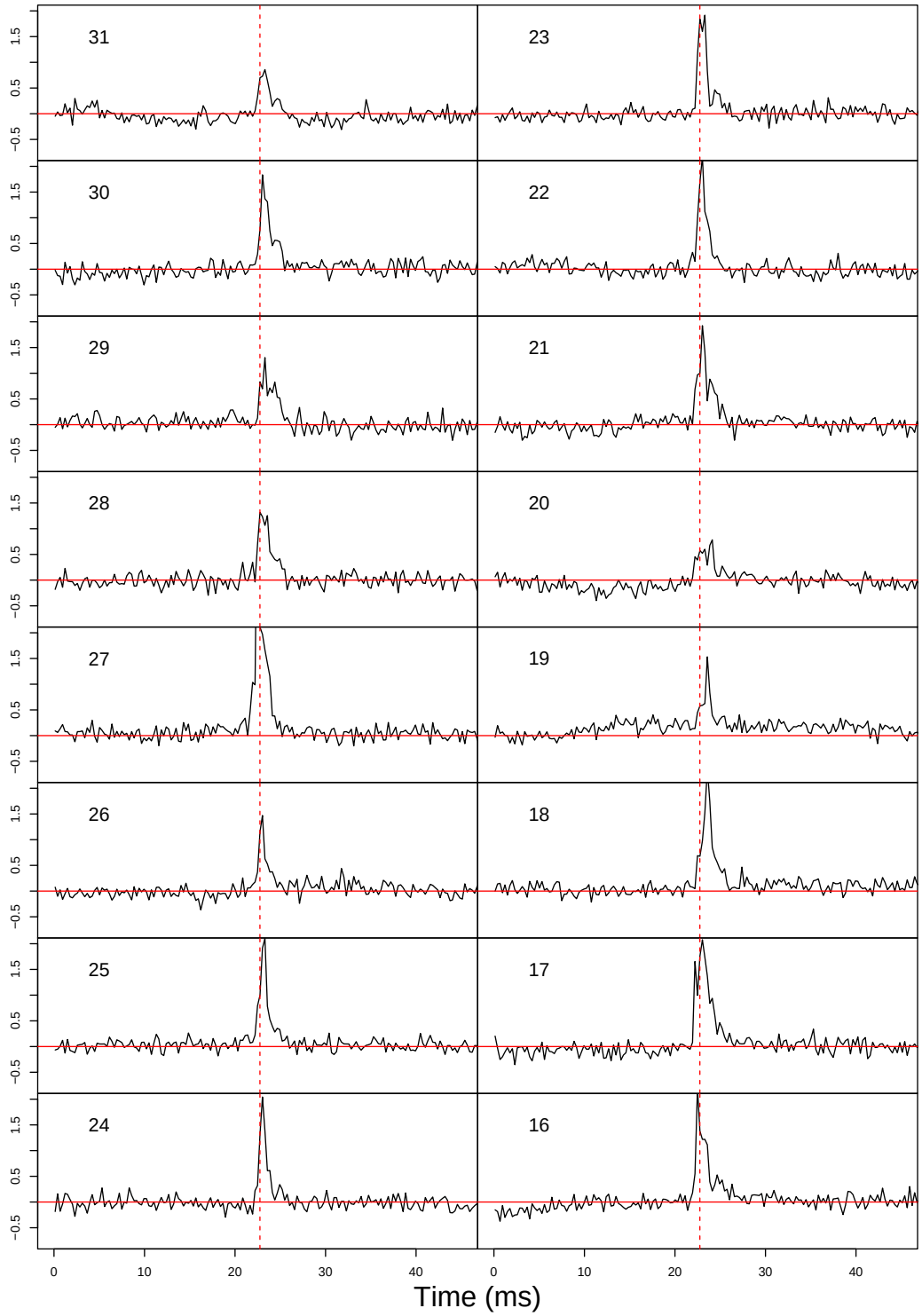

Figure 8.31: File 2016-12-12-11:36:03.ar, pulses 31-16, binned with $n = 25$. The X-axis is time in ms and the Y-axis is flux density in arbitrary units with all axes having the same scale. The solid red line marks a flux density of 0 and the dotted line marks the location of the peak of the full day's integrated pulse. Note that the full pulse period is not shown.

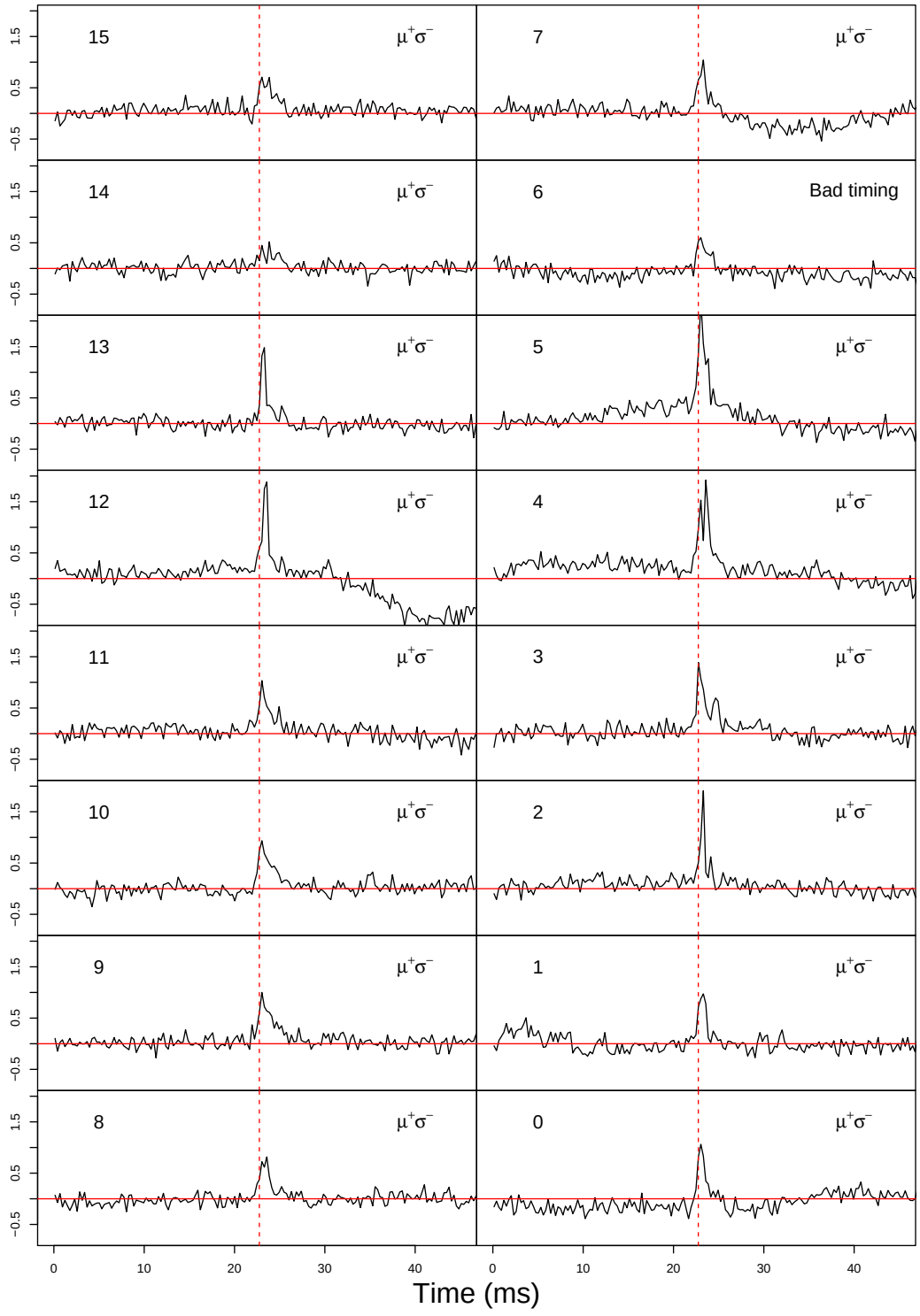

Figure 8.32: File 2016-12-12-11:36:03.ar, pulses 15-0, binned with $n = 25$. The X-axis is time in ms and the Y-axis is flux density in arbitrary units with all axes having the same scale. The solid red line marks a flux density of 0 and the dotted line marks the location of the peak of the full day's integrated pulse. Note that the full pulse period is not shown and $\mu^+\sigma^-$ indicates the section of increased mean and reduced variance discussed in the text.

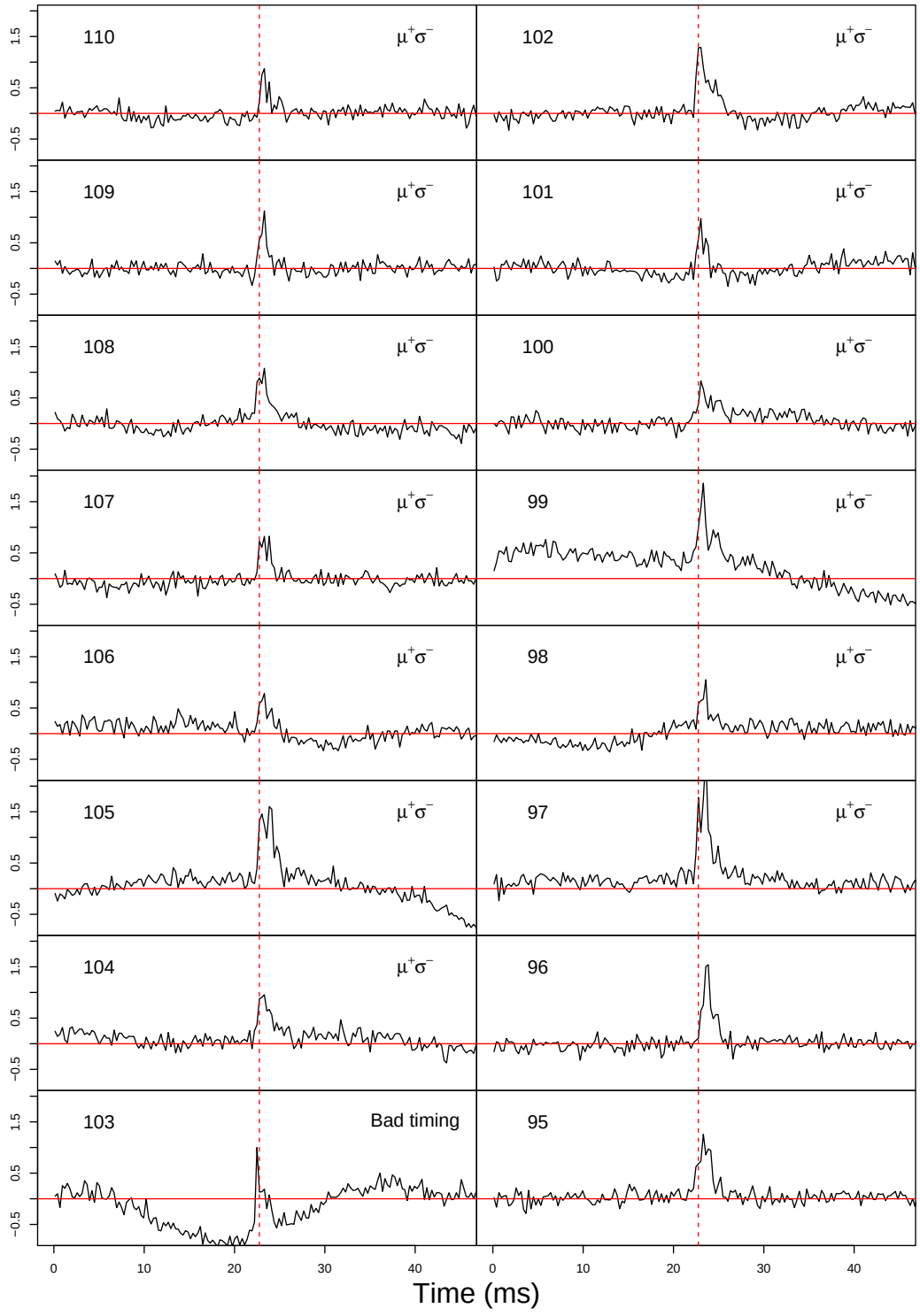

Figure 8.33: File 2016-12-12-11:35:53.ar, pulses 110-95, binned with $n = 25$. The X-axis is time in ms and the Y-axis is flux density in arbitrary units with all axes having the same scale. The solid red line marks a flux density of 0 and the dotted line marks the location of the peak of the full day's integrated pulse. Note that the full pulse period is not shown and $\mu^+\sigma^-$ indicates the section of increased mean and reduced variance discussed in the text.

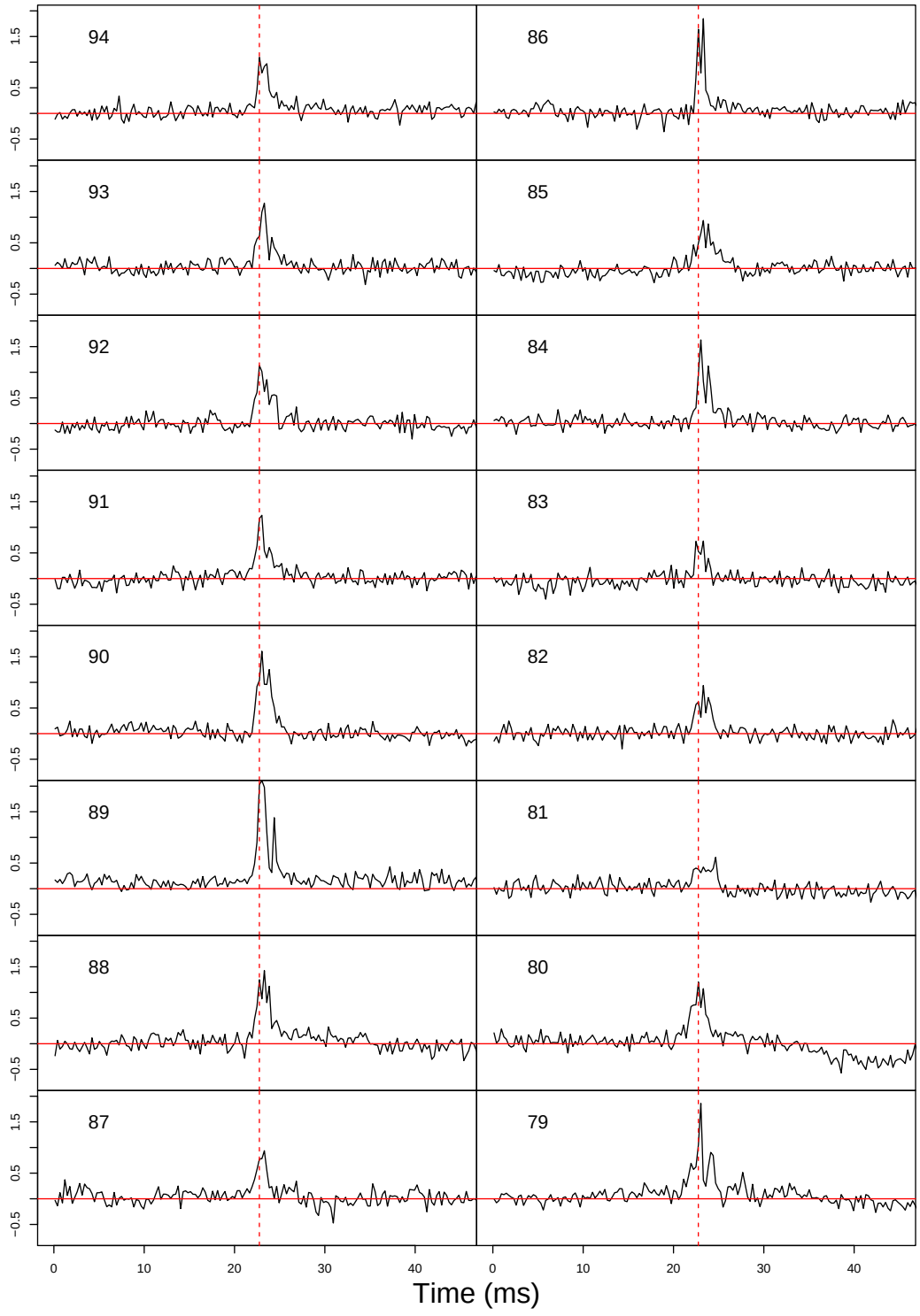

Figure 8.34: File 2016-12-12-11:35:53.ar, pulses 94-79, binned with $n = 25$. The X-axis is time in ms and the Y-axis is flux density in arbitrary units with all axes having the same scale. The solid red line marks a flux density of 0 and the dotted line marks the location of the peak of the full day's integrated pulse. Note that the full pulse period is not shown.

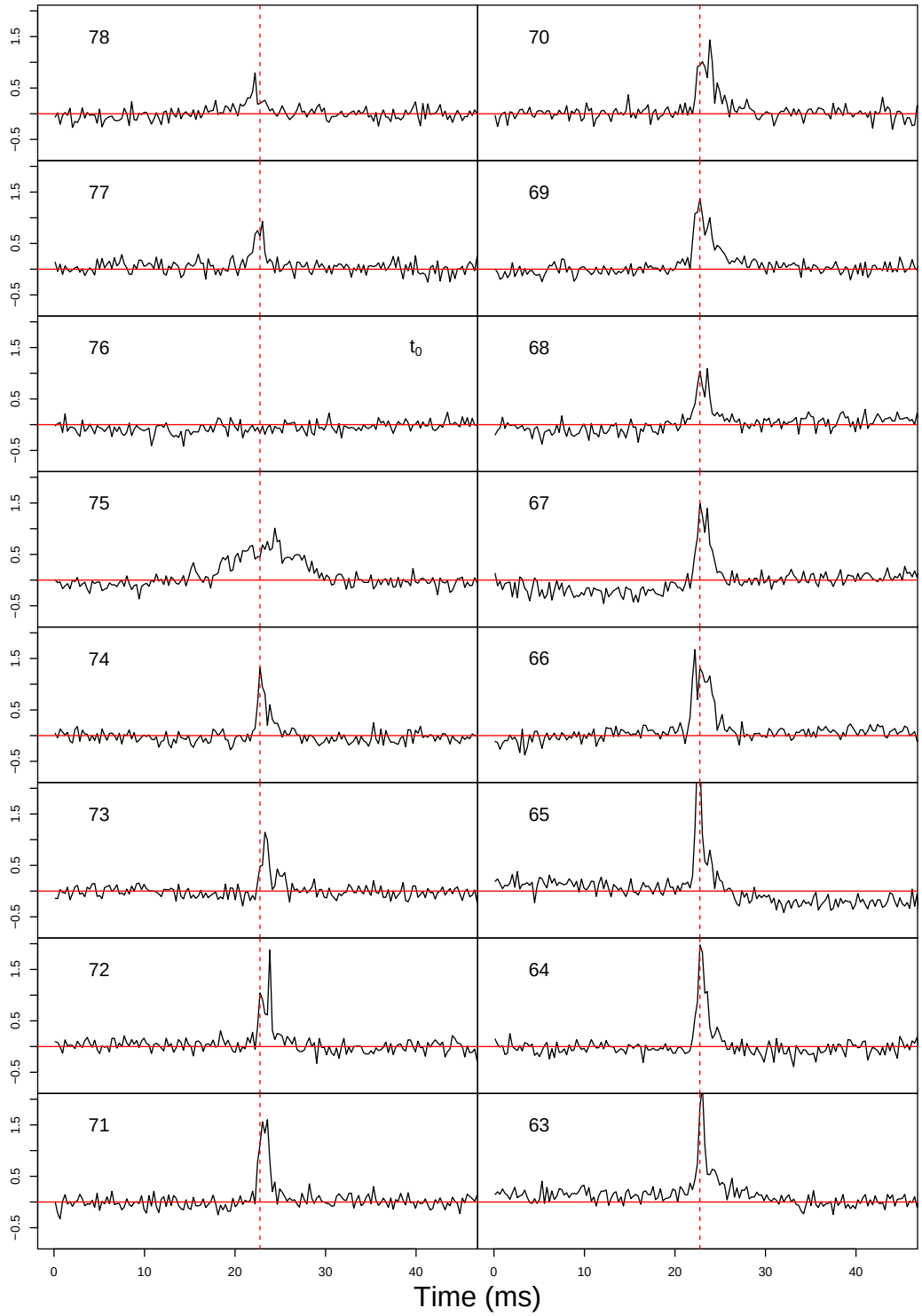

Figure 8.35: **The Glitch!** File 2016-12-12-11:35:53.ar, pulses 78-63, binned with $n = 25$. The X-axis is time in ms and the Y-axis is flux density in arbitrary units with all axes having the same scale. The solid red line marks a flux density of 0 and the dotted line marks the location of the peak of the full day's integrated pulse. Note that the full pulse period is not shown and that t_0 at pulse 76 shows the glitch.

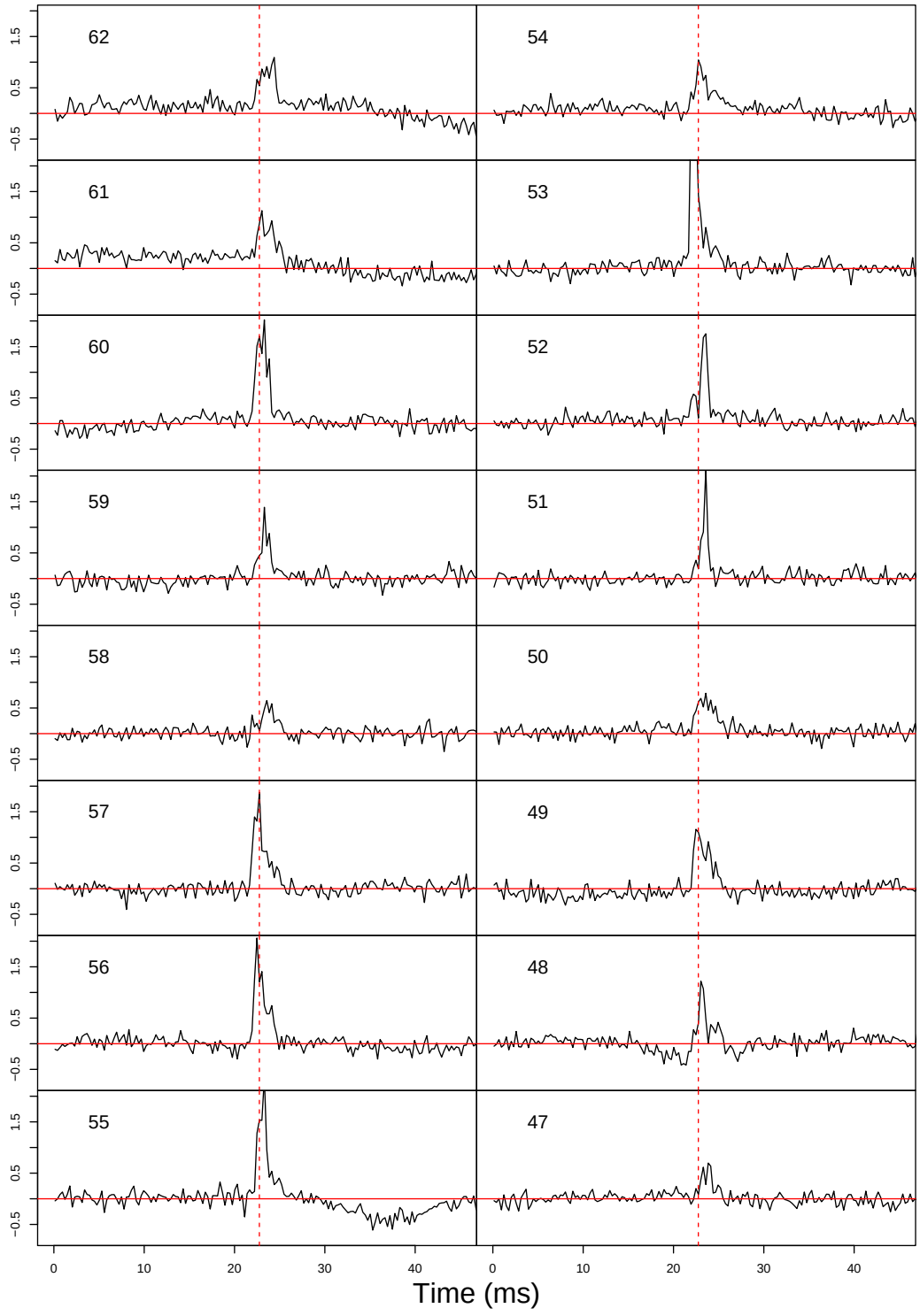

Figure 8.36: File 2016-12-12-11:35:53.ar, pulses 62-47, binned with $n = 25$. The X-axis is time in ms and the Y-axis is flux density in arbitrary units with all axes having the same scale. The solid red line marks a flux density of 0 and the dotted line marks the location of the peak of the full day's integrated pulse. Note that the full pulse period is not shown.

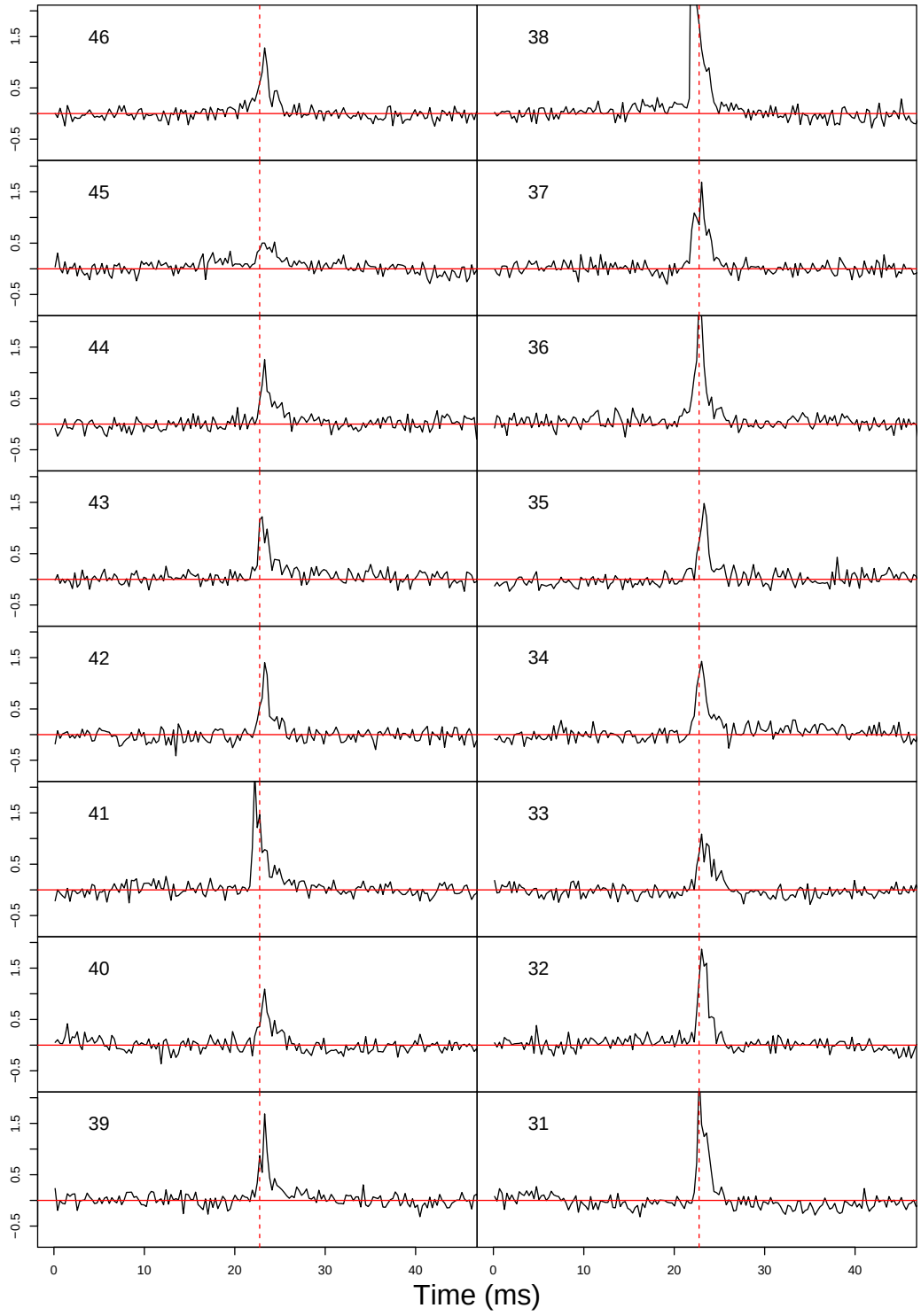

Figure 8.37: File 2016-12-12-11:35:53.ar, pulses 46-31, binned with $n = 25$. The X-axis is time in ms and the Y-axis is flux density in arbitrary units with all axes having the same scale. The solid red line marks a flux density of 0 and the dotted line marks the location of the peak of the full day's integrated pulse. Note that the full pulse period is not shown.

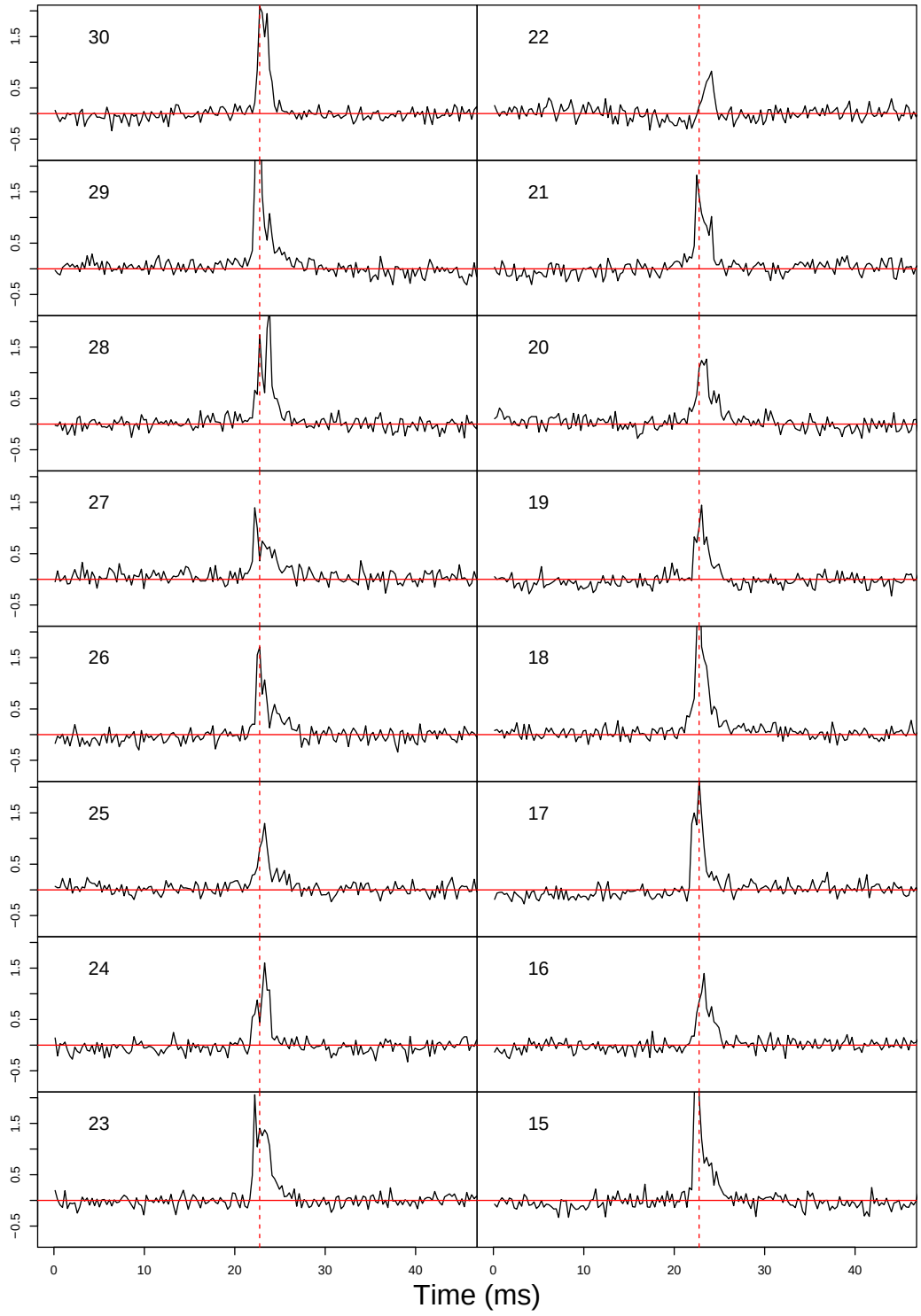

Figure 8.38: File 2016-12-12-11:35:53.ar, pulses 30-15, binned with $n = 25$. The X-axis is time in ms and the Y-axis is flux density in arbitrary units with all axes having the same scale. The solid red line marks a flux density of 0 and the dotted line marks the location of the peak of the full day's integrated pulse. Note that the full pulse period is not shown.

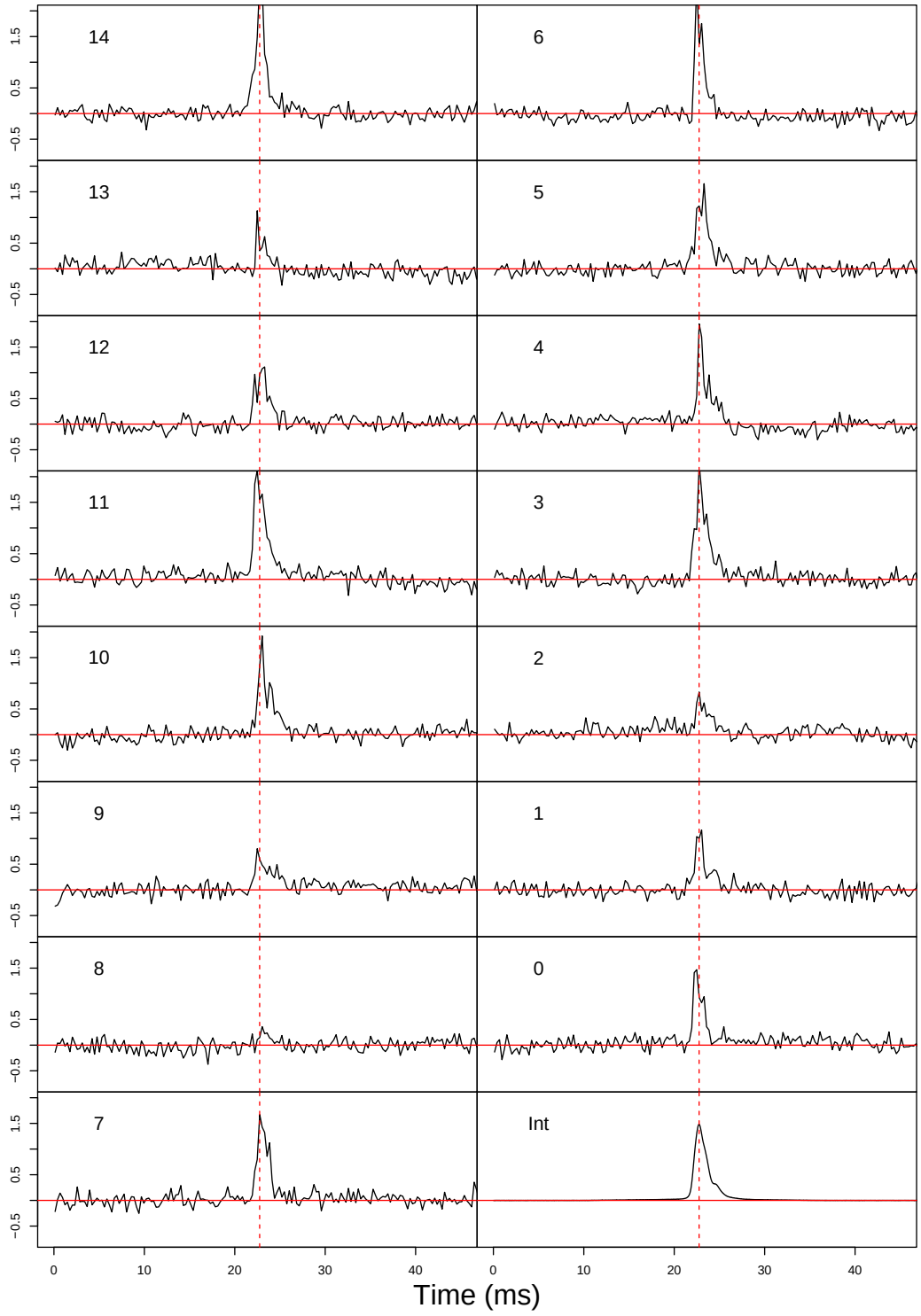

Figure 8.39: File 2016-12-12-11:35:53.ar, pulses 14-0, binned with $n = 25$. The last plot is the day's integrated plot (unbinned). The X-axis is time in ms and the Y-axis is flux density in arbitrary units with all axes having the same scale. The solid red line marks a flux density of 0 and the dotted line marks the location of the peak of the full day's integrated pulse. Note that the full pulse period is not shown.

8.2.5 Probabilities

The events described above need to be examined to decide whether their appearances are unusual or not. This will help indicate whether their close temporal relationship is a manifestation of the glitch event. Fortunately we have access to a large data set and this can be used to quantify the probabilities.

8.2.5.1 Probability of observing a null

A genuine null is potentially an extremely significant result, but to confirm how often an *apparent* null is observed using the Mount Pleasant telescope, we used two different approaches. First, we sorted all pulses on glitch day by peak flux density. Note that this day was very active with wind stows, but (fortunately) only after the glitch had occurred.

The 7000 pulses with the lowest flux density were then examined by hand[‡] and followed up to see if they were genuine nulls. Many false positives were discovered. The changeover to a new recording file every 10 s caused sub-integration 111 or 112 (the final one in a file) to be empty many times. To avoid this, we discarded this particular sub-integration from all analysis. RFI was also a large factor, but easily identified.

Wind stows or the end of an observation caused many false positives. This occurs when the telescope is moved away from Vela part way through a 10 s file. This means the early part of the file has pulses, but the rest does not, and so looks like many consecutive nulls. However, such a file still has enough data in it to produce a timing residual when integrated over the 10 s, which meant it wasn't discarded in the initial data triage. These files were discarded from the null search.

What remained was then passed through `pat` to see if an accurate timing on individual pulses could be obtained. This managed to leave 6 "pulses" out of the observation's pulse total of 684026 for which timings could not be obtained and so could be considered as apparent nulls. This give a $p = \frac{6}{684026} \approx \frac{1}{114004} = 8.77 \times 10^{-6}$.

Using an alternative approach we picked a day when Vela was at minimal activity (MJD 57661 or 2016 day 274) and also which had all files with RFI manually removed (see Table 7.1 on page 147 and the associated discussion for this procedure). Then we took the 10^4 pulses with lowest peak flux density and then used `pat` to obtain an arrival time on each of them. Pulses that had a timing residual within ± 2000 μs of the ephemeris for that day were discarded from the potential null list since it was assumed an accurate timing had been extracted. The remaining pulses were each manually examined to see

[‡]Thanks to Nicholas Bochenek and Wesley Kean Tai for assistance in this large manual task.

if a pulse was visible. After this process was complete, 9 pulses were considered to be nulls. This gives a probability of $p = \frac{9}{699672} \approx \frac{1}{77700} = 1.29 \times 10^{-5}$.

These two approaches give differing probabilities and it is interesting that the higher probability of a null ($p = \frac{1}{77700}$) occurs when Vela was at minimal bright pulse activity. This could be worthy of future research and it would be interesting to confirm if this is related to overall flux density activity and/or pulse profile width.

We will use the more conservative (higher) value ($p = \frac{1}{77700} = 1.29 \times 10^{-5}$) for future discussions here.

Of course we cannot say for certain that any of the above observations are genuine nulls in Vela as we are limited by the radiometer noise of the 26 m telescope.

Genuine nulls do occur in older pulsars (Rankin 1986), but as far as we are aware they have not occurred in young pulsars like Vela. Biggs (1992) and Johnston et al. (2001) state that not a single null pulse has been observed from Vela using the Parkes and Molongolo radio telescopes. Also, Rankin (1986) states that the nulling phenomenon is less prevalent in conal single pulsars, of which Vela is one.

We also examined $\approx$ 40000 (1 h) single pulses from the Parkes radio telescope[‡] and no nulls occurred. Using this probability, and including the 40000 pulses observed by Johnston et al. (2001), we would expect:

$$p = 1 - \left(1 - \frac{1}{77700}\right)^{80000} = 0.643 \tag{8.1}$$

to be the probability of observing a null in the Parkes data if our null statistics were genuinely correct. This figure of 64% is reasonably significant, and so we can conclude that the null we observed was extraordinary.

Future research observing a glitch with a much more sensitive telescope to confirm whether this null is genuine, or just a pulse with an extremely low flux density, would be extremely beneficial.

8.2.5.2 Probability of change in mean and variance

The null is already a low probability event and so to confirm if the change in mean and variance was rare or not, a search for other consecutive pulses of similar length and change in mean and variance was conducted. As the data is Gaussian, a simple T-test and F-test can be used. We constructed the *relative likelihood* (L_{r}) of observing a

[‡]Courtesy Willem van Straten.

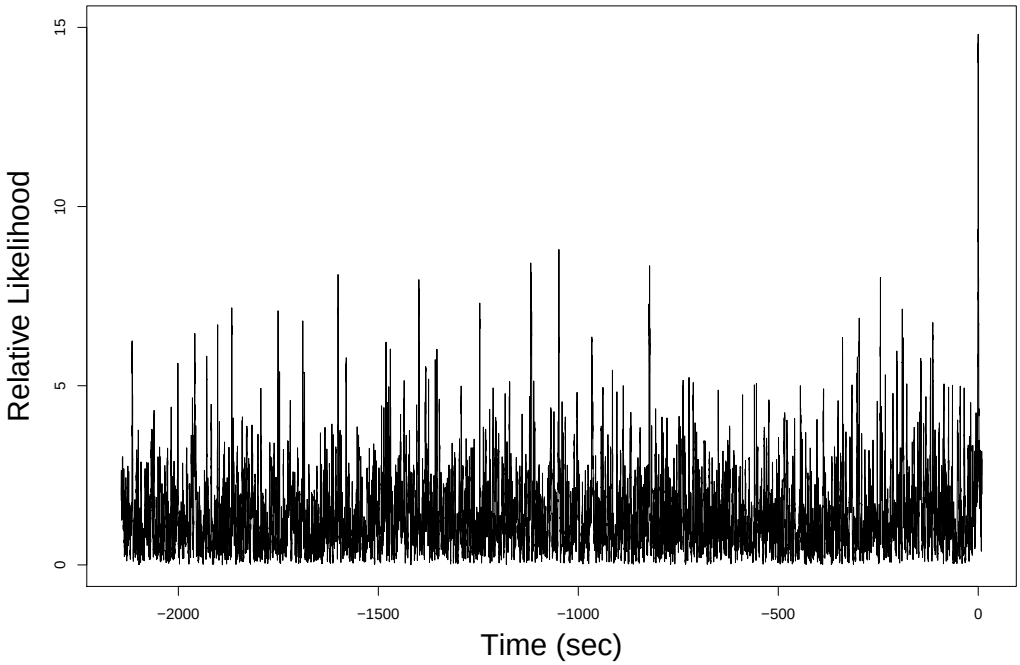

Figure 8.40: A measure of *relative likelihood* (see text) of getting 22 consecutive points with the observed mean and variance leading up to the glitch. With the X-axis, the origin represents t_0, the time of the null, and the Y-axis is a log scale.

similar change in the mean and variance of 22 consecutive points that occurred leading up to the glitch. That is,

$$L_{\mathrm{r}} = \log_{10}\left(\frac{1}{p_\mu p_\sigma}\right) \tag{8.2}$$

where p_μ and p_σ are the p-values of the T-test and F-test respectively.

Generally speaking multiplying p-values is frowned upon statistically but as long as the actual number is not used in an absolute fashion but rather in a relative fashion then the p-value can be treated as a probability (which it is) and multiplying probabilities is then subject to the recently famously proved Gaussian correlation inequality theorem by Royen (Latała and Matlak 2017).

So the actual value of L_{r} is not a meaningful (logarithmic) representation of the "odds", however it is meaningful when comparing to other L_{r} calculations in the dataset. Figure 8.40 shows L_{r} in the 30 min leading up to the glitch and shows that this event was indeed the most remarkable in that time by many orders of magnitude.

A more statistically sound method that is available to us, due to the large amount of data collected, is to search the data set for actual similar changes in mean and variance of the timing residuals. So we picked a day that all RFI had been manually removed

and then generated timings from the remaining 567966 individual pulses. This is a tedious process as TEMPO2 requires all timings processed to reside in memory at one time and so with the 4 GB RAM limit, timings had to be broken up and processed in lots of 50000 points. Once this was completed, a search of every sequence of 22[‡] timings was then conducted looking for a change in mean and variance similar (or better) to what was observed near the glitch. *None were found.* It technically would be beneficial to continue this search in other sections of the data set to establish an actual probability of this event occurring. But we can now say it has a probability $p \lesssim \frac{1}{550000} = 1.8 \times 10^{-6}$ which is vanishingly small.

8.2.6 The accurate glitch epoch

When searching other observations (for example, gamma rays, X-Rays, gravitational waves) it is useful to have a narrow epoch to search and so we will define t_0 as the time of the glitch since it is the first notable event near the glitch epoch. Table 8.3 shows times of t_0 at various locations. The null could obviously not be timed so its epoch was based on the average of the arrival times of the two pulses either side.

Table 8.3: The 2016 Glitch of the Vela pulsar showing the time of the null (t_0) at the observatory locations and the solar system barycentre. For Mount Pleasant and the barycentre, the time is calculated based on the average arrival times of the pulses either side of the null. At Ceduna only the pulse prior to the null was observable and so 1 period was added to the observed pulse. For reference and text searching purposes these are listed to the full precision provided by TEMPO2 but recall that the timing resolution is 10.9 μs.

Location	MJD	Time
Barycentre	57734.48495206727829	11:38:19.858613
Mount Pleasant	57734.48333216474613	11:35:59.899034
Ceduna	57734.48333327785134	11:35:59.995211

8.2.7 Long-term changes in flux density

Flux density changes were discussed earlier for pulses very close to the null, but longer-term changes might be prevalent. We examine these here.

[‡]since the 30 pulses of interest were interrupted by 2 bad timings, we conservatively began after the first bad timing and used the number of pulses with increased mean and decreased variance (not counting the second bad timing).

8.2.7.1 Peak flux density changes

It was stated earlier that (apart from the null) there *appeared* to be no unusual variation in pulse flux density around the time of the glitch. Plotting the flux density of each of the ≈ 40000 pulses for an hour's observation reveals little meaningful results, however a moving average can be used to highlight slower-moving changes.

If we have a sequence of $z+1$ flux densities: $f_0,\ f_1,\ f_2\ \ldots\ f_i\ \ldots\ f_z$ we have used the moving average m_i as the average of n points with the point f_i at the *centre*, where n is the window size. For convenience, n should be even. More precisely:

$$m_i = \frac{\sum_{j=i-\frac{n}{2}}^{i+\frac{n}{2}} f_j}{n} \tag{8.3}$$

and with the extra proviso that if ever $j < 0$ or $j > z$ then m_i is undefined.

Figure 8.41 on page 196 shows three moving average plots of individual pulse *peak* flux density between 11:00-12:00 UT (at the observatory) with three window sizes of n =100, 1000, and 2000 pulses wide and the vertical red line marks the null (t_0).

A strong dip appears in each plot, with the null at the nadir.[‡] Since this is a moving average, this implies that the null in peak flux density wasn't a single instant phenomena, but an event that occurred over time.

We must be careful in interpreting peak flux densities because they are heavily influenced by RFI and changes in attenuation levels. Note that this graph seems to show cycles, and the Lomb-Scargle Periodogram shows a strong signal at a period of ≈ 300, 600, and 900 s or ≈ 5, 10, and 15 min. Our automatic gain control adjusts the attenuation every 5 min and so this is almost certainly a side effect of that. Regardless, the large dip at the time of the glitch is significant.

8.2.7.2 Mean flux density changes

Figure 8.42 on page 197 shows a similar plot as Figure 8.41 on page 196 but shows mean flux density. For comparison, the same moving average window sizes (n) are used. The time of the glitch (t_0) is marked in red and there appears to be a notable increase in mean flux density, however it does not coincide with t_0. As discussed earlier,

[‡]The null isn't precisely at the nadir for $n = 2000$ since the moving average is being influenced by other data.

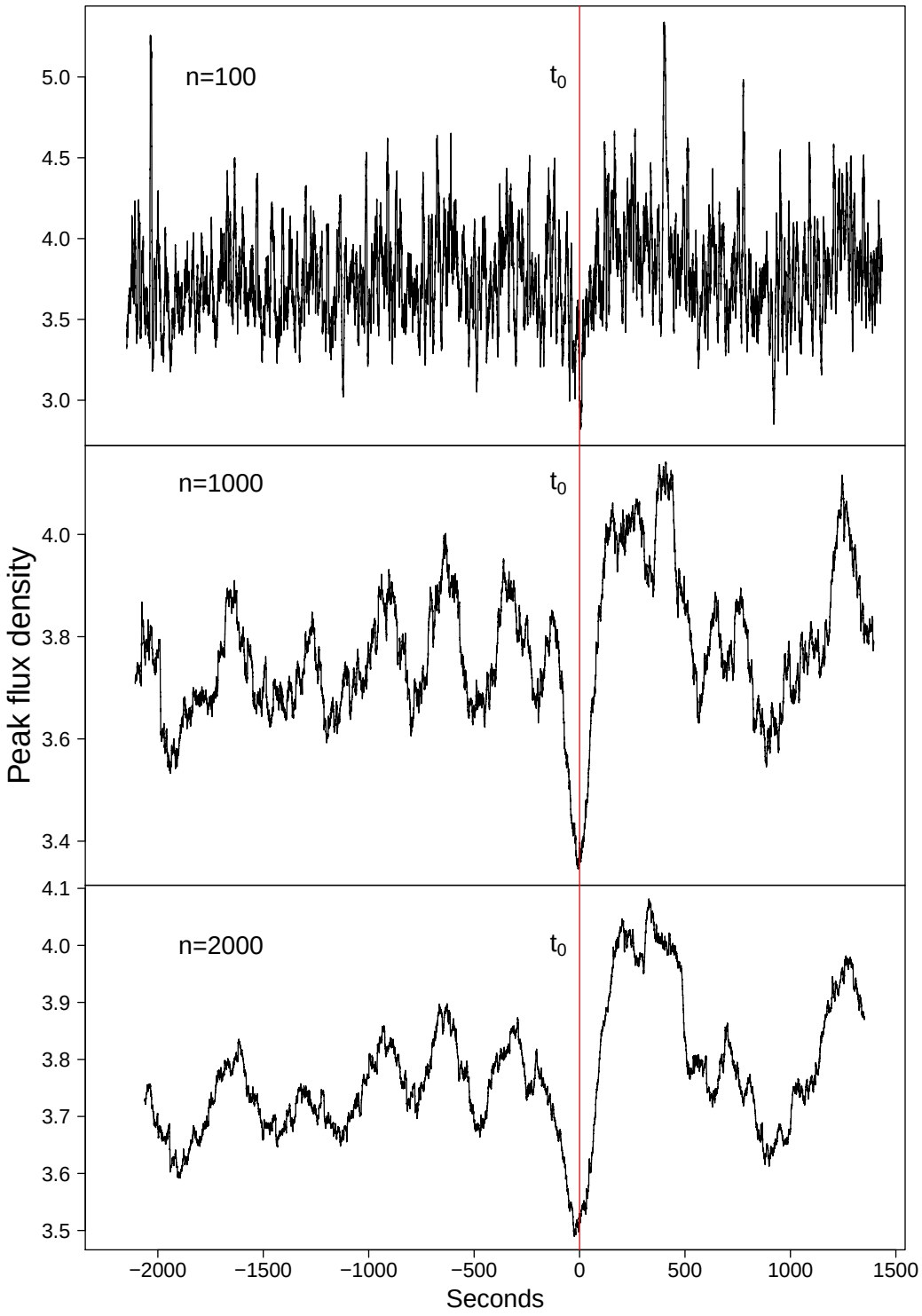

Figure 8.41: Moving averages (window size n pulses) of *peak* flux density (arbitrary units) over 1 hour of observation with the vertical red line marking the null. The moving average is affected over a long time period implying that the null is not a single event.

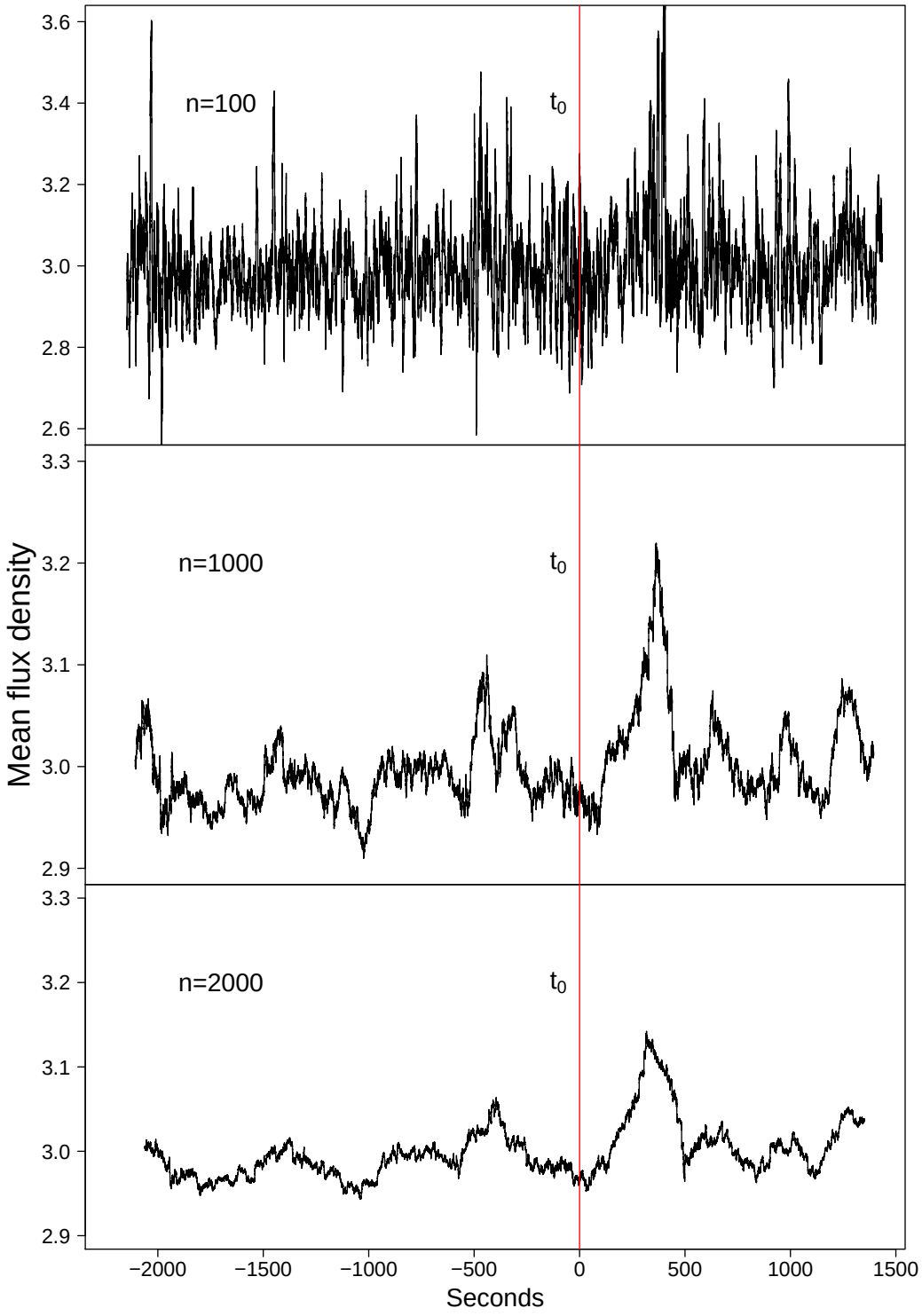

Figure 8.42: Moving averages (window size n pulses) of *mean* flux density (arbitrary units) over 1 hour of observation with the vertical red line marking the null. The increase in mean flux density that appears well after the null is most likely RFI.

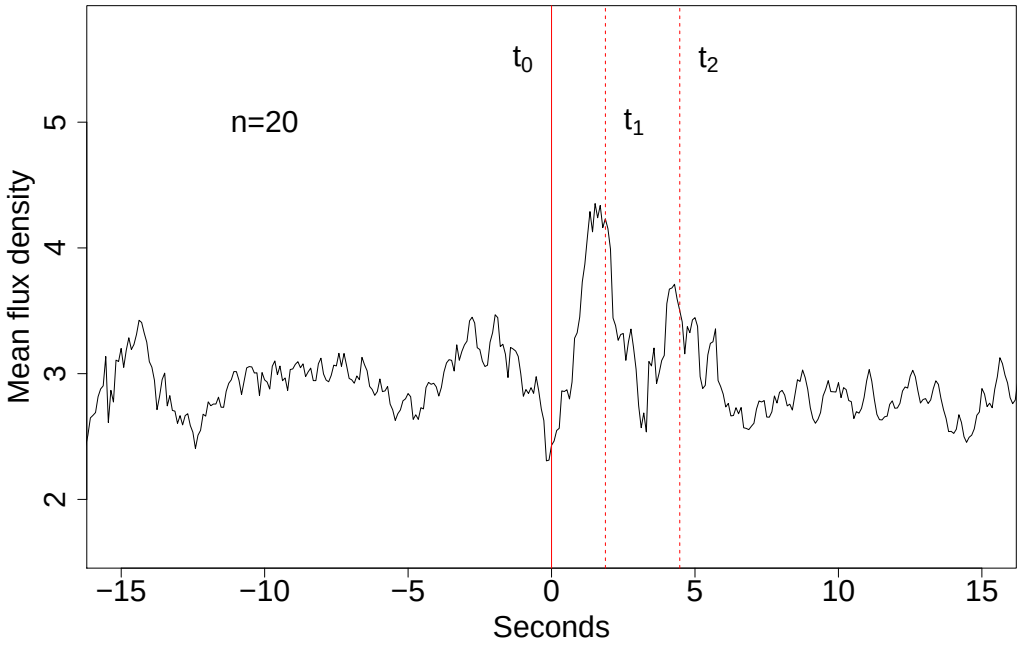

Figure 8.43: Moving averages (window size of 20 pulses) of *mean* flux density (arbitrary units) over 20 s with the vertical solid red line marking the null (t_0) and t_1 and t_2 highlighted.

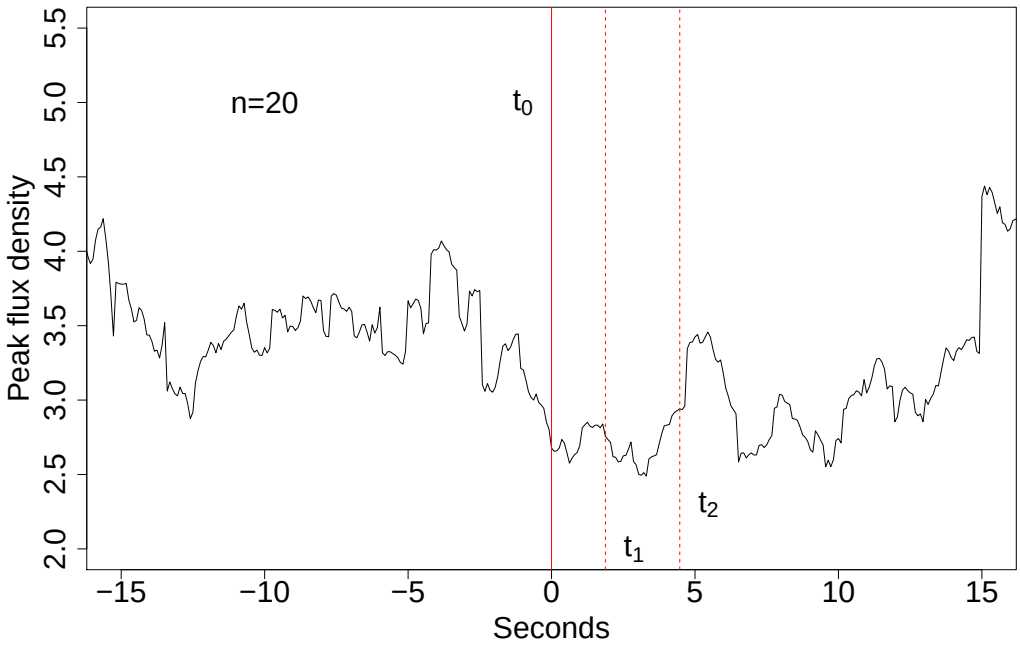

Figure 8.44: Moving averages (window size of 20 pulses) of *peak* flux density (arbitrary units) over 20 s with the vertical solid red line marking the null (t_0) and t_1 and t_2 highlighted.

out-of-band RFI causes the whole band to "lift" and hence influences mean flux density measurements. The peak to the right of t_0 is most likely RFI.

However, Figure 8.43 on page 198 shows the same data, but shown over 20 s and a moving average window of $n = 20$. The red line is t_0 and the dotted red lines are t_1 and t_2. There is a clear *increase*, a peak reached, and then a *decrease* in mean flux density in the 1.88 s between t_0 and t_1. Comparing this to a similar plot of peak flux density shown in Figure 8.44 on page 198, there is no comparable event.

This is an intriguing reversal to what's shown in earlier figures. That is, *mean* flux density shows a dip whereas *peak* flux density does not.

8.2.7.3 Binning of data

Using moving averages can sometimes provide misleading results and so here we present the same plots as in the previous section, but this time using binning. Points in the original data are grouped into n "bins" and the values of those points are averaged. As before if we have a sequence of $z + 1$ flux densities: $f_0,\ f_1,\ f_2\ \ldots\ f_i\ \ldots\ f_z$ then each bin b_i is:

$$b_i = \frac{\sum_{j=ni}^{ni+(n-1)} f_j}{n} \tag{8.4}$$

with the proviso that if $j > z$ then b_i is undefined. This will occur when n is not an exact factor of the number of data points $(z + 1)$.

Figure 8.45 on page 200 shows peak flux density over an hour's observation with t_0 being marked with the vertical red line. Binning factors of $n = 100, n = 200$, and $n = 1000$ are plotted.

Figure 8.46 on page 201 shows mean flux density over an hour's observation with t_0 being marked with the vertical red line. Identical binning factors of $n = 100, n = 200$, and $n = 1000$ are plotted. As can be seen these reflect similar results to the moving average graphs above.

8.2.8 Detail of pulses surrounding the null

Figure 8.47 on page 202 shows a selection of pulses surrounding the null that occurred at pulse number 76 (in the recorded file). Pulses 72-74 look typical, however pulse 75

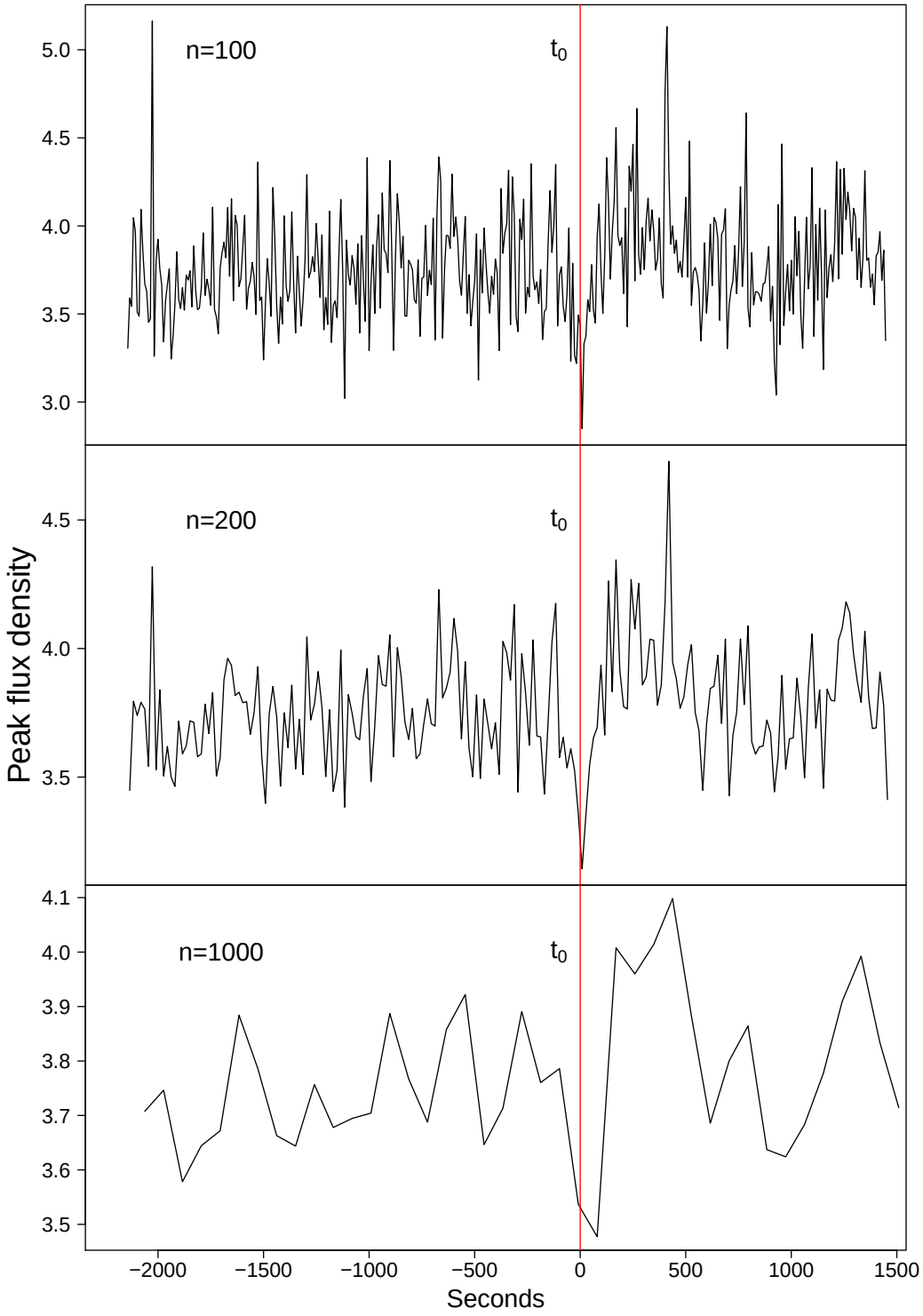

Figure 8.45: Binning of *peak* flux density (arbitrary units) over 1 h of observation with the vertical red line marking the null. The size of the bins (n) is denoted.

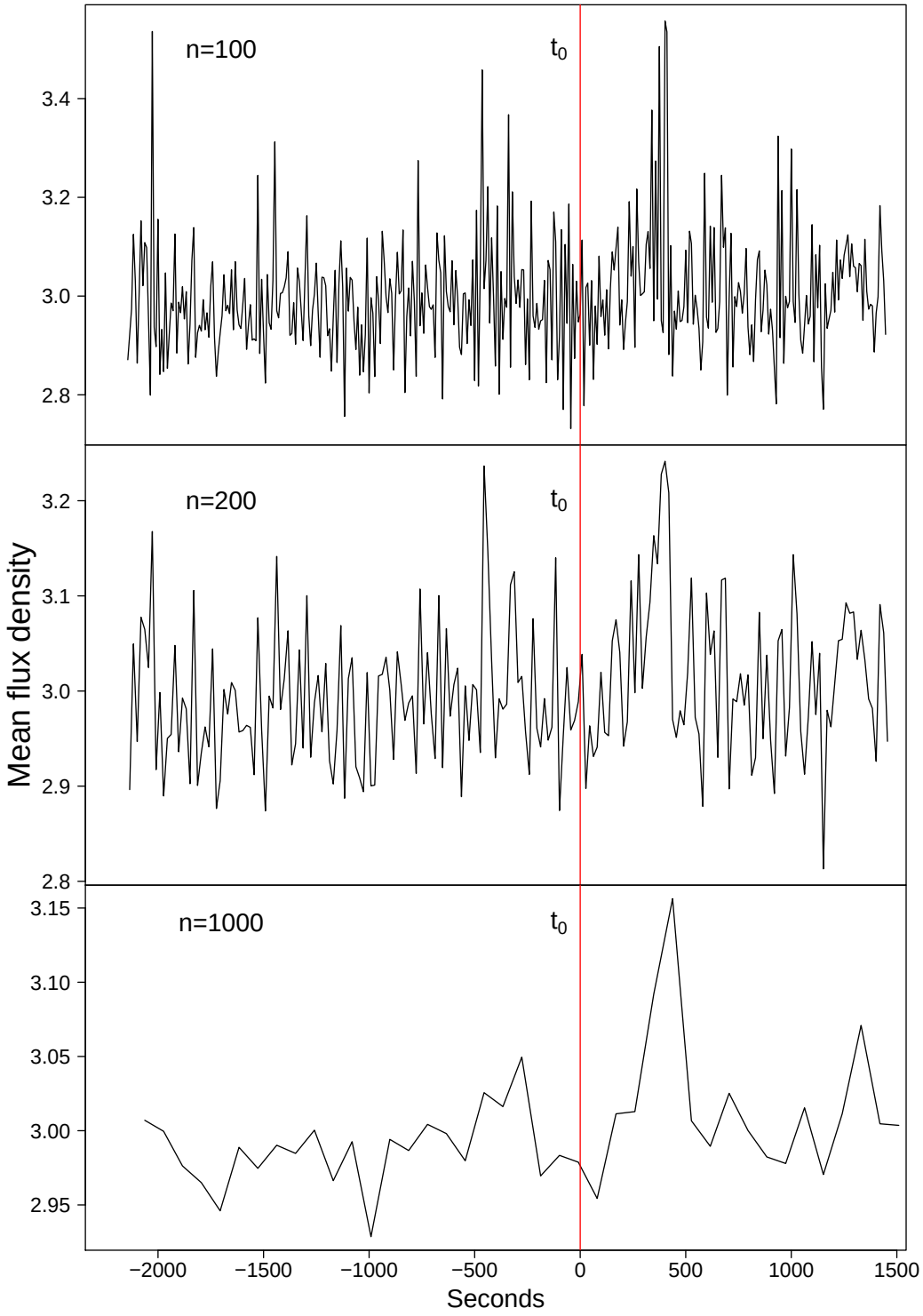

Figure 8.46: Binning of *mean* flux density (arbitrary units) over 1 h of observation with the vertical red line marking the null. The size of the bins (n) is denoted.

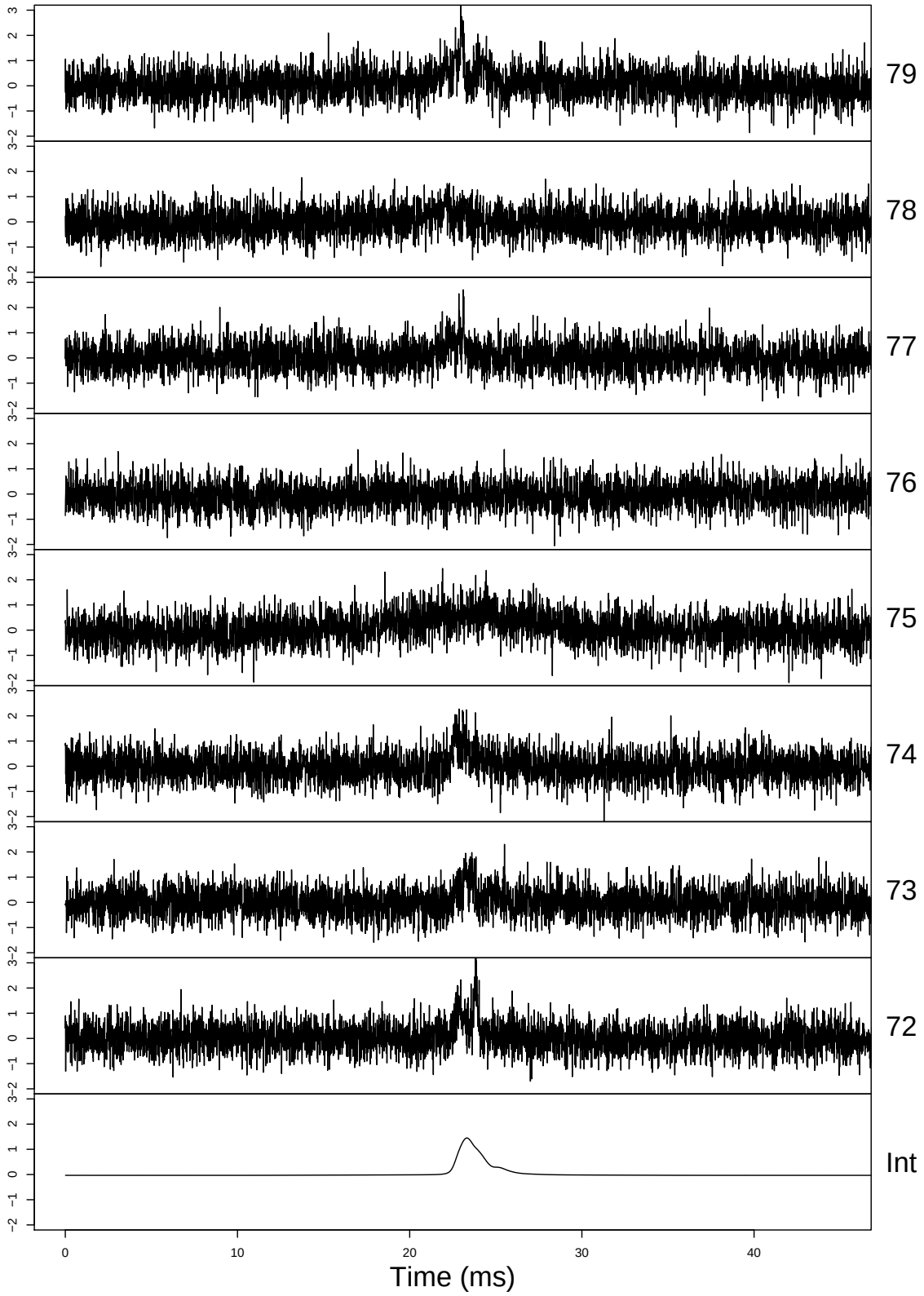

Figure 8.47: Individual pulses surrounding the null at pulse 76. The X-axis is time in ms and the Y-axis is flux density in arbitrary units with all axes having the same scale. The bottom plot is the integrated plot for the entire day's observing. Note that the full pulse period is not shown.

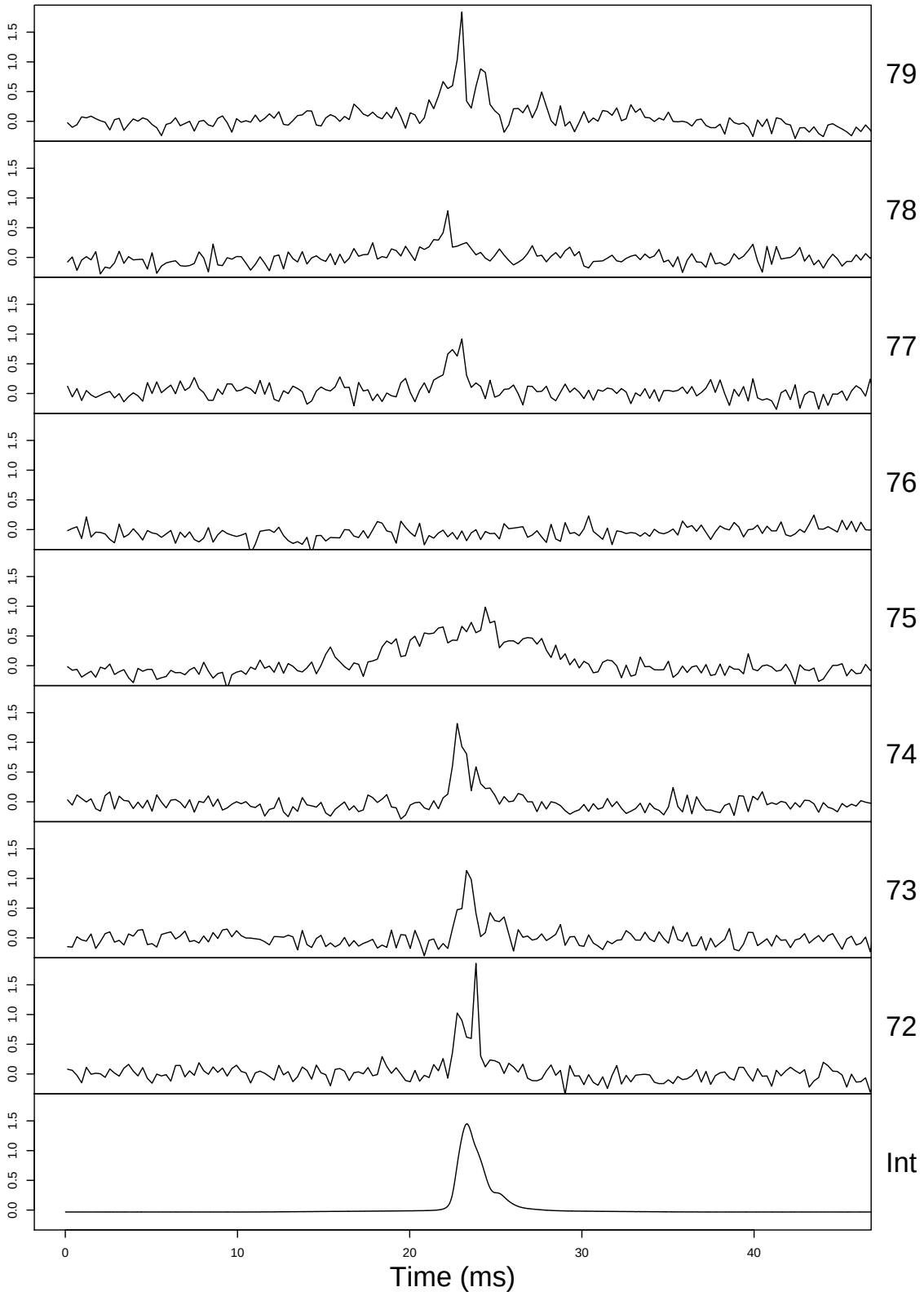

Figure 8.48: Individual pulses surrounding the null at pulse 76 but binned with $n = 25$. The X-axis is time in ms and the Y-axis is flux density in arbitrary units with all axes having the same scale. The bottom plot is the integrated plot for the entire day's observing (with no binning). Note that the full pulse period is not shown.

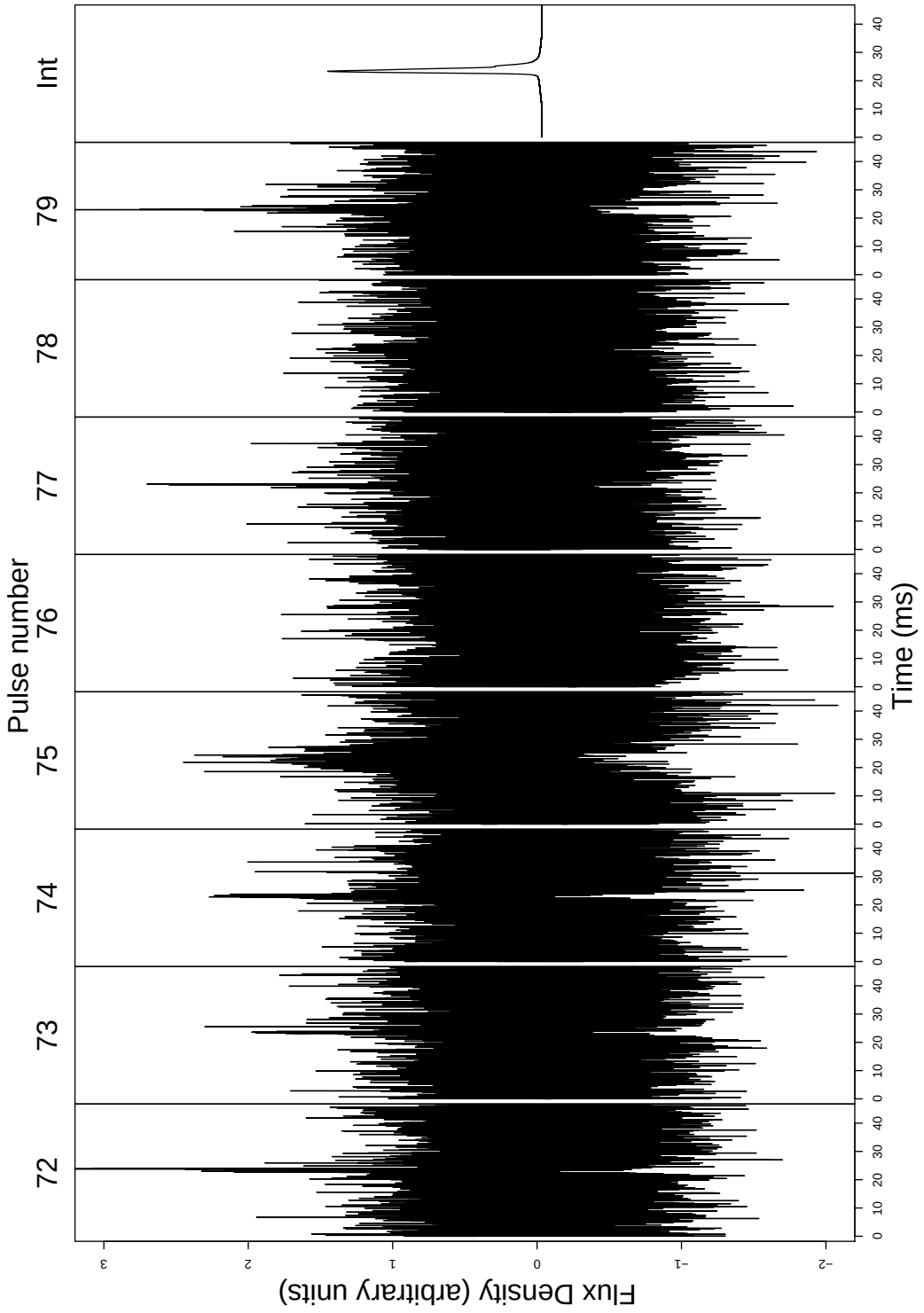

Figure 8.49: Landscape view of individual pulses surrounding the null at pulse 76. The X-axis is time in ms and the Y-axis is flux density in arbitrary units with all axes having the same scale. The far right plot is the integrated plot for the entire day's observing. Note that the full pulse period is not shown.

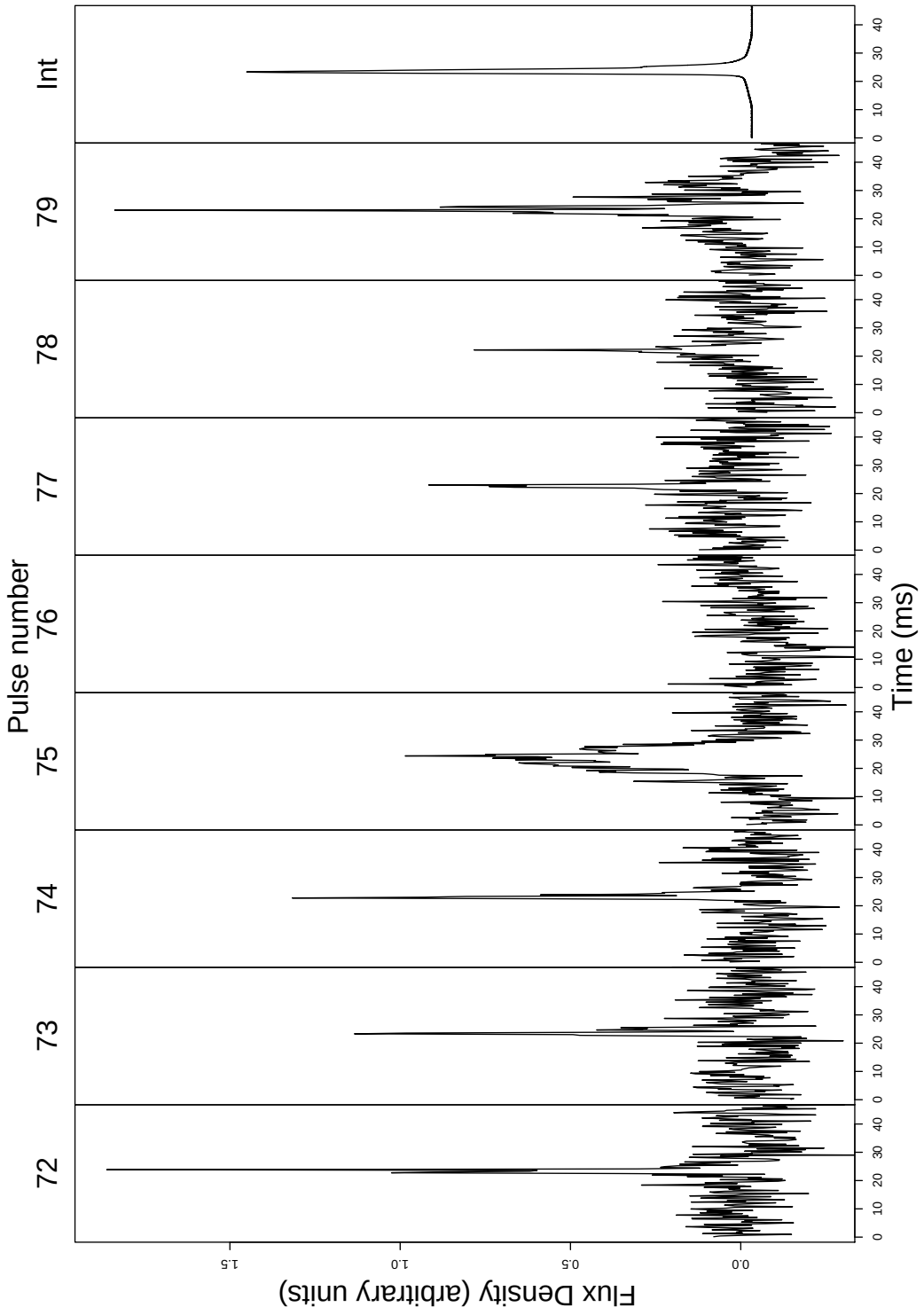

Figure 8.50: Landscape view of individual pulses surrounding the null at pulse 76 but binned with $n = 25$. The X-axis is time in ms and the Y-axis is flux density in arbitrary units with all axes having the same scale. The far right plot is the integrated plot for the entire day's observing (with no binning). Note that the full pulse period is not shown.

looks quite broad - spread over about 10 ms. Pulse 76 is the null, and then they return to typical pulses after that.

Figure 8.48 on page 203 shows the same figure but this time pulse flux density is binned and averaged in groups of $n = 25$. This highlights the individual pulse shape and in particular the null on pulse 76.

Figure 8.49 on page 204 shows the pulses from Figure 8.47 on page 202 but presented in a landscape format to highlight the lengthening of pulse 75 and the null on pulse 76, whilst Figure 8.50 on page 205 shows the same view but again with a binning of $n = 25$, and the width of pulse 75 is very clear.

8.2.8.1 Waterfall diagram of glitch

Figure 8.51 on page 207 shows a traditional "waterfall" diagram that was often used in older papers in the literature prior to availability of colour printing. These are three dimensional versions of the PSRCHIVE "Y" diagram (for example Figure 8.11 on page 166) with the X-axis representing pulse phase, the Y-axis is time, and the Z-axis is pulse flux density. The null has been shaded in black and flux density has been exaggerated for effect. This plot is a selection of 100 pulses from the combination of Figures 8.10 to 8.11 on page 166 and is not particularly useful but is included for t-shirt value.*

8.2.9 Rotational changes

Figure 8.52 on page 208 shows a timing residual plot zoomed out to 216 s (2.5×10^{-3} day) which is enough to show the larger glitch changes. Also plotted is the cumulative sum of the timing residuals and the cumulative sum of the cumulative sum of the timing residuals. These can be considered as discrete versions of the first and second integrals of the timing residuals and are used to highlight interesting changes.

This is using the similar theory behind PID (Proportional Integral Derivative) controllers in the engineering field. This states that the adjustment $a(t)$ to be applied in a system with error $e(t)$ can be calculated by:

$$a(t) = W_p e(t) + W_i \int_0^t e(\tau) d\tau + W_d \frac{de(t)}{dt} \tag{8.5}$$

The *proportional* component $W_p e(t)$ corrects for the current error, the *integral* component $W_i \int_0^t e(\tau) d\tau$ corrects for historical cumulative errors, and the *derivative* com-

*see the album cover of Unknown Pleasures from the band Joy Division.

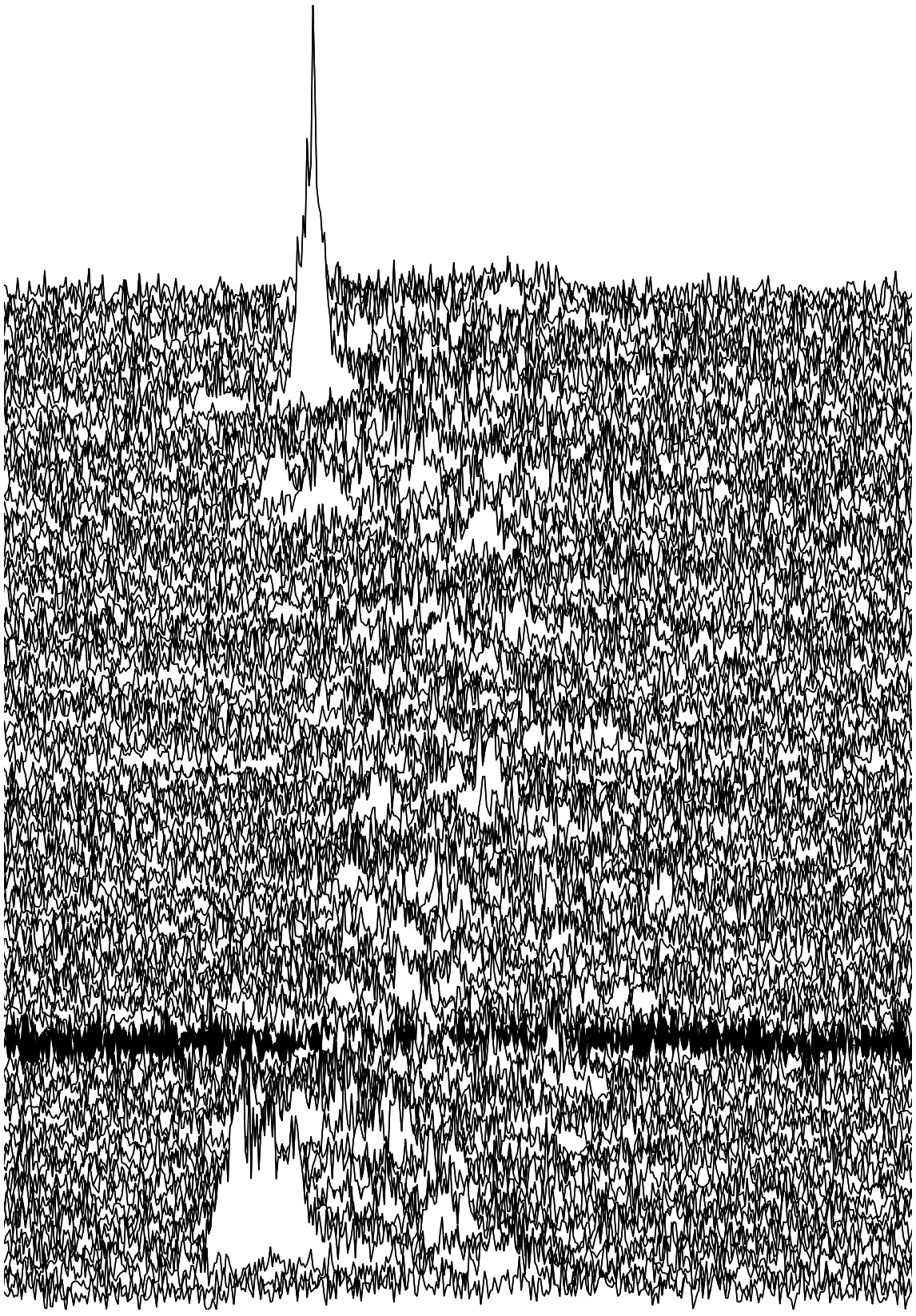

Figure 8.51: "waterfall" diagram showing pulse flux density versus time near the glitch. The null is shaded in black and 100 pulses are shown. Axes are deliberately left blank for t-shirt value.

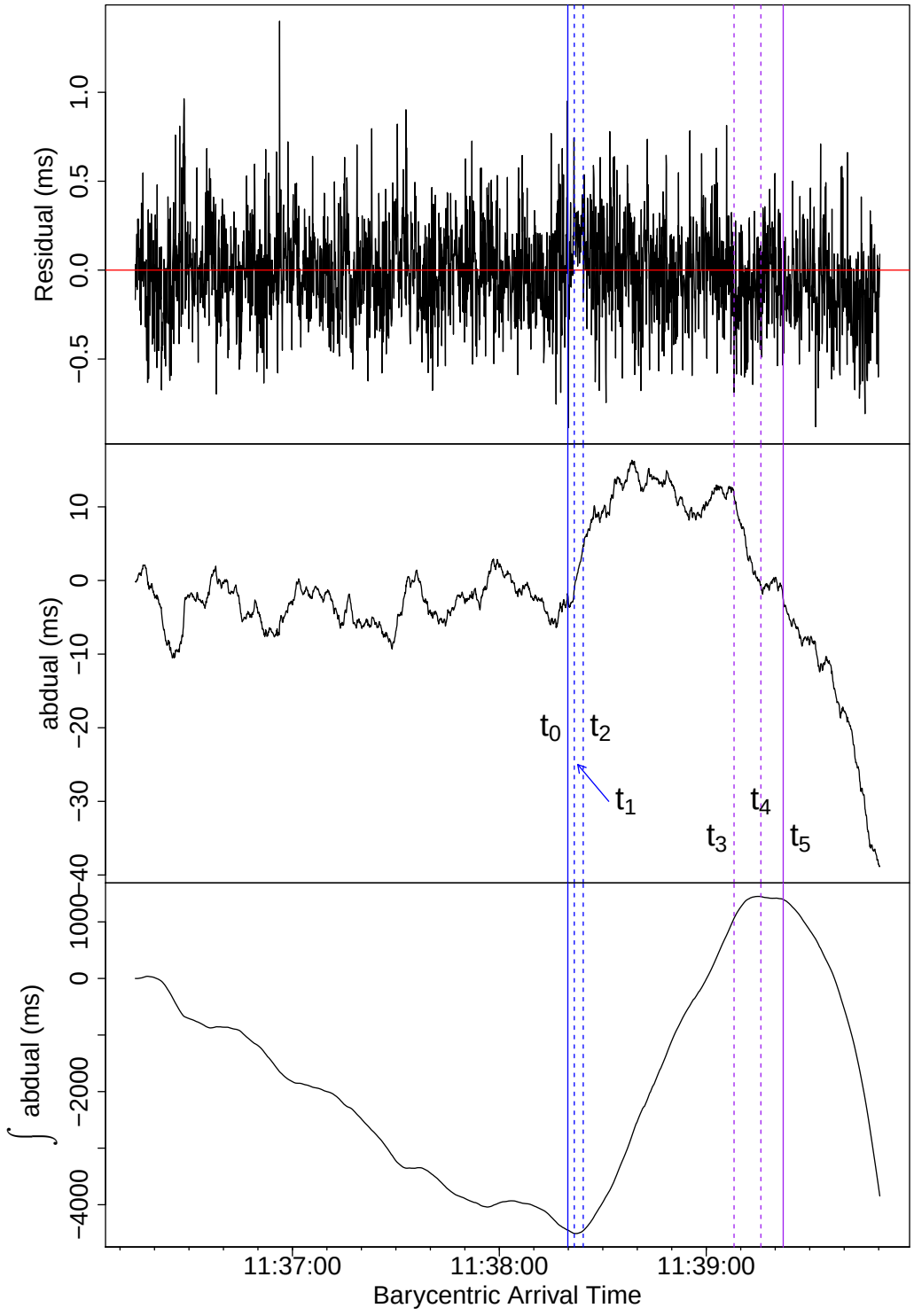

Figure 8.52: These are 216 s (2.5×10^{-3} day) plots surrounding the null at t_0 (solid blue line). The top panel is timing residuals (in ms) similar to Figure 8.4 on page 160. The middle panel is the cumulative sum, or integral, of the timing residuals (*abdual* - see text), and the bottom panel is the double integral of the timing residuals ($\int$abdual). These are used to highlight changes. Other key points t_1 to t_5 (see text) are highlighted.

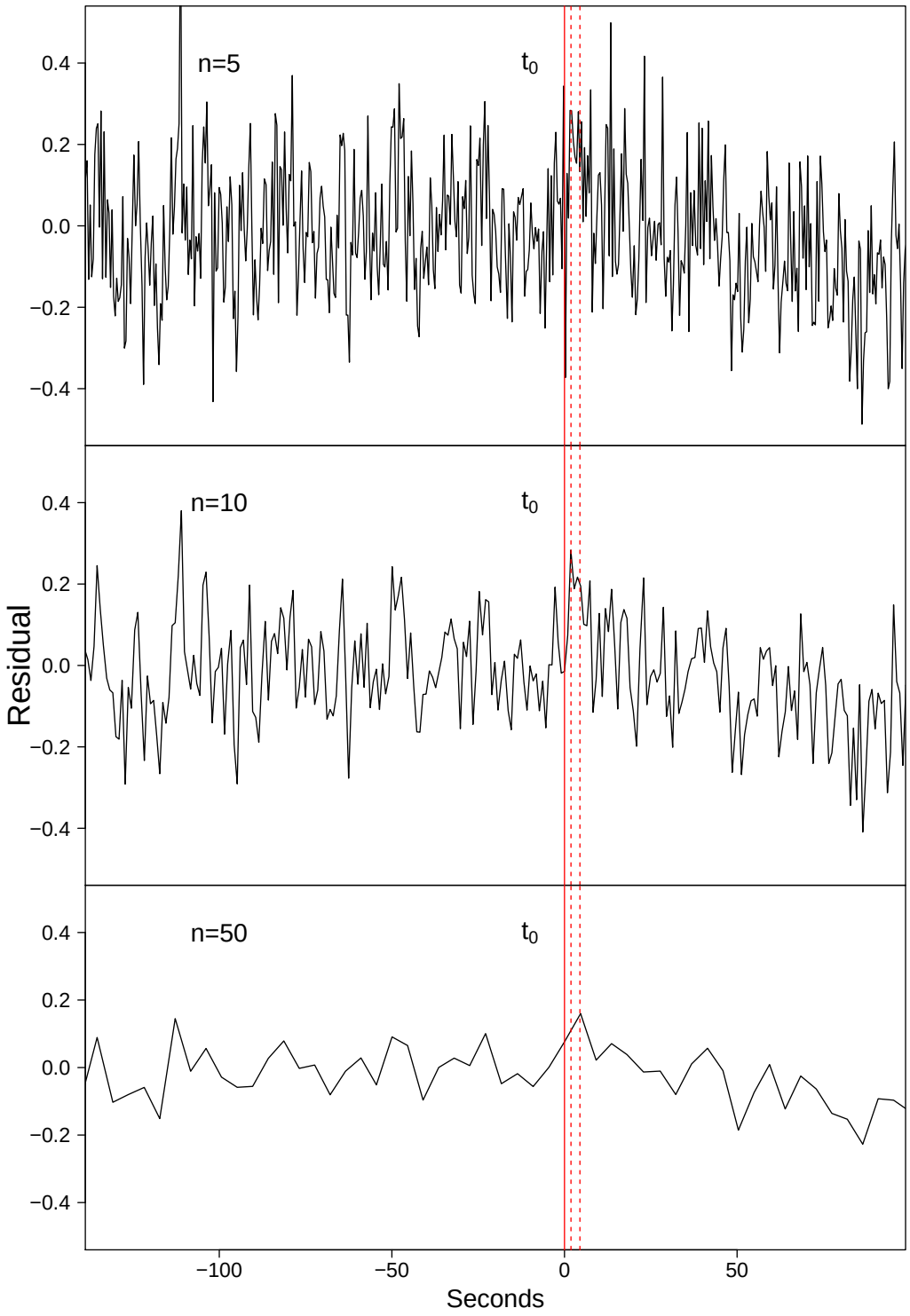

Figure 8.53: These are timing residual plots surrounding t_0 (solid red line) similar to the top panel in Figure 8.52 on page 208. However in this case residuals have been grouped together and averaged (or binned). The number of residuals in each group is denoted by n. The dotted red lines mark t_1 and t_2.

ponent $W_d \frac{de(t)}{dt}$ corrects for future errors. Each of these have a weighting W_p, W_i, and W_d applied respectively. In the case of pulsar timing residuals the *integral* component can be used to detect past cumulative changes in the timing residuals.

Just as displacement is the integral of velocity, *absement* is the name of the integral of displacement. Similarly *absity* is the integral of absement. Absement is based on the combination of the Latin prefix "ab" meaning "off" or "away" (Barnhart 1999) and the last half of the word *displacement*. For this work we have used, for simplicity, *abdual** to mean the integral of timing residual. The *integral* of abdual is also potentially interesting, in that it shows changes in abdual, but we will not name this, but simply refer to it as $\int$abdual. Hence by looking at changes in all three: timing residuals, abdual, and $\int$abdual, we can highlight some interesting features.

In Figure 8.52 on page 208 the null is marked with t_0, the beginning of a significant change in abdual is marked with t_1 and it ends at t_2. Points t_3-t_5 are other potentially interesting points, however t_3 could actually be the beginning of the proper increase in rotational frequency.

Figure 8.54 on page 211 shows a zoomed-in version of Figure 8.52 on page 208, and t_0 (marking the null) is the solid blue line followed by t_1 which begins a 2.6 s sharp and steady increase in the timing residuals that ends at t_2. The point t_2 corresponds to the end of the shift in mean and variance discussed earlier. Note that t_1 corresponds to the minimum of $\int$abdual.

Figure 8.55 on page 212 on shows a zoomed-in versions of Figure 8.52 on page 208 focusing on the areas of t_3-t_5. The abdual plot shows a sharp change at t_3 that ends at t_4, and remains quiescent until t_5 and then another change commences. By looking at $\int$abdual, t_5 appears to be the start of glitch proper and the beginning of the expected cubic.

Table 8.4: Barycentre arrival times of t_0-t_5 (see Figure 8.52 on page 208).

Event	MJD	Time	Δt (s)
t_0	57734.4849521	11:38:19.9	
			1.8
t_1	57734.4849738	11:38:21.7	
			2.6
t_2	57734.4850038	11:38:24.3	
			43.8
t_3	57734.48551	11:39:08.1	
			7.7
t_4	57734.48560	11:39:15.8	
			6.5
t_5	57734.485675	11:39:22.3	

In Figure 8.52 on page 208 this is reflected as a $-x^2$ graph in abdual and a $-x^3$ graph in $\int$abdual. In summary, 1.8 s after the null, there was an apparent 2.6 s slowing in

*Thanks to Tom van Baak for the suggestion.

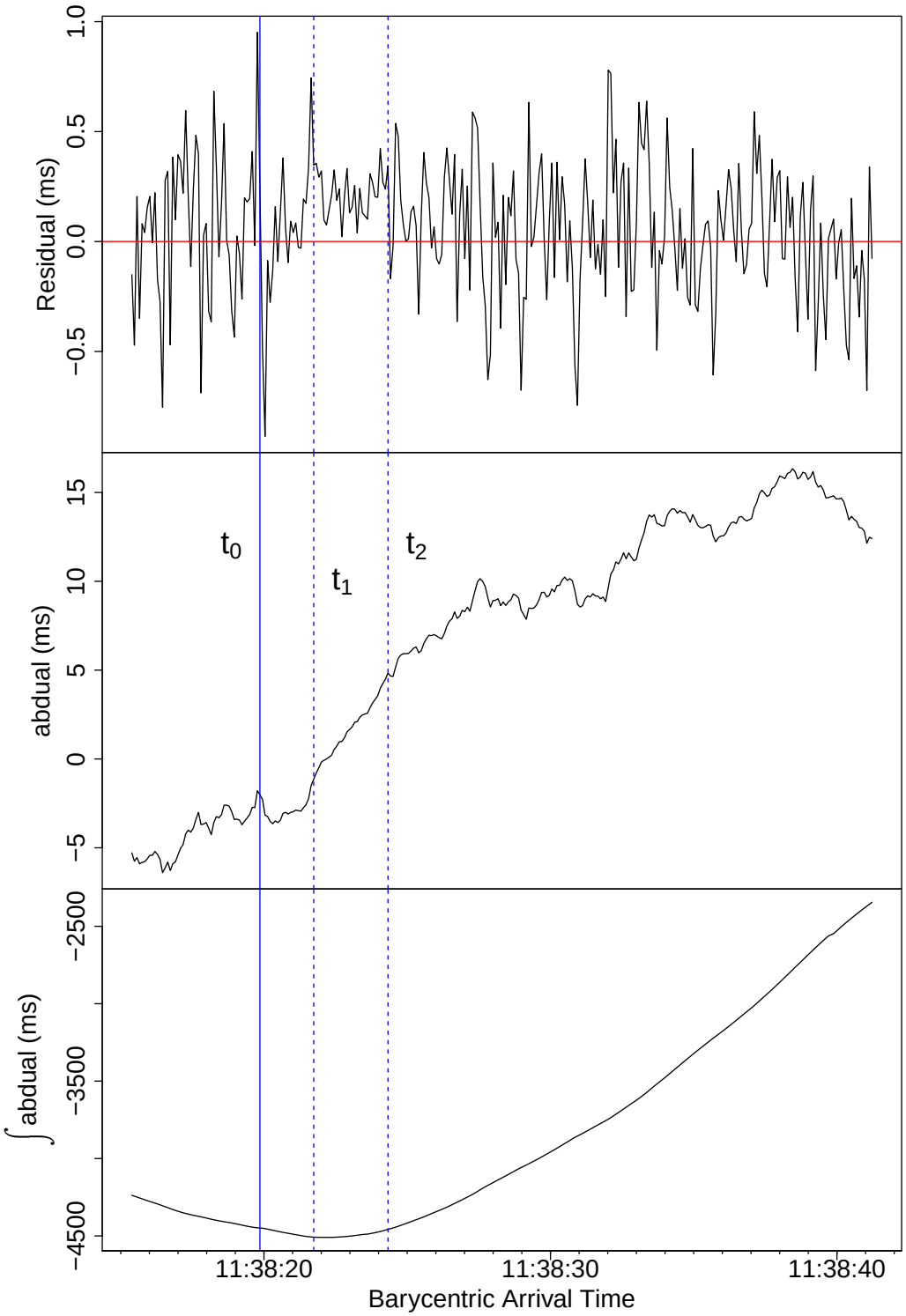

Figure 8.54: Zoomed-in to t_0 and t_1 version of Figure 8.52 on page 208. Note that t_1 corresponds with the minimum of $\int$abdual.

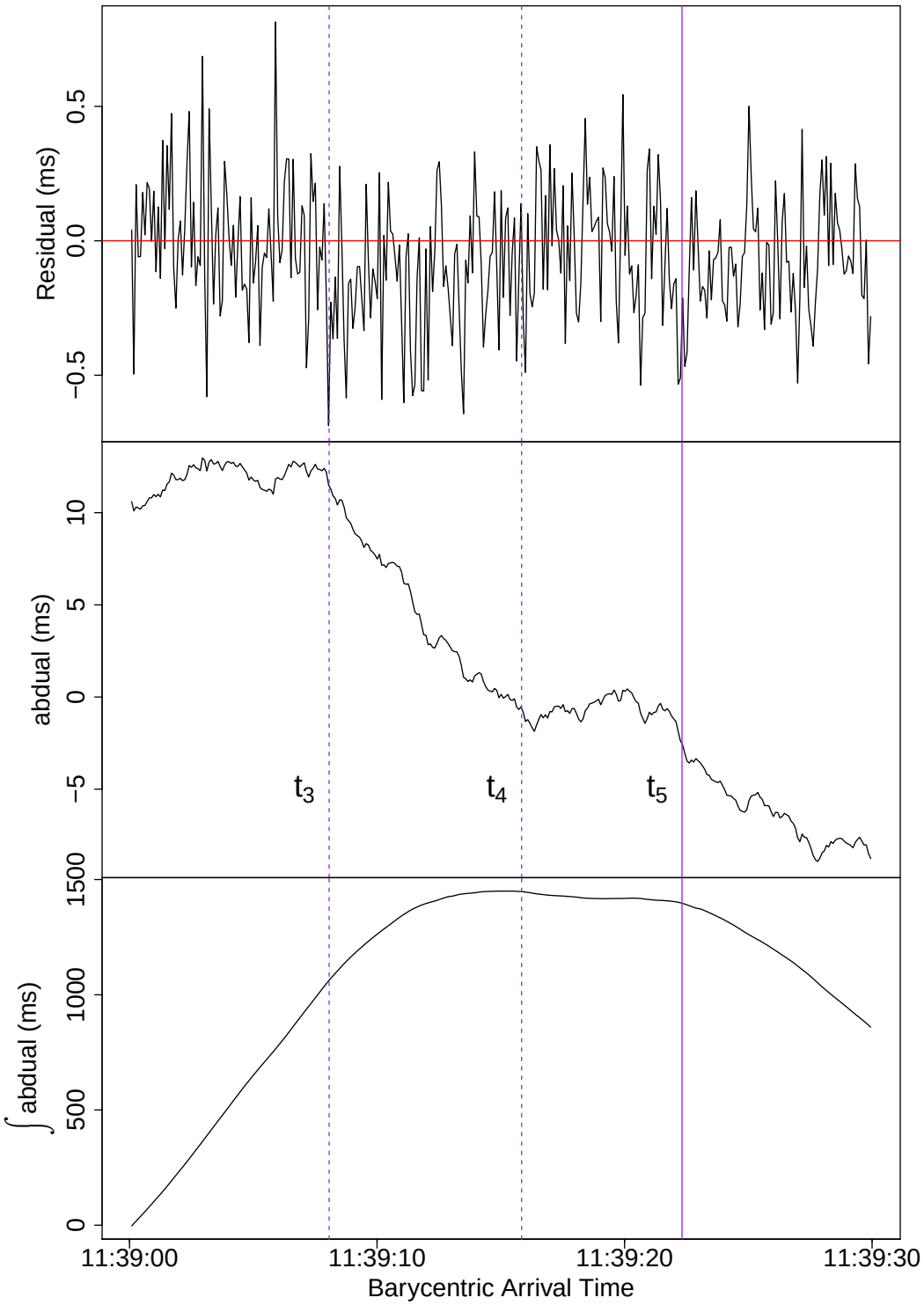

Figure 8.55: Zoomed-in to t_2-t_4 version of Figure 8.52 on page 208.

rotational frequency, followed by a return to normal rotation for 43.8 s, after which the pulsar then sped up for 7.7 s, then returned to normal for 6.5 s, then permanently sped up.

Events t_0, t_1, and t_2 appear significant (as shown earlier), but the events at t_3, t_4, and t_5 are smaller and some or all could just be typical timing noise rather than any intrinsic action occurring in the internals of the neutron star or in the magnetosphere. To resolve this question, Figure 8.56 on page 214 shows the same plots of residuals, abdual, and $\int$abdual but applied *after* the glitch model has been fitted. As can be seen from the $\int$abdual plot, there are really only two distinct regions marked by t_1 and t_2. Events t_3-t_5 just now appear as typical timing noise.

Figure 8.57 on page 215 shows the same plot but zoomed out showing a time interval of $\approx$ 17 min. $\int$abdual can be seen to head off in a strong negative direction. This is most likely due to a non-perfect fit of the glitch model and a reminder that both $\int$abdual and (to a lesser extent) abdual are extremely sensitive to departures of the timing residuals from zero.

8.2.10 Combining flux density and rotation

Combining the results of changes in peak flux density and timing residuals on the same chart using binning that maximises visibility of changes is shown in Figure 8.58 on page 216. The plot covers 1 h and the red vertical line marks t_0. We binned the data at different sizes (n) to help highlight the changes that are occurring. The peak flux density data is binned with $n = 200 \approx 17.9$ s, and the timing residuals have been binned at $n = 500 \approx 44.6$ s.

The binning hides the changes in timing residual discussed earlier, and at the wider level there appears to be no obvious correlation.

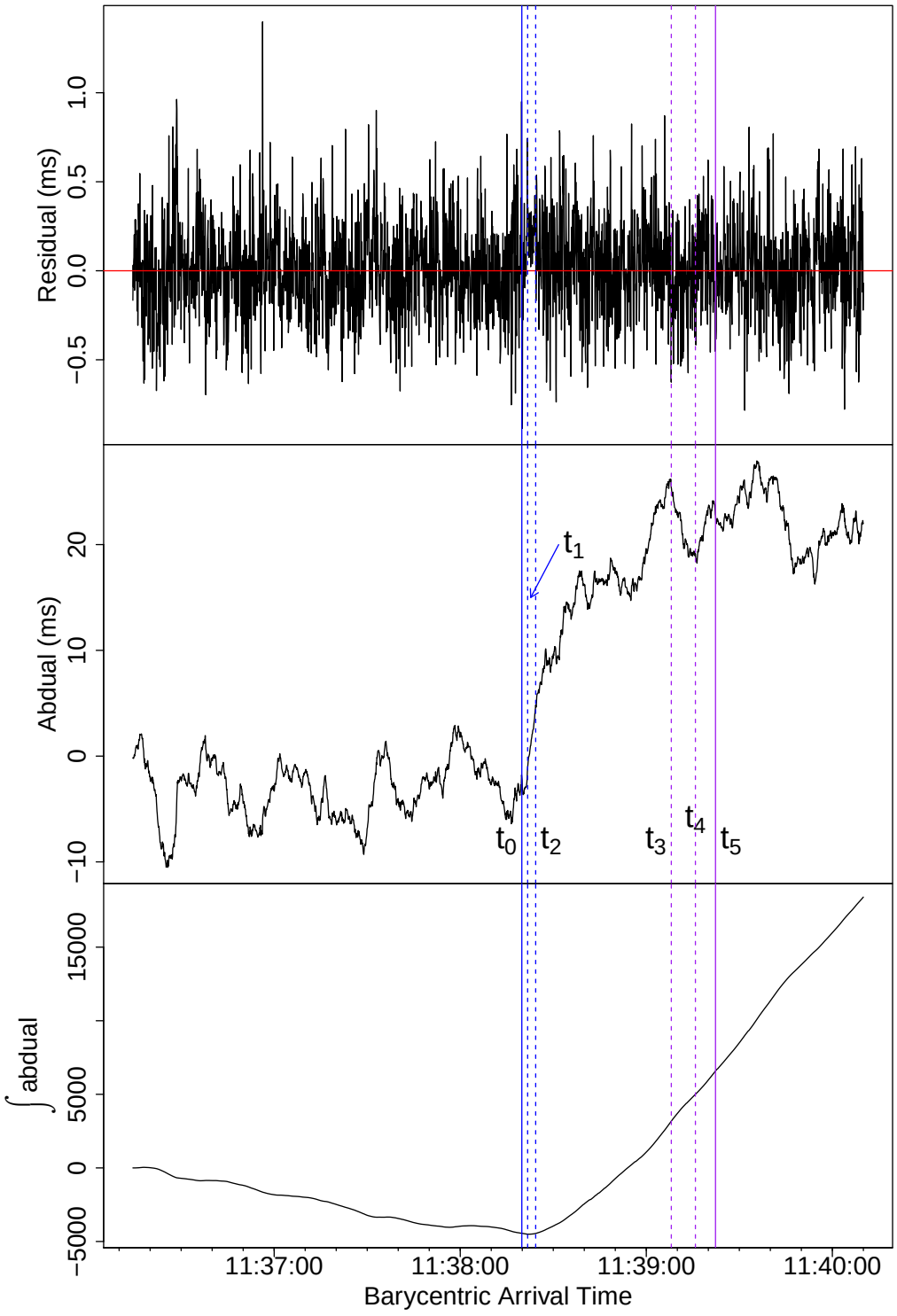

Figure 8.56: These are 216 s (2.5×10^{-3} day) plots surrounding t_0 (solid blue line) but after glitch modelling is applied. The top panel is timing residuals (in ms) and the middle panel is the cumulative sum of the timing residuals (abdual), and the bottom panel is the cumulative sum of the cumulative sum of the timing residuals ($\int$abdual). Note that the features marked by t_1 and t_2 have remained whilst t_3-t_5 appear to be just typical timing noise.

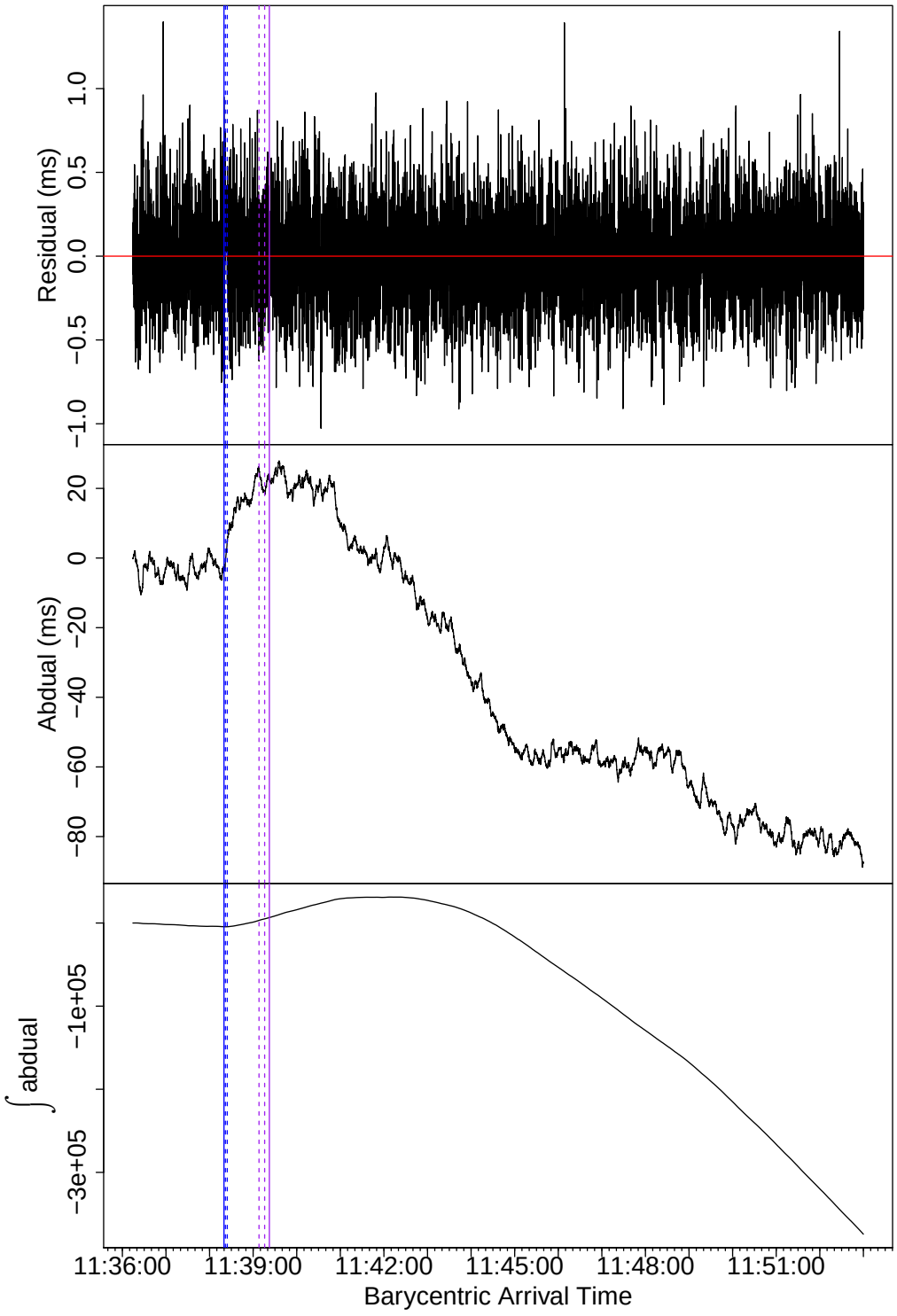

Figure 8.57: These are a zoomed-out version of Figure 8.56 on page 214 showing $\approx$ 17 min surrounding the null at t_0 (solid blue line). Glitch modelling has been applied. The top panel is timing residuals (in ms). The middle panel is abdual, and the bottom panel is $\int$abdual. This shows a wider view of the post-glitch events and the fact that abdual and $\int$abdual both head in a strong negative direction. This is most likely imperfect modelling of the glitch.

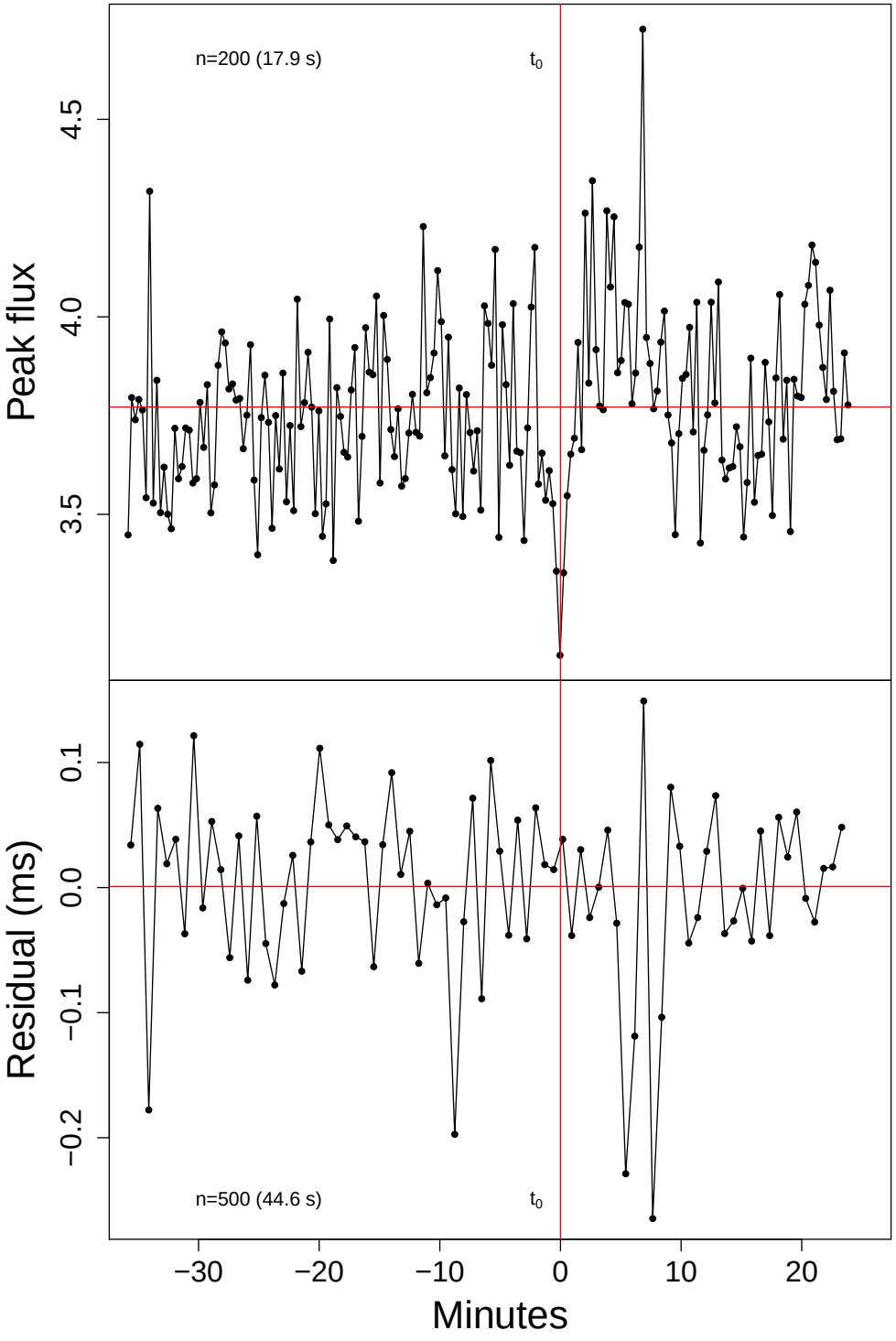

Figure 8.58: Changes in timing residual (after glitch fitting) and peak flux density over 1 h with the red line marking t_0. To highlight changes, the peak flux density data has been binned with $n = 200 \approx 17.9$ s and the timing residual data has been binned at $n = 500 \approx 44.6$ s.

8.3 Ceduna results

The Ceduna 30 m radio telescope was also observing at the time of glitch, but with some incredible bad luck a previously undetected cable fault developed ≈ 11 min prior to the glitch.

The fault was in the *twister* where cables are constantly subject to rotating stress. At least one of the cables had Type N connectors that had become partially unscrewed as the dish rotated through azimuth. Figure 8.59 on page 218 shows the cables that suffered this fault. Figure 8.60 on page 219 shows the time-of-arrival (TOA) error in μs of each of integrated pulses from the 10 s files. As can be seen the fault suddenly appeared and then slowly repaired itself.

Examination of the Ceduna data showed that the single-pulse information collected at the time of the glitch had a low signal-to-noise ratio and so individual pulses were mostly not possible to see. However the program `pat` was still able to extract arrival times for many individual pulses near the glitch. As with the Mount Pleasant data, the pulse at t_0 was also missing and fortunately the previous pulse was able to be timed. This enabled a reasonably accurate estimate of t_0 at Ceduna to be calculated. These results are shown in Table 8.3 on page 194.

Timing residuals averaged over each 10 s file were possible however and are shown in Figure 8.61 on page 220. Using these residuals, the glitch modelling feature of TEMPO2 gave the glitch times shown in Table 8.1 on page 156. The figures for $\frac{\Delta\dot{\nu}}{\dot{\nu}}$ at Ceduna were not reliable and have been omitted.

Figures 8.62 to 8.68 on pages 221–227 respectively, show 112 pulses over a period of 10 s extracted from file `2016-12-12-11:35:57.ar`. The flux density reference 0.0 on the graph (and marked with a horizontal red line) has been calculated as the mean of the off-pulse data for each pulse. The vertical dotted red line marks a timing residual of 0. The null (t_0) is "pulse" 32 in Figure 8.66 on page 225, and the sequence of 30 pulses with increased μ and decreased σ is marked on the plots as "$\mu^+\sigma^-$".

Figure 8.59: The cables and Type N connecters that partially unscrewed and caused the fault at Ceduna that prevented ideal observation of the glitch. *Photo courtesy of Bev Bedson.*

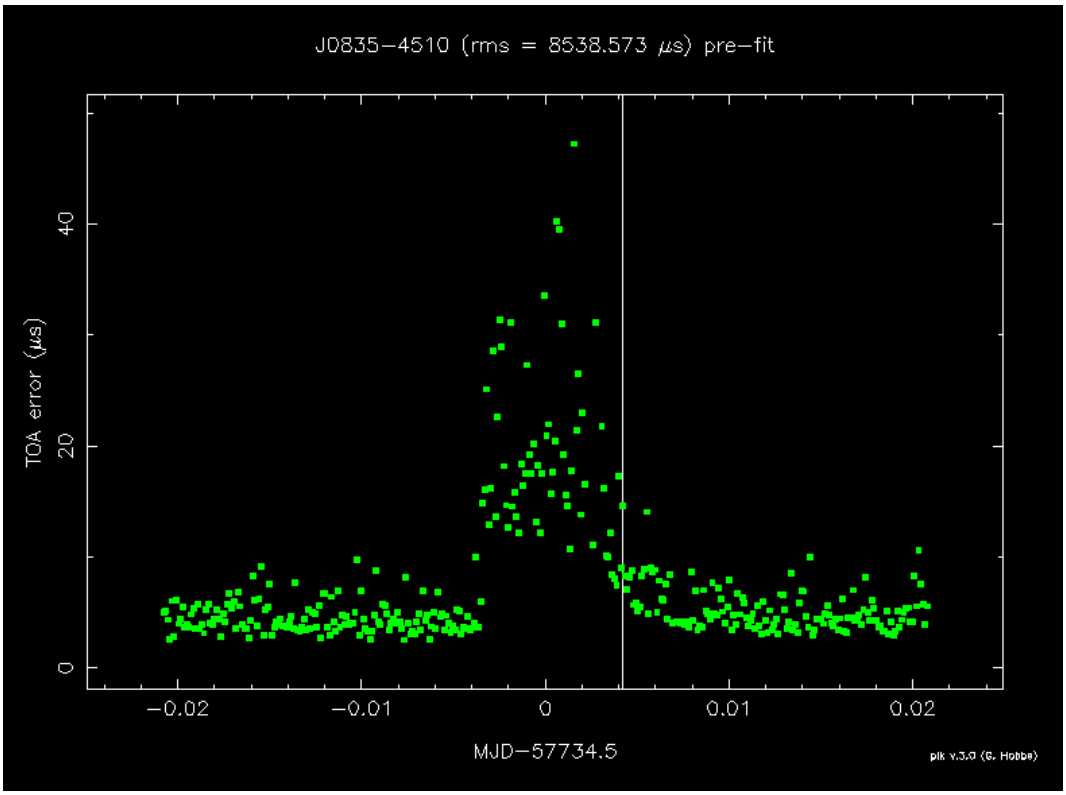

Figure 8.60: Plot of Ceduna time-of-arrival error (μs) for each 10 s file. The vertical white line marks the time of the glitch. As can be seen a fault suddenly developed prior to the glitch, but then slowly fixed itself. Note that 0.01 day=14.4 min and so each tick mark is $\approx$ 173 s $\approx$ 2.9 min.

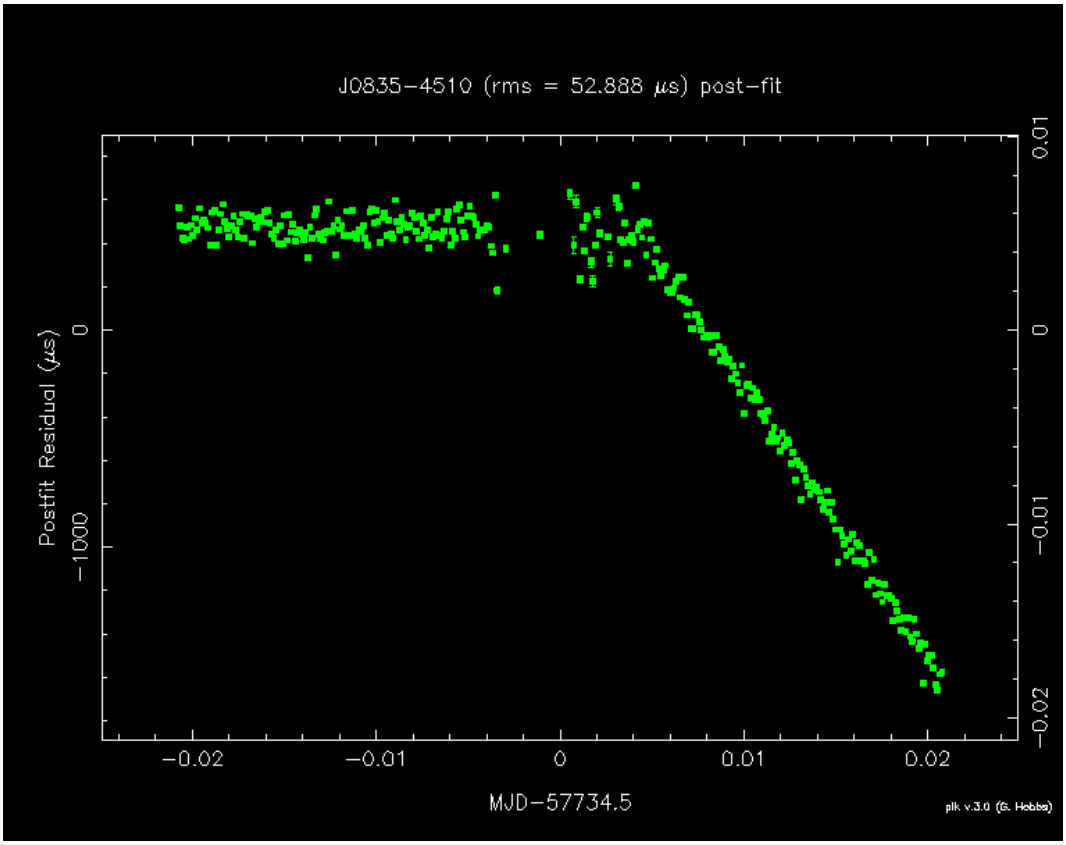

Figure 8.61: Plot of Ceduna 10 s timing residuals versus time as the glitch occurred. Note that the failure caused some data just prior to the glitch to be completely lost. Note that 0.01 day=14.4 min and so each tick $\approx$ 173 s $\approx$ 2.9 min.

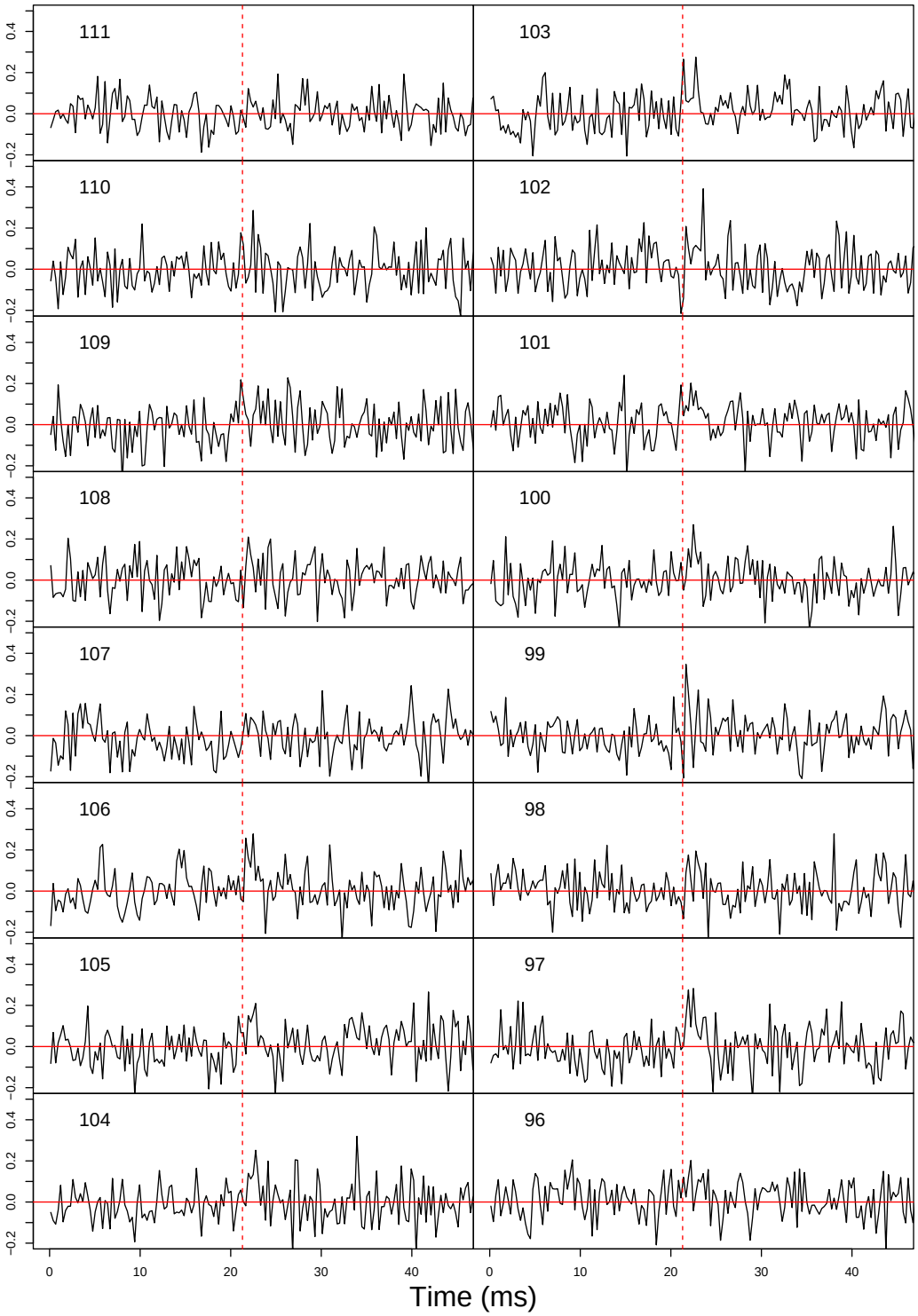

Figure 8.62: Ceduna file 2016-12-12-11:35:57.ar, pulses 111-96, binned with $n = 25$. The X-axis is time in ms and the Y-axis is flux density in arbitrary units with all axis having the same scale. The solid red line marks a flux density of 0 and the dotted line marks the location of the peak of the full day's integrated pulse. Note that the full pulse period is not shown.

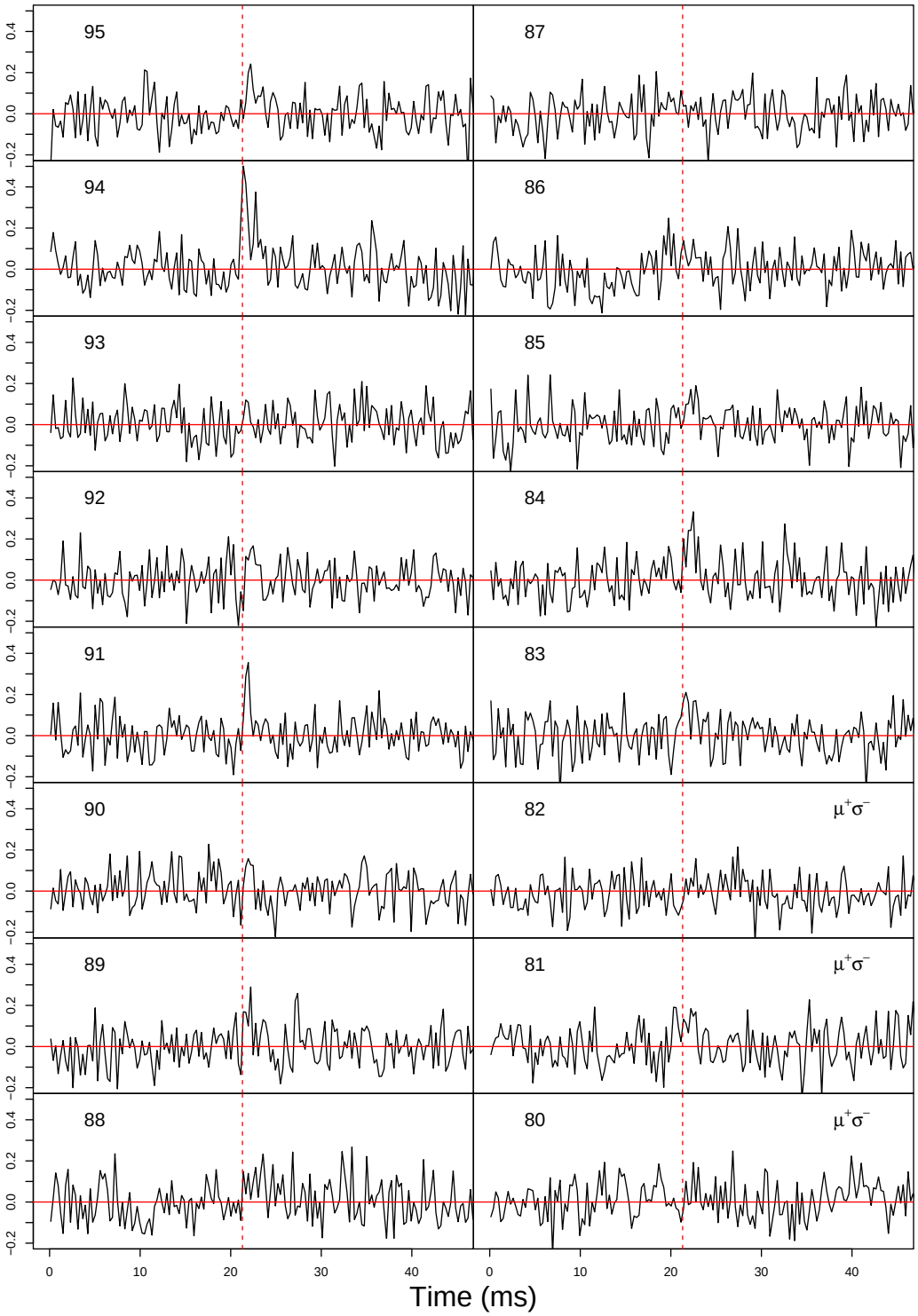

Figure 8.63: Ceduna file 2016-12-12-11:35:57.ar, pulses 95-80, binned with $n = 25$. The X-axis is time in ms and the Y-axis is flux density in arbitrary units with all axis having the same scale. The solid red line marks a flux density of 0 and the dotted line marks the location of the peak of the full day's integrated pulse. Note that the full pulse period is not shown and $\mu^+\sigma^-$ indicates the section of increased mean and reduced variance discussed in the text.

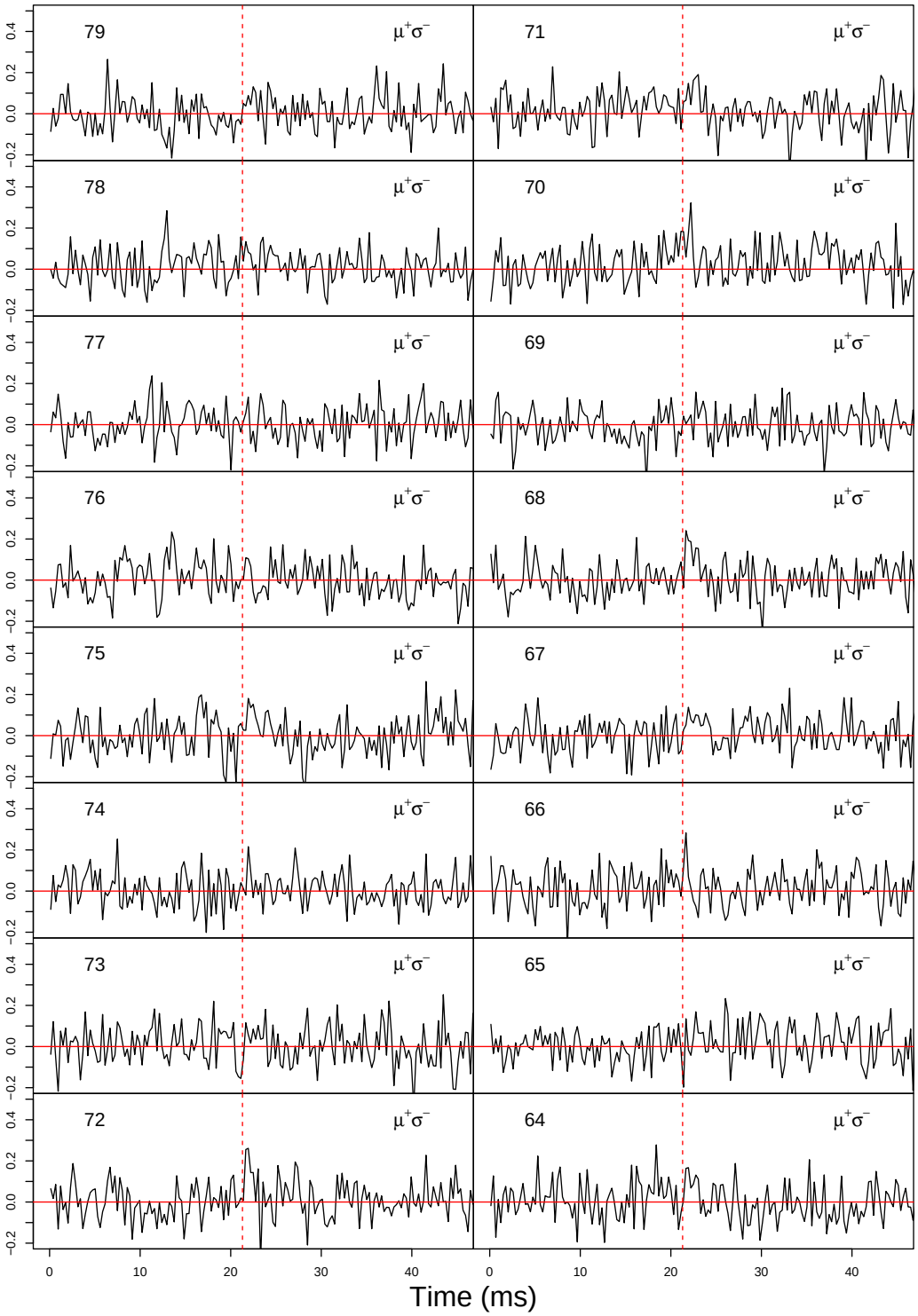

Figure 8.64: Ceduna file 2016-12-12-11:35:57.ar, pulses 79-64, binned with $n = 25$. The X-axis is time in ms and the Y-axis is flux density in arbitrary units with all axis having the same scale. The solid red line marks a flux density of 0 and the dotted line marks the location of the peak of the full day's integrated pulse. Note that the full pulse period is not shown and $\mu^+\sigma^-$ indicates the section of increased mean and reduced variance discussed in the text.

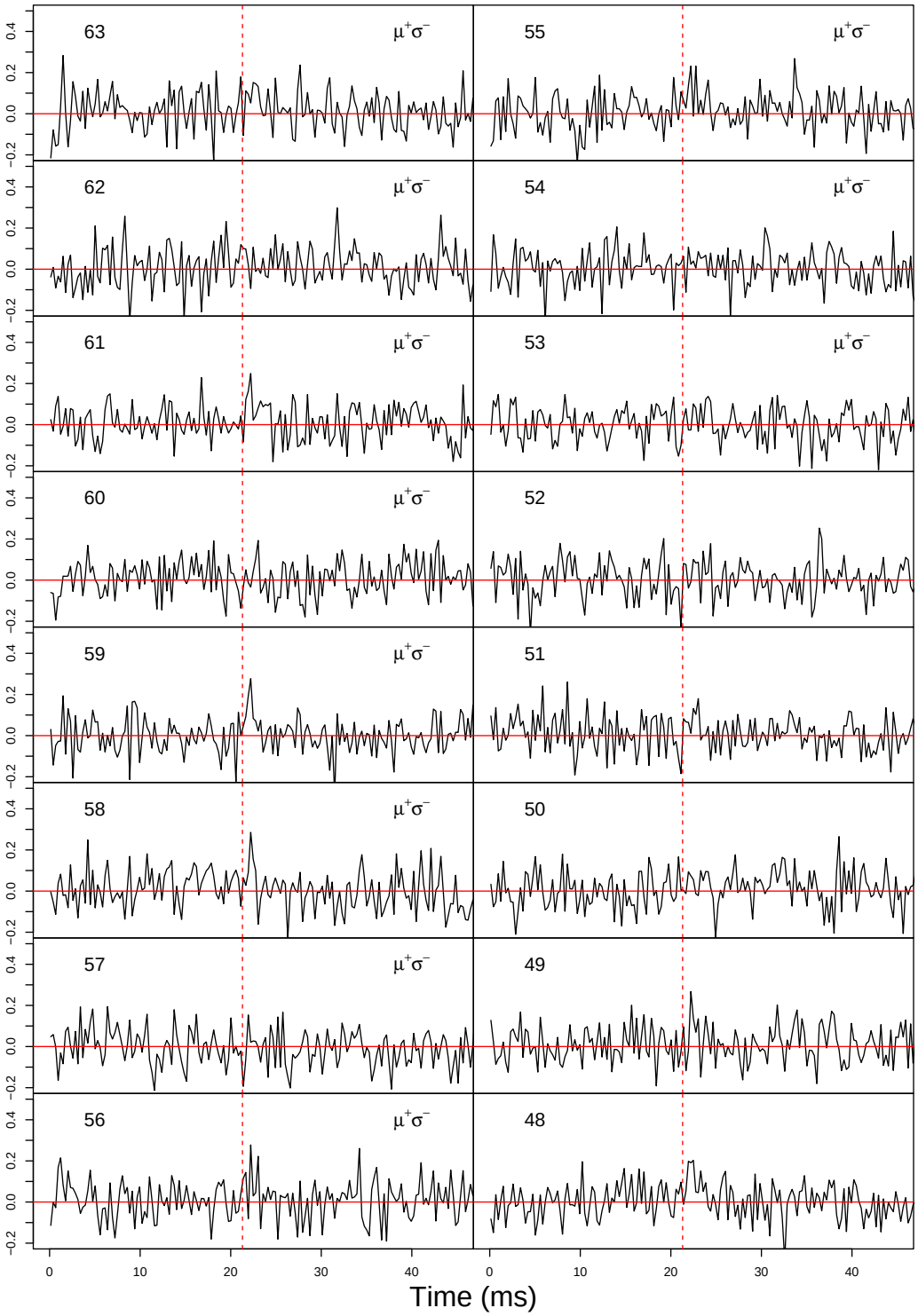

Figure 8.65: Ceduna file 2016-12-12-11:35:57.ar, pulses 63-48, binned with $n = 25$. The X-axis is time in ms and the Y-axis is flux density in arbitrary units with all axis having the same scale. The solid red line marks a flux density of 0 and the dotted line marks the location of the peak of the full day's integrated pulse. Note that the full pulse period is not shown and $\mu^+\sigma^-$ indicates the section of increased mean and reduced variance discussed in the text.

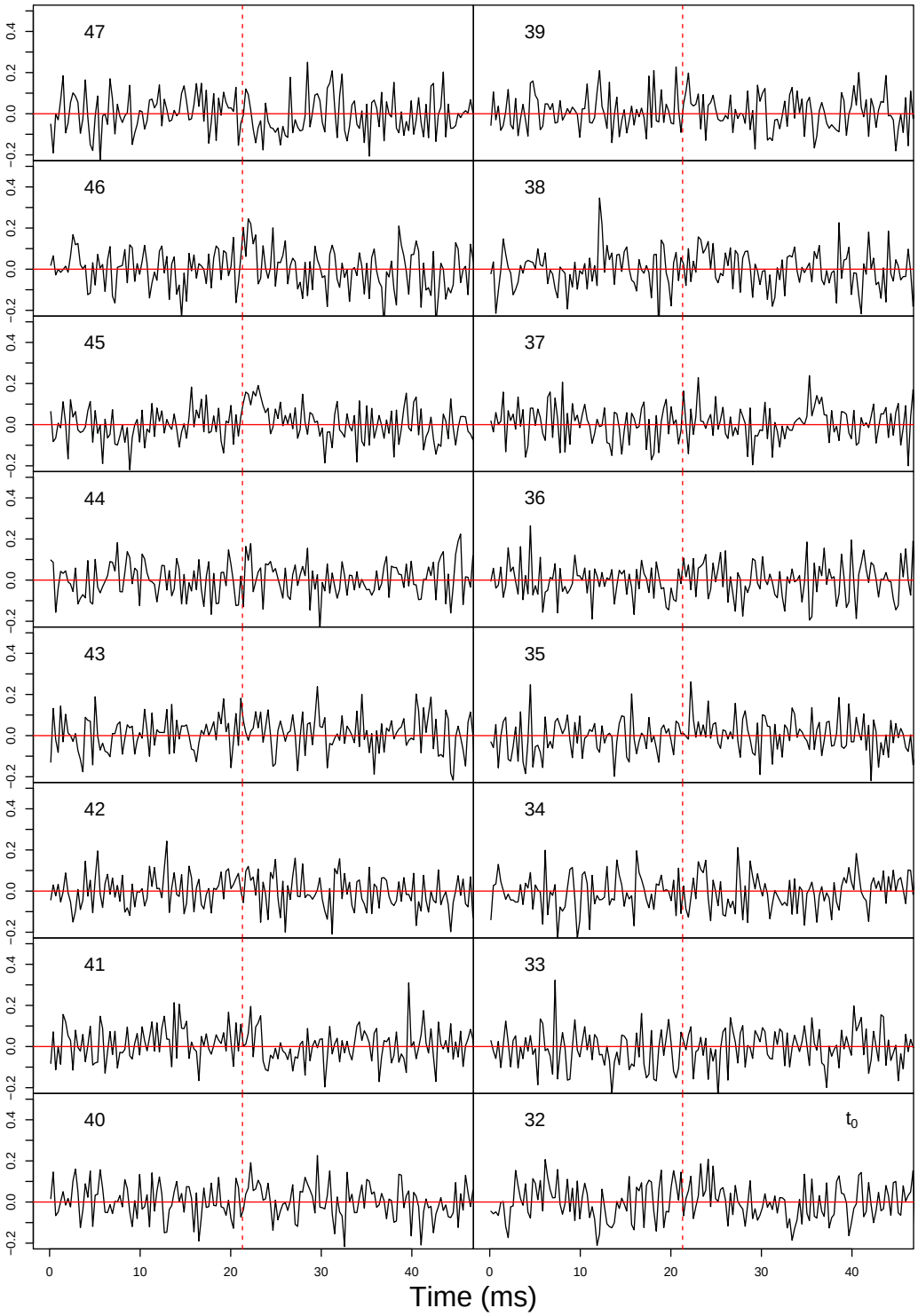

Figure 8.66: **The Glitch!** Ceduna file 2016-12-12-11:35:57.ar, pulses 47-32, binned with $n = 25$. The X-axis is time in ms and the Y-axis is flux density in arbitrary units with all axis having the same scale. The solid red line marks a flux density of 0 and the dotted line marks the location of the peak of the full day's integrated pulse. Note that the full pulse period is not shown and that t_0 at pulse 32 shows the glitch.

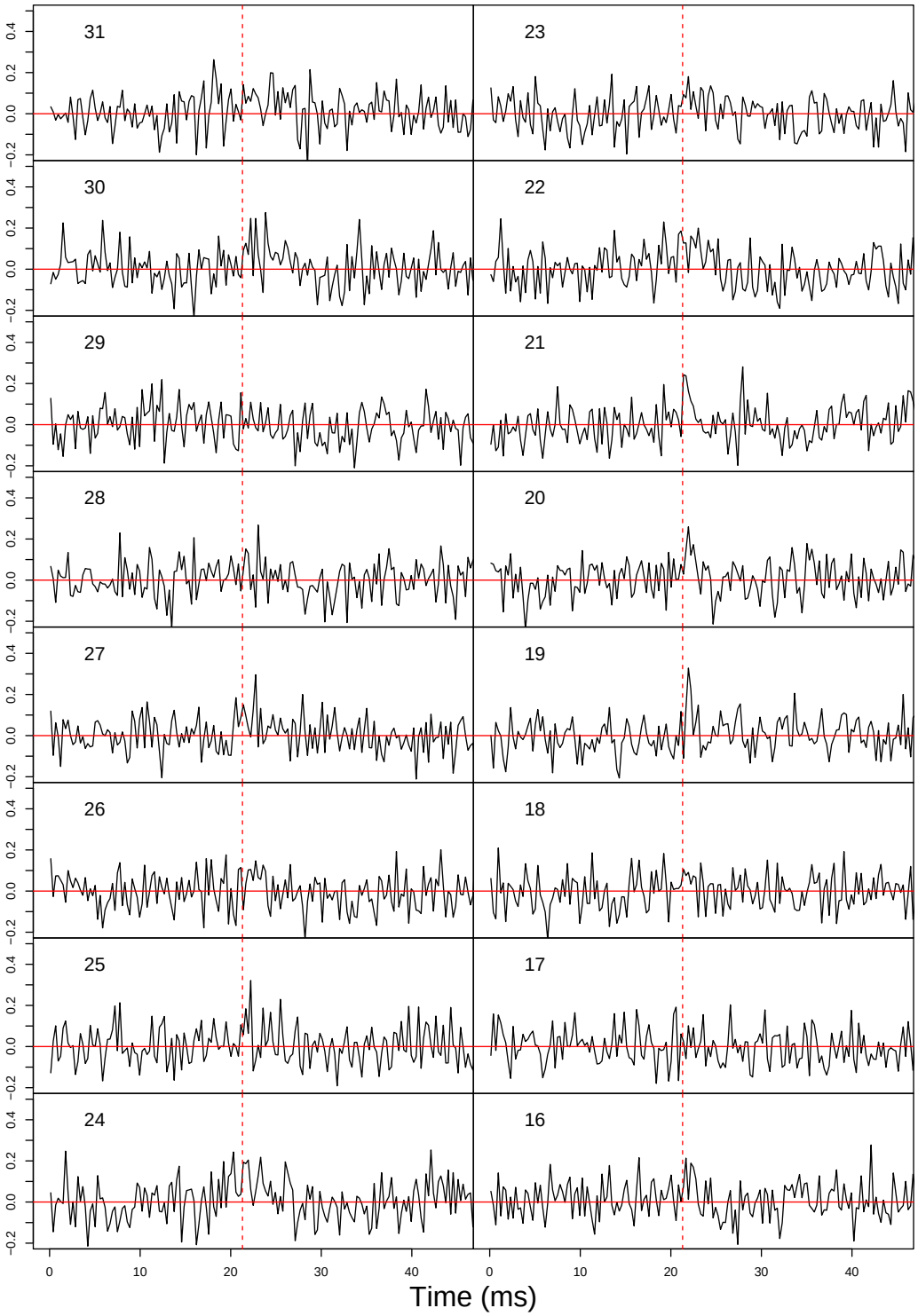

Figure 8.67: Ceduna file 2016-12-12-11:35:57.ar, pulses 31-16, binned with $n = 25$. The X-axis is time in ms and the Y-axis is flux density in arbitrary units with all axis having the same scale. The solid red line marks a flux density of 0 and the dotted line marks the location of the peak of the full day's integrated pulse. Note that the full pulse period is not shown.

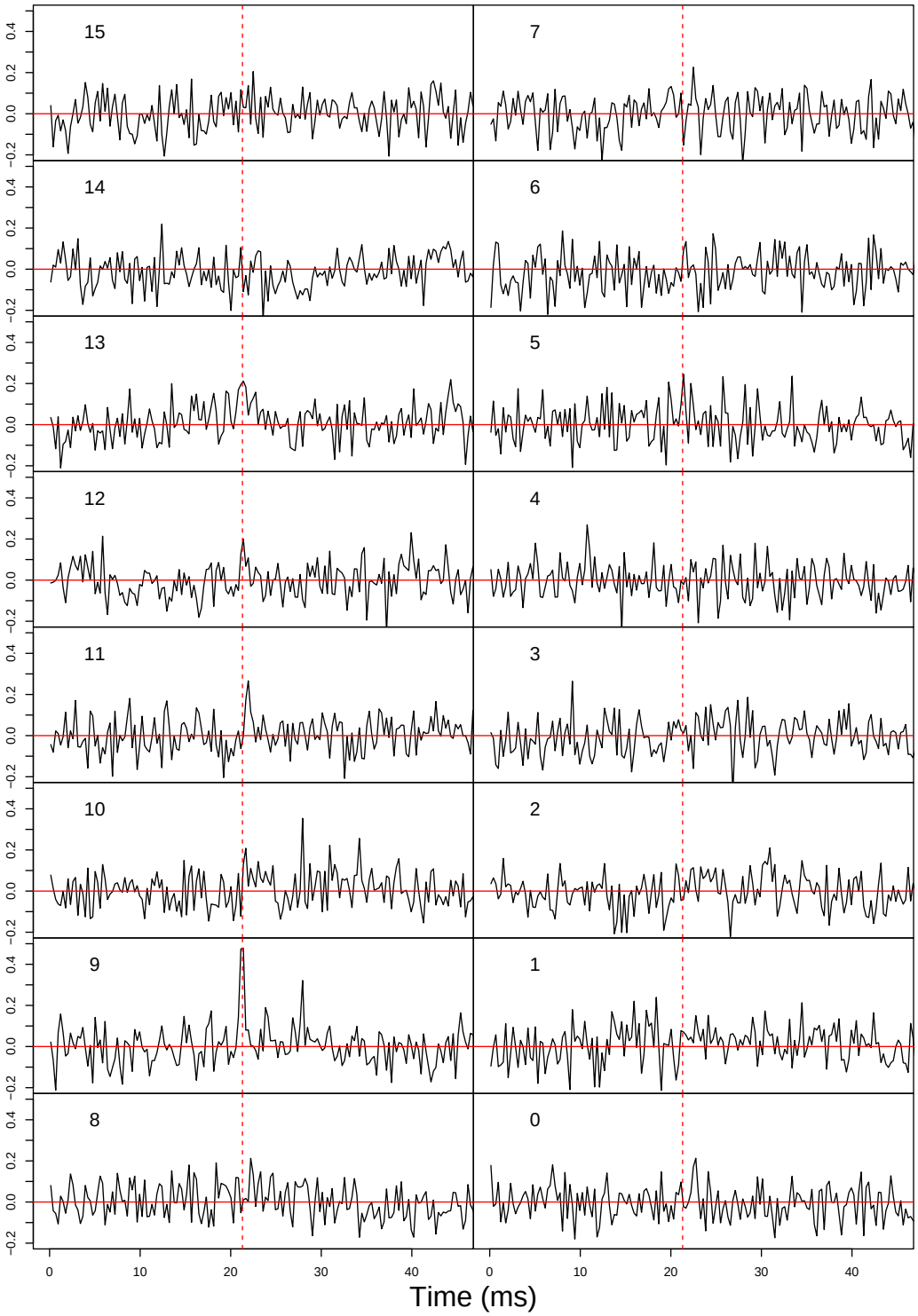

Figure 8.68: Ceduna file 2016-12-12-11:35:57.ar, pulses 15-0, binned with $n = 25$. The X-axis is time in ms and the Y-axis is flux density in arbitrary units with all axis having the same scale. The solid red line marks a flux density of 0 and the dotted line marks the location of the peak of the full day's integrated pulse. Note that the full pulse period is not shown.

8.4 Discussion

The key results presented here are that the glitch affected the magnetosphere of the pulsar. In particular, a broad pulse, followed by a null occurred. Also, the variance of the timing residuals were reduced and the arrival times were late for 2.6 s. Peak flux density also dropped for a few minutes surrounding the glitch.

The apparent change of timing residuals could be the direct result of interactions between the superfluid core and crust. However, the observed null and reduced variance in timing residuals soon after, raises the possibility that these are manifestations of changes in the magnetosphere's configuration instead.

For the moment we shall discount this second hypothesis, ignore the magnetosphere, and assume all the timing irregularities are from the interface of the core and the crust of the neutron star.

The 30 pulses between t_1 and t_2 with an *increase* in the timing residual imply a *later* pulse arrival, and hence a rotational frequency *slow-down*. Recall the spin-up time $\tau_{\rm r}$ is hypothesised to be under ≈ 6 s depending on the equation-of-state (Sourie et al. 2017). If the null (t_0) is considered the commencement of the glitch process and t_2 is the completion, then this totals 4.4 s. If t_1 is considered the commencement then the duration is 2.6 s. This change in mean and variance could be the spin-up in action as the vortices go through their unpinning. How this is reflected as a brief slow-down of the crust is unclear.

An interpretation of the observed null is that as the core transferred momentum to the crust, the magnetic field was disrupted. Perhaps the magnetic pole was temporarily pointing in a slightly different direction and so the pulse missed the Earth, or maybe the field lines were not as aligned with each other as normal and hence the normally strongly coherent radiation was dissipated somewhat.

A few of the above points are unsatisfactory. The reduced variance in timing residuals and the slowing down of the pulsar do not fit the current glitch models.

The second hypothesis mentioned above is that the magnetosphere's configuration was changed for a number of seconds. Later arrival times and reduced variance would be nicely explained if an emission zone earlier in the pulsar's phase simply did not emit (or had reduced emission) for 2.6 s. As has been noted previously, the bright pulse emission *always* leads the main pulse, and this could have been the zone affected. The null and the broad pulse prior would all fit into this scenario.

This does raise a bigger question in that how does the glitch cause this change in the magnetosphere's configuration?

As mentioned in Section 2.2.1 on page 9, intermittent or switching pulsars have the interesting property of nulling for many days (Kramer et al. 2006), and the reduction in rotation rate is slower during those times. This connection between rotation rate and magnetospheric changes is similar to what's being observed here, just with different timescales.

Another possibility (as mentioned in Section 2.7 on page 29), Sedrakian and Cordes (1999) suggest that under their model, a glitch would cause a change in the geometry and the angle of the dipole magnetic field.

Weltevrede et al. (2011) discuss J1119−6127 and show that glitches precede the commencement of the pulsar's intermittency. This also implies that glitches have an effect on the magnetosphere.

8.4.1 Solidifying superfluid?

A final speculation* that requires deeper theoretical consideration, is mentioned here for the record. Near the time of the glitch the superfluid could be "solidifying" at the boundary. This could affect the moment of inertia of the core, the vortices, and where they are pinned. This idea does not seem to be mentioned in the literature, but the idea that the boundary between the superfluid core and hard crust could change and either cause, or be a result of, the glitch is worthy of further investigation.

8.4.2 Ruling out a possible cause for FRBs

Zhang (2017) discusses the possibility of external magnetic fields (for example from supermassive black holes) briefly breaking the magnetic field lines of neutron stars and hence releasing vast amounts of energy as a Fast Radio Burst. Whilst this looks like a promising direction for the explanation of FRBs, it does mean that the glitch event does not disrupt the magnetic field in a way that produces massive ultra giant pulses, and so this rules out glitches in young neutron stars as an FRB trigger.

8.5 Glitch vs micro-glitch

The difference between glitches and micro-glitches is a little unclear in the literature. Cordes et al. (1988) drew a "line-in-the-sand" and stated that changes in rotation

*suggested by Ogilvie High School Grade 10 student Scarlett Marston during a presentation at her school by the author.

frequency that had $\frac{\Delta\nu}{\nu} \geq 1000 \times 10^{-9}$ were *glitches* and ones that had $\frac{\Delta\nu}{\nu} < 1000 \times 10^{-9}$ were *micro-glitches*.*

In 1994 (MJD=49559) a glitch of magnitude $\frac{\Delta\nu}{\nu} = 835 \times 10^{-9}$ occurred in Vela, and 32 days later (MJD=49591) it was followed by a glitch of magnitude $\frac{\Delta\nu}{\nu} = 199 \times 10^{-9}$. These can be seen in Figure 8.70 on page 234. The plot of $\dot{\nu}$ is shown in Figure 8.71 on page 234 with a zoomed-in version shown in Figure 8.72 on page 235. Given that glitches with magnitudes $\frac{\Delta\nu}{\nu} < 1000 \times 10^{-9}$ are technically classified as micro-glitches the 1994 events are intriguing. Technically both were micro-glitches, but the graph of $\dot{\nu}$ over time (Figure 8.72 on page 235) shows an interesting result.

The first glitch (magnitude $\frac{\Delta\nu}{\nu} = 835 \times 10^{-9}$) shows a sudden drop in $\dot{\nu}$ which is sustained over time. The second glitch (magnitude $\frac{\Delta\nu}{\nu} = 199 \times 10^{-9}$) also shows a sudden drop in $\dot{\nu}$ but reverts to previous $\dot{\nu}$ levels within ≈ 30 days. The first glitch did not recover to equivalent levels until ≈ 500 days. Interestingly, even though the first glitch had a magnitude ≈ 4 times greater than the second, the recovery time of $\dot{\nu}$ was ≈ 17 times greater.

Our results clearly show that glitches are different events from micro-glitches. In our data, all change in rotational frequency events that have had $0 < \frac{\Delta\nu}{\nu} \ll 100 \times 10^{-9}$ are substantially different from the single event that we observed that had $\frac{\Delta\nu}{\nu} = 1431 \times 10^{-9}$ in the sense that micro-glitches always occurred when the pulse width was a minimum, whereas the glitch occurred near a pulse width maximum. Also, some micro-glitches had $-100 \times 10^{-9} \ll \frac{\Delta\nu}{\nu} < 0$, that is some excursions were a *decrease* in rotational frequency. These did not line up with pulse width minima however.

This means that selecting an arbitrary number for $\frac{\Delta\nu}{\nu}$ like 100×10^{-9} or 1000×10^{-9} is most likely a non-ideal approach but, as shown previously, micro-glitches being related to pulse width is most likely a better indicator. This is a difficult criteria however, because measuring changes in pulse width requires a lot of dedicated telescope time.

We consider that Vela "glitches" that have appeared in the ATNF (Manchester et al. 2005) and Jodrell Bank (Espinoza et al. 2011) glitch catalogues with magnitudes as absurdly low as 0.39×10^{-9} as wrongly categorised.

So for ease of categorisation, we propose a new glitch cutoff so that if $\frac{\Delta\nu}{\nu} \geq 100 \times 10^{-9}$ then the event can be called a "glitch". Anything less can be classified as a "micro-glitch".

So we present Table 8.5 on page 231 which shows a list of all glitches of the Vela pulsar that meet this new criteria, that is, all micro-glitches have been removed.

*The wording from the original paper has been updated here from *jumps* to *glitches* for more current usage.

Table 8.5: Glitches of the Vela pulsar. Numbers 1-17 extracted from the ATNF pulsar catalogue (Manchester et al. 2005) (and referenced within) but with *micro-glitches removed*, and number 18 being a result from this work.

Glitch	Year_DOY	MJD	$\Delta\nu/\nu$ $\times 10^{-9}$	$\Delta\dot{\nu}/\dot{\nu}$ $\times 10^{-3}$	Days since previous	Days to next	Cumulative $\Delta\nu/\nu$
1	1969_059	40280	2340	10		912	2340
2	1971_241	41192	2050	15	912	1491	4390
3	1975_271	42683	1990	11	1491	1010	6380
4	1978_185	43693	3060	18	1010	1195	9440
5	1981_284	44888	1145	49	1195	304	10585
6	1982_223	45192	2050	23	304	1065	12635
7	1985_192	46257	1601	17	1065	1263	14236
8	1988_359	47519	1805	77	1263	938	16041
9	1991_201	48457	2715	600	938	1102	18756
10	1994_207	49559	835	<5	1102	32	19591
11	1994_239	49591	199	120	32	778	19790
12	1996_287	50369	2110	5.950	778	1190	21900
13	2000_016	51559	3085	6.736	1190	1634	24985
14	2004_189	53193	2100		1634	767	27085
15	2006_225	53960	2620	230	767	1449	29705
16	2010_212	55408	1940	75	1449	1147	31645
17	2013_263	56555	3100	148	1147	1179	34745
18	**2016_347**	**57734**	**1431**	**9**	**1179**		**36211**

The different processes involved for glitches, speeding-up micro-glitches, and slowing-down micro-glitches need to be considered. One possibility is that micro-glitches are changes in the line-of-sight to the emission mechanism in the magnetosphere (see Figure 5.22 on page 98) and glitches are physical changes in the neutron star rotation rate. The idea that micro-glitches are small starquakes is still a possibility, although the fact that decreases in $\frac{\Delta\nu}{\nu}$ (i.e. a slowing down) can occur seems to rule that out.

8.6 Bright pulse rates

In Palfreyman et al. (2011) it was noted that bright pulse rates appeared to increase substantially after a glitch. However, this was based on a series of observations that were not contiguous. With this study we have been able to check this hypothesis.

The glitch of 2016 did indeed occur at a peak of bright pulse activity. In fact, Vela's bright pulse activity was high at this time. However it is important to note that this activity did not commence *after*, or *at* the glitch, but well *before*.

So the glitch did not predate the bright pulse activity (and it seems unrelated to it), but it is interesting that in both this recent case, and the glitch of 2010 (MJD=55408), bright pulse activity was occurring at the time of both glitches. This could of course be a coincidence, further study is needed to confirm this.

8.7 Prediction

Accurate predictions of the Vela pulsar glitches are not available in the literature although some attempts have been made with limited accuracy (Akbal et al. 2017). We have shown that micro-glitches are predictable (see Section 7 on page 143), but unfortunately glitches appear to be a completely different type of mechanism and hence are not predictable using this method.

Here we present a method to potentially show when a glitch is approaching.

8.7.1 History

Analysis of historical data collected at the University of Tasmania (see Figures 8.69 to 8.71 on pages 233–234) shows the variation of ν and $\dot{\nu}$ over time. Figure 8.69 on page 233 shows the overall steady decline in ν and careful examination will reveal the glitches.

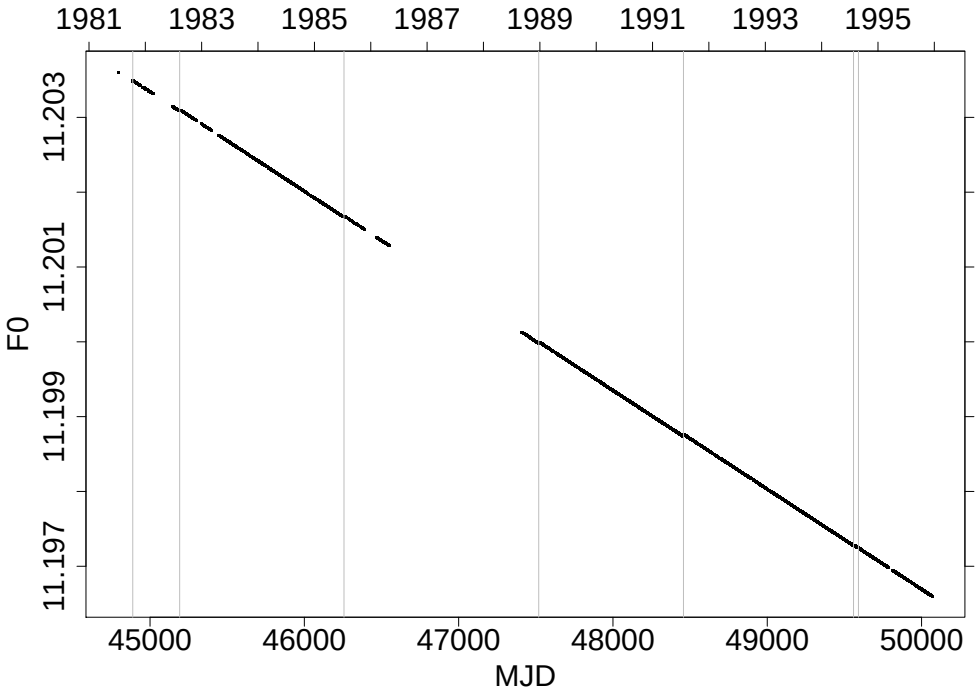

Figure 8.69: Historical data showing the change in rotation frequency (ν) over time. Glitches are marked by the vertical grey lines. For clarity, the line of best fit is not marked.

Figure 8.70 on page 234 shows the residuals of ν from the line of best fit (shown in red) and the glitches are clearly visible.

As can be seen in Figure 8.71 on page 234, the value of $\dot{\nu}$ for most glitches appears to increase to a maximum value before suddenly dropping as a glitch occurs. However with micro-glitches, visible changes in $\dot{\nu}$ are not readily apparent. Note the glitch at MJD=49559 with magnitude 835 has a marked jump in $\dot{\nu}$, whereas the glitch at MJD=49591 with magnitude 199 only shows a minor change in $\dot{\nu}$. It is worth noting that the $\frac{\Delta\dot{\nu}}{\dot{\nu}} = 120 \times 10^{-3}$ for this glitch (see Table 8.5 on page 231) is actually much larger than the previous one ($< 5 \times 10^{-3}$). These are *relative* changes in $\dot{\nu}$ whereas the plot in Figure 8.72 on page 235 is an absolute change.

In summary it would seem reasonable to classify MJD=49559 and 49591 as genuine glitches, even though their magnitudes were below 1000×10^{-9}.

Prior to the glitch of 2016, the historical data was examined and the range of values of $\dot{\nu}$ prior to each glitch are shown in Table 8.6 on page 235.

There appears to be a "maximum" $\dot{\nu}$ that is reached before a glitch occurs - although there is an apparent range. We took the approach that a "best/likely/worst" case could be adopted by using the least/median/maximum values of $\dot{\nu}$ for prediction. Figure 8.74 on page 237 shows the changes in $\dot{\nu}$ as the glitch was approaching and the glitch of

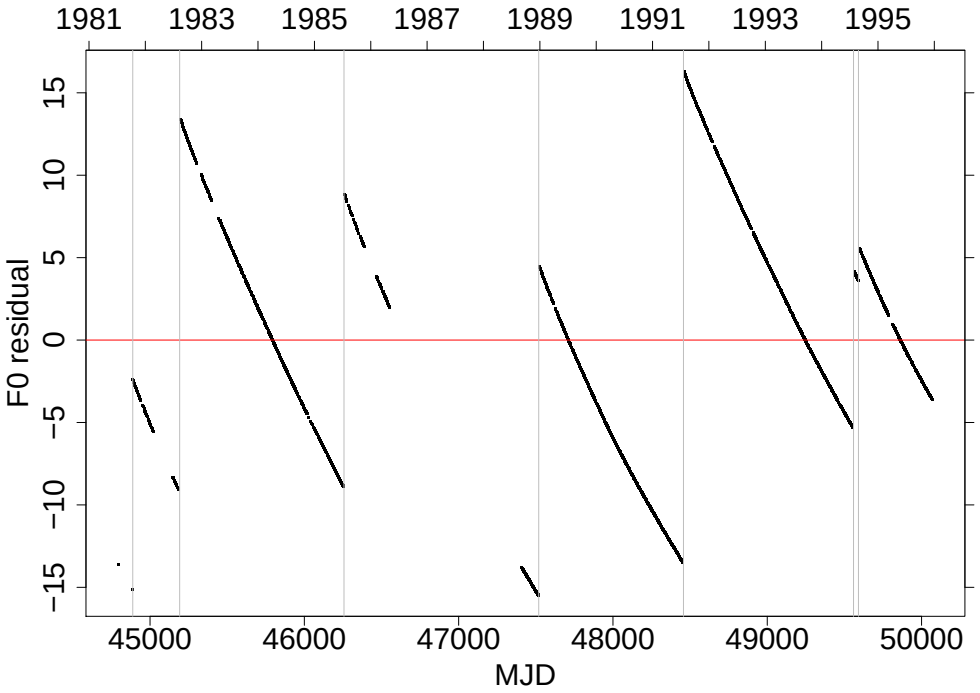

Figure 8.70: Historical data showing the residuals of frequency from the line of best fit from Figure 8.69 on page 233. The 7 glitches are clearly visible and marked with vertical grey lines. The horizontal red line shows the overall line of best fit and the Y-axis is in units of μHz.

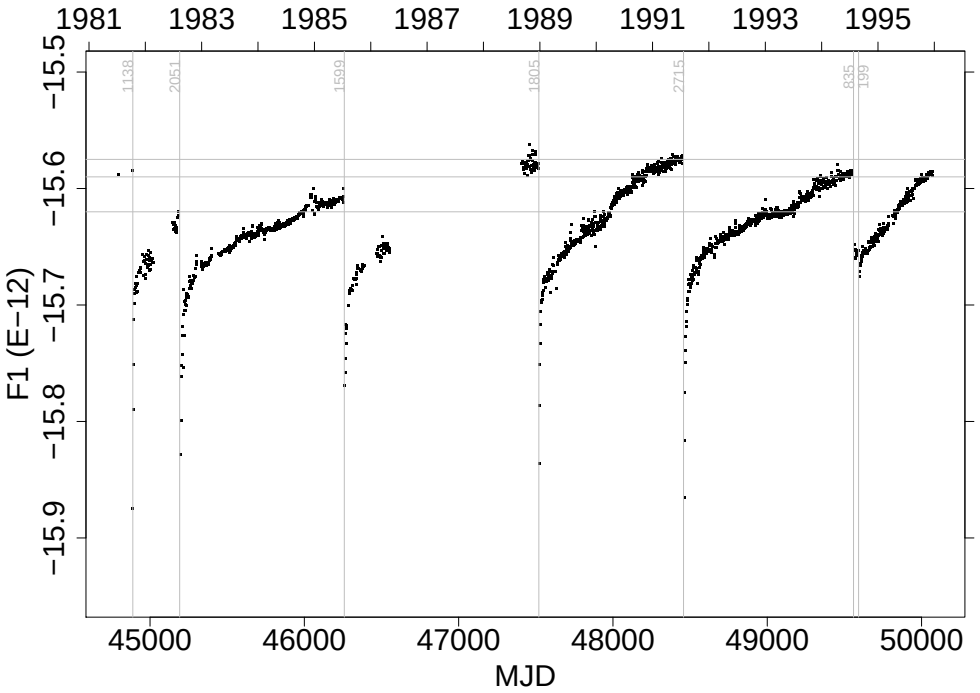

Figure 8.71: Historical data showing the change in $\dot{\nu}$ as glitches occur. Glitches are marked in grey with the magnitude $\frac{\Delta\nu}{\nu}$ shown at the top. The horizontal grey lines show the minimum, median, and maximum values of $\dot{\nu}$ just prior to a glitch.

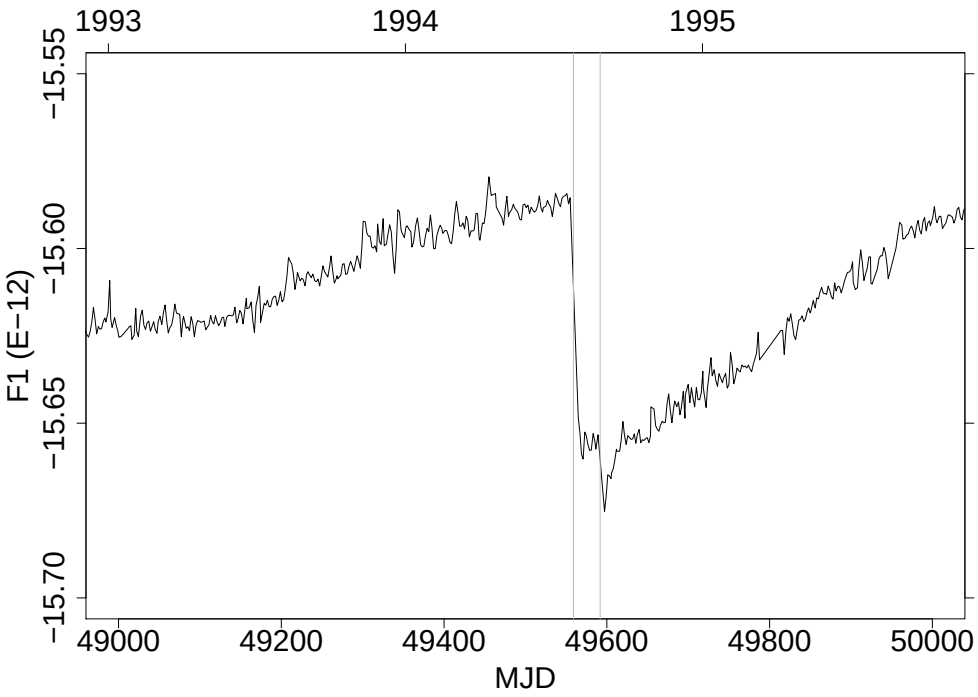

Figure 8.72: Plot of $\dot{\nu} \times 10^{-12}$ vs time for the double-glitch of 1994. This is a zoomed-in version of Figure 8.71 on page 234.

Table 8.6: Statistics of $\dot{\nu}$ just prior to each glitch.

Statistic	Value $\times 10^{-12}$ s^{-2}
Minimum	−15.62333
25 percentile	−15.59624
Median	−15.58510
25 percentile	−15.58297
Maximum	−15.57825

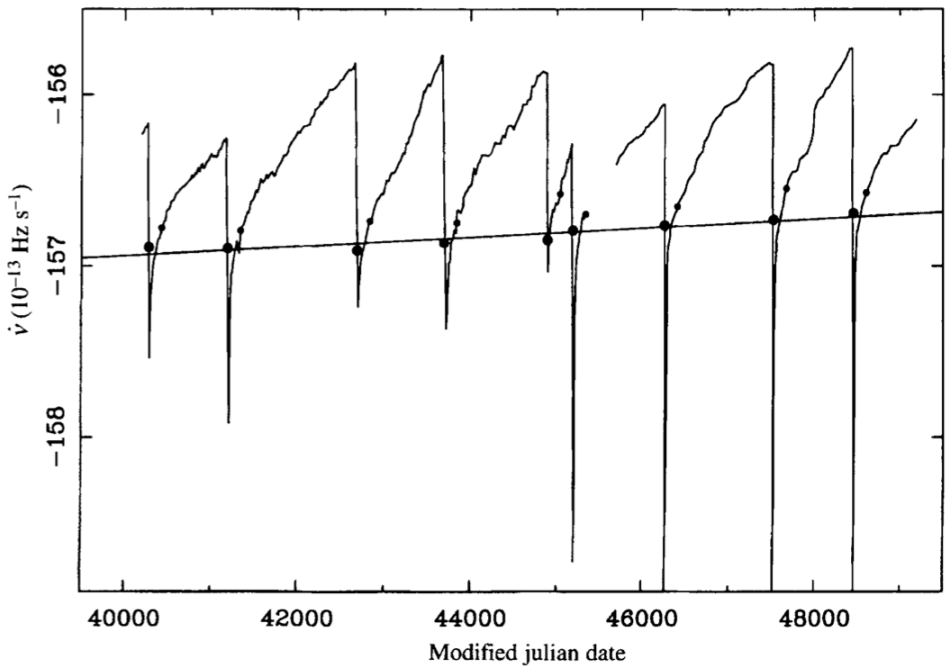

Figure 8.73: Plot from Lyne et al. (1996) showing the change in $\dot{\nu}$ over time. The gradient of the black line is $\ddot{\nu}$ and suggests a braking index of $n = 1.4$.

2016 is marked in blue.

Suffice to say, this prediction method did not work. The value of $\dot{\nu}$ exceeded the previous maximum value. Taking into account the change in $\ddot{\nu}$ by Lyne et al. (1996) may improve this prediction method.

8.7.2 Cycling of $\dot{\nu}$

In Figure 8.74 on page 237 there appears to be a slight cycling about the linear fit. Figure 8.75 on page 237 as a residual plot shows this clearly. The dotted red lines highlight micro-glitches and the horizontal red line is the line of best fit. There is clear evidence of a cyclic pattern and Figure 8.76 on page 238 is the Lomb-Scargle periodogram of this. A strong period of 572 days is evident, although this figure has high error bars due to only a portion of the 572 day cycle being present in the data. More data would be required to confirm this figure, but the glitch prevented this occurring. Small cycles of 277 and 15.7 days are also present.

Comparing the residuals from Figure 8.75 on page 237 with the historical data in which we have complete data from one glitch to the next, Figures 8.77 to 8.79 on pages 238–239 also show cyclic patterns.

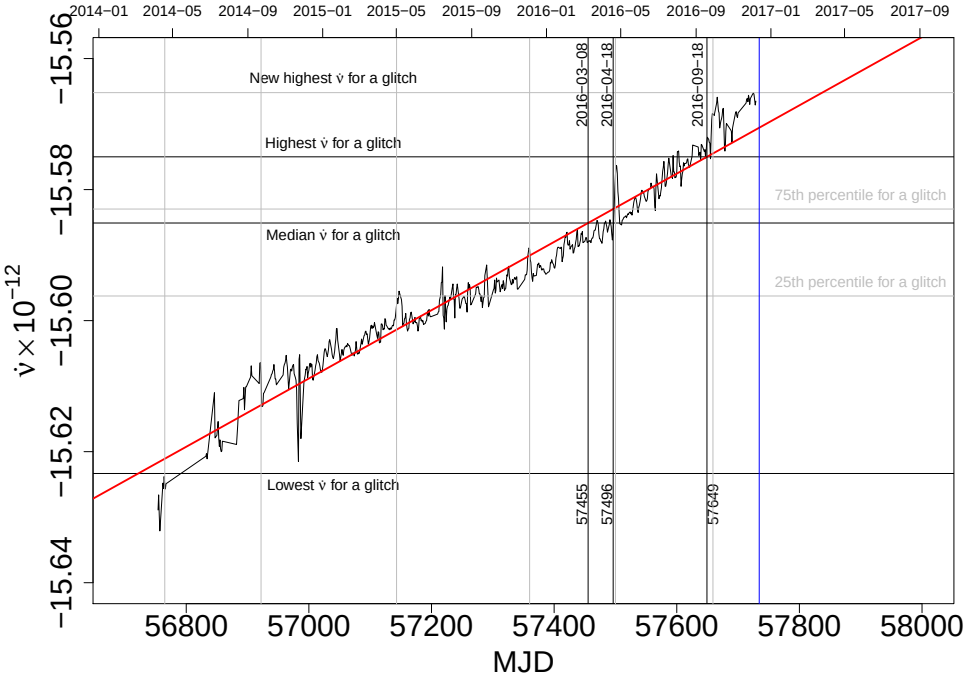

Figure 8.74: Attempted prediction of the 2016 glitch prior to occurrence. By fitting a straight line (red) to $\dot{\nu}$ and then predicting when it would hit previous values of $\dot{\nu}$ shown in Table 8.6 on page 235, we attempted to predict the glitch. In the case of 2016 glitch, $\dot{\nu}$ reached a new record high and the method did not work. Vertical grey lines mark micro-glitches.

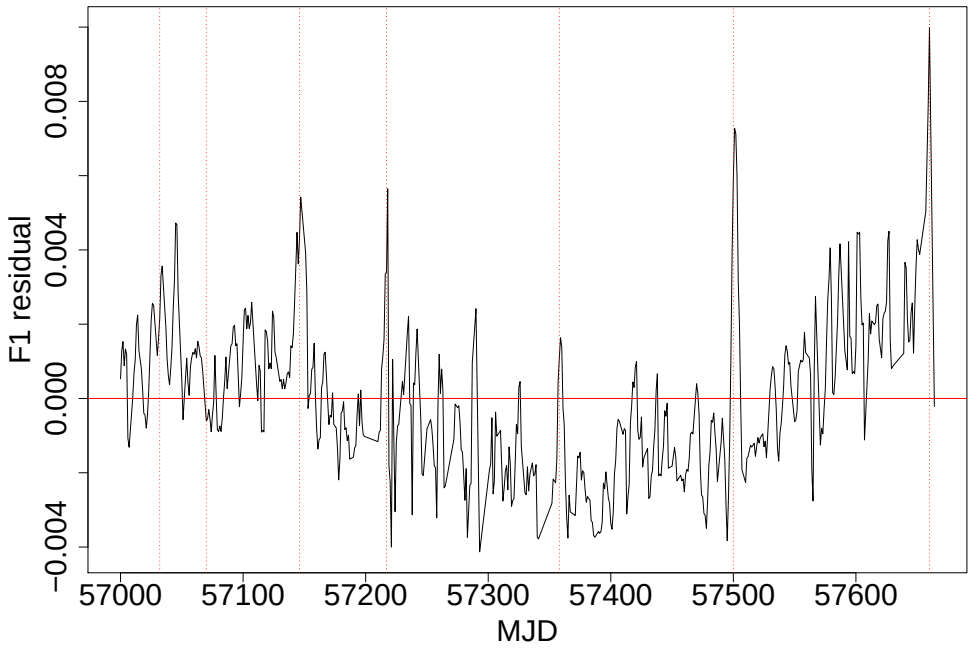

Figure 8.75: Residual from the linear fit of Figure 8.74. Y-axis is in units of 10^{-12}. Micro-glitches are shown as vertical dotted red lines and the line of best fit is the horizontal red line.

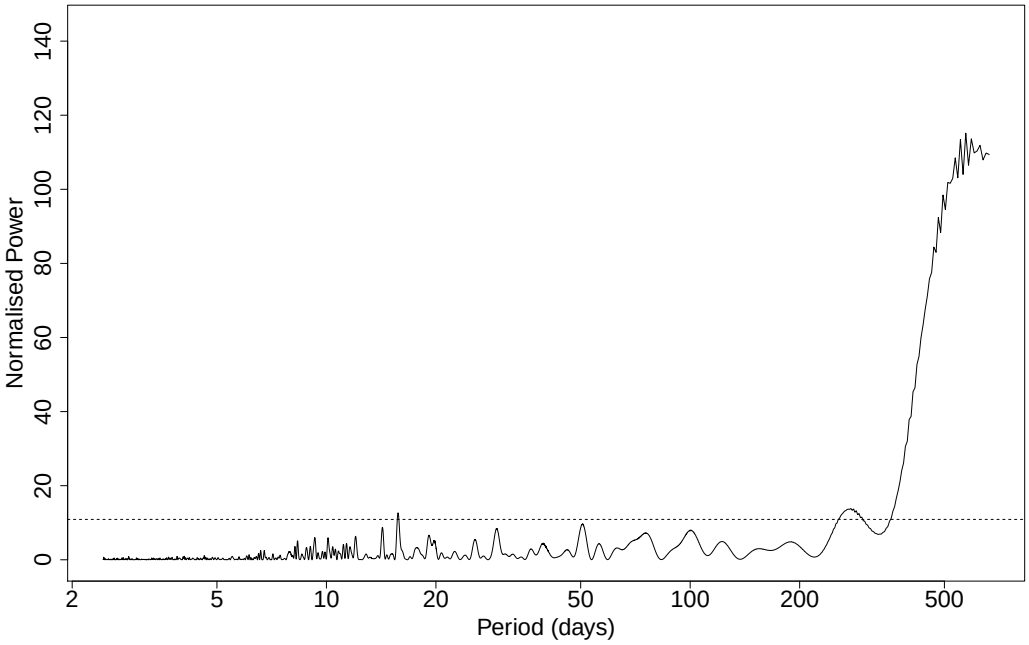

Figure 8.76: Lomb-Scargle periodogram of Figure 8.75 on page 237. Significant periods in power order: 572, 277, and 15.7 days.

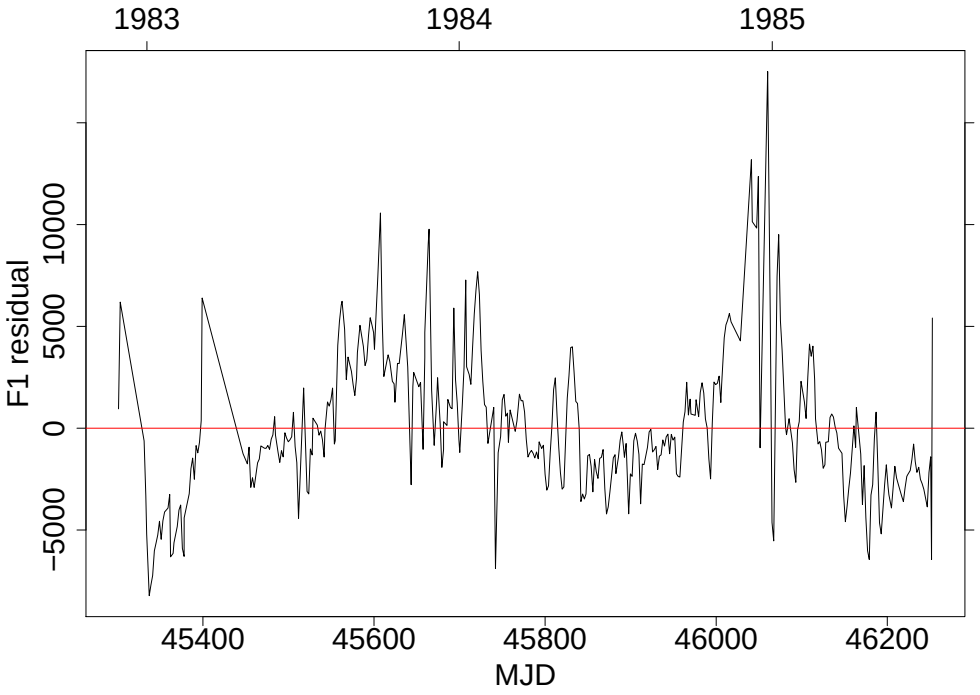

Figure 8.77: Historical data showing the residual of $\dot{\nu}$ against the line of best fit leading up to glitch 8.

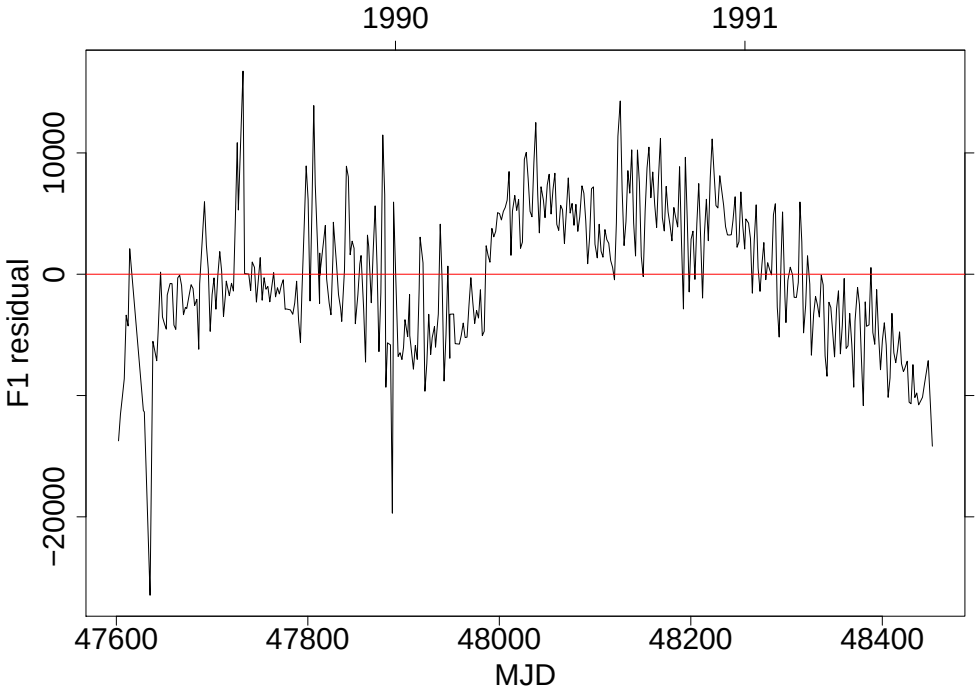

Figure 8.78: Historical data showing the residual of $\dot{\nu}$ against the line of best fit leading up to glitch 10.

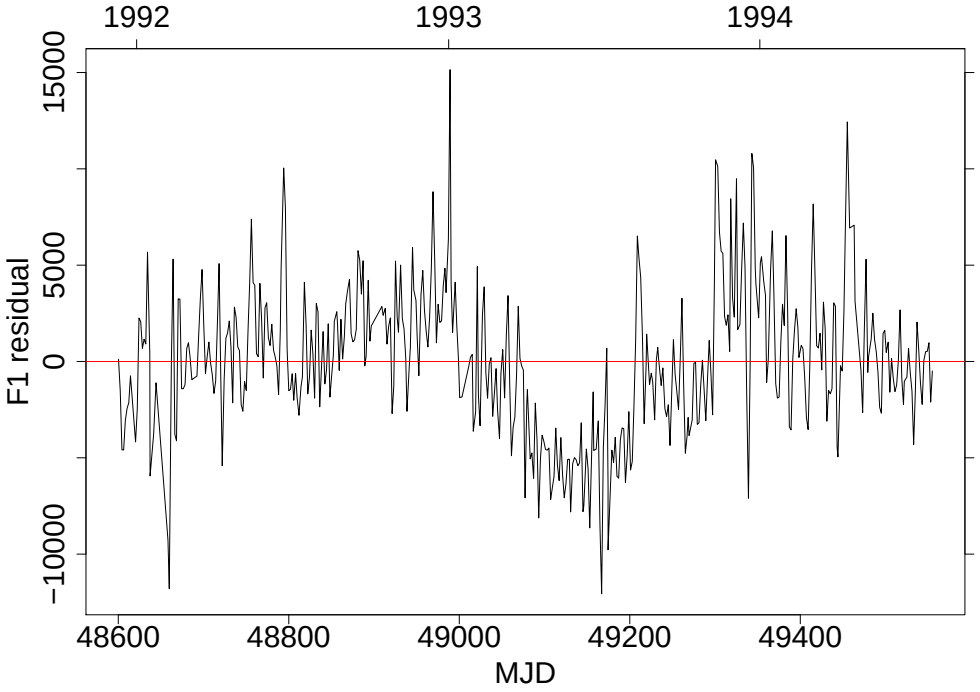

Figure 8.79: Historical data showing the residual of $\dot{\nu}$ against the line of best fit leading up to glitch 11.

8.7.3 Prediction of $\ddot{\nu}$

Interestingly, data similar to Figure 8.71 on page 234 was used in Lyne et al. (1996) (reproduced in Figure 8.73 on page 236) to predict $\ddot{\nu}$ by using $\dot{\nu}$ values 150 days* after each glitch to connect a straight line. This showed the value of $\ddot{\nu} = (31 \pm 4) \times 10^{-24}$ Hz s^{-2}. Now since a pulsar is essentially a rotating magnetic dipole we have:

$$\dot{\nu} = -K\nu^n$$
$$\ddot{\nu} = -Kn\nu^{n-1}\dot{\nu}$$

by differentiating both sides. Substituting back in and solving for n we get:

$$n = \frac{\nu\ddot{\nu}}{\dot{\nu}^2} \tag{8.6}$$

The value n is the braking index and for a rotating dipole should ideally work out to be $n = 3$. However Lyne et al. (1996) showed that for Vela the actual value is $n = 1.4 \pm 0.2$, remarkably smaller than the theoretical $n = 3$. Note that most pulsars have a measured braking index less than 3, but not normally as low as 1.4 (Lorimer and Kramer 2004).

As can be seen from Figure 8.80 on page 241, the value of $\ddot{\nu}$ has not changed since 1996 and so the value of $\ddot{\nu} = 31 \times 10^{-24}$ Hz s^{-2}, as well as the braking index of $n = 1.4$, can still be considered as unchanging using their methods. However, recently this has been challenged by Johnston and Karastergiou (2017) which is described below within Section 8.7.4 on page 242.

Also interesting is that as $\ddot{\nu}$ has caused $\dot{\nu}$ to increase over time, the peak glitching value of $\dot{\nu}$ has also appeared to increase as the latest $\dot{\nu}$ for the glitch of 2016 was at a record high.

8.7.4 Cumulative glitch frequency changes

An important plot is one of the *cumulative* $\frac{\Delta\nu}{\nu}$ used in Chamel (2013), Ho et al. (2015), and Andersson et al. (2012). It is recalculated here using genuine glitches only (including the latest from 2016) and is shown in Figure 8.81 on page 245. The red line of best fit has a gradient of 1.959×10^{-9} implying that each day this amount of $\frac{\Delta\nu}{\nu}$ is

*when all glitch recovery had supposedly completed.

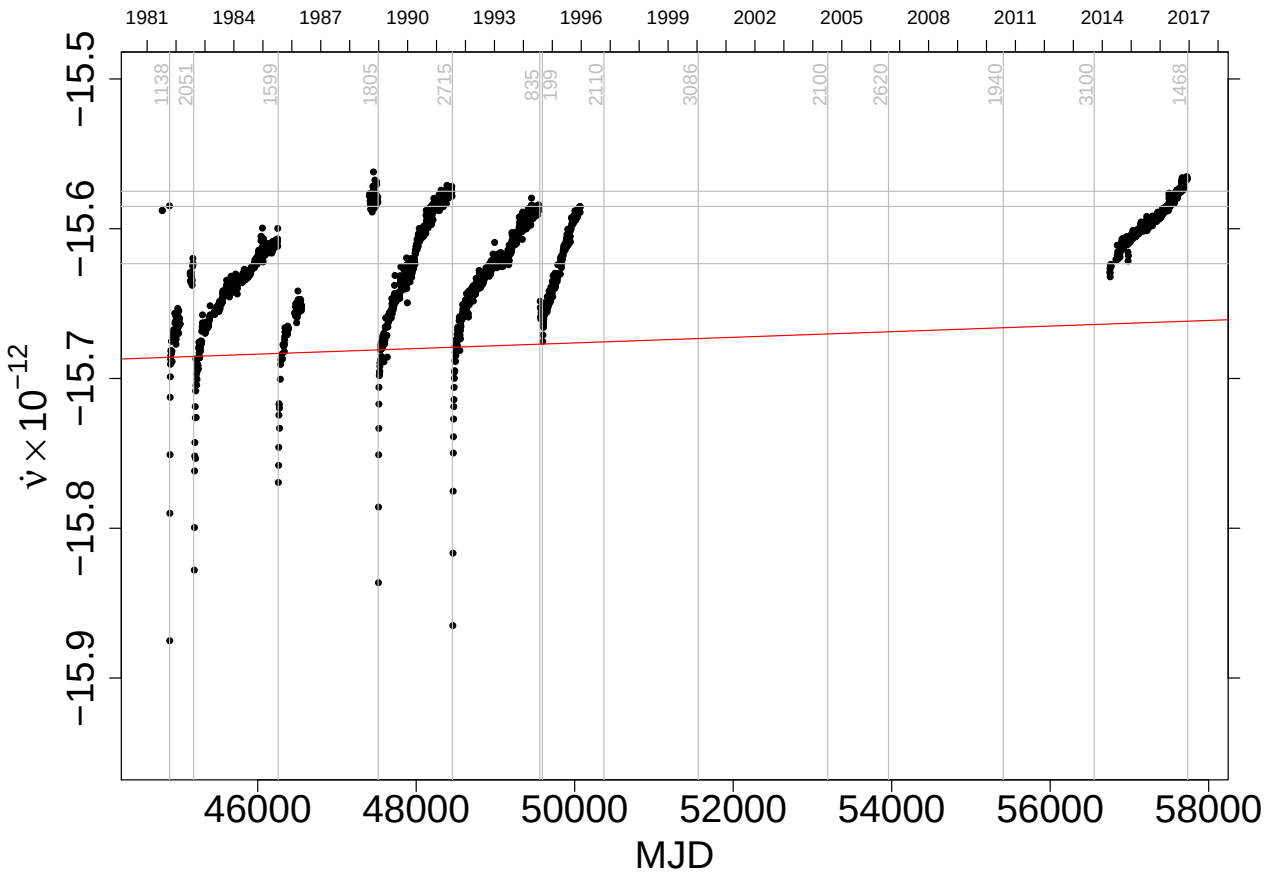

Figure 8.80: Historical data plus current data showing the change in $\dot{\nu}$ as glitches occur. Glitches are marked vertically in grey with the magnitude $\Delta\nu/\nu$ shown at the top. The horizontal grey lines show the minimum, median, and maximum values of $\dot{\nu}$ just prior to a glitch (not including 2016). The red line shows $\ddot{\nu}$ from Lyne et al. (1996).

stored in the core as the outer crust slows down. Finally, upon the glitch, most of that saved angular momentum is released.

Andersson et al. (2012) and Ho et al. (2015) define the *activity parameter*:[§]

$$\mathcal{A} = \frac{\sum \frac{\Delta\Omega}{\Omega}}{t_{\text{obs}}} \tag{8.7}$$

where Ω is the angular velocity and t_{obs} is the total time observed (which is currently ≈ 50 y for Vela). They calculate $\mathcal{A} = 1.96 \times 10^{-9} \pm 0.04$ d^{-1}. The difference between their quoted figure and our 1.959×10^{-9} is minimal.

One could argue that all micro-glitches should possibly be included in the activity parameter $\mathcal{A}$, but since our previous results show that micro-glitches and glitches are most likely separate mechanisms, we conclude that *all* micro-glitches should be excluded. Regardless, such micro-glitch data is not available for the entire time span since Vela's discovery. Also, the excellent alignment between theory and observation supports the conclusion that micro-glitches and glitches are different mechanisms.

In Ho et al. (2015) they define:

$$G \equiv 2\tau_{\text{c}}\mathcal{A} \tag{8.8}$$

where τ_{c} is the characteristic age (see Section 2.3.1 on page 13). In the case of Vela, they get $G = 0.0162$ or 1.62% (using the standard $\tau_{\text{c}} = 11.3$ kyr). This number G needs to be compared with the ratio of the crust moment of inertia and total moment of inertia which is between 3-5% (Andersson et al. 2012). This means the superfluid does *not* have enough moment of inertia I_n to cause the magnitudes of observed glitches in Vela.

There are a number of proposed solutions to this anomaly. One is that the superfluid extends deeper into the core than expected. This would require a modification to equation-of-state hypotheses.

Andersson et al. (2012) and Chamel (2013) suggest that Link et al. (1999) underestimated the ability of vortices to transfer momentum by a factor of ≈ 4.3.

However using the braking index $n = 1.4$ from (Lyne et al. 1996) and the results from Figure 2.7 on page 17 this predicts a characteristic age of $\tau_{\text{c}} = 27 \times 10^3$ years and hence $G = 2 \times 27 \times 10^3 \times 365.25 \times 1.96 \times 10^{-9} = 3.9\%$, which is a much improved fit to the ratio of crust and total moments of inertia.

[§]note that $\mathcal{A}$ is also referred to as $\langle A \rangle$ in other articles in the literature.

An improved approach is taken by Johnston and Karastergiou (2017) which drops the assumption that the braking index is constant over time. They take the idea from Tauris and Konar (2001) and expand it such that the braking index n is:

$$n(t) = n_o - \frac{3c^3 I \dot{B}(t)}{R^6 B^3(t) \sin^2(\alpha(t)) \Omega^2(t)} - \frac{3c^3 I \cos(\alpha(t)) \dot{\alpha}(t)}{R^6 B^2(t) \sin^3(\alpha(t)) \Omega^2(t)} + \mathrm{TN}(t) \qquad (8.9)$$

where n_0 is the initial braking index (*not* assumed to be 3), c is the speed of light, I is the moment of inertia of the neutron star, $B(t)$ is the magnetic field, $\dot{B}(t)$ is the rate of change of $B(t)$, R is the radius, $\alpha(t)$ is the inclination angle between the magnetic and rotational axis, $\dot{\alpha}(t)$ is the rate of change of $\alpha(t)$, $\Omega(t) = 2\pi\nu$ is the angular velocity, and $\mathrm{TN}(t)$ is a random component influenced by timing noise.[§]

They ran simulations based on these assumptions and showed that $n(t)$ "*can change significantly even on short time scales*". They also stated under their *Implications* heading: "τ_c *is significantly greater than the true age, especially for older pulsars*". Vela is, of course, a young pulsar and the implication is that the characteristic age (τ_c) is above the true age and so this contradicts the idea that $\tau_\mathrm{c} = 27 \times 10^3$ years described above. This also hints that the real age of Vela is actually less than $\tau_\mathrm{c} = 11150$ y and so the age of $t = 10746$ y shown in Section 2.3.1 on page 16 could be more accurate.

Aschenbach et al. (1995) provide an interesting insight of the age of the Vela supernova remnant based on X-Ray observations. They say that the age is $18 \times 10^3 \pm 9 \times 10^3$ years, but then go on to say there is a possibility that the age could also be $31 \times 10^3 \pm 6 \times 10^3$ years.[‡]

8.7.5 Glitch magnitudes

Plotting the residuals to the line of best fit shown in Figure 8.81 on page 245 provides an even more striking pattern as shown in Figure 8.82 on page 245. The alternation could be explained because when the Magnus force reaches a critical point, the vortices are unpinned, and the core imparts angular momentum onto the crust. Assuming that the "grip" of the core to the crust isn't perfect, not all that angular momentum will be imparted and some will remain stored in the core. Upon the next glitch, with more angular momentum stored, a larger $\frac{\Delta\nu}{\nu}$ occurs. Andersson et al. (2012) state that the remarkable regularity of the size of the Vela glitches suggests that the entire reservoir of angular momentum is transferred during a glitch whereas the alternation above and

[§]the original article also includes state changes and intermittency in this factor, but these most likely do not apply to Vela.

[‡]The actual date of the Vela supernova has implications for potential future discoveries of drawings made by Australian aboriginal populations, as it would have been prominent in the southern sky when it occurred.

below the mean as shown in Figure 8.82 on page 245 indicates that not quite all is necessarily transferred - but it's very close.

The number of zero-crossings N_z on white noise is expected to be:

$$N_z = \frac{N-1}{2} \pm \frac{\sqrt{N-1}}{2} \tag{8.10}$$

where N is the number of points. We have $N = 18$ and the predicted value $N_z = 8.5 \pm 2.06$, or $6.44 \leq N_z \leq 10.56$. We have an observed $N_z = 13$ which is greater than what's expected, and so this alternation is unlikely to be random.

This means that glitch magnitudes can generally be predicted, and that if the next glitch is in the year ≈ 2019, then it will be of a magnitude $\approx\ 3000 \times 10^{-9}$.

8.8 Prediction results

From past data, as $\dot{\nu}$ increases it then levels off before the main glitch finally arrives. However, referring back to Figure 7.1 on page 144 we can see cycles of increasing pulse width, followed by a decrease, and then finally a micro-glitch. As the main glitch occurred on one of the high-points on the pulse-width graph, this could still be used to predict future glitches. In summary for future prediction: track $\dot{\nu}$ (using a 10 day moving average) until it appears to level off, and then wait for a falling pulse width, then a rise. The glitch should happen shortly after. Future studies could easily confirm this method.

The prediction method which examined the value of $\dot{\nu}$ using 10 day averages appears to have some merit. Whilst the value of $\dot{\nu}$ exceeded the highest previous value, the pattern observed of maximising and then levelling-off appeared to hold true.

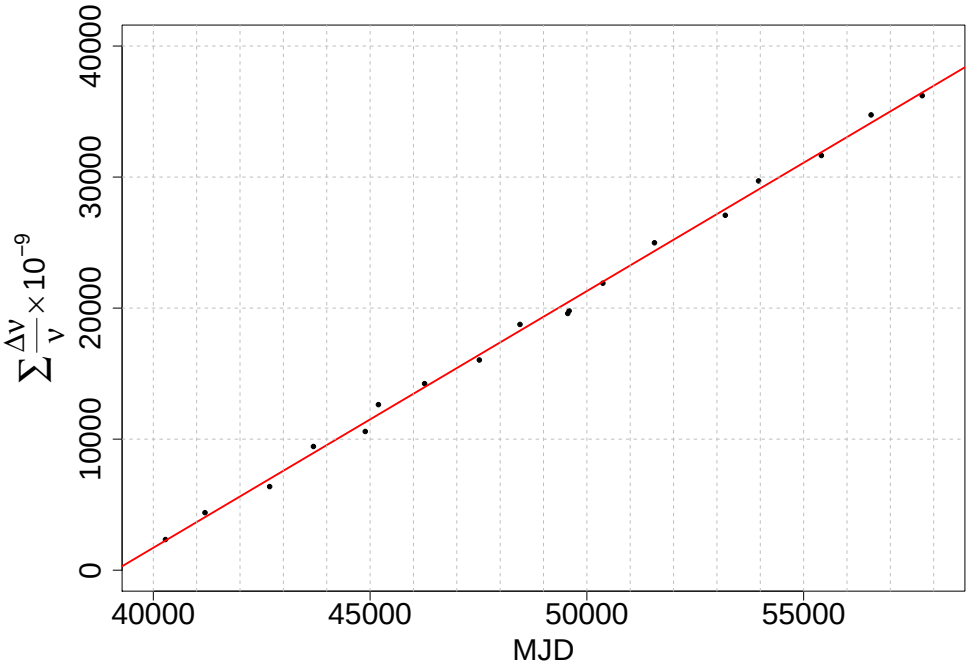

Figure 8.81: Cumulative $\frac{\Delta\nu}{\nu}$ with line of best fit having a gradient of 1.959 and a correlation R=0.9986. Only genuine glitches (see text) have been included.

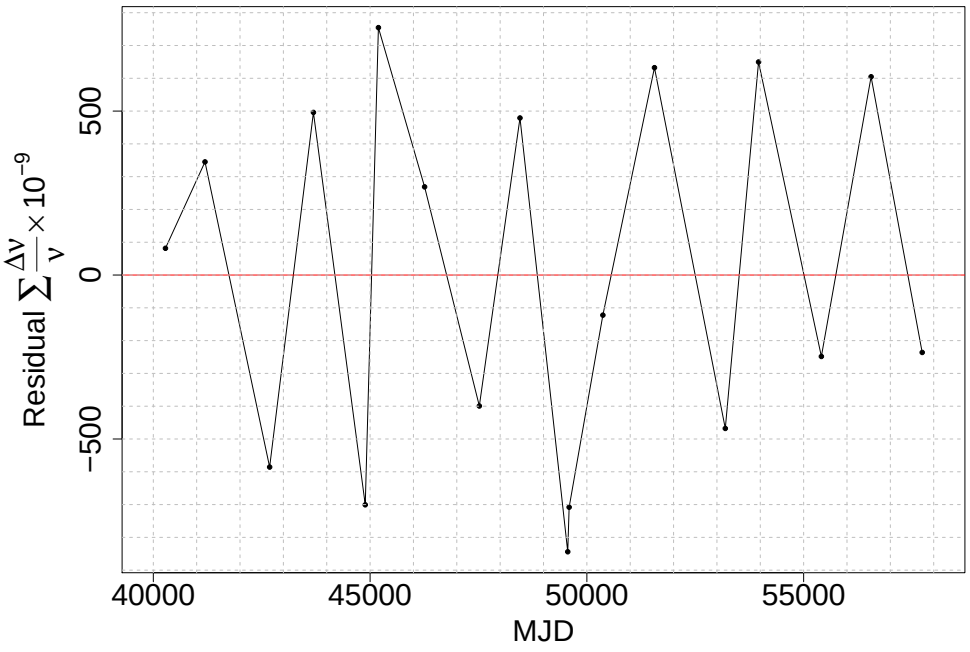

Figure 8.82: Residuals of cumulative $\frac{\Delta\nu}{\nu}$ against the line of best fit. Only genuine glitches (see text) have been included.

Chapter 9

Conclusion

9.1 Summary

After completing a nearly four year single-pulse observing program and establishing the largest single-pulse archive anywhere in the world, a number of new significant discoveries have been uncovered:

- The temporal variation of the integrated pulse width of the Vela pulsar and the possible correlation with precession has been established.
- A confirmed link between pulse-width minima and micro-glitches (with $\frac{\Delta\nu}{\nu} > 0$) has been made. This could be used to define what a micro-glitch is, but we have instead chosen to suggest a new cutoff of $\frac{\Delta\nu}{\nu} \geq 100 \times 10^{-9}$ to be the definition of a "glitch".
- Vela goes through cycles of low and high emission activity. When the pulse width is at its widest, bright pulse numbers and flux density magnitudes tend to be increased.
- The observation that the genuine glitch did *not* occur at a pulse width minimum, confirms that glitches and micro-glitches have separate origins. Glitches no doubt occur in the outer core/inner crust of the neutron star, but micro-glitches possibly have their origins in the magnetosphere.
- At the time of the glitch, a change was observed in mean and variance of the timing residuals that was most likely caused by a change in the magnetospheric configuration. This in turn was most likely caused by the glitch and may provide some clues as to the internal glitching process, and will no doubt be central to future theoretical papers on this topic.

- A null also occurred just prior to the glitch, and the pulse before was very broad. This also implies that the glitch had an effect on the magnetosphere.
- A possible method of glitch prediction (as the glitch approaches) has been proposed.
- The official "glitch" table needs revising and when done, the cumulutive $\frac{\Delta\nu}{\nu}$ and the activity parameter $\mathcal{A}$ are in strong agreement.
- J1644−4559 emitted a bright pulse, which was a rare (1 in 4.8 million) event, and such emissions had previously been excluded in the literature.

9.2 Further study

A number of questions have surfaced during the body of this work. Listed here is a brief summary. Future research could be based on any of these:

- Are there long-term temporal changes of pulse width at different frequencies?
- Are there long-term temporal changes of Gaussian emission components?
- Are there long-term temporal change of properly calibrated Stoke's parameters?
- Do bright pulses at different frequencies always occur at the same amount of time prior to the main pulse?
- Does the above change over time?
- Do glitches always happen at maximum pulse widths?
- Do nulls always happen with future glitches?
- Is a null observed at a glitch genuine? Follow up with more sensitive telescopes.
- Is the broad pulse before the null a genuine change prior to the null?
- Do nulls observed at Mount Pleasant occur at different rates depending on overall pulse flux density and/or pulse profile width?
- Search the entire dataset and gather more sound statistics on changes in mean and variance of timing residuals of individual pulses.
- Theoretical study of the glitch spin-up reflected as a brief slow-down at first. Could this happen internally?
- Does the scatterplot shown in 5.32 on page 105 change over time?
- Does the scatterplot shown in 5.32 on page 105 change before and after glitches?

- During a time of high bright-pulse activity from Vela, observe at multiple frequencies and confirm the spectral index of the bright-pulse component.
- Does the *optical* component of the Vela pulsar increase in magnitude during times of higher radio activity and/or giant pulses?
- Do bright or giant pulses occur in the emission cones on opposite magnetic poles at the same time? Observation of pulsars that exhibit bright pulse activity and with a visible interpulse ($\alpha \approx 90^\circ$) would be required.
- Does the Crab pulsar's giant pulse activity vary with time?

Bibliography

Akbal, O., Alpar, M. A., Buchner, S., and Pines, D. (2017). Nonlinear interglitch dynamics, the braking index of the Vela pulsar and the time to the next glitch. *MNRAS*, 469:4183–4192.

Anderson, P. W. and Itoh, N. (1975). Pulsar glitches and restlessness as a hard superfluidity phenomenon. *Nature*, 256:25–27.

Andersson, N., Glampedakis, K., Ho, W. C. G., and Espinoza, C. M. (2012). Pulsar Glitches: The Crust is not Enough. *Physical Review Letters*, 109(24):241103.

Aschenbach, B., Egger, R., and Trümper, J. (1995). Discovery of explosion fragments outside the Vela supernova remnant shock-wave boundary. *Nature*, 373:587–590.

Baars, J. W. M., Genzel, R., Pauliny-Toth, I. I. K., and Witzel, A. (1977). The absolute spectrum of CAS A - an accurate flux density scale and a set of secondary calibrators. *A&A*, 61:99–106.

Backer, D. C. (1970a). Correlated Subpulse Structure in PSR 1237 + 25. *Nature*, 228:752–755.

Backer, D. C. (1970b). Correlation of Subpulse Structure in a Sequence of Pulses from Pulsar PSR 1919+21. *Nature*, 227:692–695.

Barnhart, R. (1999). *Chambers dictionary of etymology*. Chambers, Edinburgh.

Basu, R., Mitra, D., and Rankin, J. M. (2015). Toward an Empirical Theory of Pulsar Emission. X. On the Precursor and Postcursor Emission. *ApJ*, 798:105.

Baym, G., Pethick, C., Pines, D., and Ruderman, M. (1969). Spin Up in Neutron Stars : The Future of the Vela Pulsar. *Nature*, 224:872–874.

Bewley, G. P., Lathrop, D. P., and Sreenivasan, K. R. (2006). SUPERFLUID HELIUM: Visualization of quantized vortices. *Nature*, 441:588.

Biggs, J. D. (1992). An analysis of radio pulsar nulling statistics. *ApJ*, 394:574–580.

Brook, P. R., Karastergiou, A., Buchner, S., Roberts, S. J., Keith, M. J., Johnston,

S., and Shannon, R. M. (2014). Evidence of an Asteroid Encountering a Pulsar. *ApJLett*, 780:L31.

Caraveo, P. A., De Luca, A., Mignani, R. P., and Bignami, G. F. (2001). The Distance to the Vela Pulsar Gauged with Hubble Space Telescope Parallax Observations. *ApJ*, 561:930–937.

Chamel, N. (2013). Crustal Entrainment and Pulsar Glitches. *Physical Review Letters*, 110(1):011101.

Chamel, N. and Haensel, P. (2008). Physics of neutron star crusts. *Living Reviews in Relativity*, 11(10).

Cooke, D. J. (1969). Intensity Variations of PSR 0833-45 at 1,720 MHz. *Nature*, 224:569.

Cordes, J. M. (1978). Observational limits on the location of pulsar emission regions. *ApJ*, 222:1006–1011.

Cordes, J. M. (1993). The detectability of planetary companions to radio pulsars. In Phillips, J. A., Thorsett, S. E., and Kulkarni, S. R., editors, *Planets Around Pulsars*, volume 36 of *Astronomical Society of the Pacific Conference Series*, pages 43–60.

Cordes, J. M., Bhat, N. D. R., Hankins, T. H., McLaughlin, M. A., and Kern, J. (2004). The Brightest Pulses in the Universe: Multifrequency Observations of the Crab Pulsar's Giant Pulses. *ApJ*, 612:375–388.

Cordes, J. M., Downs, G. S., and Krause-Polstorff, J. (1988). JPL pulsar timing observations. V - MACRO and microjumps in the VELA pulsar 0833-45. *ApJ*, 330:847–869.

Cordes, J. M. and Lazio, T. J. W. (2002). NE2001.I. A New Model for the Galactic Distribution of Free Electrons and its Fluctuations. *ArXiv Astrophysics e-prints*.

Cordes, J. M. and Shannon, R. M. (2008). Rocking the Lighthouse: Circumpulsar Asteroids and Radio Intermittency. *ApJ*, 682:1152–1165.

Cordes, J. M. and Wasserman, I. (2016). Supergiant pulses from extragalactic neutron stars. *MNRAS*, 457:232–257.

Crowder, B. (1997). *The Wonders of the Weather*. Australian Govt Pub Service.

D'Alessandro, F. (1995). *Timing Observations of Southern Pulsars*. PhD thesis, Physics Department, University of Tasmania.

Deshpande, A. A. and McCulloch, P. M. (1996). Periodic Changes in Intensity and Arrival Time of Pulses from the VELA Pulsar: Evidence for Free Precession? In Johnston, S., Walker, M. A., and Bailes, M., editors, *IAU Colloq. 160: Pulsars:*

Problems and Progress, volume 105 of *Astronomical Society of the Pacific Conference Series*, page 101.

Deshpande, A. A. and Rankin, J. M. (1999). Pulsar Magnetospheric Emission Mapping: Images and Implications of Polar CAP Weather. *ApJ*, 524:1008–1013.

Deshpande, A. A. and Rankin, J. M. (2001). The topology and polarization of sub-beams associated with the 'drifting' sub-pulse emission of pulsar B0943+10 - I. Analysis of Arecibo 430- and 111-MHz observations. *MNRAS*, 322:438–460.

Dodson, R., Lewis, D., and McCulloch, P. (2007). Two decades of pulsar timing of Vela. *Ap&SS*, 308:585–589.

Dodson, R. G., McCulloch, P. M., and Lewis, D. R. (2002). High Time Resolution Observations of the January 2000 Glitch in the Vela Pulsar. *ApJLett*, 564:L85–L88.

Drake, F. D. and Craft, H. D. (1968). Second Periodic Pulsation in Pulsars. *Nature*, 220:231–235.

Durant, M., Kargaltsev, O., Pavlov, G. G., Kropotina, J., and Levenfish, K. (2013). The Helical Jet of the Vela Pulsar. *ApJ*, 763:72.

Dyks, J. (2017). The geometry of a radio pulsar beam. *MNRAS*, 471:L131–L134.

Edwards, R. T., Hobbs, G. B., and Manchester, R. N. (2006). TEMPO2, a new pulsar timing package - II. The timing model and precision estimates. *MNRAS*, 372:1549–1574.

Espinoza, C. M., Lyne, A. G., Stappers, B. W., and Kramer, M. (2011). A study of 315 glitches in the rotation of 102 pulsars. *MNRAS*, 414:1679–1704.

Feigelson, E. D. (2017). The changing landscape of astrostatistics and astroinformatics. In *Astroinformatics*, volume 325 of *IAU Symposium*, pages 3–9.

Gold, T. (1968). Rotating Neutron Stars as the Origin of the Pulsating Radio Sources. *Nature*, 218:731–732.

Goldreich, P. and Julian, W. H. (1969). Pulsar Electrodynamics. *ApJ*, 157:869.

Hankins, T. H., Kern, J. S., Weatherall, J. C., and Eilek, J. A. (2003). Nanosecond radio bursts from strong plasma turbulence in the Crab pulsar. *Nature*, 422:141–143.

Hlavac, M. (2015). stargazer: Well-formatted regression and summary statistics tables. http://CRAN.R-project.org/package=stargazer.

Ho, W. C. G., Espinoza, C. M., Antonopoulou, D., and Andersson, N. (2015). Pinning down the superfluid and measuring masses using pulsar glitches. *Science Advances*, 1:e1500578–e1500578.

Hobbs, G. B., Edwards, R. T., and Manchester, R. N. (2006). TEMPO2, a new pulsar-timing package - I. An overview. *MNRAS*, 369:655–672.

Hotan, A. W., van Straten, W., and Manchester, R. N. (2004). PSRCHIVE and PSRFITS: An Open Approach to Radio Pulsar Data Storage and Analysis. *Publications of the Astron. Soc. of Australia*, 21:302–309.

Huth, E. J., editor (1994). *Scientific style and format : the CBE manual for authors, editors, and publishers*. Cambridge University Press, Cambridge New York.

Jankowski, F., Bailes, M., Barr, E., Bateman, T., Bhandari, S., Briggs, F., Caleb, M., Campbell-Wilson, D., Flynn, C., Green, A., Hunstead, R., Jameson, A., Keane, E., Ravi, V., Krishnan, V. V., and van Straten, W. (2015). Glitch event observed in the Vela pulsar (PSR J0835-4510). *The Astronomer's Telegram*, 6903:1.

Johnston, S. (2004). Single pulses from PSR B1641-45. *MNRAS*, 348:1229–1235.

Johnston, S. and Karastergiou, A. (2017). Pulsar braking and the $P - \dot{P}$ diagram. *MNRAS*, 467:3493–3499.

Johnston, S., Karastergiou, A., and Willett, K. (2006). High-frequency observations of southern pulsars. *MNRAS*, 369:1916–1928.

Johnston, S., Lorimer, D. R., Harrison, P. A., Bailes, M., Lyne, A. G., Bell, J. F., Kaspi, V. M., Manchester, R. N., D'Amico, N., and Nicastro, L. (1993). Discovery of a very bright, nearby binary millisecond pulsar. *Nature*, 361:613–615.

Johnston, S. and Romani, R. W. (2004). Giant Pulses - A Brief Review. In Camilo, F. and Gaensler, B. M., editors, *Young Neutron Stars and Their Environments*, volume 218 of *IAU Symposium*, page 315.

Johnston, S., van Straten, W., Kramer, M., and Bailes, M. (2001). High Time Resolution Observations of the Vela Pulsar. *ApJLett*, 549:L101–L104.

Jones, D. I. (2012). Pulsar state switching, timing noise and free precession. *MNRAS*, 420:2325–2338.

Katz, J. I. (2016). Fast radio bursts - A brief review: Some questions, fewer answers. *Modern Physics Letters A*, 31:1630013.

Katz, J. I. (2017). Fast radio bursts as pulsar lightning. *MNRAS*, 469:L39–L42.

Keith, M. J., Johnston, S., Levin, L., and Bailes, M. (2011). 17- and 24-GHz observations of southern pulsars. *MNRAS*, 416:346–354.

Kern, J. S., Hankins, T. H., and Rankin, J. M. (2000). Single Pulse Polarimetry of the Vela Pulsar. In Kramer, M., Wex, N., and Wielebinski, R., editors, *IAU Colloq.*

177: Pulsar Astronomy - 2000 and Beyond, volume 202 of *Astronomical Society of the Pacific Conference Series*, page 257.

Komesaroff, M. M. (1970). Possible Mechanism for the Pulsar Radio Emission. *Nature*, 225:612–614.

Kotera, K., Mottez, F., Voisin, G., and Heyvaerts, J. (2016). Do asteroids evaporate near pulsars? Induction heating by pulsar waves revisited. *A&A*, 592:A52.

Kramer, M., Lyne, A. G., O'Brien, J. T., Jordan, C. A., and Lorimer, D. R. (2006). A Periodically Active Pulsar Giving Insight into Magnetospheric Physics. *Science*, 312:549–551.

Krishnamohan, S. and Downs, G. S. (1983). Intensity dependence of the pulse profile and polarization of the VELA pulsar. *ApJ*, 265:372–388.

Large, M. I., Vaughan, A. E., and Mills, B. Y. (1968). A Pulsar Supernova Association? *Nature*, 220:340–341.

Latała, R. and Matlak, D. (2017). *Royen's Proof of the Gaussian Correlation Inequality*, pages 265–275. Springer International Publishing, Cham.

Link, B. and Epstein, R. I. (1997). Are We Seeing Magnetic Axis Reorientation in the Crab and VELA Pulsars? *ApJLett*, 478:L91–L94.

Link, B., Epstein, R. I., and Lattimer, J. M. (1999). Pulsar Constraints on Neutron Star Structure and Equation of State. *Physical Review Letters*, 83:3362–3365.

Lomb, N. R. (1976). Least-squares frequency analysis of unequally spaced data. *Ap&SS*, 39:447–462.

Lorimer, D. R., Bailes, M., McLaughlin, M. A., Narkevic, D. J., and Crawford, F. (2007). A Bright Millisecond Radio Burst of Extragalactic Origin. *Science*, 318:777.

Lorimer, D. R. and Kramer, M. (2004). *Handbook of Pulsar Astronomy*. Cambridge University Press.

Lyne, A. G. and Manchester, R. N. (1988). The shape of pulsar radio beams. *MNRAS*, 234:477–508.

Lyne, A. G., Pritchard, R. S., Graham-Smith, F., and Camilo, F. (1996). Very low braking index for the Vela pulsar. *Nature*, 381:497–498.

Manchester, R. N., Hobbs, G. B., Teoh, A., and Hobbs, M. (2005). The Australia Telescope National Facility Pulsar Catalogue. *AJ*, 129:1993–2006.

Manchester, R. N., Newton, L. M., Goss, W. M., and Hamilton, P. A. (1978). Detection

of a large period discontinuity in the longer period pulsar PSR 1641-45. *MNRAS*, 184:35P–37P.

Michel, F. (1991). *Theory of Neutron Star Magnetospheres*. Theoretical Astrophysics. University of Chicago Press.

Michel, F. C. (1987). A pulsar emission model - Observational tests. *ApJ*, 322:822–830.

Mitra, D. and Rankin, J. M. (2002). Toward an Empirical Theory of Pulsar Emission. VII. On the Spectral Behavior of Conal Beam Radii and Emission Heights. *ApJ*, 577:322–336.

Mitra, D. and Rankin, J. M. (2011). Toward an Empirical Theory of Pulsar Emission. IX. On the Peculiar Properties and Geometric Regularity of Lyne and Manchester's "PArtial Cone" Pulsars. *ApJ*, 727:92.

Murdin, P., Allen, D. A., and Malin, D. (1979). *Catalogue of the universe / by Paul Murdin and David Allen ; with original photographs by David Malin*. Cambridge University Press Cambridge ; New York.

Naidu, A., Joshi, B. C., Manoharan, P. K., and Krishnakumar, M. A. (2018). Detection of long nulls in PSR B1706-16, a pulsar with large timing irregularities. *MNRAS*, 475:2375–2382.

Nyquist, H. (1928). Certain Topics in Telegraph Transmission Theory. *Transactions of the American Institute of Electrical Engineers, Volume 47, Issue 2, pp. 617-624*, 47:617–624.

Ott, M., Witzel, A., Quirrenbach, A., Krichbaum, T. P., Standke, K. J., Schalinski, C. J., and Hummel, C. A. (1994). An updated list of radio flux density calibrators. *A&A*, 284:331–339.

Palfreyman, J. (2016). Glitch observed in the Vela Pulsar (PSR J0835-4510). *The Astronomer's Telegram*, 9847.

Palfreyman, J., Dickey, J. M., Hotan, A., Ellingsen, S., and van Straten, W. (2018). Alteration of the magnetosphere of the Vela pulsar during a glitch. *Nature*, 556:219–222.

Palfreyman, J. L., Dickey, J. M., Ellingsen, S. P., Jones, I. R., and Hotan, A. W. (2016). Temporal Evolution of the Vela Pulsar's Pulse Profile. *ApJ*, 820:64.

Palfreyman, J. L., Hotan, A. W., Dickey, J. M., Young, T. G., and Hotan, C. E. (2011). Consecutive Bright Pulses in the Vela Pulsar. *ApJLett*, 735:L17.

Pavlov, G. G., Zavlin, V. E., Sanwal, D., Burwitz, V., and Garmire, G. P. (2001). The

X-Ray Spectrum of the Vela Pulsar Resolved with the Chandra X-Ray Observatory. *ApJLett*, 552:L129–L133.

Pellizzoni, A., Pilia, M., Possenti, A., Fornari, F., Caraveo, P., del Monte, E., Mereghetti, S., Tavani, M., Argan, A., Trois, A., Burgay, M., Chen, A., Cognard, I., Costa, E., D'Amico, N., Esposito, P., Evangelista, Y., Feroci, M., Fuschino, F., Giuliani, A., Halpern, J., Hobbs, G., Hotan, A., Johnston, S., Kramer, M., Longo, F., Manchester, R. N., Marisaldi, M., Palfreyman, J., Weltevrede, P., Barbiellini, G., Boffelli, F., Bulgarelli, A., Cattaneo, P. W., Cocco, V., D'Ammando, F., DeParis, G., Di Cocco, G., Donnarumma, I., Fiorini, M., Froysland, T., Galli, M., Gianotti, F., Harding, A., Labanti, C., Lapshov, I., Lazzarotto, F., Lipari, P., Mauri, F., Morselli, A., Pacciani, L., Perotti, F., Picozza, P., Prest, M., Pucella, G., Rapisarda, M., Rappoldi, A., Soffitta, P., Trifoglio, M., Vallazza, E., Vercellone, S., Vittorini, V., Zambra, A., Zanello, D., Pittori, C., Verrecchia, F., Preger, B., Santolamazza, P., Giommi, P., and Salotti, L. (2009). High-Resolution Timing Observations of Spin-Powered Pulsars with the AGILE Gamma-Ray Telescope. *ApJ*, 691:1618–1633.

Perley, R. A. and Butler, B. J. (2013). An accurate flux density scale from 1 to 50 ghz. *The Astrophysical Journal Supplement Series*, 204(2):19.

Petroff, E., Barr, E. D., Jameson, A., Keane, E. F., Bailes, M., Kramer, M., Morello, V., Tabbara, D., and van Straten, W. (2016). FRBCAT: The Fast Radio Burst Catalogue. *Publications of the Astron. Soc. of Australia*, 33:e045.

Press, W. H. and Rybicki, G. B. (1989). Fast algorithm for spectral analysis of unevenly sampled data. *ApJ*, 338:277–280.

Proctor, D. E., Uytenbogaardt, R., and Meredith, B. M. (1988). VHF radio pictures of lightning flashes to ground. *J. Geophys. Res.*, 93:12.

R Core Team (2018). *R: A Language and Environment for Statistical Computing*. R Foundation for Statistical Computing, Vienna, Austria.

Radhakrishnan, V., Cooke, D. J., Komesaroff, M. M., and Morris, D. (1969). Evidence in Support of a Rotational Model for the Pulsar PSR 0833-45. *Nature*, 221:443–446.

Radhakrishnan, V. and Manchester, R. N. (1969). Detection of a Change of State in the Pulsar PSR 0833-45. *Nature*, 222:228–229.

Radhakrishnan, V. and Rankin, J. M. (1990). Toward an empirical theory of pulsar emission. V - On the circular polarization in pulsar radiation. *ApJ*, 352:258–266.

Rankin, J. M. (1983a). Toward an Empirical Theory of Pulsar Emission - Part Two - on the Spectral Behavior of Component Width. *ApJ*, 274:359.

Rankin, J. M. (1983b). Toward an empirical theory of pulsar emission. I Morphological taxonomy. *ApJ*, 274:333–368.

Rankin, J. M. (1986). Toward an empirical theory of pulsar emission. III - Mode changing, drifting subpulses, and pulse nulling. *ApJ*, 301:901–922.

Rankin, J. M. (1990). Toward an empirical theory of pulsar emission. IV - Geometry of the core emission region. *ApJ*, 352:247–257.

Rankin, J. M. (1993). Toward an empirical theory of pulsar emission. VI - The geometry of the conal emission region. *ApJ*, 405:285–297.

Rankin, J. M. (2015). Toward an Empirical Theory of Pulsar Emission. XI. Understanding the Orientations of Pulsar Radiation and Supernova "Kicks". *ApJ*, 804:112.

Rankin, J. M. and Ramachandran, R. (2003). Toward an Empirical Theory of Pulsar Emission. VIII. Subbeam Circulation and the Polarization-Modal Structure of Conal Beams. *ApJ*, 590:411–423.

Rees, M. J. and Trimble, V. L. (1971). Physical Sciences: Planet, Pulsar, "Glitch" and Wisp. *Nature*, 229:395–396.

Reichley, P. E. and Downs, G. S. (1969). Observed Decrease in the Periods of Pulsar PSR 0833-45. *Nature*, 222:229–230.

Roberts, D. H., Lehar, J., and Dreher, J. W. (1987). Time Series Analysis with Clean - Part One - Derivation of a Spectrum. *AJ*, 93:968.

Ruderman, M. (1969). Neutron Starquakes and Pulsar Periods. *Nature*, 223:597–598.

Ruf, T. (1999). The lomb-scargle periodogram in biological rhythm research: Analysis of incomplete and unequally spaced time-series. *Biological Rhythm Research*, 30(2):178–201.

Sarkissian, J. M., Reynolds, J. E., Hobbs, G., and Harvey-Smith, L. (2017). One Year of Monitoring the Vela Pulsar Using a Phased Array Feed. *Publications of the Astron. Soc. of Australia*, 34:e027.

Scargle, J. D. (1982). Studies in astronomical time series analysis. II - Statistical aspects of spectral analysis of unevenly spaced data. *ApJ*, 263:835–853.

Scholz, P., Spitler, L. G., Hessels, J. W. T., Chatterjee, S., Cordes, J. M., Kaspi, V. M., Wharton, R. S., Bassa, C. G., Bogdanov, S., Camilo, F., Crawford, F., Deneva, J., van Leeuwen, J., Lynch, R., Madsen, E. C., McLaughlin, M. A., Mickaliger, M., Parent, E., Patel, C., Ransom, S. M., Seymour, A., Stairs, I. H., Stappers, B. W., and Tendulkar, S. P. (2016). The repeating fast radio burst frb 121102: Multi-wavelength observations and additional bursts. *The Astrophysical Journal*, 833(2):177.

Sedrakian, A. and Cordes, J. M. (1999). Vortex-interface interactions and generation of glitches in pulsars. *MNRAS*, 307:365–375.

Shannon, R. M., Lentati, L. T., Kerr, M., Johnston, S., Hobbs, G., and Manchester, R. N. (2016). Characterizing the rotational irregularities of the Vela pulsar from 21 yr of phase-coherent timing. *MNRAS*, 459:3104–3111.

Slee, O. B., Alurkar, S. K., and Bobra, A. D. (1986). Flux densities, spectra and variability of pulsars at metre wavelengths. *Australian Journal of Physics*, 39:103–114.

Smoluchowski, R. (1970). Frequency of Pulsar Starquakes. *Physical Review Letters*, 24:923–925.

Sourie, A., Chamel, N., Novak, J., and Oertel, M. (2017). Global numerical simulations of the rise of vortex-mediated pulsar glitches in full general relativity. *MNRAS*, 464:4641–4657.

Staelin, D. H. and Reifenstein, III, E. C. (1968). Pulsating Radio Sources near the Crab Nebula. *Science*, 162:1481–1483.

Stairs, I. H., Lyne, A. G., and Shemar, S. L. (2000). Evidence for free precession in a pulsar. *Nature*, 406:484–486.

Stevenson, A., editor (2015). *Oxford English Dictionary*. Oxford University Press.

Tauris, T. M. and Konar, S. (2001). Torque decay in the pulsar (P,dot {P}) diagram. Effects of crustal ohmic dissipation and alignment. *A&A*, 376:543–552.

Tong, H. and Kou, F. F. (2017). Possible Evolution of the Pulsar Braking Index from Larger than Three to About One. *ApJ*, 837:117.

van Straten, W. and Bailes, M. (2011). DSPSR: Digital Signal Processing Software for Pulsar Astronomy. *Publications of the Astron. Soc. of Australia*, 28:1–14.

Wallace, P. T., Peterson, B. A., Murdin, P. G., Danziger, I. J., Manchester, R. N., Lyne, A. G., Goss, W. M., Smith, F. G., Disney, M. J., Hartley, K. F., Jones, D. H. P., and Wellgate, G. W. (1977). Detection of optical pulses from the VELA pulsar. *Nature*, 266:692–694.

Weisberg, J. M., Everett, J. E., Cordes, J. M., Morgan, J. J., and Brisbin, D. G. (2010). A Search for Neutron Star Precession and Interstellar Magnetic Field Variations Via Multiepoch Pulsar Polarimetry. *ApJ*, 721:1044–1055.

Weltevrede, P., Johnston, S., and Espinoza, C. M. (2011). The glitch-induced identity changes of PSR J1119-6127. *MNRAS*, 411:1917–1934.

Williams, G. A. and Packard, R. E. (1974). Photographs of Quantized Vortex Lines in Rotating He II. *Physical Review Letters*, 33:280–283.

Wright, G. A. E. (2003). An empirical model for the radio emission from pulsars. *MNRAS*, 344:1041–1056.

Yao, J. M., Manchester, R. N., and Wang, N. (2017). A New Electron-density Model for Estimation of Pulsar and FRB Distances. *ApJ*, 835:29.

Young, N. J., Stappers, B. W., Lyne, A. G., Weltevrede, P., Kramer, M., and Cognard, I. (2013). Long-term radio observations of the intermittent pulsar B1931+24. *MNRAS*, 429:2569–2580.

Zhang, F. (2017). Pulsar magnetospheric convulsions induced by an external magnetic field. *A&A*, 598:A88.

Zwierlein, M. W., Abo-Shaeer, J. R., Schirotzek, A., Schunck, C. H., and Ketterle, W. (2005). Vortices and superfluidity in a strongly interacting Fermi gas. *Nature*, 435:1047–1051.

Appendices

Appendix A

Scripts, commands, and daily flow

Running a continuing observing program is not too onerous. This appendix explains the key steps needed with the idea that others could continue regular observing using the existing scripts and software.

There are a number of basic stages:

1. Recording and glitch detection
2. Copying
3. Daily processing
4. Analysis
5. Calibration

A.1 Recording and glitch detection

Current observing practice has a `vnc` session running on `newsmerd` with one screen having four terminals, two to `hovsi` and two to `hobart`. Table A.1 on page 267 shows the useful commands and what they do. It is possible to get nearly 19 hours of data each day and it is highly desirable to achieve that if possible.

Real time glitch detection is also highly desirable so that an Astronomer's Telegram can be sent in a timely manner. This can assist the astrophysics community in general. Having a text template prepared in advance and being an authorised approver can help make telegrams timely. Glitch detection is run on one of the `hex` machines and the command is shown in Table A.1 on page 267 as well.

A.2 Copying

Currently data is recorded using `hovsi` but it directly stores the data over a dedicated network link to `sirius/mk5ce`. This is currently very reliable, but does crash once or twice a year. Turning both interfaces off and on again can usually recover from this issue without a reboot. `sirius` can hold about 4 days worth of recording before it needs to be moved to RDSI . Table A.1 on page 267 shows the `startcopying` command.

A.3 Daily processing

Regular daily attention makes the whole recording and processing chain quite efficient from a personal perspective. Letting unprocessed files get backed up is generally not a good idea for long-term observing. Each `hex` machine has 8 cores, and we found that utilising 7 of those cores for `dspsr` processing was the most efficient (due to memory constraints). For ease, we assign the 7 cores of a single hex machine for a single day's recording. This makes contention less of a problem. Also, large numbers of files are created and RDSI becomes less efficient the more files that are in a single directory.

Table A.3 on page 269 shows the commands that are available and Figure 4.3 on page 53 shows the data flow diagram. The command `show_nextcommand` is especially useful as it examines any number of daily directories and shows what command needs to be executed next. This can be redirected to a file for later bulk execution if desired.

A.4 Analysis

After the highly processor-intensive work has been completed, summary files (for example `pulsewidths.dat`, `daily.jodrell`) can be imported into R for further statistical analysis or to produce publication quality graphs and charts.

PSRCHIVE provides a suite of powerful tools for analysing pulsar archive (`.ar`) files. It also can produce publication quality graphs and charts. `psrhelp <query>` is a useful command to find how to achieve some tasks in PSRCHIVE .

A.5 Calibration

PSRCHIVE requires polarisation and flux calibration. Polarisation calibration needs to be done with every observation, whilst flux calibration can be performed every few

months. We found the most efficient method for polarisation calibration was to fire the noise diodes whilst actually observing Vela. This made file management more efficient and involved less telescope movement. Since the noise diodes are firing at 0.5 s intervals, when folded on that frequency, Vela has little effect on the calibration. Likewise, when the files are folded for Vela, the noise diodes appear as mild RFI. This method can work for small to medium telescopes but is less effective as aperture increases (Willem Van Straten, private communication).

A.6 Commands and tools

Figure A.1 and Figure A.2 on page 266 show the screens of the application `showdisplay` written to help observe the Vela pulsar and other key objects. Time can be easily changed using the arrow keys ("?" shows help) with an adjustment from years to seconds. A time with a * indicates the next day. This application is in the directory `timedisplay` on most machines.

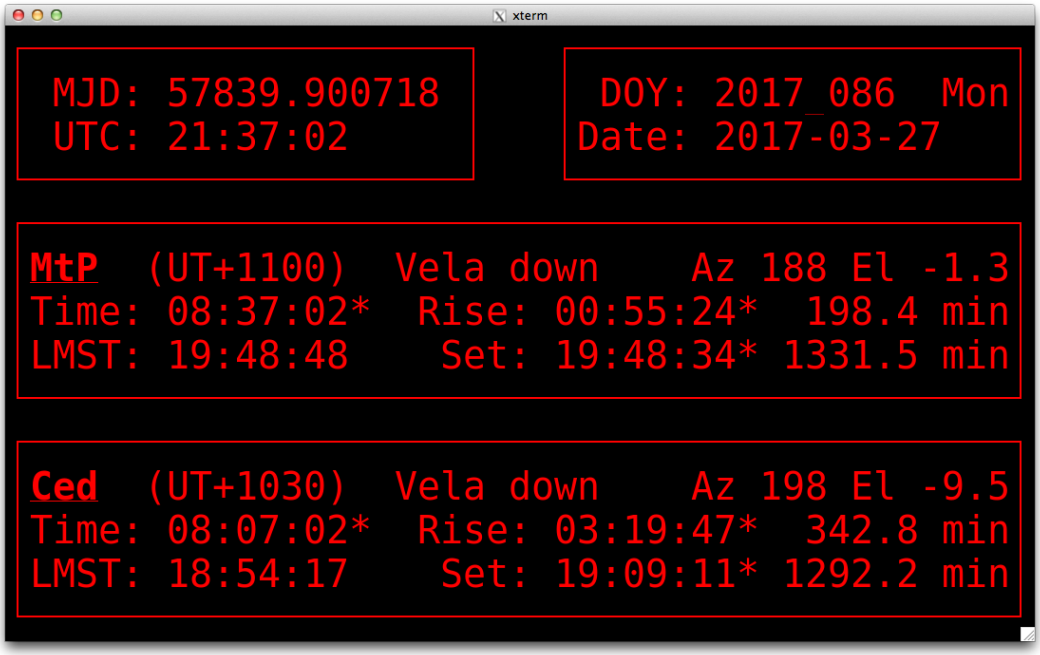

Figure A.1: Main screen of application `showdisplay`.

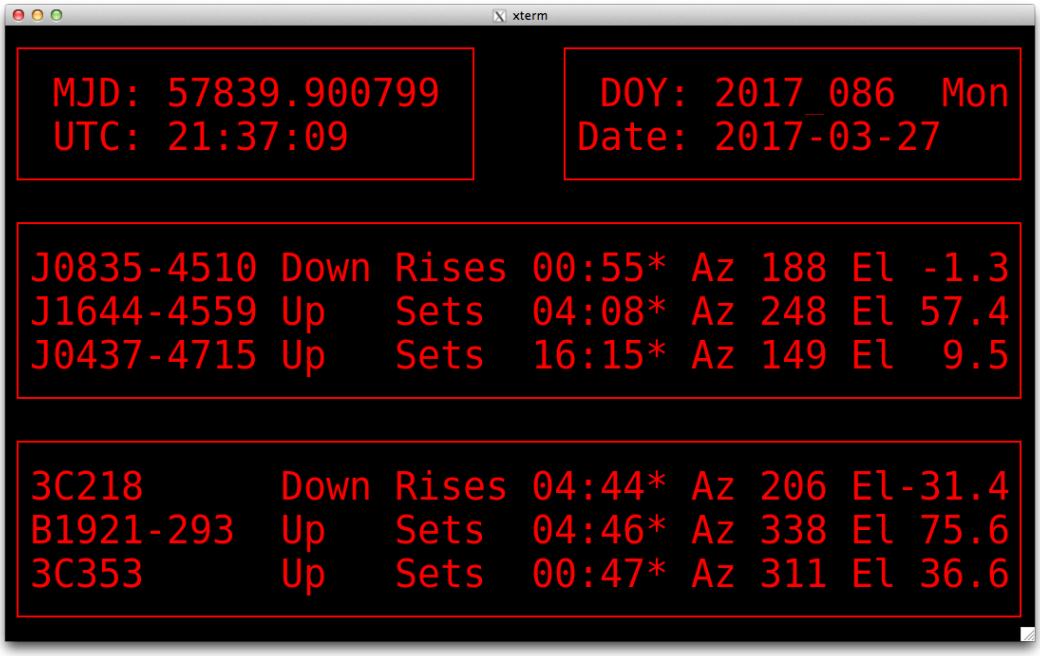

Figure A.2: Secondary screen of application `showdisplay` accessed by hitting the space-bar.

The tables below list commands and scripts that have been written for daily observation of the Vela pulsar.

Table A.1: Commands used for tracking and recording Vela in single-pulse mode.

Command with typical use	Machine	Description
`./velars -r -d`	many	Computes accurate rise/set times for Vela at the appropriate telescope. Will also sleep for the next rise/set event. Used by many scripts.
`~/jimp/track vel15333`	hobart	Waits for 15 min prior to rise, moves the telescope to the rise point and waits for Vela to rise. Then it tracks by issuing regular `onsource` commands to the Field System. If Vela is up it moves straight to it. The parameter is the Field System log file name. Is killed by `stow`.
`~/jimp/stow set`	hobart	Sleeps until Vela sets and then issues the stow command to park the telescope. Also kills `track`. "`set`" can be replaced with an hour and minute until end of observation.
`~/jimp/record 2015_333 1376 set`	hovsi	Waits until the next rise (or begins immediately if Vela is up) and then starts `vsib_record` with the appropriate parameters. Once Vela sets it will stop and kill `agc`.
`~/jimp/agc 2015_333 1376`	hovsi	Runs the 5 minute automatic gain control which checks the recorded files. Is killed when `record` finishes.
`at -f ~/jimp/fire_cal 12:00`	newsmerd	Fires the noise diode during an observation. Records date and time in logfile `~/jimp/cal.log`. Should be performed at some point during every observation.
`/exports/sirius_internal16/pulsar/startcopying_all`	sirius	Every 15 min this script copies recorded files from `sirius` to RDSI.
`~/glitch/check_glitch_15m`	hex4	Every 15 min this script copies a recent `.lba` file from `hovsi`, processes it, and returns a residual. Also sends an email and a text.

Table A.2: Commands used for tracking and recording other key pulsars.

Command with typical use	Machine	Description
`~/jimp/track_J0437`	hobart	Moves the telescope to J0437−4715. This command is killed by `stow`.
`~/jimp/record_J0437_nowait 2015_333 1376 1h`	hovsi	Immediately commence recording in *non single-pulse* mode by using `vsib_record` with the appropriate parameters. Once the indicated time has passed it will stop and kill `agc`. Note that with time, only hours, minute, or seconds can be used; not combinations.
`~/jimp/agc_J0437_nowait 2015_333 1376`	hovsi	Immediately runs the 5 minute automatic gain control which checks the levels of the recorded files. Is killed when `record` finishes.
`~/jimp/track_J1644`	hobart	Moves the telescope to J1644−4559. This command is killed by `stow`.
`~/jimp/record_J1644_nowait 2015_333 1376 1h`	hovsi	Immediately commence recording in *single-pulse* mode by using `vsib_record` with the appropriate parameters. Once the indicated time has passed it will stop and kill `agc`. Note that with time, only hours, minute, or seconds can be used; not combinations.
`~/jimp/agc_J1644_nowait 2015_333 1376`	hovsi	Immediately runs the 5 minute automatic gain control which checks the levels of the recorded files. Is killed when `record` finishes.
`~/jimp/stow 1h 15m`	hobart	Sleeps until the provided time has passed and then issues the stow command to park the telescope. Also kills `track`. When used with pulsars other than Vela, the "set" option should not be used (since that is for Vela only).

Table A.3: Commands used for processing and analysing recorded files. Commands starting with '`./`' reside in `/imports/pulsar/processing/MTP26M/J0835−4510_S`. All commands are run on `hex0-hexb`. If the example shows a wildcard directory then the command accepts wildcards, otherwise it doesn't.

Command with typical use	Description
`~/startpulsar hexb 7`	Starts up `dspsr` processing. Should be run from /imports/pulsar/processing/MTP26M/hexb/J0835−4510_S which should have a `2015_333` directory in it. Creates `.ar` files.
`./show_nextcommand 2015_3*/1376`	Shows the next command in the regular chain that needs to be executed. Can be sent to a file for running as a script if needed.
`./create_ft 2015_333/1376`	Takes each 10 s `.ar` file and creates a `.ft` file which is fully folded in time, frequency, and polarisation. Used for arrival time processing.
`./create_alltim 2015_333/1376`	Takes each 10 s `.ft` files and creates a single `.tim` file which has arrival times of each of the 10 s files.
`./create_tempo2files 2015_333/1376`	Takes the `.tim` file and starts up TEMPO2 for removal of bad data. The daily ephemeris needs to be output to `today.par` and the good timing data should be exported to `fixed.tim`.
`./create_today 2015_333/1376`	Takes the `today.par` file and uses it to line up and integrate all the good pulses (selected from `fixed.tim`) into a single profile for the day. This file is called `today.ft`. Also create `goodfiles` which lists filenames with good data in them.
`./create_pulsewidths`	Takes all the `today.ft` files and produces `pulsewidths.dat` which has the 10% and 50% pulse widths.
`./create_spa 2015_333/1376`	Takes each 10 s `.ar` file and creates `all.spa` which shows the relative flux level of every single pulse. Also installs recently created `today.par` ephemeris in all `.ar` files.
`./create_giant30_all 2015_333/1376`	Scans the `all.spa` file and `goodfiles` and creates a `png.sh` file which has a line for each giant pulse. These lines are commands for generating an image of the 10 s file.
`./create_giant30png 2015_333/1376`	Executes the `png.sh` file and creates a directory with images of all giant pulses.
`./create_verifiedgiant30 2015_333/1376`	Execute a simple graphics program to allow you to view and remove bad giants from the list.

Table A.4: Commands used for exceptional processing of recorded files. These are used for analysis of all pulses in a day. Commands starting with '`./`' reside in `/imports/pulsar/processing/MTP26M/J0835−4510_S`. All commands are run on `hex0-hexb`. If the example shows a wildcard directory then the command accepts wildcards, otherwise it doesn't.

Command with typical use	Description
`./create_pngsh_all 2015_333/1376`	Creates a `pngall.sh` file with commands to create an image of *all* `.ar` files.
`./create_png_all 2015_333/1376`	Executes the `pngall.sh` and creates a directory with images of all pulses.
`./create_verifiedall 2015_333/1376`	Execute a simple graphics program to allow you to view and remove files with RFI.

Table A.5: Miscellaneous commands used for recorded files. Commands starting with '`./`' reside in `/imports/pulsar/processing/MTP26M/J0835−4510_S`. All commands are run on `hex0-hexb`. If the example shows a wildcard directory then the command accepts wildcards, otherwise it doesn't.

Command with typical use	Description
`./show_processing`	Shows the current status of all `dspsr` processing.
`./show_stats 2015_3*/1376`	Prints a one line summary for each day of recording. Each night a `cron` job of this command is run for all data. This is stored in `./allstats`.
`./create_raw 2015_333/1376`	Moves all `.lba` and other miscellaneous processing files to the `raw` directory. Keeps things neat and is essential prior to `./create_raw.keep` being executed.
`./create_raw.keep 2015_333/1376`	Moves all "interesting" `.lba` files from `raw` to the `raw.keep` directory. The `rm` command to then delete the files in `raw` is shown for cut and paste to the command line. This is used to recover disk space. Bright pulse, consecutive bright pulse, and unprocessed `.lba` files are kept for further processing if required. Use `rm` command with care.
`./create_ar 2015_27*/*`	Moves all `.ar` files to the `ar` directory. This prevents the observing directory from being cluttered and also helps RDSI manage their storage. This should be run after all other processing has been completed. If it is re-run on a directory no damage is done.
`./create_daily`	Gathers the arrival times of all daily integrated pulses from `today.ft` files and outputs them to the timing file `daily.tim`. This has very low signal-to-noise and is excellent for showing Vela's timing residuals over time.
`./show_daily`	Starts TEMPO2 using `daily.tim` to show timing residuals. Output to `daily.jodrell` using the `ctrl-J` option is useful if desired.
`./show_tempo2 2015_333/1376`	Starts TEMPO2 using `fixed.tim`. Used to re-examine timing residuals on a day after `./create_tempo2files` has already been run.

Table A.6: Key files used in the pulsar archive. Each file is listed as relative from its observing directory. For example, `2015_333/1376`

File	Description
`spa/all.spa`	A list of peak flux densities in `spa` format of *all* pulses recorded for the observing session.
`spa/giant30_all`	An empty file to indicate processing status. Ignore.
`spa/giant30.spa`	A list in `spa` format of all pulses with a peak flux density greater than 10.
`spa/goodfiles.ar`	A list of `.ar` files that have good timings.
`spa/mavg`	A moving average of peak flux density of 100 pulses for the day's observing.
`spa/mavg.png`	A plot of `mavg`.
`spa/goodfiles.spa`	A list of individual pulses in `spa` format of all files that have good timings.
`spa/confirmed.ar`	A list of `.ar` files that contain pulses brighter than 10 (on the relative scale) and have been verified as genuine by hand.
`spa/confirmed.spa`	Verified bright pulses contained in the file `spa/confirmed.ar` listed in `spa` format.
`spa/confirmedall.ar`	A list of `.ar` files that have been verified as RFI free by hand.
`spa/confirmedall.spa`	Pulses contained in the file `spa/confirmedall.ar` listed in `spa` format.
`timing/all.tim`	Timings of every 10 s file for a day's observing.
`timing/fixed.tim`	Timings of every 10 s file for a day's observing that were good.
`timing/goodfiles`	Filenames of every 10 s file for a day's observing that were good.
`timing/today.ft`	Integrated pulse profile of the entire day's observing.
`timing/today.par`	Fitted ephemeris of the day's observing.

Appendix B

Data recording notes and summary

Reproduced here are summary tables of data that has been recorded with Table B.1 on page 274 describing the headings used. Table B.2 on page 275 shows a summary of historical data that was recorded from 2007-2010. We reprocessed this historical data using the scripts developed for this work. Table B.3 on page 278 shows the data that was captured for this project.[§]

[§]The formatting of these tables was completed using the R package *stargazer* (Hlavac 2015).

Table B.1: Headings for data recording summary

Heading	Description
year	Year of observation
doy	Day of year of observation.
freq	Frequency of observation in MHz.
mjd	Modified Julian Date.
ar_files	Number of `.ar` files.
raw_keep	Number of kept `.lba` files in raw.keep directory. These will be unprocessed baseband files of interesting events. Files with high flux density pulses are kept, so files during AGC failure sometimes were inadvertently retained.
timings	Number of timing files in `timing` directory. Should match number of `.ar` files. This will not be the case if timings are not possible on individual files - such as at higher frequencies.
good_tim	Number of "good" timing files after bad residuals have been removed.
all_spa	Number of pulses.
good_spa	Number of pulses in "good" timing files.
g30_unv	Number of bright pulses selected by the algorithm (peak flux density > 10). Unverified.
g30_ver	Number of verified bright pulses, i.e. with RFI removed.
bp_hr	Number of bright pulses per hour. Based on g30_ver figure.
g30_sel	Number of bright pulses that we selected as "interesting".
spa_unv	Number of pulses in "good" timing files detected as "bright" by `spa` program (mean flux density > 5).
spa_avg	Average peak flux density level of all files.
pcal	Time of polarisation calibration. If there is more than one then a "+" is appended. Full details will be in the file, for example, `2017_001/1376/cal`
Notes	Any notes added on the day or during processing.

Table B.2: Historical data recording summary - 2007-2010

year	doy	freq	mjd	ar_files	raw_keep	timings	good_tim	all_spa	good_spa	g30_unv	g30_ver	bp_hr	g30_sel	spa_unv	spa_avg	pcal	notes
2007	120	1440	54222	841		841	841	93224	93224	8	8	3	0	135	6.069		
2007	252	2250	54354	1267		1267	1267						0				
2007	255	2250	54357	2072		2072	1438	239					0		3.361		
2007	294	1440	54396	720		720	720	79724	79724	2	2	1	0	332	3.096		
2007	298	4800	54400	720		720	720						0				
2007	304	8400	54406	673		673	586						0				
2007	312	4800	54414	641		641							0				
2007	316	4800	54418	1800		1800							0				
2007	324	1420	54426	1446		1446	1446						0				
2007	337	4800	54439	549		549							0				
2007	340	4800	54442	1799		1799							0				
2007	344	1440	54446	360		360	360	39862	39862	14	14	14	0	230	3.260		
2007	344	4800	54446	1044		1044							0				
2007	352	1440	54454	807		807	774	89159	85500	15	14	6	0	525	3.476		
2007	353	1440	54455	720		720	720	79712	79712	9	9	4	0	394	3.102		
2007	353	4800	54455	908		908							0				
2008	28	1440	54495	1353	0	1353	1344	149704	148710	9	9	2	0	281	2.942		
2008	34	1440	54501	1203		1203	1203	133124	133124	15	15	4	0	773	3.440		
2008	34	2285	54501	1441		1441							0				
2008	41	1440	54508	617		617	615	68219	67998	12	12	7	0	373	3.273		
2008	55	1440	54522	2160		2160	2110	239125	233592	16	16	2	0	0	3.294		
2008	62	1440	54529	1439		1439	1439	159298	159298	29	29	7	0	1009	3.524		
2008	76	4800	54543	2382		2382	2362	264072					0		2.046		
2008	83	4800	54550	2880		2880							0				
2008	104	1440	54571	90		90	90	9965	9965	2	2	8	0	88	3.956		
2008	104	4800	54571	1800		1800							0				
2008	111	4800	54578	2160		2160							0				
2008	118	4800	54585	2051		2051							0				
2008	118	9999	54585	7		7							0				
2008	125	4800	54592	1440		1440							0				
2008	132	1440	54599	720		720	720	79703	79703	5	5	2	0	436	3.187		
2008	139	4800	54606	1081		1081							0				
2008	146	1440	54613	300		300	300	33210	33210	1	1	1	0	368	3.416		

Continued on next page...

Table B.2: Historical data recording summary - 2007-2010 (continued)

year	doy	freq	mjd	ar_files	raw_keep	timings	good_tim	all_spa	good_spa	g30_unv	g30_ver	bp_hr	g30_sel	spa_unv	spa_avg	pcal	notes
2008	146	4800	54613	1440		1440							0				
2008	153	4800	54620	693		693							0				
2008	167	4800	54634	2160		2160							0				
2008	181	1440	54648	1993		1993	1993	220624	220624	0	0	0	0	0	3.221		
2008	188	1440	54655	1440		1440	1438	159407	159186	26	24	6	0	1111	3.383		
2008	230	1440	54697	1438		1438	1436	160788	160565	0	0	0	0	147	2.096		Pulse shape looks wrong.
2008	237	1440	54704	1084		1084	1080	121206	120759	0	0	0	0	106	2.042		Pulse shape looks wrong.
2008	251	4800	54718	563		563							0				
2008	291	1440	54758	1020		1020	1020	114028	114028	0	0	0	0	169	1.960		Pulse shape looks wrong.
2008	307	1440	54774	360		360							0				No onsource data
2009	18	4800	54850	2160		2160	2160	241712	0	0	0		0	0	1.800		
2009	53	1440	54885	2160		2160	1498	241512	167491	0	0	0	0	59	1.882		AGC not brilliant
2009	151	1440	54983	1440		1440	1440	160998	160998	0	0	0	0	59	1.902		AGC not brilliant
2009	159	1440	54991	1798		1798	428	199795	47978	0	0	0	0	47647	0.479		Bad AGC day
2009	214	1440	55046	1439		1439	1439	160892	160892	42	42	10	2	1333	3.373		
2009	224	1440	55056	360		360	359	40251	40140	1	1	0	0	174	2.501		
2009	300	1440	55132	720		720	720	80505	80505	2	2	0	0	230	2.775		
2009	350	1440	55182	3393		3393	3391	379214	378992	64	63	6	0	2592	3.304		
2009	351	1440	55183	4968		4968	4820	554910	538889	87	86	6	0	6303	3.450		
2009	352	1440	55184	3861		3861	3854	431461	430771	65	64	5	0	7313	3.528		
2009	353	1440	55185	5667		5667	5668	633406	633406	83	82	5	0	6244	3.342		
2009	354	1440	55186	5570		5570	5569	622711	622600	0	0	0	0	5172	3.072		
2009	355	1440	55187	5059		5059	5059	565585	565585	61	60	4	0	3150	3.073		
2009	356	1440	55188	5127		5127	5126	573145	573033	73	73	5	0	3133	3.146		
2009	358	1440	55190	5218		5218	5217	583280	583168	76	76	5	0	3479	3.201		
2010	58	1440	55255	1079		1079	1079	120639	120639	11	11	3	0	611	3.200		
2010	66	1440	55263	969		969	969	108251	108251	6	6	2	0	552	3.101		
2010	107	1440	55304	582		582	577	64170	63907	5	5	3	0	265	2.933		
2010	184	1440	55381	1440		1440							0				Weird data - no good
2010	212	8400	55409	1439		1439	1274	161013					0		2.222		
2010	216	1440	55413	2159		2159	2161	241095	241095	35	34	5	0	2203	3.861		
2010	226	1440	55423	1478		1478	1296	147843	133204	0	0	0	0	7105	34.702		Some bad rfi issues
2010	236	1440	55433	1276		1276	719	125923	80385	9	6	2	0	312	3.718		Some bad rfi issues

Continued on next page...

Table B.2: Historical data recording summary - 2007-2010 (continued)

year	doy	freq	mjd	ar_files	raw_keep	timings	good_tim	all_spa	good_spa	g30_unv	g30_ver	bp_hr	g30_sel	spa_unv	spa_avg	pcal	notes
2010	240	1440	55437	1440		1440	1334	160992	149144	30	30	8	0	1505	3.735		
2010	275	1440	55472	1440		1440	1423	160983	159085	40	32	8	0	1128	3.911		
2010	278	1440	55475	1797		1797	974	200915	108898	35	35	12	0	160	8.395		AGC bad for half the session
2010	287	1390	55484	1078		1078							0				
2010	310	2285	55507	1435		1435							0				
2010	334	1390	55531	1080		1080							0				
2010	334	1440	55531	635		635	635	70997	70997	9	9	5	0	406	3.409		
2010	341	1390	55538	2206		2206							0				
2010	347	1390	55544	1276		1276							0				

Table B.3: Data recording summary 2014-2017

year	doy	freq	mjd	ar_files	raw_keep	timings	good_tim	all_spa	good_spa	g30_unv	g30_ver	bp_hr	g30_sel	spa_unv	spa_avg	pcal	notes
2014	63	1390	56720	3960	2	3960		442704					0		4.111		
2014	65	1390	56722	2880	4	2880		321867					0		4.592		
2014	66	1390	56723	3600	5	3600		402461					0		4.494		
2014	67	1390	56724	4	0	4		447					0		4.183		
2014	72	1340	56729	6		6		670					0		3.868		
2014	72	1390	56729	192		192		21463					0		3.381		
2014	73	1390	56730	5046	76	5046		564000					0		3.646		
2014	74	1390	56731	3316	28	4412		370704					0		3.868		
2014	75	1390	56732	3600		3600		402447					0		3.891		
2014	79	1390	56736	3599		3600		402288					0		13.773		Very noisy, some failed .lba files - just deleted
2014	80	1390	56737	5196		5225		580937					0		12.939		Very noisy, some failed .lba files - just deleted
2014	81	1390	56738	2876		2880		321503					0		18.031		Very noisy, some failed .lba files - just deleted
2014	82	1390	56739	3771		3960		421580					0		15.519		Very noisy, some failed .lba files - just deleted
2014	83	1390	56740	2191		2252		244928					0		20.897		Very noisy, some failed .lba files - just deleted
2014	84	1390	56741	3244		3246		362659					0		15.209		Very noisy, some failed .lba files - just deleted
2014	85	1390	56742	66		66		7374					0		4.733		
2014	87	1352	56744	12		12		1342					0		3.510		
2014	87	1376	56744	4691	11	4692	4691	524153	524153	62	62	4	0	3613	3.965		
2014	87	1390	56744	0		0		0					0		0		
2014	88	1376	56745	3960	4	3960	3960	442471	0	0	0		0	0	3.903		
2014	89	1376	56746	2269	0	2316	2269	253546	253546	69	69	10	0	1860	3.738		
2014	90	1376	56747	2863	3	2865	2863	319823	319823	39	39	4	0	2120	3.549		12:54:49, 16:02:49, 14:44:09 are all interesting.
2014	91	1376	56748	5060		5061	3636	565167	406274	54	54	5	0	4080	3.144		
2014	92	1376	56749	3234	9	3234	3234	361329	361329	46	46	5	0	2360	3.436		
2014	94	1376	56751	4332	47	4332	4332	484033	484033	85	85	7	0	3163	3.749		
2014	95	1376	56752	2324	2	2394	2297	256672	256571	36	36	5	0	1757	3.885		

Continued on next page...

Table B.3: Data recording summary 2014-2017 (continued)

year	doy	freq	mjd	ar_files	raw_keep	timings	good_tim	all_spa	good_spa	g30_unv	g30_ver	bp_hr	g30_sel	spa_unv	spa_avg	pcal	notes
2014	101	1376	56758	5406	50	5406	5406	604037	604037	182	182	12	1	4883	4.639		Some very nice bright pulses.
2014	101	8415	56758	2									0				
2014	102	1376	56759	1806	23	1806	1806	201789	201789	27	27	5	0	1631	4.619		
2014	103	1376	56760	4686	57	4686	4686	523585	523585	133	133	10	3	4397	4.933		11:52:59 and 13:45:49 has 5 in a row.
2014	104	1376	56761	5383	87	5385	5382	601668	601333	137	136	9	0	4748	4.955		
2014	105	1376	56762	3551	81	3594	3551	401564	396757	63	63	6	1	3148	4.884		Peak of 107 (08:55:39) - check.
2014	106	1376	56763	5773	76	5774	5773	645148	645036	148	148	9	1	4744	4.800		Peak of 110 04:17:35 - check. 02:38:35, 09:19:35, 06:04:45 - 5 in a row.
2014	107	1376	56764	2159	18	2159	2159	241219	241219	49	49	8	1	1635	4.695		
2014	108	1376	56765	3247	11	3247	3247	362795	362795	52	52	5	0	2561	4.490		
2014	109	1376	56766	2158	10	2158	2158	241020	241020	47	46	7	0	1577	4.350		
2014	110	1376	56767	3606	19	3606	3606	402914	402914	60	60	5	2	2575	4.566		
2014	113	1376	56770	3929	57	3930	3927	439109	438774	60	60	5	1	3240	4.844		
2014	119	1376	56776	4281	144	4322	4280	482912	478221	71	71	5	2	3750	5.113		Peak of 80 and 4 in a row. 12:57:22
2014	121	1376	56778	4326	118	4326	4326	483358	483358	73	73	6	0	4162	4.930		
2014	122	1376	56779	3606	124	3606	3606	402907	402907	68	68	6	0	3131	4.888		
2014	123	1376	56780	647		2520	647	72290	72290	15	15	8	0	609	5.280		
2014	163	1376	56820	6		6	6	670	670	0	0	0	0	5	3.184		
2014	165	1376	56822	360		360	360	40224	40224	9	9	8	0	340	3.819		
2014	166	1376	56823	4687	60	4687	4687	523689	523689	72	72	5	0	3669	3.595		
2014	167	1376	56824	9985	75	11685	9985	1115641	1115641	215	209	7	0	8435	3.616		
2014	169	1376	56826	5332	114	5333	5332	595609	595609	62	59	3	0	5673	3.830		Bad RFI?
2014	170	1376	56827	9346	71	9360	9346	1044246	1044246	260	246	9	0	9109	3.788		Bad RFI?
2014	171	1376	56828	5418	59	5419	5418	605325	605325	24	23	1	0	5912	3.872		Bad RFI?
2014	173	1376	56830	9362	128	10448	9362	1046004	1046004	90	88	3	0	8826	3.751		Base levels high sometimes (e.g. 00:12:58). OOB RFI?
2014	174	1376	56831	503	3	2173	503	56202	56202	13	13	9	0	433	3.772		
2014	175	1376	56832	5183	283	6770	5175	578230	578222	90	90	6	0	2603	4.733		Swapped servos in channels around 00:00 (see log to work out times)
2014	176	1376	56833	508	9	2615	508	56760	56760	5	5	3	0	324	3.719		
2014	178	1376	56835	6468	383	7560	6468	722691	722691	1	1	0	0	2416	5.018		
2014	179	1376	56836	4933	147	6120	4933	551173	551173	31	31	2	0	1923	4.630		
2014	180	1376	56837	5981	498	6120	5981	668273	668273	97	97	5	0	2982	4.914		

Continued on next page...

Table B.3: Data recording summary 2014-2017 (continued)

year	doy	freq	mjd	ar_files	raw_keep	timings	good_tim	all_spa	good_spa	g30_unv	g30_ver	bp_hr	g30_sel	spa_unv	spa_avg	pcal	notes
2014	181	1376	56838	2992	405	3057	1365	262760	152512	7	7	1	0	6374	2.219		
2014	183	1376	56840	3	0	3	3	268	268	0	0	0	0	2	3.855		
2014	184	1376	56841	8371	821	9364	8371	935279	935279	18	18	0	0	3075	5.476		
2014	186	1376	56843	7809	899	7902	7809	872491	872491	2	2	0	0	2833	5.492		
2014	187	1376	56844	5156	655	5272	5156	576023	576023	121	121	8	0	1982	5.340		
2014	190	1376	56847	3158	23	3158	3158	352853	352853	0	0	0	0	1606	4.177		
2014	191	1376	56848	7768	369	8100	6216	867943	694534	3	3	0	0	4771	4.283		
2014	192	1376	56849	6120	391	6120	6015	683809	672077	3	2	0	0	4465	5.217		
2014	193	1376	56850	6120	336	6120	6107	683805	682352	68	66	3	0	2546	4.649		
2014	194	1376	56851	2560	119	2560	2441	285958	272739	28	28	4	0	2054	4.017		
2014	195	1376	56852	2880	212	2880	2880	321791	321791	20	20	2	0	743	5.362		
2014	196	1376	56853	6120	193	6120	6097	683809	681239	53	51	2	0	2729	4.574		
2014	197	1376	56854	1080	1	1080	1080	120670	120670	1	1	0	0	658	3.623		
2014	198	1376	56855	2766	24	2766	2765	308980	308868	63	58	7	0	2357	4.053		
2014	199	1376	56856	6660	133	6660	5936	744144	663252	106	103	6	0	4173	4.649		
2014	200	1376	56857	6120	116	6120	6118	683813	683590	53	48	2	0	3815	4.879		
2014	201	1376	56858	6120	207	6120	6072	683809	678443	111	95	5	0	3796	4.726		
2014	202	1376	56859	3664	134	3664	3610	409359	403328	62	54	5	0	3597	4.134		
2014	203	1376	56860	8010	51	8010	8010	894968	894968	5	5	0	0	2746	4.605		
2014	204	1376	56861	1962	9	1962	1961	219151	219040	10	8	1	0	1774	3.309		
2014	205	1376	56862	4079	101	4079	48	455717	5368	2	2	14	0	69	4.345		
2014	206	1376	56863	4680	14	4680	71	522932	7938	1	1	5	0	30	3.939		re-run check_ft. Maser lost lock from MJD 56864.078125-56866.01171875
2014	207	1376	56864	4596	3	4596	4595	513553	0	0	0		0	0	3.903		Maser lost lock from MJD 56864.078125-56866.01171875
2014	208	1376	56865	6120	21	6120	2241	683787	54529	1	1	0	0	630	2.771		Maser lost lock from MJD 56864.078125-56866.01171875
2014	209	1376	56866	6120	8	6120	1283	683834	143361	2	2	0	0	6715	2.404		Very few bright or multiples.
2014	210	1376	56867	2915	10	2915	0	325634	0	0	0		0	0	2.002		Windstowed all day.
2014	212	1376	56869	7885	64	7885	4099	881067	457929	11	2	0	0	5935	2.851		Extra wide profile today. Why?
2014	213	1376	56870	8412	89	8412	7997	939922	893547	7	1	0	0	3656	3.959		
2014	214	1376	56871	6120	84	6120	5093	683790	569037	11	3	0	0	3087	3.759		
2014	215	1376	56872	4467	26	4467	3492	498323	390167	3	3	0	0	3345	3.434		

Continued on next page...

Table B.3: Data recording summary 2014-2017 (continued)

year	doy	freq	mjd	ar_files	raw_keep	timings	good_tim	all_spa	good_spa	g30_unv	g30_ver	bp_hr	g30_sel	spa_unv	spa_avg	pcal	notes
2014	217	1376	56874	8549	20	8549	2430	955211	271521	0	0	0	0	8105	2.909		
2014	218	1376	56875	2447	45	2447	2432	273340	271666	5	5	0	0	1416	4.496		
2014	219	1376	56876	4166	856	4166	4042	465411	451556	21	14	1	0	4261	6.114		Set auto agc to wrong dir. Channel 1 headed badly low from about 17:08 UTC. First attempt at zenith recording.
2014	220	1376	56877	8184	45	8184	6322	914446	706394	3	2	0	0	5029	3.800		
2014	221	1376	56878	6120	40	6120	5108	683821	570748	0	0	0	0	2869	3.930		
2014	222	1376	56879	6120	128	6120	5707	683825	637680	13	5	0	0	2694	3.995		
2014	223	1376	56880	6120	119	6120	4977	683815	556103	9	0	0	0	2470	3.707		
2014	224	1376	56881	2549	21	2549	2549	284739	284739	4	3	0	0	1676	3.732		
2014	225	1376	56882	3158	8	3158	3157	352825	352713	4	1	0	0	1815	3.497		
2014	227	1376	56884	2209	37	2209	2203	246821	246151	4	0	0	0	3055	3.329		
2014	228	1376	56885	4680	4	4680	4680	522933	522933	3	3	0	0	2251	2.911		
2014	229	1376	56886	7390	60	7390	7350	825704	821237	20	3	0	0	4726	3.035		
2014	230	1376	56887	2880	111	2880	2867	321841	320390	14	1	0	0	6993	4.070		
2014	232	1376	56889	6058	154	6058	5991	675656	669334	14	9	0	0	1813	9.265		
2014	234	1376	56891	3600	5	3600	3600	402251	402251	7	7	0	0	1935	3.196		Majestic 6 in a row at 02:25:25. Sextuple.ar shows surrounding 30 sec
2014	235	1376	56892	4320	1	4320	4318	482697	482474	3	3	0	0	2250	3.117		
2014	237	1376	56894	5611	27	5611	5587	626837	624155	19	9	0	0	4232	3.234		17:47:40 - very active.
2014	238	1376	56895	569	0	569	568	63555	63467	0	0	0	0	245	4.924		
2014	239	1376	56896	3354	0	3354	3346	374649	373753	6	0	0	0	1565	5.275		00:30:37 - weird timing - check.
2014	240	1376	56897	6120	419	6120	6101	683833	681710	0	0	0	0	5173	4.745		Direct/crossed flipped for 20sec 02-04 on day 241. 05:42:00 on 241, some interference occurred.
2014	241	1376	56898	6120	246	6120	6120	683835	683835	1	0	0	0	3598	4.535		
2014	242	1376	56899	5421	632	5421	5169	605669	577509	104	0	0	0	39815	10.306		Dodgy RFI in afternoon - Utas open day. raw.keep only partially done
2014	243	1376	56900	3594	198	3594	3552	401584	396891	21	21	2	0	1139	49.511		raw.keep partially done.
2014	245	1376	56902	6540	426	6540	6031	730766	673890	38	15	0	0	4983	4.318		
2014	246	1376	56903	5936	317	5936	5866	663191	655373	0	0	0	0	7264	4.871		
2014	247	1376	56904	4713	120	4713	4687	526439	523534	19	8	0	0	4927	3.921		2014-09-04-16:01:40.ar - drifting subpulse pattern!

Continued on next page...

Table B.3: Data recording summary 2014-2017 (continued)

year	doy	freq	mjd	ar_files	raw_keep	timings	good_tim	all_spa	good_spa	g30_unv	g30_ver	bp_hr	g30_sel	spa_unv	spa_avg	pcal	notes
2014	248	1376	56905	6014	226	6014	6006	671919	671024	2	0	0	0	2473	4.631		
2014	249	1376	56906	6120	440	6120	5996	683836	669980	29	18	1	0	3056	4.516		
2014	250	1376	56907	4100	54	4100	4097	458051	457717	5	5	0	1	3243	3.965		02:27:26.ar strange line
2014	251	1376	56908	8070	180	8070	6020	901718	672654	0	0	0	0	6138	3.915		
2014	252	1376	56909	6120	101	6120	4755	683839	531313	0	0	0	0	7535	3.578		
2014	253	1376	56910	4172	71	4172	4008	466174	447850	6	5	0	0	2833	3.645		2014-09-10-18:10:48 (4 con) and 29:48 (5 con!)
2014	254	1376	56911	2976	121	2976	2917	332535	325938	11	0	0	0	1968	3.920		
2014	255	1376	56912	2115	17	2115	2107	236254	235359	8	0	0	0	1684	3.150		
2014	256	1376	56913	9583	6	9583	9540	1070071	1065808	4	3	0	0	5680	2.297		
2014	257	1376	56914	3426	19	3426	3353	382821	374664	18	2	0	0	1142	2.298		
2014	259	1376	56916	6300	49	6300	6077	703952	679034	29	29	1	0	5749	3.638		Check out 2014-09-17-06:57:49.ar
2014	260	1376	56917	4493	111	4493	4439	502038	496007	27	13	1	0	2830	3.508		check 19:30:23
2014	266	1376	56923	2211	1	2211	1430	246972	159754	2	0	0	0	804	3.210		Mostly weird double pulse files??? Hovsi/sirius link issues?
2014	267	1376	56924	4171	23	4171	4038	466074	451209	32	32	2	0	3002	3.469		Mostly weird double pulse files??? Hovsi/sirius link issues?
2014	268	1376	56925	67		67							0				Mostly weird double pulse files??? Hovsi/sirius link issues? Not bothering for timing.
2014	269	1376	56926	7920	43	7920	7917	884987	884652	95	89	4	0	6480	3.684		Faulty link fixed.
2014	270	1376	56927	6120	6	6120	3725	683857	416226	48	48	4	0	4722	3.151		
2014	271	1376	56928	1142		1142							0				Wind stowed all day - raw files deleted. .ar files can be deleted if needed.
2014	273	1376	56930	1380	1	1380	1192	154202	133193	14	14	4	0	1044	3.715		pcal was very noisy - levels stuffed?
2014	275	1376	56932	5568	58	5568	5559	621978	621085	134	133	8	0	5996	4.640		pcal was very noisy - levels stuffed?
2014	276	1376	56933	1080	17	1080	1074	120680	120008	24	24	7	0	1023	4.732		
2014	277	1376	56934	2160	15	2160	2160	241357	241357	42	42	6	0	2739	4.890		
2014	278	1376	56935	6118	54	6118	4584	683536	512129	137	135	10	0	7189	4.072		
2014	279	1376	56936	3567	17	3567	1860	398571	207831	65	65	12	0	4749	3.314		
2014	281	1376	56938	2520	89	2520	2464	281589	275329	44	34	4	0	2968	4.146		
2014	282	1376	56939	4239	51	4239	4239	473571	473571	145	127	10	0	6437	3.897		

Continued on next page...

Table B.3: Data recording summary 2014-2017 (continued)

year	doy	freq	mjd	ar_files	raw_keep	timings	good_tim	all_spa	good_spa	g30_unv	g30_ver	bp_hr	g30_sel	spa_unv	spa_avg	pcal	notes
2014	284	1376	56941	6826	6	6826	6247	762739	698041	165	165	9	0	6335	3.531		2014-10-11-21:36:30.ar has a weird mini-jump - caused by stopping vsib_record
2014	285	1376	56942	6120	7	6120	5671	683856	633684	155	155	9	0	6170	3.626		
2014	286	1376	56943	4841	47	4841	4678	540899	522722	148	141	10	0	6351	3.918		
2014	287	1376	56944	6084	23	6084	5896	679781	658774	248	243	14	0	6827	3.941		02:36:45 four bright pulses, two >60!
2014	290	1376	56947	6690	49	6690	6686	747546	747098	235	232	12	0	7526	4.090		
2014	291	1376	56948	6114	14	6114	6097	683090	681192	193	192	11	0	6734	4.105		
2014	292	1376	56949	6120	38	6120	5826	683847	650996	180	180	11	0	6755	4.036		
2014	293	1376	56950	5888	13	5888	5161	657825	576693	210	209	14	3	6595	3.900		
2014	295	1376	56952	6360	15	6360	461	710670	51512	13	13	10	0	2061	2.115		Wind stowed most of the day. Only 461 valid points
2014	296	1376	56953	6094	188	6094	6079	680953	679278	235	224	13	0	7310	4.054		
2014	297	1376	56954	6120	62	6120	6115	683854	683294	198	198	11	0	6687	3.938		
2014	298	1376	56955	6120	17	6120	6118	683845	683623	230	230	13	0	6721	3.920		
2014	299	1376	56956	6120	11	6120	5366	683855	599604	215	213	14	0	6674	3.575		
2014	300	1376	56957	5588	11	5588	2709	624312	302700	78	78	10	0	5724	2.816		
2014	302	1376	56959	2160	95	2160	2079	241368	232310	19	18	3	0	1931	4.927		
2014	303	1376	56960	1339	2	1339	1339	149521	149521	12	11	2	0	1162	3.328		
2014	304	1376	56961	4680	4	4680	3276	522948	366061	204	204	22	0	3560	2.904		
2014	305	1376	56962	5940	14	5940	5243	663742	585860	119	116	7	0	5073	3.356		
2014	306	1376	56963	5182	30	5182	5151	578948	575486	162	151	10	0	5347	3.880		
2014	310	1376	56967	6840	128	6840	6816	764271	761590	274	264	13	0	11670	4.586		
2014	311	1376	56968	6115	76	6115	6042	683163	675004	179	175	10	0	7396	4.351		
2014	312	1376	56969	6118	60	6118	6118	683609	683609	178	177	10	0	7603	4.159		14:13:36 has 5 in a row.
2014	313	1376	56970	6019	46	6019	4069	672433	454696	12	12	1	0	13876	2.699		Much data completely stuffed.
2014	314	1376	56971	5753	47	5753	5747	642824	642153	188	179	11	0	6375	3.801		
2014	315	1376	56972	6120	241	6120	5795	683861	647538	47	32	1	0	5647	4.350		
2014	316	1376	56973	5314	85	5314	5303	593281	592049	60	51	3	0	7131	3.751		
2014	317	1376	56974	4546	35	4546	4531	507894	506217	125	119	9	0	4899	3.729		
2014	318	1376	56975	6775	177	6775	6582	756989	735499	170	138	7	1	8104	4.274		Ceduna 4800 as well from 125105-145055, bright pulses, bp timings
2014	319	1376	56976	5400	11	5400	5400	603430	603430	180	178	11	0	5559	3.893		

Continued on next page...

Table B.3: Data recording summary 2014-2017 (continued)

year	doy	freq	mjd	ar_files	raw_keep	timings	good_tim	all_spa	good_spa	g30_unv	g30_ver	bp_hr	g30_sel	spa_unv	spa_avg	pcal	notes
2014	320	1376	56977	3960	76	3960	2431	442485	271650	70	60	8	0	5710	3.395		
2014	321	1376	56978	34	0	34	34	3799	3799	3	3	31	0	30	3.716		Couldn't fit F1
2014	322	1376	56979	1800	3	1800	1800	201137	201137	40	40	7	0	1952	3.972		Very windy, sirius network card hung.
2014	323	1376	56980	5616	112	5616	5592	627547	624865	183	160	10	0	7905	4.316		Around 324:00:50 had sirius/hovsi link issues for a few minutes.
2014	324	19880	56981	30									0				Tried for fun. Nothing visible.
2014	331	1376	56988	5760	3	5760	5248	643631	586421	142	142	9	0	5459	3.440		
2014	332	1376	56989	3960	19	3960	3923	439509	437211	130	116	10	0	4459	3.479		
2014	334	1376	56991	5689	134	3825	3737	634027	417540	117	87	8	0	5953	4.173		Auto attenuation stuffed up toward end of day 334. Also RAKBUS being fixed. Antenna stuck slewing.
2014	335	1376	56992	4953		4953	2786	553451	311309	147	137	17	0	371	17.012		See warmed.tim for attenuation and warming issues. Can probably delete all raw.keep files here.
2014	336	1376	56993	5269	34	5269	4618	588690	516017	15	15	1	0	6798	3.153		Receiver warmed to 132/128 for 20/70K stage.
2014	338	1376	56995	6213	27	6213	6203	694174	693058	516	513	29	0	5847	3.585		Receiver still slightly warm. 16K (20K stage) at 12:28, horizon test.
2014	339	1376	56996	5755	4	5755	5735	643058	640835	199	196	12	1	5391	3.444		
2014	340	1376	56997	6127	0	6127	6125	684561	684337	28	28	1	0	5263	3.405		
2014	341	1376	56998	5928	1	5928	5676	662365	634242	66	65	4	0	5006	3.279		
2014	342	1376	56999	5072	17	5072	5070	566672	566449	216	213	15	2	4473	3.390		
2014	343	1376	57000	360	0	360	359	40226	40114	3	3	2	0	223	2.773		
2014	346	1376	57003	6660	29	6660	6646	744194	742630	228	207	11	0	7101	3.631		
2014	347	1376	57004	6120	7	6120	6119	683853	683742	213	212	12	1	5867	3.838		
2014	348	1376	57005	5260	9	5260	4793	587690	535580	188	188	14	0	5600	3.910		
2014	349	1376	57006	5421	12	5421	4856	605707	542611	212	212	15	0	6051	4.050		Late 348/early 349 and late 349: stopped during recording for maintenance of bolts.
2014	350	1376	57007	5317	31	5317	4741	593843	529761	217	217	16	1	6354	4.243		~350_22:00 moved to service (for s/x vacuuming).

Continued on next page...

Table B.3: Data recording summary 2014-2017 (continued)

year	doy	freq	mjd	ar_files	raw_keep	timings	good_tim	all_spa	good_spa	g30_unv	g30_ver	bp_hr	g30_sel	spa_unv	spa_avg	pcal	notes
2014	351	1376	57008	3042	13	3042	3013	339248	336676	124	124	14	0	3281	4.418		351_03:30:00 backend rewired. Should make no difference. 1160 failed due to RD1412 experiment taking over around 351_17:41:31
2014	352	1376	57009	1704	47	1704	1395	190365	155834	39	37	9	0	1775	4.214		
2014	353	1376	57010	5280	15	5280	5280	589990	589990	167	167	11	0	5985	4.105		
2014	354	1376	57011	5218	9	5218	5217	583034	582923	150	148	10	0	5640	3.964		
2014	355	1376	57012	5004	10	5004	4968	559070	555121	163	163	11	0	5269	3.927		
2014	356	1376	57013	6000	11	6000	6000	670438	670438	197	197	11	0	6216	3.784		Ceduna 356_12:02:02 to 22:02:02. 2014-12-22-14:50:30.ar has a bright pulse
2014	357	1376	57014	6120	3	6120	6120	683849	683849	211	211	12	0	6310	3.837		Ceduna 357_11:43:03 to 21:43:03
2014	358	1376	57015	6300	11	6300	6299	703940	703829	232	230	13	0	6242	3.898		
2014	359	1376	57016	6298	13	6298	6297	703637	703525	236	233	13	1	6702	3.994		
2014	360	1376	57017	6300	15	6300	6300	703952	703952	220	220	12	0	6628	4.074		16:01:15.ar looks interesting.
2014	361	1376	57018	6120	25	6120	6120	683824	683824	205	203	11	0	6660	4.158		
2014	362	1376	57019	6118	25	6118	6118	683624	683624	216	215	12	0	6387	4.143		
2014	363	1376	57020	6116	20	6116	6115	683322	683210	206	203	11	0	6258	4.168		
2014	364	1376	57021	6390	27	6390	6380	714020	712902	247	247	13	0	6833	4.007		Biggest giant found so far. 2014-12-30-14:38:24.ar subint 25 flux=96.92 Single pulse timing data here.
2014	365	1376	57022	6115	8	6115	6115	683216	683216	188	187	10	0	6108	3.708		
2015	1	1376	57023	6120	1	6120	6117	683844	683509	126	126	7	0	5387	3.365		
2015	2	1376	57024	6360	0	6360	6334	710666	707761	119	118	6	0	5277	3.082		
2015	3	1376	57025	6210	939	6210	6008	693888	671340	9	9	0	0	54305	5.350		Lightning around 090000-100000. A few systems failed.
2015	4	1376	57026	6120	7	6120	6119	683848	683736	103	103	6	0	4902	3.020		
2015	5	1376	57027	6268	7	6268	6267	700355	700243	101	99	5	0	4789	3.007		
2015	6	1376	57028	6330	47	6330	6314	707295	705506	273	265	15	0	6278	3.238		23:33:27 is weird. Single bright pulse. Possibly off pulse? Nope just RFI.
2015	7	1376	57029	6120	96	6120	6070	683848	678263	117	111	6	0	6383	3.402		Lightning around 21:30.
2015	8	1376	57030	6360	55	6360	6342	710663	708651	80	76	4	0	6340	3.343		
2015	9	1376	57031	6390	12	6390	6388	714008	713784	101	98	5	0	5551	3.245		

Continued on next page...

Table B.3: Data recording summary 2014-2017 (continued)

year	doy	freq	mjd	ar_files	raw_keep	timings	good_tim	all_spa	good_spa	g30_unv	g30_ver	bp_hr	g30_sel	spa_unv	spa_avg	pcal	notes
2015	10	1376	57032	5493	6	5493	5489	613704	613256	79	78	5	0	4088	3.323		
2015	11	1376	57033	6120	53	6120	6063	683845	677478	104	101	5	0	5010	3.436		
2015	12	1376	57034	6120	6	6120	6119	683845	683733	120	119	6	0	5245	3.351		
2015	13	1376	57035	6390	29	6390	6174	714011	689877	37	35	2	0	7068	3.382		Strange gap at 013_15:30 UT. Like Vela drifted out of view and came back.
2015	14	1376	57036	6120	28	6120	5117	683845	571775	107	103	7	0	5223	3.315		
2015	15	1376	57037	5274	44	5274	5242	589309	585736	133	128	8	0	5070	3.983		Bad wind.
2015	16	1376	57038	6300	78	6300	3858	703945	431086	107	105	9	0	2	82.269		Bad wind.
2015	17	1376	57039	6390	9	6390	3961	714004	442590	110	110	9	0	7575	3.306		Bad wind.
2015	18	1376	57040	6390	151	6390	6321	714005	706299	221	208	11	0	6627	4.318		today.par installed in first and last .ar file.
2015	19	1376	57041	2841	107	2841	2647	296100	295773	104	104	14	0	2349	3.999		Power failure - most likely the cause of the failed files. Create_tim: model profile failed 2710 times.
2015	20	1376	57042	711	3	711	359	79409	40112	6	5	4	0	649	2.599		Clock setting error after power failure, not pointing at Vela!
2015	21	1376	57043	6360	14	6360	6347	710652	709199	151	149	8	0	5750	3.509		
2015	22	1376	57044	4032	39	4032	4019	450490	449036	56	53	4	0	3497	3.472		Wrong DAS profile loaded. Raw files deleted.
2015	23	1376	57045	6480	5	6480	6465	724067	722389	141	141	7	0	5765	3.301		
2015	24	1376	57046	6480	3	6480	6468	724052	0	0	0		0	0	19.031		hovsi / disk full. Pulsar AGC didn't work. Very dodgy data. Day 023 should be ok, but check.
2015	25	1376	57047	6540	29	6540	6104	730770	682052	91	90	5	0	8000	3.385		Strange jump from 25.748 to 25.752
2015	26	1376	57048	6537	21	6537	6367	730339	711433	160	159	8	0	6522	3.475		
2015	27	1376	57049	2160	0	2160	1953	241351	218222	62	62	11	0	2114	3.448		
2015	28	1376	57050	630	0	630	630	70396	70396	18	18	10	0	613	3.805		
2015	29	1376	57051	6480	8	6480	6479	724052	723940	185	185	10	0	6362	3.706		
2015	30	1376	57052	6547	6	6547	6546	731470	731432	215	215	11	1	6599	3.750		Extra long observing. Had dish at X=-83, Y=28.8 before source command
2015	31	1376	57053	6540	11	6540	6540	730754	730754	209	209	11	2	6626	3.800		
2015	32	1376	57054	4680	7	4680	4669	522926	521699	178	178	13	0	4672	3.851		Short day - Radioastron

Continued on next page...

Table B.3: Data recording summary 2014-2017 (continued)

year	doy	freq	mjd	ar_files	raw_keep	timings	good_tim	all_spa	good_spa	g30_unv	g30_ver	bp_hr	g30_sel	spa_unv	spa_avg	pcal	notes
2015	33	1376	57055	6120	12	6120	6120	683831	683831	185	184	10	1	6130	3.933		16:41:45 is a stunning file! Accidentally overwrote this file with folded data. original lba file in raw.keep
2015	34	1376	57056	3600	10	3600	3600	402255	402255	117	117	11	0	3461	4.012		
2015	35	1376	57057	1239	38	1239	1170	138400	130733	24	17	5	0	1513	3.705		At 22:45:00 drvoff until signal faded. At 22:49:30 onsource. At 22:50:05 reacquired. At 22:54:44 drvoff and tracked manually in Y and X in focus cabin.
2015	36	1376	57058	4770	7	4770	4770	532994	532994	102	100	7	0	4575	3.891		09:36:09 is very interesting.
2015	37	1376	57059	6840	8	6840	6819	764220	761874	180	179	9	1	6471	3.853		Start and finished with new X limit of -85. 12:39:58 is very interesting!
2015	38	1376	57060	6787	4	6787	6783	758255	757883	208	208	10	1	6354	3.856		
2015	39	1376	57061	6720	10	6720	6719	750867	750756	216	216	11	0	6382	3.897		
2015	40	1376	57062	6719	15	6720	6713	750751	749969	165	164	8	1	6264	3.844		test png directory.
2015	41	1376	57063	6419	17	6419	5212	717213	582370	165	162	11	0	6360	3.631		
2015	42	1376	57064	6801	46	6801	6762	759863	755504	178	178	9	1	6406	3.902		
2015	43	1376	57065	6288	56	6288	6260	702587	699456	165	159	9	0	6830	4.010		
2015	44	1376	57066	6450	12	6450	6449	720691	720579	177	174	9	0	5957	3.975		
2015	45	1376	57067	6480	22	6480	6480	724046	724046	203	203	11	0	6736	4.143		09:13:05 is 6 consecutive!
2015	46	1376	57068	6538	72	6538	6536	730527	730303	164	148	8	0	7138	4.261		
2015	47	1376	57069	5413	12	5413	5412	604709	604708	137	137	9	0	4985	4.182		
2015	48	1376	57070	6780	22	6780	6778	757566	757344	166	163	8	1	6163	4.067		Stopped recording using new sidereal time script.
2015	49	1376	57071	6840	14	6840	6324	764275	706619	147	147	8	0	6986	3.891		Bug in script meant dish parked for an hour or so.
2015	50	1376	57072	6838	144	6838	6768	763955	756223	189	170	8	1	8057	4.016		Using brand new velars for first time at set. Current end of png directory.
2015	51	1376	57073	6798	34	6798	6767	759573	756107	157	153	8	0	7389	3.758		S band receiver installed. Lots of RFI at start. Is it new?
2015	52	1376	57074	6798	4	6798	6798	759572	759572	138	138	7	0	5884	3.590		
2015	53	1376	57075	6024	5	6024	6019	672985	672425	131	130	7	0	5126	3.519		Lightning! 08:18:44 and 10:18:24. sirius/hovsi link died at 200424.

Continued on next page...

Table B.3: Data recording summary 2014-2017 (continued)

year	doy	freq	mjd	ar_files	raw_keep	timings	good_tim	all_spa	good_spa	g30_unv	g30_ver	bp_hr	g30_sel	spa_unv	spa_avg	pcal	notes
2015	54	1376	57076	2719	1	2719	2719	303728	303728	62	62	8	0	2109	3.459		
2015	55	1376	57077	6798	129	6798	6737	759572	752753	64	61	3	0	8660	3.786		Bad start to observation. Wrong coordinates (1950) and then wrong levels.
2015	56	1376	57078	6794	17	6794	6791	759044	758787	153	149	7	0	5774	3.565		
2015	57	1376	57079	6798	16	6798	6798	759579	759579	172	172	9	0	6359	3.661		
2015	58	1376	57080	6536	5	6536	6534	730211	729988	150	148	8	0	5707	3.661		Plane possibly flew through beam. 06:09 UTC; stopped by radioastron; 06:09:08 or 06:09:18 both have rfi
2015	59	1376	57081	6798	4	6798	2637	759571	294647	83	80	10	0	2528	3.648		
2015	60	1376	57082	6798	56	6798	6760	759566	755321	198	192	10	0	7133	3.817		
2015	61	1376	57083	6798	6	6798	6796	759562	759339	169	168	8	0	6230	3.695		
2015	62	1376	57084	6798	8	6798	6798	759565	759565	156	154	8	0	6162	3.783		Added todaynof2.par
2015	63	1376	57085	6798	36	6798	6797	759565	759454	182	166	8	0	8630	3.963		Misc onsource fails dec=-3? Around 07h Probably false. Check if clean observation. All clean.
2015	64	1376	57086	6509	23	6509	3463	727195	386936	96	96	9	0	7512	3.046		Started late due to wind speed recalibration, high wind for most of the night.
2015	65	1376	57087	6794	21	6794	6790	759103	758655	219	214	11	0	7108	3.878		
2015	66	1376	57088	6798	14	6798	6798	759553	759553	172	166	8	0	6795	3.721		
2015	67	1376	57089	6798	3	6798	6797	759564	759452	182	182	9	1	6568	3.557		
2015	68	1376	57090	6792	5	6792	6791	758870	758759	190	187	9	0	6516	3.486		Break in recording and dodgy file at 19:14:17. Weird. Also, potential mini-glitch on this day?
2015	69	1376	57091	6750	17	6750	6741	754192	753184	177	176	9	1	6210	3.420		
2015	70	1376	57092	6798	16	6798	6256	759559	698999	144	143	8	1	6013	3.310		Wind stows at start. University-wide internet outage from 10pm-1am UT+11
2015	71	1376	57093	6120	3	6120	6116	683799	683351	153	152	8	0	5893	3.493		
2015	72	1376	57094	6798	72	6798	6768	759559	756206	186	165	8	0	8423	3.680		Circuit breaker 22 popped and lights flashed near start of observation.
2015	73	1376	57095	6798	4	6798	5613	759559	627157	163	163	10	0	7139	3.427		Wind stowed at start. 2015_073/1376/2015-03-14-12:19:01.ar is nice. 3 consecutive and then 2

Continued on next page...

Table B.3: Data recording summary 2014-2017 (continued)

year	doy	freq	mjd	ar_files	raw_keep	timings	good_tim	all_spa	good_spa	g30_unv	g30_ver	bp_hr	g30_sel	spa_unv	spa_avg	pcal	notes
2015	74	1376	57096	6795	7	6795	6795	759175	759175	240	238	12	0	7124	3.788		
2015	75	1376	57097	6123	3	6123	6123	684037	684037	237	237	13	0	6461	3.814		vsib_record died at 18:44:59
2015	76	1376	57098	6324	1	6324	6324	706590	706590	167	167	9	0	5752	3.577		Started late due to hovsi network card fault. Needed power cycle.
2015	77	1376	57099	6795	5	6795	6719	759153	750662	146	141	7	0	5242	3.532		Created 02_S.tim which has single pulse arrival times
2015	78	1376	57100	6678	49	6678	6042	746044	675086	35	33	1	0	4035	3.266		Bad start to observation. S/X being vacuumed. Then palfreymans client on rx26m broken. OK after 01:53:00. Imogen at observatory. RFI from her phone. Lot's of wind stows
2015	79	1376	57101	6008	27	6008	5984	671251	668645	31	22	1	0	3823	3.050		
2015	80	1376	57102	6798	27	6798	6794	759554	759107	14	9	0	0	4320	3		
2015	81	1376	57103	6798	4	6798	6798	759557	759557	82	82	4	0	3803	2.986		
2015	82	1376	57104	6793	342	6793	6062	758997	677313	38	37	2	0	1803	4.384		Bad levels until 02:15 or so.
2015	83	1376	57105	6796	91	6796	6771	759194	756401	99	76	4	0	6467	3.615		08:24:02 and 15:37:12 failed, but .ar files exist. Are they on the boundary of a stoppage?
2015	84	1376	57106	296	0	296	296	33070	33070	2	2	2	0	178	2.935		
2015	85	1376	57107	341	33	341	324	38098	36198	5	2	2	0	481	5.040		
2015	87	1376	57109	246	15	246	139	27486	17206	2	2	4	0	298	3.248		LBA - got 30 min in. Drive PC crashed at end.
2015	92	1376	57114	6648	54	6648	5763	742786	643902	115	114	7	0	7961	4.223		Imogen had her phone on from start to 02:19:00. 7 in a row! 10:53:08
2015	93	1376	57115	6798	220	6798	6686	759551	747034	260	236	12	0	6840	4.955		Around 00:48:00 had DAS level issues. 05:48:33 has interesting stuff. Removed all timings up to 00:56
2015	94	1376	57116	6798	70	6798	6791	759544	758762	37	36	1	0	7646	4.187		
2015	95	1376	57117	6797	9	6797	6796	759395	759283	176	175	9	1	6436	3.935		
2015	96	1376	57118	6798	13	6798	6593	759545	736639	193	189	10	0	6651	3.806		
2015	100	1376	57122	6630	12	6630	6630	740769	740769	152	148	7	0	6247	3.498		
2015	102	1376	57124	6762		6762	5978	755527	667923	66	42	2	0	7766	5.845		Bad RFI day from timing file it seems. 213 in png dir.

Continued on next page...

Table B.3: Data recording summary 2014-2017 (continued)

year	doy	freq	mjd	ar_files	raw_keep	timings	good_tim	all_spa	good_spa	g30_unv	g30_ver	bp_hr	g30_sel	spa_unv	spa_avg	pcal	notes
2015	103	1376	57125	6798	45	6798	6775	759541	756971	114	109	5	0	6516	3.460		
2015	104	1376	57126	1160	0	1160	1160	129566	129566	33	33	10	0	934	3.142		
2015	105	1376	57127	6734	65	6734	5382	752252	601325	89	84	5	0	5280	3.271		DAS profile incorrect until 03:12:30 (during windstow). Non inverted with AGC (64MHZ_F.PRO). Did pcal during windstow. May be dodgy, couldn't do calu -m sam26m
2015	106	1376	57128	6732	38	6732	6220	752161	694956	151	141	8	0	6297	3.535		
2015	107	1376	57129	6675	101	6675	6633	745793	741101	179	167	9	0	6975	3.803		Cal on 3C218 done. Giant calib and .txt output
2015	108	1376	57130	6647	5	6647	5603	742618	625970	116	116	7	1	5896	3.276		
2015	109	1376	57131	6798	9	6798	6798	759530	759530	161	161	8	0	6085	3.538		
2015	110	1376	57132	6798	19	6798	6798	759544	759544	184	181	9	1	7162	3.530		
2015	111	1376	57133	6798	19	6798	6790	759536	758643	170	166	8	0	1365	7.084		
2015	112	1376	57134	6798	21	6798	6771	759537	756520	154	153	8	0	236	10.465		Strange thing happened 01:51-01:55.
2015	113	1376	57135	6798	46	6798	6383	759444	713144	165	160	8	0	2387	5.523		Cryo pump installed - looks like a wind stow. Good attenuation restored at 01:40:30
2015	114	1376	57136	6798	55	6798	6796	759531	759307	159	150	7	0	8757	3.617		Imogen at observatory - phone off mostly.
2015	115	1376	57137	6763	36	6763	6753	755592	754474	199	192	10	0	7290	3.650		
2015	116	1376	57138	6053	95	6053	5993	676266	669563	155	138	8	0	6324	3.754		
2015	117	1376	57139	6798	3	6798	6798	759531	759531	197	197	10	0	6215	3.673		
2015	118	1376	57140	6798	5	6798	6798	759533	759533	195	194	10	0	6232	3.712		
2015	119	1376	57141	6798	11	6798	6797	759537	759425	188	185	9	0	6111	3.788		
2015	120	1376	57142	5455	10	5455	5454	609487	609376	157	153	10	0	5311	3.910		Gap due to cryo pump install. Also did 15m simulanteous at 4816 MHz at Ceduna as a test.
2015	121	1376	57143	841	743	841	833	93385	92934	35	28	12	0	992	3.827		Large gap due to cryo pump install. Agilent dies after a short time now.
2015	124	1376	57146	3141	4	3141	3139	350929	350713	55	53	6	0	2921	3.934		Agilent restored. Brief observing until cryo pneumatic line installed. Micro glitch (Could be 57143-57146)

Continued on next page...

Table B.3: Data recording summary 2014-2017 (continued)

year	doy	freq	mjd	ar_files	raw_keep	timings	good_tim	all_spa	good_spa	g30_unv	g30_ver	bp_hr	g30_sel	spa_unv	spa_avg	pcal	notes
2015	125	1376	57147	6798	28	6798	1724	759528	192620	43	43	8	0	5807	2.613		Very windy day and night.
2015	127	1376	57149	6618	50	6618	6237	739420	696852	72	69	3	0	4911	3.564		Bad start - recording to wrong directory. Played around with headset at around 06:30:00
2015	128	1376	57150	6798	12	6798	5718	759528	638863	64	62	3	0	5293	3.316		
2015	129	1376	57151	6798	1	6798	6798	759527	759527	99	98	5	0	4568	3.396		No bad timing data - gt30 file and single pulse analysis
2015	130	1376	57152	6798	15	6798	4273	759527	477415	65	64	5	1	4093	2.832		
2015	131	1376	57153	6797	10	6797	6519	759370	728353	104	101	5	1	4590	3.203		
2015	132	1376	57154	6795	166	6795	6025	759195	673164	64	50	2	0	5625	3.306		Gamma Ray Collaboration! Ceduna at 4816 MHz as well.
2015	133	1376	57155	6789	19	6789	5629	758251	628921	48	47	2	0	4270	2.914		Oil pump maintenance.
2015	134	1376	57156	6349	46	6349	4558	709316	509251	46	39	3	0	3849	2.880		vela_levels.log has bad data because it was left on after observing. Strange timing at 57154..2919 on glitch_check.
2015	135	1376	57157	6472	34	6472	6468	723038	722591	108	82	4	0	6705	3.238		Stopped early as network link hung.
2015	136	1376	57158	6792	103	6792	6774	758851	756839	60	45	2	1	5420	3.309		Accidentally trashed vela_levels.log
2015	137	1376	57159	258	0	258	258	28825	28825	2	2	2	0	75	2.673		Short day because AOV003 takes over. Files started with test_*.lba. Should be fine.
2015	138	1376	57160	5849	14	5849	5845	653434	652987	3	2	0	0	2640	3.333		
2015	139	1376	57161	6774	31	6774	6772	756860	756636	44	34	1	1	5692	3.478		
2015	140	1376	57162	6554	43	6554	6539	732282	730605	107	92	5	0	5737	3.600		CRD experiment. Also shifted days here. Turbo pump on multifeed continuously. 02:25:00 chainsaw rfi
2015	141	1376	57163	5914	181	5914	5826	660775	650942	49	24	1	0	11273	4.133		Levels went dodgy at the start.
2015	142	1376	57164	6798	28	6798	6779	759539	757416	110	110	5	0	5066	3.455		
2015	143	1376	57165	6798	49	6798	6767	759535	756069	337	325	17	1	5175	3.393		
2015	144	1376	57166	5415	47	5415	4570	605007	510591	180	178	13	0	4166	3.300		Multifeed needed cooling.
2015	145	1376	57167	6642	13	6642	6642	742096	742096	124	121	6	0	5022	3.420		No bad timing data.
2015	146	1376	57168	6798	9	6798	6796	759524	759301	398	393	20	1	5106	3.465		Photographer here from 030000-040000 on day 147 - check for RFI
2015	147	1376	57169	6774	23	6774	6624	756842	740082	126	123	6	0	5472	3.566		Microwave on at 148_000800 for 10 min or so.

Continued on next page...

Table B.3: Data recording summary 2014-2017 (continued)

year	doy	freq	mjd	ar_files	raw_keep	timings	good_tim	all_spa	good_spa	g30_unv	g30_ver	bp_hr	g30_sel	spa_unv	spa_avg	pcal	notes
2015	148	1376	57170	6766	38	6766	6745	755814	753526	133	130	6	0	6141	3.699		Accidentally changed receivers at around 149_00:19 or so
2015	149	1376	57171	2416	51	2416	1638	269915	182991	47	47	10	0	2090	3.231		Recording stopped for most of the day for some reason. :-(
2015	152	1376	57174	5445	6	5445	5442	608323	607988	81	79	5	0	4424	3.910		
2015	153	1376	57175	6798	79	6798	6793	759522	758963	191	178	9	0	6614	3.938		
2015	154	1376	57176	6798	62	6798	6778	759522	757286	158	149	7	0	5927	3.885		Levels were a bit off from 11:27-13:00 (vela AGC finished early)
2015	155	1376	57177	5021	44	5021	5007	560985	559419	124	113	8	0	4819	3.748		Satellite observation interupted for 2 hours.
2015	156	1376	57178	6590	27	6590	6586	736283	735837	116	113	6	0	5499	3.721		Recorded 10 min at 4816
2015	156	4816	57178	60									0				
2015	157	1376	57179	6798	5	6798	6798	759524	759524	141	141	7	1	5231	3.615		Nice clean day. Minimal RFI. Good sample choice
2015	158	1376	57180	6798	3	6798	1622	759526	181224	46	46	10	0	4467	2.377		Windy. Very very windy. Lucky to get anything in today. Levels bad until 10:27:09. Copying interrupted. Check duplicate copied files.
2015	159	1376	57181	6051	11	6051	1939	676019	216639	52	51	9	0	4998	2.450		sirius link to switch died. Reboot didn't work. Recording continuing until power cycle possible.
2015	160	1376	57182	6280	155	6280	6229	701644	695947	146	125	7	0	6135	3.783		
2015	161	1376	57183	6795	170	6795	6766	759164	755929	192	157	8	0	8134	3.959		
2015	162	1376	57184	6798	109	6798	6760	759524	755277	160	145	7	0	7483	3.979		162_002105 air conditioner turned on
2015	163	1376	57185	6108	194	6108	6017	682439	672270	99	81	4	0	6047	4.385		163_003830 flash 021800 + others + 062415 + microwave start 062630, door 062640 + Imogen reported weird rfi at 0437
2015	164	1376	57186	6798	233	6798	6720	759517	750805	170	138	7	0	5780	4.042		Lot's of that single pulse sporadic RFI. All week basically.
2015	165	1376	57187	6798	41	6798	6791	759534	758751	211	207	10	0	6487	4.044		Lot's of that single pulse sporadic RFI. All week basically.
2015	166	1376	57188	3576	13	3576	3576	399541	399541	63	63	6	0	3160	4.064		Lot's of that single pulse sporadic RFI. All week basically.

Continued on next page...

Table B.3: Data recording summary 2014-2017 (continued)

year	doy	freq	mjd	ar_files	raw_keep	timings	good_tim	all_spa	good_spa	g30_unv	g30_ver	bp_hr	g30_sel	spa_unv	spa_avg	pcal	notes
2015	167	1376	57189	5916	75	5916	5907	660983	659978	113	108	6	0	5475	4.172		Lot's of that single pulse sporadic RFI. All week basically.
2015	168	1376	57190	5562	186	5562	5434	621431	607127	127	119	7	0	4806	4.250		Eric reported short burst of RFI during tour at 23:54 (UT) day 167. Short day as drove telescope into limit night before. 2h at Ceduna at 6.7 GHz as well.
2015	169	1376	57191	5190	171	5190	5073	579876	566808	157	132	9	0	5407	4.071		Lot's of that single pulse sporadic RFI. All week basically.
2015	170	1376	57192	6774	300	6774	6625	756370	739721	238	184	9	0	6374	4.020		Lot's of that single pulse sporadic RFI. All week basically.
2015	171	1376	57193	6763	243	6763	6693	755587	747769	189	153	8	0	5955	3.838		Lot's of that single pulse sporadic RFI. All week basically.
2015	172	1376	57194	6797	50	6797	6766	759392	755929	134	125	6	0	5573	3.632		Lot's of that single pulse sporadic RFI. All week basically.
2015	173	1376	57195	6651	842	6651	5609	742565	626624	95	71	4	0	635	7.171		Levels stuffed from 01:52:26-04:30:50
2015	174	1376	57196	6798	6	6798	6795	759534	759199	113	111	5	0	4963	3.336		CME and auroras
2015	175	1376	57197	4966	16	4966	4955	554772	553541	95	94	6	0	3772	3.363		CME and auroras
2015	177	1376	57199	6350	13	6350	6077	709442	678941	14	14	0	1	3411	3.103		Some weird slewing at 13:49:00 and 30 min earlier
2015	178	1376	57200	6798	0	6798	3934	759528	439541	6	6	0	1	3606	39.651		Bad timing at start. Levels off? 03:42:10 6 bright with gap
2015	179	1376	57201	6798	4	6798	4884	759527	545680	32	32	2	0	4260	2.981		
2015	180	1376	57202	2819	0	2819	2818	314908	314852	29	29	3	0	1889	3.361		RFI seems to have gone
2015	181	1376	57203	6797	229	6797	6624	759337	740007	116	95	5	0	7510	3.740		
2015	182	1376	57204	6524	46	6524	3644	728917	407141	237	231	22	1	4446	2.944		Leap Second. Note dUTC was set incorrectly. Timing went bizarrely off exactly 1 hour before leap second.
2015	183	1376	57205	3619	0	3619		404349	0	0	0		0	0	3.367		Weird jump in timing for a few hours. Restarted recording on hovsi. Fixed it.
2015	184	1376	57206	6686	104	6686	6663	746782	744211	435	383	20	1	6758	3.429		Fixed dUTC on telescope clock. May not have had impact.
2015	185	1376	57207	6733	7	6733	6732	752267	752155	349	338	17	0	4882	3.218		Pcal today was on Vela.

Continued on next page...

Table B.3: Data recording summary 2014-2017 (continued)

year	doy	freq	mjd	ar_files	raw_keep	timings	good_tim	all_spa	good_spa	g30_unv	g30_ver	bp_hr	g30_sel	spa_unv	spa_avg	pcal	notes
2015	186	1376	57208	6798	3	6798	6797	759526	759415	419	406	21	0	4885	3.196	02:32:03	
2015	187	1376	57209	6798	19	6798	6798	759541	759541	359	337	17	0	5635	3.207	02:02:03+	
2015	188	1376	57210	6798	79	6798	6754	759532	754621	195	161	8	0	6465	3.309	02:02:03	
2015	190	1376	57212	5526	154	5526	5445	617402	608358	99	75	4	0	5600	3.760	01:02:03	Compressor at 01:12:58 - RFI? Brett had wireless from 00:00-01:18
2015	191	1376	57213	6798	74	6798	6783	759535	757855	137	122	6	0	7580	3.490	03:02:03	Hobart rebooted around 02:30. Wireless on 03:27, off ~06:30
2015	192	1376	57214	6798	7	6798	5523	759530	617079	102	99	6	0	6399	3.254		Late start due to sys26m needing reboot
2015	193	1376	57215	6798	6	6798	6798	759524	759524	143	142	7	0	5517	3.504	03:02:03	No RFI seen on timing.
2015	194	1376	57216	6798	12	6798	6795	759531	759196	151	150	7	0	5836	3.577	08:02:02	
2015	195	1376	57217	6798	40	6798	6786	759543	758202	167	160	8	1	6688	3.647	02:02:02	
2015	196	1376	57218	2687	3	2687	1436	300183	160408	35	35	8	1	2927	3.022	01:02:03	pcal at 0100 most likely missed due to LBA.
2015	201	1376	57223	4992	14	4992	4992	557749	557749	104	102	7	1	4677	3.859	01:02:03	No RFI deleted timings.
2015	204	1376	57226	2022	10	2022	2013	225917	224910	28	27	4	0	1780	3.556		Encoder and brake resistor fault.
2015	205	1376	57227	5653	41	5653	5648	631606	631047	174	163	10	0	6054	3.645	06:22:03	
2015	206	1376	57228	6798	1	6798	6797	759543	759431	135	133	6	0	5853	3.503	01:02:02	
2015	207	1376	57229	6798	89	6798	3663	759535	409260	76	75	7	0	4806	2.689		
2015	208	1376	57230	6798	7	6798	6797	759556	759444	38	37	1	0	3895	3.095	01:02:03	
2015	210	1376	57232	5100	12	5100	5096	569822	569374	35	35	2	0	2935	3.236		
2015	213	1376	57235	4926	14	4926	4052	550383	452730	32	31	2	0	3421	3.013	06:42:03	dodgy timing - levels at 07:00-08:00 went bad
2015	214	1376	57236	6798	19	6798	3669	759547	409938	193	192	18	0	4034	2.736		Very windy
2015	215	1376	57237	6798	73	6798	6765	759541	755854	409	384	20	0	5627	3.461	07:02:03	
2015	216	1376	57238	6798	66	6798	4111	759545	459327	188	178	15	2	4987	2.829		
2015	218	1376	57240	3789	9	3789	3789	423345	423345	26	26	2	0	2502	3.344	00:59:21+	
2015	220	1376	57242	3959	283	3959	3581	422228	400088	44	37	3	0	0	100.674	01:02:03	Power failure.
2015	221	1376	57243	6798	29	6798	6775	759540	756969	65	55	2	1	5472	3.258		
2015	222	1376	57244	3540	9	3540	3539	395526	395414	61	60	6	0	2671	3.210	01:02:03	No bad timing data.
2015	223	1376	57245	1336	0	1336	1334	149272	149048	6	6	1	0	872	2.964		
2015	227	1376	57249	5274	11	5274	5273	589270	589158	102	101	6	0	4420	3.692		Up to 6:03:26 (EST) had 64MHZ.PRO loaded

Continued on next page...

Table B.3: Data recording summary 2014-2017 (continued)

year	doy	freq	mjd	ar_files	raw_keep	timings	good_tim	all_spa	good_spa	g30_unv	g30_ver	bp_hr	g30_sel	spa_unv	spa_avg	pcal	notes
2015	228	1376	57250	6798	1	6798	3844	759549	429496	109	109	10	0	5983	2.859		Windy day.
2015	229	1376	57251	6798	36	6798	6784	759549	757988	156	150	7	0	5144	3.745	01:02:03	
2015	231	1376	57253	1800	22	1800	1752	201116	195754	38	33	6	0	2034	3.926	01:02:03	
2015	232	1376	57254	1350	8	1350	1343	150835	150056	10	10	2	0	953	3.440		
2015	234	1376	57256	4776	13	4776	4776	533638	533638	82	78	5	1	4082	3.715	01:02:03	
2015	235	1376	57257	6798	29	6798	6797	759565	759454	20	19	0	1	3574	3.580	01:02:03	
2015	236	1376	57258	6798	165	6798	6567	759464	733651	69	60	3	1	4507	4.147	02:02:03	
2015	238	1376	57260	4770	6	4770	4767	532962	532626	89	88	6	0	4055	3.876	03:02:03	
2015	241	1376	57263	5058	5	5058	2731	565130	305142	46	46	6	0	4768	2.937		
2015	242	1376	57264	6798		6798	3772	759574	421465	102	100	9	1	611	7.693	06:02:03	UTas open day - bad RFI.
2015	243	1376	57265	6661	47	6661	6048	740660	675668	181	178	10	0	2331	6.072	01:00:03+	Power outage. 0100 pcal may be no good.
2015	246	1376	57268	5514	109	5514	5493	616097	613750	107	84	5	0	7210	4.410	01:02:03	
2015	247	1376	57269	4518	121	4518	4079	504746	455699	127	119	10	2	4213	4.144	01:02:03	
2015	250	1376	57272	1428	14	1428	1427	159513	158156	8	8	2	0	1899	3.762	06:02:03	Bad AGC data manually removed for bright pulses.
2015	251	1376	57273	6798	17	6798	6793	759559	759001	156	152	8	1	5521	3.631	01:02:03	
2015	253	1376	57275	5251	47	5251	4292	586710	479554	64	51	4	0	5555	3.271	01:02:03	vsib_record updated on hovsi and cdvsi.
2015	254	1376	57276	3433	142	3433	3285	383505	366961	30	23	2	0	2866	4.335	01:02:02	
2015	255	1376	57277	6798	6	6798	6796	759561	759337	129	127	6	0	5430	3.609	01:02:03+	
2015	256	1376	57278	2880	1	2880	2880	321793	321793	83	83	10	0	2438	3.686		
2015	257	1376	57279	6798	20	6798	6798	759553	759553	137	130	6	0	5090	3.793	01:02:06	
2015	259	1376	57281	3966	31	3966	3891	443141	434760	104	101	9	0	4332	4.425	01:02:04	
2015	260	1376	57282	6506	132	6506	6447	726944	720353	226	208	11	0	7150	4.811	01:03:10	
2015	262	1376	57284	3654	132	3654	3548	408278	396430	92	90	9	0	4014	4.928	01:03:09	AST open night.
2015	263	1376	57285	6798	51	6798	6794	759570	759122	261	260	13	0	6942	4.494	01:03:10+	
2015	264	1376	57286	3594	12	3594	3323	401425	371144	43	43	4	0	3607	4.430	04:03:09	
2015	267	1376	57289	3616	146	3616	3577	404032	399672	103	75	7	1	5492	4.484	01:03:09	
2015	269	1376	57291	1870	11	1870	1870	208859	208859	39	35	6	0	2399	3.624	19:37:06	
2015	275	1376	57297	3282	7	3282	183	366715	20449	7	7	13	0	803	2.123		Very windy day.
2015	276	1376	57298	4065	8	4065	2830	454053	316209	62	60	7	0	3711	3.231		Power failure.

Continued on next page...

Table B.3: Data recording summary 2014-2017 (continued)

year	doy	freq	mjd	ar_files	raw_keep	timings	good_tim	all_spa	good_spa	g30_unv	g30_ver	bp_hr	g30_sel	spa_unv	spa_avg	pcal	notes
2015	277	1376	57299	6798	13	6798	6167	759588	689084	47	46	2	0	4911	3.258	01:00:00+	Recorded reportedly with channels crossed. Could be not true due to power failure.
2015	278	1376	57300	1440	1	1440	1440	160899	160899	11	11	2	0	741	3.422	13:00:00	
2015	279	1376	57301	3930	7	3930	3929	439119	439008	92	89	8	0	4240	4.131	21:00:00	
2015	280	1376	57302	1710	4	1710	1710	191071	191071	69	69	14	0	2045	4.026		
2015	282	1376	57304	3863	5	3863	3863	431634	431634	69	69	6	0	3322	4.114	21:00:00	
2015	283	1376	57305	6798	20	6798	6707	759575	749406	216	216	11	0	6734	4.111	13:00:00	
2015	284	1376	57306	6695	9	6695	6695	747990	747990	224	224	11	0	6394	4.189		
2015	286	1376	57308	1800	0	1800	1800	201122	201122	47	47	9	0	1472	3.980	13:00:00	
2015	287	1376	57309	2945	101	2945	1444	328992	161346	54	46	11	0	3321	3.560	21:00:00	
2015	288	1376	57310	2220	429	2220	2220	248056	248056	93	93	14	0	2264	7.081	12:00:01	Started AGC on wrong dir. Data bad.
2015	289	1376	57311	3996	24	3996	2044	446500	228395	72	72	12	0	5788	3.488		Very windy
2015	290	1376	57312	6798	38	6798	6796	759577	759354	197	196	10	0	7240	4.235	12:00:00	Cryo started to warm ~2000
2015	291	1376	57313	6062	6	6062	6060	677342	677118	90	88	5	0	4846	2.983	12:00:00	Warming
2015	292	1376	57314	1800	40	1800	1800	201126	201126	42	39	7	0	4677	3.898	12:00:00	Warmed
2015	293	1376	57315	3570	2	3570	3570	398897	398897	60	59	5	0	2845	3.492	21:00:01	20K stage at 100K
2015	294	1376	57316	6424	37	6424	6412	717753	716411	134	132	7	0	7451	3.851	12:00:00	Cooling commenced 0430
2015	295	1376	57317	2430	15	2430	2430	271524	271524	125	124	18	0	2403	4.298	12:00:00	
2015	296	1376	57318	3822	22	3822	3821	427054	426943	21	21	1	0	2715	4.254	20:00:01	
2015	297	1376	57319	6178	24	6178	5323	596984	594695	200	200	13	0	5718	4.359	12:00:00	2100-0100 AGC problems in one channel.
2015	298	1376	57320	6798	22	6798	5944	759578	243854	100	100	16	0	1	4.003	12:00:00	
2015	299	1376	57321	1811	1	1811	1811	202313	202313	137	136	26	0	1703	3.984	12:00:00	
2015	300	1376	57322	3516	40	3516	3385	392859	378219	53	49	5	0	5221	3.739	22:00:01	
2015	301	1376	57323	6798	214	6798	6420	759588	523711	296	282	21	0	0	4.869	23:00:00	
2015	302	1376	57324	2520	2	2520	2519	281574	281462	63	63	8	0	2203	3.390		
2015	303	1376	57325	3300	4	3300	3268	368731	365156	36	35	3	0	2862	3.565	21:00:00	Bad start, Ross stowed 26m
2015	304	1376	57326	6798	10	6798	6798	759579	759579	154	154	8	0	6657	3.552	12:00:01	
2015	305	1376	57327	6798	5	6798	6109	759601	682605	176	174	10	1	6095	3.556	12:00:00	
2015	306	1376	57328	6798	8	6798	6478	759559	723799	150	150	8	1	5965	3.781	12:00:00	
2015	307	1376	57329	1441	6	1441	1398	160914	156112	41	40	10	0	1345	4.120	12:00:00+	
2015	308	1376	57330	3048	16	3048	3045	340563	340227	49	46	5	0	3185	3.987	22:00:00	

Continued on next page...

Table B.3: Data recording summary 2014-2017 (continued)

year	doy	freq	mjd	ar_files	raw_keep	timings	good_tim	all_spa	good_spa	g30_unv	g30_ver	bp_hr	g30_sel	spa_unv	spa_avg	pcal	notes
2015	309	1376	57331	2568	3	2568	2568	286946	286946	94	94	13	0	2264	3.955	12:00:00	
2015	310	1376	57332	3228	5	3228	3031	360683	338685	65	65	7	0	3272	4.008	21:00:01	
2015	311	1376	57333	6798	18	6798	6797	759613	759501	211	211	11	1	6810	4.132	12:00:00	
2015	312	1376	57334	6798	20	6798	5932	759585	662809	148	148	8	0	6043	3.752	12:00:00	Bright pulses: 19:26:23
2015	314	1376	57336	3012	40	3012	3001	336431	335202	29	29	3	0	2848	4.082	22:00:00	
2015	315	1376	57337	2610	5	2610	2605	291618	291060	92	91	12	0	2369	3.853	12:00:00	
2015	317	1376	57339	3054	2	3054	3050	341119	340672	57	57	6	0	2775	3.671	22:00:00	
2015	318	1376	57340	6798	13	6798	6783	759572	757896	173	173	9	1	6230	3.702	12:00:00	
2015	319	1376	57341	5988	55	5988	5983	669108	668549	220	208	12	0	5900	3.689	13:00:00	80 person tour
2015	323	1376	57345	2382	507	2382	1993	266182	222724	51	10	1	0	4790	7.605	22:00:00	Very bad RFI day
2015	324	1376	57346	6798	3	6798	6101	759558	681692	120	120	7	0	4894	3.242	12:00:00	
2015	325	1376	57347	6798	10	6798	6491	759620	725314	177	175	9	0	6401	3.382	12:00:00	
2015	326	1376	57348	6798	12	6798	4225	759303	472106	115	115	9	0	6378	2.986	12:00:00	
2015	327	1376	57349	6786	31	6786	3611	758289	403492	120	108	10	0	7738	3.119		
2015	328	1376	57350	6799	26	6799	3934	759544	439595	13	12	1	0	5128	3.115	01:15:00+	
2015	329	1376	57351	2459	3	2459	2244	274746	250745	19	19	3	0	1604	3.741	12:00:00	
2015	330	1376	57352	2700	30	2700	1985	301678	221822	51	47	8	0	3366	3.672	21:00:00	
2015	331	1376	57353	6798	38	6798	6649	759566	742916	54	51	2	0	7938	4.007	12:00:00	
2015	332	1376	57354	6798	7	6798	6798	759617	759617	194	194	10	0	6351	4.102		
2015	333	1376	57355	6798	106	6798	6778	759618	757381	191	179	9	0	7449	4.314	02:00:00+	
2015	335	1376	57357	1860	10	1860	1858	207803	207579	43	43	8	0	1637	4.272	12:00:00	
2015	336	1376	57358	3012	150	3012	2960	336542	330728	54	36	4	0	3479	4.592	20:00:00	
2015	337	1376	57359	6798	251	6798	6713	759385	749885	182	153	8	0	10223	4.706	12:00:00	
2015	338	1376	57360	6798	8	6798	6793	759548	758990	117	117	6	1	4886	3.820	12:00:01	
2015	339	1376	57361	6798	14	6798	6790	759582	758688	104	103	5	0	4313	3.811	12:00:00	
2015	340	1376	57362	4780	2	4780	4778	534065	533843	65	63	4	0	3024	3.509	12:00:00	
2015	341	1376	57363	6798	3	6798	6797	759576	759465	83	82	4	0	4298	3.397	12:00:00	
2015	342	1376	57364	5934	11	5934	2864	662977	319959	0	0	0	0	4393	2.737	05:01:52+	
2015	343	1376	57365	6670	264	6670	5352	745291	598025	26	0	0	0	6390	3.395	14:00:01	
2015	344	1376	57366	4579	9	4579	4392	511564	490748	82	82	6	0	489	6.441		
2015	347	1376	57369	798	28	798	762	89165	85143	5	5	2	0	881	4.018		
2015	348	1376	57370	6450	44	6450	6432	720700	718688	173	171	9	1	6296	4.146	12:00:01	
2015	349	1376	57371	6560	5	6560	6560	732974	732974	172	171	9	0	5961	4.122	12:00:01	

Continued on next page...

Table B.3: Data recording summary 2014-2017 (continued)

year	doy	freq	mjd	ar_files	raw_keep	timings	good_tim	all_spa	good_spa	g30_unv	g30_ver	bp_hr	g30_sel	spa_unv	spa_avg	pcal	notes
2015	350	1376	57372	6795	159	6795	6748	759213	753963	196	182	9	0	7861	4.326	12:00:01	
2015	351	1376	57373	6751	155	6751	6652	754281	743218	178	173	9	0	8833	4.395	12:00:00	
2015	352	1376	57374	6798	14	6798	6798	759577	759577	177	177	9	0	7050	3.860		
2015	353	1376	57375	6798	16	6798	6798	759578	759578	156	155	8	0	6348	3.625	12:00:00	
2015	354	1376	57376	6740	11	6740	6353	753078	709836	93	93	5	0	5953	3.453	22:00:00	
2015	355	1376	57377	6798	186	6798	6672	759580	745497	145	134	7	2	5241	3.945	12:00:00	
2015	356	1376	57378	6798	31	6798	6777	759574	757227	97	95	5	0	4454	3.476	12:00:00	
2015	357	1376	57379	6566	22	6566	4333	733587	484154	21	21	1	1	3394	2.756	12:00:00	15:31:17 has 10 with 2 gaps
2015	358	1376	57380	6798	10	6798	6798	759582	759582	361	359	18	1	5440	3.357	12:00:00	
2015	359	1376	57381	5970	13	5970	5965	667059	666501	76	73	4	0	1272	6.185	12:00:00	
2015	360	1376	57382	6798	5	6798	6798	759571	759571	350	348	18	0	5174	3.555	12:00:00	
2015	361	1376	57383	6798	3	6798	6798	759576	759576	137	137	7	0	5016	3.681	12:00:00	
2015	362	1376	57384	6797	3	6797	6796	759439	759327	153	153	8	0	5240	3.828	12:00:00	
2015	363	1376	57385	6798	27	6798	6782	759576	757787	199	198	10	1	187	13.030	12:00:00	
2015	364	1376	57386	6798	509	6798	6413	759575	716560	163	144	8	1	3676	5.623	12:00:00	
2015	365	1376	57387	6798	34	6798	6798	759574	759574	190	188	9	0	7024	4.186		
2016	1	1376	57388	6798	305	6798	6569	759572	733982	170	160	8	0	3714	5.466		Slight blip in timing. Bad AGC maybe.
2016	2	1376	57389	6798	16	6798	6798	759572	759572	209	208	10	1	6325	4.115	12:00:00	
2016	3	1376	57390	6798	21	6798	6794	759570	759123	172	168	8	0	6479	4.024	12:00:00	
2016	4	1376	57391	6798	7	6798	6798	759572	759572	156	156	8	0	5703	3.804	12:00:00	
2016	5	1376	57392	6798	15	6798	6798	759574	759574	34	34	1	0	4008	3.610	12:00:00	
2016	6	1376	57393	6798	56	6798	6752	759570	754438	173	171	9	0	5542	3.946	12:00:00	
2016	7	1376	57394	6798	70	6798	6767	759572	756106	181	175	9	0	6605	4.017	12:00:01	
2016	8	1376	57395	6798	23	6798	6517	759563	728167	169	166	9	0	6412	3.918	12:00:00	
2016	9	1376	57396	6798	20	6798	6798	759588	759588	202	201	10	0	6125	4.056	12:00:01	
2016	10	1376	57397	6000	20	6000	5999	670408	670296	190	189	11	0	6118	4.113	12:00:00	
2016	11	1376	57398	5144	17	5144	5138	574633	574076	204	203	14	0	5324	4.239	12:00:00	
2016	12	1376	57399	6798	27	6798	6789	759565	758559	200	200	10	0	4502	4.894	12:00:00	
2016	13	1376	57400	3962	19	3962	3962	442411	442411	171	170	15	0	3888	4.272	12:00:01	
2016	14	1376	57401	1987	8	1987	1986	221755	221655	12	11	1	0	2008	4.137	20:00:00	
2016	15	1376	57402	3168	14	3168	3167	353784	353773	107	107	12	0	3822	4.092	12:00:00	
2016	16	1376	57403	3149	10	3149	3144	351740	351180	117	117	13	0	871	6.579		

Continued on next page...

Table B.3: Data recording summary 2014-2017 (continued)

year	doy	freq	mjd	ar_files	raw_keep	timings	good_tim	all_spa	good_spa	g30_unv	g30_ver	bp_hr	g30_sel	spa_unv	spa_avg	pcal	notes
2016	17	1376	57404	6798	21	6798	6797	759572	759460	51	50	2	0	4690	3.483		
2016	18	1376	57405	6798	54	6798	6772	759569	756664	192	188	9	1	7242	3.681	12:00:00	
2016	19	1376	57406	6788	19	6788	6786	758356	758132	178	173	9	0	6245	3.686	08:00:00	
2016	20	1376	57407	4320	5	4320	4320	482689	482689	183	182	15	0	4147	3.734	12:00:01	
2016	22	1376	57409	6798	39	6798	6788	759564	758447	250	243	12	0	7724	4.012	12:00:00	
2016	23	1376	57410	6792	27	6792	6790	758850	758626	284	281	14	0	8042	4.169	12:00:00	
2016	24	1376	57411	6798	154	6798	6757	759554	754974	293	290	15	1	8094	4.562	22:00:00	09:36:47.ar,27,102.38
2016	25	1376	57412	6798	62	6798	6790	759561	758668	291	290	15	0	5951	4.946		
2016	26	1376	57413	6798	88	6798	6780	759556	757551	292	287	15	0	8574	4.288	12:00:00	
2016	27	1376	57414	3304	5	3304	3304	369006	369006	153	153	16	1	3774	4.083	12:00:00	Nice very bright 5 consecutive
2016	29	1376	57416	6213		6213	3117	694120	348198	16	16	1	1	0	38.046	12:00:01	Radioastron. Freq set wrong on restart. Fixed at 21:36. Things weird after that. Discarded.
2016	30	1376	57417	6798	72	6798	6780	759560	757549	2	0	0	0	7248	3.723	12:00:00	
2016	31	1376	57418	6798	0	6798	6797	759555	759443	509	508	26	0	6801	3.489	12:00:00	
2016	32	1376	57419	6799	31	6799	6789	759459	758339	190	185	9	0	7425	3.515	12:00:00	
2016	33	1376	57420	4500	3	4500	4499	502792	502680	154	153	12	0	4444	3.398	12:00:00	
2016	34	1376	57421	132	12	132	126	14747	14077	1	0	0	0	103	3.843		
2016	35	1376	57422	6798	103	6798	6712	759551	749939	197	194	10	0	7568	3.636	12:00:00	
2016	36	1376	57423	6798	73	6798	6753	759550	754521	173	160	8	0	6786	3.662		
2016	37	1376	57424	3102	1	3102	3100	346519	346295	112	112	12	1	3088	3.395	12:00:00	
2016	38	1376	57425	4749	8	4749	4746	530499	530243	147	142	10	0	5263	3.375	10:00:00	
2016	39	1376	57426	6798	11	6798	6798	759551	759551	188	187	9	0	6900	3.501	12:00:00	
2016	40	1376	57427	6798	25	6798	6795	759552	759216	57	54	2	1	4711	3.493	12:00:00	
2016	41	1376	57428	6798	14	6798	6797	759543	759431	269	269	14	0	7597	3.694	12:00:00	
2016	42	1376	57429	6798	19	6798	6798	759543	759543	452	449	23	4	7940	3.828	12:00:00	
2016	43	1376	57430	6798	28	6798	6790	759541	758648	500	492	25	0	7137	4.060	02:58:41+	
2016	44	1376	57431	6798	77	6798	6779	759544	757420	315	305	16	1	8462	4.172	12:00:01	
2016	45	1376	57432	6798	512	6798	5411	759552	604582	651	620	40	0	55818	7.939	12:00:00	Bad AGC after 21:12
2016	46	1376	57433	2717	13	2717	1498	303536	167338	58	58	13	0	3821	3.503	10:20:00	
2016	47	1376	57434	6798	38	6798	6084	759542	679768	246	245	14	0	8380	4.046	12:00:00	
2016	48	1376	57435	6792	30	6792	6791	758868	758756	282	281	14	0	7843	4.077	12:00:01	
2016	49	1376	57436	6798	22	6798	6793	759464	758904	221	219	11	0	7342	4.122	12:00:00	

Continued on next page...

Table B.3: Data recording summary 2014-2017 (continued)

year	doy	freq	mjd	ar_files	raw_keep	timings	good_tim	all_spa	good_spa	g30_unv	g30_ver	bp_hr	g30_sel	spa_unv	spa_avg	pcal	notes
2016	50	1376	57437	6798	31	6798	6785	759540	758085	233	223	11	0	7542	3.885	12:00:00	
2016	51	1376	57438	6472	28	6472	6472	723119	723119	35	34	1	3	4510	3.645	12:00:00	
2016	52	1376	57439	6798	14	6798	6798	759541	759541	220	218	11	1	6887	3.882	12:00:00	
2016	53	1376	57440	6798	10	6798	6798	759545	759545	625	621	32	0	7454	3.787	12:00:00	
2016	54	1376	57441	4301		4301	3682	480518	411357	986	133	12	0	40185	14.818	12:00:00	Bad AGC after 13:06
2016	56	1376	57443	1344	0	1344	604	150165	67486	9	9	5	0	1001	2.640	20:30:01	A short day.
2016	57	1376	57444	6744	46	6744	6505	753506	726805	214	210	11	1	7944	4.175	12:00:00	
2016	58	1376	57445	6798	15	6798	6797	759536	759424	234	230	12	2	7047	4.118	12:00:00	
2016	59	1376	57446	6798	61	6798	6760	759525	755282	237	231	12	1	6773	4.247	12:00:00	
2016	60	1376	57447	6685	23	6685	6680	746557	746280	246	243	13	0	7306	4.096	12:00:00+	
2016	61	1376	57448	6798	11	6798	6798	759542	759542	140	140	7	1	5514	3.762	12:00:00	
2016	62	1376	57449	4973	8	4973	4972	555580	555468	116	116	8	1	4953	3.792	12:00:00	
2016	63	1376	57450	6798	31	6798	6784	759531	757968	210	207	10	0	3024	5.973	12:00:00	
2016	66	1376	57453	6798	630	6798	5968	759544	666796	119	119	7	0	1390	6.723	12:00:00	
2016	67	1376	57454	6798	19	6798	6795	759530	759194	211	210	11	2	6451	4.041	12:00:00	Giant of 98.7 at 18:02:13, subint 42
2016	68	1376	57455	6780	49	6780	6773	757532	756749	220	207	10	1	8031	4.297	12:00:00	
2016	69	1376	57456	6799	140	6799	6009	759508	671299	186	178	10	1	7873	4.599	12:00:00	Bad RFI near the start
2016	70	1376	57457	6798	58	6798	6790	759494	758599	256	254	13	0	7605	4.620	12:00:01	
2016	71	1376	57458	6558	81	6558	6557	732687	732575	134	133	7	0	9032	4.533	12:00:01	
2016	72	1376	57459	6798	186	6798	6595	759527	736844	220	220	11	0	4542	5.436	12:00:00	
2016	73	1376	57460	6798	91	6798	6795	759522	759186	246	240	12	0	8975	4.916	12:00:00	
2016	74	1376	57461	6798	92	6798	6796	759526	759302	277	277	14	2	8391	4.998	12:00:00	3 bright pulses over 100. 104.85, 103.8, 101.21
2016	75	1376	57462	6798	106	6798	6798	759521	759521	299	294	15	0	8850	4.930	12:00:00	
2016	76	1376	57463	6798	80	6798	6795	759521	759186	228	227	11	1	7565	4.866	12:00:00	
2016	77	1376	57464	6798	77	6798	6547	759522	731477	215	207	11	1	7469	4.677	12:00:00	
2016	78	1376	57465	6798	97	6798	5610	759437	626712	219	213	13	0	8468	4.524	12:00:00	Check for 100 Hz in one channel 05:00
2016	79	1376	57466	6798	100	6798	6798	759517	759517	250	248	13	1	7493	4.992	12:00:01	New giant record. 107.47. 11:28:32
2016	80	1376	57467	6693	89	6693	6683	747674	746557	220	220	11	1	6354	4.952	12:00:00	
2016	84	1376	57471	6798	26	6798	6797	759519	759407	193	192	10	0	6353	4.505	12:00:01	
2016	85	1376	57472	6798	42	6798	6798	759513	759513	196	194	10	1	6513	4.443	12:00:00	
2016	86	1376	57473	6798	40	6798	6792	759520	758850	196	196	10	0	5977	4.694	12:00:00	
2016	87	1376	57474	6798	79	6798	6798	759515	759515	208	208	10	1	6555	5.030	12:00:00	

Continued on next page...

Table B.3: Data recording summary 2014-2017 (continued)

year	doy	freq	mjd	ar_files	raw_keep	timings	good_tim	all_spa	good_spa	g30_unv	g30_ver	bp_hr	g30_sel	spa_unv	spa_avg	pcal	notes
2016	88	1376	57475	6798	223	6798	6755	759514	754710	260	259	13	2	6981	5.439	12:00:00+	
2016	89	1376	57476	6798	249	6798	6787	759515	758287	254	252	13	0	7161	5.668	12:00:00	
2016	90	1376	57477	6798	281	6798	6798	759519	759519	242	242	12	2	7743	5.381	12:00:01	7 consecutive
2016	91	1376	57478	6798	260	6798	6797	759520	759408	245	245	12	0	7246	5.402	12:00:01	Used for APJ2
2016	92	1376	57479	6280	133	6280	4272	701602	477255	133	133	11	0	7966	4.591	12:00:00	ultragiant directory here
2016	93	1376	57480	5023	399	5023	3485	561095	389313	75	74	7	0	607	11.033	04:00:00	
2016	94	1376	57481	6798	60	6798	6798	759513	759513	251	250	13	0	7219	4.692		
2016	95	1376	57482	6798	273	6798	6663	759521	744438	195	177	9	0	9044	5.020	04:00:00	
2016	96	1376	57483	5841	27	5841	4074	652466	455054	138	132	11	0	5337	4.137	04:00:00	
2016	97	1376	57484	5586	54	5586	5567	624063	621940	202	200	12	0	775	12.194	04:00:00	
2016	98	1376	57485	306	0	306	306	34188	34188	3	3	3	0	266	3.379		
2016	99	1376	57486	6798	69	6798	6797	759504	759392	188	172	9	0	7643	4.311	12:00:00	
2016	100	1376	57487	6798	28	6798	4548	759504	508127	108	107	8	1	7640	3.527	12:00:00	
2016	101	1376	57488	6798	29	6798	3578	759506	399753	101	97	9	0	7449	3.146	12:00:00	
2016	102	1376	57489	6798	5	6798	6798	759508	759508	183	183	9	0	5911	4.040	12:00:00	
2016	103	1376	57490	6390	2	6390	6389	713850	713738	174	173	9	0	5181	4.026	12:00:01	
2016	104	1376	57491	380	0	380	380	42456	42456	3	3	2	0	290	3.176	18:00:00	
2016	105	1376	57492	6798	22	6798	6796	759506	759282	181	173	9	1	6450	4.010	12:00:00	00:05:19 subint 90 weird rabbit-ears giant pulse
2016	106	1376	57493	6798	65	6798	6796	759504	759280	193	178	9	0	7539	4.169	12:00:00	
2016	107	1376	57494	6798	27	6798	6798	759502	759502	189	189	9	0	6832	4.324	12:00:00	
2016	108	1376	57495	3724	40	3724	3717	415986	415204	101	92	8	0	4113	4.238	12:00:00	
2016	109	1376	57496	6763	22	6763	6757	755567	754897	115	115	6	0	2829	5.268	12:00:00	
2016	110	1376	57497	4349	17	4349	3161	485562	352839	162	157	17	0	3884	3.332	12:00:00	
2016	111	1376	57498	4656	10	4656	3295	520152	368133	36	36	3	0	2923	3.291	12:00:00	
2016	113	1376	57500	4572	5	4572	4572	510801	510801	28	27	2	0	2463	3.445	12:00:00	
2016	114	1376	57501	6798	14	6798	6794	759501	759053	53	51	2	0	3675	3.328	12:00:00	
2016	115	1376	57502	6796	28	6796	6785	759224	757994	35	35	1	0	3	26.179	12:00:00	
2016	116	1376	57503	6798	28	6798	6788	759494	758376	43	41	2	0	1098	8.126	12:00:00	
2016	117	1376	57504	6071	18	6071	6060	678254	677048	28	28	1	0	3175	3.217	12:00:00	
2016	118	1376	57505	6678	1	6678	4540	746020	507154	93	93	7	0	3239	2.948	12:00:01+	
2016	119	1376	57506	5846	11	5846	5845	652973	652862	238	233	14	0	4602	3.400	12:00:00	
2016	120	1376	57507	4562	4	4562	4562	509598	509598	71	70	5	0	3650	3.673	12:00:01	

Continued on next page...

Table B.3: Data recording summary 2014-2017 (continued)

year	doy	freq	mjd	ar_files	raw_keep	timings	good_tim	all_spa	good_spa	g30_unv	g30_ver	bp_hr	g30_sel	spa_unv	spa_avg	pcal	notes
2016	121	1376	57508	6734	22	6734	6724	752174	751164	130	127	6	0	5711	3.916	12:00:00	
2016	122	1376	57509	6798	28	6798	4974	759494	555711	137	131	9	0	7047	3.611	12:00:00	
2016	123	1376	57510	4902	1	4902	1620	547592	180917	39	39	8	0	4589	2.680	12:00:00	
2016	124	1376	57511	5788	25	5788	5747	646574	641994	120	120	7	0	0	37.431	12:00:00	
2016	125	1376	57512	6798	27	6798	6797	759501	759389	102	102	5	0	5148	4.108	12:00:00	
2016	126	1376	57513	5929	44	5929	4895	662322	546886	107	103	7	0	187	15.705	12:00:00	
2016	127	1376	57514	4613	25	4613	4038	515347	451106	60	60	5	0	3430	3.990	12:00:00	
2016	128	1376	57515	6786	21	6786	6769	758150	756252	108	108	5	0	2484	5.628	12:00:00	
2016	129	1376	57516	6798	40	6798	6781	759489	757588	114	112	5	1	126	14.362		
2016	130	1376	57517	6798	57	6798	6795	759498	759162	118	114	6	0	6520	3.985	12:00:00	
2016	131	1376	57518	6744	16	6744	5450	753416	608850	128	127	8	0	4796	3.676	12:00:00	
2016	132	1376	57519	6342	17	6342	1163	708549	129936	24	24	7	0	4448	2.461	12:00:00	
2016	133	1376	57520	6798	56	6798	3263	759496	364554	42	38	4	0	6177	3.002	12:00:00	
2016	134	1376	57521	2200	1	2200	2200	245757	245757	38	38	6	0	1389	3.628		
2016	135	1376	57522	4110	10	4110	3339	459178	373038	30	29	3	0	2618	3.626	12:00:01	
2016	136	1376	57523	6798	35	6798	4195	759487	468673	81	79	6	0	4444	3.296	12:00:00	
2016	137	1376	57524	4599	22	4599	4592	513671	512890	101	98	7	0	3697	4.088	12:00:01	
2016	138	1376	57525	816	0	816	816	91166	91166	6	6	2	0	543	3.157		
2016	139	1376	57526	4418	17	4418	4415	493512	493176	63	58	4	0	2998	4.021	12:00:00	
2016	141	1376	57528	6563	78	6563	6550	733165	731713	70	65	3	1	5635	3.806	12:00:00	
2016	142	1376	57529	6798	8	6798	6792	759488	758817	488	484	25	0	3038	4.273	12:00:00	
2016	143	1376	57530	6798	11	6798	6798	759493	759493	321	318	16	1	4342	3.572	12:00:00+	
2016	144	1376	57531	1999	2	1999	1999	223334	223334	56	56	10	0	1265	3.517		
2016	145	1376	57532	2496	2	2496	2495	278860	278748	3	3	0	0	1379	3.931	12:00:00	
2016	146	1376	57533	5387	25	5387	5352	601818	597906	84	84	5	0	3289	4.097	12:00:00	
2016	147	1376	57534	6756	50	6756	6756	754794	754794	109	109	5	0	5892	4.124	12:00:00	
2016	148	1376	57535	5969	73	5969	5954	666800	665122	124	119	7	0	6984	3.840	12:00:00	
2016	149	1376	57536	6798	19	6798	6797	759463	759351	67	64	3	1	5002	3.411	12:00:00	Double-peaked consecutive
2016	150	1376	57537	6798	18	6798	6797	759490	759378	147	144	7	1	6606	3.711	12:00:00	
2016	151	1376	57538	6798	6	6798	6798	759491	759491	307	306	16	0	6058	3.587		
2016	152	1376	57539	6798	97	6798	6704	759491	748985	173	169	9	0	7187	3.715	12:00:00	
2016	153	1376	57540	6612	5	6612	6611	738692	738580	120	119	6	2	5575	3.428	12:00:00	
2016	154	1376	57541	5902	39	5902	5887	659301	657626	86	79	4	0	6092	3.512	12:00:00	

Continued on next page...

Table B.3: Data recording summary 2014-2017 (continued)

year	doy	freq	mjd	ar_files	raw_keep	timings	good_tim	all_spa	good_spa	g30_unv	g30_ver	bp_hr	g30_sel	spa_unv	spa_avg	pcal	notes
2016	155	1376	57542	6664	66	6664	6645	744440	742315	129	122	6	0	6432	3.530	12:00:00	
2016	156	1376	57543	6798	10	6798	6795	759490	759155	171	169	8	0	6017	3.530	12:00:00	
2016	157	1376	57544	6798	30	6798	6590	759491	736250	127	125	6	0	488	9.530	12:00:00	
2016	158	1376	57545	6342	37	6342	5724	708543	639498	100	96	5	1	6170	3.907	12:00:00	Amazing double drifting subpulses
2016	159	1376	57546	6798	104	6798	6403	759493	715362	169	169	9	0	4288	4.547	12:00:00	
2016	160	1376	57547	6798	31	6798	6098	759492	681286	168	166	9	0	6474	4.227	13:00:01	
2016	162	1376	57549	6774	60	6774	5539	756809	618834	211	209	13	1	7914	4.291	12:00:00	
2016	163	1376	57550	6798	89	6798	4711	759494	526327	131	127	9	0	6576	4.461	12:00:00	AGC not running from start until 12:30UT
2016	164	1376	57551	6798	120	6798	4500	759525	502786	107	27	2	0	12956	4.128	12:00:00	Strong signal in R at 00:00UT
2016	165	1376	57552	6475	608	6475	5250	723328	586467	687	130	8	0	62624	8.842	22:00:00	Bad AGC at end
2016	166	1376	57553	1928	17	1928	354	215281	39513	11	11	11	0	1658	2.734		
2016	167	1376	57554	6690	30	6690	6689	747426	747315	157	154	8	1	5546	4.332	12:00:00	
2016	168	1376	57555	6798	37	6798	6797	759488	759376	147	143	7	1	6133	4.152	12:00:00	
2016	169	1376	57556	6798	253	6798	6745	759492	753569	171	128	6	0	6614	6.253	12:00:00	
2016	170	1376	57557	6798	26	6798	6795	759489	759154	112	107	5	0	5366	3.896	12:00:01	
2016	171	1376	57558	6798	15	6798	6798	759495	759495	75	74	3	0	3748	3.667	12:00:00	
2016	172	1376	57559	6802	21	6802	6799	758826	758493	469	455	23	0	5322	3.828		
2016	173	1376	57560	6798	5	6798	6657	759497	743745	396	394	21	0	4629	3.833	12:00:00	
2016	174	1376	57561	6799	35	6799	4992	759366	557582	121	115	8	0	7732	3.388	12:00:00	
2016	175	1376	57562	6798	40	6798	6793	759500	758941	182	174	9	0	6114	4.236	12:00:00+	
2016	176	1376	57563	3911	57	3911	3909	436945	436722	150	139	12	1	5145	4.376		
2016	183	1376	57570	5244	45	5244	5229	585879	584203	92	90	6	0	4437	4.474	12:00:00	
2016	184	1376	57571	6502	189	6502	6325	726424	706648	154	154	8	0	3091	5.338	12:00:00	Radiostron took over
2016	185	1376	57572	6163	18	6163	6163	688269	688269	93	93	5	0	4270	3.978	12:00:00	Power fail and accidental receiver change. 012000
2016	186	1376	57573	6798	3	6798	6794	202000	202000	41	41	8	0	0	4.033	12:00:01	
2016	187	1376	57574	6796	24	6796	6788	759252	758357	142	140	7	0	5526	4.077	12:00:00	
2016	188	1376	57575	5810	2	5810	5809	649020	648909	112	106	6	0	4316	3.948		hovsi failed
2016	189	1376	57576	6798	31	6798	6796	759493	759269	146	142	7	0	5561	3.875	12:00:00	
2016	190	1376	57577	5702	29	5702	5691	637041	635813	100	92	5	1	4124	3.911	00:00:00	
2016	191	1376	57578	5249	8	5249	5225	586241	583661	91	88	6	0	3441	3.772	00:00:00	
2016	192	1376	57579	5485	16	5485	5460	612398	609760	40	40	2	0	3357	3.530	00:00:00	Strange double pulse files, corrupt hovsi recordings.

Continued on next page...

Table B.3: Data recording summary 2014-2017 (continued)

year	doy	freq	mjd	ar_files	raw_keep	timings	good_tim	all_spa	good_spa	g30_unv	g30_ver	bp_hr	g30_sel	spa_unv	spa_avg	pcal	notes
2016	193	1376	57580	5362	17	5362	5018	598905	560472	600	595	42	0	4456	4.143	00:00:00	
2016	194	1376	57581	2919	79	2919	1381	326110	154291	43	42	10	0	3632	3.209	02:00:00	
2016	197	1376	57584	1767	106	1767	1750	197419	195521	44	33	6	1	3496	5.955	03:05:00	
2016	198	1376	57585	4530	18	4530	4528	506111	505888	137	136	10	0	3569	4.804		
2016	199	1376	57586	4830	23	4830	4830	539630	539630	67	67	4	1	3810	4.636		
2016	200	1376	57587	6798	36	6798	5032	759499	562195	191	189	13	2	6492	3.926		
2016	201	1376	57588	6798	5	6798	4513	759501	504210	82	82	6	0	6525	3.537	01:00:00	
2016	204	1376	57591	4384	23	4384	2047	489744	228644	28	25	4	0	4644	3.074	02:00:00	
2016	207	1376	57594	3642	64	3642	3284	406905	366904	41	38	4	0	642	8.894	05:00:00	
2016	208	1376	57595	1776	12	1776	1775	198421	198310	0	0	0	0	1526	3.790		
2016	209	1376	57596	5935	109	5935	4534	662938	506483	133	132	10	0	5455	3.593	01:00:00	
2016	211	1376	57598	3325	107	3325	3315	371452	370334	88	69	7	0	5066	4.545	04:00:00	
2016	212	1376	57599	1592	3	1592	1588	177700	177419	1	1	0	0	1213	3.682	08:00:00	
2016	213	1376	57600	1957		1957	1957	218612	218612	29	27	4	0	1403	37.523		Weird timing. AGC stuffed.
2016	214	1376	57601	3984	7	3984	3982	445110	444887	68	67	6	0	2856	4.103	09:00:01	
2016	215	1376	57602	5014	106	5014	5008	560198	559529	150	133	9	0	5951	4.279	01:00:00	
2016	216	1376	57603	1530	0	1530	1518	170938	169599	3	3	0	0	1178	3.541		
2016	217	1376	57604	4830	3	4830	4830	539629	539629	96	95	7	0	3819	4.152		
2016	218	1376	57605	6797	18	6797	6797	759363	759363	82	82	4	0	4472	4.017	04:00:00	
2016	219	1376	57606	2406	3	2406	886	268792	98990	32	32	12	0	1654	2.754	01:00:00	
2016	221	1376	57608	2221	3	2221	2196	247762	245172	8	8	1	0	1647	4.246		
2016	222	1376	57609	6798	90	6798	5538	759512	618738	190	188	12	1	7425	3.987		
2016	224	1376	57611	5965	41	5965	5140	666416	574275	76	76	5	0	3631	4.547		
2016	225	1376	57612	6798	24	6798	6795	759511	759176	175	173	9	0	5381	4.442	01:00:00	
2016	226	1376	57613	6798	13	6798	4946	759505	552588	177	173	12	0	6712	3.626	01:00:00	
2016	227	1376	57614	6253	14	6253	3944	698513	440647	134	134	12	0	6295	3.304	01:00:00	
2016	228	1376	57615	6784	3	6784	6784	757920	757920	160	159	8	0	5406	3.909	01:00:00	
2016	229	1376	57616	4235	135	4235	3983	472742	445011	74	64	5	0	4687	4.366	01:00:00	
2016	230	1376	57617	6708	12	6708	6704	749461	749013	113	109	5	0	4895	3.792	01:00:00	
2016	231	1376	57618	6798	73	6798	6755	759515	754710	447	434	22	0	5013	3.895	01:00:00	
2016	232	1376	57619	6798	6	6798	6795	759518	759183	403	402	21	0	4167	4.003	01:00:00	
2016	233	1376	57620	6798	9	6798	6797	759514	759403	281	281	14	0	5160	3.802	01:00:00	
2016	234	1376	57621	6606	4	6606	6606	738074	738074	141	141	7	2	5201	3.845	01:00:00	

Continued on next page...

Table B.3: Data recording summary 2014-2017 (continued)

year	doy	freq	mjd	ar_files	raw_keep	timings	good_tim	all_spa	good_spa	g30_unv	g30_ver	bp_hr	g30_sel	spa_unv	spa_avg	pcal	notes
2016	235	1376	57622	6798	45	6798	6793	759514	758956	162	162	8	1	7218	3.986	01:00:00	
2016	236	1376	57623	6798	16	6798	6798	759529	759529	160	160	8	0	6195	3.952	01:00:00	Scintillation test here.
2016	237	1376	57624	5717	15	5717	5713	638742	638295	124	122	7	0	4617	4.073	01:00:00+	
2016	238	1376	57625	417	0	417	417	46516	46516	11	11	9	0	334	3.563		
2016	239	1376	57626	5682	11	5682	5182	634835	578972	21	21	1	0	5036	4.105	01:00:01	
2016	240	1376	57627	6798	12	6798	5562	759509	621418	157	157	10	0	6905	3.748	01:00:00	
2016	241	1376	57628	6798	26	6798	6797	759519	759408	200	198	10	0	6322	4.362	01:00:00	
2016	242	1376	57629	6798	53	6798	6728	759526	751705	191	188	9	0	7140	4.401		
2016	243	1376	57630	6797	24	6797	6796	759375	759263	179	176	9	0	6384	4.371	01:00:00+	
2016	244	1376	57631	1359	788	1359	1359	151676	151676	25	25	6	0	2480	19.687		AGC stuffed.
2016	245	1376	57632	2280	7	2280	2280	254739	254739	13	13	2	0	1744	4.382	04:00:00	
2016	246	1376	57633	6798	35	6798	6798	759524	759524	230	229	12	0	6931	4.473	01:00:00+	
2016	247	1376	57634	6148		6148	5719	686892	638961	69	68	4	0	37933	18.236	20:00:01	AGC maybe stuffed at start. Weird vsib_record jump.
2016	248	1376	57635	6798	17	6798	6401	759528	715172	177	177	9	1	6133	4.039		
2016	249	1376	57636	6204	132	6204	6108	692764	682444	159	147	8	0	5582	5.106		
2016	250	1376	57637	6798	93	6798	5408	759546	604239	209	198	13	0	9716	3.680		
2016	251	1376	57638	6798	5	6798	6798	759531	759531	157	157	8	0	5727	3.949	01:00:00+	
2016	252	1376	57639	5057	166	5057	4997	564922	558223	101	79	5	2	5415	4.208		
2016	253	1376	57640	6795	69	6795	6788	759170	758388	183	172	9	2	7024	3.999	01:00:00	
2016	254	1376	57641	6795	157	6795	6396	759172	714611	107	106	5	0	3932	4.339		
2016	255	1376	57642	6798	26	6798	6798	759527	759527	225	221	11	0	6463	4.340	01:00:00	
2016	256	1376	57643	6798	92	6798	6761	759527	755394	219	216	11	0	7263	4.576	01:00:00	
2016	257	1376	57644	6796	122	6796	6794	759070	758846	263	213	11	1	9284	4.601		
2016	258	1376	57645	680	0	680	680	75977	75977	28	28	14	0	646	3.605	01:00:00	
2016	259	1376	57646	5346	58	5346	5221	597295	583329	117	114	7	0	5805	4.541	01:00:00	
2016	260	1376	57647	5994	1179	5994	5228	669628	584040	109	43	2	1	12115	9.387	01:00:00+	
2016	261	1376	57648	1617	11	1617	1608	180591	179660	66	66	14	0	1343	4.665		
2016	262	1376	57649	4752	25	4752	4752	530933	530933	113	113	8	1	4674	4.529	01:00:00	
2016	263	1376	57650	6798	25	6798	6798	759525	759525	211	211	11	0	6381	4.478	01:00:00	pngall up to 200
2016	264	1376	57651	9213		9213	9194	1029138	1027152	54	53	2	1	102769	10.175	01:00:00	AGC bad at start
2016	265	1376	57652	4013	20	4013	1272	448113	142047	24	24	6	0	673	4.148		
2016	266	1376	57653	6800	15	6800	6797	759561	759336	182	182	9	1	5968	4.138	03:00:00	

Continued on next page...

Table B.3: Data recording summary 2014-2017 (continued)

year	doy	freq	mjd	ar_files	raw_keep	timings	good_tim	all_spa	good_spa	g30_unv	g30_ver	bp_hr	g30_sel	spa_unv	spa_avg	pcal	notes
2016	267	1376	57654	6798	5	6798	6798	759534	759534	114	114	5	1	5110	3.985	01:00:00	1000 file pulse widths
2016	268	1376	57655	6798	8	6798	6782	759529	757741	110	110	5	1	5086	3.925	01:00:00+	
2016	269	1376	57656	762	0	762	761	85061	84949	16	16	7	0	528	3.181	18:00:00	
2016	270	1376	57657	3322	12	3322	3316	371149	370478	10	10	1	1	2621	3.594		
2016	271	1376	57658	1476	1	1476	1475	164840	164802	60	60	14	0	917	3.722	07:00:01	
2016	272	1376	57659	5004	10	5004	5004	559083	559083	79	79	5	1	3754	4.156		
2016	273	1376	57660	6714	17	6714	6263	750071	699759	96	96	5	0	5361	4.075	14:00:00	
2016	274	1376	57661	6294	39	6294	6263	703227	699762	121	120	6	1	2458	6.322	22:00:00	pngall dir
2016	275	1376	57662	6798	21	6798	6796	759540	759316	101	99	5	1	6854	4.216	18:00:00	
2016	276	1376	57663	6798	9	6798	6798	759540	759540	129	129	6	1	5720	4.085	18:00:00	
2016	277	1376	57664	5997	55	5997	5992	670045	669487	114	106	6	0	5181	4.296		
2016	278	1376	57665	3336	64	3336	1784	372733	199327	16	16	3	0	5245	3.117		
2016	279	1376	57666	1605	0	1605	1530	179256	170875	14	14	3	0	796	3.720		
2016	280	1376	57667	4848	40	4848	4845	541665	541330	79	75	5	1	4892	4.025		
2016	281	1376	57668	2688	7	2688	2688	300332	300332	15	15	1	0	1205	3.679		
2016	282	1376	57669	3526	118	3526	3386	393926	378321	67	50	5	0	2562	4.293	20:00:00	
2016	283	1376	57670	5669	72	5669	5376	630856	600658	99	90	5	0	5081	4.162	20:00:00	
2016	284	1376	57671	6798	31	6798	6792	759532	758862	148	145	7	0	5331	4.316	20:00:00	
2016	285	1376	57672	4993	8	4993	4993	557832	557832	77	77	5	1	3676	4.368	20:00:00	
2016	286	1376	57673	1311	114	1311	1224	146444	136759	5	0	0	0	757	5.500	20:00:00	Power lost. Receivers warmed. A bad day.
2016	287	1376	57674	6228	71	6228	6199	695742	692618	340	314	18	0	589	12.932	22:00:00	
2016	288	1376	57675	6798	9	6798	5688	759544	635522	96	95	5	0	4317	3.679	23:00:00	
2016	289	1376	57676	6365	3	6365	5666	711059	632960	101	101	6	1	3934	3.790	20:00:00	
2016	290	1376	57677	6223	17	6223	6215	695157	694263	129	129	7	0	4757	4.038		
2016	291	1376	57678	5267	10	5267	5264	588443	588109	114	114	7	0	3543	4.048	03:00:00+	
2016	294	1376	57681	2916	39	2916	2897	325813	323690	15	12	1	0	2056	3.902		
2016	295	1376	57682	2553	0	2553	2553	285248	285248	42	42	5	0	1825	3.266	03:00:00	
2016	296	1376	57683	3936	4	3936	3936	439770	439770	22	20	1	0	2782	3.159	20:00:00	
2016	297	1376	57684	1848	1	1848	1848	206424	206424	2	1	0	0	761	2.869	20:00:00	
2016	298	1376	57685	4321	1	4321	4280	63577	63577	13	13	8	1	0	3.394	20:00:00	Stunning 4 consecutive
2016	299	1376	57686	6798	45	6798	6786	759550	758207	103	96	5	0	5848	3.231	20:00:00	
2016	300	1376	57687	4704	98	4704	4674	525498	522147	84	69	5	0	5252	3.478	20:00:00	20:39:31.ar (subint 12) for an interesting small double pulse

Continued on next page...

Table B.3: Data recording summary 2014-2017 (continued)

year	doy	freq	mjd	ar_files	raw_keep	timings	good_tim	all_spa	good_spa	g30_unv	g30_ver	bp_hr	g30_sel	spa_unv	spa_avg	pcal	notes
2016	304	1376	57691	2547	39	2547	2180	283882	243079	27	21	3	1	2371	3.331		Maser change, SML02 removed. Drop this day.
2016	305	1376	57692	6292	20	6292	6278	702943	701379	94	91	5	3	585	8.333		
2016	306	1376	57693	6327	4	6327	6321	706853	706215	123	121	6	0	5443	3.362	22:00:00	
2016	307	1376	57694	2053	0	2053	2045	229276	228382	19	19	3	0	1181	3.183	22:00:00	
2016	308	1376	57695	2959	21	2959	1835	330563	204978	50	47	9	1	3224	3.346		
2016	309	1376	57696	3940	15	3940	3934	440207	439535	119	116	10	1	3655	3.991	01:00:00+	
2016	310	1376	57697	4463	19	4463	4461	498552	498328	154	151	12	1	5152	4.180	23:30:00	
2016	311	1376	57698	2092	4	2092	2091	233642	233531	92	92	15	0	2276	4.147	05:58:36+	
2016	312	1376	57699	4314	16	4314	4314	482009	482009	66	65	5	0	4029	3.990	22:00:01	
2016	313	1376	57700	6798	42	6798	6797	759557	759557	578	567	29	0	8608	4.146	22:00:00	
2016	314	1376	57701	6798	147	6798	6757	759552	754968	221	202	10	2	11257	4.237	22:00:00	X drifting subpulse
2016	315	1376	57702	6799	19	6799	6661	759530	744109	203	202	10	1	6920	3.917	22:00:00	
2016	316	1376	57703	6798	13	6798	6794	759545	759099	204	204	10	3	959	8.647	22:00:00	
2016	317	1376	57704	6702	17	6702	6686	748826	747039	81	81	4	0	4840	3.919	22:00:00	
2016	318	1376	57705	6204	104	6204	6201	693063	692727	384	366	21	2	8844	4.258	22:00:00+	
2016	319	1376	57706	12		12	4	1340	446	0	0	0	0	3	2.676		
2016	320	1376	57707	6774	74	6774	6412	756868	716421	189	184	10	0	7278	4.225	22:00:00	
2016	322	1376	57709	1836	2	1836	264	29496	29496	1	1	1	0	365	3.470		
2016	323	1376	57710	6758	3339	6758	3367	755047	376198	250	250	26	0	1	27.251	12:00:00	
2016	324	1376	57711	3216	5	3216	3216	359321	359321	44	44	4	1	2734	4.073	20:00:00	
2016	325	1376	57712	6798	74	6798	6776	743757	741303	188	178	9	0	0	4.087	20:00:00	spa not quite finished
2016	326	1376	57713	5168	9	5168	4811	577343	537456	171	170	12	0	4618	3.907	20:00:00	
2016	327	1376	57714	1428	125	1428	1306	159559	145915	13	9	2	0	1449	5.079		
2016	328	1376	57715	3725	3	3725	3725	416198	416198	132	132	12	0	3804	4.038	01:00:00+	
2016	330	1376	57717	2730	9	2730	1787	305027	199666	32	32	6	0	2945	3.749	22:00:00	
2016	331	1376	57718	6276	41	6276	6260	701109	699324	261	261	14	2	6442	4.561	12:00:00	
2016	332	1376	57719	6798	234	6798	6640	759548	741898	299	286	15	2	8796	5.085	22:00:00	
2016	333	1376	57720	6798	269	6798	6746	759551	753744	345	322	17	0	9465	5.200	22:00:00	
2016	334	1376	57721	3102	24	3102	3102	346591	346591	195	195	22	0	3654	4.563		
2016	335	1376	57722	3516	176	3516	3472	392845	387930	104	96	9	0	6323	5.010	22:00:00	
2016	337	1376	57724	6283	46	6283	6273	702011	700893	256	255	14	2	8194	4.352		
2016	338	1376	57725	6564	54	6564	6564	733409	733298	268	265	14	1	8285	4.295	22:00:00	

Continued on next page...

Table B.3: Data recording summary 2014-2017 (continued)

year	doy	freq	mjd	ar_files	raw_keep	timings	good_tim	all_spa	good_spa	g30_unv	g30_ver	bp_hr	g30_sel	spa_unv	spa_avg	pcal	notes
2016	339	1376	57726	6769	181	6769	5736	756151	640891	251	233	14	1	1663	10.962	22:00:01+	
2016	340	1376	57727	6504	197	6504	6459	726701	721673	208	192	10	0	9633	4.396	22:00:00	
2016	341	1376	57728	6798	62	6798	6796	759549	759325	140	135	7	4	7315	3.717	22:00:00	
2016	342	1376	57729	6798	84	6798	6492	759549	725360	532	512	28	2	8218	3.901	22:00:00	
2016	343	1376	57730	6300	276	6300	3791	703907	423568	116	102	9	2	9469	3.852	22:00:00	
2016	344	1376	57731	3603	4	3603	3603	402565	402565	134	134	13	2	3641	3.855	12:00:00	
2016	345	1376	57732	2681	5	2681	2519	299516	281448	47	47	6	0	2422	3.535	20:00:00	
2016	346	1376	57733	6798	35	6798	6786	759545	758203	477	471	24	1	6064	3.699	20:00:00	
2016	347	1376	57734	6799	25	6798	6123	759561	684026	112	112	6	0	6651	3.531	20:00:00	The GLITCH
2016	348	1376	57735	6086	3	6086	3042	679917	339877	102	101	11	0	5559	2.890	20:00:00	
2016	349	1376	57736	6402	105	6402	6391	715310	714083	249	235	13	7	9081	3.941		
2016	350	1376	57737	6798	80	6798	6783	759545	757864	295	287	15	5	1297	10.965	20:00:00	
2016	351	1376	57738	6799	14	6799	6308	759496	704637	277	276	15	3	6638	3.789	03:08:37+	
2016	352	1376	57739	6798	45	6798	6519	759545	728370	240	238	13	1	7043	4.107	20:00:00	
2016	353	1376	57740	6798	52	6798	6783	759540	757863	346	343	18	0	7295	4.260	20:00:00	
2016	354	1376	57741	2528	12	2528	2528	282382	282382	125	125	17	1	2622	4.143	09:00:00	
2016	355	1376	57742	2207	6	2207	2207	246577	246577	36	36	5	1	2308	4.120	22:00:01	Long consecutive 00:36:32
2016	356	1376	57743	3532	21	3532	3532	394636	394636	204	203	20	1	4134	4.242	09:00:00	
2016	357	1376	57744	1950	79	1950	1936	217876	216312	44	34	6	1	3231	4.192	22:00:01	
2016	358	1376	57745	6798	15	6798	6797	759546	759434	240	240	12	1	6869	3.861	22:00:00	
2016	359	1376	57746	6798	11	6798	6798	759543	759543	255	253	13	1	6956	3.790	22:00:00	
2016	360	1376	57747	6798	6	6798	6798	759544	759544	231	231	12	1	6008	3.705	22:00:00	
2016	361	1376	57748	6798	26	6798	6797	759550	759439	379	369	19	1	7364	3.783	22:00:00	
2016	362	1376	57749	6420	10	6420	6416	717311	716865	214	212	11	0	6476	3.800	22:00:00	
2016	363	1376	57750	6999	19	6999	6985	781560	780410	345	345	17	1	7179	4.057	22:00:00	
2016	365	1376	57752	6798	37	6798	6797	759535	759423	352	350	18	1	7595	4.268	22:00:01	
2016	366	1376	57753	6798	43	6798	6798	759554	759554	339	339	17	0	7712	4.362	22:00:00	
2017	1	1376	57753	6798	46	6798	6697	759544	748260	336	334	17	1	7754	4.378	22:00:00	
2017	2	1376	57754	6798	59	6798	6798	759540	759540	561	556	29	4	8038	4.488	22:00:01	
2017	3	18605	57755	6798									0				
2017	4	1376	57756	6798	158	6798	6587	759534	735959	317	304	16	2	4196	6.423	21:00:00	
2017	5	1376	57757	120	1	120	34	13409	3800	6	6	63	0	110	2.656		
2017	6	1376	57758	120	0	120	30	13408	3352	1	1	11	0	102	2.475		

Continued on next page...

Table B.3: Data recording summary 2014-2017 (continued)

year	doy	freq	mjd	ar_files	raw_keep	timings	good_tim	all_spa	good_spa	g30_unv	g30_ver	bp_hr	g30_sel	spa_unv	spa_avg	pcal	notes
2017	8	1376	57760	120		120	29	13407	3240	0	0	0	0	62	2.550		
2017	9	1376	57761	120	0	120	35	13407	3910	2	2	20	0	92	2.678		
2017	10	1376	57762	120	0	120	33	13407	3688	0	0	0	0	92	2.569		
2017	13	1376	57765	120	0	120	32	13407	3574	2	2	22	0	105	2.501		
2017	14	1376	57766	120	0	120	32	13406	3574	4	4	44	0	115	2.744		
2017	16	1376	57768	120	0	120	27	13407	3016	0	0	0	0	76	2.595		
2017	21	1376	57773	450	3	450	447	50268	49932	5	5	4	1	432	3.237		
2017	22	1376	57774	6798	50	6798	6716	759509	750349	295	292	15	2	765	9.535	21:00:00	
2017	23	1376	57775	6000	36	6000	4547	670377	508034	155	152	11	1	6231	3.968	15:00:00	
2017	30	1376	57782	4617	9	4617	3773	515762	421464	94	94	8	1	4867	3.816	12:00:00	Changed ephemeris file half way through processing.
2017	31	22214	57783	5618		5618	5620	628385	628385	0	0	0	0	1	2.867		
2017	32	22214	57784	6648		6648	6649	743685	743685	0	0	0	0	1	2.864		
2017	33	8425	57785	6558		6558	4947	733616	553398	0	0	0	0	1	2.311		
2017	34	6658	57786	6302		6302	5250	704904	587298	0	0	0	0	4	2.220		
2017	35	1376	57787	6468	18	6468	6468	722634	722634	171	171	9	0	6514	3.836	12:00:00	
2017	36	1376	57788	6798	11	6798	6798	759516	759516	166	166	8	0	6579	3.720	12:00:00	
2017	37	1376	57789	6798	1	6798	6797	759528	759417	180	180	9	2	6054	3.555	12:00:00	
2017	38	1376	57790	6798	26	6798	6784	759517	757953	123	121	6	0	1801	5.660	12:00:00	
2017	39	12200	57791	6798		6798							0				
2017	40	1376	57792	6768	25	6768	6756	756165	754824	97	92	4	0	5877	3.206	12:00:01	
2017	41	2230	57793	261		261	200	29122	22376	0	0	0	0	5	3.115		
2017	41	4800	57793	5155		5155	5069	576585	567037	0	0	0	0	6	1.911		12:50:11 subint 84 is a giant
2017	43	2230	57795	6798		6798	4518	760440	505402	0	0	0	0	1700	3.094		
2017	44	1376	57796	6738	6	6738	6738	752810	752810	104	104	5	1	5641	3.381	12:00:00	
2017	45	1376	57797	6589	10	6589	6588	736084	735973	119	119	6	1	5091	3.365	12:00:00	Weird curvey RFI
2017	46	1376	57798	6798	68	6798	3882	759502	433720	58	48	4	1	5609	2.855	12:00:00	
2017	47	1376	57799	6678	13	6678	6675	746102	745767	109	106	5	0	5354	3.327	00:17:10+	
2017	48	1376	57800	6798	3	6798	6212	160885	160773	27	27	6	0	1145	3.549		
2017	49	1376	57801	6600	65	6600	6585	737381	735708	137	121	6	2	817	9.173	12:00:00	
2017	50	1376	57802	179		179	179						0			12:00:00	Drone RFI test - not on pulsar
2017	53	1376	57805	5772	21	5772	5772	644884	644884	16	16	0	0	3764	3.604	12:00:01	
2017	61	1376	57813	6168	4	6168	6167	689112	689001	108	108	6	1	5384	3.448	12:00:00	

Continued on next page...

Table B.3: Data recording summary 2014-2017 (continued)

year	doy	freq	mjd	ar_files	raw_keep	timings	good_tim	all_spa	good_spa	g30_unv	g30_ver	bp_hr	g30_sel	spa_unv	spa_avg	pcal	notes
2017	69	1376	57821	5886	46	5886	5882	657513	657067	130	111	6	0	5767	3.876	12:00:00	
2017	71	1376	57823	6744	6	6744	6744	753460	753460	141	141	7	1	5594	3.706	12:00:00	Dip in mavg. Check for micro glitch.
2017	72	1376	57824	6132	7	6132	6131	685081	684969	102	100	5	2	5069	3.693	12:00:00	
2017	73	1376	57825	6045	4	6045	6027	675330	673355	106	106	6	2	4646	3.535	12:00:00	
2017	74	1376	57826	6096	6	6096	6095	681061	680949	103	102	5	1	4923	3.421	12:00:00	
2017	79	1376	57831	5698	1	5698	5698	636551	636551	84	84	5	0	4878	3.572	12:00:00	BG3 cable out at start. VSOP_HO used in error.
2017	80	1376	57832	6756	36	6756	6750	754794	754122	158	148	7	0	6453	3.567	12:00:00	VSOP_HO used in error
2017	82	1376	57834	6798	13	6798	6797	759484	759372	180	175	9	1	5857	3.876	12:00:00	
2017	84	1376	57836	5544	8	5544	5541	619382	619046	146	145	9	0	5401	3.940	12:00:00	
2017	85	1376	57837	5568	5	5568	5567	622064	621953	125	125	8	0	5477	3.954	12:00:00	
2017	86	1376	57838	1055	21	1055	758	117674	84684	10	10	4	0	563	3.449		
2017	87	1376	57839	190	0	190	172	21191	19216	2	2	4	0	165	3.302	12:00:00	
2017	92	1376	57844	6258	24	6258	6258	699151	699151	139	132	7	1	5832	3.499	12:00:00	
2017	94	1376	57846	5877	76	5877	5868	656511	655507	186	155	9	0	3852	5.365	12:00:00	
2017	96	1376	57848	6798	72	6798	6786	759475	758131	453	424	22	1	8357	3.814	12:00:00	
2017	97	1376	57849	90	1	90	90	10055	10055	0	0	0	0	79	3.579		
2017	99	1376	57851	5934	16	5934	5934	662944	662944	168	167	10	0	6479	4.085		
2017	100	1376	57852	6798	205	6798	6639	759417	741653	227	200	10	0	6857	4.302	12:00:00	
2017	101	1376	57853	6696	18	6696	6696	748076	748076	238	237	12	0	7035	4.129	12:00:00	
2017	102	1376	57854	25	0	25	25	2756	2756	4	4	57	0	24	3.782		
2017	106	1376	57858	6709	11	6709	6709	749360	749360	205	200	10	1	7555	3.920	12:00:00	
2017	107	6658	57859	6030		6030	5358	674506	599340	0	0	0	0	9	2.226		
2017	108	1376	57860	5936		5936	5926	663122	662004	82	-82	-4	0	519	8.319	08:15:00+	
2017	108	2230	57860	23		23	11	1701	1154	0	0	0	0	19	1.714		
2017	111	12200	57863	6798		6798	6798	760412	760412	0	0	0	0	10	3.440		
2017	114	1376	57866	182	0	182	180	20259	20109	4	4	7	0	176	3.938		
2017	115	1376	57867	6798		6798							0			12:00:00	

Appendix C

Nature paper

This paper was submitted to *Nature* prior to this thesis being sent for examination. However the Nature Referees required polarisation data to be considered. The polarisation calibration and analysis process took many months and so these results were not included in this thesis.

Appendix C has been removed for copyright or proprietary reasons.

It has been published as: Palfreyman, J., Dickey, J. M., Hotan, A., Ellingsen, S., van Straten, W., 2018. Alteration of the magnetosphere of the Vela pulsar during a glitch, Nature, 556, 219-222

Index